https://ntrs.nasa.gov/search.jsp?R=19960016651 2020-06-16T04:31:26+00:00Z

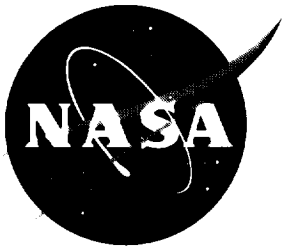

NASA Contractor Report 4706

Structural Damage Prediction and Analysis for Hypervelocity Impacts – Handbook

N.C. Elfer

Contract NAS8–38856
Prepared for Marshall Space Flight Center

February 1996

NASA Contractor Report 4706

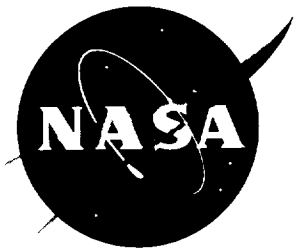

Structural Damage Prediction and Analysis for Hypervelocity Impacts – Handbook

N.C. Elfer
Lockheed Martin Marietta Manned Space Systems

National Aeronautics and Space Administration
Marshall Space Flight Center • MSFC, Alabama 35812

Prepared for Marshall Space Flight Center
under Contract NAS8–38856

February 1996

FOREWORD

This handbook was prepared under contract NAS8-38856 from NASA Marshall Space Flight Center. The study contract title was "Structural Damage Prediction and Analysis for Hypervelocity Impacts." The Technical Monitors were Dr. Joel Williamsen, Greg Olsen, and Jennifer Robinson. The work was performed between October, 1989, and September, 1995.

In the area of ballistic limits and fracture mechanics, there are often several different philosophies in the technical community. The author has his own opinions which are reflected in this work. The author's opinions are based on his interpretation of test and analysis data, which may be different than others in the scientific community. Furthermore, the reader is urged to consult the references quoted in this work, other literature, and investigators currently active in the field to ensure the accuracy and relevance of the equations and trends quoted here.

TABLE OF CONTENTS

Foreword ii

Table of Contents v

Appendices vi

Figures vii

1 INTRODUCTION 1-1

2 ENVIRONMENT 2-1

2.1 Meteoroids 2-1

2.2 Space Debris 2-1

3 PENETRATION MECHANISMS 3-1

3.1 Penetration Definitions 3-1

3.2 Single Wall Damage Mechanisms 3-1

3.3 Double Wall Penetration Mechanisms 3-2

3.3.1 Fragment Penetration 3-2

3.3.2.1 Projectile Shape Effects 3-4

3.3.2 Momentum Failure 3-4

3.3.2.1 Wilkinson Model 3-4

3.3.2.2 Modifications to the Wilkinson Model 3-5

3.3.2.3 Grove's Model 3-5

3.3.2.4 Housen and Schmidt's Scaled Velocity Model 3-5

3.3.3 Spall Failure 3-6

3.3.4 Oblique Impact Effects 3-7

3.3.5 Christiansen's High Velocity Extrapolation 3-8

3.3.6 Comparison of High Velocity Predictions 3-8

4 PROBABILITY ANALYSIS 4-1

4.1 Probability of No Impact 4-1

4.2 Probability of No Penetration 4-1

4.3 Probability of No Critical Damage 4-2

4.4 Probability Analysis Codes 4-3

5 ADVANCED SHIELD CONCEPTS 5-1
5.1 Bumper Material Selection 5-1
5.2 Multiple Bumpers 5-2
5.3 Intermediate Catcher Shields 5-3
5.3.1 Catcher materials 5-3
5.3.2 Impregnated Catcher materials 5-4
5.3.3 Catcher Location 5-4
5.4 Analysis of Advanced Shield Designs 5-5
5.5 Geometric Bumper Shapes 5-5
6 DEFORMATION ANALYSIS 6-1
6.1 Bulge Deformation Analysis 6-1
6.1.1 Deformation 6-2
6.2 Hole Size 6-3
6.2.1 Effect of wall thickness on hole size 6-4
6.2.2 Effect of projectile size 6-4
6.2.3 Tearing of petal ends 6-5
7 DAMAGE TOLERANCE 7-1
7.1 Initial Crack Length 7-1
7.1.1 Crack Propagation Energy Balance 7-1
7.2 Structural Failure 7-2
7.2.1 Material Properties for Fracture Analysis 7-2
7.2.2 Cylinder Effect 7-4
7.2.3 Hole Effect 7-5
7.2.4 Influence Function for a Cylinder 7-5
7.2.5 Cylinder with integrally machined stiffeners 7-6

APPENDICES

A. Equations
B. Bibliography
C. Hypervelocity Test Databases
- Martin Marietta IRAD M01S Test Database (Tests performed at UDRI)
- MSFC Test Database (July 1991)
- JSC Space Station Test Database (July 1991)

D. Modeling the Response of a Thin Sheet Due to a Hypervelocity Debris Cloud Impact

FIGURES

Fig. 1-1 Rupture of a pre-loaded 2219-T851 panel due to a hypervelocity impact with a 3 gram projectile at 6.4 km/s.....1-3

Fig. 1-2 Bumper and Kevlar 29 cloth in front of rear wall in Fig. 1-1 after the impact.....1-4

Fig. 1-3 Front of the fractured rear wall in Fig. 1-1. Integrally machined stiffeners could not stop the crack.....1-5

Fig. 2-1 Impact flux for space debris or meteoroids of diameter shown and larger. Flux is defined for a randomly tumbling surface. [as published in Williamsen94].....2-3

Fig. 2-2 Impact flux for space debris of diameter shown and larger, with and without 100% effective collision avoidance.....2-4

Fig. 2-3 Angular and velocity distribution of debris flux.....2-5

Fig. 3-1. Multi-layer penetration mechanisms.....3-9

Fig. 3-2. Typical ballistic limit as a function of impact velocity and obliquity for a multi-layer design.....3-10

Fig. 3-3 Typical Whipple bumper fragment damage.....3-11

Fig. 3-4. Post impact debris cloud radiographs from a spherical projectiles. [UDRI shot in Rajendran89].....3-12

Fig. 3-5 Post impact debris cloud radiographs from a cylindrical projectile. [UDRI shot in Rajendran89].....3-13

Fig. 3-6 Rear wall damage from a cylindrical projectile that impacted the bumper without yaw. (UDRI shot 4-0411).....3-14

Fig. 3-7 Front of rear wall from Fig. 3.6. Note central crater probably from the tip of the bumper debris cloud.....3-15

Fig. 3-8 Rear of rear wall from Fig. 3.6 showing wide area spall.....3-16

Fig. 3-9 Rear wall damage due to a cylindrical projectile that had yaw. (UDRI shot 4-0436).....3-17

Fig. 3-10 Front of rear wall from Fig. 3.9.....3-18

Fig. 3-11 Rear of rear wall from Fig. 3.9. Penetration and spall from aligned projectile fragments, and spall probably from the tip of the bumper debris cloud.....3-19

Fig. 3-12 Wilkinson type momentum bulge and failure with Kevlar intermediate shields to prevent fragment damage.....3-20

Fig. 3-13 Ballistic limit determined from aluminum rear wall with cadmium projectile and bumper tests, scaled to equivalent all aluminum test. [Schmidt94]. 3-21
Fig. 3-14 Oblique impact schematic..... 3-22
Fig. 3-15 Oblique impact bumper damage. (UDRI shot 4-0657)..... 3-23
Fig. 3-16 Oblique impact ricochet damage. (same as Fig 3-14) 3-24
Fig. 3-17 Oblique impact rear wall damage (back side) due to a fragment normal to the bumper. The fragment was likely bumper material. (same as Fig 3-14)..... 3-25
Fig. 3-18 Comparison of high velocity penetration equations. [Hayashida95] 3-26
Fig. 4-1 Flux times the exposed area times the exposure time versus velocity and obliquity from SD_SURF. 4-4
Fig. 5-1 Multi-shock aluminum bumper compared to Whipple bumper (Fig. 3-3). MSFC tests. [Elfer88] 5-6
Fig. 5-2 Double bumper (equal weight) test results. MSFC tests. [Elfer88].... 5-7
Fig. 5-3 Kevlar cloth intermediate shield (catcher) UDRI tests. Same designs as Fig. 1-1, with (no penetration) and without Kevlar 29 cloth (penetration) for a 1 gram projectile. [Elfer88] 5-8
Fig. 5-4 Multiple layers of aluminum bumper and Kevlar cloth can prevent penetration for the same conditions as Fig. 1-1. (UDRI 4-0675)[Elfer88]..... 5-9
Fig. 6-1 Rear wall deformation (same design as Fig. 1-1) 1 gram projectile 6.4 km/s. (UDRI 4-0508) [Elfer] 6-6
Fig. 6-2 Rear wall deformation (same design as Fig. 1-1 except -T62 rear wall) 1.3 gram projectile 6.4 km/s. (UDRI 4-0508) [Elfer]..... 6-7
Fig. 6-3 Projectile mass for no penetration (or rupture) is proportional to S^2 for adequate bumpers and catchers. 6-8
Fig. 6-4 Comparison of debris spray dispersion angle between HULL results and Wilkinson's vaporization equation. 6-9
Fig. 6-5 STEALTH models of rear wall deformation. 6-10
Fig. 6-6 Measured thinning of rear wall. Maximum thinning may occur at the centerline or in a circle away from the centerline. 6-11
Fig. 6-7 Measured thinning of rear wall compared to a HULL analysis. .. 6-12
Fig. 6-8 Comparison of measured permanent deformation, HULL analyses and simple NASTRAN sheet element analyses. 6-13

Fig. 6-9 Correlation between maximum effective rear wall strain as predicted by EPIC simulation and Grove's dimensionless design parameter. 6-14
Fig. 6-10 Summary of pre-stressed panel test results. Large panels similar to Fig. 1-1. [Elfer] 6-15
Fig. 6-11 Same as Fig.1-1 except for 5456 rear wall material and impact occurred on a stiffener. 6-16
Fig. 6-12 Same as Fig. 6-10 except that stiffener was removed prior to impact 6-17
Fig. 6-13 Same as Fig. 6.11 except sheet was used instead of machining plate down to same 1/8 inch thickness 6-18
Fig. 6-14 Same as Fig. 6.12 except thinner sheet. 6-19
Fig. 6-15 Same as Fig. 6.12 and 6-13 except thinner sheet 6-20
Fig. 6-16 Same as Fig. 6-10 and 1.1 except 6061-T6 material used. 6-21
Fig. 6-17 Reverse of Fig. 6-12, showing torn petals, catcher cloth, and bumper. 6-22
Fig. 6-18 The petals were bent back in on the rear wall shown in Fig. 6-13. Note that the impact area is approximately one third the diameter of the final hole size. 6-23
Fig. 7-1. An illustration of the energy balance for rear wall crack propagation. 7-7
Fig. 7-2. Tear Resistance of 0.063 in. thick aluminum sheet. [Kaufman and Hunsicker] 7-8
Fig. 7-3. Unit propagation energy of some aluminum alloys at various temperatures. [Kaufman and Hunsicker] 7-9
Fig. 7-4. Failure stress versus flaw size in 61 cm wide sheet of 2219 and 5456. [Elfer 88] 7-10
Fig. 7-5. R-curve versus physical flaw size a 61 cm wide sheet of 2219-T87 and 5456-H116. [Elfer 88] A flaw length was not necessarily measured at max stress. 7-11
Fig. 7-6 Stress intensity magnification factor for a cylinder relative to a flat plate 7-12
Fig. 7-7 Influence function for a flat plate. 7-13
Fig. 7-8 Effect of a Hole (modeled as depressurized zone) on the Stress Intensity in a Cylinder. [Rajendran in Elfer88] 7-14
Fig. 7-9 NASTRAN 1/4 cylinder symmetric model 7-15

Fig. 7-10 Effect of mesh size on the calculated stress intensity for a cylinder (using NASTRAN crack tip element)..... 7-16
Fig. 7-11 Influence function for a crack in a cylinder..... 7-17

1 INTRODUCTION

This handbook provides a reference for the prediction and analysis of structural damage due to hypervelocity impact. It is applicable to Space Station habitable module walls and other similar spacecraft . Hypervelocity impact includes both meteoroid and space debris impacts. The emphasis of the discussion is stretching, petaling, and tearing of a module wall by either meteoroid or debris impacts.

The analyses and comments are general design guidelines and not necessarily applicable to final Space Station designs since several configuration and detail design changes were being made during the course of this contract. Rather, the analyses and comments may indicate either a point-in-time concept analysis, available test data, or desirable protection goals, not hindered by the design and operation constraints faced by Space Station designers. The baseline design for debris protection was nominally:

- bumper of 0.13 cm (0.050 inch) 6061-T6 aluminum
- 30 layers of 1.3 μm (0.0005 inch) thick Multi-Layer Insulation (MLI)
- standoff of 10.2 cm (four inch) and
- rear wall of 0.32 cm (0.125 inch) age-formed 2219-T87 aluminum.

However, this does not reflect the final space station design and is a point of reference only.

Selected equations are included in appendix A. A Bibliography for the report and appendix A is included as Appendix B. Appendix C contains several light gas gun hypervelocity test databases.

The typical space vehicle design requirement is to meet a specified probability of no penetration or failure in the design lifetime. Large area and long duration spacecraft require a substantial weight of protective shielding. For example, an object the size of the Space Station Freedom, will require on the order of 10 kg/m^2 or more for meteoroid and space debris protection. Part of the problem in determining a shield to meet a given reliability is understanding the threat. Rather than having a unique threat size and velocity which must be defeated, there is a spectrum of sizes, velocities, and obliquities, and consequently a variety of penetration mechanisms which must be considered.

To design these shields accurate analysis of the probability of penetration must consider the flux, velocity and angular distributions of debris, as well as the debris shape and density distributions, the spacecraft geometry, and the penetration resistance of the structure. Each has a high level of uncertainty. Penetration resistance is analyzed with a combination

of light gas gun simulation testing, and computer models. Routine testing is possible up to 7 km/s which encompasses a portion of the possible debris impact velocities. A three stage light gas gun has been developed at Sandia National Laboratory, as well as an inhibited shaped charge launcher at Southwest Research Institute (SWRI), to achieve 10 km/s, but in each case the state of the projectile at impact needs to be better characterized. The average space debris impact velocity is 10 km/s but impacts can occur at up to 16 km/s. Meteoroid impact velocities can be up to 72 km/s.

Damage tolerance in manned systems is essential to provide fail-safe vehicles. A goal is to have pressure vessels leak, but not burst in the event of an impact beyond the design considerations. However, this is not practically achievable for all situations. "No-burst" analysis for a hypervelocity penetration must consider a damage zone on the order of 25 cm, which is much larger than the typical flaw size analyzed in aerospace structures.

Figure 1-1 shows the catastrophic results possible for an impact beyond a design's capability. This was tested at the University of Dayton Research Institute (UDRI) as a Martin Marietta IR&D project. [Elfer88]* The projectile was a 12.7 mm (0.5 inch) sphere of 2017 aluminum, weighing 3 grams and fired at 6.4 km/s. The rear wall was 2219-T851, nominally 3.2 mm (0.125 inch) thick, pre-loaded with Bellville washers to a stress of 130 MPa (19 ksi). The wall had an 2 mm (0.080 inch) 6061 bumper held 114 mm (4.5 inches) in front of the wall, with 4 layers of style 710 Kevlar 29 cloth held 38 mm (1.5 inch) from the wall. The Kevlar cloth was essential to this type of failure, as will be discussed in Sec. 6. Figure 2 shows the bumper and Kevlar cloth after the impact. Figure 3 shows the front of the rear wall. Integrally machined stiffeners, 3.2 mm (0.125 inch) thick and 32 mm high, could not stop the crack from running.

---

* References in the Bibliography, Appendix B, are shown in square brackets. A number refers to the year of publication of the referenced author's document.

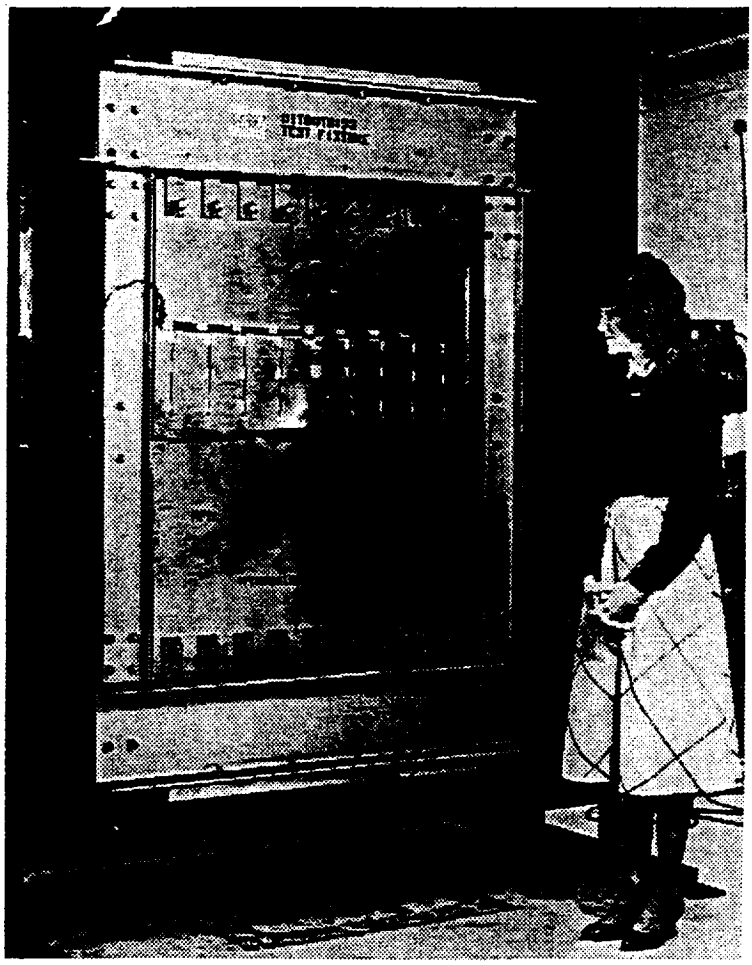

Fig. 1-1 Rupture of a pre-loaded 2219-T851 panel due to a hypervelocity impact with a 3 gram projectile at 6.4 km/s.

Fig. 1-2 Bumper and Kevlar 29 cloth in front of rear wall in Fig. 1-1 after the impact.

Fig. 1-3 Front of the fractured rear wall in Fig. 1-1. Integrally machined stiffeners could not stop the crack.

2 ENVIRONMENT

Equations for the meteoroid and debris flux are given in NASA SSP 30425 (Rev. A with change A1) "Space Station Program Natural Environment Definition." and are built into the BUMPERII analysis code. [Graves; Coronado] Figure 2-1 shows the meteoroid and debris flux. The definition of the flux is for the diameter shown *and larger*. The diameter shown is the minimum diameter with that flux. Fig. 2-2 shows that if trackable debris, 10 cm and larger, can be completely avoided then there is a significant impact on the flux of particles in the 1 cm to 10 cm *and larger* sizes. Note that the graphs in Fig. 2-1 and 2-2 are for specific years, inclinations, altitudes and solar activity. The EnviroNET computer system is a convenient method of checking the currently accepted definition of the orbital environment. [The EnviroNET user guide is available from Dr. Michael Lauriente, Code 400.1, Goddard Space Flight Center, Greenbelt MD 20771, phone (301)-286-5690.]

2.1 Meteoroids

The meteoroid environment is dominated by low density (0.5 to 2 g/cm^3) loosely packed ice rather than the more dense iron-nickel meteoroids. However, the loosely packed ice can be very damaging at the high impact velocities. The meteoroid environment is better seen in relationship to the Earth rather than the spacecraft. The earth regularly moves through streams (densely populated orbits) which produce meteoroid showers. There is also a random "sporadic" flux. The earth also tends to focus the meteoroids due to gravitational attraction. The spacecraft then moves through this changing environment, shadowed by the Earth, accumulating most impacts on the forward and then the skyward facing surfaces.

2.2 Space Debris

For a large-area, long-duration spacecraft the debris flux will by more significant, as shown in Fig. 2-1. Much of the environment definition has been driven by D. Kessler at NASA-JSC and it is continually subject to updates because significant break-up events, or possibly the lack thereof. Users of this document will either have a contractual requirement, or they should consult EnviroNET as mentioned at the start of this section.

The debris environment is predominantly aluminum particles, although a variety of other materials are present, including paint, electronic components, composites, titanium, and steel.

Space debris is very directional. For low earth orbit (LEO) debris may be described by the intersection of circular orbits. Besides the dominant polar, 60°(e.g.. Baikonur, Tyuratam) and 28° (Cape Canaveral, Fl) inclinations, precession of orbits can result in high impact velocities from orbits with the same inclination. Figure 2-2 shows the fraction of the total flux coming from angles relative to the direction of flight in 5° increments. The relative impact velocity for the intersection of 500 km orbits is also labeled on the plot. The relative impact velocity in LEO is determined by the orbital velocity and the intersection angle of the two orbits.

If the spacecraft is not fixed relative to the earth then it can be treated as randomly tumbling. There will be a spectrum of relative impact velocities and obliquities which must be considered in the penetration analysis with the different penetration mechanisms which will be discussed later.

When the spacecraft attitude is fixed relative to the earth, each facet of the surface will have its own distribution of probable obliquity angles and velocities. While no debris overtakes from the rear, a rear facing facet can be impacted by debris which appears to come from the side (an orbit with a shallow intersection angle). Debris cannot intercept a LEO spacecraft from more than 10° above or below a plane tangent to the local Earth normal, since the debris would otherwise enter the Earth's atmosphere and be removed as a threat. The typical angle is only 3° for a 500 km orbit being crossed by trackable debris.

It must be noted that the definition of flux used is the flux, F, on a randomly rotating object. This means that the area will spend half of its time with no exposure to a given stream. However, when a stream from a particular direction is used with the projected area in that direction, then the flux, J, is given by

$$J = 4\,F$$

The simplest derivation of this is that the projected area of a sphere, πr^2, is one fourth of the surface area of a sphere, $4\pi r^2$. While each will receive the same number of impacts from a stream perpendicular to the disk, the impacts per square meter are four times higher for the disk. An alternative definition is

$$j = F/\pi = J/(4\pi)$$

where j is the flux in terms of impacts per square meter per year per steradian.

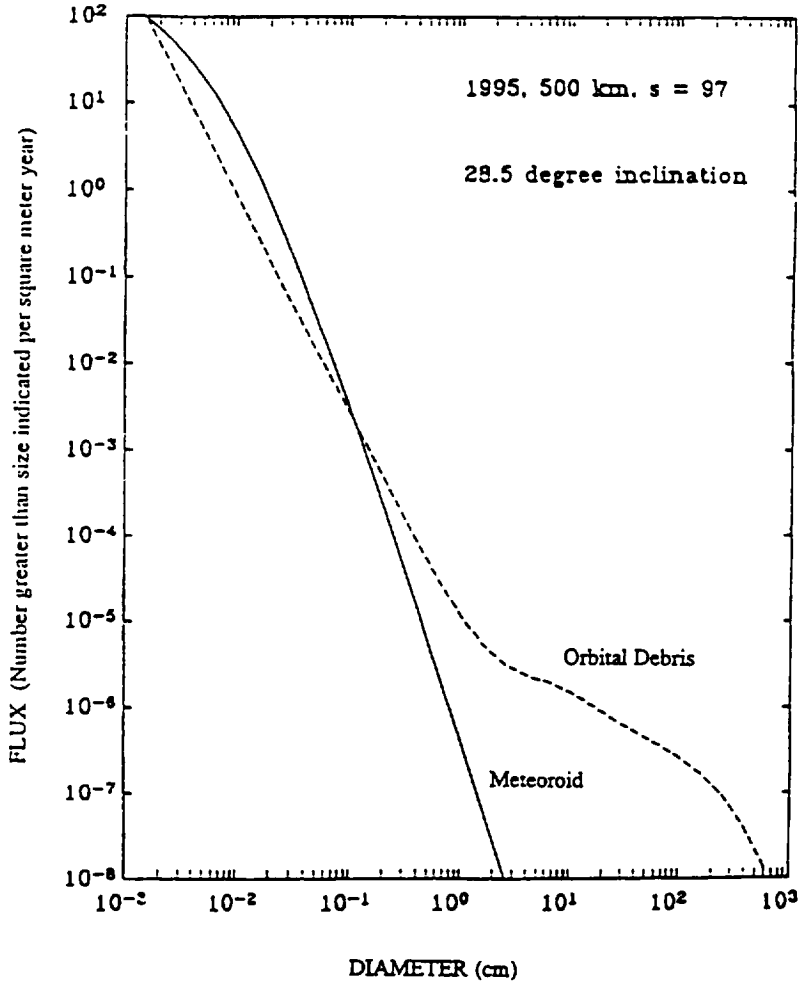

Fig. 2-1 Impact flux for space debris or meteoroids of diameter shown and larger. Flux is defined for a randomly tumbling surface. [as published in Williamsen94]

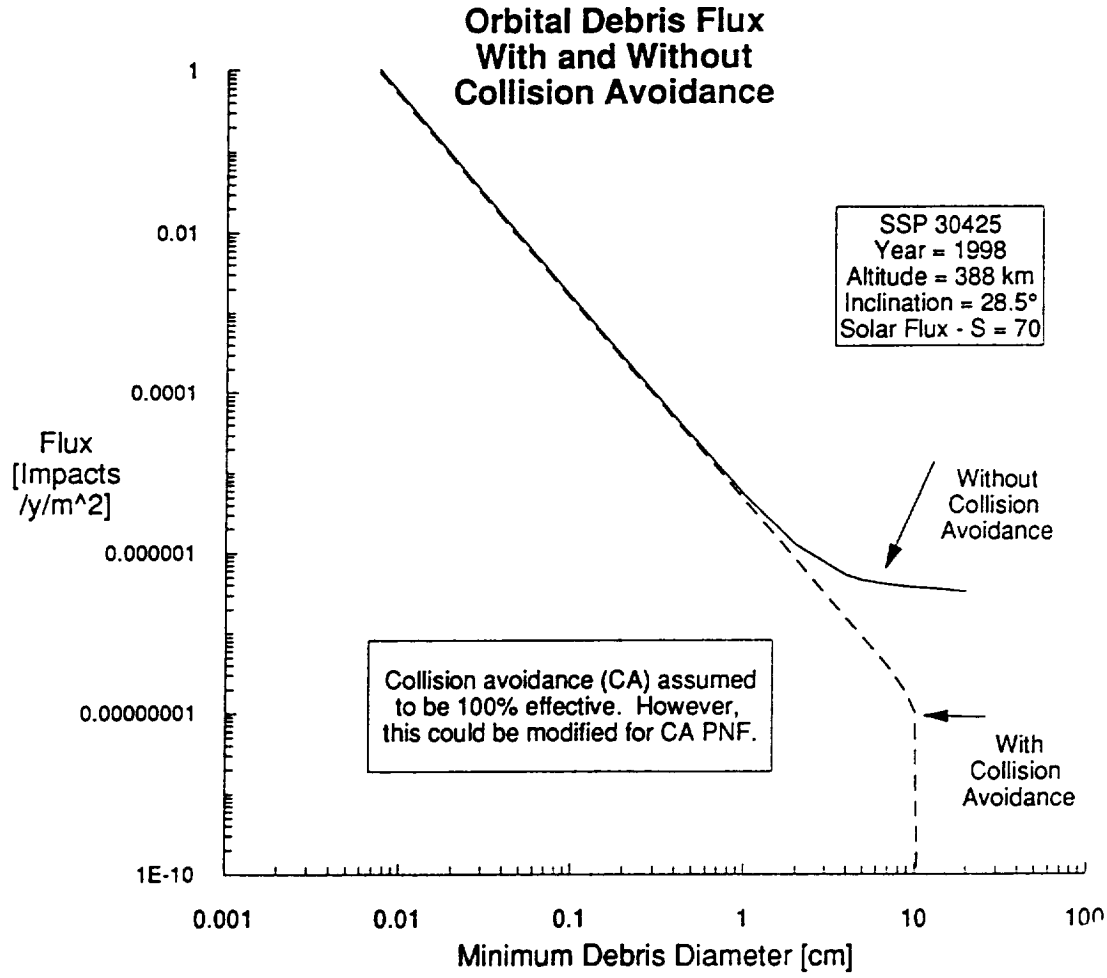

Fig. 2-2 Impact flux for space debris of diameter shown and larger, with and without 100% effective collision avoidance.

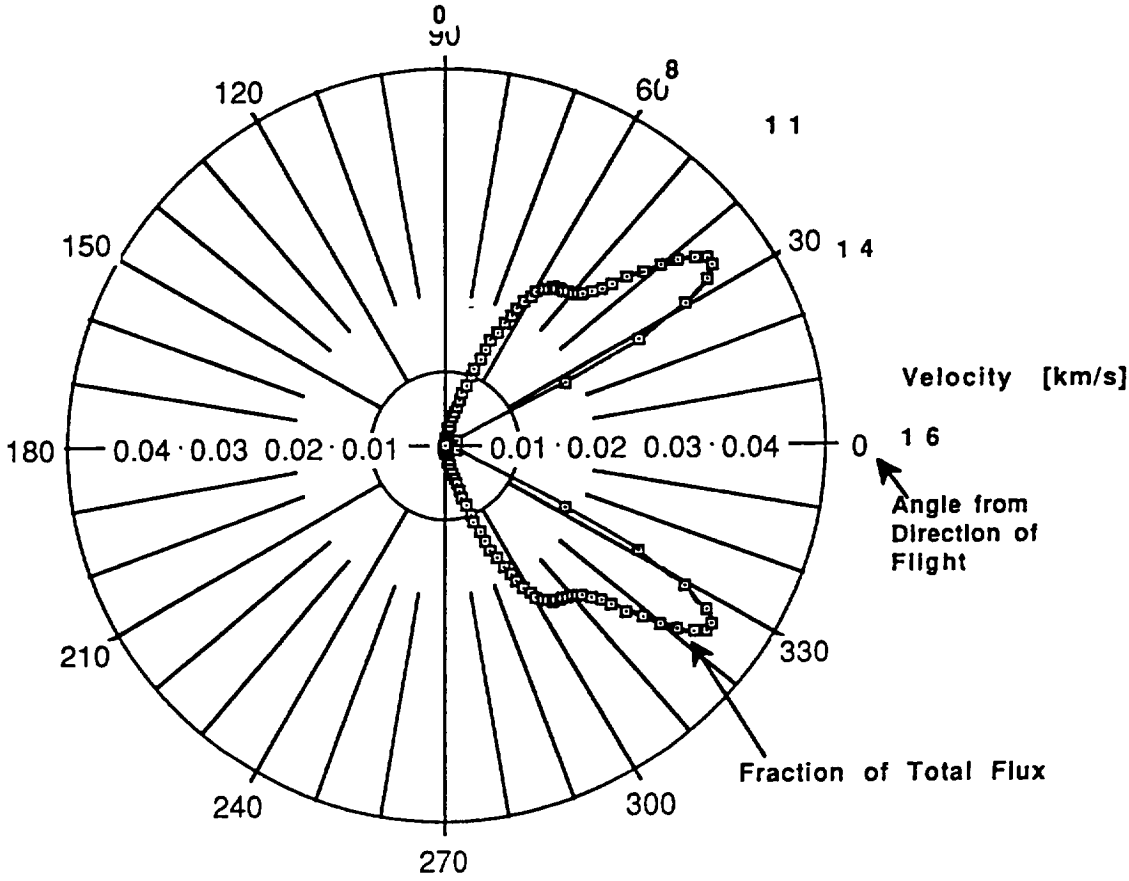

Fig. 2-3 Angular and velocity distribution of debris flux.

3 PENETRATION MECHANISMS

There are a variety of penetration mechanisms that work in unison or compete with each other to cause a failure. Penetration predictions based on one penetration mechanism may lead to a gross error when extrapolated to conditions for which another penetration mechanism is occurring. Appendix C contains hypervelocity impact test data from NASA-MSFC, NASA-JSC and Martin Marietta IR&D M-01S.

Debris cloud analysis characterization was reviewed by Piekutowski. [Piekutowski 95]

3.1 Penetration Definitions

The definition of penetration used in most recently in hypervelocity testing for the Space Station, is no detached spall or no visible hole through the thickness. Leaking helium, or penetration of a witness sheet behind the rear wall are alternate definitions of penetration that have been used on other programs. (Note that while detached spall is considered a failure, it does not appear to make a significant difference compared to the no-visible-hole definition, at least for Space Station shields up to 7 km/s.)

3.2 Single Wall Damage Mechanisms

A single wall can be very vulnerable to hypervelocity impact. At low velocities, the depth of the crater is controlled by erosion of the projectile. However, as velocity increases, the crater becomes hemispherical and the volume of material removed is roughly proportional to the energy of the impacting particle. Tests indicate oblique impacts should use only the normal component of the impact velocity to calculate energy and crater volume.[Summers59] As the obliquity angle becomes large, greater than 45°, the crater becomes elongated, and at greater than 65° from the normal, the projectile primarily ricochets from the surface (as small fragments).

For a finite thickness sheet, the threshold of penetration is reached when the bottom of the crater links up with spall from the back of the sheet. Spall occurs when the compressive shock wave accelerates the rear of the sheet and reflects as a tensile wave above the ultimate strength of the material.

Five single wall penetration equations were reviewed by Hayashida and Robinson. The Fish-Summers and JSC (Modified Cour-Palais) are given in Appendix A. Both found to adequately fit recent test data. The Schmidt-Holsapple equation was found to predict significantly higher diameters to

cause penetration, and it significantly overestimate the penetration threshold on at least one test.

3.3 Double Wall Penetration Mechanisms

At different impact velocities and obliquities, multi-wall designs may be penetrated by projectile or bumper shield fragments, spall, melting, or by a late time momentum failure of the final wall. Intermediate shields are useful in further breaking up projectile fragments and reducing spall in a rear wall. At very high velocities the bumper and projectile will melt or even vaporize. If the final wall is not penetrated by fragments it must still absorb the momentum of the initial projectile.

The ballistic limit is dictated by the operative penetration mechanism. The reaction of a multiwall shield to a projectile impact is shown schematically in Fig. 3-1. With increasing shock pressures the original projectile will first fragment into smaller and smaller sizes, then melt and even vaporize. Subsequent layers must stop the fragments from the initial impact, resist spall, and also absorb the momentum. Tests at the University of Dayton Research Institute (UDRI) and at Marshall Space Flight Center (NASA-MSFC) have demonstrated that an intermediate layer of thermal insulation material can be very effective in preventing cratering and spallation of the rear wall, but the momentum of the initial impact must still be absorbed by the rear wall. Even if the original particle is fragmented and "ricochets" from the bumper, bumper fragments may still penetrate the rear wall.

The ballistic limit for a given shield can be plotted as a function of impact velocity and obliquity as shown in Fig. 3-2. This will be called the ballistic limit surface, the shape of which will change radically for changes in shield design. For example, a change in spacing will strongly influence momentum failure, have a mild influence on fragment penetration, and almost no effect on single particle, or ricochet penetration. It is interesting to note that in the valley, or "bucket" of the surface, an oblique impact can be more penetrating than a normal impact because the projectile is not as effectively fragmented.

3.3.1 Fragment Penetration

For penetrations less than 1.5 km/s, there will typically be a single hole in the bumper and the rear wall. As impact velocity increases the projectile begins to fragment into smaller and smaller pieces. Figure 3-3 shows typical rear wall damage that may result from normal incidence hypervelocity impact. There may be one or many rear wall holes.

Individual holes may be due to single particles, multiple craters occurring at the same location, or then interaction of rear wall momentum and a weakened and cratered rear wall. Piekutowski showed that for thin bumpers (relative to the projectile diameter) a single large, and lethal, fragment may remain at the center of the post impact fragment debris cloud.

As a rule of thumb, to be effective at 6 km/s impacts the bumper should be 0.15 to 0.25 times the projectile diameter, although much lighter bumpers can work well at these high velocities if the standoff is large. [Christiansen91,92]

There have been several attempts at empirically determining the ballistic limit for fragment penetration. Projectile break-up is analyzed with a combination of experimental data, scaling, hydrocodes, and phenomenological models. The test databases in Appendix C contain a wealth of information, but much of it remains anecdotal in terms of different shield parameters. Jolly and Williamsen [93] performed a curve fit to the data for 0.125 inch rear walls, but even this was difficult due to the go/no-go nature of penetration tests and the results contained both conservative and non-conservative predictions.

The ballistic limit diameter for normal impact reaches a low, on the order of the total shield thickness, at approximately 3 km/s, and goes up to almost twice the total shield thickness for standoffs of 30 times the projectile diameter.

The available penetration equations in BUMPERII appear to be adequate in the regime less than 7 km/s. Christiansen's equations in Appendix A have a simple expression for the ballistic limit below 3 km/s and use linear interpolation between there and the transition to the high velocity penetration mechanism at 6 to 7 km/s, depending on the shield. The THOR equations in BUMPERII were not included in Appendix A due to their complexity, but they are more general and can be used for different materials besides aluminum-on-aluminum. The Burch equations, also included in Appendix A, are particularly useful for prediction of penetration through multiple plates. Although Jolly and Williamsen note they may not reflect oblique impact results accurately. Only the Burch aluminum-on-aluminum equations were included in appendix A, but the original paper has steel-on-aluminum as well.

For the initial baseline design, the fragment penetration equations do not have a strong influence on the probability of no penetration [Elfer92a] as will be discussed in Sec. 4.

3.3.2.1 Projectile Shape Effects

Cylinders with a length to diameter ratio of 1 (L/D = 1) have been found to be much less penetrating than equivalent mass spheres at low velocities, 3 km/s, but the ranking reversed at 6+ km/s.[Morrison72, Elfer 88] This was because the cylinder shatters more easily than the sphere at 3 km/s. At 6+ km/s, in normal impacts the cylinder creates a debris cloud with a spike, of which the tip is the most lethal. The tip appears to be a spall fragment from the bumper, normal to the flat of the cylinder, that can penetrate the rear wall. This is illustrated in Fig. 3-4 and 3-5. Morrison described this: "for cylindrical projectiles, the shock [in the rear surface of the bumper} near the axis is planar, whereas for the sphere the shock is more hemispherical."

Schmidt et al [1992] showed that a disk with a small L/D could be very penetrating even for a cadmium on cadmium impact. A flat fragment, including all or part of the bumper, tended to continue in the line of flight with very little dispersion. This easily penetrated the rear wall.

The fragments from a yawed cylinder (as opposed to the bumper) can tend to line up and penetrate the rear wall, rather than being spread over a large area like the sphere fragments. A typical penetration is shown in Fig. 3-6 through Fig. 3-11.

3.3.2 Momentum Failure

If the wall is not penetrated by fragments then it must absorb the debris cloud momentum. The failure of the rear wall from this blast loading can be very sensitive to the momentum distribution, the rate of loading, momentum multiplication due to rebound and/or cratering, and damage to the surface from early time cratering. Generally, the failure models have either relied on an assumed momentum distribution in the rear wall, or a critical momentum intensity. This will be discussed briefly in the following sections and in greater detail in Section 6. This failure mode can be achieved in typical light gas gun tests only with intermediate shields or by the use of cadmium projectiles and cadmium bumpers (Cd-on-Cd) to simulate vaporization. [Schmidt92] Figure 3-12 shows a momentum bulge and failure in specimens with a Kevlar intermediate shield to prevent fragment damage. The specimen that failed was impact by the same size projectile with slightly higher velocity.

3.3.2.1 Wilkinson Model

The Wilkinson model for momentum failure was based on McMillan's hydrocode models of impacts at velocities sufficient to cause complete vaporization of the projectile and bumper. The dispersion of the debris

cloud momentum intensity on the rear wall is given in Appendix 1. Note that the dispersion angle corresponds to one standard deviation on a Gausian momentum distribution. A significant amount of momentum was assumed to be outside of the dispersion angle.

The rear wall failure criterion was determined by Wilkinson from two dimensional analyses of a strip bulging under a Gausian momentum intensity distribution.

3.3.2.2 Modifications to the Wilkinson Model

Elfer [88] modified the Wilkinson dispersion angle for aluminum impacts based on two reasons. The first reason was to select a constant to fit the equation to observed failures in Whipple bumpers with Kevlar cloth intermediate shields. The second reason was that the dispersion angle observed from HULL hydrocode analyses, as well as observed rear wall damage rings, was smaller than the dispersion angle that Wilkinson used. This is simply a manifestation of the fact that Wilkinson's analysis was for aluminum vaporization at meteoroid impact velocities while complete vaporization does not occur for aluminum except over 12 km/s impact speeds. For a t/d ratio of 0.252, Wilkinson's equation predicted a dispersion angle of 16 degrees. Note that Wilkinson's angle is for one standard deviation, approximately 1/3 of the mass was at higher dispersion angles. Hull hydrocode results were closer to 11 degrees at 7 to 13 km/s. Piekutowski's analysis [95] of post-impact radiographs shows the dispersion angle of the outer bubble can be up to 18 degrees, but the momentum distribution may not be consistent with Wilkinson's assumed Gausian distribution.

Bjorkman [91] also suggested modifying the Wilkinson equation to 80% of the original value, similar to Elfer. However, this was based on the potential for elastic rebound which could double the momentum, rather than due to a dispersion angle effect.

3.3.2.3 Grove's Model

Grove and Rajendran modeled rear wall bulge, and necking, with varying the input parameters. [Appendix D] Their equation summarizing rear wall thinning is also given in Appendix B. The analyses were for Gausian momentum distribution, so that using either the Wilkinson or a modified Wilkinson equation, failure can be predicted for a wide variety of rear wall material characteristics.

3.3.2.4 Housen and Schmidt's Scaled Velocity Model

Schmidt et al [94] performed tests with cadmium bumpers and projectiles with a standoff from aluminum rear walls. The cadmium bumper and projectile were assumed to produce the same damage in the

aluminum rear wall as for an aluminum bumper and projectile (Al-on-Al) at 3.1 times higher velocity. The 3.1 scales both the energy of melting and vaporization of the debris cloud, as well as the cloud's momentum, due to the density ratio of cadmium to aluminum. [Holsapple93]

Figure 3-13 shows the experimental scaled ballistic limit based on Cd-on-Cd, and a comparison to Christiansen's Whipple shield equation. The remarkable feature is that the ballistic limit increases from 12 to 18 km/s (Cd-on-Cd test velocities 3.9 to 5.8 km/s). This is probably due a transition from liquid to all vapor as the impact velocity increases. In terms of the previous models, the there would be a transition from a modified Wilkinson model to an un-modified Wilkinson equation, although even that would not account for the increase in penetration diameter observed in the test. And the reason for the transition is not clear. The tests at UDRI [Schmidt94] show the shape of the cloud is similar for both velocities. This means that either there is a different mass distribution in the cloud which affects the rate of loading of the rear wall, or there is less rebound and momentum multiplication for the higher velocity test. Both of these benefits could actually be changed or even negated by intermediate shields.

There is still a question of whether cadmium-on-cadmium can adequately simulate rear wall damage for aluminum-on-aluminum impacts at a higher scaled velocity. While the state and momentum of the debris cloud is adequately reproduced by the scaled tests, the rate of load application on the rear wall is not simulated. Without an intermediate shield, the debris cloud impulse will have 3.1 times longer duration for Cd-on-Cd surrogate tests. For that case, shear waves can extend from the initial impact location before the remainder of the debris cloud can impact the rear wall. This can over-estimate the penetration resistance, but is probably the worst case for tearing.

This is certainly one of the most revealing means of analyzing 10 to 18 km/s impacts. However, surrogate material tests are also potentially misleading if intermediate shield and rear wall loading rates are not considered.

3.3.3 Spall Failure

Spall of a large area is possible due to an impulse from the liquid or gaseous debris cloud. Wide area spall of a 0.64 cm thick sheet is shown in Fig. 3-8. It has also be observed in 0.32 cm thick 2219. Spall failure should extrapolate with projectile energy rather than momentum. (The peak pressure would vary linearly with impact velocity for the same momentum.) This is not favorable for PNP predictions, but should decrease

the chance of critical damage if more of the momentum passes through the wall.

Without an intermediate shield, the debris cloud momentum is transferred over a short time span. Even without fragments in the debris cloud, gas and droplets can generate pressures which exceed the spall strength of the rear wall. This failure mode can be difficult to achieve in light gas gun testing. Fragment penetration is usually observed for shields of interest, and similitude testing does not typically address this failure mode. Most hydrocode models do not consider this failure mode.

The debris cloud model by Piekutowski was used by Rajendran [89] to predict that spall will be associated with the initial bumper material in the cloud. A typical spall strength for aluminum is on the order of 800 to 1200 MPa (110 to 170 ksi). At 6.5 km/s, with out an intermediate catcher, the cloud model produced pressures of 6000 MPa.

Schmitt et al [94] noted that spall occurred for aluminum-on-aluminum impacts but not for Cd-on-Cd for the same dimensionless impact speed. This shows that Cd-on-Cd scaled velocity tests may adequately model the physical state and momentum of the debris cloud, the tests do not properly scale rear wall effects.

As impact velocity increases, the threshold mass to cause penetration should scale with projectile velocity squared, modified for debris cloud dispersion angles. The time duration of the momentum transfer is inversely proportional to the velocity of the leading edge of the debris cloud. To maintain the same peak pressure at high velocity, the total momentum must by smaller.

Spall has been observed even with intermediate shields. A rigid intermediate shield, if it is uniformly accelerated, can act as a flyer plate and cause spall.

3.3.4 Oblique Impact Effects

Above 60° obliquity, the projectile tends to ricochet off the bumper as illustrated in Fig. 3-14. Fragments of the projectile or bumper can still cause penetrating craters in the rear wall. Figures 3-15 to 3-17 show a ricochet test result.

Tests at 30 to 55 degrees obliquity and 5 to 7 km/s show that a much smaller particle can penetrate a given design than would be possible for an impact at normal obliquity.[Gehring, Brewer, Coronado, Elfer, Christiansen, Jolly, and others]

Increased penetration for oblique impacts appears to be contrary to normal logic for penetration when the projectile does not fragment. The

reason is that the projectile does not fragment (and possibly disperse) as well as for a normal incidence impact. Just as cratering volume is related to the normal component of velocity of the projectile relative to the target, shatter of the projectile appears to be related to the normal component of velocity relative to the bumper.

The initial contact point of an oblique impact is on the side of a spherical projectile. Release waves reduce the stress compared to a normal incidence impact. Furthermore, the bumper material along the centerline of the projectile is imparted a velocity before projectile material would even hit it. Hydrocode analysis shows the material along the bumper centerline has a significant component of velocity radial to the shotline after impact.

3.3.5 Christiansen's High Velocity Extrapolation

Christiansen has high velocity penetration equations for several different shield designs. [Appendix A contains several of the equations.] In general they extrapolate from 6 to 7 km/s, the maximum test velocity or an observed transition to a different failure mode, using either constant energy or constant momentum. Considering the uncertainties in fragment penetration, spall, and load rate effects on the rear wall, constant energy extrapolation may be somewhat conservative but it is warranted for simple Whipple shields.

3.3.6 Comparison of High Velocity Predictions

Hayashida [95] plotted ballistic limits for several penetration equations as shown in Fig. 3-18. The new Cour-Palais equation is from a modification with Christiansen. The Housen-Schmidt equation, shown on Fig. 3-13, has a larger diameter to penetrate than the un-modified Wilkinson equation at the high velocity range. The author of this handbook has an opinion on which equations are most appropriate, but he also recommends the use of each in a PNP analysis [Section 4] to estimate design sensitivity. Without an intermediate shield [Section 5] constant energy extrapolation is probably appropriate due to the potential for spall, bumper fragment penetration, or a "trap door" failure mode rather than a Wilkinson type momentum failure [see Sec. 6]. When an intermediate shield is used, the modified Wilkinson equation will probably be appropriate. There may be a transition to an un-modified Wilkinson equation around 10 to 12 km/s, based on Housen-Schmidt results, but how the intermediate shield interacts with the cloud and the rear wall is not known and cannot be relied on with existing data.

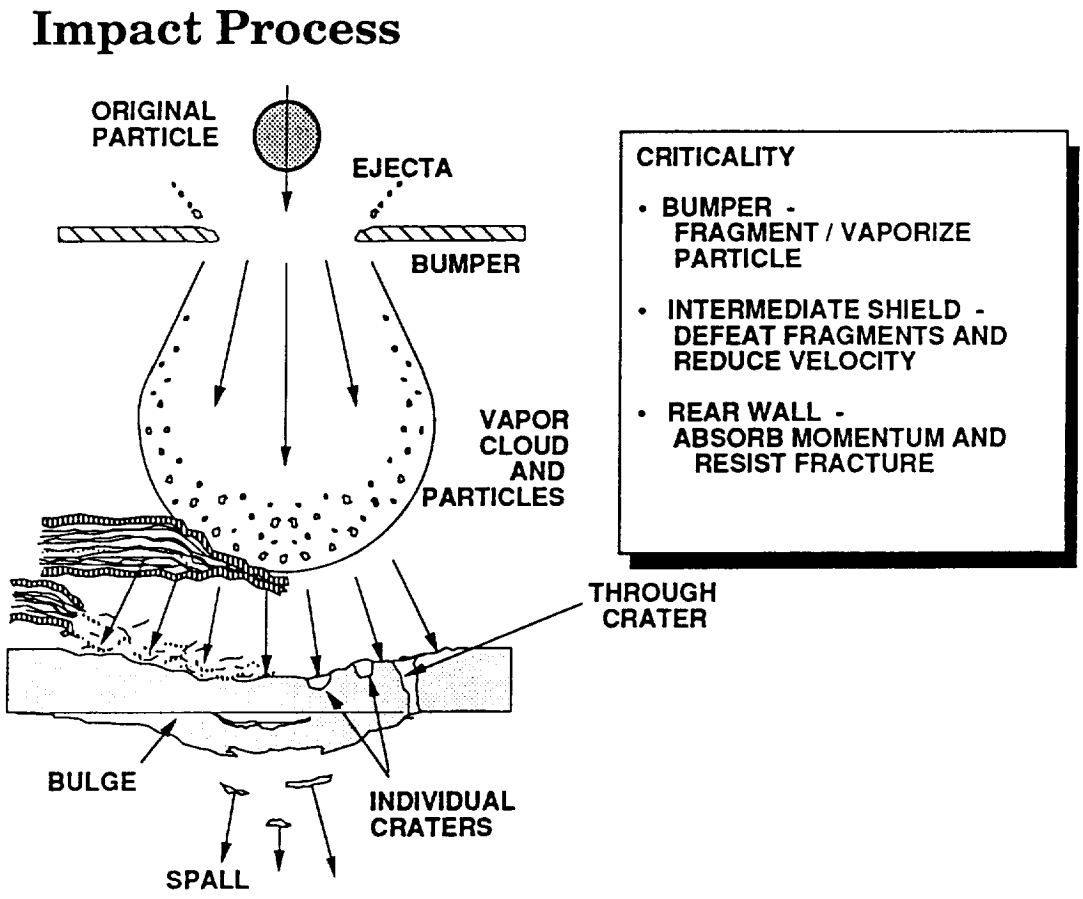

Fig. 3-1. Multi-layer penetration mechanisms.

The Ballistic Limit Surface Separates Penetration (All Points Above the Surface) from No Penetration (Below the Surface).

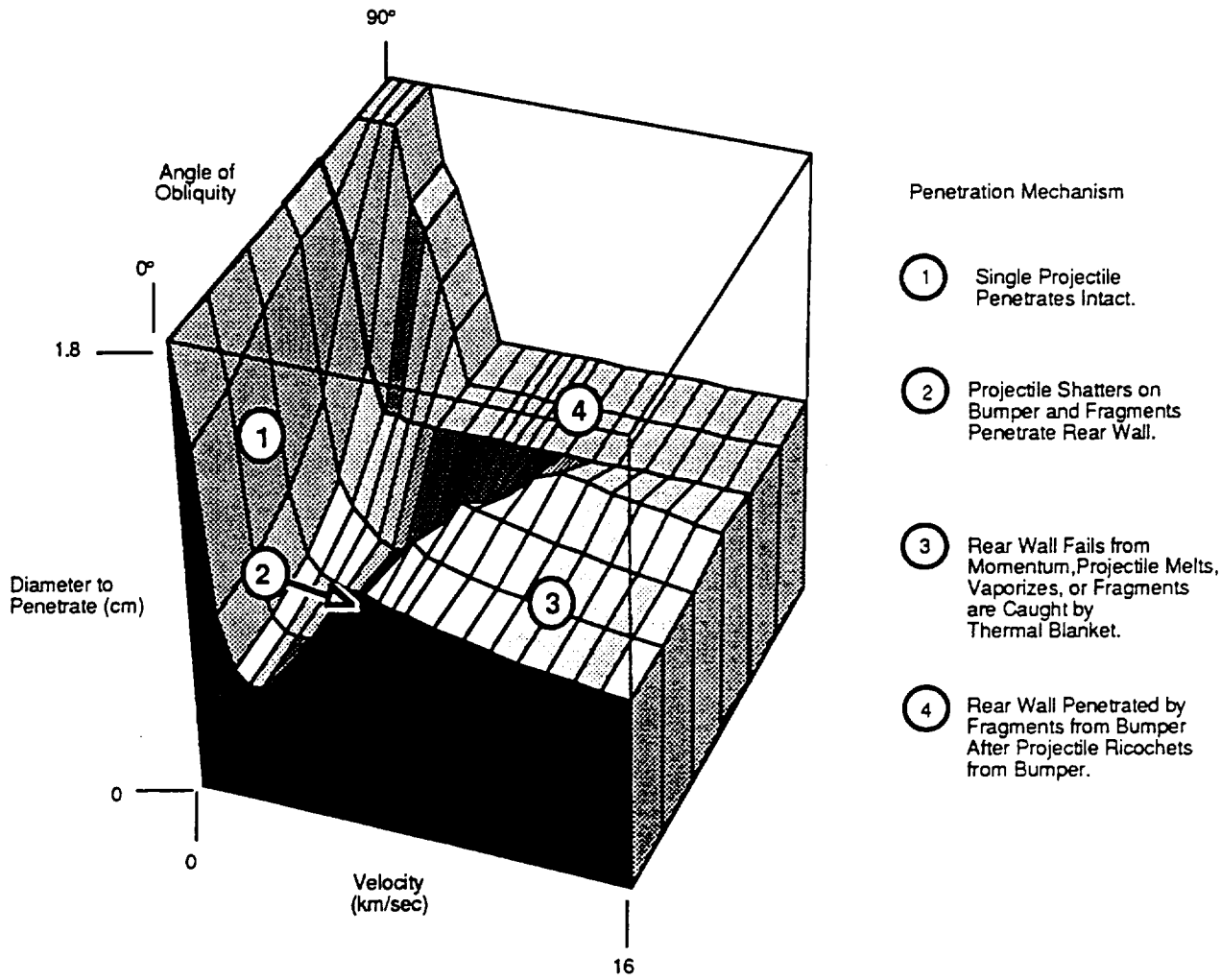

Fig. 3-2. Typical ballistic limit as a function of impact velocity and obliquity for a multi-layer design.

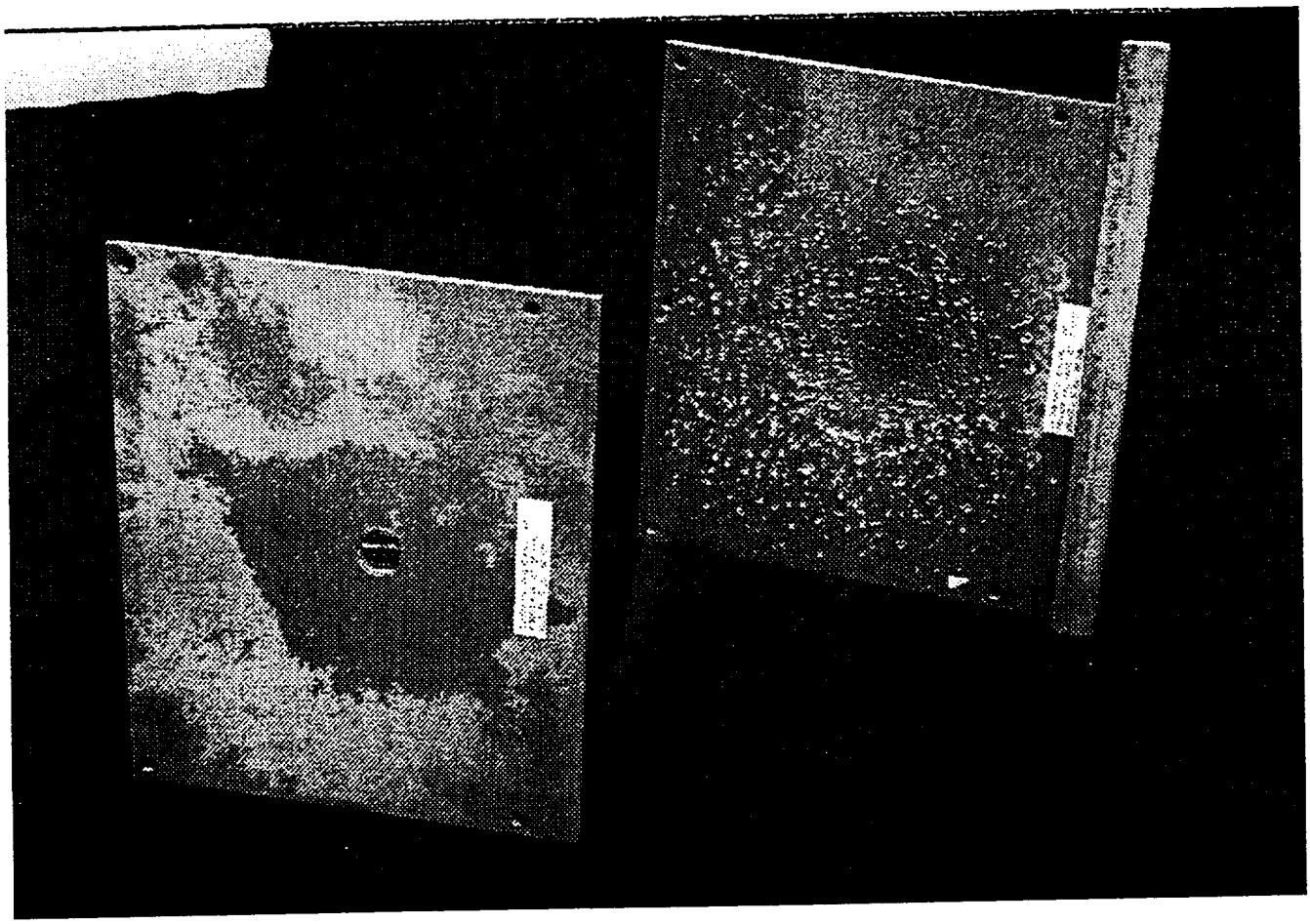

Fig. 3-3 Typical Whipple bumper fragment damage.
(305 mm (12 inch) standoff.) (MSFC shot.)

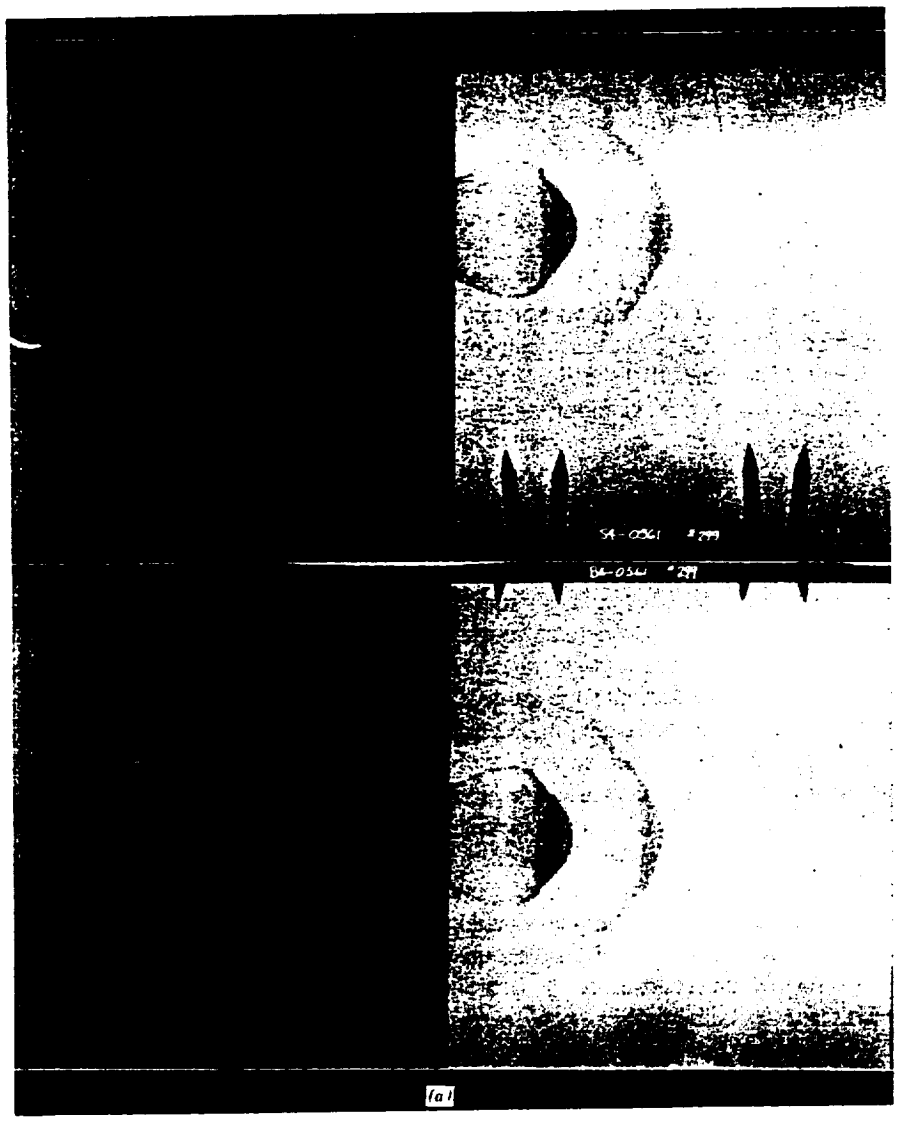

Fig. 3-4. Post impact debris cloud radiographs from a spherical projectiles. [UDRI shot in Rajendran89]

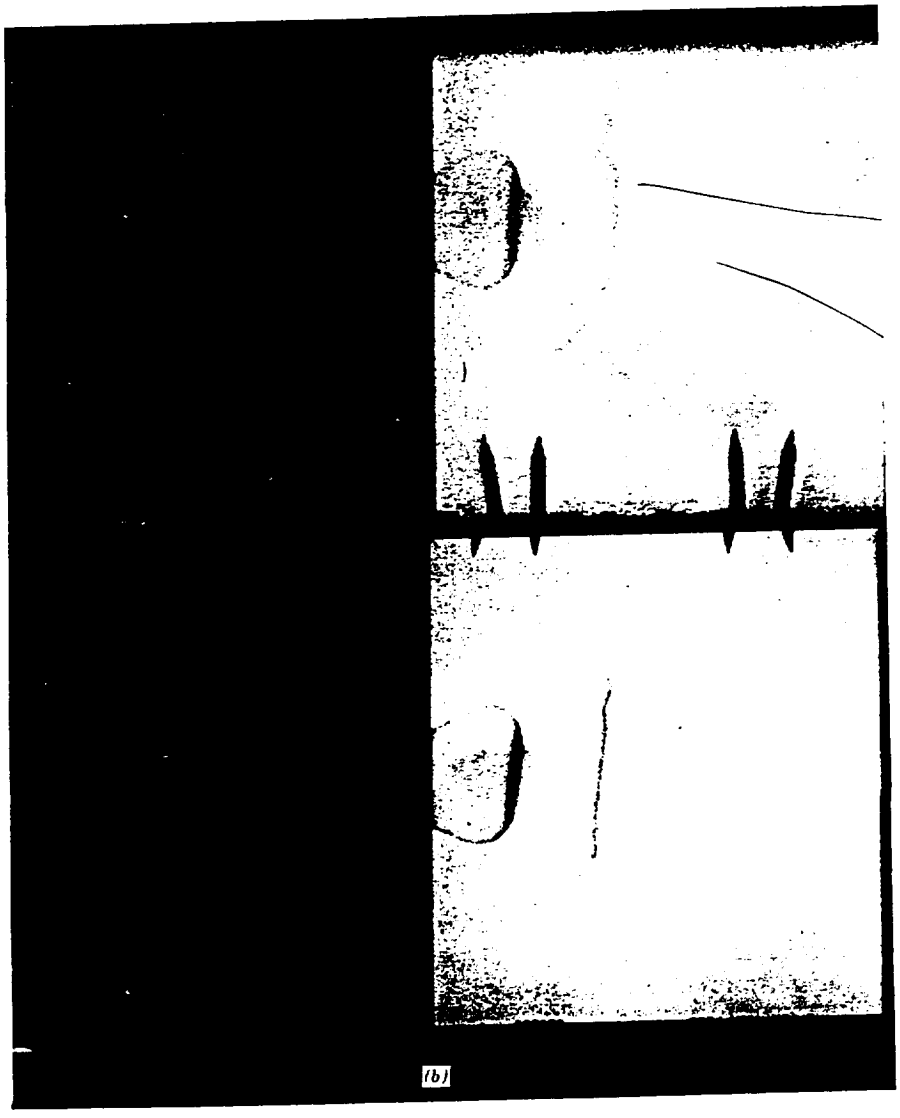

Fig. 3-5 Post impact debris cloud radiographs from a cylindrical projectile. [UDRI shot in Rajendran89]

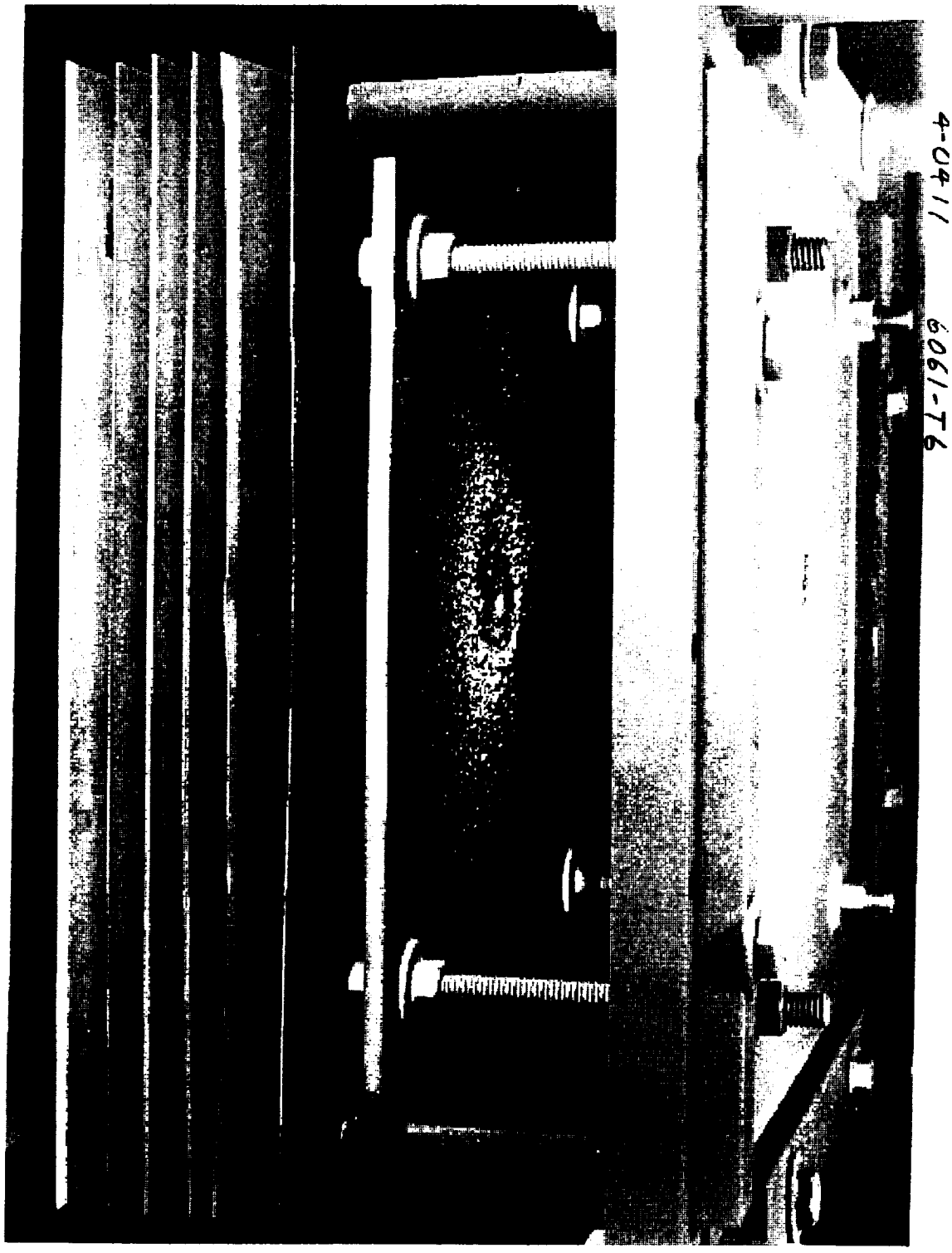

Fig. 3-6 Rear wall damage from a cylindrical projectile that impacted the bumper without yaw. (UDRI shot 4-0411)

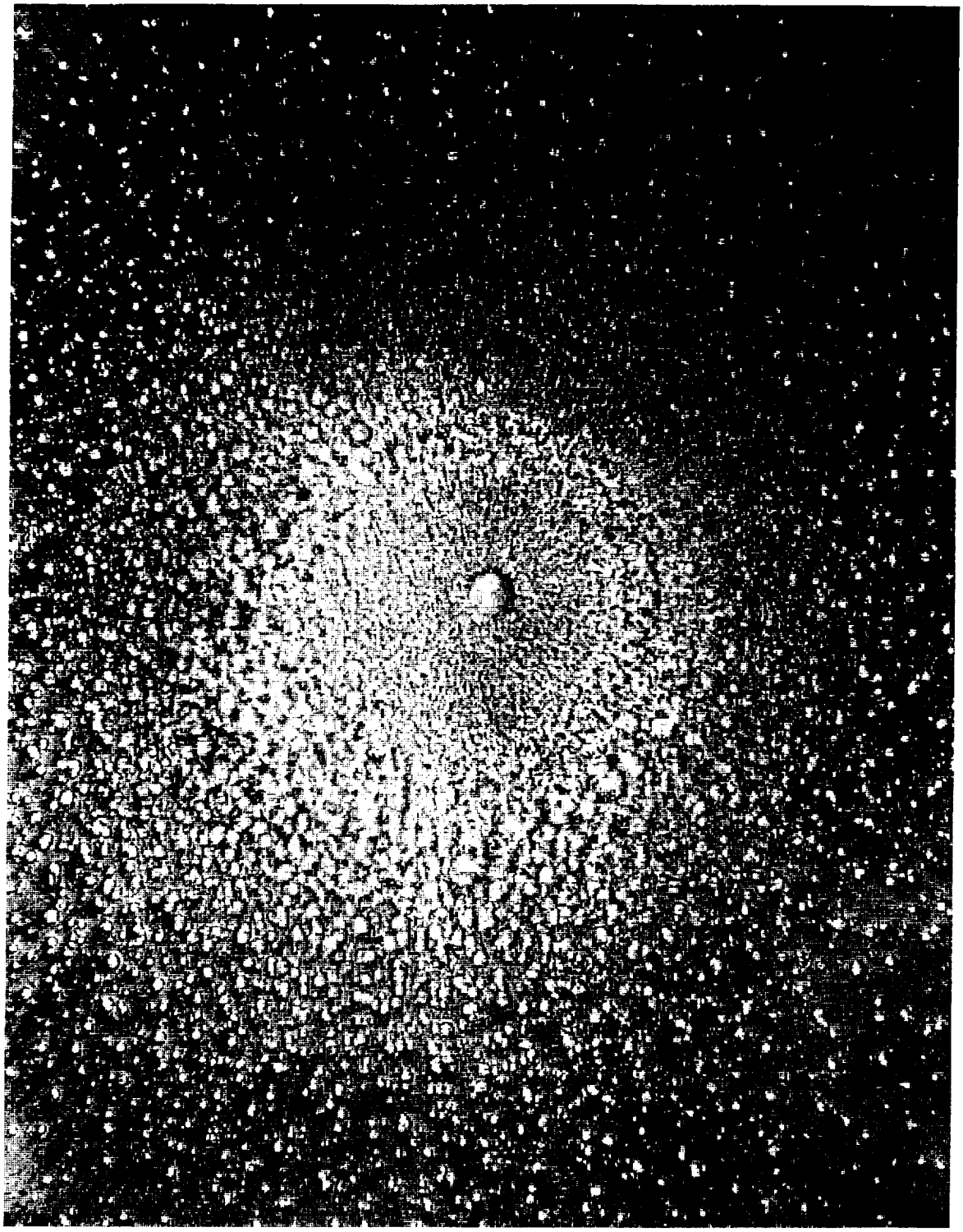

Fig. 3-7 Front of rear wall from Fig. 3.6. Note central crater probably from the tip of the bumper debris cloud.

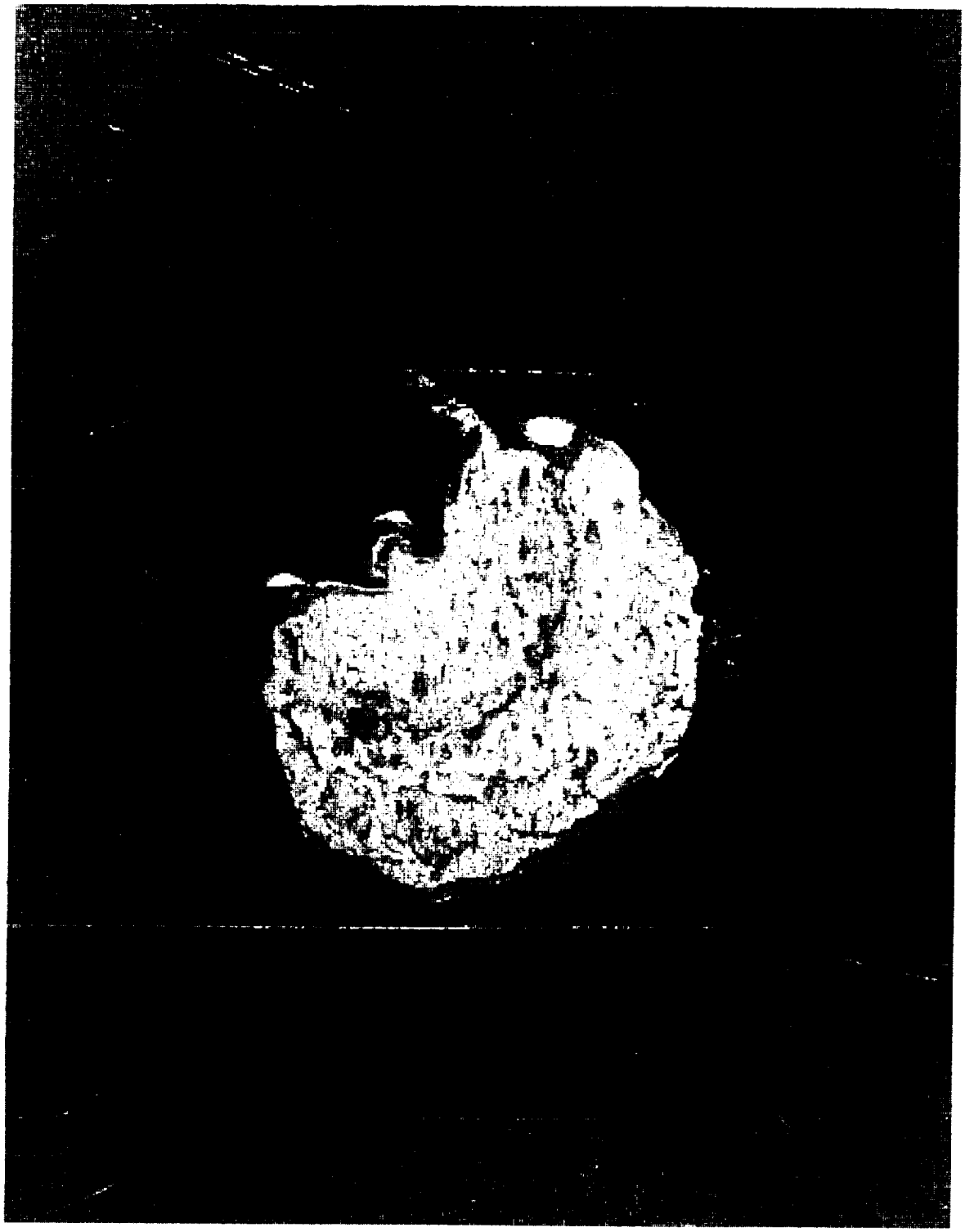

Fig. 3-8 Rear of rear wall from Fig. 3.6 showing wide area spall.

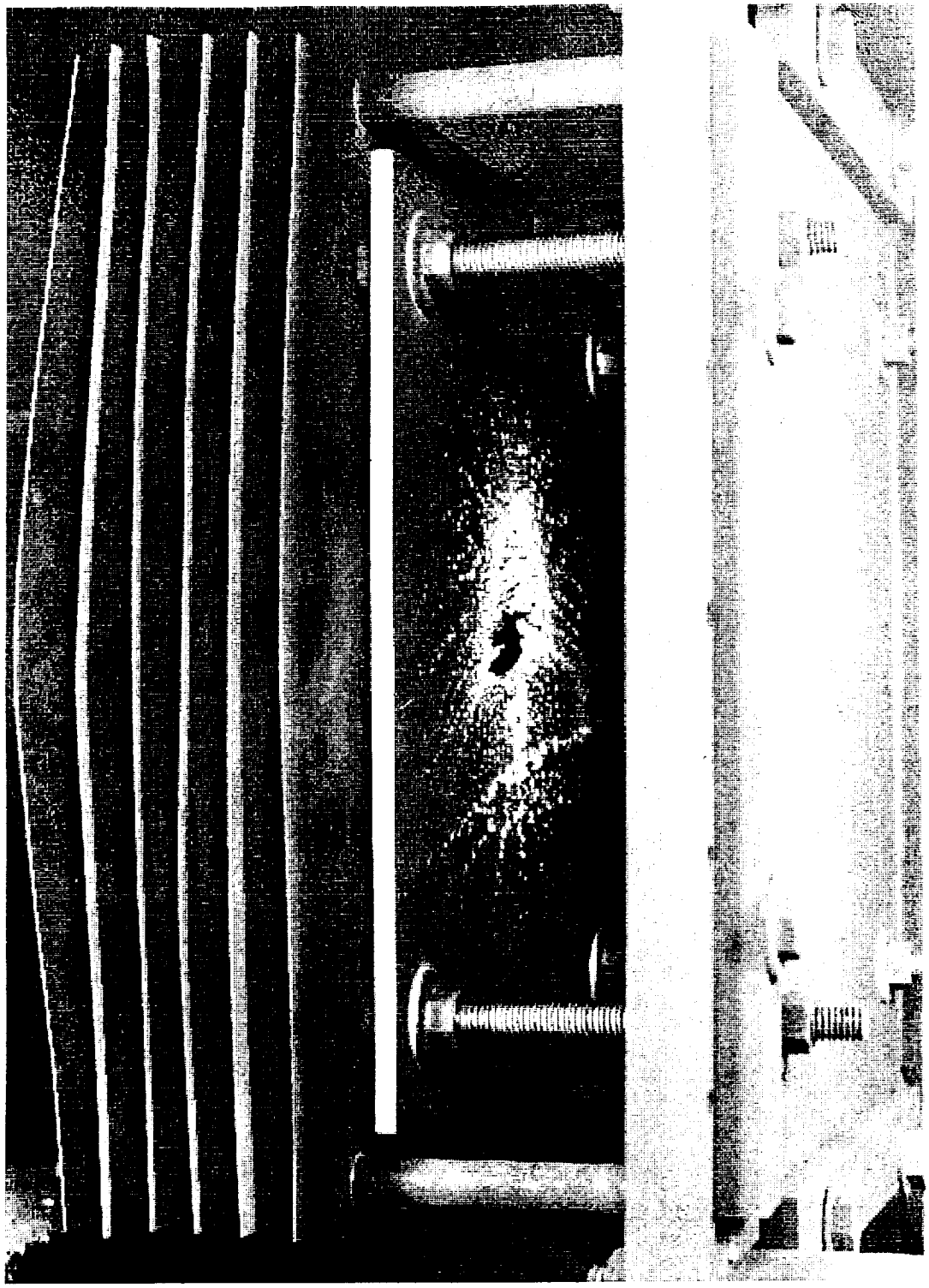

Fig. 3-9 Rear wall damage due to a cylindrical projectile that had yaw. (UDRI shot 4-0436)

Fig. 3-10 Front of rear wall from Fig. 3.9.

Fig. 3-11 Rear of rear wall from Fig. 3.9. Penetration and spall from aligned projectile fragments, and spall probably from the tip of the bumper debris cloud.

Fig. 3-12 Wilkinson type momentum bulge and failure with Kevlar intermediate shields to prevent fragment damage.

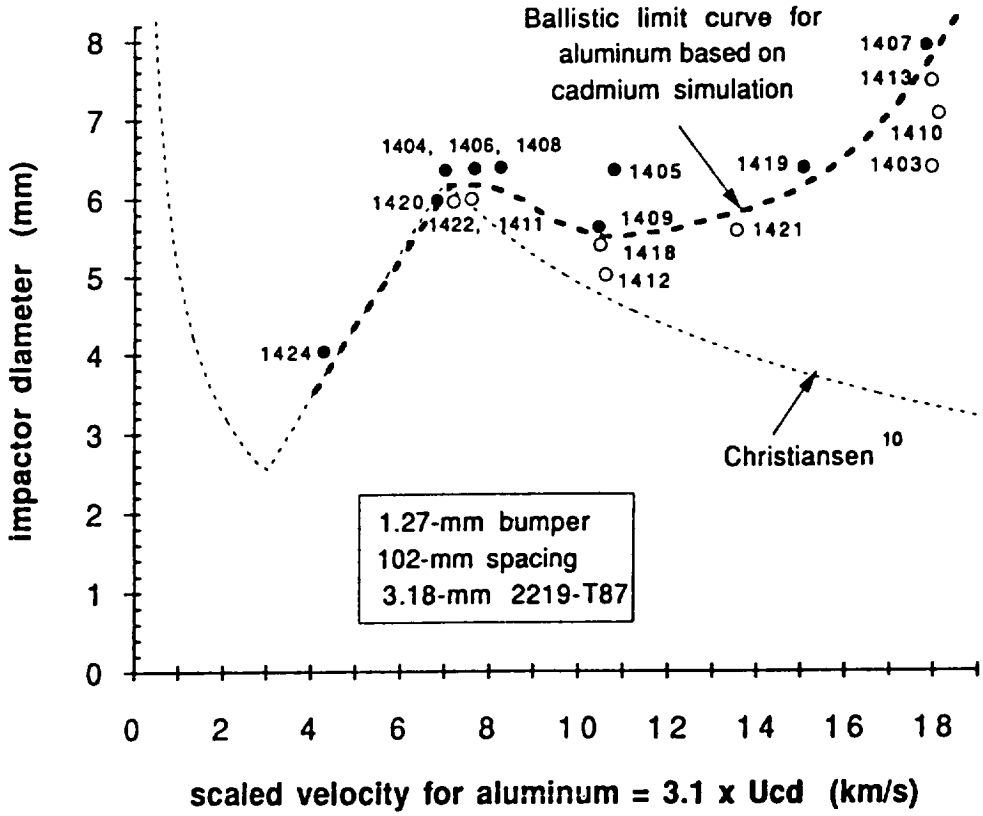

Fig. 3-13 Ballistic limit determined from aluminum rear wall with cadmium projectile and bumper tests, scaled to equivalent all aluminum test. [Schmidt94]

Ricochet

- Above 65° projectiles will ricochet off the bumper
- Projectile fragments come off in streams
- Bumper fragments (spall) may penetrate the pressure wall

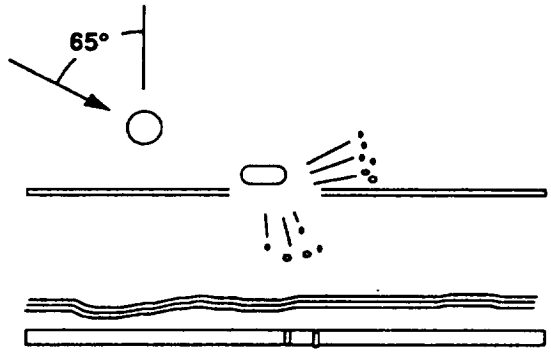

- BAC approach for ricochet stream PNP seems conservative
- Analysis of multiple impacts in same location maybe needed.
  - Depends on operations (removeable log modules vs permanent hangar)

Fig. 3-14 Oblique impact schematic.

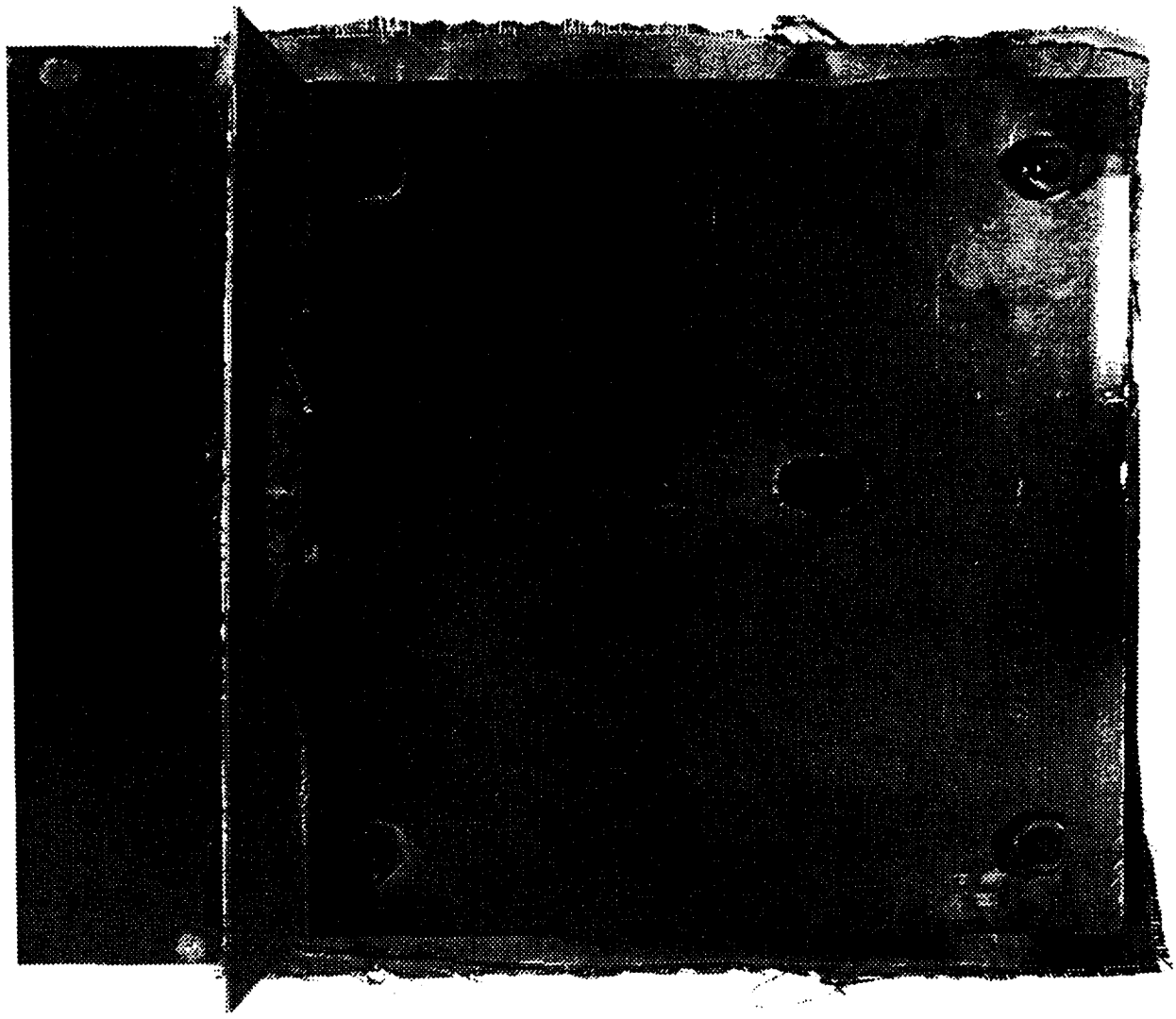

Fig. 3-15 Oblique impact bumper damage. (UDRI shot 4-0657)

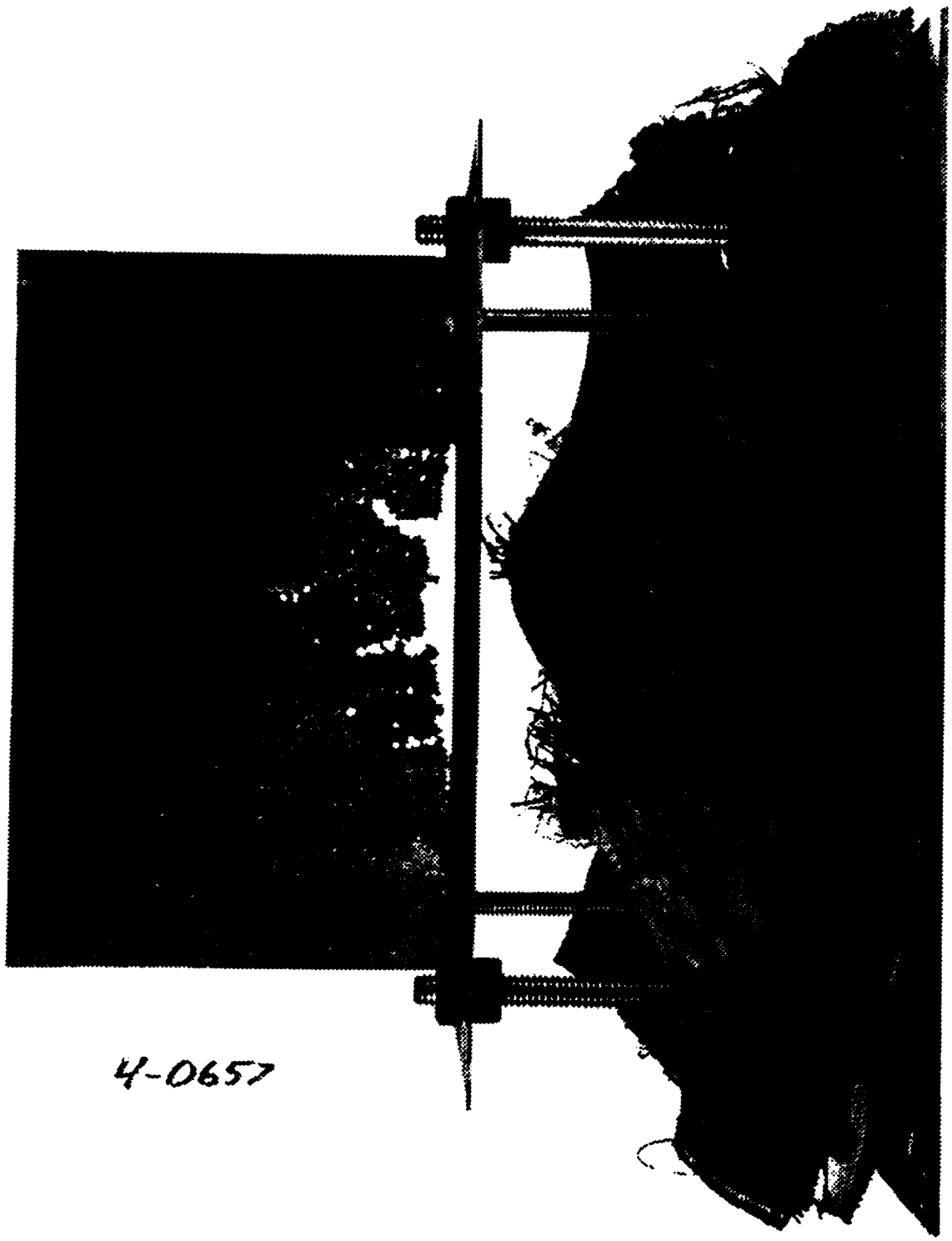

Fig. 3-16 Oblique impact ricochet damage. (same as Fig 3-15)

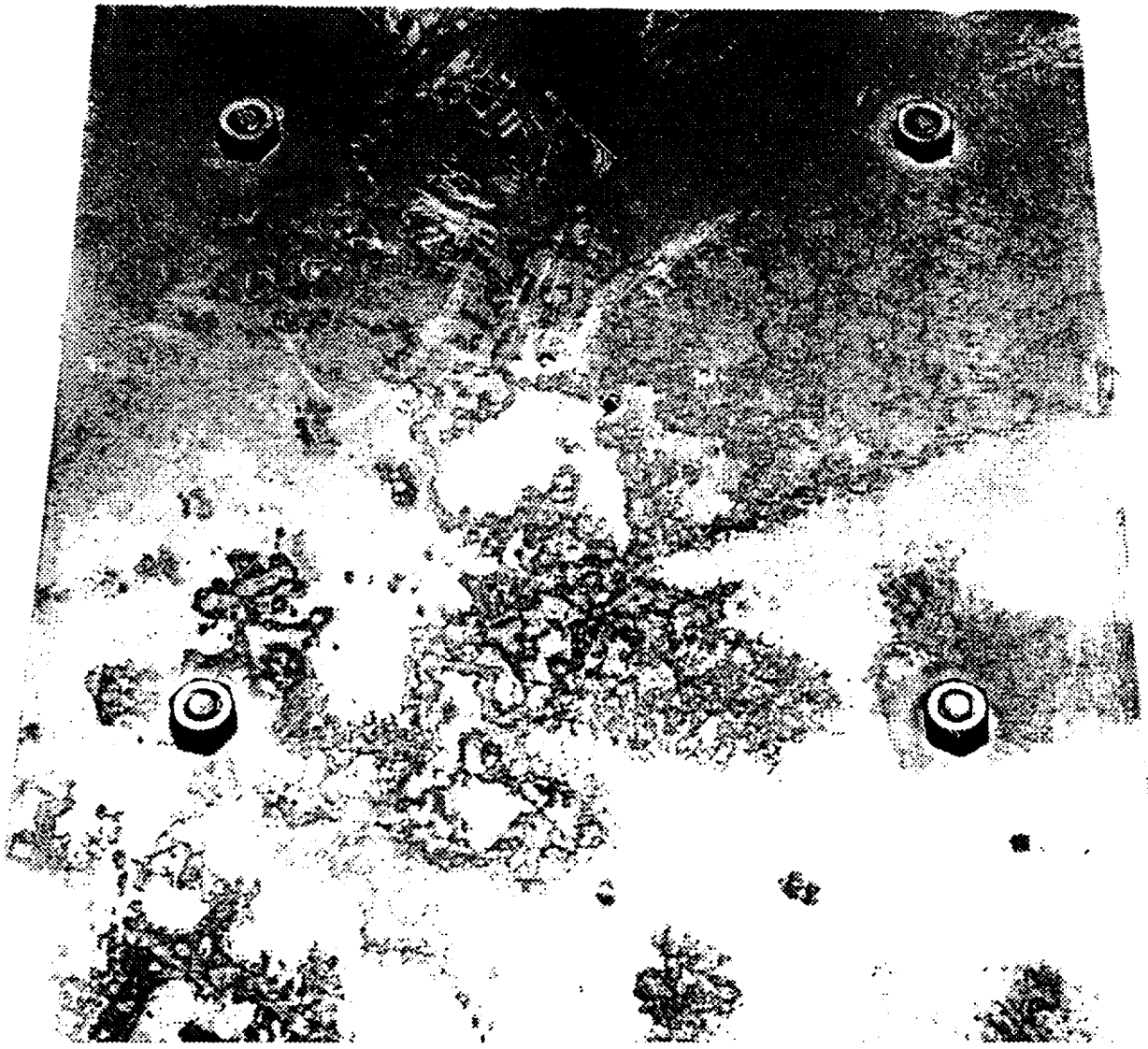

Fig. 3-17 Oblique impact rear wall damage (back side) due to a fragment normal to the bumper. The fragment was likely bumper material. (same as Fig 3-15)

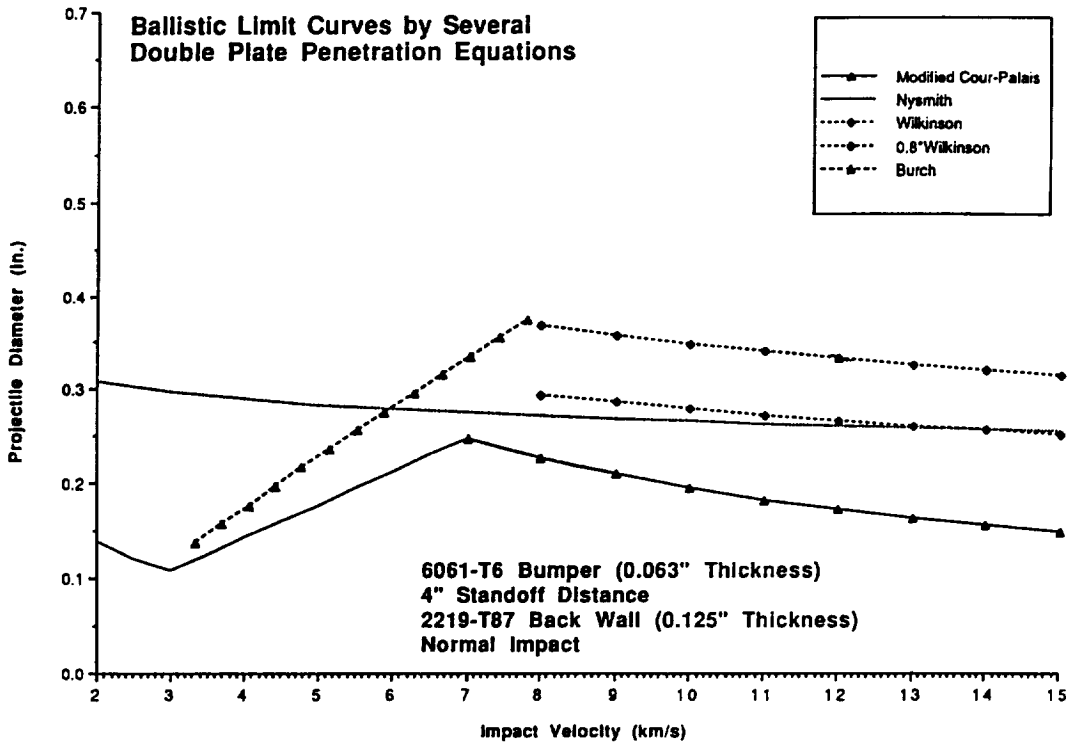

Fig. 3-18 Comparison of high velocity penetration equations. [Hayashida95]

4 PROBABILITY ANALYSIS

The probability analysis approach is based on the use of the BUMPERII [Graves] and SD_SURF [Elfer 92] computer codes. These computer code integrate the probability of no penetration (PNP) on a faceted spacecraft model. The programs work with an earth oriented spacecraft in low earth orbit . The codes do the bookkeeping on the spacecraft geometry, ballistic limit and meteoroid and debris flux. A separate analysis of the environment and impact probabilities was developed by Klindrad and Jehn.[92]*

These codes are very useful in doing sensitivity analyses for assumed variations in the ballistic limit surface, spacecraft design or operation, or the environment definition. The particulars of many parts of the analysis are subject to debate, and it is important to understand the effect on the overall PNP to put their significance into perspective.

4.1 Probability of No Impact

The traditional analysis is based on a the Poisson distribution for a probability, P, of zero impacts:

$$P = (F \times A \times T)n \quad x \exp(- F \times A \times T) / n!$$

where F is the flux, A is the exposure area, n is the number of impacts, and t is time, all in consistent units. The simplest approach is to use the total surface area of the space craft, or the area of a simple shape which envelopes the spacecraft. Given the area, the design lifetime, and the required reliability, a flux can be determined and from that a particle size can be determined which has that probability of no impact. If this size can be stopped by the basic structure at all velocities and obliquities, then the requirement has been met.

4.2 Probability of No Penetration

If the design is driven by the penetration resistance, then a proper weighting of probable velocities and obliquities must be done. For a spacecraft with a fixed orientation relative to the earth, a more accurate calculation is possible. The space debris and meteoroid threats can be broken down into streams of flux from different directions, i, at specific velocities. The diameter to penetrate every area on the spacecraft is determined for each stream element (reference the ballistic limit surface in

Fig. 3-2). The flux for each diameter is determined from the N_r relationship shown in Fig. 2-1 or 2-2 and then multiplied by the fraction of the flux, f_i, in each stream as adapted from Fig.2-3.

The probability of no penetration (PNP) from each direction and for each element is based on the Poisson distribution for zero events:

$$PNP_{el} = \exp\left(- \sum_{i=1}^{nthreats} (N_i \cdot A_i) \cdot t \right)$$

where (with consistent units)

N_i = flux which penetrates from each threat direction, i.
= $4 \cdot f_i \cdot N_r(d_i)$

N_r = flux on a randomly tumbling plate of diameter d_i or larger. (As defined in the specifications.)

d_i = diameter to penetrate at the velocity and obliquity of the ith threat.

f_i = fraction of flux from threat direction

A_i = projected area of the facet in the flux direction.

t = exposure time.

The total PNP is determined by the product of the PNP for each element.

$$PNP_{total} = \prod_{j=1}^{nelements} PNP_j$$

4.3 Probability of No Critical Damage

The probability on no critical damage (PNCD) is determined in the same way as PNP, except that the projectile diameter to cause critical damage is used instead of the diameter to penetrate. Williamsen has performed a complete analysis for crew loss due to debris impact. [Williamsen94] Critical damage to a module can result from:

- a hole size that leads to too rapid depressurization of a module.
- a crack that will propagate due to structural loads (catastrophic rupture of a module) as shown in Fig. 1-1.
- damage to a critical system.

For these definitions, the particle to cause this damage will generally be larger than the ballistic limit. For some other design considerations, critical damage could occur for a non-penetrating particle. This could

include deformation, cratering or spall on a critical component before penetration occurs.

4.4 Probability Analysis Codes

The BUMPERII computer code may be used alone or in combination with SD_SURF to analyze a spacecraft's PNP (or PNCD). [Graves91, Elfer 92] BUMPERII can show threat contours on the spacecraft geometry model. The threat contours can be generated by BUMPERII to show which areas of the spacecraft are most responsible for reducing the PNP. SD_SURF works alone or with BUMPERII to calculate PNP and to show which impact velocities and obliquities are most responsible for reducing the PNP. Figure 4-1 shows the results of a SD_SURF analysis.

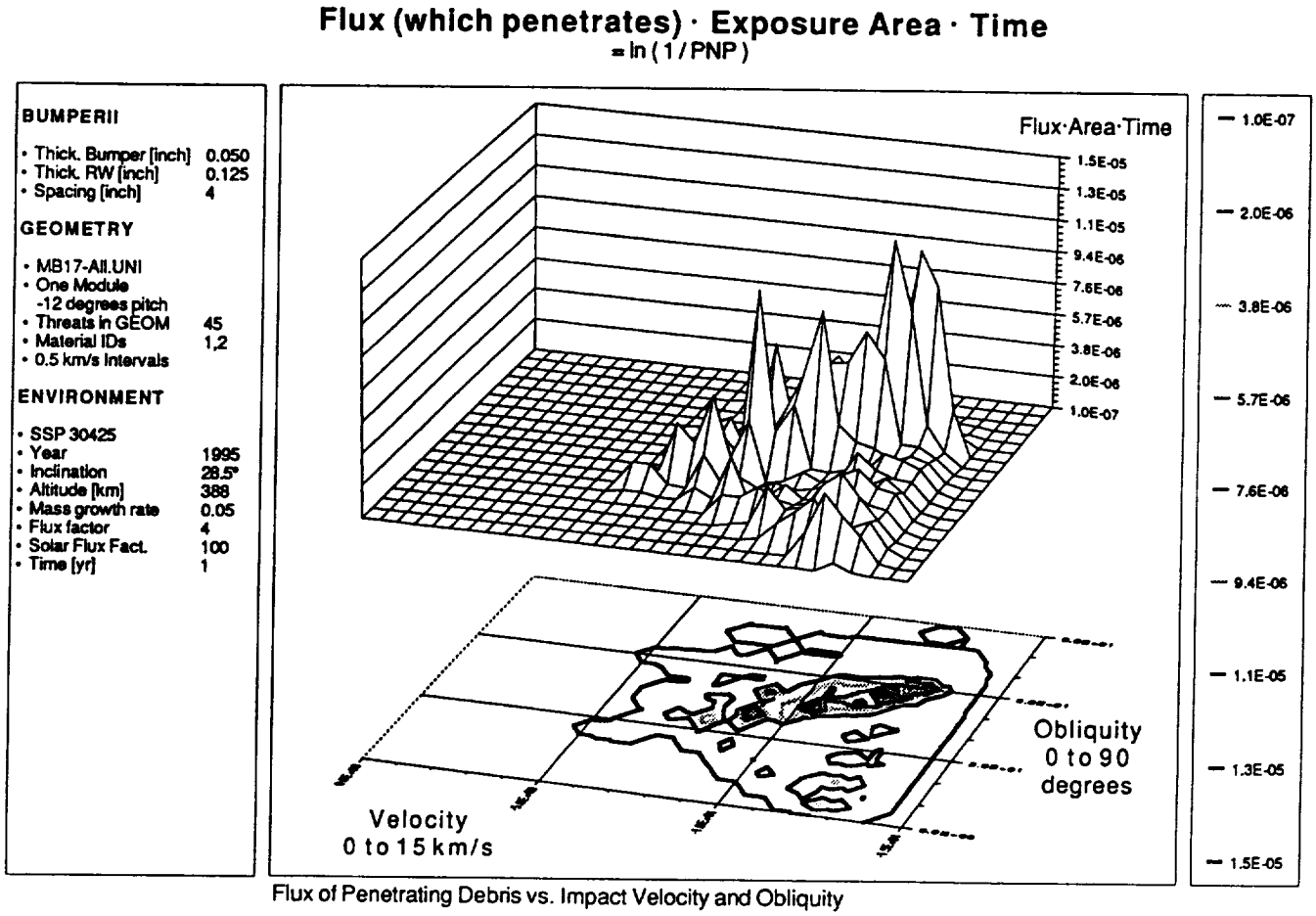

Flux of Penetrating Debris vs. Impact Velocity and Obliquity

Fig. 4-1 Flux times the exposed area times the exposure time versus velocity and obliquity from SD_SURF.

5 ADVANCED SHIELD CONCEPTS

Advanced shields have been designed using a variety of intermediate shields and customized geometries. Intermediate shields have several important roles:

- Shock fragments.
- Catch fragments.
- Reduce debris cloud velocity by adding mass.
- Reduce debris cloud momentum (depending on support structure).
- Reduce momentum multiplication (rebound or cratering) on the rear wall.

5.1 Bumper Material Selection

Swift [70, 82] came to the conclusion that the bumper material should have the same density as the projectile to be shattered. Lower density was not sufficient, and higher densities (especially with higher melting temperatures) tended to cause rear wall failure from bumper fragments.

It is of interest to compare the ballistic limit of single sheets of aluminum and steel. For the same impacting projectile the volume of material removed is much larger in aluminum. However, the lower density is an advantage in preventing perforation. If equal weights of steel and aluminum are equally effective bumpers for a large design projectile, then aluminum is the better choice for a bumper for spacecraft applications, because it will not be penetrated as frequently as the steel bumper. Hence the thermal insulation layers beneath the bumper and the rear wall will suffer less degradation from micrometeoroids which will certainly impact the spacecraft.

Low density fiber resin composites have been shown to be less effective in fragmenting aluminum projectile than aluminum bumpers. [Christiansen87, Elfer87, ESA] However, the fiber composites do not create fragments that can penetrate the rear wall. This feature makes them extremely attractive for protection against icy meteoroids, which would be expected to vaporize. Also, if composites could deflect debris projectiles at high obliquities, then composites would be better than monolithic aluminum bumpers which generate penetrating fragments.

Ceramic plates can be effective bumpers, but multi-impact capability is limited and they need to be supported to avoid completely shattering.

Christiansen [87] showed that an equal weight of an alumina-boro-silica ceramic cloth (tradename Nextel) should shock the projectile to higher

pressures and temperatures than an aluminum bumper. However, a cloth can have a lower apparent density and is best used as an intermediate shield in an advanced shield system.

Metal matrix and ceramic matrix composites appear to be marginally better than monolithic aluminum bumpers as debris bumpers [McGill92] but a more complete analysis is necessary to quantify the benefit. Again, the effects on numerous non-critical meteoroid impacts needs to be evaluated.

5.2 Multiple Bumpers

Intermediate shields may further shock the fragments, thereby increasing fragment temperature, reducing fragment size, and increasing the debris cloud dispersion angle. This is similar to the performance of the bumper as discussed previously.

The use of multiple bumpers can significantly improve penetration resistance compared to a single bumper with the same total weight as shown in Fig. 5-1. The repeated impacts do a better job by fragmenting and raising the temperature of the initial impact fragments.[Richardson, Cour-Palais89,-91] Figure 5-1 shows that for an overall 12 inch spacing, and 0.125" 2219-T87 rear wall, a 0.5" diameter 6061 projectile was stopped by 3 bumpers of 0.040" Al, each 4 inches apart. The rear wall was coated with molten aluminum. However, in a similar test, penetration occurred both for a single 0.125" bumper, and for six 0.020" bumper with 2" spacing between the sheets.

Multiple bumpers can be more effective at shattering the projectile, but they do not tend to spread the momentum over as large an area as a thicker single bumper with the same areal density. Therefore a larger standoff distance is required to resist momentum failure. Christiansen's equations for the mesh double bumper versus multi-shock bumpers tend to bear this out.

Figure 5-2 shows the results at MSFC for two equal weight bumpers. The total spacing was restricted in this example. The second bumper performed best when close to the front bumper to provide a better dispersion of fragments on the rear wall. However, the Richardson multiple bumper was more effective when the second bumper was about 20% of the thickness of the first bumper and places just above the rear wall.

Multiple bumpers appear to be very effective means of building up the performance of a spacecraft on orbit. An initial low weigh configuration can be flown, and as the environment increases, successive layers, with greater standoff can be added.

5.3 Intermediate Catcher Shields

Intermediate shields may catch fragments. While the net momentum that impinges on the rear wall is not decreased, the mass is increased and the velocity is decreased. The benefit is illustrated in Fig. 5-3.

The intermediate shield will also affect rebound and momentum multiplication on the rear wall. If fragments impact the rear wall, cratering may occur that causes momentum multiplication. Cratering can eject more momentum than the momentum of the initial fragment. Even if cratering does not occur, elastic rebound from the rear wall can double the momentum transferred to the rear wall.

The impact of the cloth intermediate shield on the rear wall will not increase the momentum of the rear wall significantly over the initial projectile momentum. The bumper was often bulged out away from the intermediate shield after impact. The bulge was not as significant as rear wall bulges, even though the bumper was always thinner. The bulge may be due to impact of the debris cloud with the intermediate shield or rebound of the intermediate shield from the rear wall. Whatever the cause, limited bumper deformation is evidence of a contribution of some small fraction of the initial momentum to the rear wall. Momentum doubling at the rear wall does not occur.

5.3.1 Catcher materials

As an intermediate debris cloud catcher, Kevlar cloth was found to be very weight efficient in preventing cratering of the rear wall from impact velocities at 5 to 7 km/s.[Elfer 88] This is illustrated in Fig. 5-3. In one test program, Spectra 900 cloth was not as effective as Kevlar cloth.[Elfer 88] This is probably due to differences in the thermal properties of the materials. Other test programs have shown Spectra to be as effective as Kevlar even though melting of the fibers was obvious.[Christensen92] This emphasizes the need for accurate material properties as well as penetration models for extrapolation beyond test velocity.

Considering its outstanding performance in multi-shock shields, Nextel is expected to be as good or better than Kevlar as an intermediate shield catcher material. However, Christiansen's sizing equations (Appendix A) for Mesh Double-Bumpers indicate that up to 50% higher areal density is required for Nextel catcher layers, compared to Spectra or Kevlar catcher layers. Nextel also has a design advantage in that it is more stable than Kevlar or Spectra, which will degrade from exposure to either atomic oxygen or UV.

5.3.2 Impregnated Catcher materials

It should be noted that there are potential contamination issues associated with Nextel fibers breaking off. This may be true of any blanket material. Impregnation may control fiber loss. Impregnation materials should not be too stiff and have relatively weak interfacial bonds with the fibers so as not to affect ballistic performance.

Elfer found that in nominally identical tests, a monolithic Kevlar-Epoxy intermediate shield allowed rear wall failure while an equivalent weight of Kevlar cloth did not cause rear wall failure. In normal ballistic testing dry Kevlar fabric can outperform due to ability of fibers to slip and stretch. However, there was no apparent difference in cratering of the rear wall, and it was suspected that the difference in elastic rebound from the rear wall caused a different momentum multiplication.

Another problem with epoxy composites is that if the catcher is stiff, then the acoustic environment of launch must be considered. This can present severe design constraints that are not applicable to a flexible cloth catcher.

Teflon impregnated beta cloth may also have an added benefit beyond just mechanically catching projectile fragments. The Teflon can chemically react with the fragments to promote further reduction in fragment size. It is not known whether this is a significant contribution to penetration resistance but it warrants further investigation as a possible means of enhancing penetration resistance.

5.3.3 Catcher Location

The location of the cloth was shown to be critical to effective performance. If the cloth was against the bumper, fragments would overwhelm the cloth; too close to the rear wall and the momentum could not be transferred to the cloth. The momentum transfer to the cloth is necessary for higher mass and lower velocity than the initial debris cloud so that the rear wall will not spall. Christiansen suggested that the catcher be four projectile diameters from the rear wall.

Momentum absorption by the cloth was negligible due to tearing of the cloth. A six inch square of material was just as effective as a 12 inch square fixed on the edges. After the impact the cloth was shredded but remained fluffed up in the same location. The shreds of the cloth could be a significant enhancement for multi-hit capability.

5.4 Analysis of Advanced Shield Designs

Determination of the ballistic limit surface of advanced shield designs has depended more on empirical data and less on modeling capability. Momentum failure is discussed in greater detail in Sec. 6.

Test data is the best method of anchoring the Wilkinson momentum failure analysis. If tests cannot generate a momentum failure it would be conservative to use just the outer bumper and the total standoff to predict the dispersion angle for failure. This assumes that the intermediate layers only reduce fragment penetration and do not contribute to dispersing the momentum. An alternative approach was used by Elfer: an effective bumper was assumed to be equal to the total thickness of the two bumpers and at a standoff two thirds of the distance from the front bumper to the second bumper. The areal density is expected to be conservative, and the reduced standoff (rather than just using the standoff distance to the front bumper) was an estimate believed to be adequate to describe the reduce area of the spray.

Figure 5-4 shows the benefit of adding multiple bumpers and catchers. The bumper and catcher configuration used in Fig. 1-1 was repeated 3 times and was able to prevent penetration for the same projectile as used in Fig. 1-1.

5.5 Geometric Bumper Shapes

Christiansen [92] noted that mesh bumpers are effective in breaking up projectiles at 3 to 5 km/s. However, it was only effective in combination with a second bumper plate to further shock the fragments. Along a similar vein, a geometric disrupter was developed by Martin Marietta, the University of Dayton Research Institute (UDRI), and Kaman Sciences. UDRI succeeded in rolling a plate into a hexagonal ribbed configuration, similar to side-by-side wires. An oblique impact at greater than six km/s did not show it to be significantly different than a homogeneous bumper sheet in preventing rear wall penetration and no further testing was performed.

A faceted or corrugated bumper may be useful in turning an oblique impact into a locally normal impact. The facets should probably be on the order of one-half to one times the anticipated projectile diameter. While this increases the surface area of the bumper, the bumper may be so much more effective that the overall weight requirement could be reduced. However, to effectively use this concept, the relationship of the facets to debris would have to be thoroughly modeled for all spacecraft orientations.

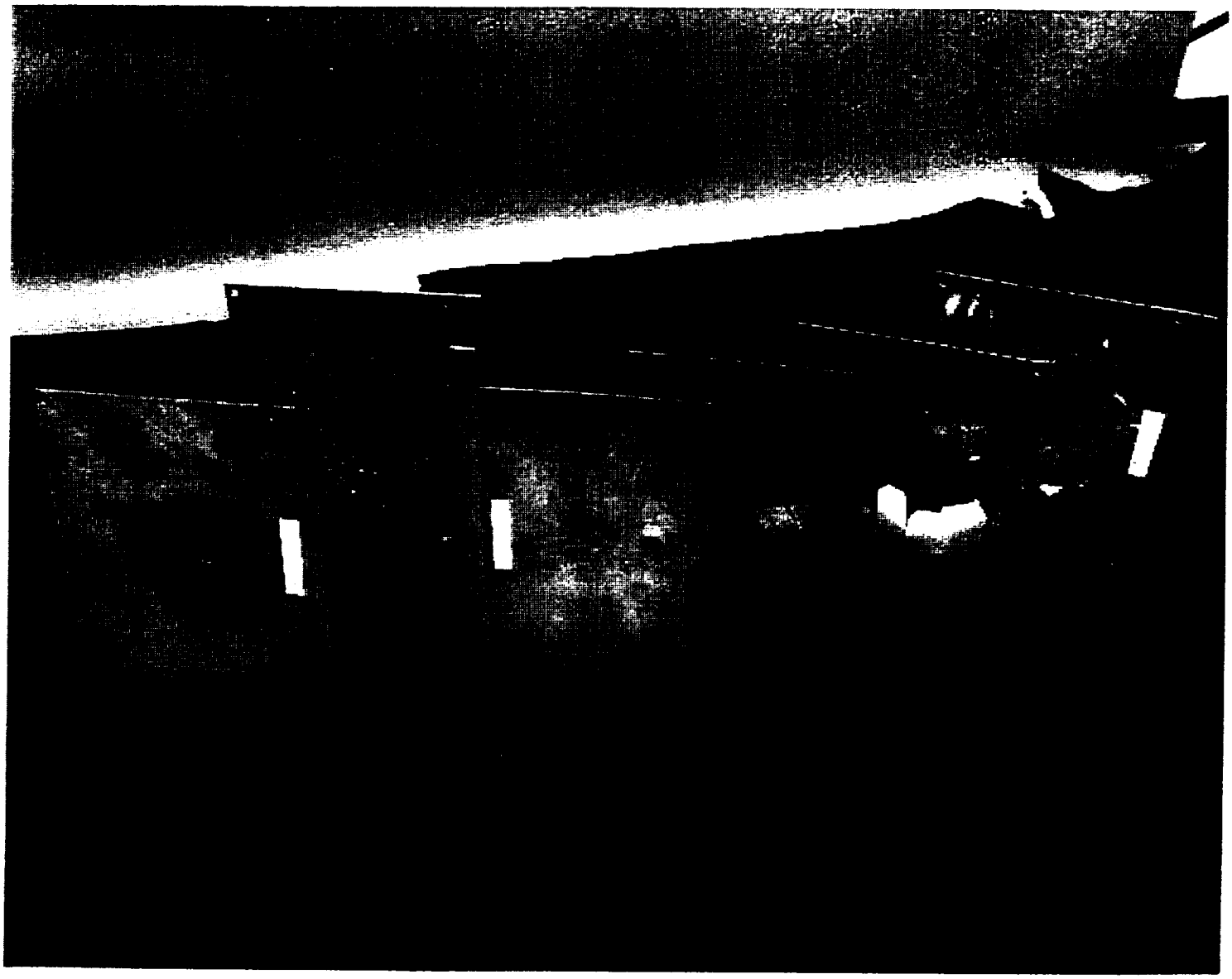

Fig. 5-1 Multi-shock aluminum bumper compared to Whipple bumper (Fig. 3-3). MSFC tests. [Elfer88]

Double Bumper System

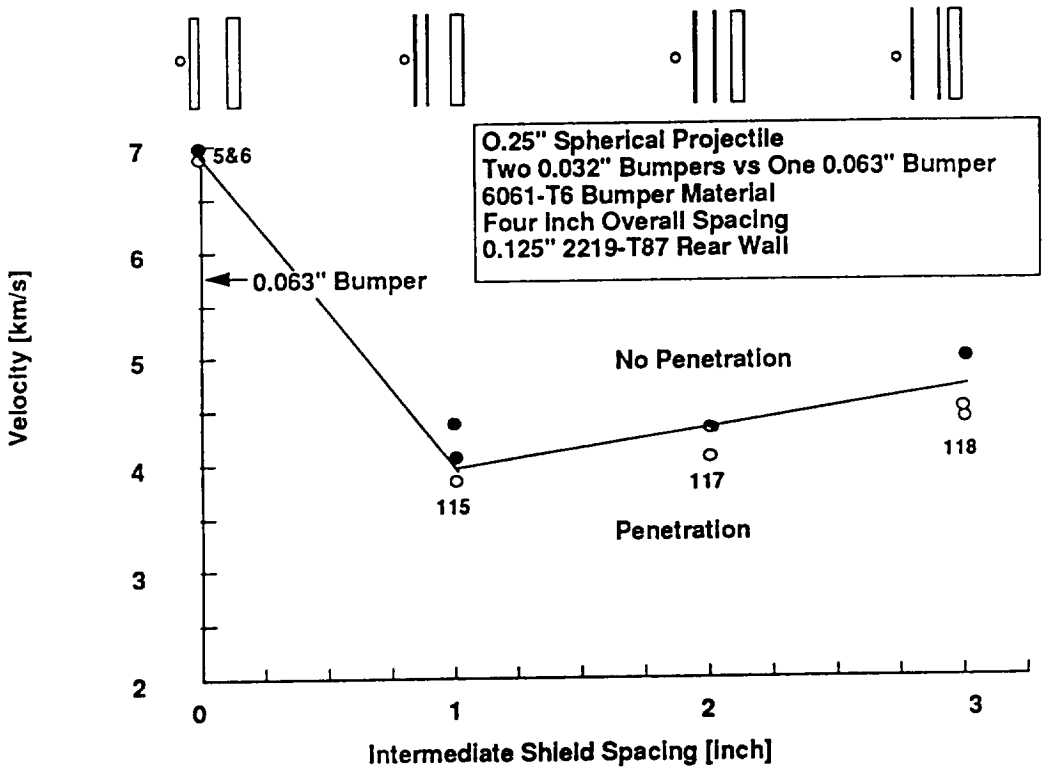

Fig. 5-2 Double bumper (equal weight) test results. MSFC tests. [Elfer88]

Fig. 5-3 Kevlar cloth intermediate shield (catcher) UDRI tests. Same designs as Fig. 1-1, with (no penetration) and without Kevlar 29 cloth (penetration) for a 1 gram projectile. [Elfer88]

Fig. 5-4 Multiple layers of aluminum bumper and Kevlar cloth can prevent penetration for the same conditions as Fig. 1-1. (UDRI 4-0675)[Elfer88]

6 DEFORMATION ANALYSIS

6.1 Bulge Deformation Analysis

Figures 6-1 and 6-2 show rear wall bulge for 2219-T87 and 2219-T62 for 1 g and 1.27 g projectiles respectively, at 6.4+ km/s.

The starting point of the analysis is an assumed distribution of momentum on the rear wall. The assumed distribution in both time and position can have a large influence on rear wall failure.

The Christiansen equations for multi-shock shields and mesh-double-bumpers (Appendix A) assume that for velocities greater than 6 km/s, the rear wall will fail for constant projectile momentum normal to the wall. The equation assumes that the allowable momentum is proportional to $1/S^2$. Note that oblique effects are only assumed in the normal component of velocity, while any beneficial effect on the effective spacing, S, is conservatively ignored. The equation also includes a yield strength term to account for different rear wall materials, but tests and analysis, in the following sections, show that rear wall ductility have a larger influence, and should be included in a general penetration equation.

For velocities greater than 6 km/s, the Wilkinson equation for momentum failure has been used successfully for shields with intermediate catchers. (See Fig. 6-2 with next paragraph) This is slightly less conservative than a constant momentum approach, since for a larger t/d ratio there will be a larger dispersion angle. A larger t/d ratio occurs for constant momentum at higher impact velocities.

However, Elfer used Wilkinson's equation with a modified dispersion angle from the original Wilkinson equation. The dispersion angle used was 25% lower than Wilkinson proposed. because the lower angle agrees with rear wall damage, with HULL analysis, (Fig. 6-3) and it also predicts the observed momentum failure in specimens. The lower angle was likely a result of melting of the aluminum particle in the 6 to 8 km/s range, while Wilkinson's analysis was for vaporization at higher impact velocities.

Momentum multiplication occurs in both elastic collisions and cratering events. McMillan assumed elastic rebound of vaporized gas and that the rear wall momentum was twice that of the original projectile. If the debris "sticks" to the rear wall, then the rear wall will be approximately equal to the original projectile. However, if ablation or cratering of the rear wall occur, then the momentum can be up to five times that of the original projectile. Although bumper debris may be spread over too large an area to significantly affect the rear wall loading, the uncertainty associated with

momentum multiplication can mean a factor of two difference in the rear wall thickness to resist penetration.

A general test observation is that the bumper is not deformed as much as the rear wall, even though the bumper is much thinner. See Figures 6-1 and 6-2. Therefore, the momentum in the rear wall probably does not approach the upper limits theoretically possible for even the rebound case. This lends credibility to just using the initial projectile momentum as the starting assumption for rear wall models.

A curve fit to Lagrangian rear wall deformation predictions was generated by Grove and Rajendran to provide an alternate analysis method provided the original Gausian distribution of momentum can be applied. The curve fit is included in Appendix A.

6.1.1 Deformation

This type of failure mode leads to large petaled holes, potentially more dangerous than the relatively clean holes produced by fragment penetration.

The analysis of bulging is different than the initial impact analysis. The use of an Lagrangian model is best for late time momentum failure to accurately track deformations and strain. The deformation usually occurs over about 50 to 100 microseconds after the initial impact of the debris cloud on the rear wall. It is impractical to run the Lagrangian models from Eulerian hydrocode input because computer memory and time requirements. This is true for two dimensional calculations much less for three dimensional calculations. Furthermore, the pressure distribution from hydrocode analyses tends to be too jagged, resulting in failure.

Most models of rear wall deformation derive the loading from either simple models of vaporized clouds or assume that the momentum intensity is deposited either uniformly or with a Gausian distribution over some area on the rear wall.

STEALTH and EPIC calculations of rear wall deformation were done at the University of Dayton. [Rajendran] When models of the debris cloud were used to drive the calculation, the stresses exceeded the spall strength by several times. When an intermediate shield is used, the extra mass involved can slow down the impact sufficiently so that spall should not be predicted.

Figure 6-5 shows rear wall deformation models. Thinning can occur at the centerline or also away from the centerline depending on the starting momentum distribution. Figure 6-6 shows measured thinning on two different specimens and it can be seen that the maximum strain can occur

either on or away from the centerline. Figure 6-7 shows Roberts' HULL predicted thinning versus measured thinning. While the absolute agreement is not good, the relative shape of the two curves was judged acceptable. The HULL standard properties for aluminum were used which were low relative to the measured strength of the alloys of interest, and this accounts for the discrepancy. HULL uses a strength of approximately 300 MPa while Rajendran measured a flow stress of 480 MPa for 2219 and 5456 using a split Hopkinson bar tensile test. While the dynamic strength was similar for the two materials, 5456 had 30% elongation compared to 12% for 2219.[Elfer88] The effects of strength and strain were included in Grove's parametric analyses to give a general solution.

Figure 6-8 shows rear wall deformation on two specimens as well as HULL and NASTRAN analyses performed by Roberts. (The 5456 specimen deformation was measured before and after sectioning. There were no residual stress effects.) The HULL analyses again gave the correct qualitative shape, although more analyses would be required to completely match the correct momentum (with rebound), momentum distribution, and material properties. The NASTRAN 3D sheet elements appeared to accentuate the thinning and deformation at the center of the specimen. This was true for 10.16 and 30.48 cm radius pie slices. While the simpler model would be useful for petaling type of analysis, this may be inadequate for accurate simulations.

Groves performed parametric analyses of rear wall deformation using EPIC (similar to the HULL analyses) and fit the results to a dimensionless parameter to predict failure (Appendix A) Figure 6-9 shows the correlation between Groves dimensionless parameter and calculated rear wall strain. [Analysis in Final Report Attachment 7]

6.2 Hole Size

The hole size depends on the penetration mechanism that forms the hole and the amount of momentum that remains in the rear wall after the initial penetration. Hole sizes are related to:

- single fragments crater damage (with sizes as little as a crack to leak gas)
- debris cloud diameter, with a hole formed immediately after impact (multiple fragments, spall enhanced penetration, or a shear plug)
- petaled holes larger than the debris cloud diameter. Theses are formed 10s of milliseconds after the wall is penetrated.

There is no lower limit on hole size. A front wall crater may be linked by a minute crack to allow a gas leak. If the hole is created by a fragment,

then bumper holes size equations are appropriate. Larger size holes may be estimated from the debris cloud diameter.

The larger holes, associated with a petaled hole, are the greatest concern for critical damage to a manned module. Notwithstanding, most tests have been designed for penetration resistance testing rather than hole size characterization.

6.2.1 Effect of wall thickness on hole size

There appears to be an upper limit on hole size for a given wall design and a given impact velocity. Figure 6-10 shows how petaled hole size varied with rear wall thickness for a series of specimens. Several of the specimens are shown in Fig. 6-10 to 6-17. The specimens were each impacted by a 1.27 cm aluminum projectile with a nominal velocity of 6.4 km/s. Each rear wall was protected by a 0.2 cm thick 6061 aluminum bumper at 11.4 cm and 4 layers of style 710 Kevlar 29 cloth at 5.7 cm.

The exact amount of momentum absorbed by the rear wall is not known. The bumper and Kevlar cloth probably allowed a large central particle to penetrate the rear wall. The remainder of the debris cloud (including Kevlar cloth) imparted some of its momentum to the rear wall. After tearing the rear wall, and giving it an initial momentum, the rest of the debris cloud continued along the shot direction.

The initial velocity was higher for the thinner rear walls, due to their lower mass. Also thinner rear walls, will absorb less momentum from the debris cloud. If the rear wall mass is small relative to the debris cloud mass, the rear wall will attain cloud velocity as it is pushed out of the way.

Figure 6-18 show the rear wall in Fig. 6-13 with the petals bent back in. Note that the impact area is approximately one third the diameter of the final hole size. This would be a good estimate for maximum petaled hole size. Also note that the petals overlap. It is obvious that cracks or tears that make the petals form after the bulging is complete, which is a relatively late time effect.

Measurements of thinning were made on some of the petaled holes to try and compare to the data in Fig. 6-6 and 6-7. However, due to difficulties with craters raising or lowering the thickness measurement, it can only be said the data appeared to be similar. The strain at failure was approximately 11 percent.

6.2.2 Effect of increasing the projectile size

Once the hole is "fully developed," further increases in projectile size are not expected to significantly increase the hole size. Most of the additional projectile momentum will go into the central fragments. Any additional

momentum in the cloud will have a smaller effect on rear wall velocity. For the 2219 and 5456 walls described in the previous section, the "fully developed" hole size is approximately 22 centimeters.

6.2.3 Tearing of petal ends

Examination of the petals (described in Sec 6.2.1) showed that the tips were torn off some petals. The tip was torn approximately two to five centimeters behind the initial fragment penetration hole. See Fig. 6-17 for a partial tear. The petals with torn tips did not open up as much as the other petals. Some of the momentum to open the petal was lost to the tip. It is not known whether the torn petal tips were related to initial crater damage, to a neck generated early during the initial deformation (before the petal formed), or whether it is a natural consequence of having so much momentum that the tip tears off the end of the petal. If the latter is the case, then this is a mechanism to limit the maximum momentum transferred to the rear wall.

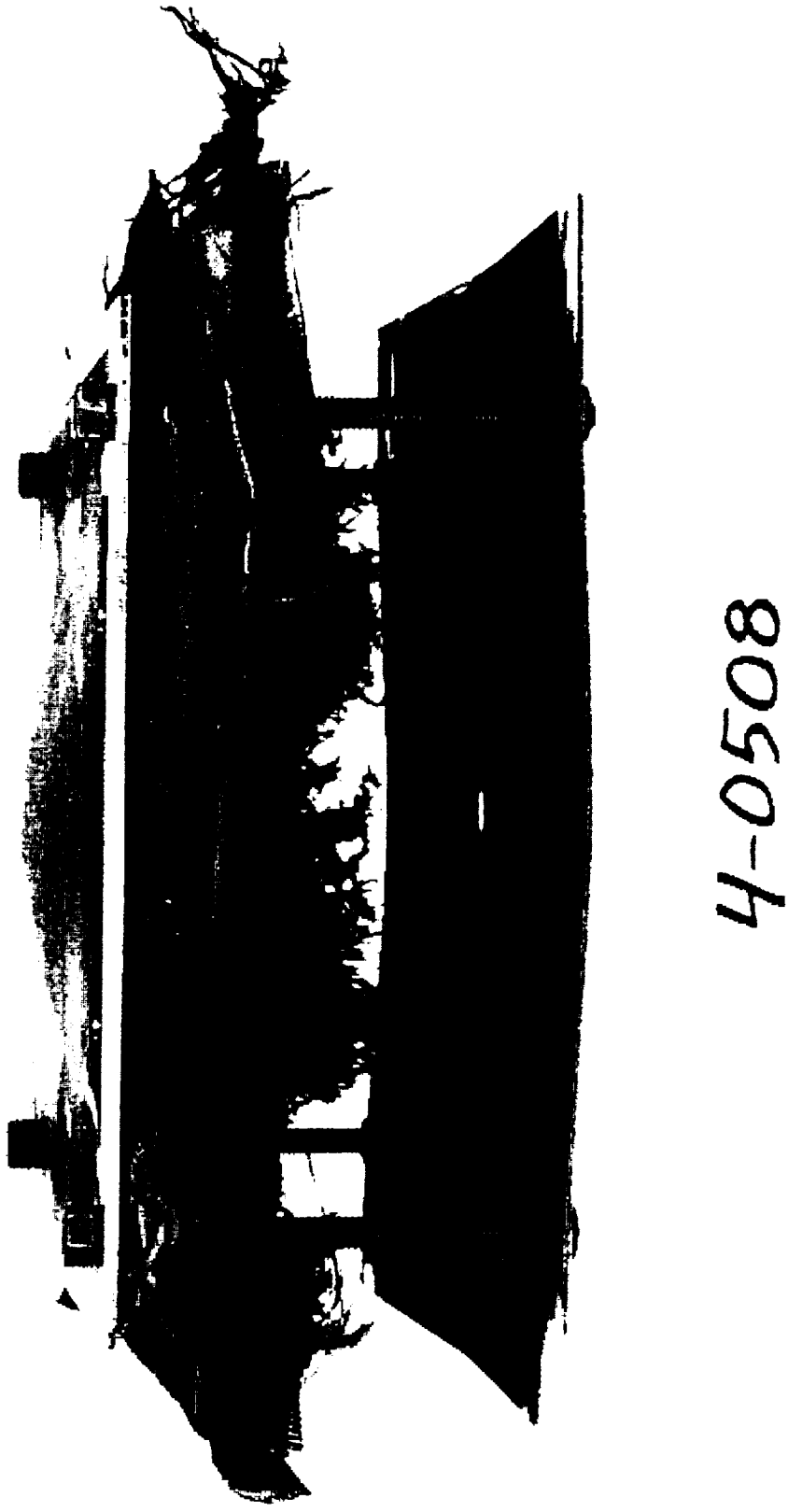

Fig. 6-1 Rear wall deformation (same design as Fig. 1-1) 1 gram projectile 6.4 km/s. (UDRI 4-0508) [Elfer]

Fig. 6-2 Rear wall deformation (same design as Fig. 1-1 except -T62 rear wall) 1.3 gram projectile 6.4 km/s. (UDRI 4-0508) [Elfer]

Standoff Distance with Kevlar

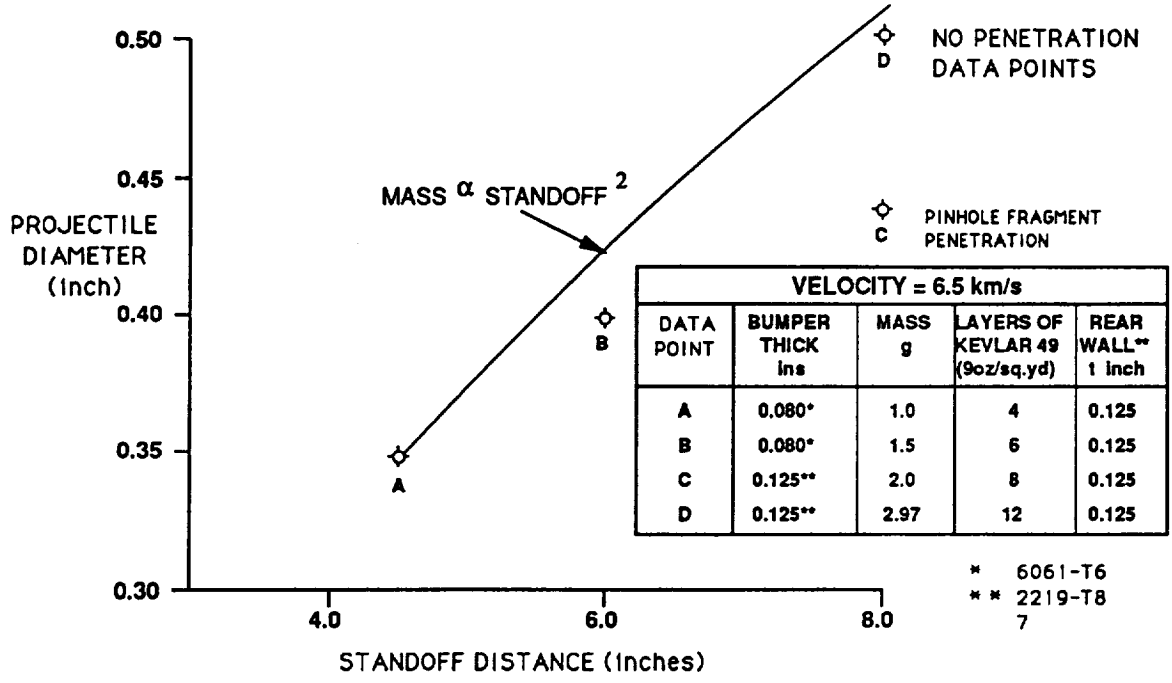

VELOCITY = 6.5 km/s				
DATA POINT	BUMPER THICK ins	MASS g	LAYERS OF KEVLAR 49 (9oz/sq.yd)	REAR WALL** 1 inch
A	0.080*	1.0	4	0.125
B	0.080*	1.5	6	0.125
C	0.125**	2.0	8	0.125
D	0.125**	2.97	12	0.125

* 6061-T6
** 2219-T87

Fig. 6-3 Projectile mass for no penetration (or rupture) is proportional to S^2 for adequate bumpers and catchers.

Spray Angle

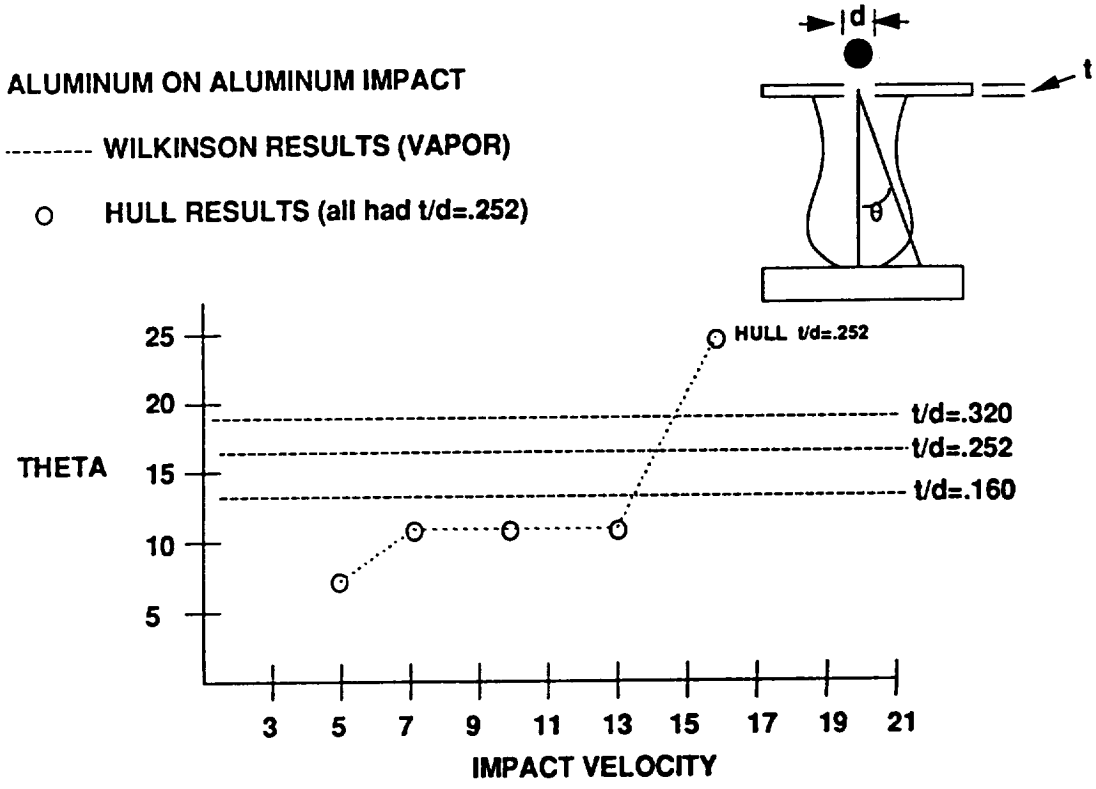

Fig. 6-4 Comparison of debris spray dispersion angle between HULL results and Wilkinson's vaporization equation. Note that HULL results are outer diameter of spray while Wilkinson's dispersion angle is one standard deviation on a Gausian distribution.

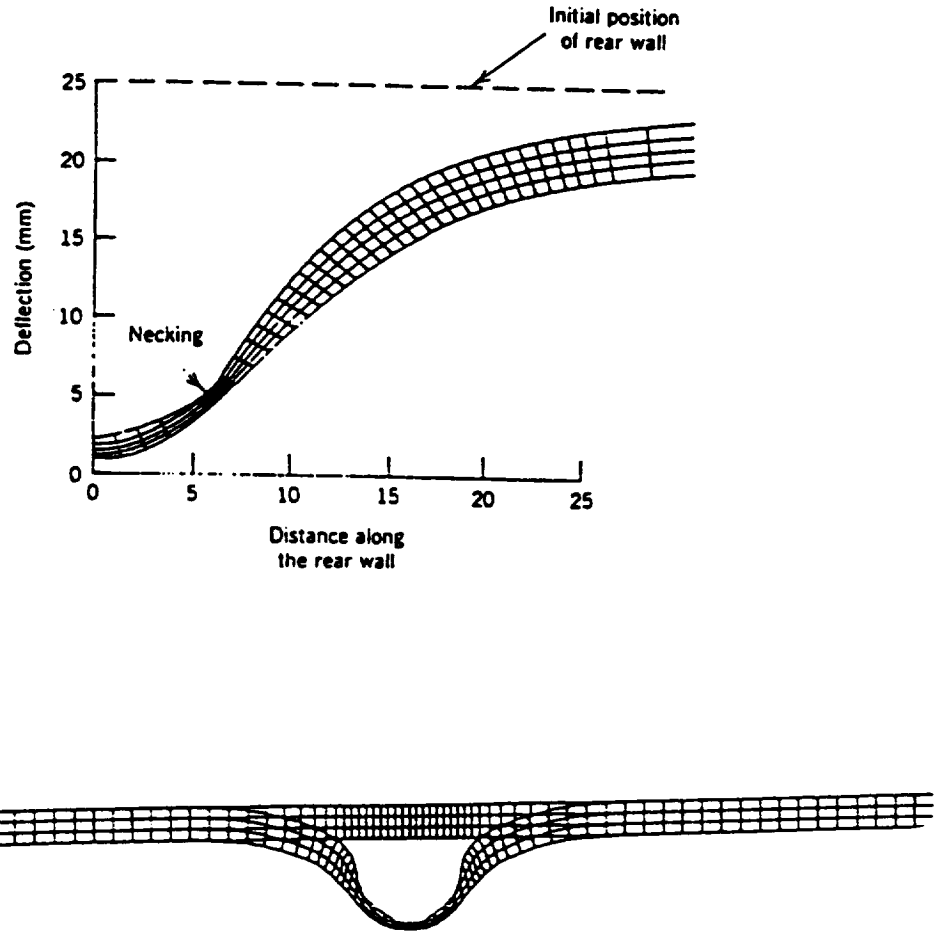

Fig. 6-5 STEALTH models of rear wall deformation.

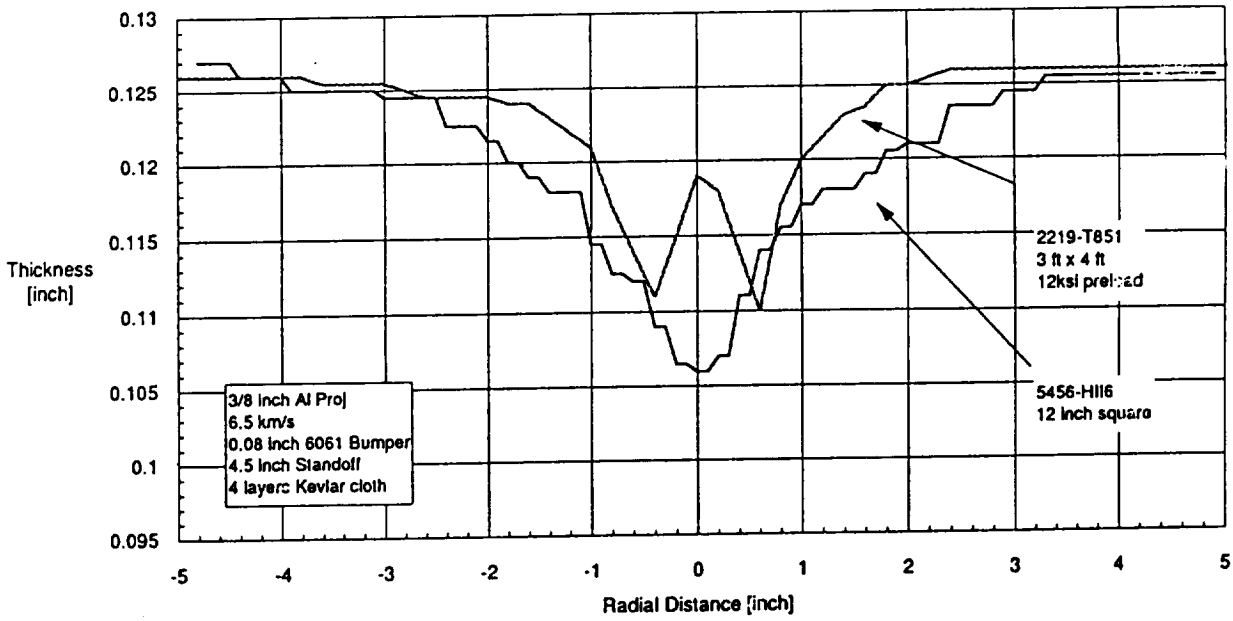

Fig. 6-6 Measured thinning of rear wall. Maximum thinning may occur at the centerline or in a circle away from the centerline.

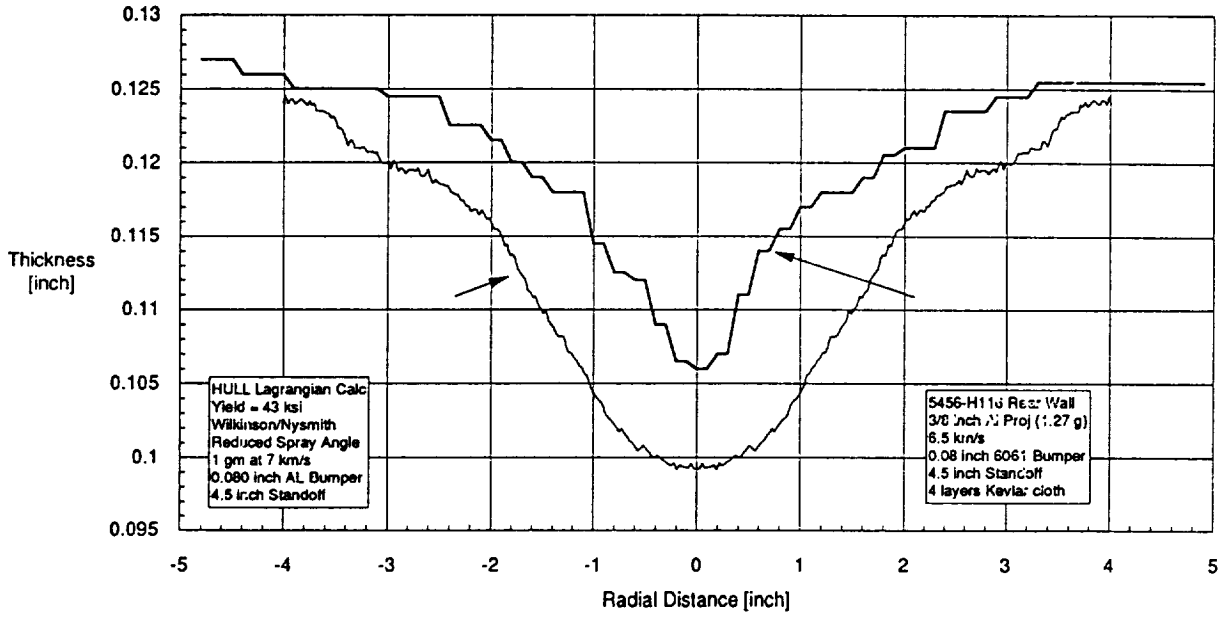

Fig. 6-7 Measured thinning of rear wall compared to a HULL analysis. The low strength in the HULL model ended with more thinning than the test, but the relative shape of the curves was in agreement.

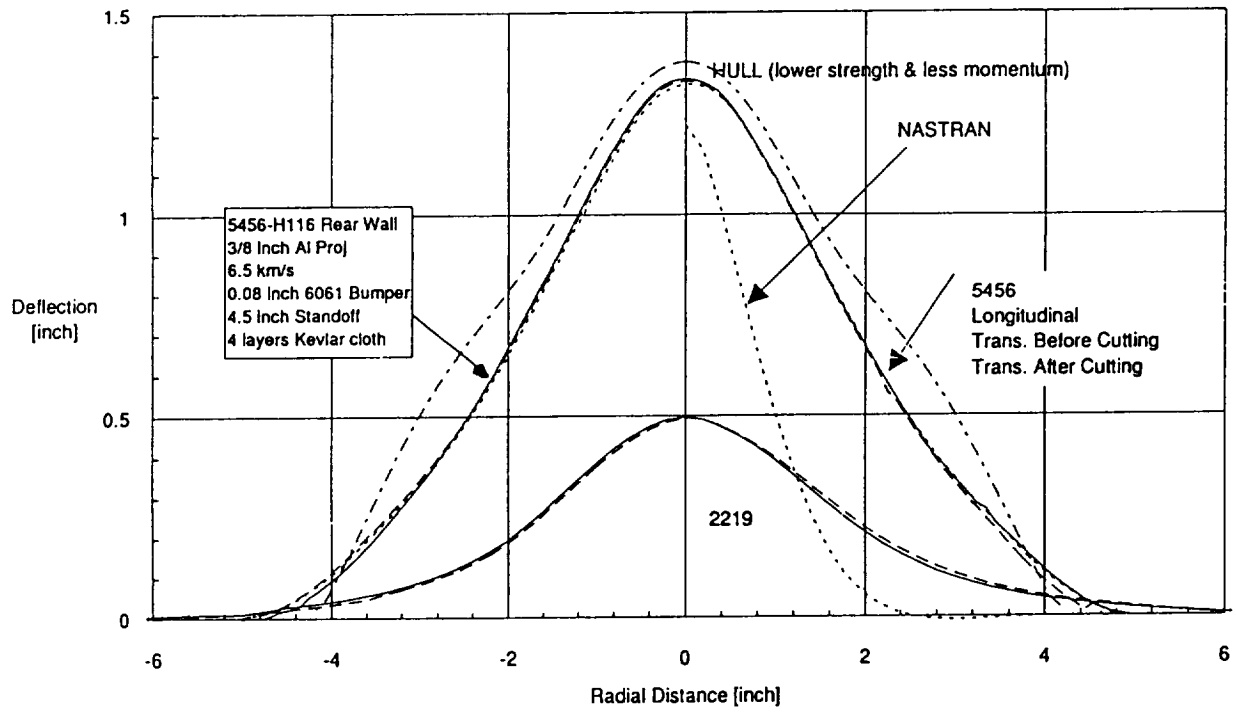

Fig. 6-8 Comparison of measured permanent deformation, HULL analyses and simple NASTRAN sheet element analyses.

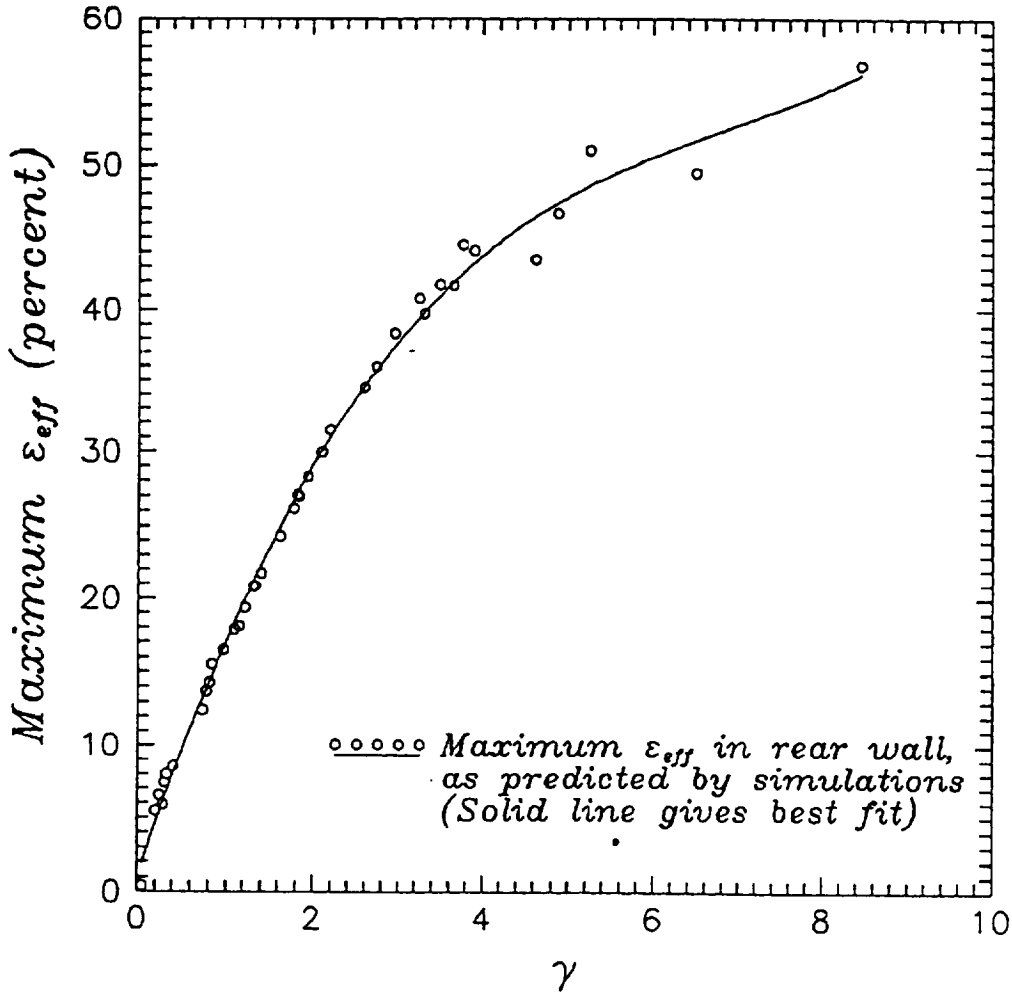

Fig. 6-9 Correlation between maximum effective rear wall strain as predicted by EPIC simulation and Groves dimensionless design parameter.

STRESSED PANEL DEBRIS TESTS

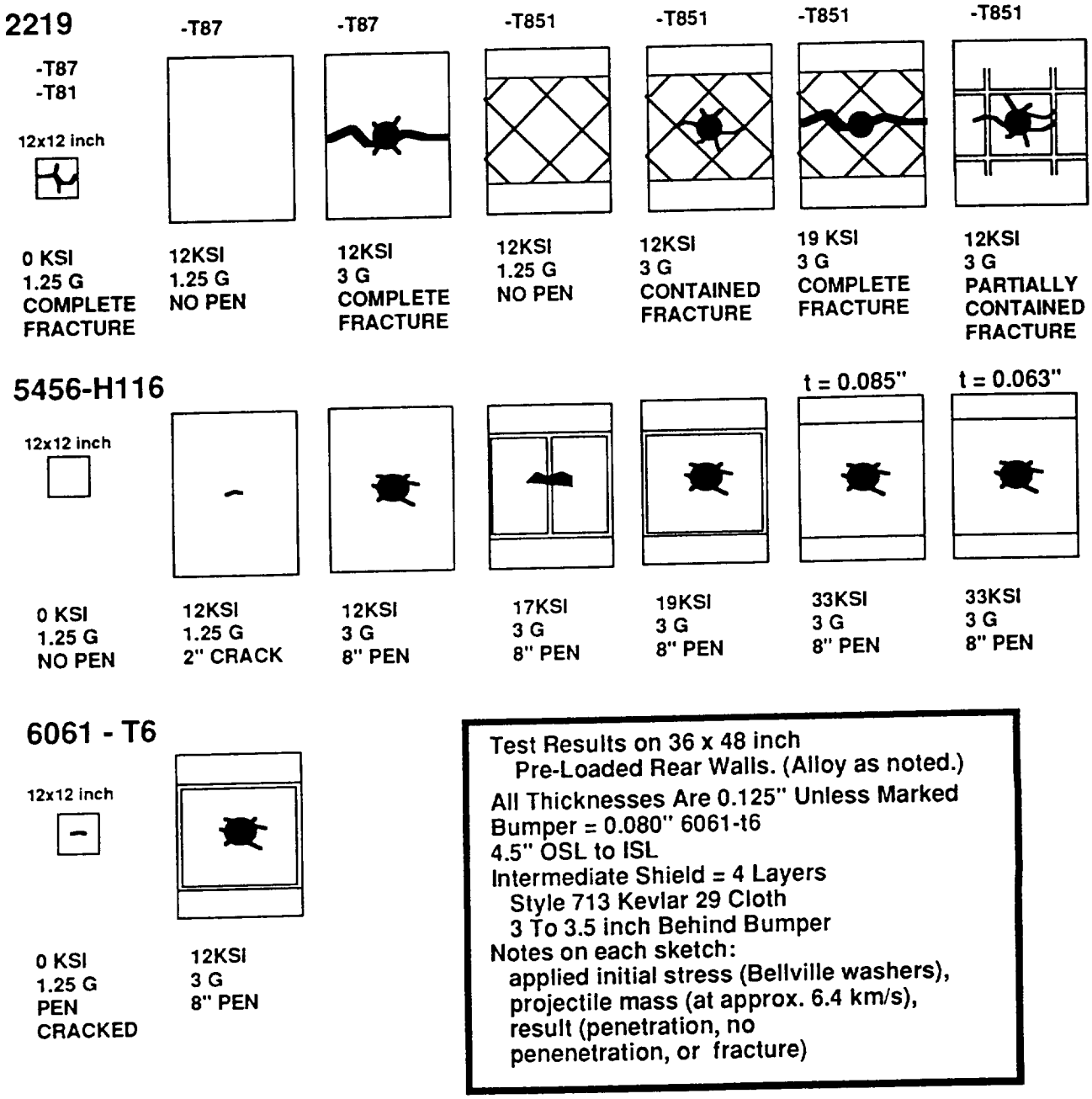

Fig. 6-10 Summary of pre-stressed panel test results. Large panels similar to Fig. 1-1. [Elfer]

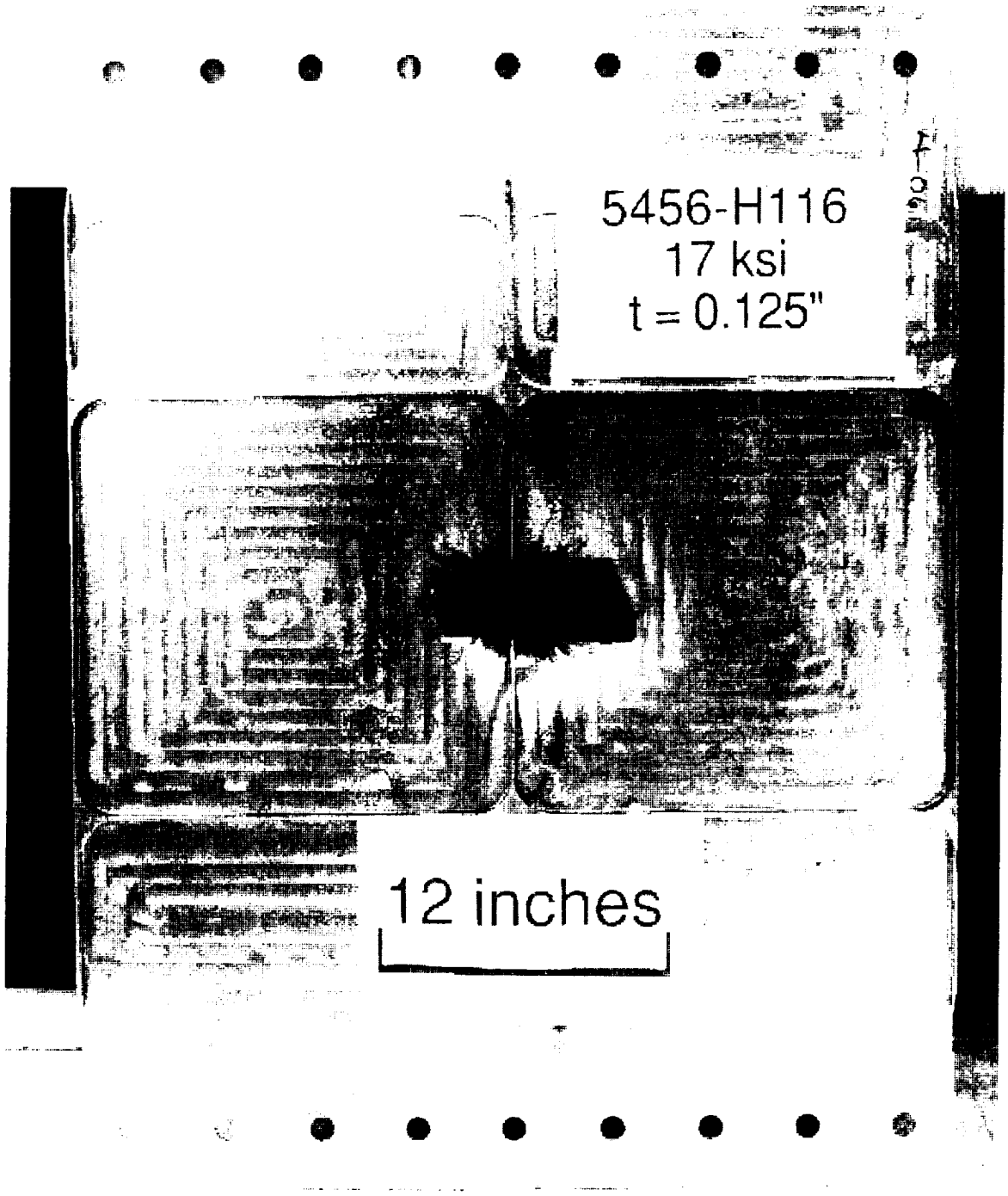

Fig. 6-11 Same as Fig.1-1 except for 5456 rear wall material and impact occurred on a stiffener.

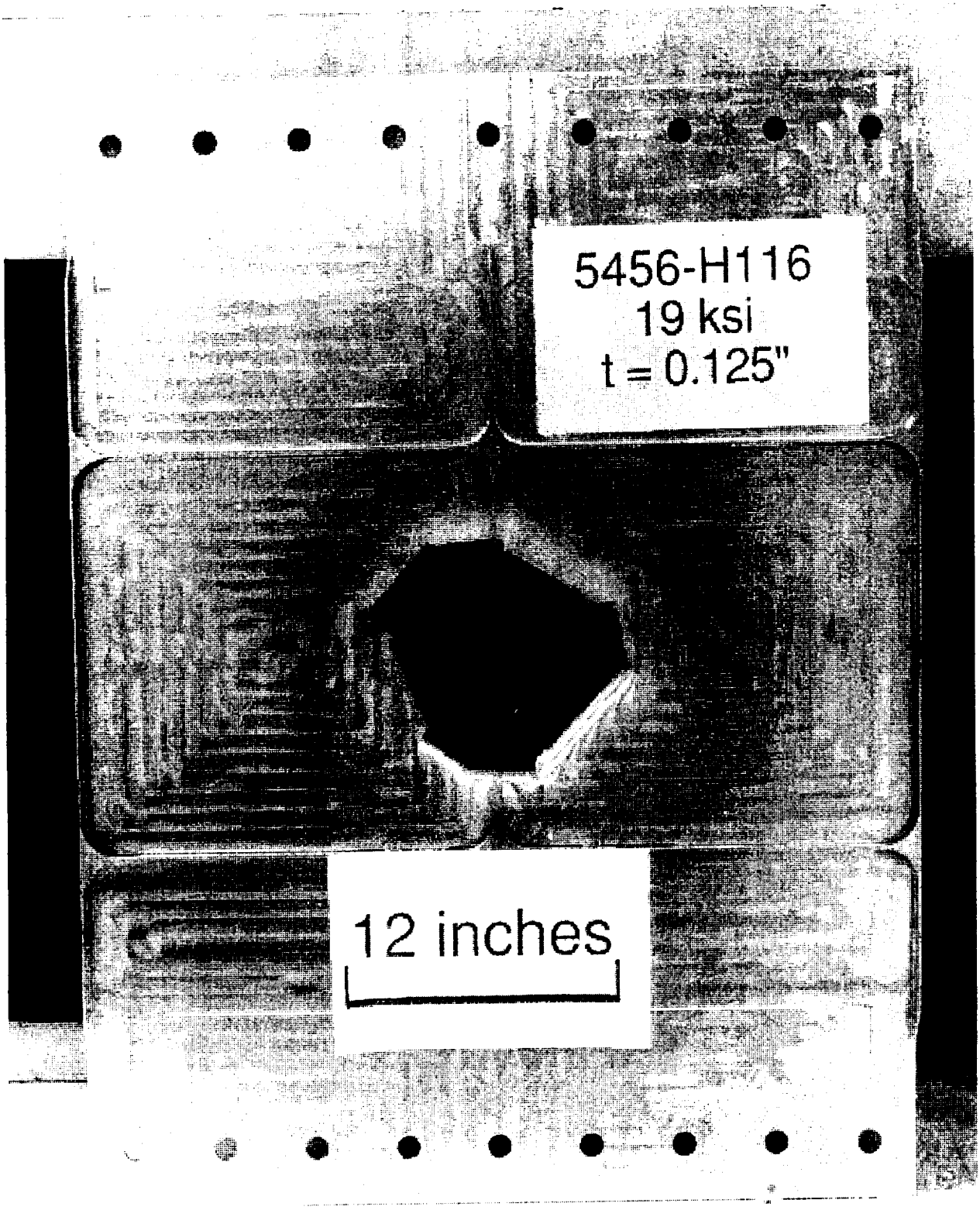

Fig. 6-12 Same as Fig. 6-10 except that stiffener was removed prior to impact.

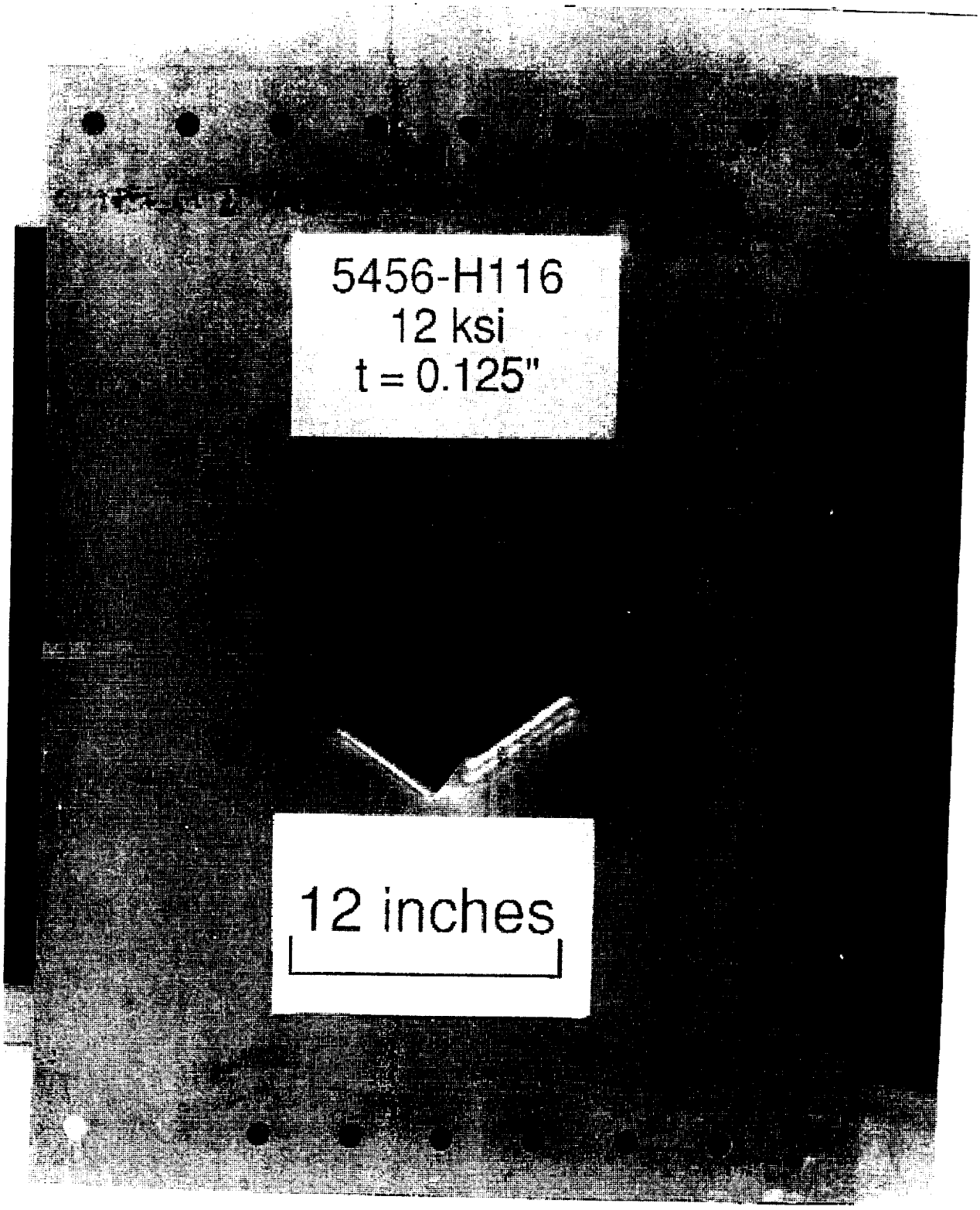

Fig. 6-13 Same as Fig. 6.11 except sheet was used instead of machining plate down to same 1/8 inch thickness.

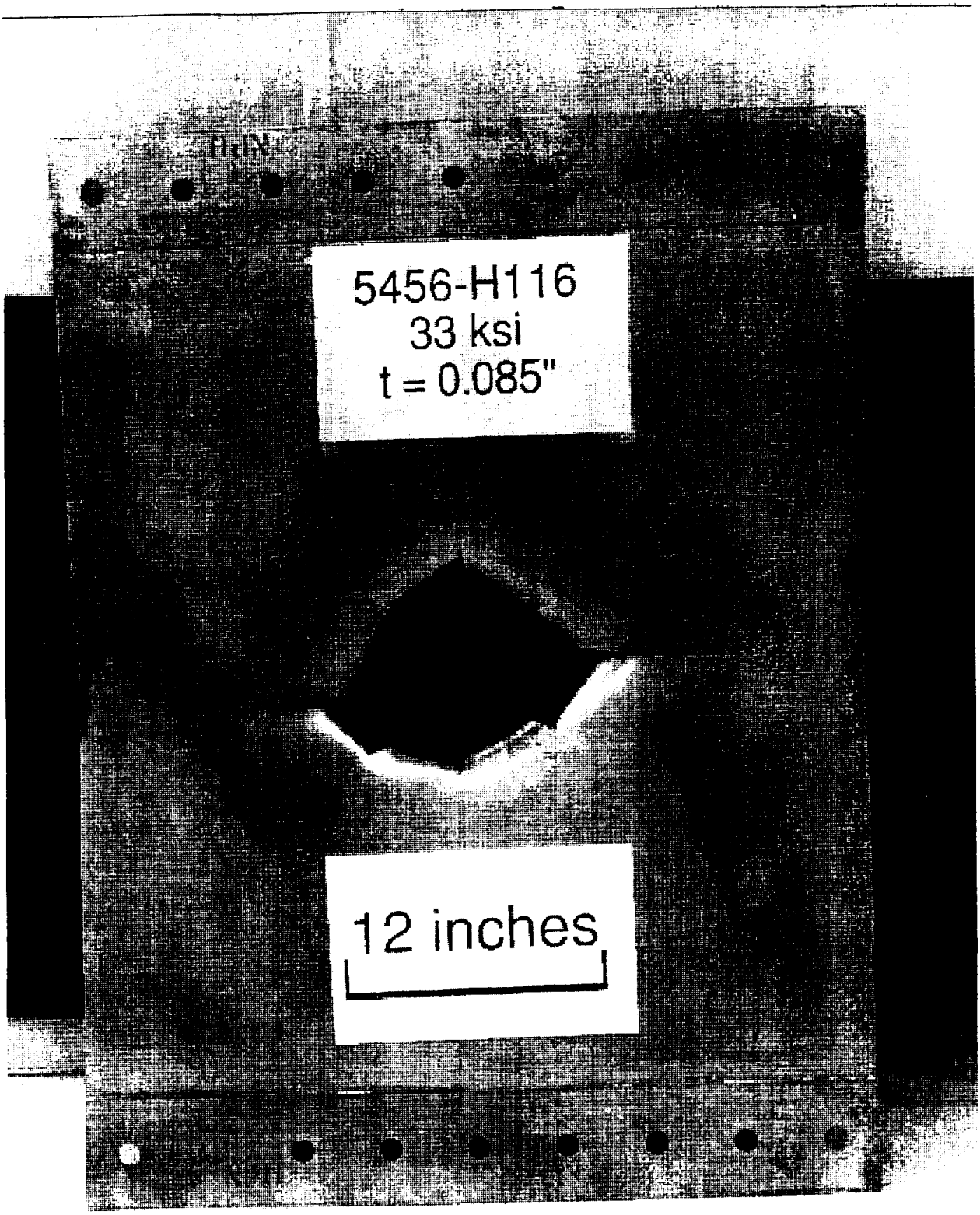

Fig. 6-14 Same as Fig. 6.12 except thinner sheet.

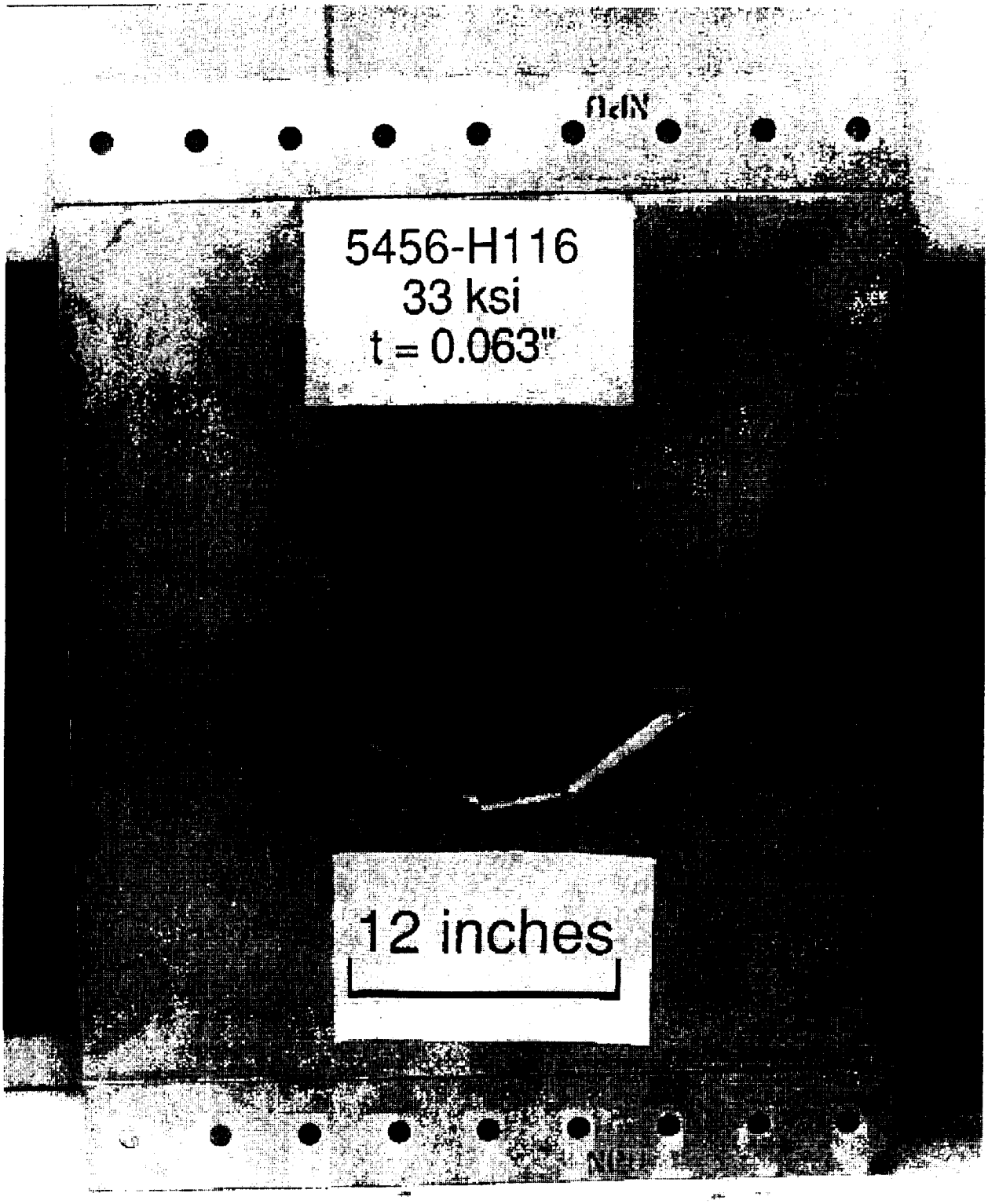

Fig. 6-15 Same as Fig. 6.12 and 6-13 except thinner sheet.

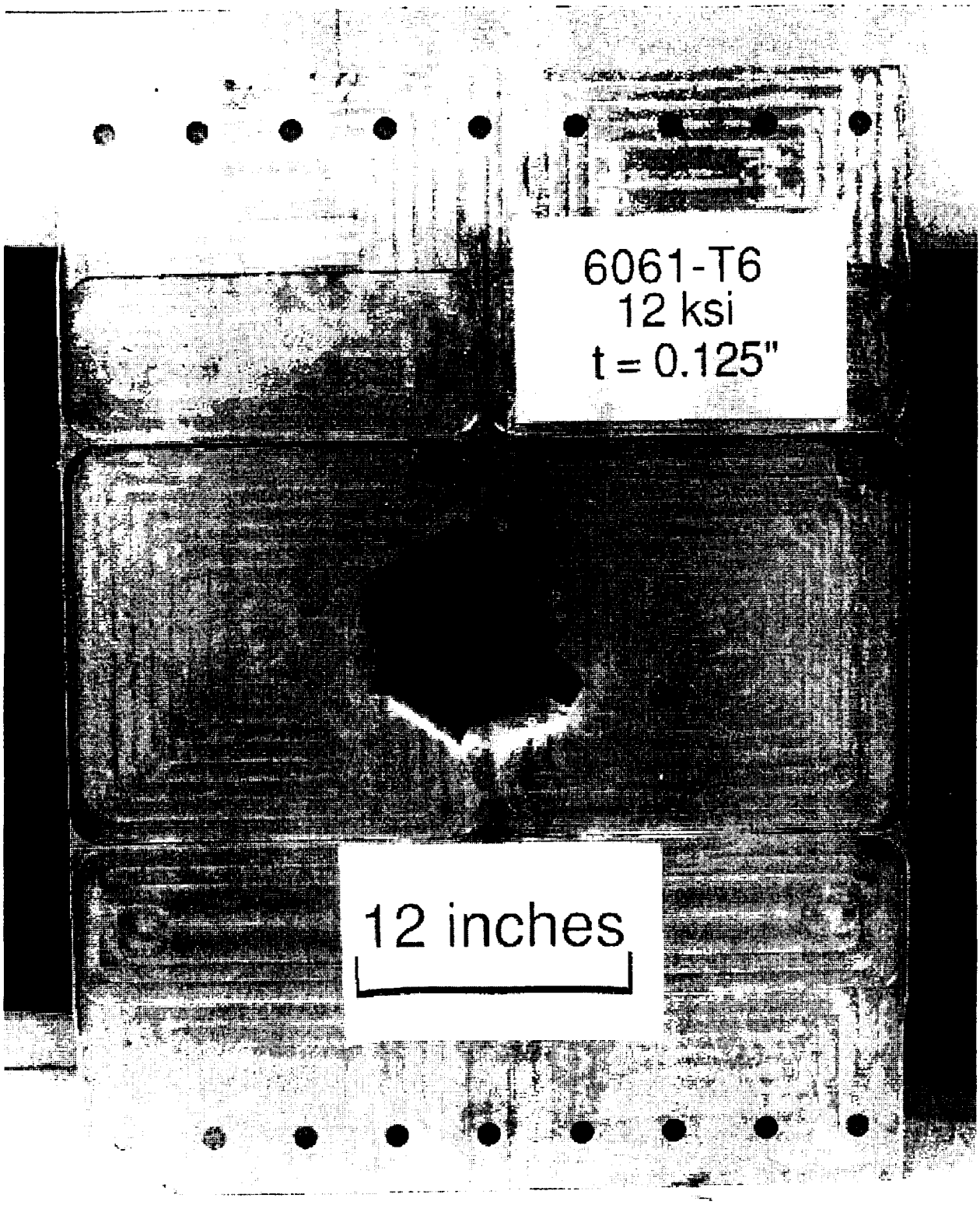

Fig. 6-16 Same as Fig. 6-10 and 1.1 except 6061-T6 material used.

Fig. 6-17 Reverse of Fig. 6-12, showing torn petals, catcher cloth, and bumper.

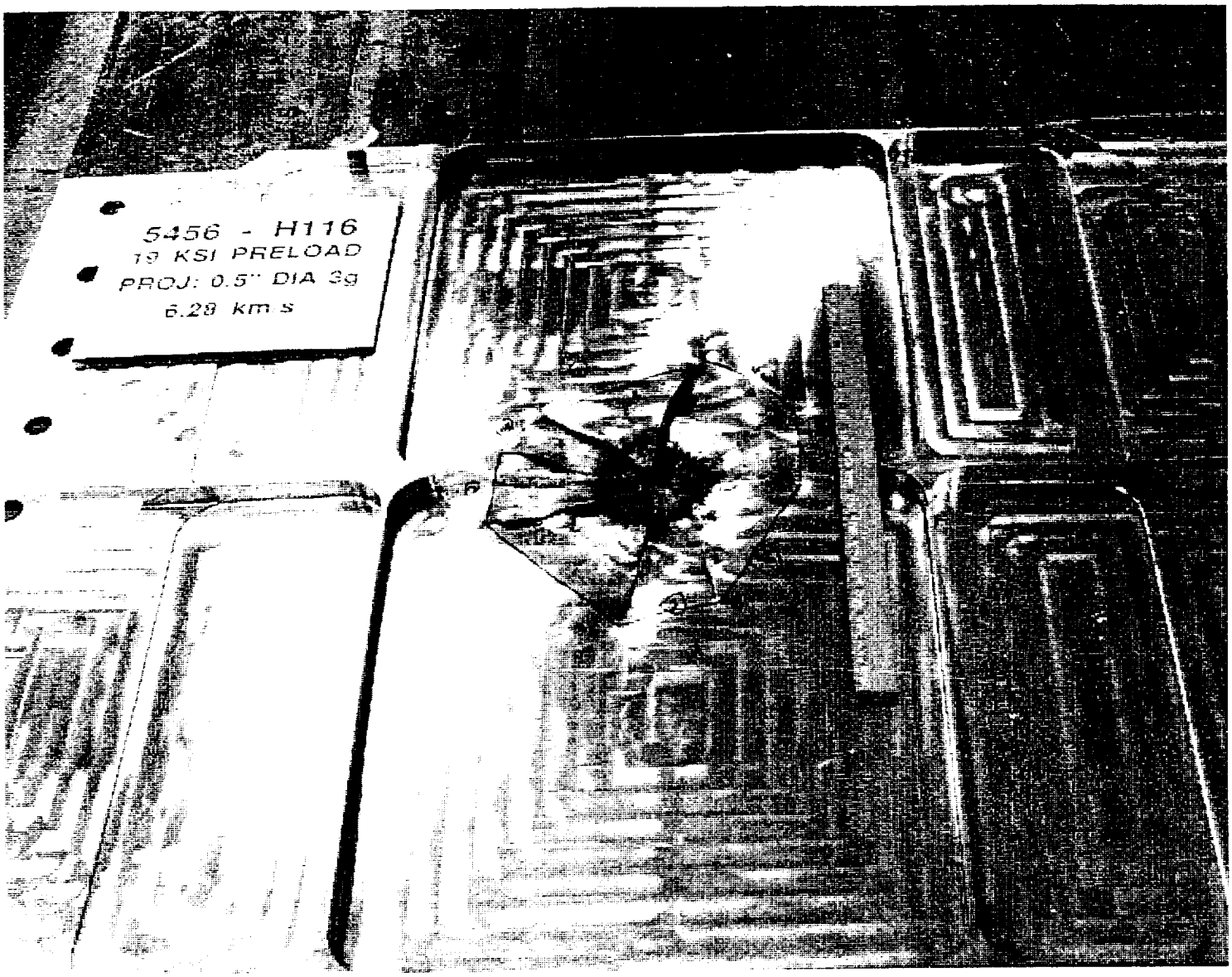

Fig. 6-18 The petals were bent back in on the rear wall shown in Fig. 6-13. Note that the impact area is approximately one third the diameter of the final hole size.

7 DAMAGE TOLERANCE

The section addresses the potential for a meteoroid or debris impact to create a large crack which will propagate to complete fracture of a module. The first step in this process is a penetration which forms petals or cracks. This occurs due to the inward bulging that occurs as projectile momentum is absorbed. The crack driving force due to impact decrease as the crack gets longer. The next step in the process is to determine whether internal loads will cause catastrophic crack growth. As will be discussed, the separation of these processes is appropriate. The impact bends the metal inward, whereas the internal pressure is the prime structural load, and it bends the petals back out. (The hoop stress is constant but it has less than one half of the crack driving force.)

7.1 Initial Crack Length

Prediction of crack length after penetration is very difficult. One must know the residual momentum distribution left in the specimen and how this affects crack length.

For a given shield design, there may be a maximum rear wall crack length generated regardless of impact projectile size. As momentum increases beyond the penetration threshold, more petals are formed up to an experimentally observed limiting number of eight to twelve. As projectile size increases further, most of the momentum just continues along the shot line, rather than being deposited in the rear wall. This is illustrated in the first block in Fig. 7-1.

7.1.1 Crack Propagation Energy Balance

The following approach to predicting fracture is based on an energy balance. The Wilkinson equation provides a starting estimate of the rear wall momentum distribution. The momentum deposited in the rear wall is used to determine the initial kinetic energy. This is much different than the initial kinetic energy of the projectile since the total mass is much higher and the velocity is lower. Furthermore, a significant fraction of the initial momentum may propagate through the wall.

K.E.(rear wall) = Work of deformation + Fracture Energy + K.E.(torn fragments)

where

Fracture Energy = No. of petals x length of tear x energy of fracture per unit length

It is assumed that the elastic energy absorbed by the rear wall is negligible. Assume that the kinetic energy is absorbed initially by plastic deformation (bulging) of the rear wall, and when radial cracks initiate, the remainder of the energy is consumed by crack propagation.

The crack propagation energy is dependent on the number of cracks formed. Assume that the maximum number of cracks/petals is eight. Although more petals may form (as many as twelve), this is a conservative upper limit. (It is conservative to estimate fewer petals, since the cracks must be longer to account for the same amount of energy.) The actual number of petals to be used in the analysis depends on the amount of kinetic energy available beyond that required to fail the rear wall by bulging.

Figure 7-1 schematically shows the processes that will occur for increasing momentum. A key assumption is that the rear wall was optimized to the bumper shield system to allow momentum failure before fragment penetration could occur. However, if the rear wall always fails by fragment pentration, spall, or plug failure, before bulging and momentum failure can occur, then significant crack propagation will not occur.

Figure 7-2 shows Kaufman and Hunsicker's results on crack propagation energy per unit length. The numbers are not actual material properties. The resistance to crack propagation is dependent on specimen geometry and increases as the crack gets longer (R-Curve effect), but the chart shows relative rankings of several alloys. Figure 7-3 shows crack propagation energy per unit length for three alloys as a function of temperature. These charts help explain why the 5456 and 6061 aluminum rear walls did not have as much crack growth as the 2219 rear walls (which will be similar to 2014).

7.2 Structural Failure

One simplifying approach to predicting failure, is the separation of the initial flaw size from the analysis of the structure of with a crack. This is supported by the tests on pre-loaded specimens as shown in Fig. 6-10 through 6-17. [Elfer87] In those tests the crack growth perpendicular to the tensile load was not significantly larger than the crack growth in the same direction as the principal stress. This section reviews the damage tolerance analysis after the initial impact induced damage.

7.2.1 Material Properties for Fracture Analysis

Figure 7-4 shows the fracture stress for different initial flaw lengths in a 61 cm wide sheets of 2219-T87 and 5456-H116. [Elfer88] For 2219, there is only a small R-curve effect, and linear elastic fracture mechanics with a

toughness of 60 ksi·√in appears to adequately model the failure. Measured R-curves versus physical flaw size are shown in Fig. 7-5. [Elfer88] This is in contrast to the values reported in the Air Force Damage Tolerant Design Handbook. There values in excess of 100 ksi·√in were reported for wide specimens of 0.100 inch material. Those specimens exhibited a definite R-curve effect, longer flaws failed at higher toughness values. Both test programs used anti-buckling restraints on the specimens.

One possible cause for the difference in the toughness between the two test programs, was that values from the Damage Tolerant Design Handbook were from a 1962 report by Eichenberger[62]. However, in 1963 the aging heat treatment for 2219-T87 was changed from 14 to 24 hours at 325°F to prevent the possibility of stress corrosion cracking. The specimens with the shorter aging time, especially at lower aging temperatures, could have higher ductility, and hence higher toughness, than the current heat treatment. Kaufman and Hunsicker showed that for 2014 alloy the peak aged condition has the lowest unit propagation energy, and that for equal stregths, the underaged condition is much tougher than the overaged condition.

Pfluger[64] also reported through flaw toughness for 2219-T87. The toughness (~60 ksi√in) appear to be consistent with Elfer's results based on maximum load and initial flaw size. However, the toughness was reported as approximately 100 ksi√in based on maximum load and the flaw size at onset of rapid crack growth. This is not a typical way of quoting the R-curve. The load level typically drops before unstable crack growth, although Pfluger may not have been able to measure the load drop.

For 2219 aluminum considerations, the lower values reported by Elfer are more representative, but specimens actually matching the heat treatment would be preferred. For example, age-forming can use higher temperatures and relatively longer times to reduce spring-back. The age-forming practice could further reduce strength and/or ductility compared to the standard heat treat, so it is important to test the actual heat treat conditions.

One issue is whether an impact induced crack length should be evaluated using the K from the initial flaw size or from the final flaw size. The tearing associated with the impact has already moved the crack tip up the R-curve. It is conservative to start the R-curve at the final flaw size from the impact (assume the crack will continue to grow at low R-curve levels). However, it may be more realistic to use the peak value on the R-curve (K-max). This simplifies the analysis to a simple linear elastic fracture mechanics analysis.

Dynamic fracture toughness, K_{Id}, should be considered for impact induced flaws. For several materials K_{Id} is lower than the static K_{Ic}. However, for 2219-T87, like several other aluminum alloys, the dynamic toughness is always greater than the static toughness. This may be inferred for the increase in toughness under cryogenic conditions, and this was confirmed by dynamic toughness measurements. [Kanninen93] While the higher dynamic toughness is of interest in trying to predict the crack growth during impact, the lower static toughness is what should be used to analyze whether the structure is stable due to internal pressure.

7.2.2 Cylinder Effect

A cylinder with internal pressure, and a longitudinal crack, has a much higher stress intensity than would be predicted in a flat plate with a similar hoop stress. Several solutions are given in Appendix A and Newman's solution in NASA-FLAGRO is preferred. Fig. 7-6 shows a magnification factor for a cylinder relative to a flat plate.

It has been shown that biaxial loads can cause a significant increase in toughness, but this does not appear to be significant to large cracks in manned modules. Tests by Erdogan and Ratwani [1972] showed a large (30%) improvement in toughness in 6061-T6 aluminum for a biaxial load equal to half of the opening load. This appears to be due to biaxial effects on the crack tip strain response (provided adequate anti-buckling restraints were used in uni-axial testing). While Erdogan's test showed a significant effect, the flaw was relatively small (1.3 inch) and the biaxial load was large. For larger flaws, of concern to a manned module, the hoop stress is small and so is the biaxial stress (on the order of 5 ksi for a 0.125 inch thick manned module). At the crack tip, the opening stresses will be above yield, but the biaxial stress will still be small, and there will be a negligible effect. This says that the magnitude of the stress parallel to the crack is much more important than the biaxial stress ratio. R-curve calculations by Nied [93] verified that a biaxial stress had a negligible effect on the R-curve of the 24 inch wide specimens tested by Elfer [section 7.2.1].

A possible conservatism in the analysis is the fact that some of the stress intensity is due to through-the-thickness bending. However, bending is not generally as detrimental as pure tension. The material may exhibit a higher toughness for a bending induced stress intensity. This effect has been observed in 2219-T87 surface flaws [Elfer92] and may be related to loss of constraint. However, considering Zahoor's fit of Erdogan's data (Appendix A) the bending contribution is less than 10% of the total stress intensity in the flaw sizes of interest to Space Station.

It is worth noting that the bending induced by the internal pressure is opposite to the bending induced by the initial impact. This substantiates the approach of separating the initial impact from the structural effects.

7.2.3 Hole Effect

A crack emanating from the edge of hole in a cylinder is more representative of a petaled hole than a simple crack in a cylinder. This significantly reduces the stress intensity at the crack tip since internal pressure would not work over a large area. To analyze these effects Rajendran and Grove modeled a cylinder with a depressurized area at the center of the crack.[in Elfer88] This is shown in Fig. 7-7. A generalized curve fit to their results is given in Appendix A. The curve fit is based on simple modification to the Folias equation (also in Appendix A) and used to ratio the Newman solution. As the radius of the area without pressure approached the half crack length, the closer the results came to the solution for a flat plate.

There is one caution in using the hole size directly in the analysis. Due to the petals bending inward, there will still be a bending moment on the petal. A somewhat smaller hole size should probably used to account for this.

Solutions for a star crack in a flat plate are included in Appendix A. While this looks like petals and should be applicable to a flat plate, this is probably not an accurate modification for a crack in a cylinder. Nevertheless, the petals are expected to reduce the stress intensity compared to a single longitudinal crack in a cylinder.

7.2.4 Influence Function for a Cylinder

Influence functions provide a means of analyzing a crack in an arbitrary stress field. This is illustrated for a flat plate in Fig. 7-8.

Influence functions were calculated for a longitudinal crack in a cylinder using a NASTRAN model with a crack tip element as shown in Appendix A. The geometry is shown in Fig. 7-9. Even though NASTRAN has special crack tip elements available, the analysis only converged on the FLAGRO solution for 3D brick elements when the mesh size was 0.25 inch square or twice the wall thickness, as shown in Fig. 7-10. The influence funtion was developed by applying point loads along the crack length. Since the model was only a quarter of the cylinder the influence funtion is for symmetric loads about the center of the crack. The analysis results for a particular flaw are shown in Fig. 7-11. An equation for the influence funtion is in Appendix A. The typical influence funtion for a center cracked plate, Green' function, is also included. The cylinder equation includes

components for Green's function in a flat plate and a cylindrical component so that the whole equation will integrate to Newman's solution for a uniform load. It is obvious that the cylinder is much more sensitive to loads at the center of the crack, compared to the flat plate. The influence function does converge to the flat plate solution close to the crack tip.

7.2.5 Cylinder with integrally machined stiffeners

Most manned modules require stiffeners for launch. There is a natural desire to determine if these stiffeners can prevent catastrophic rupture due to the large cracks that can be generated by debris impacts. In general, analysis of aircraft structures has shown that mechanically attached stiffeners, which can bridge a crack, are better than integrally machined stiffeners to slow fatigue crack growth and provide damage tolerance.

The integrally machined stiffeners originally planned for manned modules were in a 45° diamond pattern with 20.95 inches on diagonal. The stiffeners were 0.090 inches thick on a cylinder with a 0.125 inch membrane. An analysis by Eidinoff showed that the stiffeners have a significant influence on the stress intensity of centrally located crack in the membrane of cylinder.[Eidinoff93] This was based on a 3D analysis with 2D elements. On the other hand, separate 2D hoop stress analyses by Rajendran [in Elfer88] and Nied[93] did not predict as significant a reduction in the stress intensity except at the stiffener, and for that large a crack the stress intensity was so large that the crack would continue to propagate. The stress intensity away from the stiffener could be estimated on the smeared thickness. The influence funtion by Elfer (section 7.2.4) shows that pressure loads at the center of the crack to have a large influence on the stress intensity. If there are no stiffeners at the center of the crack, then the stiffener effects should not be significant.

The stiffeners do appear to have a significant effect on the impact induced crack growth. Impacts centered on the stiffener may not fracture the stiffener and, even when the stiffener failed, rear wall petaling was significantly reduced. Compare Fig. 6-11 and 6-12.

A conservative approach is to assume that the impact induced crack length will be limited by the stiffener spacing and then determine if the resultant crack is critical without including the stiffener influence on stress intensity.

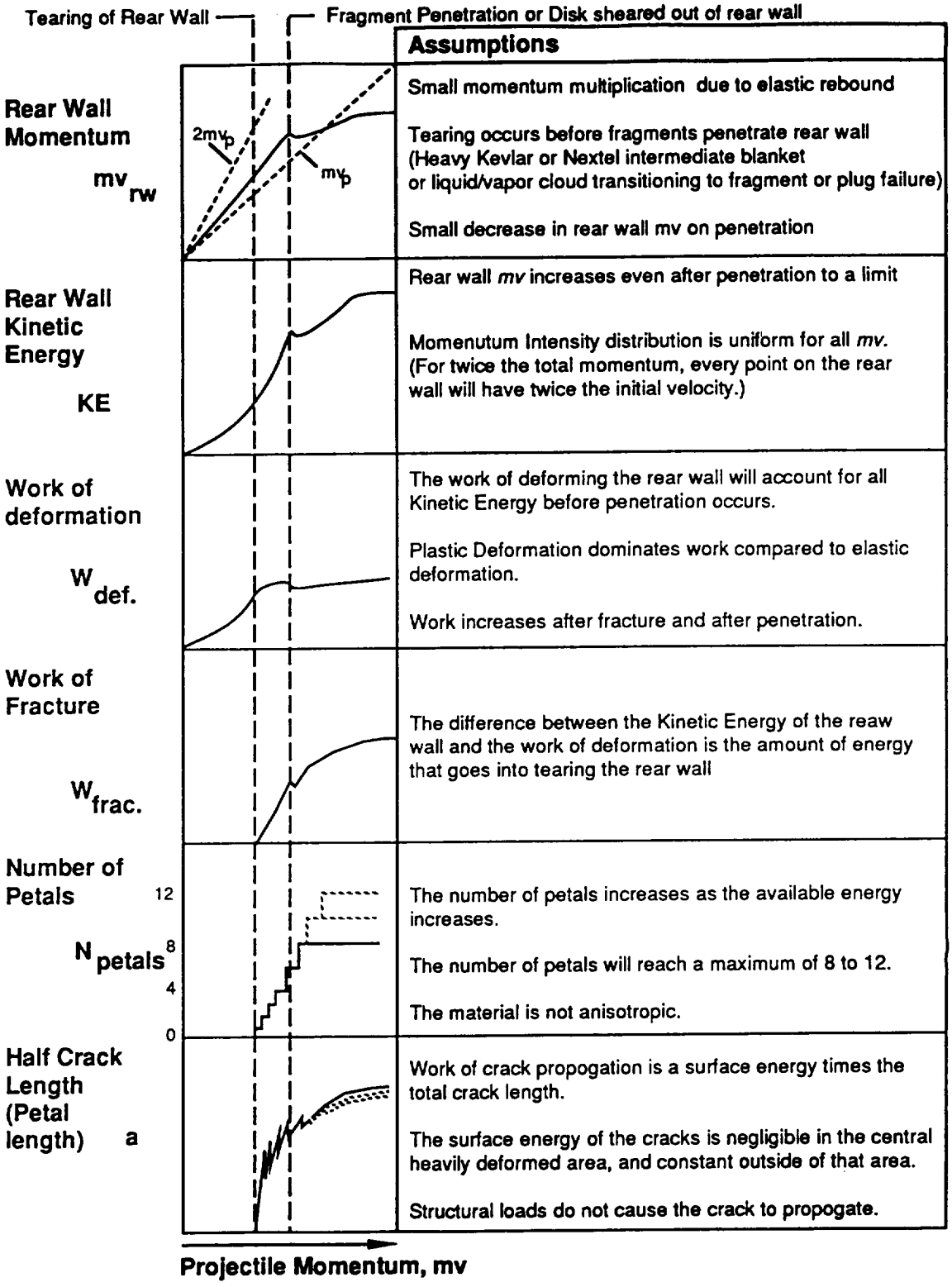

Fig. 7-1. An illustration of the energy balance for rear wall crack propagation.

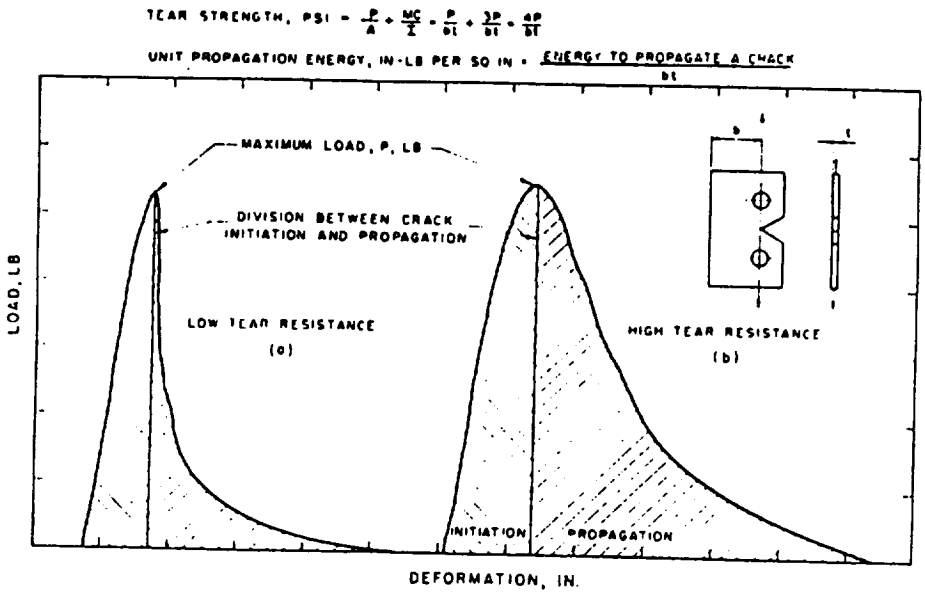

FRACTURE TOUGHNESS TESTING

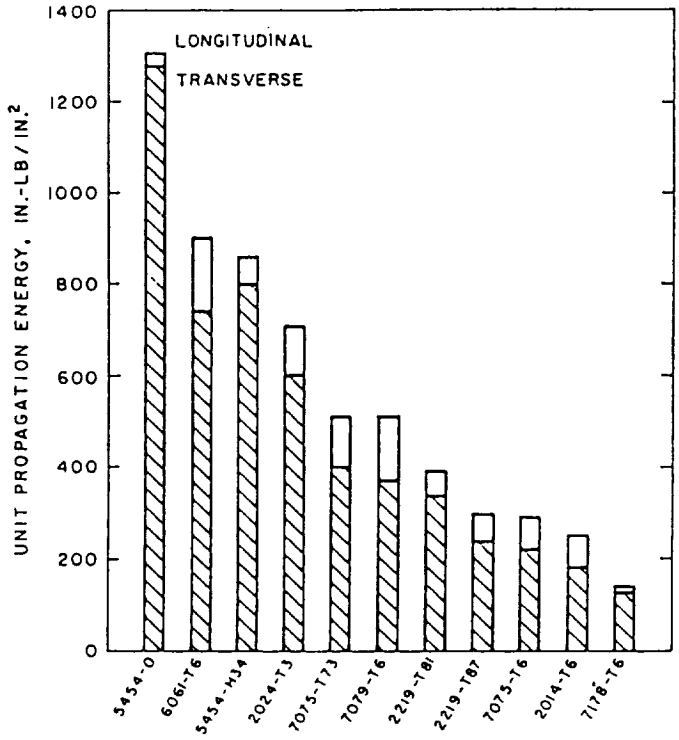

Fig. 7-2. Tear Resistance of 0.063 in. thick aluminum sheet. [Kaufman and Hunsicker]

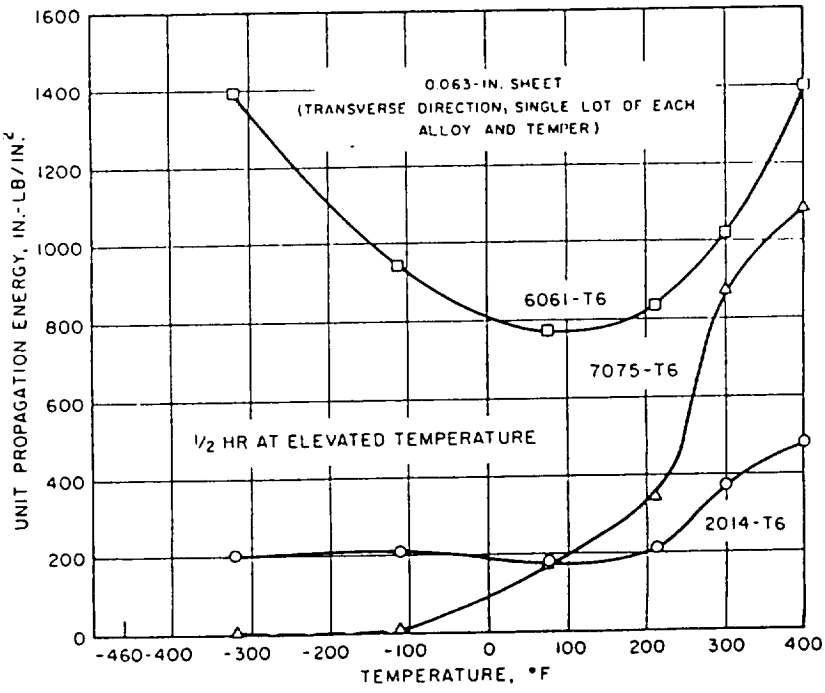

Fig. 7-3. Unit propagation energy of some aluminum alloys at various temperatures. [Kaufman and Hunsicker]

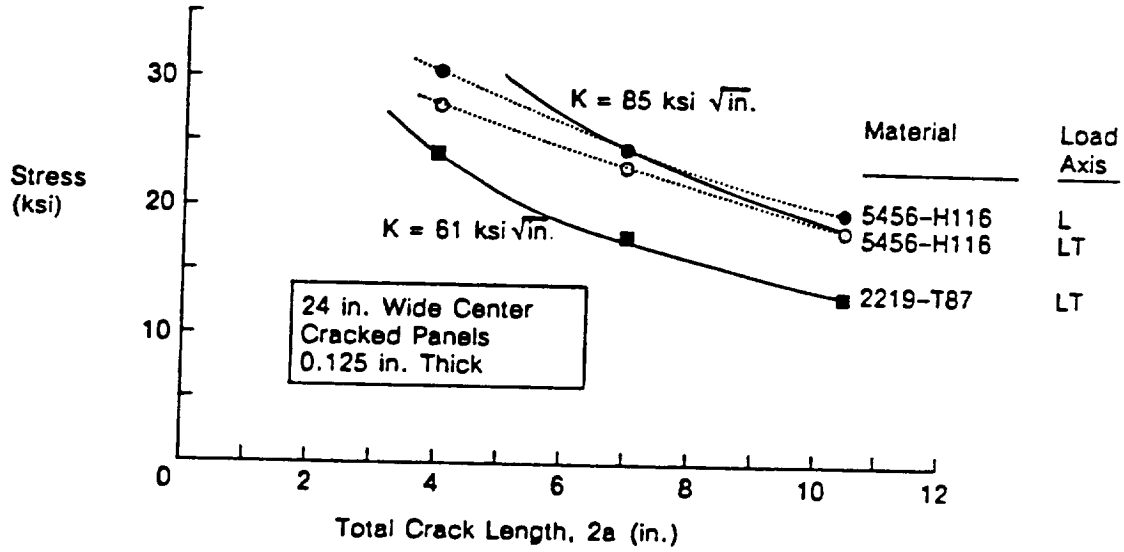

Fig. 7-4. Failure stress versus flaw size in 61 cm wide sheet of 2219 and 5456. [Elfer 88]

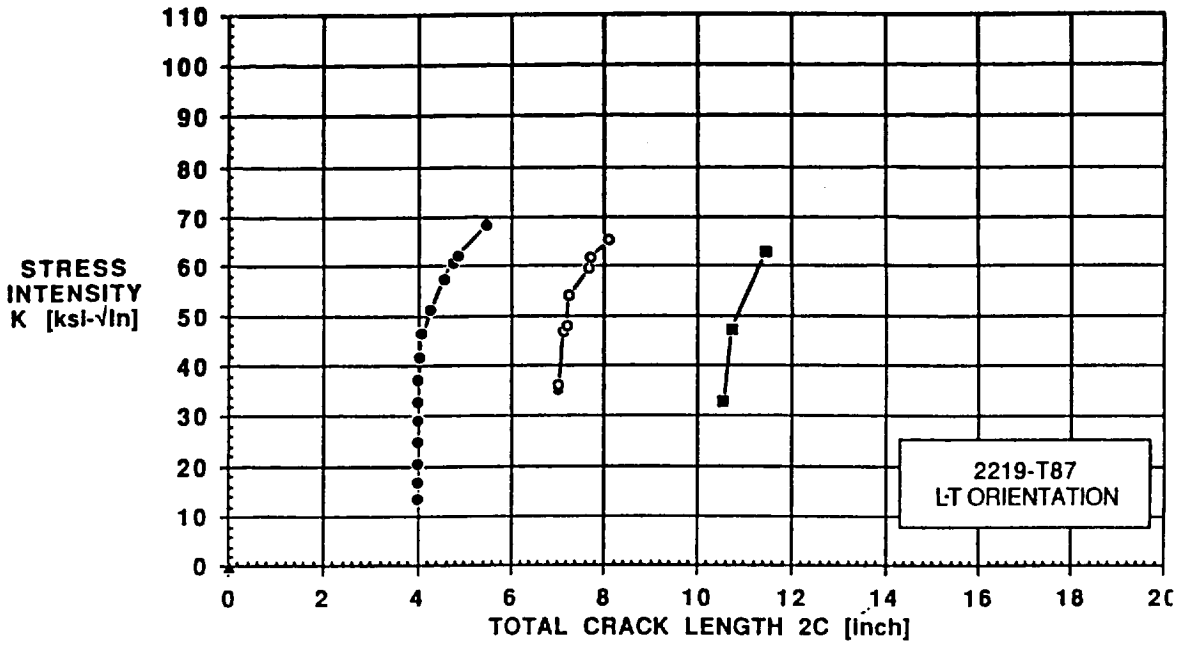

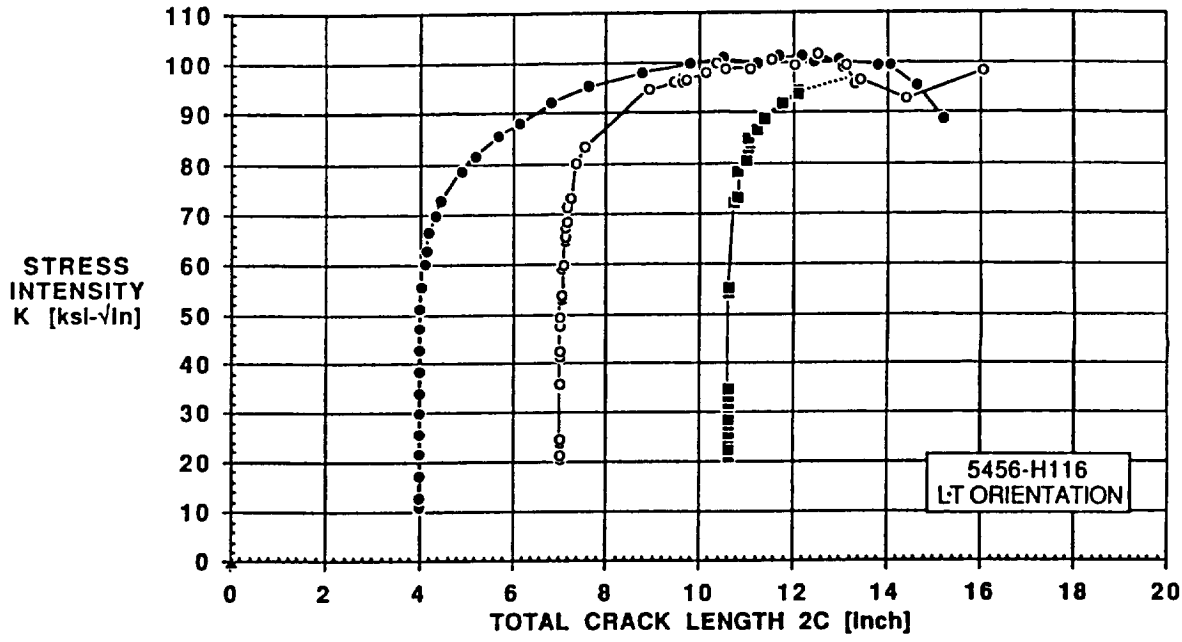

Fig. 7-5. R-curve versus physical flaw size a 61 cm wide sheet of 2219-T87 and 5456-H116. [Elfer 88] A flaw length was not necessarily measured at max stress.

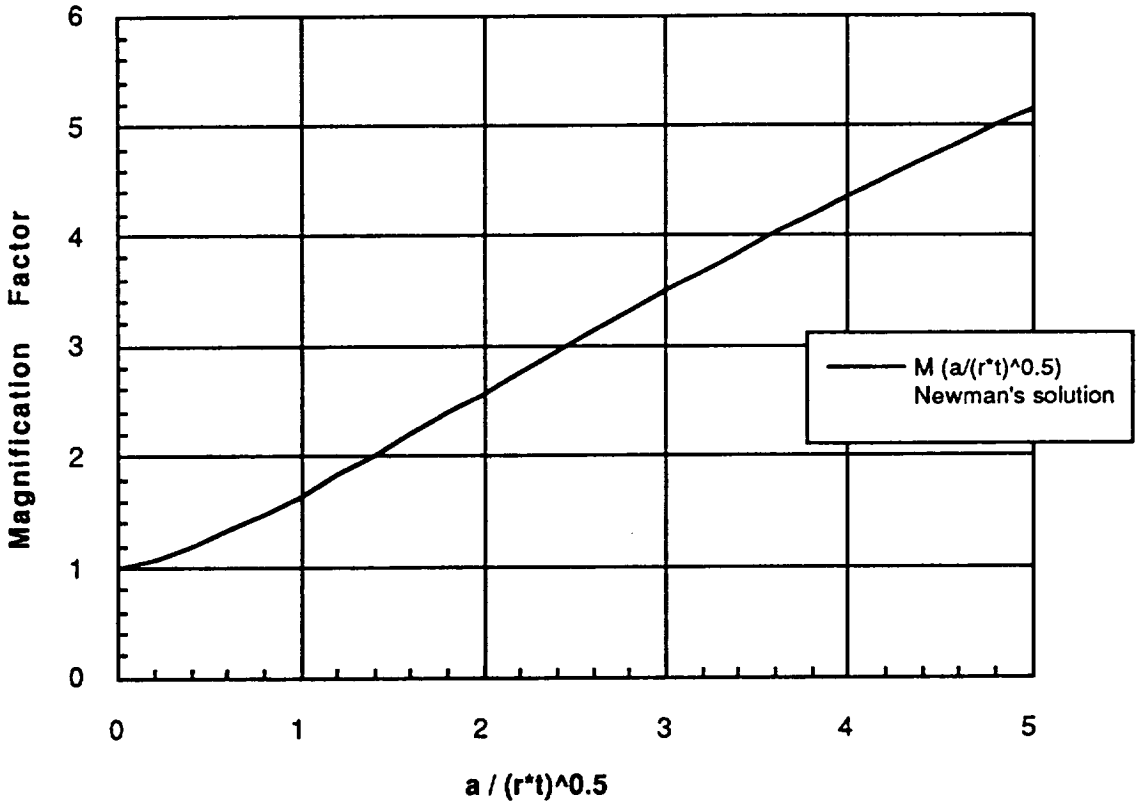

Fig. 7-6 Stress intensity magnification factor for a cylinder relative to a flat plate.

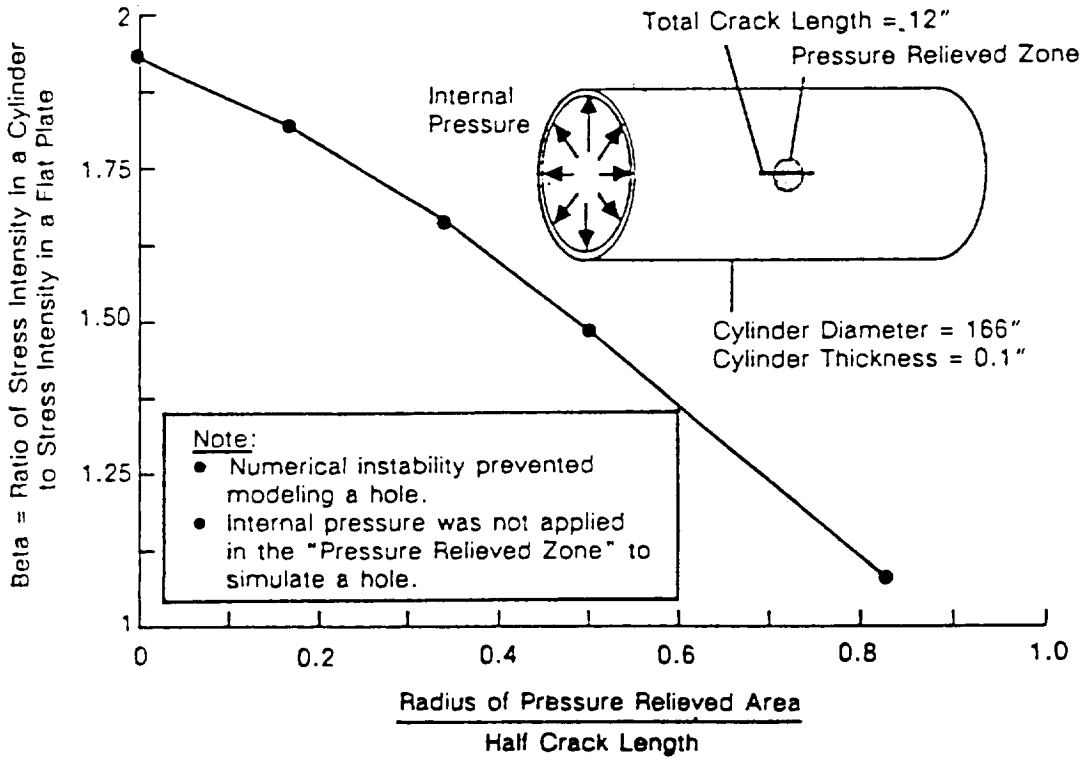

Fig. 7-7 Effect of a Hole (modeled as depressurized zone) on the Stress Intensity in a Cylinder. [Rajendran in Elfer88]

Influence Function

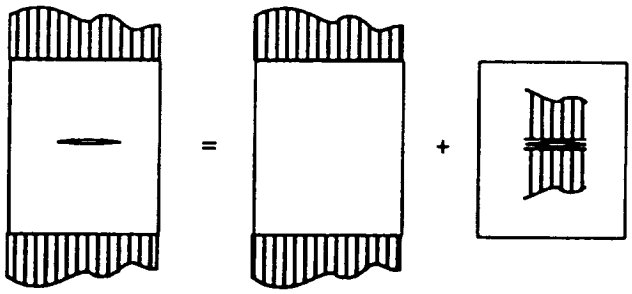

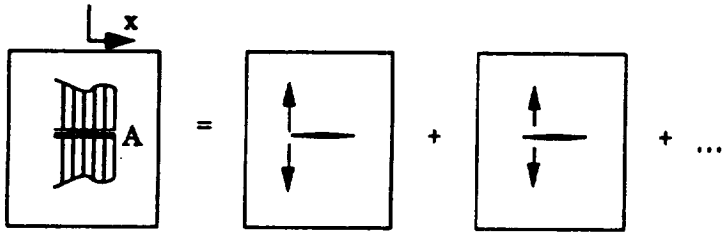

for a flat plate (solved using Green's function):

$$K_{IA} = \frac{P}{\sqrt{\pi a}} \frac{\sqrt{(a+x)}}{\sqrt{(a-x)}}$$

Fig. 7-8 Influence function for a flat plate.

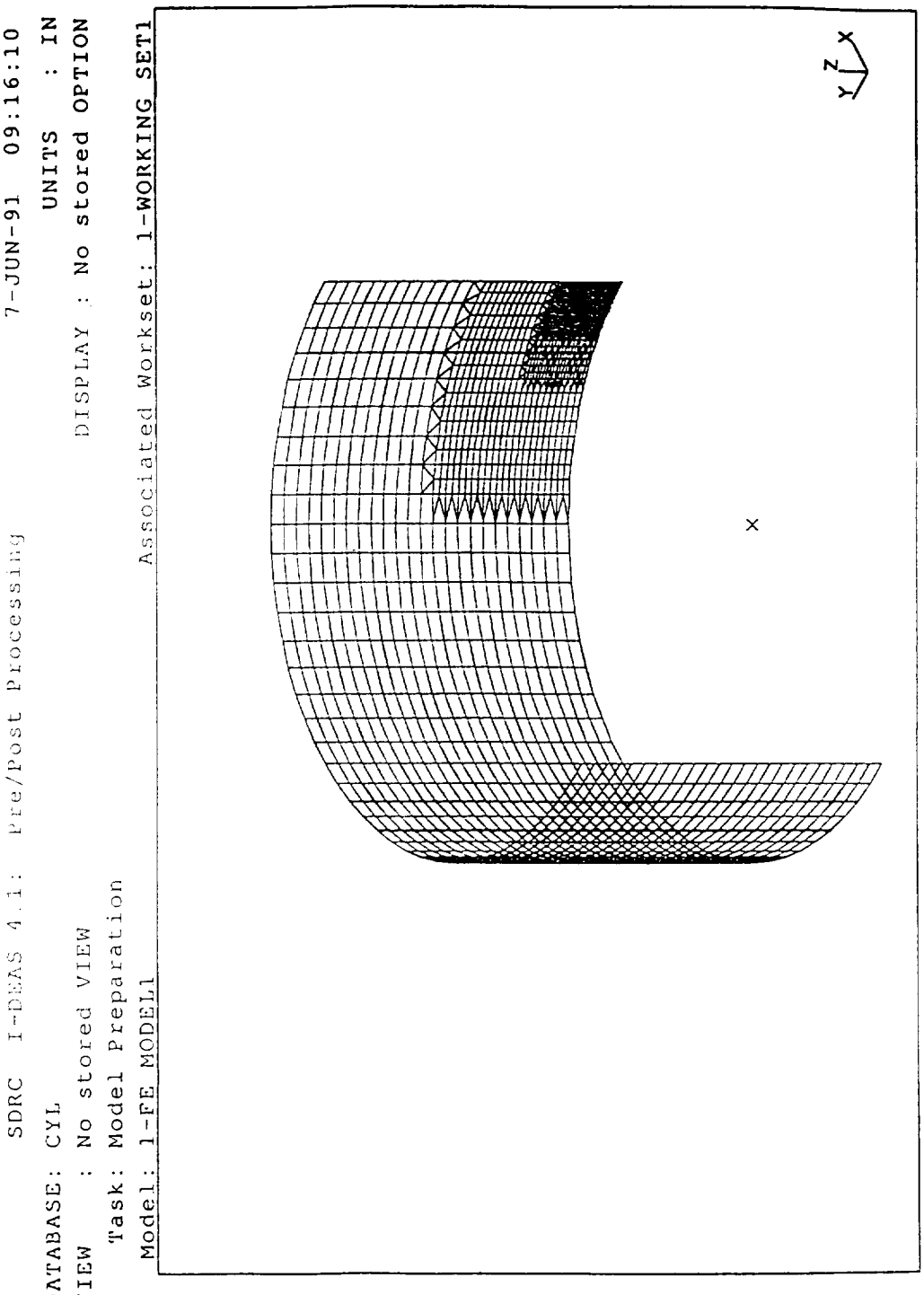

Fig. 7-9 NASTRAN 1/4 cylinder symmetric model.

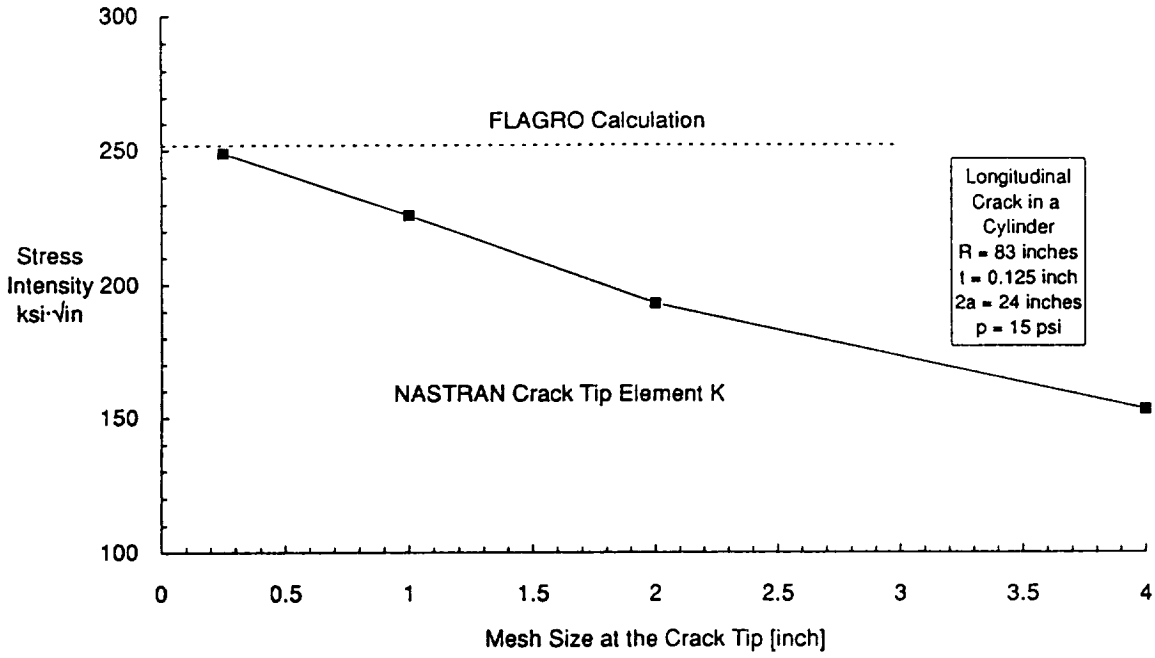

Fig. 7-10 Effect of mesh size on the calculated stress intensity for a cylinder (using NASTRAN crack tip element).

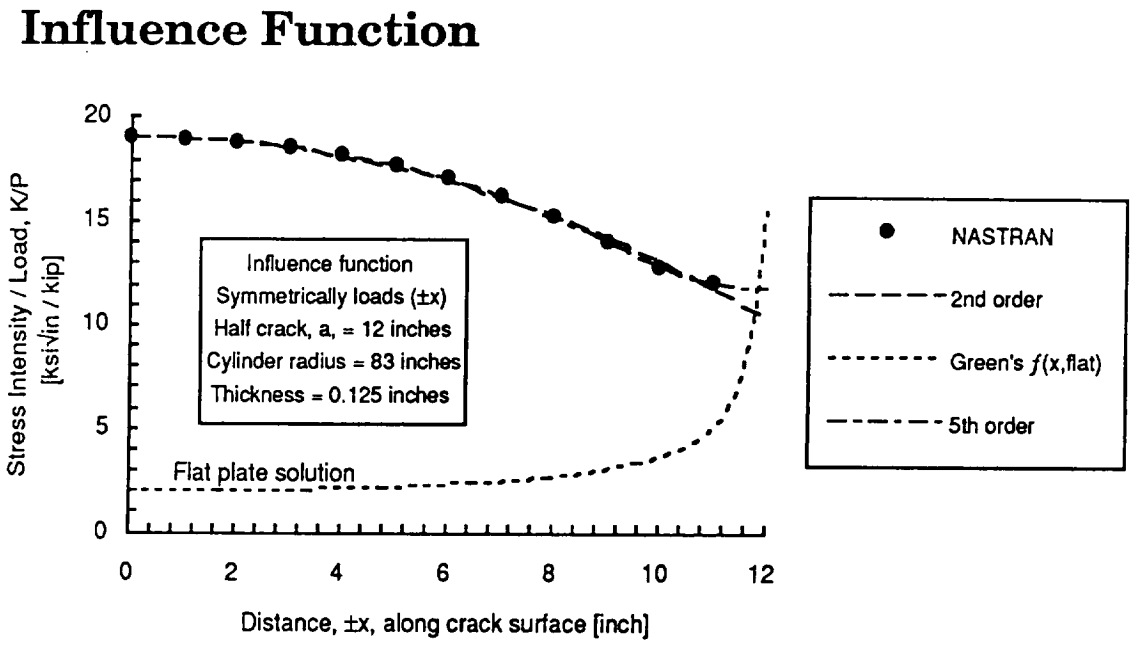

Fig. 7-11 Influence function for a crack in a cylinder.

CONTRACT NAS8-38856

Structural Damage Prediction and Analysis for Hypervelocity Impact

APPENDIX A

EQUATIONS

APPENDIX A - TABLE OF CONTENTS

TABLE OF CONTENTS III

GLOSSARY VI

UNIT CONVERSIONS VII

Probability

Binomial Distribution 1

Penetration - Cratering/Single Wall Penetration

Fish and Summers 2

JSC (Modified Cour-Palais) 3

Penetration - Multisheet Fragment Penetration

Burch 4

Nysmith 6

Penetration - Equations for Specific Shields

Whipple Bumper (Modified Cour-Palais) 7

Nextel/Kevlar Intermediate Shield 9

Multishock Shield (Christiansen) 11

Mesh Double-Bumper (Christiansen) 13

Penetration - Dispersion Angle

Wilkinson 15

Penetration - Momentum Failure

Wilkinson 17

Grove and Rajendran 19

Housen and Schmidt 20

Fracture Mechanics - Longitudinal Through Crack in a Cylinder

Tada solution 22

Folias solution 23

Plastic Zone correction by Hahn et al. to Folias solution 24

Zahoor solution 25

Zahoor limt load solution 26

Newman solution 27

Depressurized Area at Center of Crack

(or Hole at center of crack) - Elfer, Grove and Rajendran 29

Membrane Load - Zahoor solution 31

Wedge loads - Influence function 33

Fracture Mechanics - Through Crack in a Sphere
Tada solution 35
Erdogan and Kibler solution 36
Fracture Mechanics Flat Plate
Radial cracks - Tada solution 37
Wedge loads - Influence function 38
Through cracks from a hole in a plate - Tada 39
Through cracks from a hole in a plate - FLAGRO 40
Fracture mechanics - Influence function
General equation for influence function 41

GLOSSARY

Variable

Subscript

c ---------- Speed of sound [km/s]
d ---------- Diameter [cm]
  frag .....fragment diameter from bumper impact
  p .....projectile diameter (spherical unless noted)
E---------- Young's Modulus [MPa]
G ---------- Shear Modulus [MPa]
h ---------- Spacecraft altitude from earth's surface [km]
H ---------- Energy per unit mass for melt/vaporization []
m---------- Mass [g]
PNCD---------- Probabilty of no Critical Damage
PNP ---------- Probability of no Penetration
POP ---------- Probability of (one or more) Penetrations (1-PNP)
r ---------- Radial distance
S---------- Spacing (front of bumper to rear of rear wall unless noted [cm]
  1,2,...n .....first, second, nth bumper to rear wall spacing. Bumpers counted from the initial projectile impact.
t ---------- Thickness [cm]
  b .....bumper
  rw .....rear wall
t ---------- time [s, or as listed]
v ---------- Velocity [km/s]
  E. .....initial projectile
  frag .....largest fragment from bumper impact
  orb .....orbital velocity of a spacecraft

β ----------Obliquity angle
ε----------Strain
ρ ---------- Density [g/cm^3]
σ ---------- Stress [dynes/cm^2 or MPa]
  sp, ult, y .....spall, ultimate or yield strength
θ---------- Average semivertex cone angle of debris cloud [rad]

Subscripts
  b .....bumper
  frag .....fragment from bumper impact
  p .....projectile
  rw .....rear wall
  t.....target (for a single wall experiment)
  1,2,...n .....first, second, nth bumper to rear wall.

UNIT CONVERSIONS

To Convert from	Multiply by	To Get

Length		
Angstrom	1.0 E+10	meters [m]
centimeters [cm]	0.3937	inches [in]
centimeters [cm]	3.281 E-2	feet [ft]
feet [ft]	1.894 E-4	miles [mi]
feet [ft]	1.645 E-4	nautical miles
feet [ft]	30.48	centimeters [cm]
inches [in]	2.54	centimeters [cm]
kilometers [km]	0.6214	miles [mi]
kilometers [km]	0.5396	nautical miles
meters [m]	1.0 E-10	Angstrom
miles [mi]	0.86842	nautical miles
miles [mi]	1.6093	kilometers [km]
miles [mi]	5,280.	feet [ft]
nautical miles	1.8532	kilometers [km]
nautical miles	6,080.	feet [ft]
nautical miles	1.1515	miles [mi]

Mass		
grain	1.42857 E-4	Pound mass [lbm]
grain	6.47989 E-2	gram (g)
gram (g)	3.52741 E-2	ounce (oz)
gram (g)	2.20462 E-3	Pound mass [lbm]
gram (g)	15.4324	grain
kilogram [kg]	6.85218 E-2	slug
ounce (oz)	28.3494	gram (g)
ounce (oz)	28.3494	gram (g)
Pound mass [lbm]	32.174	slug
Pound mass [lbm]	7,000.	grain
Pound mass [lbm]	453.5924	gram (g)
slug	3.1081 E-2	Pound mass [lbm]
slug	14.5939	kg

Velocity		
cm/s	0.	km/s
ft/s	6.8182 E-1	mi/hr
ft/s	3.048 E-3	km/s
in/s	2.54 E-4	km/s
km/s	1.0 E+5	cm/s
km/s	3,937.	in/s
km/s	328.08	ft/s
km/s	6.2137 E-2	mi/hr
mi/hr	16.0934	km/s
mi/hr	1.4663	ft/s

Density		
gm/cm^3	3.613 E-2	lbm/in^3
lbm/in^3	27.6798	gm/cm^3

To Convert from	Multiply by	To Get

Force		
dyne	1.0 E-5	Newton (N)
kg·m/s^2	1.	Newton (N)
kilogram-force	9.8067	Newton (N)
kip (1000 lbs)	4,448.	Newton (N)
Newton (N)	1.0 E+0	kg·m/s^2
Newton (N)	2.24809 E-1	Pound-force [lbf]
Newton (N)	2.2482 E-4	kip (1000 lbs)
Newton (N)	1.01972 E-1	kilogram-force [kgf]
Newton (N)	100,000.	dyne
Pound-force [lbf] avoirdupois	4.4482	Newton (N)

Areal Density		
gm/cm^2	0.2276	oz/in^2
gm/cm^2	32.7708	oz/ft^2
gm/cm^2	98.3123	oz/yd^2
gm/cm^2	1.422 E-2	lbm/in^2
gm/cm^2	2.0482	lbm/ft^2
gm/cm^2	6.1445	lbm/yd^2
gm/cm^2	10.	kg/m^2
kg/m^2	0.1	gm/cm^2
lbm/ft^2	0.4882	gm/cm^2
lbm/in^2	70.3066	gm/cm^2
lbm/yd^2	0.1627	gm/cm^2
oz/ft^2	0.0305	gm/cm^2
oz/in^2	4.3942	gm/cm^2
oz/yd^2	0.0102	gm/cm^2

Pressure - Stress		
atm (normal 760 Torr)	101,325.	Pascal
atm (technical (1kgf/cm^2))	98,066.5	Pascal
bar	1.000 E+5	Pascal (Pa)
dyne/cm^2	1.000 E-1	Pascal (Pa)
kg-force/cm^2	98,070.	Pascal (Pa)
ksi (1000 psi)	6.895	MPa
MPascal [MPa]	1.450 E-1	ksi
Pascal (Pa)	1.020 E-5	kg-force/cm^2
Pascal (Pa)	9.869 E-6	atm (normal 760 Torr)
Pascal (Pa)	1.020 E-5	atm (technical (1kgf/cm^2))
Pascal (Pa)	1.450 E-4	psi
Pascal (Pa)	1.0 E-5	bar
Pascal (Pa)	10.	dyne/cm^2
lbf/sq inch [psi]	6,895.	Pascal (Pa)

Momentum		
g·km/s	5.59974 E+2	lbm·in/s
lbm·in/s	1.7858 E-3	g·km/s

To Convert from	Multiply by	To Get

Stress Intensity		
ksi√in	1.099	MPa√m
MPa√m	0.9099	ksi√in
MPa√m	31.6228	MPa√mm
MPa√mm	0.0316	MPa√m

Energy		
British Thermal Unit BTU (Int. Table)	1,055.1	Joule
Calorie (Int. Table)	4.1868	Joule
dyne-cm	1.0 E-7	Joule
Electronvolt (eV)	1.6022 E-19	Joule
erg	1.0 E-7	Joule
ft·lbf	1.3558	Joule
Joule	1.	Newton-meter
Joule	1.	Watt-second
Joule	9.4782 E-4	BTU (Int. Table)
Joule	0.7376	ft·lbf
Joule	6.24146 E+18	Electronvolt (eV)
Joule	0.2388	Calorie (Int. Table)
Joule	1.0 E+7	dyne-cm
Joule	1.0 E+7	erg
Joule	0.10197	Kgf-m
Kgf-m	9.8067	Joule
Newton-meter	1.	Joule
Watt-second	1.	Joule

Energy per unit area		
ft·lbf/in^2	0.2102	Joule/cm^2
in·lbf/in^2	1.75127 E-2	Joule/cm^2
in·lbf/in^2	24.9089	Pascal (Pa-cm)
Joule/cm^2	4.7585	ft·lbf/in^2
Joule/cm^2	57.1015	in·lbf/in^2

Power		
BTU/s	107.58	Kgf·m/s
Ft-lbf/s	1.81818 E-3	Horsepower
ft-lbf/s	1.3558	Watt
ft-lbf/s	0.1383	Kgf·m/s
Horsepower	550.	Ft-lbf/s
Joule/s	1.	Watt
Kgf·m/s	9.295 E-3	BTU/s
Kgf·m/s	7.233	ft-lbf/s
Watt	1.0	Joule/s
Watt	0.73756	ft-lbf/s

Probability - Binomial Distribution
Probability of n impacts or penetrations

Reference NASA SP-8042

Relationship $P = (F \cdot A \cdot t)^n \cdot (\exp(- F \cdot A \cdot t))/n!$

where

P = Probability of *n* impacts or penetrations

F = flux [consistent units]

A = area [consistent units]

t = time [consistent units]

and

n = number of impacts or penetrations

Limitations Binomial theory

Comments Flux and area must have similar definitions (e.g. flux and area for randomly tumbling plate vs. for a projected area. The flux and *n* may be determined in terms or impacts, penetrations or other phenomena.

Penetration - Cratering/Single Wall Penetration
Fish and Summers

Reference Frost (NASA SP-8042)

Relationship

$P = K_i\, m_p^{0.352}\, \rho_p^{0.167}\, (V_p \cdot \cos(\beta))^{0.667}$ (CRATERING)

where

P = depth of penetration in cm

K_i = material constant for semi-infinite material
= 0.42 for Al alloys
= 0.25 for 304 and 316 stainless steel

and

$V_p \cdot \cos(\beta)$ = projectile velocity normal to the surface [km/s].

$t = K_i\, m_p^{0.352}\, \rho_p^{0.167}\, (V_p \cdot \cos(\beta))^{0.875}$ (PENETRATION)

where

t = thickness of plate penetrated [cm]

K_i = material constant for penetration (pressure)
= 0.54 for visual penetration in Al alloys
= 0.57 in Al alloys
= 0.32 for 304 and 316 stainless steel
= 0.38 for 17-4 PH annealed CRES

Limitations $\beta < 45°$. Spherical cratering. Other variables unknown. Empirical fit to data.

Comments Tests indicate oblique impacts should use only the normal component of the impact velocity to calculate energy and crater volume. As the obliquity angle became large, greater than 45°, the crater becomes elongated, and at greater than 65° from the normal, the projectile primarily ricochets from the surface.

Hayashida and Robinson found that this equation and the JSC Cour-Palais equations gave adequate predictions of independent aluminum impact test data. Fish-Summers was the most conservative.

Penetration - Cratering/Single Wall Penetration
JSC (Modified Cour-Palais)

Reference Christiansen 1981

Relationship

$$p = 5.24\, d_p^{19/18} \cdot BH^{-.25} \cdot \left(\frac{\rho p}{\rho t}\right)^{0.5} \left(\frac{V_p \cdot \cos(\beta)}{C}\right)^{0.667}$$

where

p = depth of penetration [cm]

C = speed of sound in target [km/s]

$= \sqrt{E_t/\rho t}$

BH = Brinell Hardness for target.

$V_p \cdot \cos(\beta)$ = projectile velocity normal to the surface [km/s]

$t_{pen} = 1.8 \cdot p$ (PENETRATION)

$t_{spall} = 2.2 \cdot p$ (SPALL)

where

t = thickness of plate penetrated or spalled [cm]

Limitations $\beta < 45°$. Spherical cratering. Other variables unknown. Empirical fit to data.

Comments Tests indicate oblique impacts should use only the normal component of the impact velocity to calculate energy and crater volume. As the obliquity angle became large, greater than 45°, the crater becomes elongated, and at greater than 65° from the normal, the projectile primarily ricochets from the surface.

Hayashida and Robinson found that this equation and the Fish-Summers equations gave adequate predictions of independent aluminum impact test data. Fish-Summers was the most conservative.

Penetration - Multisheet Fragment Penetration

Penetration and Dispersion Angle - Burch

Reference Burch[67]

Relationship N_0 = Number of sheets penetrated following the first sheet.

$$= \left(\frac{V}{C}\right)^{-4/3} \cdot \left(\frac{t_2}{D}\right)^{-7/12} \cdot \left(\frac{S_1}{D}\right)^{-5/12} f\left(\frac{t_1}{D}\right)$$

where

$$f\left(\frac{t_1}{D}\right) = 2.42 \cdot \left(\frac{t_1}{D}\right)^{-1/3} + 4.26 \cdot \left(\frac{t_1}{D}\right)^{+1/3} - 4.18$$

C = speed of sound in first sheet (16,650 f/s in aluminum)

S1 is the distance between the first and second sheets. Subsequent sheets are the same thickness as the second sheet. To equate the number of sheets of thickness "b" to sheets of thickness "a" use the following formula.

$$n_b \cdot (t_b)^{7/12} = n_a \cdot (t_a)^{7/12}$$

For oblique impacts the number of sheets after the first sheet, N_f, penetrated along the flight path was:

$$N_f = N_0 + 0.63 \cdot f(\beta, t_1/D) \cdot \left(\frac{V}{C}\right)^{-4/3} \cdot \left(\frac{t_2}{D}\right)^{-7/12} \cdot \left(\frac{S_1}{D}\right)^{-5/12}$$

where

$$f(\beta, t_1/D) = \{0.5 - 1.87 \cdot \left(\frac{t_1}{D}\right)\} + \{5 \cdot \left(\frac{t_1}{D}\right) - 1.6\} \cdot \chi + \{1.7 - 12 \cdot \left(\frac{t_1}{D}\right)\} \cdot \chi$$

$$\text{for } \left(\frac{t_1}{D}\right) \leq 0.32;$$

$$= -(0.6 + 0.8 \cdot \chi^{-3}) \quad \text{for } \left(\frac{t_1}{D}\right) = 0.64$$

$$\chi = (\tan\beta - 0.5)$$

For oblique impacts the number of sheets after the first sheet, N_n, penetrated normal to the bumper was:

$$N_n = [0.32 \cdot \left(\frac{t_1}{D}\right)^{5/6} + 0.48 \cdot \left(\frac{t_1}{D}\right)^{1/3} \cdot \sin^3(\beta)] \cdot \left(\frac{V}{C}\right)^{-4/3} \cdot \left(\frac{D}{t_2}\right)$$

The major damage diameter, D_{90}, for aluminum on aluminum impacts was expressed as:

$$\left(\frac{D_{90}}{D}\right) = \left(\frac{t_1}{D \cdot \cos(\beta)}\right)^{1/4} \cdot \left(\frac{S_l}{D \cdot \cos(\beta)}\right)^{1/2} \cdot \lambda$$

where

$$\lambda = 5.55 \cdot V \cdot \cos(\beta)/C - 2.52 \qquad \text{for } 0.6 \le V \cdot \cos(\beta)/C \le 1.05$$

$$= 1.56 \cdot V \cdot \cos(\beta)/C + 1.66 \qquad \text{for } 1.05 \le V \cdot \cos(\beta)/C$$

and this was independent of second sheet material.

The equation for major spray diameter was

$$\left(\frac{D_{MS}}{D}\right) = \left(\frac{t_1}{D \cdot \cos(\beta)}\right)^{1/4} \cdot \left(\frac{S_l}{D \cdot \cos(\beta)}\right)^{1/2} \cdot \lambda_{MS}$$

where

$$\lambda_{MS} = 3.12 \cdot V/C + 3.32 \qquad \text{for } 0.6 \le V \cdot \cos(\beta)/C \le 1.05$$

Limitations

The models were appropriate between 0.6 and 1.3 times the speed of sound.

Penetration - Whipple Bumper
Nysmith

Reference Nysmith[69]

Relationship The Ballistic Limit Velocity (km/s) is given by

$$V = 2.88 \cdot 10^{-3} \cdot \left(\frac{t_b}{d}\right)^{1.9} \cdot \left(\frac{t_{rw}}{d}\right)^{3.6} \cdot \left(\frac{S}{d}\right)^{5}$$

and also

$$V = 7.8 \cdot 10^{-5} \cdot \left(\frac{t_b + t_{rw}}{d}\right)^{5.5} \cdot \left(\frac{S}{d}\right)^{5}$$

(All terms are defined in the glossary.)

Limitations Developed by pyrex-glass spheres (2.23 g/cm^3) to simulate meteoroids. Tests up to 8.8 km/s. Targets were

$0.81 \text{ mm} \le t_b \le 1.24 \text{ mm}$

$1.63 \text{ mm} \le t_{rw} \le 3.18 \text{ mm}$

$17.5 \text{ mm} \le S \le 42.9 \text{ mm}$

Comments By combining the two equations Nysmith found the optimum ratio of bumper to rear wall thickness was 0.35.

Penetration - Whipple Bumper
Modified Cour-Palais Equations

Reference Christiansen [93]

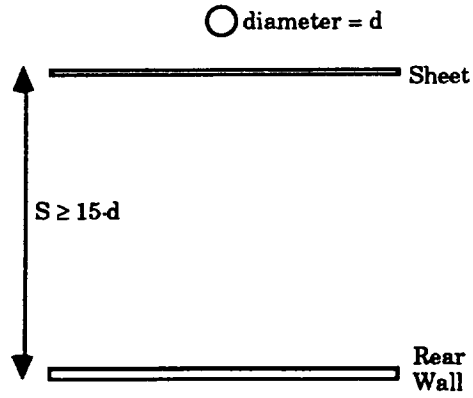

Relationship The critical diameter, d_p, to penetrate a given shield is

$$d_p = 3.918\, t_{rw}^{2/3}\cdot\rho_b^{-1/9}\cdot\rho_p^{-1/3}\cdot(V_p\cdot\cos(\beta))^{-2/3}\cdot S^{1/3}\cdot(\sigma_y/70)^{1/3}$$

for $V_n > 7$ km/s

$$= \left(\frac{t_{rw}\cdot\sqrt{\sigma_y/40}+t_b}{1.248\cdot\rho_p^{0.5}\cos(\beta)}\right)^{\frac{18}{19}}\cdot(1.75-V_n/4) +$$

$$(1.071\cdot t_{rw}^{2/3}\cdot\rho_b^{-1/9}\cdot\rho_p^{-1/3}\cdot S^{1/3}\cdot(\sigma_y/70)^{1/3})\cdot(V_n-3)/4$$

for 3 km/s $< V_n <$ 7 km/s

$$= \left(\frac{t_{rw}\cdot\sqrt{\sigma_y/40}+t_b}{0.6\cdot\rho_p^{0.5}\cdot V_n^{2/3}\cdot\cos^{5/3}(\beta)}\right)^{\frac{18}{19}} \quad \text{for } V_n < 3 \text{ km/s}$$

Above 65° obliquity the critical diameter is set to the 65° critical diameter.

$V_n = V_p\cdot\cos(\beta)$

= projectile velocity normal to the surface [km/s]

S = Total spacing [cm]

and

σ_y = rear wall yield strength (NB: standard units) [ksi]

The minimum design requirements for the above equations to be applicable are

$$t_b = c_b \cdot m_p/\rho_b = c_b \cdot d_p \cdot \rho_p/\rho_b$$

where

$$c_b = 0.25 \quad \text{when } S/d < 30$$
$$= 0.20 \quad \text{when } S/d \geq 30$$

$$t_w = c_w \cdot d^{0.5} \cdot (\rho_p \cdot \rho_b)^{1/6} \cdot M^{1/3} \cdot V_n/S^{0.5} \cdot (70/\sigma_y)^{0.5}$$

where

$$c_w = 0.16 \text{ cm}^2 \cdot \text{sec}/\text{g}^{2/3} \cdot \text{km}$$

Limitations $S/d_p > 15$; above provisions on minimum bumper thickness.

Comments The equation assumes constant initial projectile energy to penetrate. The low velocity equations provide a very compact alternate to the BUMPERII equations developed from the THOR equations. The 3 to 7 km/s regime is an interpolation between the low velocity equation and Christiansen's high velocity equation.

Penetration - Nextel/Kevlar Intermediate Shield Enhanced Shield Equations

Reference Christiansen et al [92b]

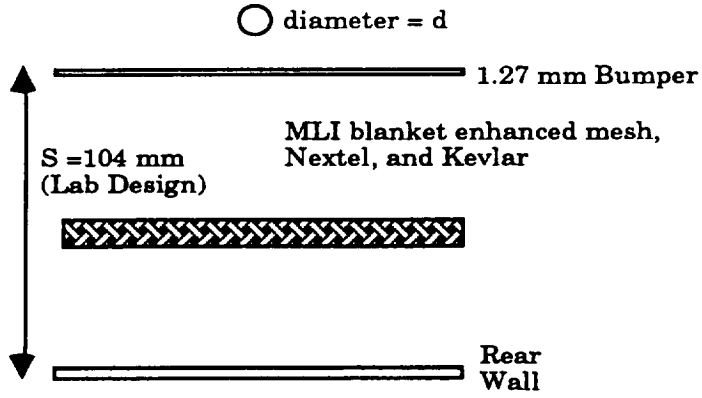

Relationship The critical diameter, d_p, to penetrate a given shield is

$$d_p = 0.62\,(t_{rw}\cdot\rho_{rw})^{1/3}\cdot\rho_p^{-1/3}\cdot V_p^{-1/3}\cdot\cos^{-1/2}(\beta)\cdot S^{2/3}\cdot(\sigma_y/40)^{1/6}$$

for $V\cdot\cos^{1/3}(\beta) > 6.5$ km/s

$$= 1.031\cdot\rho_p^{-1/2}\cdot[t_{rw}\cdot(\sigma_y/40)^{1/2}+0.37\cdot m_b]\cdot\cos^{-4/3}(\beta)$$
$$\cdot\{[6.5\cdot\cos^{-1/3}(\beta)-V]/[6.5\cdot\cos^{-1/3}(\beta)-2.7\cdot\cos^{-1/2}(\beta)]\}$$
$$+ 0.332\cdot(t_{rw}\cdot\rho_{rw})^{1/3}\cdot\rho_p^{-1/3}\cdot\cos^{-7/18}(\beta)\cdot S^{2/3}\cdot(\sigma_y/40)^{1/6}$$
$$\cdot\{[V-2.7\cdot\cos^{-1/2}(\beta)]/[6.5\cdot\cos^{-1/3}(\beta)--2.7\cdot\cos^{-1/2}(\beta)]\}$$

for $2.7/\cos^{1/2}(\beta)$ km/s $< V < 6.5/\cos^{1/3}(\beta)$ km/s

$$= 2\left(\frac{t_{rw}\cdot\sqrt{\sigma_y/40}+0.37\cdot m_b}{\rho_p^{0.5}\cdot V_n^{2/3}\cdot\cos^{5/3}(\beta)}\right)$$

for $V\cdot\cos^{1/2}(\beta) \le 2.7$ km/s

$V = V_p$

= projectile velocity normal to the surface [km/s]

m_b = Areal density of all bumpers and intermediate shields [g/cm^2]

and

σ_y = rear wall yield strength (NB: standard units) [ksi]

The design is shown in the sketch.

Limitations

For 1.3 mm bumper and intermediate shield of MLI plus $0.03 g/cm^2$ mesh; $0.3 g/cm^2$ Nextel and $0.136 g/cm^2$ Kevlar. Blanket midway between bumper and rear wall.

Comments

High velocity curve is constant momentum extrapolation. This is different that Wilkinson, which assumes that there is an enhanced dispersion angle for smaller projectiles at higher velocities.

Penetration - Multishock

Modified Cour-Palais Multi-Shock

Reference Christiansen 1992

Relationship The critical diameter, d_p, to penetrate a given shield is

$$d_p = 0.354\, t_{rw}^{1/3} \cdot \rho_{rw}^{1/3} \cdot \rho_p^{-1/3} \cdot (V_p \cdot \cos(\beta))^{-1/3} \cdot S^{2/3} \cdot (40/\sigma_y/40)^{1/6}$$

for $V_n > 6$ km/s

$$= \left(\frac{t_{rw} \cdot \sqrt{\sigma_y/40} + 0.37 \cdot m_b}{0.624 \cdot \rho_p^{0.5} \cos(\beta)} \right)^{\frac{18}{19}} \cdot (2 - V_n/3) +$$

$$(0.1948 \cdot t_{rw}^{1/3} \cdot \rho_{rw}^{1/3} \cdot \rho_p^{-1/3} \cdot S^{2/3} \cdot (\sigma_y/40)^{1/6}) \cdot (V_n/3 - 1)$$

for 3 km/s $< V_n <$ 6 km/s

$$= \left(\frac{t_{rw} \cdot \sqrt{\sigma_y/40} + 0.37 \cdot m_b}{0.3 \cdot \rho_p^{0.5} \cdot V_n^{2/3} \cdot \cos(\beta)} \right)^{\frac{18}{19}} \quad \text{for } V_n < 3 \text{ km/s}$$

The design is defined by:

$$m_b = 0.19\, m_p = 0.19 \cdot d_p \cdot \rho_p$$

$$m_{rw} = 43.1 \cdot M_p \cdot V_n / S^2 \cdot \sqrt{40/\sigma_y}$$

where

m_b = required total areal density of four bumper layers of alumina-boro-silica ceramic cloth (Nextel by 3M) [g/cm^2]

m_p = areal density projectile [g/cm^2]

m_{rw} = required areal density aluminum rear wall [g/cm^2]

M_p = projectile mass [g]

$V_n = V_p \cdot \cos(\beta)$

= projectile velocity normal to the surface [km/s]

S = Total spacing with each layer located successively at one quarter of the total spacing [cm]

and

σ_y = rear wall yield strength (NB: standard units) [ksi]

Limitations $S/d_p > 15$; with the stated provisions on minimum bumper thickness.

Comments Tested with aluminum projectiles to 0.32 cm. Primary weight savings is in rear wall required to stop a given threat particle. The required bumper thickness is not reflected in the rear wall equations. The rear wall equation accounts for strength but not for ductility, which may be more important.

Penetration - Mesh Double-Bumper
Christiansen Equations

Reference Christiansen 1992

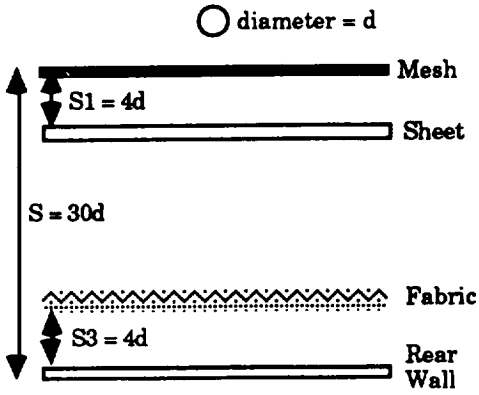

Relationship The critical diameter, d_p, to penetrate a given shield is

$$d_p = 0.38\, t_{rw}^{1/3} \cdot \rho_{rw}^{1/3} \cdot \rho_p^{-1/3} \cdot (V_p \cdot \cos(\beta))^{-1/3} \cdot S^{2/3} \cdot (\sigma_y/40)^{1/6}$$

for $V_n > 6$ km/s

$$= \left(\frac{t_{rw} \cdot \sqrt{\sigma_y/40} + 0.37 \cdot m_{b+I}}{0.83 \cdot \rho_p^{0.5} \cos(\beta)} \right)^{\frac{18}{19}} \cdot (2 - V_n/3) +$$

$$(0.209 \cdot t_{rw}^{1/3} \cdot \rho_{rw}^{1/3} \cdot \rho_p^{-1/3} \cdot S^{2/3} \cdot (\sigma_y/40)^{1/6}) \cdot (V_n/3 - 1)$$

for 3 km/s $< V_n <$ 6 km/s

$$= \left(\frac{t_{rw} \cdot \sqrt{\sigma_y/40} + 0.37 \cdot m_b}{0.4 \cdot \rho_p^{0.5} \cdot V_n^{2/3} \cdot \cos(\beta)} \right)^{\frac{18}{19}} \quad \text{for } V_n < 3 \text{ km/s}$$

Optimum design parameters:

$m_1 = c_1 \cdot d_p \cdot \rho_p$ (where $0.035 < c_1 < 0.057$)

= required total areal density of fine aluminum mesh first part of bumper [g/cm^2]

$m_2 = 0.93 \cdot d_p \cdot \rho_p$

= required total areal density of aluminum plate second part of bumper at spacing $S_1 = 4 \cdot d_p$ from first bumper [g/cm^2]

$m_3 = c_3 \cdot d_p \cdot \rho_p$

= required total areal density of intermediate catcher cloth (Nextel, Spectra or Kevlar) at spacing $S_3 = 4 \cdot d_p$ in front of rear wall [g/cm^2]

c_3 = 0.095 for Nextel

c_3 = 0.064 for Kevlar or Spectra

$$m_{rw} = 34.8 \cdot M_p \cdot V_n / S^2 \cdot \sqrt{40/\sigma_y}$$

where

m_{rw} = required areal density aluminum rear wall [g/cm^2]

m_{b+I} = total areal density of mesh, sheet and fabric [g/cm^2]

M_p = projectile mass [g]

$V_n = V_p \cdot \cos(\beta)$

= projectile velocity normal to the surface [km/s]

$S = 30 \cdot d_p$

= Optimum total spacing [cm]

and

σ_y = rear wall yield strength (NB: standard units) [ksi]

Limitations $S/d_p > 15$; the stated provisions on minimum bumper thickness

Comments Tested with aluminum projectiles to 0.32 cm. Primary weight savings is in rear wall required to stop a given threat particle. The rear wall equation accounts for strength but not for ductility, which may be more important.

Penetration - Dispersion Angle

Dispersion Angle - Wilkinson

Reference Wilkinson

Relationship θ = Average cone angle of debris cloud
(Note: "Average" is defined below with a limiting condition and modifications defined in the comments.)

$$\theta = \arctan\left(0.6 \cdot \frac{\rho_b \cdot t_b}{\rho_p \cdot d_p}\right) \quad \text{for} \quad \left(\frac{\rho_b \cdot t_b}{\rho_p \cdot d_p}\right) < 1$$

$$\theta = \arctan(0.6) = .54 \text{ rad} = 31° \quad \text{for} \quad \left(\frac{\rho_b \cdot t_b}{\rho_p \cdot d_p}\right) \geq 1$$

where

ρ_b, t_b, ρ_p, and d_p are the density and thickness of the bumper and projectile respectively.

$$\tan\theta = \frac{1}{S} \cdot \frac{\int_0^\infty r^2 \cdot D(r)dr}{\int_0^\infty r \cdot D(r)dr}$$

where

$D(r)$ = the momentum intensity distribution

and

S = Spacing of bumper to location of $D(r)$.

The standard deviation of the momentum intensity distribution is given as:

$\Delta = (2/\pi)^{1/2} \cdot S \cdot \tan(\theta)$

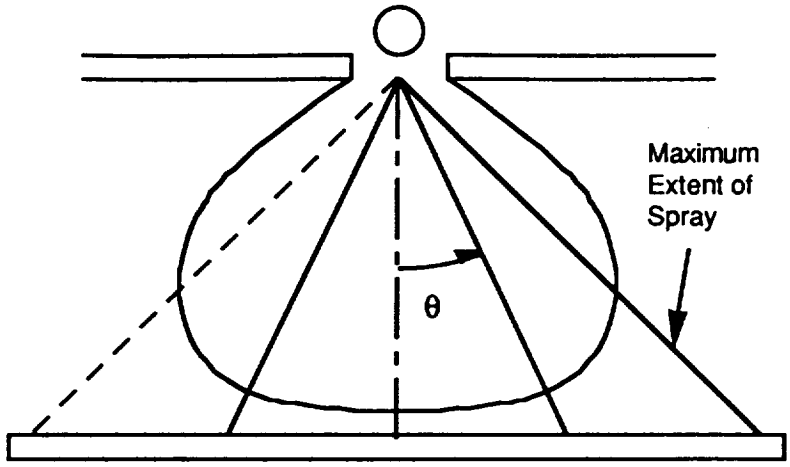

Limitations

Based on hydrocode calculations in vaporization regime, as well as cadmium-on-cadmium tests at 6 to 7 km/s.

Comments

Wilkinson's equation is based on vaporization, which is not appropriate to all space debris impacts. Average cone angle contains most of the mass but not all. If the momentum distribution is a step function, 1 inside r_0 and 0 outside of r_0, then $\tan\theta = 2/3 \cdot (r_0 / S)$.

Elfer used 0.475 instead of 0.6 in the equation to correlate momentum failures at 6 to 7 km/s with aluminum projectiles on aluminum bumpers with Kevlar intermediate shields. This modification is probably appropriate up to 12 to 14 km/s when more aluminum-on-aluminum impacts will transition from predominantly liquid to vapor, thus increasing the dispertion angle to the original Wilkinson equation.

Penetration Mechanics - Momentum Failure
Wilkinson Equation with Modifications

Reference Wilkinson, modifications by Elfer [77] and Bjorkman [91]

Relationship For penetration to occur:

$$m_p V = 1.44 \cdot c_2 (\xi/c_2)_a \cdot m_2 \cdot S^2 \quad \text{for} \quad \left(\frac{\rho_b \cdot t_b}{\rho_p \cdot d_p}\right) \geq 1$$

or

$$m_p V \rho_p d_p = 1.44 \cdot c_2 \left(\frac{\xi}{c_2}\right)_a \cdot m_2 \cdot S^2 \cdot m_1 \quad \text{for} \quad \left(\frac{\rho_b \cdot t_b}{\rho_p \cdot d_p}\right) \geq 1$$

where

c_2 = speed of sound in the rear wall

$m_2 = \rho_{rw} \cdot t_{rw}$

$m_1 = \rho_b \cdot t_b$

and

$\left(\frac{\xi}{c_2}\right)_a$ = $f(\varepsilon_{max}, E/\sigma_y)$ given in the figure:

Limitations Assumes Wilkinson dispersion angle. Assumes rear wall loading can be modeled as a Gausian momentum intensity distribution. Assumes $\Delta/t_{rw} > 20$, and that the strain to failure is independent of Δ/t_{rw}, where Δ is the standard deviation of the momentum intensity distribution given previously.

Comments Wilkinson assumed vaporization, and did not include loading rate effects in the rear wall, such as spall.

Elfer [88] and Bjorkman [91] suggested revising the critical projectile diameter to 80 percent of the original Wilkinson equation prediction, consistent with the observed critical diameters using intermediate shields. Elfer suggested this was due to a lower dispersion angle, caused by melting rather than vaporization of the projectile. Schmidt's cadmium-on-cadmium tests [94] did not show a change in the shape of the cloud with the transition from melting to vaporization, although there may be a different mass distribution within the cloud to account for the dramatic increase in penetration resistance. Bjorkman suggested the modification based on elastic

rebound. 100% rebound was not observed with intermediate shields or with Schmidt's tests which had vaporization.

For 2219-T87 using the normal strain rate room temperature typical yield strength, E/σ_y = (72.4GPa/395MPa) = 184. The typical strain to failure is only 10 percent. This gives $(\xi/c_2)_a$ approximately 0.8 km/s. A uniaxial flow stress of 485 MPa and 30% strain to failure were measured at UDRI using a tensile Hopkinson bar at a strain rate of 10^3 [Rajendran]. Using this flow stress E/σ_y = 149, and a using a strain to failure of 25% percent, gives $(\xi/c_2)_a$ closer to the value of 0.27 km/s used by BUMPER and BUMPERII. Under biaxial load conditions, the effective flow stress will increase further, but the strain to failure will decrease.

It can be seen that a 10% improvement in the strain to failure should give a 25% improvement in the momentum that can be absorbed. However, for a 20% improvement in strength momentum absorption capability will increase by only about 10%. This is qualitatively consistent with the improvement seen in using 5456-H116 compared to 2219-T87 [Elfer]. When tested by UDRI at a high strain rate, 5456 showed similar strength to the 2219-T87 results mentioned in the preceding paragraph.

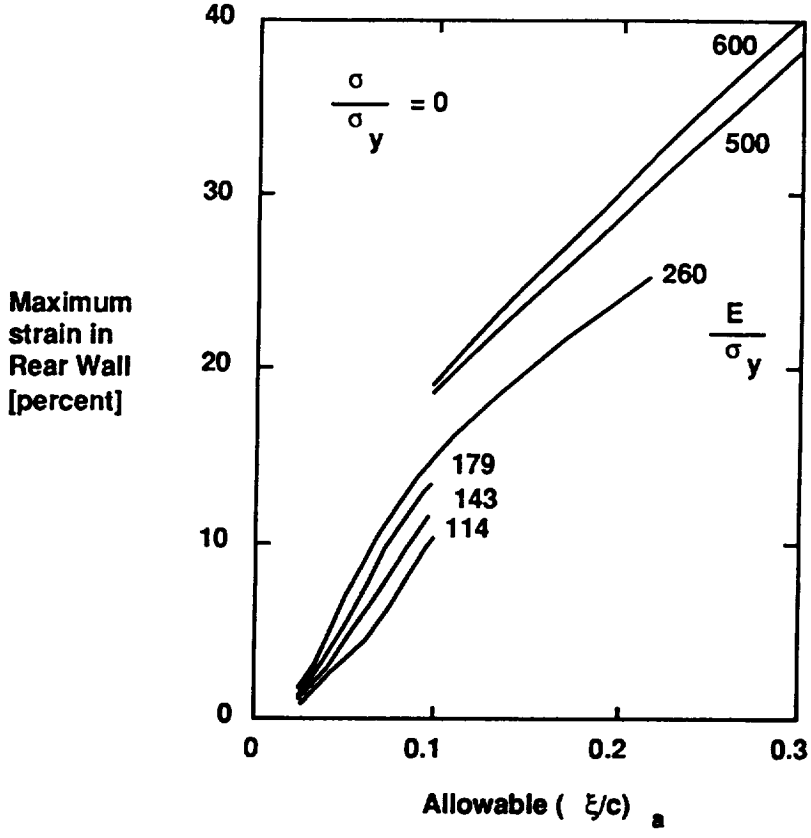

Figure - Wilkinson failure criteria, $(\xi/c_2)_a$, in km/s.

Penetration Mechanics - Momentum Failure
Grove and Rajendran

Reference

Grove [Appendix D]

Relationship

For penetration to occur:

$$\gamma \geq -7.71338 \cdot 10^{-3} + 2.64191 \cdot 10^{-2} \cdot \varepsilon + 3.61467 \cdot 10^{-3} \cdot \varepsilon^2 - 1.24587 \cdot 10^{-4} \cdot \varepsilon^3 + 1.74572 \cdot 10^{-6} \cdot \varepsilon^4$$

where

ε = effective rear wall strain at failure in percent

γ = dimensionless parameter

$= \xi^2 \cdot \rho_{rw} \cdot e^{(t_{rw}/\Delta)} / \sigma_y$

$\xi = m_p \cdot V / \{4 \cdot \rho_{rw} \cdot t_{rw} \cdot S^2 \cdot \tan^2(\theta)\}$ (as in Wilkinson)

$\Delta = \sqrt{2/\pi} \cdot S \cdot \tan(\theta)$ (as in Wilkinson)

and

θ = Wilkinson dispersion angle (although Wilkinson constant of 0.6 may be adjusted as necessary.)

Alternative formula for ε as a function of γ.

$$\varepsilon = 1.01152 + 18.295 \cdot \gamma - 2.35542 \cdot \gamma^2 + 0.113756 \cdot \gamma^3$$

Limitations

Assumes rear wall loading can be modeled as a Gausian momentum intensity distribution. Assumes Wilkinson dispersion angle or a modification.

Comments

Curve fit to maximum strain as a function of the dimensionless parameter, γ. To use as a ballistic limit equation solve for the mass of the projectile as a function of the other variables. For 2219-T87 aluminum, a critical strain of 0.2 (20%) was found to be appropriate from Hopkinson bar tensile tests.

Penetration Mechanics - Momentum Failure
Housen and Schmidt

Reference

Housen and Schmidt [95]

Relationship

For penetration to occur (aluminum-on-aluminum):

$$\frac{d}{t_b} \geq A + B\cdot\exp[-0.17(V\cdot\cos\beta - 7.5)^2] + C\cdot\exp[0.3\cdot V\cdot\cos\beta]$$

where

$$A(\pi_1) = \begin{cases} 0.87\cdot\pi_1^{0.157} & \pi_1 \leq 1.6\cdot10^4 \\ 0.218\cdot\pi_1^{0.3} & \pi_1 > 1.6\cdot10^4 \end{cases}$$

$$B(\pi_1) = \begin{cases} 0.003\cdot\pi_1^{0.624} & \pi_1 \leq 7000 \\ 0.75 & \pi_1 > 7000 \end{cases}$$

$$C(\pi_1) = \begin{cases} 0.001 & \pi_1 \leq 2000 \\ 2.17\cdot10^{-7}\cdot\pi_1^{1.11} & 7000 \leq \pi_1 \leq 1.6\cdot10^4 \\ 3.8\cdot10^{-3}\cdot\pi_1^{0.1} & \pi_1 > 1.6\cdot10^4 \end{cases}$$

and

$$\pi_1 = t_{rw}\cdot S^2/t_b$$

Limitations

$7 \text{ km/s} < V < 18\text{km/s}$ and $500 < \pi_1 < 10^5$

Comments

Empirical fit to cadmium-on-cadmium tests using a 3.1 velocity scaling factor. The diameter to penetrate increases between approximately 12 and 18 km/s. This is due to the transition from liquid to vapor in the debris cloud, and is comparable to a shift between modified Wilkinson and normal Wilkinson. Note that while the simulation has the correct debris cloud shape and momentum, the rate of momentum transfer to the rear wall is also 3.1 times slower than for an aluminum-on-aluminum impact. This effectively distributes the momentum over a larger area using Cd-on-Cd instead of Al-on-Al. This could overestimate the diameter to penetrate.

(Continued next page)

For penetrations below 3 km/s, Housen and Schmidt recommend Christiansen's Whipple shield equation and then they give a linear interpolation between this 3 and 7 km/s using a similar procedure as Christiansen. The equation is:

d_p = Critical diameter to penetrate a given shield [cm]

$$= 0.5 \cdot \left(\frac{t_{rw} \cdot 1.14 + t_b}{\cos(\beta)} \right)^{\frac{18}{19}} \cdot (7 - V_n)/4$$

$$+ t_b \cdot (A + 0.958 \cdot B + 8.17C) \cdot (V_n - 3)/4$$

for 3 km/s < V_n < 7 km/s

where all A, B, and C were previously defined.

Fracture Mechanics - Cylinder

Longitudinal Through Crack in a Cylinder - Tada solution

Reference Tada 83, Tada 85

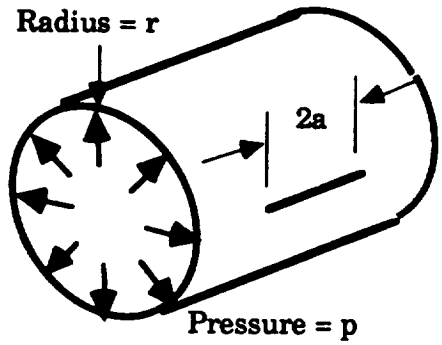

Relationship

K = Stress intensity.

A = Crack opening area.

$$K = \sigma \cdot \sqrt{\pi \cdot a} \cdot F(\lambda)$$

where

$$\sigma = p \cdot r/t$$

= pressure·(pressure vessel radius)/thickness

$$\lambda = a/\sqrt{r \cdot t}$$

and

$$F(\lambda) = \sqrt{1 + 1.25 \cdot \lambda^2} \quad \text{for } 0<\lambda\leq 1$$

$$= 0.6 + 0.9 \cdot \lambda \quad \text{for } 1\leq\lambda\leq 5$$

$$A = \sigma/E \cdot (2 \cdot \pi \cdot r \cdot t) \cdot G(\lambda)$$

where

$$G(\lambda) = \lambda^2 + .625 \cdot \lambda^4 \quad \text{for } 0<\lambda<1$$

$$= .14 + .36 \cdot \lambda^2 + .72 \cdot \lambda^3 + .405 \cdot \lambda^4 \quad \text{for } 1<\lambda<5$$

Limitations $\lambda<5$

Fracture Mechanics - Cylinder

Longitudinal Through Crack in a Cylinder - Folias solution

Reference Folias, Broeck

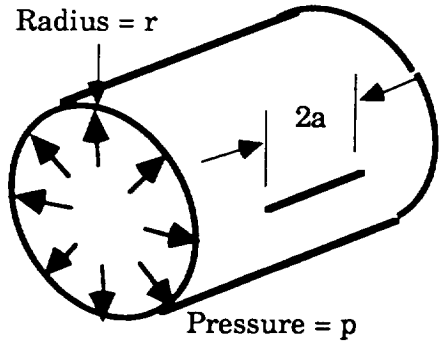

Relationship

K = Stress intensity.

$$K = \sigma \cdot \sqrt{\pi \cdot a} \cdot M_f(\lambda)$$

where

$$\sigma = p \cdot r/t$$

$$\lambda = a/\sqrt{r \cdot t}$$

and

$$M_f(\lambda) = \sqrt{1 + 1.61 \cdot \lambda^2}$$

Limitations Linear elastic fracture mechanics; unknown in other terms.

Comments

Fracture Mechanics - Cylinder
Longitudinal Through Crack in a Cylinder - Plastic Zone correction by Hahn et al. to Folias solution

Reference Hahn et al. as referenced in Broeck

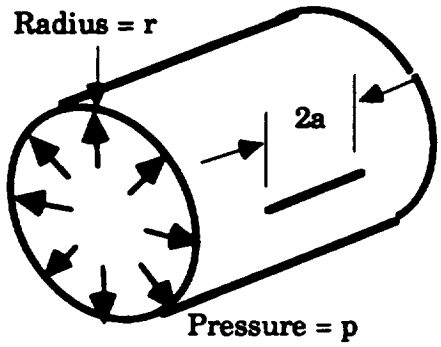

Relationship

K = Stress intensity.

$$K = \sigma \cdot \sqrt{\pi \cdot a \cdot \phi} \cdot M_f(\lambda)$$

where

$$\sigma = p \cdot r / t$$

$$\lambda = a / \sqrt{r \cdot t}$$

$$M_f(\lambda) = \sqrt{1 + 1.61 \cdot \lambda^2}$$, the Folias magnification factor.

$$\phi = 2 \cdot \left(\frac{2 \cdot \sigma_f}{\pi \cdot M_f \cdot \sigma} \right)^2 \cdot \ln \sec \left(\frac{\pi \cdot M_f \cdot \sigma}{2 \cdot \sigma_f} \right)$$

and

σ_f = the effective yield or flow stress

$$\approx (\sigma_{yield} + \sigma_{ult}) / 2 .$$

Limitations Unknown.

Comments Verified for a variety of tough materials [Hahn et al.] including aluminum pressure vessels. [Anderson] The plastic zone correction only gives a 6% increase in K for $\sigma_f/\sigma = 6$ and $M_f = 3$.

Fracture Mechanics - Cylinder

Longitudinal Through Crack in a Cylinder - Zahoor solution

Reference Zahoor 89

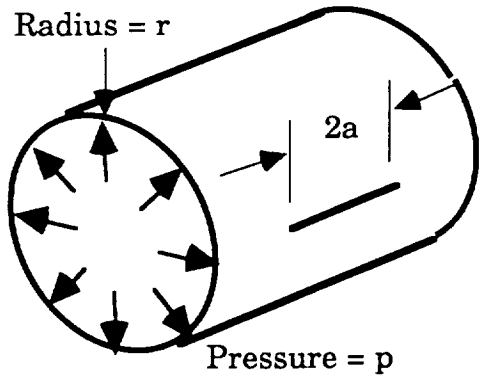

Relationship

K = Stress intensity.

$$K = \sigma \cdot \sqrt{\pi \cdot a} \cdot M(\lambda)$$

where

$$\sigma = p \cdot r/t$$

$$\lambda = a/\sqrt{r \cdot t}$$

and

$$M(\lambda) = 1 + .72449 \cdot 10^{-2} \cdot \lambda + 0.64856 \cdot \lambda^2 - 0.2327 \cdot \lambda^3 + 3.8154 \cdot 10^{-2} \cdot \lambda^4 - 2.3487 \cdot 10^{-3} \cdot \lambda^5$$

Limitations $\lambda \leq 5$.

Comments Accuracy within 1% of [Erdogan and Kibler 69].

Fracture Mechanics - Cylinder
Longitudinal Through Crack in a Cylinder - Zahoor limt load solution

Reference Zahoor 89

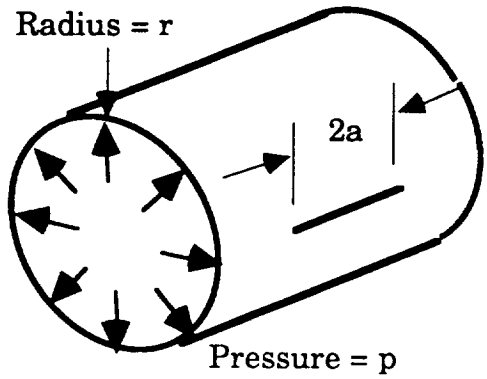

Relationship

p_l = limit pressure.

$$p_l = \sigma_f \cdot (t/R) \cdot M(\lambda)$$

where

σ_f = reference stress (average of yield and ultimate)

$$\lambda = a/\sqrt{r \cdot t}$$

and

$$M(\lambda) = [1 + 1.2987\lambda^2 - 0.026905 \cdot \lambda^4 + 5.3549 \cdot 10^{-4} \cdot \lambda^6]^{0.5}$$

Limitations $0 \le \lambda \le 5$.

Comments Empirical solution.

Fracture Mechanics - Cylinder

Longitudinal Through Crack in a Cylinder-Newman solution

Reference Newman 76; Forman

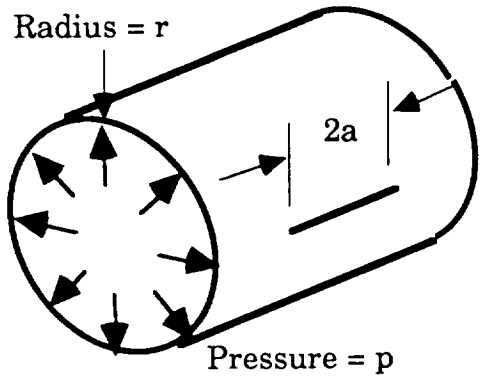

Relationship

K = Stress intensity.

$$K = \sigma \cdot \sqrt{\pi \cdot a} \cdot M(\lambda)$$

where

$$\sigma = p \cdot r/t$$

$$\lambda = a/\sqrt{r \cdot t}$$

and

$$M(\lambda) = \sqrt{1 + .52 \cdot \lambda + 1.29 \cdot \lambda^2 - 0.074 \cdot \lambda^3}$$

Limitations $\lambda \leq 10$.

Comments TC07 in FLAGRO 2.0.

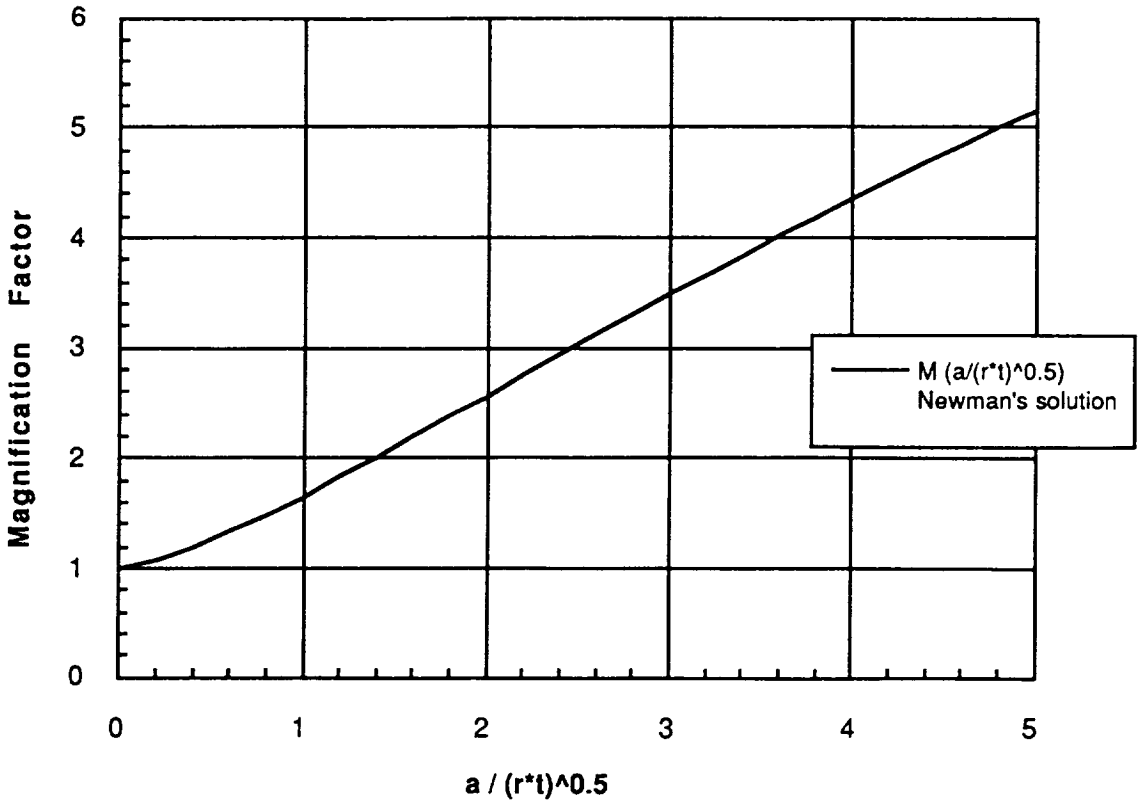
Magnification Factor
6
5
4
3
2
1
0
0
1
2
3
4
5
a / (r*t)^0.5
M (a/(r*t)^0.5)
Newman's solution

Fracture Mechanics - Cylinder

Longitudinal Through Crack in a Cylinder - Depressurized Area at Center of Crack (or Hole at center of crack)

Reference Elfer, Groove and Rajendran.

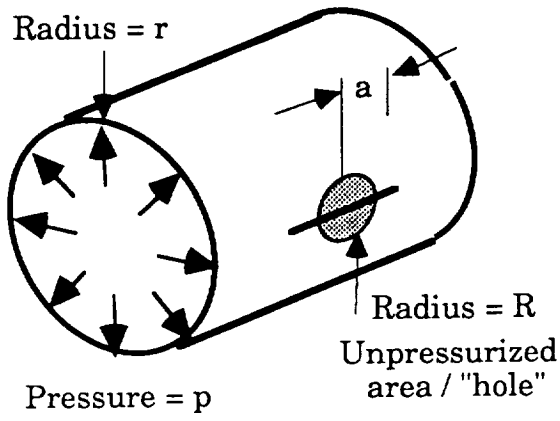

Relationship

K = Stress intensity.

$$K = \sigma \cdot \sqrt{\pi \cdot a} \cdot M_n(\lambda) \cdot (M_h/M_f)$$

where

$$\sigma = p \cdot r/t$$

$$\lambda = a/\sqrt{r \cdot t}$$

and

$$M_n(\lambda) = \sqrt{1 + .52 \cdot \lambda + 1.29 \cdot \lambda^2 - 0.74 \cdot \lambda^3}$$

= Newman Magnification factor

$$M_f = \sqrt{1 + 1.61 \cdot a^2/(r \cdot t)}$$

= Folias Magnification factor

$$M_h = \sqrt{1 + 1.61 \cdot a \cdot (a-R)/(r \cdot t)}$$

= Folias modified for a hole (depressurized area)

$2a$ = crack tip to crack tip distance

and

R = Radius of hole (depressurized area)

Limitations Unknown. Newman magnification factor limited to ≤ 10. Estimate $a/r \geq 1.2$ due to modeling of hole as a depressurized zone.

Comments A hole was modeled as an unpressurized area and this will not be accurate as the size of the unpressurized area approaches the flaw length. If used to model a petalled hole, the pressure on the inward turned petals should also be considered. This may be used to model hydraulic ram effects by superposition.

Fracture Mechanics - Cylinder
Uniform Membrane Load Through Crack in a Cylinder
- Zahoor solution

Reference Zahoor 89

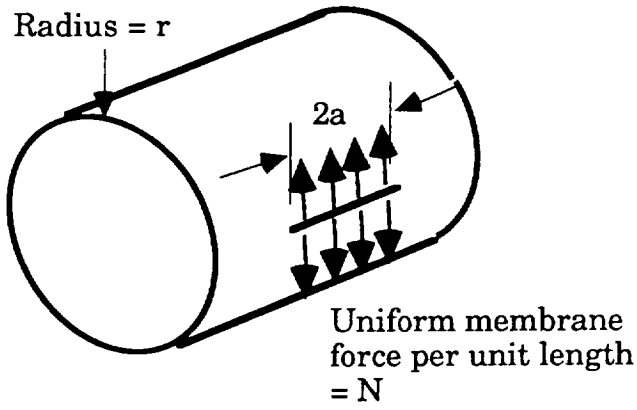

Relationship

K = Stress intensity.

$$K = \sigma \cdot \sqrt{\pi \cdot a} \cdot (M_m(\lambda) + (2 \cdot z/t) \cdot M_b(\lambda))$$

where

σ = N/t

N = uniform membrane force per unit length

λ = $a/\sqrt{r \cdot t}$

z = $+t/2$ at outer surface

= $-t/2$ at innersurface

$M_m(\lambda)$ = Membrane component magnification factor

$$= 1 + .72449 \cdot 10^{-2} \cdot \lambda + 0.64856 \cdot \lambda^2 - 0.2327 \cdot \lambda^3 + 3.8154 \cdot 10^{-2} \cdot \lambda^4 - 2.3487 \cdot 10^{-3} \cdot \lambda^5$$

and

$M_b(\lambda)$ = bending component magnification factor

$$= .36811\cdot\lambda + 0.067692\cdot\lambda^2 - 0.14558\cdot\lambda^3 + .036931\cdot\lambda^4 - 3.0961\cdot10^{-3}\cdot\lambda^5$$

Limitations $\lambda \leq 5$.

Comments Accuracy within 1% of [Erdogan and Kibler 69].

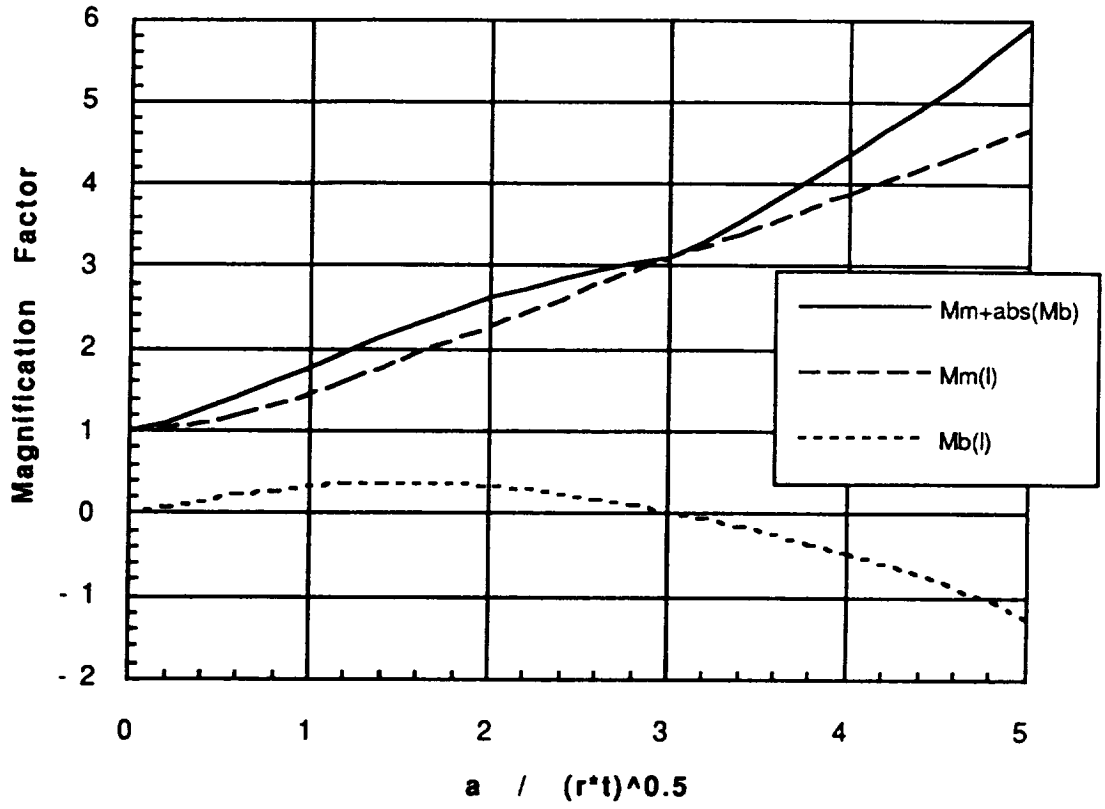

Fracture Mechanics - Through crack in a Cylinder
Wedge loads on a Longitudinal Through Crack-
- Influence function by Elfer

Reference Elfer92

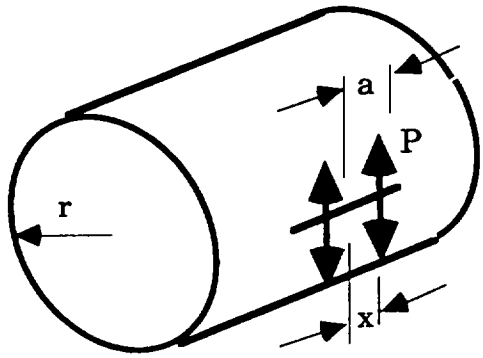

P typ 4 places

Relationship K_I = Stress intensity at either crack tip due to wedge loads P at ±x.

$$K_I/P = \left(\frac{\sqrt{\pi \cdot a}}{(a \cdot t)} (M_{cyl}(\lambda)-1) \cdot h_{cyl}(x) + H_{plate}(x) \right)$$

where

$$M_{cyl}(\lambda) = \sqrt{1 + .52 \cdot \lambda + 1.29 \cdot \lambda^2 - 0.74 \cdot \lambda^3}$$

$$\lambda = a / \sqrt{r \cdot t}$$

$$h_{cyl}(x) = (1.269 - 0.070 \cdot y - 0.235 \cdot y^2 - 0.623 \cdot y^3)$$

$$y = x/a$$

$$H_{plate} = 2 \cdot \sqrt{a} / \sqrt{\pi \cdot (a^2 - x^2)} / t$$

P = load

and

x = load location, $0 \le x \le a$, with symmetric load at -x.

Limitations Unknown. Estimated ±5%. Integrates to Newman's solution for longitudinal

Comments The equations are based on a curve fit to NASTRAN symmetric wedge load solutions for 14.6 and 29.8 cm half crack lengths in a cylinder with thickness of 2.54*0.125 cm and a radius of 2.13 m. The equation uses Broeck's [82] solution for a flat plate and it integrates to the FLAGRO solution [Newman76].

Fracture Mechanics - Sphere

Through Crack in a Sphere - Tada solution

Reference Tada 85

Relationship

K = Stress intensity.
A = Crack opening area.

$$K = \sigma \cdot \sqrt{\pi \cdot a} \cdot F(\lambda)$$

where

$$\sigma = p \cdot r/(2 \cdot t)$$

$$\lambda = a/\sqrt{(r \cdot t)}$$

and

$$F(\lambda) = (1+1.41 \cdot \lambda^2+0.04 \cdot \lambda^3)^{0.5} \quad \text{for } 0<\lambda\leq 3.$$

$$A = \sigma/E \cdot (2 \cdot \pi \cdot r \cdot t) \cdot G(\lambda)$$

where

$$G(\lambda) = \lambda^2 + .705 \cdot \lambda^4 + 0.016 \cdot \lambda^5 \quad \text{for } 0<\lambda\leq 3.$$

Limitations $\lambda \leq 3$. Accuracy given as 1% on K and 2% on A.

Comments a is along a great meridian.

Fracture Mechanics - Sphere

Through Crack in a Sphere - Erdogan and Kibler solution

Reference Erdogan and Kibler; Forman

Relationship K = Stress intensity.

$$K = \sigma \cdot \sqrt{\pi \cdot a} \cdot F(\lambda)$$

where

$$\sigma = p \cdot r/(2 \cdot t)$$

$$\lambda = a/\sqrt{(r \cdot t)}$$

and

$$F(\lambda) = (1+3 \cdot \lambda^{1.9})^{0.4} \qquad \text{for } 0<\lambda\leq 3.$$

Limitations $\lambda \leq 3$.

Comments TC06 dsolution in FLAGRO 2.0

Fracture Mechanics - Infinite plate.
Infinite plate with radiating cracks - Tada solution

Reference Tada 85 (21.12)

Relationship K = Stress intensity.

$$K = \sigma \cdot \sqrt{\pi \cdot a} \cdot F_A(n)$$

where

$$F_A(n) = (1/\sqrt{n}) \cdot (3 - 3.25 \cdot n^{-1} - .64 \cdot n^{-2} + 1.6 \cdot n^{-3}) \quad \text{for } n \geq 1$$

$$F_A(n) \rightarrow 3/\sqrt{n} \quad \text{as } n \rightarrow \infty$$

Limitations Accuracy quoted as "expected to be within 1%." Infinite plate solution.

Comments Cracks are radial at $2\pi/n$ angle. Solution is for first crack which is normal to tensile direction. Estimated by Tada from solutions for n = 1, 2, 4, and infinity.

Fracture Mechanics - Flat Plate
Wedge loads - Influence function

Reference Broeck 82

Relationship

K_{IA} = Stress intensity at A (+a) location.

K_{IB} = Stress intensity at B (-a) location.

$$K_{IA} = P/t/\sqrt{\pi \cdot a} \cdot \sqrt{(a+x)/(a-x)}$$

and

$$K_{IB} = P/t/\sqrt{\pi \cdot a} \cdot \sqrt{(a-x)/(a+x)}$$

where

P = load

and

x = load location, $-a \le x \le a$.

Special cases

$$K_{IA,B} = P/t/\sqrt{\pi \cdot a} \quad \text{for } x = 0.$$

$$K_{IA,B} = 2 \cdot P\sqrt{a}/t/\sqrt{\pi \cdot (a^2 - x^2)}$$

for symmetric loads, P at both $\pm x$.

Limitations

Comments Infinite plate solution.

Fracture mechanics - Infinite Plate

Through cracks (symmetric) from a hole in a plate - Tada

Reference Tada, Newman 71

Relationship

$K = \sigma \cdot \sqrt{\pi \cdot a} \cdot F_\lambda$

$F_\lambda = (1-\lambda) \cdot F_0 + \lambda \cdot F_1$

λ = Ratio of (stress normal to crack/stress in crack direction)

$F_0 = 0.5 \cdot (3-s) \cdot (1+1.243 \cdot (1-s)^3)$

$F_1 = 1+(1+s) \cdot (0.5+0.743 \cdot (1-s)^2)$

$s = a / (R+a)$

and

R = Radius of hole.

Limitations Unknown.

Comments Tada solution includes additional mode 3 loading, which is not included here. As $s \rightarrow 0$, $F1 \rightarrow 2.243$ and $F2 \rightarrow 3.365$.

Fracture mechanics - Flat Plate
Through crack from a hole in a plate - FLAGRO

Reference Forman

Relationship

$$K = \sigma \cdot \sqrt{\pi \cdot a} \cdot F_0$$

$$F_0 = G_0 \cdot G_w$$

$$G_0 = 0.7071 + 0.7548 \cdot z + 0.3415 \cdot z^2 + 0.642 \cdot z^3 + 0.9196 \cdot z^4$$

$$z = (1 + 2 \cdot a/D)^{-1}$$

D = hole diameter

a = crack length from hole edge

$$G_w = [\sec(\cdot (\sin((D/t\text{-}D/W))/(D/t\text{-}D/W)]^{0.5}$$

and

$$\lambda = (\pi/2) \cdot (1 + a/D)/(2 \cdot t/D - a/D)$$

Limitations Unknown.

Comments The FLAGRO solution includes pin loading of the hole, which is ignored here.

Fracture mechanics - Influence function
General equation for influence function

Reference NASCRAC 89, Besuner 81

Relationship

$$K = t \cdot \int_{o \text{ or } -a}^{a} \sigma(x) \cdot h(x)\, dx$$

or

$$K = 1/(t(a)) \cdot \int_{o \text{ or } -a}^{a} t(x) \cdot \sigma(x) \cdot h(x)\, dx$$

where

$t(x)$ = thickness variation,

$\sigma(x)$ = stress variation along the crack face,

and

$h(x)$ = K/P solution for a point load P at location x along the crack face.

$= 1/ t / \sqrt{\pi \cdot a} \cdot \sqrt{(a-x)/(a+x)}$ for a flat plate.

Limitations

Comments Linear superposition of K solutions.

APPENDIX B - BIBLIOGRAPHY

TABLE OF CONTENTS

Table of Contents.....i

Hypervelocity Impact 1

Fracture 7

HYPERVELOCITY IMPACT BIBLIOGRAPHY

Baker, W. E. et al.: Workbook for Predicting Pressure Wave and Fragment Effects of Exploding Propellant Tanks and Gas Storage Vessels, NASA CR-134906 (Nov. 1975).

Bjork, R. L.: The Physics of Hypervelocity Lethality, *Int. J. of Impact Engr.*, **5**, 129-154 (1987).

Bjorkman, M.: Proceedings of the APS 1991 Topical Conference on Shock Compression on Condensed Matter, Williamsburg, VA, June 17-20, (1991).

Bodner, S. R.: Modelling Ballistic Perforation, *Int. Conf. on Structural Impact and Crashworthiness*, Imperial College, London, (1984).

Brewer, E. D.; Hendrich, W. R.; Thomas, D. G. and Smith, J. E.: Effects of Oblique Impact on Hypervelocity Shield Performance, ORNL/TM-11390 (1990).

Bruce, E. P.: Review and Analysis of High Velocity Impact Data, *Proceedings of the Fifth Symposium on Hypervelocity Impact*, Vol 1-Part 2, 439-474 (1961)

Burch, G. T.: Multiplate-Damage Study, AFATL-TR-67-116, (1967)

Chhabildas, L. C.: *A New Hypervelocity Launcher (HVL) for Space Science Applicaitons*, AIAA 92-1639, AIAA Space Programs and Technologies Conference, Huntsville, AL (1992).

Christiansen, E. L.: *Evaluation of Space Station Meteoroid Debris Shielding Materials*, NASA Contract NAS9-15800, Eagle Engineering Report 87-163 (1987).

Christiansen, E. L.: *Shield Sizing and Response Equations*, NASA SN3-91-42, (1991).

Christiansen, E. L.: Private Communication.(1991a)

Christiansen, E. L., Hyde, J. L. and Snell, G.: *Spacecraft Survivablility in the Meteoroid and Debris Environment*, AIAA 92-1409, AIAA Space Programs and Technologies Conference, Huntsville, AL (1992).

Christiansen, E. L.: *Performance Equations for Advanced Orbital Debris Shields*, AIAA 92-1462, AIAA Space Programs and Technologies Conference, Huntsville, AL (1992a).

Christiansen, E.L.; Crews, J.; Nolen, A.; Robinson, J. and Willaimsen, J.: The Space Station Freedom Shielding Tiger Team: Results of the Protection Enhancement Plan Shielding Study, attachment: Ballistic Limit Equations for SSF Shielding Enhancement Plan, NASA/JSC Memo SN3-92-175, (1992b).

Christiansen, E. L.: Design and Performance Equations for Advanced Meteoroid and Debris Shields, *Int. J. Impact Engng*, 14, 145-156 (1993)

Christman, D. R.; Gehring, J. W.; Maiden, C. J. and Wenzel, A. B.: *Study of the Phenomena of Hypervelocity Impact*, General Motor Defense Laboratories Report TR 63-216 (1963).

Coronado, A.R., Wright, M.A., and Stern, P.H.: Space Station Integrated Wall Design and Penetration Damage Control Contract NAS8-36426 Report D180-30550, July, 1987.

Cour-Palais, B. G. and Crews, J. L.: A Multi-Shock Concept for Spacecraft Shielding, *Hypervelocity Impact, Proceedings of the 1989 Symposium, Int. J. of Impact Engineering*, Vol.10, 135-146 (1989).

Cour-Palais, B. G. and Piekutowski, A. J.: The Multi-Shock Hypervelocity Impact Shield, *Proceedings of the American Physical Society 1991 Topical Conference on Shock Compression on Condensed Matter*, Williamsburg, VA.

Dickinson, D.L.; Yatteau, J.D. and Recht R.F.: Fragment breakup, *Int. J. of Impact Engr.*, 5, 249-260 (1987).

Eftis, J. and Nemes, J.A.: Modeling of Impact Induced Spall Fracture And Post Spall Behavior of a Circular Plate, *Int. J. Fracture*, **53**, 301-324 (1992).

Elfer, N. C.: *Space Debris and Meteoroid Protection*, Martin Marietta IR&D Report 826-2307, (1988).

Elfer, N. C.; Baillif, F. and Robinson, J.: *External Tank Space Debris Considerations*, AIAA 92-1411, AIAA Space Programs and Technologies Conference, Huntsville, AL (1992).

Elfer, N. C.; Meibaum, R. and Olsen, G.: *Space Debris Surfaces SD_SURF (Computer Program): Probability of No Penetration versus Impact Velocity and Obliquity*, AIAA 92-1407, AIAA Space Programs and Technologies Conference, Huntsville, AL (1992a).

Elfer, N. C.: *Structural Damage Pediction and Analysis for Hypervelocity Impact*, (This Handbook) Contract NAS8-38856 Report (1995).

Elfer, N. C.: *User's Manual for SD_SURF*, Contract NAS8-38856 Report 1995a.

Fish, R. H. and Summers, J. L.: The Effect of Material Properties on Yhreshold Penetration, *Proceedings of the Seventh Hypervelocity Impact Symposium*, VI, (1965).

Frost, V. C.: *Meteoroid Damage Assessment*, Aerospace Corporation, NASA SP-8042, (1970).

Gehring, J. W.: Theory of Impact on Thin Targets and Shields and Correlation with Experiment, *High Velocity Impact Phenomena*, R. Kinslow ed., Academic Press, New York, 105-156 (1970).

Gehring, J. W.: Engineering Considerations in Hypervelocity Impact, *High Velocity Impact Phenomena*, R. Kinslow ed., Academic Press, New York, 463-514 (1970).

Gilman, J. J. and Tuler, F. R.: Dynamic Fracture by Spallation in Metals, *Int. J. of Fracture Mech.*, **6**, 169-182 (1970).

Grady, D.E. and Kipp, M. E.: Fragmentation of Solids Under Dynamic Loading, *Structural Failure*, T. Weirzbicki ed., John Wiley & Sons, New York, 1-40 (1989).

Graves, R. and Smiley, J.: User's Guide for Design Analysis Code BUMPER-II, Report XD683-99402-1 on Contract NAS8-50000 (1991).

Grove, D. J. and Rajendran, A. M.: Modeling the Response of a Thin Sheet due to a Hypervelocity Debris Cloud Impact, Appendix D, Contract NAS8-38856 Report (1992).

Gurson, A. L.: The Effect of Geometric Scale on Impact Induced Fragmentation and its Application to the Design of Dual Plate Armor, *Hypervelocity Impact, Proceedings of the 1989 Symposium, Int. J. of Impact Engineering*, Vol.10, 135-146 (1989).

Hayashida, K. B. and Robinson, J. H.: *Single Wall Penetration Equations*, NASA TM 103565, (1991).

Hayashida, K. B. personal communication, NASA-MSFC (1995).

Henderson, B.J. and Zimmerschied, A.B.: Very High Velocity Penetration Model, NSWC TR 83-189, (1983).

Herrmann, W. and Wilbeck, J. S.: Review of Hypervelocity Penetration Theory, *Int. J. of Impact Engr.*, **5**, 307-322 (1987).

Holsapple, K. A.: Hypervelocity Impacts: Testing In Surrogate Materials, *Int. J. of Impact Engr.*, **14**, 335-345 (1993).

Holsapple, K. A. and Schmidt, R. M.: On the Scaling of Crater Dimensions to Impact Process, *J. Geophysical Research*, N87 vol B3 (1982).

Housen, K. R. and Schmidt, R. M.: Whipple Shields Characterized by a Nondimensional Geometry Parameter, *J. Spacecraft and Rockets.*, 32-1, 162-168 (1995).

Jolly, W. H. and Williamsen, J.E.: Statistical Ballistic Limit Curve Regression for Space Station Freedom Meteoroid/Orbital Debris Shielding, *Int. J. Impact Engng.*, **14**, 395-406 (1993).

Klinkrad, H. and Jehn, R.: The Space Debris Environment, *ESA Journal*, 16, 1-11 (1992).

Kulesz, J. J. and Vargas, L. M.: Prediction of fragment velcoities and trajectories, *Shock and Vibration Journal*, **1** (1979).

Lawrence, R. J.: *A Simple Approach for the Design and Optimization of Standoff Hypervelocity Particle Shields*, AIAA 92-1465, AIAA Space Programs and Technologies Conference, Huntsville, AL (1992).

McGill, P. and Mount, A.: Effectiveness of Metal Matrix and Ceramic Matrix Composites as Orbital Debris Shield Materials, AIAA 92-1461, AIAA Space Programs and Technologies Conference, Huntsville, AL (1992).

Mechtly, E. A.: The International System of Units Physical Constants and Conversion Factors, NASA SP-7012, 2nd Revision (1973).

Morrison, R. H.: A Preliminary Investigation of Projectile Shape Effects in Hypervelocity Impact of a Double-Sheet Structure, NASA TN D-6944 (1972).

Mullin, S. A.; Anderson, C. E. Jr.; and Wilbeck, J. S.: *Dissimilar Material Scaling Relationships for Hypervelocity Impact*, DNA-TR-89-112, Feb. 1989.

NASA SP-8042 see (Frost, V. C.: *Meteoroid Damage Assessment*, Aerospace Corporation, NASA SP-8042, (1970).)

Nicholas, T. and Rajendran, A. M.: Material Characterization at High Strain Rates, *High Velocity Impact Dynamics*, J. A. Zukas ed., John Wiley & Sons, New York, 127-297 (1990).

Nysmith, R. C.: An Experimental Impact Investigation of Aluminum Double Sheet Structures, AIAA Paper 69-374 (1969).

Piekutowski, A.J.: Debris Clouds Generated by Hypervelocity Impact of Cylindrical Projectiles with Thin Aluminum Plates, *Int. J. of Impact Engr.*, Vol. 5, pp.509-518, 1987.

Piekutowski, A. J.: A simple dynamic model for the formation of debris clouds, *Hypervelocity Impact, Proceedings of the 1989 Symposium, Int. J. of Impact Engineering,* Vol.10, 453-472 (1989).

Piekutowski, A. J.: Formation and Description of Debris Clouds Produced by Hypervelocity Impact, UDR-TR-95-46 (1995).

Rajendran, A. M. and Elfer, N. C.: Debris Protection of Space Structures, *Structural Failure*, T. Weirzbicki ed., John Wiley & Sons, New York, 41-78 (1989).

Recht, R. F.: High Velocity Impact Dynamics: Analytical Modeling and Plate Penetration Dynamics, *High Velocity Impact Dynamics*, J. A. Zukas ed., John Wiley & Sons, New York, 443-514 (1990).

Richardson, A.J.: Theoretical Penetration Mechanics of Multisheet Structures Based on Discrete Particle Modeling, *J. of Spacecraft and Rockets,* vol.7, pp.486-489, 1970.

Richardson, A.J., and Sanders, J.P.: Development of Dual Bumper Wall Construction for Advanced Spacecraft, *J. of Spacecraft and Rockets,* vol.9, pp448-451, 1972.

Schmidt, R. M.; Housen, K. R.; Piekutowski, A. J. and Poorman, K. L.: Cadmium Simulations of Orbital Debris Shield Performance to Scaled Velocities of 18 km/s, *J. of Spacecraft and Rockets,* 31-5, pp866-877 (1994).

Summers, J. L.: Investigation of High Speed Impact: Regions of Impact and impact at Oblique Angles, NASA TN D-94 (1959).

Swift, H. F. and Hopkins, A. K.: Effects of Bumper Material Properties on the Operation of Spaced Meteoroid Shields, AFML-TR-68-257 (1968) and *J. Spacecraft and Rockets*, vol. 7, no. 1, pp 73-77 (1970).

Swift, H. F.: Hypervelocity Impact Mechanics, *Impact Dynamics*, John Wiley and Sons, (1982)

Swift, H. F.; Bamford, R, and Chen, R.:Designing Dual Plate Meteoroid Shields - A New Analysis, NASA CR-169143, (1982).

Swift, H. F.: On Predicting Projectile Breakup During Thin Plate Impact, *Hypervelocity Impact, Proceedings of the 1989 Symposium, Int. J. of Impact Engineering*, Vol.10, 579-586 (1989).

Taylor, D. E. and Price, C. F.: Velocities of Fragments From Bursting Gas Reservoirs, *J. Engr. for Industry, Trans. ASME*, 981-985 (1971).

Trucano, T. G.; Grady, D. E. and McGlaun, J. M.: Fragmentation Statistics from Eulerian Hydrocode Calculations, *Hypervelocity Impact, Proceedings of the 1989 Symposium, Int. J. of Impact Engineering*, Vol.10, 587-599 (1989).

Tullos, R. J.; Mullen, S. A. and Graef, R.C.: An Evaluation of the Response of Advanced Structural Materials to Hypervelocity Impacts, SwR Final Report 06-1974-130 Air Force Contract F41608-87-A237 (1990)

Weldon, W. F.: Development of Hypervelocity Electromagnetic Launchers, *Int. J. of Impact Engr.*, **5**, 671-680 (1987).

Williamsen, J. E.: Orbital Debris Risk Analysis and Survivability Enhancement for Freedom Station Manned Modules, AIAA-92-1410, AIAA Space Programs and Technologies Conference, Huntsville, AL (1992).

Williamsen, J. E.: Vulnerability of Manned Spacecraft to Crew Loss from Orbital Debris Penetration, NASA TM-108452, (1994)

Yatteau, J.D.: *High Velocity Penetration Model*, NSWC TR 82-123 1982.

Zukas, J. A.: Survey of Computer Codes for Impact Simulation, *High Velocity Impact Dynamics*, J. A. Zukas ed., John Wiley & Sons, New York, 593-714 (1990).

FRACTURE MECHANICS BIBLIOGRAPHY

Aminpour, M. A. and Holsapple, K. A.: Finite Element Solutions for Propagating Interface Cracks with Singular Elements, Engr. Fracture Mechanics, 39 no. 3, 451-468 (1991).

Anderson, R. B. and Sullivan, T. L.: *Fracture Mechanics of Through-Cracked Cylindrical Pressure Vessels*, NASA TN D-3252 (1966).

Atluri, S. N.; Nishioka, T.; Nakagaki, M.: Numerical Modeling of dynamic and nonlinear crack propagation in finite bodies by moving singular elements, Nonlinear and Dynamic Fracture Mechanics, N. Perrone and S. N. Atluri, ed., ASME, 35, 37-66 (1979).

Atkins, A. G.: Tearing of Thin Metal Sheet, Structural Failure, T. Weirzbicki ed., John Wiley & Sons, New York, 107-159 (1989).

Baker, B. R.: Dynamic Stresses Created by a Moving Crack, J. Applied Mech., 29, 449-545 (1962).

Besuner, P. M.: BIGIF - Fracture Mechanics Code for Structures, Electric Power Research Institute Report NP-1830-CCM, Palo Alto, CA (1981)

Broeck, D.: Elementary Engineering Fracture Mechanics, Martinus Nijhoff, Boston (1982).

Couque, H.; O'Donoghue, P.; Mullin, S.; and Kanninen, M.: Investigation of Crack Initiation and Unstable Propagation due to Meteoroid or Orbital Debris Impact into Space Station Freedom Pressure Vessels, Southwest Research Institute Project No. 06-5537 (1993).

Eichenberger, T. W.: *Fracture Resistance Data Summary*, Report DA-20947, (1962).

Eidinoff, H., Meyers,W. and Balderes: Fracture Mechanics Analysis of the Space Station Freedom Common Module, Grumman ASD Report SAR-93-01, Bethpage, N.Y., Presented at the 7th Meeting of the Space Station Freedom Meteoroid/Oribital Debris Advanced Fracture Mechanics Group, at Southwest Research Institute, San Antonio, (March 1993)

Elfer, N. C.: Space Debris and Meteoroid Protection, Martin Marietta IR&D Report 826-2307, 1988.

Elfer, N. C.: R-Curve Analysis of Surface Flaws, Final Report for TD 812, TBD [1991]

Erdogan, F. and Kibler, J. J.: Cylindrical and Spherical Shells with Cracks, *Int. J. of Frac. Mechanics*, **5** no. 3, 229-237 (1969).

Erdogan, F. and Ratwani, M.: Fracture of Cylindrical and Spherical Shells Containing a Crack, *Nuclear Engineering and Design*, Paper G6/4, p. 265-286, (1972).

Ernst, H.: Recent Developments in Elastic Plastic Crack Growth Characterization, *22nd National Fracture Mechanics Symposium*, ASTM STP 1131, 136-157 (1992).

Ernst, H.: Material Resistance and Instability Beyond J-Controlled Crack Growth, *Elastic-Plastic Fracture: Second Symposium, Vol.1 Inelastic Crack Analysis*, ASTM STP 803, C.F. Shih and J. P. Gudas, Eds., 191-213 (1983).

Folias, E. S.: A Finite Line Crack In A Pressurized Cylindrical Shell, *Int. J. of Fracture Mech.*, 1, 104-113 (1965).

Forman, R. G., Fatigue Crack Growth Computer Program "NASA/FLAGRO," NASA-Johnson Space Center Materials Branch Report 85-ES5-1 (1986).

Fruend, L. B.: Dynamic Crack Propagation, *The Mechanics of Fracture*, F. Erdogan ed., ASME Publ. No. AMD-19, 1976.

Gunther, C. K.; Holsapple, K. A. and Kobayashi, A. S.: Finite Element Analysis of Cracking Bodies, *AIAA J.* 19, 789-795 (1981).

Hahn, G. T.; Sarrate, M. and Rosenfield, A. R.: Criteria for Crack Extension In Cylindrical Pressure Vessels, *Int. J. Fracture Mechanics*, 5, 187-210 (1969).

Kanninen, M. F. and Popelar, C. H.: Dynamic Fracture Mechanics, *Advanced Fracture Mechanics*, Oxford Univ. Press, New York, 193-280, (1985).

Kanninen, M. F. Preliminary Dynamic Toughness Measurements on 2219-T87, Southwest Research Institute, San Antonio, TX, Presentation at the Eighth Meeting of the Space Station Freedom Meteoroid/Oribital Debris Advanced Fracture Mechanics Group, at GE Corporate Research and Development, Schenectady N.Y.(June, 1993). see Couque et al.

Kaufman, J. G., and Hunsicker: Fracture Toughness Testing at Alcoa Research Laboratories, ASTM STP.

Newman, J. C. Jr: *An Improved Method of Collocation for the Stress Analysis of Cracked Plates with Various Shaped Boundaries*, NASA TN D-6376, (1971).

Newman, J. C. Jr: *Fracture Analysis of Surface and Through Cracks in Cylindrical Pressure Vessels*, NASA TN D-8325, (1976).

Nied, H.F. and Bachrach, W. E. Several Topics in Fracture Mechanics, GE Corporate Research and Development (GE CR&D) Presentation at the Eighth Meeting of the Space Station Freedom Meteoroid/Oribital Debris Advanced Fracture Mechanics Group, at GE Corporate Research and Development, GE CR&D Schenectady N.Y.(June, 1993).

Pfluger, A. R.: *Fracture Toughness of 2219-T87 Aluminum*, NASA CR-60285 (1964). (note that toughness reported for maximum flaw length at maximum load, while max load actually occurs at shorter lengths.)

Poe, C.C.: Fatigue Crack Propagation in Stiffened Panels, *Damage Tolerance in Aircraft Structures*, ASTM STP 486, 79-97 (1971).

Schmidt, R.: Linear-Shaped Charge Experiments: Crack Geometry Effects on Unzipping. Boeing Defense and Space Group, Seattle Wa., Presentation at the Eighth Meeting of the Space Station Freedom Meteoroid/Oribital Debris Advanced Fracture Mechanics Group, at GE Corporate Research and Development, Schenectady N.Y.(June, 1993).

Tada, H.: The Effects Of Shell Corrections On Stress Intensity Factors And The Crack Opening Areas Of A Circumferential And A Longitudinal Through Crack In A Pipe, *The Application of Fracture Proof Design Methods Using Tearing Instability Theory to Nuclear Piping Postulating Circumferential Through Wall Cracks*, P. C. Paris and H. Tada ed., U.S. Nuclear Regulatory Commision, NUREG/CR-3464, Section III (1983).

Tada, H.; Paris, P. C. and Irwin, G.: The Stress Intensity Analysis of Cracks Handbook, Paris Productions Inc. (and Del Research Corporation) 226 Woodburne Dr. St. Louis, Mo 63105 (1985).

Zahor, A.: Axial Throughwall Crack, chapter 6 in *Ductile Fracture Handbook*, EPRI NP-6301-D (1989),

APPENDIX C - TEST DATABASES

TABLE OF CONTENTS

Table of Contents i

Martin Marrietta IR&D Tests at UDRI [N. Elfer - Lockheed Martin]..... 1

NASA-MSFC 'Meteroid' Database (7/91) [D. Williams - Boeing]..... 7

JSC Whipple Database (7/91) [E. Christiansen - JSC]..... 36

JSC Mesh Double Bumper Database (7/91) [E. Christiansen - JSC]..... 46

JSC Multi-Shock Bumper Database (7/91)[E. Christiansen - JSC] 49

		PROJECTILE CHARACTERISTICS						BUMPER			REAR WALL			
UDRI	PROJECTILE	CYL.	MASS	DIA.	VELOC.	OBL.	BUMPER	THICK.	HOLE	SPACE	REAR WALL	THICK.	HOLEOUT	PEN
ID.NO.	MATERIAL	/SPHERE	g	in	km/s	deg	MATERIAL	in	DIA. in	in	MATERIAL	in	DIA. in	Y,N,T
	CELOTEX WITNESS MATERIALS													
	2.54-4.0	KM/SEC					Aluminum				1st Witness Plate			
4-0327	2024-T4	C	1.0018	0.304	2.64	0	6061-T6	0.080	0.53	4	2024-T3	0.02	2	
4-0330	2017-T4	S	1.272	0.375	2.79	0	6061-T6	0.080	0.56	4	2024-T3	0.02	0.9	
4-0405	2024-T4	C	1	0.304	3.09	0	6061-T6	0.125	0.63	4	2024-T3	0.02	1.5	
4-0416	2024-T4	C	1	0.304	3.06	0	6061-T6	0.080	0.55	4	2024-T3	0.02	1.7	
4-0421	2024-T4	C	1	0.304	3.11	0	6061-T6	0.080	0.55	4	2024-T3	0.02	2	
4-0422	2024-T4	C	1	0.304	2.97	0	6061-T6	0.080	0.585	4	2024-T3	0.02	0.5x1.0	
4-0423	2024-T4	C	1.28	0.329	2.98	0	6061-T6	0.080	0.585	4	2024-T3	0.02	2	
							Composites							
4-0368	2024-T4	C	1	0.304	3.03	0	IM6/3501	0.200	0.65	4	2024-T3	0.02	1.0x1.2	
4-0369	2024-T4	C	1	0.304	3.09	0	S2/3501	0.100	0.5	4	2024-T3	0.02	1.5	
4-0370	2024-T4	C	1	0.304	3.03	0	IM6/8551	0.200	0.65	4	2024-T3	0.02	1.0x1.5	
4-0371	2024-T4	C	1	0.304	3.08	0	IM6-S2/3501	0.175	0.61	4	2024-T3	0.02	1.0x1.5	
4-0396	2024-T4	C	1	0.304	3.16	0	KEVLAR 49/3501	0.160	0.54	4	2024-T3	0.02	0.7x1.5	
4-0397	2024-T4	C	1	0.304	3.13	0	IM6/3501	0.150	0.6x0.9	4	2024-T3	0.02	1.5	
4-0419	2024-T4	C	1	0.304	3.04	0	Al-Si C	0.071	0.55	4	2024-T3	0.02	1.0x1.7	
4-0428	2024-T4	C	1.0011	0.304	3.01	0	3 PLIES VM3063 KEVLAR	TBD	TBD	4	2024-T3	0.02	0.7	
4-0431	2024-T4	C	0.9985	0.304	3.02	0	2 PLIES VM3063 KEVLAR	0.120	0.6	4	2024-T3	0.02	0.5x0.9	
4-0467	2024-T4	C	0.9996	0.304	3.12	0	MMA II.2-06-001	0.175	0.75	6	2024-T3	0.02	0.5	
4-0486	2024-T4	C	0.9998	0.304	3.06	0	2(Al203)/Al	0.075	0.865	6	2024-T3	0.02	1.5	
4-0589	2024-T4	C	1.0043	0.304	3.04	0	7740 GLASS/SiC	0.100	0.8	4	2024-T3	0.02	1.8	
	4-6 KM/SEC						Aluminum							
4-0331	2017-T4	S	1.27	0.375	5.1	0	6061-T6	0.080	0.72	4	2024-T3	0.02	3	
4-0333	2024-T4	C	1	0.304	4.82	0	6061-T6	0.080	0.8	4	2024-T3	0.02	1.5x2.5	
4-0334	2024-T4	C	1	0.304	4.98	0	6061-T6	0.080	0.63	4	2024-T3	0.02	2.5	
4-0424	2024-T4	C	1.28	0.329	4.91	0	6061-T6	0.080	0.7	4	2024-T3	0.02	5	
	6+ KM/SEC						Aluminum							
4-0335	2024-T4	C	1	0.304	6.09	0	6061-T6	0.080	0.76	4	2024-T3	0.02	5.0x6.0	
4-0336	2024-T4	C	2.01	0.383	6.17	0	6061-T6	0.080	0.85	4	2024-T3	0.02	9	
4-0338	2024-T4	C	1	0.304	6.3	0	6061-T6	0.080	0.7	2	2024-T3	0.02	2	
4-0339	2017-T4	S	0.373	0.25	6.35	0	6061-T6	0.080	0.8	4	2024-T3	0.02	2.0-2.5	
4-0404	2024-T4	C	1	0.304	6.42	0	6061-T6	0.125	0.81	4	2024-T3	0.02	3	
4-0433	2024-T4	C	0.998	0.304	6.23	0	6061-T6	0.080	0.685	4	2024-T3	0.02	2.5	
4-0434	2024-T4	C	1.0039	0.304	6.34	0	6061-T6	0.080	0.65	4	2024-T3	0.02	4	
							Composites							
4-0360	2024-T4	C	0.9968	0.304	6.45	0	IM6/3501	0.200	0.95	4	2024-T3	0.02	4.5	
4-0361	2024-T4	C	1	0.304	6.3	0	S2/3501	0.100	0.65	4	2024-T3	0.02	3	
4-0362	2024-T4	C	1	0.304	6.42	0	IM6/8551	0.200	0.95	4	2024-T3	0.02	2	
4-0363	2024-T4	C	1	0.304	6.54	0	IM6-S2/3501	0.150	0.8	4	2024-T3	0.02	2.5	
4-0398	2024-T4	C	1	0.304	6.38	0	KEVLAR 49/3501	0.160	0.7	4	2024-T3	0.02	2.5	
4-0415	2024-T4	C	1	0.304	6.33	0	IM6/3501	0.150	7.75	4	2024-T3	0.02	2.5x3.0	
4-0420	2024-T4	C	1	0.304	6.43	0	Al-Si C	0.071	0.67	4	2024-T3	0.02	4	
4-0427	2024-T4	C	0.9984	0.304	6.36	0	2 PLIES KEVLAR 3063-1	TBD	TBD	4	2024-T3	0.02	4	
4-0430	2024-T4	C	1.0024	0.304	6.3	0	3 PLIES VM3063 KEVLAR	TBD	TBD	4	2024-T3	0.02	8	
4-0468	2024-T4	C	0.9816	0.304	6.51	0	MMA II.2-06-002	0.175	0.425	6	2024-T3	0.02	0	
4-0469	2024-T4	C	0.9805	0.304	6.54	0	MMA II.2-06-003	0.175	0.95	6	2024-T3	0.02	4	
4-0485	2024-T4	C	1.0049	0.304	6.4	0	Al02/Al 3 PLIES	0.075	1	6	2024-T3	0.02	3	
4-0487	2024-T4	C	1.0028	0.304	6.46	0	8 PLIES TRIAX KEVLAR	0.035	TBD	6	2024-T3	0.02	9.5	
4-0503	2024-T4	C	1.0035	0.304	6.4	0	Al02/Al 3 PLIES	0.075	1.0x1.26	4	2024-T3		3	
4-0504	2024-T4	C	1.0028	0.304	6.36	0	MMA II.2-10-001	TBD	0.9	4	2024-T3	0.02	9	
4-0588	2024-T4	C	1.0043	0.304	6.49	0	MML 7740 GLASS/SiC	0.080	1.7 X 2.5	4	2024-T3	0.02	3.5	

UDRI ID.NO.	WITNESS MATERIALS	SPACING in	THICK. in	DEPTH of PEN. in	HOLEOUT DIA. in	COMMENTS
4-0327	CELOTEX	0	UNLIMITED	2.05	2	6 CELOTEX PENETRATED
4-0330	CELOTEX	0	UNLIMITED	4	1.6	8 SMALL HOLES OUTSIDE OF HOLEOUT
4-0405	CELOTEX	0	UNLIMITED	2.67	1.5	THICKER BUMPER,5 CELOTEX PENETRATED,1 CRUSH/DENTED
4-0416	CELOTEX	0	UNLIMITED	1.63	1.0x1.7	4 FRAGMENTS THROUGH 2ND CELOTEX
4-0421	CELOTEX	0	UNLIMITED	1.9	2	4 CELOTEX PENETRATED,1 CRUSH/DENTED, 7" DIA. CRATER AREA ON WITNESS PLATE
4-0422	CELOTEX	0	UNLIMITED	3.61	0.7x1.5	7 CELOTEX PENETRATED,1 CRUSH/DENTED, 7" DIA. CRATER AREA ON WITNESS PLATE
4-0423	CELOTEX	0	UNLIMITED	2.2	1.5x2.0	4 CELOTEX PENETRATED,1 CRUSH/DENTED, 7" DIA CRATER AREA ON WITNESS PLATE
4-0368	CELOTEX	0	UNLIMITED	2.1	1.5	EQUIVALENT 0.110" Al,GRAPHITE BUMPER
4-0369	CELOTEX	0	UNLIMITED	1.68	1.5x2.0	EQUIVALENT 0.080" Al,FIBERGLASS BUMPER
4-0370	CELOTEX	0	UNLIMITED	2.52	0.5x1.5	EQUIVALENT 0.110" Al,FIBERGLASS BUMPER
4-0371	CELOTEX	0	UNLIMITED	3.04	1.0x1.5	ALTERNATING S-2 GLASS & IM6,EQUIVALENT 0.095" Al
4-0396	CELOTEX	0	UNLIMITED	2.2	1.0x1.5	EQUIVALENT 0.080" Al,3 CELOTEX PENETRATED,1 CRUSHED ,2 DENTED
4-0397	CELOTEX	0	UNLIMITED	2.3	1.5	EQUIVALENT 0.080" Al ,4 CELOTEX PENETRATED,1 CRUSHED,1DENTED
4-0419	CELOTEX	0	UNLIMITED	2.2	2	4 CELOTEX PENETRATED,1 CRUSH/DENTED , 7" DIA CRATER AREA ON WITENSS PLATE
4-0428	CELOTEX	0	UNLIMITED	3.78	1	8 CELOTEX PENETRATED 1 CRUSH/DENTED, (SMALL DIA), 5" DIA CRATER AREA ON WITNESS PLATE
4-0431	CELOTEX	0	UNLIMITED	4.25	1.2	8 CELOTEX PENETRATED, 4" DIA CRATER AREA ON WITNESS PLATE
4-0467	CELOTEX	0	UNLIMITED	3.76	1.5	8 CELOTEX SHEETS PENETRATED
4-0486	CELOTEX	0	UNLIMITED	2.67	1.5x2.0	AlO2 BUMPER 1PLY Al CREST4-0487,5 CELOTEX PENETRATED 2 CRUSH/DENTED
4-0589	CELOTEX	0	UNLIMITED	2.37	1.8	5 CELOTEX PENETRATED, 1 DENTED
4-0331	CELOTEX	0	UNLIMITED	2.67	3	
4-0333	CELOTEX	0	UNLIMITED	1.8	2.5	PARTIAL SABOT FAILURE
4-0334	CELOTEX	0	UNLIMITED	1.88	2.5	4 CELOTEX PENETRATED,8.5" CRATER AREA ON WITNESS PLATE
4-0424	CELOTEX	0	UNLIMITED	3.31	3	5 CELOTEX PENETRATED,1 CRUSH/DENTED,12 BROKEN,8" DIA CRATER AREA ON WITNESS PLATE
4-0335	CELOTEX	0	UNLIMITED	2.68	3.5	PETALLING OF WITNESS PLATE
4-0336	CELOTEX	0	UNLIMITED	2.37	9	WITNESS PLATE TOO DAMAGED TO MEASURE; 1ST SEVEN CELOTEX FRACTURED,SABOT DAMAGE
4-0338	CELOTEX	0	UNLIMITED	3.14	2.5x3.0	SABOT DAMAGE, 7 CELOTEX PENETRATED
4-0339	CELOTEX	0	UNLIMITED	0.49	0	
4-0404	CELOTEX	0	UNLIMITED	2.1	2.5	2 CELOTEX PENETRATED,1 CRUSH/DENTED,2 DENTED,SLIGHT SABOT DAMAGE
4-0433	CELOTEX	0	UNLIMITED	2.37	3	3 CELOTEX PENETRATED, 9" DIA CRATER AREA ON WITNESS PLATE
4-0434	CELOTEX	0	UNLIMITED	2.84	3	9" DIA CRATER AREA ON WITNESS PLATE
4-0360	CELOTEX	0	UNLIMITED	2.975	2.0x3.0	EQUIVALENT 0.095" Al,GRAPHITE EPOXY BUMPER
4-0361	CELOTEX	0	UNLIMITED	2.94	3.0x3.5	EQUIVALENT 0.080" Al, FIBERGLASS BUMPER
4-0362	CELOTEX	0	UNLIMITED	2.15	2	EQUIVALENT 0.110" Al, GRAPHITE BUMPER
4-0363	CELOTEX	0	UNLIMITED	2.17	2	EQUIVALENT 0.110" Al,GRAPHITE BUMPER
4-0398	CELOTEX	0	UNLIMITED	1.81	3.5	EQUIVALENT 0.080" Al,4 CELOTEX PENETRATED, 4 PANELS CRACKED ENTIRELY, 1 DENTED
4-0415	CELOTEX	0	UNLIMITED	2.67	2	EQUIVALENT 0.080" Al, 4 CELOTEX PENTRATED,1 CRUSH /DENTED,2 DENTED
4-0420	CELOTEX	0	UNLIMITED	2.84	2.5	EQUIV. 0.080", 4 CELOTEX PENETRATED,1 CRUSH/ DENTED,2 DENTED,9" DIA CRATER AREA ON WIT. PLT.
4-0427	CELOTEX	0	UNLIMITED	3.09	2.5	2 PLIES KEVLAR VM 3063-1 BUMPER,5 CELOTEX PEN.,1 C/D,2 DENTED, 7" DIA CRATER AREA ON WIT. PLT
4-0430	CELOTEX	0	UNLIMITED	2.37	3.5	3 PLIES KEVLAR VM 3063-1 BUMPER,8" DIA CRATER AREA ON WITNESS PLATE
4-0468	CELOTEX	0	UNLIMITED	0.005	0	SABOT TURNED ?, ONE HALF AHEAD OF PROJECTILE,SMALL DENTS IN WITNESS PLATE
4-0469	CELOTEX	0	UNLIMITED	2.35	3.74	EQUIVALENT 0.080" Al BUMPER, 5 CELOTEX PENETRATED
4-0485	CELOTEX	0	UNLIMITED	1.43	3.5	2 PLIES Al203/1 PLY Al/CREST,AlO2 TOWARD PROJECTILE,2 CELOTEX PENETRATED,2 CRACKED
4-0487	CELOTEX	0	UNLIMITED	1.9	3.5	4 CELOTEX PENETRATED,2 CRUSH/DENT,WITNESS PLATE DESTROYED
4-0503	CELOTEX	0	UNLIMITED	1.9	3.5	2 PLIES Al203/1 PLY Al/CREST,4 CELOTEX PENETRATED,2 CRACKED
4-0504	CELOTEX	0	UNLIMITED	2.82	4	5 CELOTEX PENETRATED
4-0588	CELOTEX	0	UNLIMITED	2.37	3	3 CELOTEX PENETRATED

		PROJECTILE CHARACTERISTICS						BUMPER			REAR WALL			
UDRI	PROJECTILE	CYL.	MASS	DIA.	VELOC.	OBL.	BUMPER	THICK.	HOLE	SPACE	REAR WALL	THICK.	HOLEOUT	PEN
ID.NO.	MATERIAL	/SPHERE	g	in	km/s	deg	MATERIAL	in	DIA. in	in	MATERIAL	in	DIA. in	Y,N,T
	MULTIWALL DESIGNS													
		ALL ALUMINUM												
PRELIM.	2024-T4	C	0.75	0.23	5.2	0	6061-T6	0.040	TBD	2	2219-T87	0.07	2	Y
PRELIM.	2024-T4	C	0.75	0.23	5.2	0	6061-T6	0.020	TBD	4	2219-T87	0.125	0	N
4-0316	2024-T4	C	0.75	0.23	5.2	0	6061-T6	0.080	1.0x1.25	4	2219-T87	0.125	0.3x0.675	Y
4-0317	2024-T4	C	0.75	0.23	5.2	0	6061-T6	0.125	0.825	4	2219-T87	0.125	0.3x2.3	Y
4-0402	2024-T4	C	0.9991	0.304	6.31	0	6061-T6	0.080	0.735	4	2219-T851	0.125	1.5x2.5	Y
4-0408	2024-T4	C	1	0.304	6.38	0	6061-T6	0.080	0.7	4	2219-T851	0.2	0.5x1.5	Y
4-0417	2024-T4	C	1	0.304	6.27	0	6061-T6	0.080	0.675	4	2219-T851	0.25	0	N
4-0435	2024-T4	C	1	0.304	6.26	0	6061-T6	0.080	0.65	12	2219-T851	0.15	0.04	Y
4-0436	2024-T4	C	1.0018	0.304	6.24	0	6061-T6	0.080	0.63x0.75	4	2219-T851	0.225	0.7x2.2	Y
4-0438	2024-T4	C	1.0007	0.304	6.34	0	6061-T6	0.080	0.66x0.74	9/3	(0.02") 2024-T3/2219-T851	0.15	0	N
4-0446	2024-T4	C	0.9988	0.304	6.28	0	6061-T6	0.080	TBD	12	2219-T851	0.175	TBD	Y
		Fabric Catchers + Aluminum Rear Walls												
4-0454	2024-T4	C	1.0004	0.304	6.44	0	6061-T6	0.080	0.69	2.5/1/1	2 PLIES (2X) TRIAXIAL KEVLAR/2219-T81	0.125	0	N
4-0455	2024-T4	C	1.0031	0.304	3.06	0	6061-T6	0.080	0.575	2.5/1/1	2 PLIES (2X) TRIAXIAL KEVLAR/2219-T81	0.125	0.3	Y
4-0456	2024-T4	C	1.2731	0.327	6.3	0	6061-T6	0.080	0.65x0.8	2.5/1/1	2 PLIES (2X) TRIAXIAL KEVLAR/2219-T81	0.125	0.2x1.0	Y
4-0457	2024-T4	C	0.4975	0.383	3	0	6061-T6	0.080	0.485	2.5/1/1	2 PLIES (2X) TRIAXIAL KEVLAR/2219-T81	0.125	0	N
4-0459	2024-T4	C	1.0024	0.304	6.24	0	6061-T6	0.080	0.725	3.5/1	MMA II.2-08-005/2219-T81	0.125	0.5x7.0	Y
4-0462	2024-T4	C	1.0045	0.304	3.17	0	6061-T6	0.080	0.575	2.5/1/1	0.02" 2024/2 PLIES TRIAX KEVLAR/2219-T81	0.125	0.25	Y
4-0463	2024-T4	C	1.0011	0.304	6.43	0	6061-T6	0.080	0.685	2.5/1/1	0.02" 2024/2 PLIES TRIAX KEVLAR/2219-T81	0.125	0	N
4-0465	2024-T4	C	1.0021	0.304	6.37	0	6061-T6	0.080	0.675	2.5/.5/.5/1	(3X)KEVLAR 49/EPOXY / 2219-T81	0.125	0	N
4-0466	2017-T4	S	1.2728	0.375	6.23	0	6061-T6	0.080	TBD	2.5/1/1	2 PLIES (2X) TRIAXIAL KEVLAR/2219-T81	0.125	0.7	Y
4-0474	2024-T4	C	0.9868	0.304	6.44	0	6061-T6	0.080	0.675	2.5/2	3 PLIES TRIAXIAL KEVLAR/2219-T81	0.125	0	N
4-0477	2024-T4	C	0.9869	0.304	6.39	0	6061-T6	0.080	0.71	2.5/2	2 PLIES TRIAXIAL KEVLAR/2219-T81	0.125	0	N
4-0478	2024-T4	C	1.2475	0.327	6.4	0	6061-T6	0.080	0.685	2.5/1/1	2 PLIES (2X) TRIAXIAL KEVLAR/2219-T81	0.125	0.5	Y
4-0479	2024-T4	C	1.0021	0.304	6.55	0	6061-T6	0.080	0.65	1/3.5	2 PLIES TRIAXIAL KEVLAR/2219-T81	0.125	0.4	Y
4-0480	2024-T4	C	1.0018	0.304	6.39	0	6061-T6	0.080	0.675	3.5/1	2 PLIES TRIAXIAL KEVLAR/2219-T81	0.125	0	N
4-0482	2024-T4	C	1.0028	0.304	6.36	0	6061-T6	0.080	0.62x0.75	2.5/2	6 PLIES SPECTRA 900 / 2219-T81	0.125	0.5x2.5	Y
4-0484	2024-T4	C	1.0019	0.304	6.42	0	6061-T6	0.063	0.69	2.5/2	2 PLIES TRIAXIAL KEVLAR/2219-T81	0.125	1.5	Y
4-0491	2024-T4	C	0.4973	0.241	2.96	0	6061-T6	0.080	0.465	3.5/1	2 PLIES TRIAX KEVLAR/ 2219-T87	0.125	0.29	Y
4-0492	2024-T4	C	2.015	0.383	6.36	0	6061-T6	0.080	0.765	4/1/1	2 PLIES (2X) TRIAXIAL KEVLAR/2219-T87	0.125	1.5	Y
4-0501	2024-T4	C	1.5095	0.348	6.42	0	6061-T6	0.080	0.735	4/1/1	2 PLIES (2X) TRIAXIAL KEVLAR/2219-T87	0.125	0.1	T
4-0502	2024-T4	C	1.0028	0.304	6.49	0	6061-T6	0.080	0.68	2.5/2	4 PLIES 8 OZ KEVLAR/2219-T87	0.125	0	N
4-0505	2024-T4	C	1.0053	0.304	6.42	0	6061-T6	0.080	0.678	3.5/1	2 PLIES 8 OZ KEVLAR/2219-T87	0.125	0.1	Y
4-0506	2024-T4	C	2.0232	0.383	6.36	0	2219-T87	0.125	0.95	9/3	8 PLIES 8 OZ KEVLAR/2219-T87	0.125	0	N
4-0507	2017-T4	S	1.2735	0.375	6.42	0	6061-T6	0.080	0.725	3.5/1	8 PLIES 8 OZ KEVLAR/ 5456-H116	0.125	0	N
4-0508	2024-T4	C	1.0038	0.304	6.42	0	6061-T6	0.080	0.69	3.5/1	4 PLIES 8 OZ KEVLAR/2219-T87	0.125	0	T
4-0509	2024-T4	C	1.0025	0.304	6.79	0	6061-T6	0.080	0.68	3.5/1	4 PLIES 8 OZ KEVLAR/2219-T87	0.125	0	N
4-0510	2024-T4	C	1.0038	0.304	6.96	0	6061-T6	0.080	TBD	3.5/1	4 PLIES 8 OZ KEVLAR/2219-T87	0.125	TBD	Y
4-0511	2017-T4	S	1.2747	0.375	6.42	0	6061-T6	0.080	0.73	2/1/1	2 PLIES (2X) 17 OZ KEVLAR /5456-H116	0.125	0	N
4-0512	2017-T4	S	1.2718	0.375	6.31	0	6061-T6	0.080	TBD	3.5/1	4 PLIES 8 OZ KEVLAR/5456-H116	0.125	TBD	N
4-0513	2024-T4	C	1.5053	0.348	6.34	0	6061-T6	0.080	0.74	3.5/1	8 PLIES 8 OZ KEVLAR/5456-H116	0.125	4.0 X 3.0	Y
4-0515	2017-T4	S	0.3733	0.25	3.01	0	6061-T6	0.080	0.43	3.5/1	4 PLIES 8 OZ KEVLAR 5456-H116	0.125	0.31	Y
4-0516	2017-T4	S	0.3729	0.25	3.93	0	6061-T6	0.080	0.48	3.5/1	4 PLIES 8 OZ KEVLAR 5456-H116	0.125	0	N
4-0517	2024-T4	C	2.025	0.383	6.3	0	2219-T87	0.125	0.92	6/2	8 PLIES 8 OZ KEVLAR/2219-T87	0.125	0.01	Y
4-0527	2024-T4	C	1.0021	0.304	6.31	0	6061-T6	0.080	0.71	4.5/0	4 PLIES 8 OZ KEVLAR/2219 -T87	0.125	2.0" SPLIT	Y
4-0528	2024-T4	C	1.002	0.304	6.16	0	6061-T6	0.080	0.675	3.5/1	4 PLIES 8 OZ KEVLAR/2219-T87	0.125	0	N
4-0529	2024-T4	C	1.0004	0.304	6.17	0	6061-T6	0.063	0.625	3.5/1	4 PLIES 8 OZ KEVLAR/2219-T87	0.125	0.9 X 1.2	Y
4-0530	2024-T4	C	1.0004	0.304	6.1	0	2024-T3	(3)0.020	0.40,1.47	3.5/1	4 PLIES 8 OZ KEVLAR/2219-T87	0.125	0.4 x0.56	Y
4-0531	2024-T4	C	1.0033	0.304	6.34	0	COPPER	0.026	0.525	3.5/1	4 PLIES 8 OZ KEVLAR/2219-T87	0.125	0	N
4-0533	2024-T4	C	1.0079	0.304	6.95	0	6061-T6	0.080	0.7	3.5/1	4 PLIES 8 OZ KEVLAR/ 5456-H116	0.1	0	N
4-0534	2024 -T4	C	1.0061	0.304	7	0	6061-T6	0.080	0.71	3.5/1	4 PLIES 8 OZ KEVLAR/5456-H116	0.08	1.5	Y
4-0535	2024-T4	C	1.0066	0.304	6.98	0	6061-T6	0.080	0.695	3.5/1	4 PLIES 8 OZ KEVLAR/5456-H116	0.1	1.28	Y
4-0541	2024-T4	C	2.0189	0.383	6.37	45	6061-T6	0.080	0.82x1.3	3.5/1	4 PLIES 8 OZ KEVLAR/5456-H116	0.125	3.5x5.0	Y
4-0542	2024-T4	C	1.5087	0.348	6.48	45	6061-T6	0.080	0.76x0.96	3.5/1	4 PLIES 8 OZ KEVLAR/ 5456-H116	0.125	0.65x1.0	Y
4-0543	2024-T4	C	1.2493	0.327	6.36	45	6061-T6	0.080	0.76x0.93	3.5/1	4 PLIES 8 OZ KEVLAR/ 5456-H116	0.125	1.2	Y

UDRI ID.NO.	WITNESS MATERIALS	SPACING in	THICK. in	DEPTH of PEN. in	HOLEOUT DIA. in	COMMENTS
PRELIM.						PETALLED HOLE
PRELIM.	NONE					1 " HOLE IN HEAT PIPE
4-0316	2024-T3	4	0.002	0.02+	0.25	1 PINHOLE ONLY WALL,6 PENETRATIONS > 0.25" IN 1ST WITNESS PLATE, SABOT DAMAGE
4-0317	2024-T3	4	0.02	0.02+	0.25	BAD SHOT SABOT DAMAGE
4-0402	2024-T3	0.5	0.02	0.02+	2.0x5.0	7" DIAMETER CRATER AREA ON WITNESS PLATE
4-0408	2024-T3	4	0.02	0.1	3	5 WITNESS PLATES PENETRATED
4-0417	2024-T3	0.5	0.02	0.04	0.5x2.5	2 WITNESS PLATES PENETRATED BY SPALL, 2" DIA. SPALL AREA
4-0435	2024-T3	0.5	0.02	0.03	0	SMALL DENT AND10"DIA CRATER AREA ON WITNESS PLATE
4-0436	2024-T3	0.5	0.02	1.2	3	5 WITNESS PLATES PENETRATED,5" DIA CRATER ON 1ST WITNESS PLATE
4-0438	NONE	-	-	-	-	0.02" 2024-T3 9" FROM BUMPER,12" SPACING, 6" DIA. CRATER ON WALL, 0.125" MAX CRATER DEPTH
4-0446	TBD	TBD	TBD	TBD	TBD	WITNESS PLATE DENTED
4-0454	2024-T3	0.5	0.02	0	0	0.3" DEEP, 3.8" DIA DENT IN WALL
4-0455	2024-T3	0.5	0.02	0.04	TBD	1 FRAGMENT THROUGH WALL AND 2 WITNESS PLATES
4-0456	2024-T3	0.5	0.02	0.8	0.75	WALL SPLIT IN HALF, 4 WITNESS PLATES PENETRATED, 1 DENTED
4-0457	2024-T3	0.5	0.02	0	0	SMALL BULGE IN WALL NO FAILURE, DEEPEST CRATER 0.100"
4-0459	2024-T3	0.5	0.02	0.06	PLATE SPLIT	WALL SPLIT IN HALF- HIGH STRAIN FAILURE,3 WITNESS PLATES PENETRATED, 2 DENTED
4-0462	2024-T3	0.5	0.02	0.02	0.5	0.02" 2024 &2 KEVLAR INTERMEDIATE LAYERS,2 SPLITS ~0.7" LONG IN WALL
4-0463	2024-T3	0.5	0.02	0	0	0.02" 2024 &2 KEVLAR INTERMEDIATE LAYERS, WALL BULGE- 2.5"x 3.5", DENT IN FIRST WITNESS PLATE
4-0465	2024-T3	0.5	0.02	0	0	3 SHEETS INTERMEDIATE KEVLAR/EPOXY,1.5" DIA BULGE IN WALL
4-0466	2024-T3	0.5	0.02	0.6	1.7	WALL SPLIT IN HALF
4-0474	2024-T3	0.5	0.02	0	0	3 PLIES TRIAXIAL KEVLAR (2.5"); 0.2" DENT IN WALL; TARGET CLAMPED IN FOLLOWING TESTS
4-0477	2024-T3	0.5	0.02	0	0	2 PLIES TRIAXIAL KEVLAR (2.5"); 0.25" DENT IN WALL
4-0478	2024-T3	0.5	0.02	0.04	SPLIT	2 PLIES (2X) TRIAXIAL KEVLAR (2.5"/3.5"); PLATE SPLIT
4-0479	2024-T3	0.5	0.02	0.08	1.5	2 PLIES TRIAXIAL KEVLAR (1"); "JET" HOLE THROUGH WALL AND WITNESS PLATES
4-0480	2024-T3	0.5	0.02	0	0	2 PLIES TRIAXIAL KEVLAR (3.5"); 0.5 " DENT,WITNESS PLATE ALSO DENTED
4-0482	2024-T3	0.5	0.02	0.06	1.1	3 WITNESS PLATES SPLIT , 1 DENTED
4-0484	2024-T3	0.5	0.02	0.04	1.5	2 PLIES TRIAXIAL KEVLAR (2.5"),WALL SPLIT,2 WITNESS PLATES PENETRATED, 2 DENTED
4-0491	TBD	TBD	TBD	TBD	TBD	2 WITNESS PLATES TORN,7 FRAGMENTS THROUGH WALL
4-0492	2024-T3	0.5	0.02	0.12	2	(4) 4.0" AVG LENGHT PETALS IN WALL, 6 WITNESS PLATES PETAL DAMAGED
4-0501	2024-T3	0.5	0.02	0	0	10" DIA , 0.5" DEEP DENT IN WALL, 1ST WITNESS PLATE DENTED
4-0502	2024-T3	0.5	0.02	0.02	0	SOME Al SPRAY, 0.40" DEEP, 9.0" DIA. DENT IN WALL
4-0505	2024-T3	0.5	0.02	0.02	0.5	0.5" BULGE IN WALL
4-0506	2024-T3	0.5	0.02	0	0	3" DIA. CRATER PATTERN ON WALL, DEEPEST CRATER 0.02"
4-0507	2024-T3	0.5	0.02	0	0	FIBER PATTERN & 10" DIA,~1.325 DEEP DENT IN WALL ,3 WITNESS PLATES DENTED
4-0508	2024-T3	0.5	0.02	0	0	10.0" DIA. , 0.60" DEEP DENT IN WALL
4-0509	2024-T3	0.5	0.02	0	0	9.5" DIA ,0.7" DEEP DENT IN WALL, 1.5" DIA CRATER AREA AND DENT ON WITNESS PLATE
4-0510	2024-T3	0.5	0.02	0.04	0.5x5	4 TEARS IN WALL , 2 WITNESS PLATES PENETRATED
4-0511	2024-T3	0.5	0.02	0	0	10" DIA, 0.98" DEEP DENT IN WALL, 2 WITNESS PLATES DENTED
4-0512	2024-T3	0.5	0.02	0	0	1.125" DEEP DENT IN WALL , 3 WITNESS PLATES DENTED
4-0513	2024-T3	0.5	0.02	0.04	2	(4) 3.0" AVG LENGHT PETALS IN WALL, 4 WITNESS PLATES DENTED
4-0515	2024-T3	0.5	0.02	0.04	0.415	2.5" DIA CRATER AREA ON WALL
4-0516	2024-T3	0.5	0.02	0	0	SEVERAL DIMPLES,0.125" DEEP DENT IN WALL
4-0517	2024-T3	0.5	0.02	0	0	0.375" DEEP DENT SEVERAL PINHOLES & DIMPLES IN WALL, WITNESS PLATE DAMAGED
4-0527	2024-T3	0.5	0.02	0.08	1.0 SPLIT	CRESCENT SHAPED SPLIT IN WALL,4 WITNESS PLATES SPLIT, 2 DENTED
4-0528	2024-T3	0.5	0.02	0	0	DENT IN WALL, 0.05" DEEP DENT IN WITNESS PLATE
4-0529	2024-T3	0.5	0.02	0.06	1.3	(4) 2" AVG LENGHT PETALS IN WALL, 3 WITNESS PLATES PENETRATED, 1 DENTED
4-0530	2024-T3	0.5	0.02	0.12	1.7	MULTIPLE BUMPER TEST, 6 WITNESS PLATES PENETRATED
4-0531	2024-T3	0.5	0.02	0	0	~ 0.5" DEEP DENT IN WALL , 0.03" DEEP DENT IN WITNESS PLATE
4-0533	2024-T3	0.5	0.02	0	0	1.2" DEEP, 9.0" DIA DENT IN WALL;3 WITNESS PLATES DENTED
4-0534	2024-T3	0.5	0.02	0.04	1	(5)PETALS 2.0"AVG LENGTH IN WALL; 2 WITNESS PLATES BROKEN,2 DENTED
4-0535	2024 T3	0.5	0.02	0	0	"TRAPDOOR" FAILURE, NO WITNESS PLATES PENETRATED
4-0541	2024-T3	0.5	0.02	0.04	2.5x3.0	45° OBLIQUE SHOT, (4) 2.0"AVG LENGHT PETALS IN WALL,2 WITNESS PLATES PENETRATED
4-0542	2024-T3	0.5	0.02	0.04	1.7	(2) 1" AVG LENGHT PETALS IN WALL , 2 WITNESS PLATES PENETRATED
4-0543	2024-T3	0.5	0.02	0.04	0.2x1.7	2 WITNESS PLATES PENETRATED

		PROJECTILE CHARACTERISTICS						BUMPER			REAR WALL			
UDRI	PROJECTILE	CYL.	MASS	DIA.	VELOC.	OBL.	BUMPER	THICK.	HOLE	SPACE	REAR WALL	THICK.	HOLEOUT	PEN
ID.NO.	MATERIAL	/SPHERE	g	in	km/s	deg	MATERIAL	in	DIA. in	in	MATERIAL	in	DIA. in	Y,N,T
4-0544	2024-T4	C	0.9988	0.304	6.43	45	6061-T6	0.080	0.71x0.87	3.5/1	4 PLIES 8 OZ KEVLAR/5456-H116	0.125	0.65	Y
4-0545	2024-T4	C	1.0054	0.304	6.34	45	CORR.Al 0.08 Eff.	0.75(.08)	5.0x0.68	3.5/1	4 PLIES 8 OZ KEVLAR/5456-H116	0.125	0	N
4-0571	2017-T4	S	1.2719	0.375	6.37	0	6061-T6	0.080	0.72	3.5/1	4 PLIES 8 OZ KEVLAR/ 6061-T6	0.125	0	N
4-0572	2024-T4	C	1.004	0.304	6.37	0	CORR.Al 0.08 Eff.	0.75(.08)	0.47x0.61	3.5/1	4 PLIES 8 OZ KEVLAR/ 5456-H116	0.125	0.7	Y
4-0573	2017-T4	S	1.2728	0.375	6.54	65	6061-T6	0.080	0.74x1.25	3.5/1	4 PLIES 8 OZ KEVLAR/5456-H116	0.125	0.22	Y
4-0590	2024-T4	C	1.5085	0.348	6.51	0	6061-T6	0.080	0.755	3.5/1	8 PLIES 8 OZ KEVLAR/6061-T6	0.125	0.3x4.0	N
4-0591	2017-T4	S	1.2715	0.375	6.58	0	6061-T6	0.080	0.8	3.25/1.25	4 PLIES 8 OZ KEVLAR/5456-H116	1.25	0	N
4-0592	2024-T4	C	1.5055	0.348	6.57	0	6061-T6	0.080	0.74	3.25/1.25	6 PLIES 8 OZ KEVLAR/5456-H116	1.25	2.5x3.5	Y
4 -0593	2024-T4	C	2.0283	0.383	6.51	0	6061-T6	0.080	0.775	3.25/1.25	6 PLIES 8 OZ KEVLAR/5456-H116	1.25	3 x3.5	Y
4-0594	Al	S	0.1582	0.1875	2.79	0	6061-T6	0.080	0.325	3.5/1	4 PLIES 8 OZ KEVLAR/5456-H116	0.125	0	N
4-0595	Al	S	3.0072	0.5	6.42	0	2219-T87	0.125	1.1	6/2	12 PLIES 8 OZ KEVLAR/ 2219-T87	0.125	0	N
4-0597	2017-T4	S	2.9879	0.5	6.36	0	6061-T6	0.080	TBD	3.5/1	4 PLIES 8 OZ KEVLAR/2219-T87	0.125	TBD	Y
4-0599	2017-T4	S	1.2712	0.375	6.49	0	6061-T6	0.080	0.72	3.5/1	4 PLIES 8 OZ KEVLAR/2219-T62	0.125	0	T
4-0600	2024-T4	C	1.5049	0.348	6.48	0	6061-T6	0.080	0.75	3.5/1	8 PLIES 8 OZ KEVLAR/6061-T6	0.125	2.4	Y
4-0602	2017-T4	S	2.988	0.5	6.36	0	6061-T6	0.08	TBD	3.5/1	4 PLIES 8 OZ KEVLAR/5456-H116	0.125	8	Y
4-0603	2017-T4	S	1.2724	0.375	6.6	0	6061-T6	0.08	0.732	3.5/1	4 PLIES 8 OZ KEVLAR/5456-H116	0.125	2.5x0.4	Y
4-0604	2024-T4	C	1.0039	0.304	5.64	0	6061-T6	0.080	TBD	3.5/1	6 PLIES 8 OZ KEVLAR/5456-H116	0.125	1x2	Y
4-0605	2017-T4	S	0.3732	0.25	2.97	0	6061-T6	0.080	0.425	3.5/1	6 PLIES 8 OZ KEVLAR/5456-H116	0.125	0.275	Y
4-0608	2017-T4	S	1.2714	0.375	6.57	0	6061-T6	0.08	0.734	3.25/1.25	4 PLIES 8 OZ KEVLAR/2219-T851	0.125	8	Y
4-0609	2017-T4	S	2.9888	0.5	6.42	0	6061-T6	0.08	0.855	3.25/1.25	4 PLIES 8 OZ KEVLAR/2219-T851	0.125	8	Y
4-0610	2017-T4	S	1.2727	0.375	6.55	0	6061-T6	0.08	0.745	3.5/1	4 PLIES 8 OZ KEVLAR/2219-T87	0.125	0	N
4-0611	2017-T4	S	2.9885	0.5	6.28	0	6061-T6	0.08	0.84	3.25/1.25	4 PLIES 8 OZ KEVLAR/5456-H116	0.2	TBD	Y
4-0612	2017-T4	S	2.9881	0.5	6.28	0	6061-T6	0.08	0.85	3.25/1.25	4 PLIES 8 OZ KEVLAR/2219-T851	0.125	TBD	Y
4-0613	2017-T4	S	3.0014	0.5	6.36	0	6061-T6	0.08	TBD	3.5/1	4 PLIES 8 OZ KEVLAR/2219-T851	TBD	TBD	
4-0614	2017-T4	S	2.9999	0.5	6.28	0	6061-T6	0.08	TBD	3.5/1	4 PLIES 8 OZ KEVLAR/5456-H116	TBD	TBD	
4-0646	2017-T4	S	0.7336	0.312	6.74	0	6061-T6	0.063		3/1.5	3 PLIES 8OZ KEVLAR/ 5456-H116	0.1		Y
4-0647	2017-T4	S	0.1589	0.187	3.08	0	6061-T6	0.063		3/1.5	3 PLIES 8OZ KEVLAR/ 5456-H116	0.1		Y
4-0648	2017-T4	S	0.045	0.125	2.84	0	6061-T6	0.063		3/1.5	3 PLIES 8OZ KEVLAR/ 5456-H116	0.1		N
4-0650	2017-T4	S	0.3762	0.25		45	6061-T6	0.063		3/1.5	3 PLIES 8OZ KEVLAR/ 5456-H116	0.1		
4-0651	2017-T4	S	0.3726	0.25	6.69	45	6061-T6	0.063		3/1.5	3 PLIES 8OZ KEVLAR/ 5456-H116	0.1		N
4-0652	2017-T4	S	0.3733	0.25	6.28	45	6061-T6	0.063		3/1.5	3 PLIES 8OZ KEVLAR/ 5456-H116	0.1		Y
4-0653	2017-T4	S	0.1588	0.187	5.1	45	6061-T6	0.063		3/1.5	3 PLIES 8OZ KEVLAR/ 5456-H116	0.1		Y
4-0654	2017-T4	S	0.1583	0.187	5.97	45	6061-T6	0.063		3/1.5	3 PLIES 8OZ KEVLAR/ 5456-H116	0.1		N
4-0655	2017-T4	S	0.3727	0.25	6.82	65	6061-T6	0.04		3/1.5	3 PLIES 8OZ KEVLAR/ 5456-H116	0.1		N
4-0656	2017-T4	S	0.3724	0.25	6.85	65	6061-T6	0.063		3/1.5	3 PLIES 8OZ KEVLAR/ 5456-H116	0.1		N
4-0657	2017-T4	S	0.7313	0.312	6.61	65	6061-T6	0.063		3/1.5	3 PLIES 8OZ KEVLAR/ 5456-H116	0.1		Y
4-0660	2017-T4	S	1.2716	0.375	6.67	0	6061-T6	0.63		3/1.5	3 PLIES (2X) 8OZ KEVLAR/5456-H116	0.1		N
4-0661	2017-T4	S	3.0014	0.5	6.24	0	6061-T6	0.63		3/1.5	3 PLIES (3X) 8OZ KEVLAR/5456-H116	0.1		N
4-0662	2017-T4	S	0.3725	0.25	6.33	45	6061-T6	0.63		3/1.5	3 PLIES 8OZ KEVLAR/5456-H116	0.125		N
4-0671	1100	S	0.0059	0.0625	6.75	0	3 PLIES 8OZ KEVLAR			4	5456-H116	0.1	0	N
4-0673	2017-T4	S	0.3731	0.25	6.8	45	7075-T6	0.063		3/1.5	3 PLIES 8OZ KEVLAR/5456-H116	0.1		Y
4-0674	2017-T4	S	0.3731	0.25	6.8	45	7075-T6	0.04		3/1.5	3 PLIES 8OZ KEVLAR/5456-H116	0.1		Y
4-0675	2017-T4	S	3.0032	0.5	5.72	0	3 LAYERS 6061-T6	0.063		3x(3/1.5)	3 PLIES (3X) 8OZ KEVLAR/5456-H116	0.1		N
4-0724	2017-T4	S	1.275	0.375	6.38	0	6061-T6	0.08		3/1.5	2519-T81 (NOT 2219)	0.125		Y
4-0736	2017-T4	S	3.0028	0.5	4.37	0	3 LAYERS 6061-T6	0.063		3x(3/1.5)	3 PLIES (3X) 8OZ KEVLAR/5456-H116	0.1		N
4-0737	2017-T4	S	1.2727	0.375	2.83	0	3 LAYERS 6061-T6	0.063		3x(3/1.5)	3 PLIES (3X) 8OZ KEVLAR/5456-H116	0.1		N

		WITNESS MATERIALS				
UDRI	WITNESS	SPACING	THICK.	DEPTH of	HOLEOUT	COMMENTS
ID.NO.	MATERIALS	in	in	PEN. in	DIA. in	
4-0544	2024-T3	TBD	0.02	0.02	0.01	1 WITNESS PLATE PENETRATED
4-0545	2024-T3	TBD	0.02	0	0	CORRUGATED BUMPER (32/20/20MILS 0.75" THICK) SPLIT, DEPEST CRATER IN WALL 0.080"
4-0571	2024-T3	0.5	0.02	0	0	1.0" DEEP,9.0" WIDE DENT IN WALL
4-0572	2024-T3	0.5	0.02	0.04	0.2	(4) 1" AVG LENGHT PETALS IN WALL, 2 WIT. PLT. PENETRATED, CORR.BUMPER(32/20/20MILS 0.75 THICK)
4-0573	2024-T3	0.5	0.02	TBD	TBD	65° OBLIQUE SHOT, 3 SMALL HOLES IN WALL
4-0590	2024-T3	0.5	0.02	0	0	10" X 10" AND 1.6 " DEEP DENT IN WALL,2 WITNESS PLATES DENTED
4-0591	2024-T3	0.5	0.02	0	0	~ 0.625" DOUBLE BULGE, 0.60" DEEP DENT IN WALL
4-0592	2024-T3	0.5	0.02	0	0	3"X 3.5" KITE-SHAPED HOLE, WALL TORN ON RIGHT SIDE OF RIB, WAFFLE WALL
4 -0593	2024-T3	0.5	0.02	0	0	TORN ON BOTH SIDES RIB,WAFFLE WALL
4-0594	2024-T3	0.5	0.02	0	0	WALL DENTED/CRATERED 1" X 2" CRATER AREA, DEEPEST CRATER 0.110" AND 0.215" DIA.
4-0595	2024-T3	0.5	0.02	0	0	1.8" DEEP DENT IN 12" X12" WALL PANEL
4-0597						WALL LOADED 1500#/IN
4-0599	2024-T3	0.5	0.02	0	0	1.1" DEEP DENT IN WALL,NOTE: 0.60" LONG CRACK ON BACKSIDE BUT NO PENETRATRATION
4-0600	2024-T3	0.5	0.02	0.04	1.0x2.0	(3) 4" AVG LENGHT PETALS IN WALL, 2 WITNESS PLATES PENETRATED
4-0602	2024-T3					WALL LOADED 1500#/IN
4-0603	2024-T3	0	0.02	0	0	WALL LOADED 1500#/IN,WITNESS STANDOFF 4.625", WITNESS PLATE DENTED
4-0604	2024-T3	0.5	0.02	TBD	TBD	(4)1.5" AVG LENGHT PETALS IN WALL
4-0605	2024-T3	0.5	0.02	0.02	0.275x0.43	1 CELOTEX PENETRATED AND 1 DENTED
4-0608	2024-T3	4.125	0.02	7.02	4.0x2.0	(7) PETALS IN WALL AVG LENGHT 7" (1.25",45°,WAFFLE WALL LOADED 1500#/IN)
4-0609	2024-T3	4.125	0.02	7.02	4.0x2.0	(7) 7" AVG LENGHT PETALS IN WALL (LOADED 1500#/IN)
4-0610	2024-T3	4.125	0.02	0	0	8" DIA,0.5" DEEP DENT IN WALL (LOADED 1500#/IN)
4-0611	2024-T3	4.625	0.02	> 0.490	0.5x0.3	1" ORTHGONAL WALL (LOADED 2050#/IN)
4-0612	2024-T3	4.625	0.02	0.49	1.5	WALL CRACKED IN HALF (LOADED 2400#/IN),0.8"x0.6" HOLE IN CELOTEX
4-0613	2024-T3	4.625	0.02	TBD	TBD	WALL LOADED 1500#/IN
4-0614	2024-T3	4.625	0.02	TBD	TBD	CENTER RIB REMOVED FROM WALL (LOADED 2400#/IN)
4-0646						
4-0647						
4-0648						
4-0650						SABOT FAILED
4-0651						
4-0652						
4-0653						
4-0654						
4-0655						RICOCHET PANEL RIVETED TO BUMPER
4-0656						
4-0657						
4-0660						
4-0661						
4-0662						
4-0671						
4-0673						
4-0674						
4-0675						
4-0724						PLATE SPLIT LIKE 2219.
4-0736						
4-0737						

C-6

	standoff inch	rearwall gage inch	bumper gage inch	rearwall alloy	bumper alloy	mli present	mli location	prj. len to dia	prj. material	obliquity	projectile size	velocity avg km/s	near penet'n	rearwall inch	rearwall spall	bumper hole inch	vel hall km/s	vel xray km/s	witness panel	rico con	test number	data source	test	date	comments
1	0	0.13		2219-T87	B CLOTH	TPS			1100-O	0	0.13	7.7		0.4			7.6	7.8			730		GRIT-9	08/16/88	
2	4	0.05	0.05	2219-T87	6061-T6	B	3.75		1100-O	75	0.31	7.1	N	0	N	1.53	7.1	7	0	CRATERED	1181		4108-D	11/27/90	WALL CRATERED ONLY.
3	4	0.06	0.03	2219-T87	6061-T6	NO			1100-O	0	0.31	6	Y	0.8	Y	0.49	5.9	6.1	4		406	IWALL	SS-228A	12/11/86	
	4	0.06	0.03	2219-T87	6061-T6	NO			1100-O	0	0.31	6.8	Y	0.8	Y	0.5		6.8	4		407	IWALL	SS-228B	12/11/86	
4	4	0.06	0.03	2219-T87	6061-T6	YES			1100-O	45	0.25	5.6	Y	0.5	N	0.6	5.5	5.6	3	CAVITIES	399	IWALL	SS-227A	12/04/86	
	4	0.06	0.03	2219-T87	6061-T6	YES			1100-O	45	0.25	7.2	Y	1	N	0.6	7.1	7.3	2	CAVITIES	410	IWALL	SS-227B	12/12/86	
5	4	0.1	0.03	2219-T87	6061-T6	YES			1100-O	45	0.25	4.5	Y	0.5	N	0.51	4.4	4.5	4	CAVITIES	394	IWALL	SS-226A	11/24/86	
	4	0.1	0.03	2219-T87	6061-T6	YES			1100-O	45	0.25	5.5	Y	0.8	N	0.56		5.5	4	CAVITIES	397	IWALL	SS-226B	12/01/86	
	4	0.1	0.03	2219-T87	6061-T6	YES			1100-O	45	0.25	6.7	Y	0.4	N	0.7	6.7	6.8	2	CAVITIES	398	IWALL	SS-226C	12/03/86	
6	4	0.1	0.04	2219-T87	6061-T6	YES	W		1100-O	0	0.25	4.4	Y	0.3	N	0.48		4.4	0		178	ADP SM1	SS-P-034C-1	03/14/86	
	4	0.1	0.04	2219-T87	6061-T6	YES	W		1100-O	0	0.25	5.5	N	0	N	0.51		5.5	0		177	ADP SM1	SS-P-034C	03/13/86	
7	4	0.13	0.03	2219-T87	6061-T6	NO			1100-O	45	0.3	3.5	Y	0.5	N	0.63		3.5	3		175	MARTIN	SS-114B	03/12/86	
8	4	0.13	0.03	2219-T87	6061-T6	YES	B		1100-O	0	0.19	7.2	Y	0.2	Y	0.34	7.3	7.2			897		MLI-B3	12/12/89	SPALL AROUND HOLES
	4	0.13	0.03	2219-T87	6061-T6	YES	B		1100-O	0	0.19	7.8	S	0	Y	0.38	7.8	7.8			898		MLI-B4	12/13/89	COUNT SPALL AS FAILURE
9	4	0.13	0.03	2219-T87	6061-T6	YES	W		1100-O	0	0.19	4	Y	0.4	Y	0.28		4	2		798		3001-A	09/08/89	SMALL CRATERS UP TO 0.12" DIA X 0.05" DEEP IN AREA APPROX. 3.5" DIA. NO DIMPLES ON REAR, SPALLING AROUND HOLE APPROX. 0.06" WIDE AND 0.05" DEEP. OTHER CRATERS 0.2" DIA AND 0.2" DEEP FEW VERY SLIGHT DIMPLES ON REAR.
	4	0.13	0.03	2219-T87	6061-T6	YES	W		1100-O	0	0.19	5.8	Y	0.2	N	0.35	5.8	5.8	1		799		3001-B	09/14/89	2 HOLES: APPROX. 0.2" DIA AND ONE PIN HOLE. NO SINK AREA, VERY FEW CRATERS, 2 CRATERS AT EDGE OF HOLE APPROX. .2" DIA AND .05" DEEP. OTHER CRATERS 0.2" DIA AND .02" DEEP, FEW VERY SLIGHT DIMPLES ON REAR.
	4	0.13	0.03	2219-T87	6061-T6	YES	W		1100-O	0	0.19	6.3	Y	0.2	N	0.35	6.2	6.3	0		800		3001-C	09/14/89	3 HOLES, APPROX. 0.2" DIA X 0.1" DIA, 0.06" DIA AND 0.03" DIA, FEW SMALL CRATERS, SLIGHT BULGE ON REAR.
	4	0.13	0.03	2219-T87	6061-T6	YES	W		1100-O	0	0.19	6.8	Y	0.2	N	0.35	6.8	6.9	0		802		3001-E	09/18/89	HOLE .2X.1", MOST OF DAMAGE APPROX. 1" DIA, ONE CRATER APPROX. .2" I 10m HOLE APPROX. .15" DIA AND .07 DEEP, FEW SMALL CRATERS LESS THAN 0.060" DIA.
	4	0.13	0.03	2219-T87	6061-T6	YES	W		1100-O	0	0.19	7.2	N	0	N	0.52	7.2	7.3			801		3001-D	09/15/89	3 VERY SLIGHT CRATERS
10	4	0.13	0.03	2219-T87	6061-T6	YES	W		1100-O	0	0.25	7	Y	0.9	N	0.46	7	7.1			803		3002-A	09/18/89	HOLE APPROX. .2" DIA X .1" DIA WITH CRACKS IN METAL APPROX. .7" AND .9" SINK APPROX. 2.5" DIA WITH MOST OF DAMAGE APPROX. 7" DIA. BULGE ON REAR APPROX .3"
	4	0.13	0.03	2219-T87	6061-T6	YES	W		1100-O	0	0.25	7.4	Y	2	N	0.42	7.3	7.5	2		804		3002-B	09/19/89	HOLE 2X1". MOST OF DAMAGE AT ONE END OF PETALED HOLE APPROX. " DIA, 2 HOLES APPROX. .1" DIA x .2" DIA APPROX. .2" FROM HOLE. SEVERAL CRATERS IN PETAL AND EDGE OF HOLE

	standoff inch	rearwall gage inch	bumper gage inch	rearwall alloy	bumper alloy	mli present	mli location	prj. len to dia	prj. material	obliquity	projectile size	velocity avg km/s	rear penetrn	rearhole inch	rearwall spall	bumper hole inch	vel hail km/s	vel xray km/s	witness penet.	rico con	test number	data source	test	date	comments
	4	0.13	0.03	2219-T87	6061-T6	YES	W		1100-O	0	0.25	7.7	N	0	N	0.46	7.5	7.8			806		3002-C	09/20/89	SINK .3" DIA X .3" DIA DEEP WITH SMALL CRATERS,..FEW SMALL CRATERS....
11	4	0.13	0.03	2219-T87	6061-T6	YES	W		1100-O	45	0.19	8.1	Y	0.3	N	0.44	6.1	6.1	0		963		3203	03/19/90	
	4	0.13	0.03	2219-T87	6061-T6	YES	W		1100-O	45	0.19	6.6	Y	0.1	N	0.48	6.6	6.7	0		810		3004-B	09/22/89	HOLE 0.1" DIA, ONE CRATER APPROX. 0.25" DIA WITH CRACK ON REAR. FEW VERY SMALL CRATERS.
	4	0.13	0.03	2219-T87	6061-T6	YES	W		1100-O	45	0.19	7	Y	0	N	0.43	6.8	7.2			807		3004-A	09/21/89	PINHOLE, DAMAGE AREA APPROX. 1.5" DIA X 1" DIA SEVERAL CRATERS IN THIS AREA UP TO .2" DIA AND .05" DEEP ALL IN PROJECTILE PATH. VERY SLIGHT CRATERING UNDER BUMPER HOLE. 4 SMALL DIMPLES ON REAR.
	4	0.13	0.03	2219-T87	6061-T6	YES	W		1100-O	45	0.19	7.7	C	0	N	0.54	7.7	7.7	0		964		3204	03/19/90	REAR SURFACE CRACK ON WALL, COUNT AS FAILURE
12	4	0.13	0.03	2219-T87	6061-T6	YES	W		1100-O	45	0.25	6.5	Y	0.5	N	0.57	6.5	6.5	2		970		3207	03/23/90	
	4	0.13	0.03	2219-T87	6061-T6	YES	W		1100-O	45	0.25	7.5	Y	0.2	N	0.63	7.4	7.6	0		808		3005-A	09/21/89	2 HOLES IN PROJECTILE PATH APPROX. .20" DIA X .12" DIA AND APPROX. .1" DIA, MOST OF DAMAGE IN AREA APPORX. 1.2" DIA. FEW CRATERS UP TO .2" DIA AND .05" DEEP. FEW DIMPLES ON REAR.
	4	0.13	0.03	2219-T87	6061-T6	YES	W		1100-O	45	0.25	7.7	N	0	N	0.64	7.6	7.8	0		811		3005-B	09/26/89	DAMAGE AREA IN PROJECTILE PATH 1.7" DIA X 1" DIA WITH FEW CRATERS UP TO .12" DIA AND .040" DIA DEEP. FEW VERY SMALL CRATERS UNDER BUMPER PROJECTILE HOLE. SLIGHT BULGE ON REAR.
13	4	0.13	0.03	2219-T87	6061-T6	YES	W		1100-O	45	0.31	7.1	Y	0.8	N	0.75	7	7.2	3		812		3006-A	09/26/89	SEVERE CRACKS DAMAGE APPROX. 2/3 CIRCUMFERENCE OF HOLE
14	4	0.13	0.03	2219-T87	6061-T6	YES	W		1100-O	65	0.19	3.4	N	0	N	0.58	3.4	3.4			820		3007-C	10/02/89	VERY LITTLE DAMAGE, FEW SMALL CRATERS UNDER BUMPER HOLE, NO DIMPLES ON REAR.
	4	0.13	0.03	2219-T87	6061-T6	YES	W		1100-O	65	0.19	4.8	N	0	N	0.54	4.8	4.9	0		819		3007-B	10/02/89	CRATER IN PROJECTILE PATH APPROX. .2" DIA WITH DIMPLE ON REAR. FEW CRATERS BEGINNING UNDER BUMPER HOLE AND EXTENDING FOR AREA APPROX .3" DIA WIDE AND .3" DIA TOWARD PROJECTILE PATH. ONE CRATER .15" DIA AND .040" DIA DEEP WITH DIMPLE ON REAR. OTHER CRATER
	4	0.13	0.03	2219-T87	6061-T6	YES	W		1100-O	65	0.19	6.6	N	0	N	0.85	6.5	6.6	0		818		3007-A	09/29/89	NO DAMAGE IN PROJECTILE PATH. FEW CRATERS BEGINNING UNDER BUMPER HOLE UP TO APPROX. .1" DIA. 3 VERY SMALL DIMPLES ON REAR.
15	4	0.13	0.03	2219-T87	6061-T6	YES	W		1100-O	65	0.25	3.8	N	0	N	0.78	3.8	3.8	0		971		3208	03/23/90	
	4	0.13	0.03	2219-T87	6061-T6	YES	W		1100-O	65	0.25	4.3	Y	0.1	N	0.74	4.3	4.3	0		822		3008-B	10/03/89	FEW SMALL CRATERS IN SAME AREA. FEW SMALL CRATERS UNDER BUMPER HOLE NO DIMPLES ON REAR.
	4	0.13	0.03	2219-T87	6061-T6	YES	W		1100-O	65	0.25	4.7	N	0	N	0.77	4.6	4.7	0		821		3008-A	10/03/89	CRATER IN PROJECTILE PATH APPROX. .267" DIA X .17" DIA AND .08" DIA DEEP WITH DIMPLE ON REAR. FEW SMALL CRATER IN SAME AREA UNDER BUMPER HOLE SLIGHT DAMAGE TO AREA APPROX. .4" DIA FEW CRATERS UP TO .1" DIA WITH 3 SMALL DIMPLES ON REAR.
	4	0.13	0.03	2219-T87	6061-T6	YES	W		1100-O	65	0.25	5.6	N	0	N	0.95		5.6	0		974		3210	03/27/90	
16	4	0.13	0.03	2219-T87	6061-T6	YES	W		1100-O	65	0.31	3.6	Y	0.3	N	0.95	3.6	3.6	1		982		3212-1	04/05/90	

	standoff inch	rearwall gage inch	bumper gage inch	rearwall alloy	bumper alloy	mli present	mli location	prj. len to dia	prj. material	obliquity	projectile size	velocity avg km/s	rear penetrn	rearhole inch	rearwall spall	bumper hole inch	vel hall km/s	vel xray km/s	witness penet.	rico con	test number	data source	test	date	comments
	4	0.13	0.03	2219-T87	6061-T6	YES	W		1100-O	65	0.31	4.8	C	0	N	1	4.5	4.6	0		824		3009-B	10/04/89	NO HOLE, NO LIGHT CAN BE SEEN THROUGH CRATER IN PROJECTILE PATH THAT IS APPROX. .26" DIA X .18" DIA AND .15" DIA DEEP. DIMPLE ON REAR WITH VERY SMALL CRACK (COUNT CRACK AS FAILURE. SEVERAL SMALL CRATERS. UNDER BUMPER HOLE DAMAGE AREA IS APPROX. .4" DIA W
	4	0.13	0.03	2219-T87	6061-T6	YES	W		1100-O	65	0.31	5.2	Y	0	N	0.93	5.1	5.2			823		3009-A	10/04/89	PIN HOLE IN PROJECTILE PATH, SMALL CRACK IN METAL AT BOTTOM OF CRATER THAT IS APPROX. .24" DIA X .2" DIA, 2 CRATERS IN AREA APPROX. .2" DIA WITH DIMPLES ON REAR, FEW OTHER SMALL CRATERS UNDER BUMPER HOLE CRATER COVER AN AREA APPROX. 3.5" DIA FEW CRATERS
	4	0.13	0.03	2219-T87	6061-T6	YES	W		1100-O	65	0.31	6.1	C	0	N	1.05		6.1	0		979		3217	04/02/90	REAR SURFACE CRACK, COUNTED AS FAILURE
17	4	0.13	0.04	2219-T87	6061-T6	NO		1	LEXAN	0	0.38	6.4	Y	3	N	0.71	6.4		4		387	IWALL	SS-225D-1	11/06/86	
18	4	0.13	0.04	2219-T87	6061-T6	NO			1100-O	0	0.19	3.3	Y	0.1	Y	0.31	3.2	3.4			481	MSFC	SS-T2-2	02/26/87	
19	4	0.13	0.04	2219-T87	6061-T6	NO			1100-O	0	0.25	4.9	Y	0.2	N	0.44		4.9	1		182	ADP SM1	SS-P-033B	03/20/86	
	4	0.13	0.04	2219-T87	6061-T6	NO			1100-O	0	0.25	5.3	Y	0.3	Y	0.44		5.3	1		183	ADP SM1	SS-P-033B-1	03/24/86	
	4	0.13	0.04	2219-T87	6061-T6	NO			1100-O	0	0.25	5.5	C	0	N	0.44		5.5	0		184	ADP SM1	SS-P-033C	03/24/86	REAR SURFACE CRACK COUNTED AS FAILURE
	4	0.13	0.04	2219-T87	6061-T6	NO			1100-O	0	0.25	7.2	Y	0.1	Y	0.52		7.2	2		181	ADP SM1	SS-P-033	03/17/86	
20	4	0.13	0.04	2219-T87	6061-T6	NO			1100-O	0	0.31	4.3	Y	1	N	0.56	4.3	4.3			391	MSFC	SS-PT6A	11/19/86	
	4	0.13	0.04	2219-T87	6061-T6	NO			1100-O	0	0.31	4.6	Y	1	Y	0.48	4.6	4.7			475	MSFC	SS-T2-6	02/23/87	
21	4	0.13	0.04	2219-T87	6061-T6	NO			1100-O	0	0.38	5.4	Y	1.8	N	0.53	5.4	5.5			495	MSFC	SS-T2-16	03/11/87	
22	4	0.13	0.04	2219-T87	6061-T6	NO			1100-O	45	0.13	3.3	N	0	N	0.29	3.3	3.3	0	CAVITIES	359	IWALL	SS-222C	10/15/86	
	4	0.13	0.04	2219-T87	6061-T6	NO			1100-O	45	0.13	5	N	0	N	0.34		5	0	CAVITIES	358	IWALL	SS-222B	10/14/86	
	4	0.13	0.04	2219-T87	6061-T6	NO			1100-O	45	0.13	5.6	N	0	N	0.36		5.6	0	CAVITIES	357	IWALL	SS-222A	10/14/86	
23	4	0.13	0.04	2219-T87	6061-T6	NO			1100-O	45	0.19	3.2	Y	0.3	N	0.42	4.2	4.3	1		215	IWALL	SS-202B	06/05/86	
	4	0.13	0.04	2219-T87	6061-T6	NO			1100-O	45	0.19	3.5	Y	0.1	N	0.42	3.5	3.5	0		214	IWALL	SS-202A	06/05/86	
	4	0.13	0.04	2219-T87	6061-T6	NO			1100-O	45	0.19	5.3	Y	0.4	N	0.47	5.2	5.3	2	SPRAY	259	IWALL	SS-202C	07/14/86	
	4	0.13	0.04	2219-T87	6061-T6	NO			1100-O	45	0.19	6	Y	0.2	Y	0.48	5.9	6	0		504	MARTIN	SS-154B	04/02/87	
	4	0.13	0.04	2219-T87	6061-T6	NO			1100-O	45	0.19	6.4	Y	0.3	N	0.46	6.4	6.5	1	SPRAY	261	IWALL	SS-202D	07/14/86	
	4	0.13	0.04	2219-T87	6061-T6	NO			1100-O	45	0.19	6.8	N	0	N	0.55	6.8	6.9	0		503	MARTIN	SS-154A	04/02/87	
	4	0.13	0.04	2219-T87	6061-T6	NO			1100-O	45	0.19	7.2	Y	0.1	N	0.51	7.2	7.2	0	SPRAYED	262	IWALL	SS-202E	07/15/86	
	4	0.13	0.04	2219-T87	6061-T6	NO			1100-O	45	0.19	7.5	Y	0.2	N	0.54		7.5	0		263	IWALL	SS-202F	07/15/86	
24	4	0.13	0.04	2219-T87	6061-T6	NO			1100-O	65	0.25	3.2	N	0	N	0.72		3.2	0	HOLES	265	IWALL	SS-204D	07/16/86	
	4	0.13	0.04	2219-T87	6061-T6	NO			1100-O	65	0.25	4.3	N	0	N	0.83	4.2	4.3	0	2HOLES	247	IWALL	SS-204C	07/01/86	
	4	0.13	0.04	2219-T87	6061-T6	NO			1100-O	65	0.25	4.8	Y	0.1	N	0.78	4.7	4.8	0	HOLES	245	IWALL	SS-204A	06/30/86	

	standoff inch	rearwall gage inch	bumper gage inch	rearwall alloy	bumper alloy	mli present	mli location	prj. len to dia	prj. material	obliquity	projectile size	velocity avg km/s	rear penetrn	rearhole inch	rearwall spall	bumper hole inch	vel hall km/s	vel xray km/s	witness penet.	rico con	test number	data source	test	date	comments
	4	0.13	0.04	2219-T87	6061-T6	NO			1100-O	65	0.25	5.9	C	0	N	0.88	5.9	5.9	0	HOLES	246	IWALL	SS-204B	07/01/86	CRACK ON BACK SIDE OF A DIMPLE.
25	4	0.13	0.04	2219-T87	6061-T6	NO			LEXAN	0	0.35	4.3	N	0	N	0.51		4.3	0		384	IWALL	SS-225C	11/05/86	
	4	0.13	0.04	2219-T87	6061-T6	NO			LEXAN	0	0.35	4.9	N	0	N	0.51		4.9	0		383	IWALL	SS-225B	11/04/86	
	4	0.13	0.04	2219-T87	6061-T6	NO			LEXAN	0	0.35	5.8	S	0	Y	0.53		5.8	0		379	IWALL	SS-225A	10/31/86	
26	4	0.13	0.04	2219-T87	CADMIUM	NO			CADMIUM	0	0.22	3.7	Y		N	0.5		3.7	0		298	MARTIN	CD-134B	08/20/86	
	4	0.13	0.04	2219-T87	CADMIUM	NO			CADMIUM	0	0.22	4.6	Y		Y	0.55		4.6	0		297	MARTIN	CD-134A	08/19/86	
	4	0.13	0.04	2219-T87	CADMIUM	NO			CADMIUM	0	0.22	4.8	N		N	0.55		4.8	0		299	MARTIN	CD-134C	08/21/86	
27	4	0.13	0.04	2219-T87	CADMIUM	NO			CADMIUM	0	0.24	2.8	Y	0.5	N	0.47		2.8	1		300	MARTIN	CD-134D	08/21/86	
	4	0.13	0.04	2219-T87	CADMIUM	NO			CADMIUM	0	0.24	3.5	Y	1	N	0.51		3.5	0		293	MARTIN	CD-133A	08/15/86	
	4	0.13	0.04	2219-T87	CADMIUM	NO			CADMIUM	0	0.24	4.6	Y	1.1	N	0.54		4.6	3		294	MARTIN	CD-133B	08/15/86	
	4	0.13	0.04	2219-T87	CADMIUM	NO			CADMIUM	0	0.24	5	Y	0.2	N	0.7		5	0	N	295	MARTIN	CD-133C	08/18/86	
	4	0.13	0.04	2219-T87	CADMIUM	NO			CADMIUM	0	0.24					0.5		5.4			296		CD-133D	08/18/86	
28	4	0.13	0.04	2219-T87	CADMIUM	NO			CADMIUM	0	0.26	6	Y	0.1	Y	0.51		6	0		291	MARTIN	CD-132C	08/14/86	
	4	0.13	0.04	2219-T87	CADMIUM	NO			CADMIUM	0	0.26	6.5	Y	0.6	N	0.46		6.5	1		290	MARTIN	CD-132B	08/13/86	
29	4	0.13	0.04	2219-T87	6061-T6	YES	W	1	1100-O	0	0.2	3.9	Y	0.2	N	0.39	3.8	3.9			493	MSFC	SS-T2-14	03/10/87	
30	4	0.13	0.04	2219-T87	6061-T6	YES	W	1	6061-T6	45	0.26	5.7	Y	0.4	N	0.67		5.7	4	CAVITIES	372	IWALL	SS-223C	10/27/86	
	4	0.13	0.04	2219-T87	6061-T6	YES	W	1	6061-T6	45	0.26	6.6	Y	0.3	N	0.7		6.6	1	NO CAVS	370	IWALL	SS-223A	10/24/86	
	4	0.13	0.04	2219-T87	6061-T6	YES	W	1	6061-T6	45	0.26	6.8	Y	0.4	N	0.8		6.8	1	SPRAY	371	IWALL	SS-223B	10/24/86	
31	4	0.13	0.04	2219-T87	6061-T6	YES	W	1	6061-T6	65	0.26	3.7	N	0	N	0.89		3.7	0	5HOLES	376	IWALL	SS-224C	10/29/86	
	4	0.13	0.04	2219-T87	6061-T6	YES	W	1	6061-T6	65	0.26	4.8	N	0	N	1		4.8	0	3HOLES	375	IWALL	SS-224B	10/28/86	
	4	0.13	0.04	2219-T87	6061-T6	YES	W	1	6061-T6	65	0.26	6.5	N	0	N	1.02		6.5	0	HOLES	374	IWALL	SS-224A	10/28/86	
32	4	0.13	0.04	2219-T87	6061-T6	YES	W		1100-O	0	0.19	2.5	Y	0.3	N	0.27	2.6	2.5			483	MSFC	SS-T2-1	03/02/87	
	4	0.13	0.04	2219-T87	6061-T6	YES	W		1100-O	0	0.19	6	Y	0.6	Y	0.36	5.9	6	1		813		3010-A	09/27/89	2 HOLES, 0.6X0.25", 0.05" DIA. DAMAGE MOSTLY IN 1.2" DIA AREA FEW CRATERS IN THIS AREA APPROX. .1" DIA AND .03" DIA DEEP. VERY SLIGHT EDGE ON REAR WITH SPALL AROUND HOLE APPROX. .1" DIA WIDE AND THIN LAYER OF METAL
	4	0.13	0.04	2219-T87	6061-T6	YES	W		1100-O	0	0.19	6.6	Y	0.2	N	0.39	6.6	6.6	0		965		3201	03/20/90	

	standoff inch	rearwall gage inch	bumper gage inch	rearwall alloy	bumper alloy	mli present	mli location	prj. len.to dia	prj. material	obliquity	projectile size	velocity avg km/s	rear penetrn	rearhole inch	rearwall spall	bumper hole inch	vel hall km/s	vel xray km/s	witness penet.	rico con	test number	data source	test	date	comments
	4	0.13	0.04	2219-T87	6061-T6	YES	W		1100-O	0	0.19	7.1	Y	0.2	N	0.32		7.1	0		814		3010-B	09/27/89	2 HOLES, 0.2X0.12", 0.05" DIA. DAMAGE IN AREA APPROX. 1" DIA ONE CRATERS APPROX. .2" DIA AND .06" DIA DEEP WITH DIMPLE ON REAR SEVERAL OTHER SMALL CRATERS. LARGER HOLE HAS APPROX. .06" DIA WIDE SOME ARE AND EDGE AT HOLE. SLIGHT EDGE IN METAL ON REAR.
	4	0.13	0.04	2219-T87	6061-T6	YES	W		1100-O	0	0.19	7.2	N	0	N	0.42	7.2	7.2	0		966		3202	03/20/90	
	4	0.13	0.04	2219-T87	6061-T6	YES	W		1100-O	0	0.19	7.5	Y	0.1	N	0.04	7.3	7.6	0		815		3010-C	09/28/89	HOLE 0.06" DIAM IN A CRATER APPROX. .15" DIA WITH ANOTHER CRATER JOINING APPROX. .12" DIA FEW VERY SMALL CRATERS WITHIN .3" DIA OF THE LARGER CRATERS.
33	4	0.13	0.04	2219-T87	6061-T6	YES	W		1100-O	0	0.25	6.8	N	0	N	0.5	6.8	6.8	0		967		3205	03/21/90	
	4	0.13	0.04	2219-T87	6061-T6	YES	W		1100-O	0	0.25	6.8	Y	0.2	Y	0.46		6.8	0		969		3206	03/22/90	4 HOLES, SMALL SPALL AROUND HOLES
	4	0.13	0.04	2219-T87	6061-T6	YES	W		1100-O	0	0.25	6.8	Y	0.3	N	0.46	6.8	6.9	0		817		3010-B1	09/29/89	HOLE 0.25" DIA, SLIGHTLY JAGGED, SINK IN AN AREA APPROX. .2" DIA, WITH MOST OF THE CRATERS IN AN AREA APPROX. .6" DIA X 1.5" DIA, MANY SMALL CRATERS IN THIS AREA UP TO .1" DIA AND .040" DIA DEEP. FEW CRATERS OUT TO 2" DIA AREA BULGE ON REAR WITH A SLIGH
	4	0.13	0.04	2219-T87	6061-T6	YES	W		1100-O	0	0.25	7.3	N	0	N	0.51	7.2	7.4	0		816		3010-A1	09/28/89	SINK AREA APPROX. .2" DIA WITH FEW CRATERS LESS THAN .1" DIA, SLIGHT BULGE OR REAR WITH ONE DIMPLE.
34	4	0.13	0.04	2219-T87	6061-T6	YES	W		1100-O	0	0.31	4	Y	1	N	0.46	3.9	4			476	MSFC	SS-T2-5	02/23/87	PETALED
	4	0.13	0.04	2219-T87	6061-T6	YES	W		1100-O	0	0.31	6.8	Y	2	N	0.52	6.8	6.9	1		825		3011-B	10/05/89	HOLE APPROX. 2" DIA WITH 5 PETALS PUSHED OUTWARDS APPROX. 2". METAL SPLIT ALONG PETALS APPROX. 3.5" DIA, 2.5" DIA, 4" DIA, 1.5" DIA AND 3" DIA.
	4	0.13	0.04	2219-T87	6061-T6	YES	W		1100-O	0	0.31	7.1	Y	2.5	N	0.54	7	7.1	3		826		3011-A	10/05/89	HOLE 2.5X2". 6 PETALS PUSHED OUTWARD APPROX. 2." SPLIT IN METAL ALONG PETALS APPROX. 3", 2.5", 2.5", 2.5", 2.2" AND 2.1"
35	4	0.13	0.04	2219-T87	6061-T6	YES	W		1100-O	0	0.38	5	Y	6	N	0.52	5	5.1			494	MSFC	SS-T2-15	03/10/87	PETALING
36	4	0.13	0.04	2219-T87	6061-T6	YES	W		1100-O	30	0.19	2.7	Y	0.3	N	0.33	2.7	2.7	1		827		3012-B	10/06/89	HOLE 0.324X0.266" OBLONG IN PROJECTILE PATH. FEW SHALLOW CRATERS UNDER BUMPER HOLE
	4	0.13	0.04	2219-T87	6061-T6	YES	W		1100-O	30	0.19	4	N	0	N	0.36	4	4	0		829		3012-C	10/10/89	NO HOLE, 2 CRATERS APPROX. .2" DIA X .08" DEEP, AMD .18" DIA X .08" DEEP WITH LARGE DIMPLES ON REAR SEVERAL SMALLER CRATERS. ALL DAMAGE IN AREA OF PROJECTILE PATH
	4	0.13	0.04	2219-T87	6061-T6	YES	W		1100-O	30	0.19	4.3	N	0	N	0.39	4.3	4.3	0		828		3012-D	10/06/89	CRATERS APPROX. .15" DIA X .11 DEEP, .018" DIA X d.09" DEEP, .19" DIA X .11 DEEP. ALL WITH LARGE DIMPLES ON REAR. SEVERAL SMALLER CRATERS. DAMAGE ALL IN PROJECTILE PATH
37	4	0.13	0.04	2219-T87	6061-T6	YES	W		1100-O	30	0.25	7	Y	1.4	N	0.48	7	7.1	0		830		3013-A	10/10/89	HOLE IN PROJECTILE PATH APPROX. 1.4" X .8" WITH 2 PETALS PUSHED OUT ON BACK APPROX 0.8" WIDE X 1.0" LONG AND 0.6" WIDE X 1.2" LONG. FEW SMALL CRATERS IN PETALS AND ABOUND EDGE OF HOLE

	standoff inch	rearwall gage inch	bumper gage inch	rearwall alloy	bumper alloy	mil present	mil location	prj. len to dia	prj. material	obliquity	projectile size	velocity avg km/s	rear penet'n	rearhole inch	rearwall spall	bumper hole inch	vel hall km/s	vel xray km/s	witness penet.	nico con	test number	data source	test	date	comments
38	4	0.13	0.04	2219-T87	6061-T6	YES	W		1100-O	45	0.19	2.9	N	0	N	0.4	2.9	3	0	CAVITIES	535	MSFC	SS-333	05/11/87	
	4	0.13	0.04	2219-T87	6061-T6	YES	W		1100-O	45	0.19	3.7	N	0	N	0.4	3.6	3.7	0	CAVITIES	533	MSFC	SS-334	05/07/87	
	4	0.13	0.04	2219-T87	6061-T6	YES	W		1100-O	45	0.19	4.1	c	0	N	0.46	4	4.1	0	CAVITIES	347	IWALL	SS-221D	10/06/86	COUNT REAR SURFACE CRACK AS FAILURE
	4	0.13	0.04	2219-T87	6061-T6	YES	W		1100-O	45	0.19	4.6	N	0	N	0.45	4.6	4.6	0	CAVITIES	346	IWALL	SS-221C	10/03/86	
	4	0.13	0.04	2219-T87	6061-T6	YES	W		1100-O	45	0.19	5.9	N	0	N	0.54	5.9	6	0	CAVITIES	345	IWALL	SS-221B	10/03/86	
	4	0.13	0.04	2219-T87	6061-T6	YES	W		1100-O	45	0.19	6.4	N	0	N	0.48	6.4	6.5	0	NODAMAG	344	IWALL	SS-221A	10/02/86	
39	4	0.13	0.04	2219-T87	6061-T6	YES	W		1100-O	45	0.25	4.1	Y	0.5	N	0.52	4	4.2	1	CAVITIES	531	MSFC	SS-335	05/05/87	
	4	0.13	0.04	2219-T87	6061-T6	YES	W		1100-O	45	0.25	4.3	Y	0.4	N	0.55		4.3	1	SPRAYED	266	IWALL	SS-201A	07/17/86	
	4	0.13	0.04	2219-T87	6061-T6	YES	W		1100-O	45	0.25	4.5	Y	0.6	N	0.53	4.5	4.6	2	CAVITIES	532	MSFC	SS-336	05/06/87	
	4	0.13	0.04	2219-T87	6061-T6	YES	W		1100-O	45	0.25	5.5	Y	0.5	N	0.53		5.5	4	CAVITIES	267	IWALL	SS-201B	07/17/86	
	4	0.13	0.04	2219-T87	6061-T6	YES	W		1100-O	45	0.25	5.8	C	0	N	0.57	5.7	5.8	0	CAVITIES	536	MSFC	SS-336A	05/13/87	"SMALL CRACK IN DIMPLE ON BACK"--COUNT AS PENETRATION
	4	0.13	0.04	2219-T87	6061-T6	YES	W		1100-O	45	0.25	7.2	Y	0.1	N	0.53		7.2	0	CAVITIES	268	IWALL	SS-201C	07/18/86	
	4	0.13	0.04	2219-T87	6061-T6	YES	W		1100-O	45	0.25	7.6	Y	0.6	N	0.65	7.5	7.7	2	CAVITIES	269	IWALL	SS-201D	07/21/86	
40	4	0.13	0.04	2219-T87	6061-T6	YES	W		1100-O	45	0.31	3	Y	1	N	0.65	2.9	3	4	CAVITIES	524	MSFC	SS-319	04/24/87	
	4	0.13	0.04	2219-T87	6061-T6	YES	W		1100-O	45	0.31	4.1	Y	0.8	N	0.65	4.1	4.2	4	CAVITIES	527	MSFC	SS-324	04/29/87	
	4	0.13	0.04	2219-T87	6061-T6	YES	W		1100-O	45	0.31	6.5	Y	3	N	0.76	6.5	6.6	4		497	MSFC	SS-003A	03/25/87	
	4	0.13	0.04	2219-T87	6061-T6	YES	W		1100-O	45	0.31	6.9	Y	1.1	N	0.77	6.8	7	4	CAVITIES	540	MSFC	SS-337	05/18/87	
	4	0.13	0.04	2219-T87	6061-T6	YES	W		1100-O	45	0.31	7	Y	1	N	0.84	7	7.1	2	CAVITIES	538	MSFC	SS-338	05/14/87	
41	4	0.13	0.04	2219-T87	6061-T6	YES	W		1100-O	45	0.38	6.5	Y	2	N	0.83	6.5		3	1HOLE	544	MSFC	SS-339	05/21/87	
42	4	0.13	0.04	2219-T87	6061-T6	YES	W		1100-O	65	0.25	4.6	N	0	N	0.88	4.6	4.5	0		983		3209-1	04/06/90	
	4	0.13	0.04	2219-T87	6061-T6	YES	W		1100-O	65	0.25	4.8	N	0	N	0.81		4.8			833		3017-C	10/12/89	NO HOLE, DAMAGE BOTH IN PROJ PATH AND UNDER BUMPER HOLE, CRATERS APPROX. SAME SIZE AND DEPTH, MORE CRATERS UNDER BUMPER HOLE, CRATERS UP TO .12" DIA X .04" DEEP WITH FEW VERY SLIGHT DIMPLES ON REAR.
	4	0.13	0.04	2219-T87	6061-T6	YES	W		1100-O	65	0.25	5.7	N	0	N	0.8	5.7	5.7	0		973		3211	03/26/90	
	4	0.13	0.04	2219-T87	6061-T6	YES	W		1100-O	65	0.25	5.8	N	0	N	0.79	5.8	5.8	0		972		3209	03/26/90	
	4	0.13	0.04	2219-T87	6061-T6	YES	W		1100-O	65	0.25	6.3	Y	0.1	N	0.8	6.3	6.4			832		3017-B	10/11/89	2 HOLES, ONE IN PROJ PATH AND ONE UNDER BUMPER HOLE, DAMAGE AREA IN PROJ PATH APPROX .4" X .3" WITH HOLE APPROX .13" X .1. DAMAGE AREA UNDER BUMPER HOLE APPROX. 4.0" WIDE X 2.5" LONG (WITH PROJ TRAVEL), HOLE APPROX .09" DIA, CRATERS .1" DIA AND SMALLER
	4	0.13	0.04	2219-T87	6061-T6	YES	W		1100-O	65	0.25	7	N	0	N	0.88	7	7.1			831		3017-A	10/11/89	NO HOLE, NO DAMAGE INPROJECTILE PATH DAMAGE AREA UNDER PROJECTILE HOLE APPROX 3.5" DIA, ONE CRATER APPROX. .17" DIA AND .06" DEEP WITH DIMPLE ON BACK, OTHER CRATERS .1" DIA AND LESS WITH FEW SMALL DIMPLES ON REAR
43	4	0.13	0.04	2219-T87	6061-T6	YES	W		1100-O	65	0.3	2.7	N	0	N	0.86	2.7	2.7	0	HOLES	255	IWALL	SS-203C	07/09/86	
	4	0.13	0.04	2219-T87	6061-T6	YES	W		1100-O	65	0.3	3.7	N	0	N	0.87	3.6	3.7	0	HOLES	254	IWALL	SS-203B	07/08/86	
	4	0.13	0.04	2219-T87	6061-T6	YES	W		1100-O	65	0.3	4.8	N	0	N	0.94		4.8	0	HOLES	253	IWALL	SS-203A	07/08/86	
	4	0.13	0.04	2219-T87	6061-T6	YES	W		1100-O	65	0.3	5.6	N	0	N	0.93		5.6	0	HOLES	256	IWALL	SS-203D	07/09/86	
	4	0.13	0.04	2219-T87	6061-T6	YES	W		1100-O	65	0.3	6.7	N	0	N	1.18	6.7	6.8	0	HOLES	270	IWALL	SS-203E	07/21/86	

	standoff inch	rearwall gage inch	bumper gage inch	rearwall alloy	bumper alloy	mli present	mli location	pp_len_to_dia	pr. material	obliquity	projectile size	velocity avg km/s	rear penetr'n	rearhole inch	rearwall spall	bumper hole inch	vel hall km/s	vel xray km/s	witness penet.	rico con	test number	data source	test	date	comments
44	4	0.13	0.04	2219-T87	6061-T6	YES	W		1100-O	65	0.31	3.4	Y	0.3	Y	0.88	3.4	3.4	0		975		3212	03/28/90	
	4	0.13	0.04	2219-T87	6061-T6	YES	W		1100-O	65	0.31	4.4	N	0	N	1.27	4.5	4.4	0		976		3213	03/28/90	
	4	0.13	0.04	2219-T87	6061-T6	YES	W		1100-O	65	0.31	5.2	N	0	N	0.97	5.2	5.2	0		977		3214	03/29/90	
	4	0.13	0.04	2219-T87	6061-T6	YES	W		1100-O	65	0.31	5.7	N	0	N	1.04		5.7	0		978		3215	04/02/90	
	4	0.13	0.04	2219-T87	6061-T6	YES	W		1100-O	65	0.31	6.3	S	0	Y	1.02	6.3	6.3	0		980		3216	04/04/90	COUNT SPALL AS FAILURE
	4	0.13	0.04	2219-T87	6061-T6	YES	W		1100-O	65	0.31	6.5	N	0	N	1.03	6.5	6.5	0		981		3218	04/05/90	
45	4	0.13	0.04	2219-T87	6061-T6	YES	W		1100-O	65	0.35	3.1	C	0	N	0.98	3.1	3	0	HOLES	277	IWALL	SS-203F	08/01/86	SURFACE CRACK ON REAR OF WALL
	4	0.13	0.04	2219-T87	6061-T6	YES	W		1100-O	65	0.35	4.6	Y	0.2	N	1.1	4.6	4.7	0	HOLES	278	IWALL	SS-203G	08/01/86	
46	4	0.13	0.05	2219-T87	2024-T3	B	3.75		1100-O	45	0.31	4.1	Y	1	N	0.71	4.1	4.1	2	CRATERED	1189		4102-B	12/04/90	3 WALL HOLES, LARGEST 0.95X0.5, OTHERS 0.35,0.25 DIA.
47	4	0.13	0.05	2219-T87	6061-T6	B	3.75		1100-0	75	0.31	4	N	0	N	1.25	4	4	0	CRATERED	1179		4108-B	11/26/90	WALL CRATERED ONLY.
48	4	0.13	0.05	2219-T87	6061-T6	B	3.75		1100-O	45	0.25	6	N	0	N	0.67	5.9	6	0		1173		9001-C	11/15/90	WALL CRATERED ONLY.
	4	0.13	0.05	2219-T87	6061-T6	B	3.75		1100-O	45	0.25	6	Y	0.3	N	0.66	6	6	0		1171		9001-A	11/14/90	WALL CRATERED PLUS HOLE.
	4	0.13	0.05	2219-T87	6061-T6	B	3.75		1100-O	45	0.25	6.1	Y	0.2	N	0.65	6.1	6.1	0 ?		1174		9001-D	11/16/90	WALL CRATERED PLUS HOLE.
	4	0.13	0.05	2219-T87	6061-T6	B	3.75		1100-O	45	0.25	6.4	N	0	N	0.7	6.4	6.4	0		1177		9002-C	11/20/90	WALL CRATERED ONLY.
	4	0.13	0.05	2219-T87	6061-T6	B	3.75		1100-O	45	0.25	6.4	N	0	N	0.65	6.4	6.4	0		1178		9002-D	11/21/90	WALL CRATERED ONLY.
	4	0.13	0.05	2219-T87	6061-T6	B	3.75		1100-O	45	0.25	6.4	Y	0.2	N	0.65	6.4	6.4	2		1175		9002-A	11/19/90	HOLE SIZES NEED TO BE VERIFIED.
	4	0.13	0.05	2219-T87	6061-T6	B	3.75		1100-O	45	0.25	6.4	N	0	N	0.7	6.4	6.5	0		1176		9002-B	11/20/90	WALL CRATERED ONLY.
49	4	0.13	0.05	2219-T87	6061-T6	B	3.75		1100-O	45	0.31	3	Y	0.6	N	0.67	3		2	CRATERED	1190		4102-A	12/04/90	WALL ALSO CRATERED.
50	4	0.13	0.05	2219-T87	6061-T6	B	3.75		1100-O	60	0.31	2.9	Y	0.4	N	0.83	2.9	2.9	2	CRATERED	1185		4105-A	11/29/90	WALL JAGGED HOLE, PLUS CRATERS.
	4	0.13	0.05	2219-T87	6061-T6	B	3.75		1100-O	60	0.31	3	N	0	N	0.85	3	3	0	CRATERED	1187		4105-A1	12/03/90	WALL CRATERED & REAR BUMPS.
	4	0.13	0.05	2219-T87	6061-T6	B	3.75		1100-O	60	0.31	4	N	0	N	0.9	4	4.1	0	CRATERED	1184		4105-B	11/29/90	WALL CRATERED & REAR BUMPS.
	4	0.13	0.05	2219-T87	6061-T6	B	3.75		1100-O	60	0.31	6.2	N	0	N	0.98	6.2	6.1	0	CRATERED	1182		4105-C	11/27/90	WALL CRATERED, SOME REAR BUMPS.
	4	0.13	0.05	2219-T87	6061-T6	B	3.75		1100-O	60	0.31	7.3	N	0	N	1.1	7.2	7.3	0	CRATERED	1183		4105-D	11/28/90	CRATERED ONLY.
51	4	0.13	0.05	2219-T87	6061-T6	B	3.75		1100-O	75	0.31	3	N	0	N	1.29	3	3	0	CRATERED	1188		4108-A1	12/03/90	WALL CRATERED & 1 REAR BUMP.
	4	0.13	0.05	2219-T87	6061-T6	B	3.75		1100-O	75	0.31	3.1	N	0	N	1.08	3.1	3.1	0	CRATERED	1186		4108-A	11/30/90	CRATERED ONLY.
	4	0.13	0.05	2219-T87	6061-T6	B	3.75		1100-O	75	0.31	6	N	0	N	1.5	6	5.9	0	CRATERED	1180		4108-C	11/26/90	WALL CRATERED ONLY.
52	4	0.13	0.05	2219-T87	6061-T6	NO	3.75		1100-O	45	0.25	6	Y	0.6	N	0.65	5.9	6	2		1172		9001-B	11/15/90	2 HOLES IN WALL, PLUS CRATERS
53	4	0.13	0.05	2219-T87	6061-T6	YES	3.75		1100-O	45	0.19	3	N	0	N	0.41	3	3	0	SPRAY	1105		4100-A	09/05/90	
	4	0.13	0.05	2219-T87	6061-T6	YES	3.75		1100-O	45	0.19	3.8	N	0	N	0.45	3.8	3.8	0	SPRAYED	1106		4100-B	09/06/90	
	4	0.13	0.05	2219-T87	6061-T6	YES	3.75		1100-O	45	0.19	5.6	N	0	N	0.48	5.7	5.6	0	SPRAYED	1108		4100-C	09/07/90	
	4	0.13	0.05	2219-T87	6061-T6	YES	3.75		1100-O	45	0.19	7.2	N	0	N	0.52	7.2	7.1	0	SPRAYED	1109		4100-D	09/07/90	
54	4	0.13	0.05	2219-T87	6061-T6	YES	3.75		1100-O	45	0.25	3.2	Y	0.4		0.59	3.1	3.2	1	SPRAYED	1110		4101-A	09/10/90	
	4	0.13	0.05	2219-T87	6061-T6	YES	3.75		1100-O	45	0.25	4.1	Y	0.4	N	0.66	4.1	4.2	1	CRATERED	1111		4101-B	09/10/90	
	4	0.13	0.05	2219-T87	6061-T6	YES	3.75		1100-O	45	0.25	6.1	Y	0.4	N	0.65	6.1	6.1	2	CRATERED	1112		4101-C	09/11/90	
	4	0.13	0.05	2219-T87	6061-T6	YES	3.75		1100-O	45	0.25	7.5	Y	0.1	N	0.68	7.5	7.4	0	SPRAYED	1113		4101-D	09/12/90	
55	4	0.13	0.05	2219-T87	6061-T6	YES	3.75		1100-O	60	0.19	2.9	N	0	N	0.56	2.9	2.9	0	SPRAYED	1114		4103-A	09/12/90	
	4	0.13	0.05	2219-T87	6061-T6	YES	3.75		1100-O	60	0.19	3	N	0	N	0.52	3.1	3	0	CRATERED	1125		4106-A	09/24/90	

	standoff inch	rearwall gage inch	bumper gage inch	rearwall alloy	bumper alloy	mli present	mli location	prj. len to dia	prj. material	obliquity	projectile size	velocity avg km/s	rear penetr'n	rearhole inch	rearwall spall	bumper hole inch	vel hall km/s	vel xray km/s	witness panel	rear con	test number	data source	test	date	comments
	4	0.13	0.05	2219-T87	6061-T6	YES	3.75		1100-O	60	0.19	4	N	0	N	0.54	4	4	0	CRATERED	1115		4103-B	09/13/90	
	4	0.13	0.05	2219-T87	6061-T6	YES	3.75		1100-O	60	0.19	4.1	N	0	N	0.59	4.1	4.1	0	CRATERED	1126		4106-B	09/25/90	
	4	0.13	0.05	2219-T87	6061-T6	YES	3.75		1100-O	60	0.19	5.9	N	0	N	0.69	5.9	5.9	0	SPRAYED	1116		4103-C	09/13/90	
	4	0.13	0.05	2219-T87	6061-T6	YES	3.75		1100-O	60	0.19	7.4	N	0	N	0.87	7.4		0	SPRAYED	1121		4103-D	09/20/90	
56	4	0.13	0.05	2219-T87	6061-T6	YES	3.75		1100-O	60	0.25	3.2	N	0	N	0.71	3.2	3.2	0	CRATERED	1118		4104-A	09/17/90	
	4	0.13	0.05	2219-T87	6061-T6	YES	3.75		1100-O	60	0.25	4.2	N	0	N	0.76	4.2	4.2	0	CRATERED	1122		4104-B	09/20/90	
	4	0.13	0.05	2219-T87	6061-T6	YES	3.75		1100-O	60	0.25	6.1	N	0	N	0.88	6.1	6.1	0	CRATERED	1123		4104-C	09/21/90	
	4	0.13	0.05	2219-T87	6061-T6	YES	3.75		1100-O	60	0.25	7.6	N	0	N	0.76	7.5	7.6	0	SPRAYED	1124		4104-D	09/24/90	
57	4	0.13	0.05	2219-T87	6061-T6	YES	3.75		1100-O	75	0.19	3.1	N	0	N	0.73	3.1	3.1	0	CRATERED	1133		4106-A1	10/09/90	
	4	0.13	0.05	2219-T87	6061-T6	YES	3.75		1100-O	75	0.19	4	N	0	N	0.59	4	4.1	0	CRATERED	1134		4106-B1	10/09/90	
	4	0.13	0.05	2219-T87	6061-T6	YES	3.75		1100-O	75	0.19	6	N	0	N	0.75	6	6	0	CRATERED	1137		4106-C	10/11/90	
	4	0.13	0.05	2219-T87	6061-T6	YES	3.75		1100-O	75	0.19	7.6	N	0	N	0.93	7.6	7.6	0	CRATERED	1136		4106-D	10/10/90	
58	4	0.13	0.05	2219-T87	6061-T6	YES	3.75		1100-O	75	0.25	3.1	N	0	N	1.09	3.1	3.1	0	CRATERED	1128		4107-A	09/26/90	
	4	0.13	0.05	2219-T87	6061-T6	YES	3.75		1100-O	75	0.25	4.1	N	0	N	1.04	4.1	4.2	0	CRATERED	1130		4107-B	10/03/90	
	4	0.13	0.05	2219-T87	6061-T6	YES	3.75		1100-O	75	0.25	6.2	N	0	N	1.37	6.2	6.3	0	CRATERED	1131		4107-C	10/04/90	
	4	0.13	0.05	2219-T87	6061-T6	YES	3.75		1100-O	75	0.25	7.7	N	0	N	0.92	7.6	7.7	0	CRATERED	1132		4107-D	10/05/90	
59	4	0.13	0.06	2219-T87	6061-T6	2.0	2.0		1100-O	0	0.25	3.1	Y	0.5	N	0.43		3.1	2		1165		3405-A	11/06/90	30 LAYER MLI. WALL CRATERED PLUS HOLE.
	4	0.13	0.06	2219-T87	6061-T6	2.0	2.0		1100-O	0	0.25	3.1	Y	0.3	Y	0.45	3.1	3.1	1		1161		3406-A	11/01/90	2 BUMHOLES .45" DIA. 20 LAYER MLI.
	4	0.13	0.06	2219-T87	6061-T6	2.0	2.0		1100-O	0	0.25	3.9	Y	0	N	0.48	3.8	3.9	1		1166		3405-B	11/07/90	30 LAYER MLI. WALL CRATERED PLUS HOLE.
	4	0.13	0.06	2219-T87	6061-T6	2.0	2.0		1100-O	0	0.25	4.1	N	0	N	0.5	4.1	4.1	0		1162		3406-B	11/01/90	WALL CRATERED ONLY. 20 LAYER MLI.
	4	0.13	0.06	2219-T87	6061-T6	2.0	2.0		1100-O	0	0.25	5.1	N	0	N	0.53	5.1	5.2	0		1167		3405-C	11/07/90	30 LAYER MLI. WALL CRATERED ONLY.
	4	0.13	0.06	2219-T87	6061-T6	2.0	2.0		1100-O	0	0.25	5.2	N	0	N	0.48	5.2	5.2	0		1163		3406-C	11/05/90	WALL CRATERED ONLY. 20 LAYER MLI.
	4	0.13	0.06	2219-T87	6061-T6	2.0	2.0		1100-O	0	0.25	5.6	N	0	N	0.5	5.6	5.6	0		1164		3406-D	11/06/90	WALL CRATERED ONLY. 20 LAYER MLI.
	4	0.13	0.06	2219-T87	6061-T6	2.0	2.0		1100-O	0	0.25	6.1	Y	0.3	N	0.5	6.1	6.2	0		1169		3406-D1	11/09/90	20 LAYER MLI. WALL CRATERED PLUS 2 HOLES.
	4	0.13	0.06	2219-T87	6061-T6	2.0	2.0		1100-O	0	0.25	6.2	N	0	N	0.52	6.2	6.2	0		1168		3405-D	11/09/90	30 LAYER MLI. WALL CRATERED ONLY.
60	4	0.13	0.06	2219-T87	6061-T6	2.0	2.0		1100-O	0	0.38	5.5	Y	6	N	0.7	5.5	5.5	2		1156		3404-D	10/29/90	WALL 7 PETALS TO 3" FROM IMPACT POINT. 20 LAYER MLI.
	4	0.13	0.06	2219-T87	6061-T6	2.0	2.0		1100-O	0	0.38	6.2	Y	6	N	0.64	6.2		3		1154		3404-C	10/26/90	WALL PETALED 6 WAYS TO 3" FROM IMPACT POINT. 20 LAYER MLI (NEW).
61	4	0.13	0.06	2219-T87	6061-T6	B	3.75		1100-O	0	0.25	2.9	Y	0.5	N	0.44		2.9	3		1160		3407-A	10/31/90	WALL HOLE JAGGED, APPROX. ROUND. 20 LAYER MLI.
	4	0.13	0.06	2219-T87	6061-T6	B	3.75		1100-O	0	0.25	4	Y	1	N	0.47		4	3		1159		3407-B	10/31/90	WALL JAGGED HOLE 1.04X0.65 INCHES. 20 LAYER MLI.
	4	0.13	0.06	2219-T87	6061-T6	B	3.75		1100-O	0	0.25	4.8	Y	0.2	N	0.52	4.8	4.8	0		1158		3407-C	10/30/90	20 LAYER MLI
	4	0.13	0.06	2219-T87	6061-T6	B	3.75		1100-O	0	0.25	5.8	N	0	N	0.53	5.8	5.8	0		1157		3407-D	10/30/90	WALL CRATERED ONLY. 20 LAYER MLI.
62	4	0.13	0.06	2219-T87	6061-T6	B	3.75		1100-O	45	0.25	6.1	N	0	N	0.74	6	6.1	0		1170		9001-1	11/13/90	WALL CRATERED ONLY.
63	4	0.13	0.06	2219-T87	6061-T6	CPR	CPR		1100-O	0	0.25	3.6	Y	0.6	N	0.43		3.6	0		426	MARTIN	SS-148C	01/06/87	
	4	0.13	0.06	2219-T87	6061-T6	CPR	CPR		1100-O	0	0.25	4.6	S	0	Y	0.46		4.6			425	MARTIN	SS-148B	01/05/87	
	4	0.13	0.06	2219-T87	6061-T6	CPR	CPR		1100-O	0	0.25	5.7	N	0	N	0.5		5.7	N		424	MARTIN	SS-148A	12/22/86	

	standoff inch	rearwall gage inch	bumper gage inch	rearwall alloy	bumper alloy	mli present	mli location	prj. len to dia	prj. material	obliquity	projectile size	velocity avg km/s	rear penet'n	rearhole inch	rearwall spall	bumper hole inch	vel hall km/s	vel xray km/s	witness penet.	rico con	test number	data source	test	date	comments
64	4	0.13	0.06	2219-T87	6061-T6	NO		1	1100-O	0	0.26	5.1	Y	2	N	0.58		5.1	2		131	ADP SM1	SS-P-022	01/14/86	
	4	0.13	0.06	2219-T87	6061-T6	NO		1	1100-O	0	0.26	6.9	Y	0.3	N	0.67		6.9	2		133	ADP SM1	SS-P-022B	01/15/86	AFT PLATE ZIGZAG SPLIT C. 2" LONG, PLUS 1" SPLIT AT TOP OF ZIGZAG SPLIT.
65	4	0.13	0.06	2219-T87	6061-T6	NO			1100-O	0	0.13	3	N	0	N	0.34		3	0		121	ADP SM1	SS-P-028	12/18/85	
66	4	0.13	0.06	2219-T87	6061-T6	NO			1100-O	0	0.19	3.9	Y	0.2	N	0.38		3.9	0		116	ADP SM1	SS-P-027A	12/13/85	
	4	0.13	0.06	2219-T87	6061-T6	NO			1100-O	0	0.19	4.2	Y	0.1	N	0.41		4.2	0		117	ADP SM1	SS-P-027B	12/16/85	
	4	0.13	0.06	2219-T87	6061-T6	NO			1100-O	0	0.19	4.5	N	0	N	0.41		4.5	0		115	ADP SM1	SS-P-027	12/12/85	
67	4	0.13	0.06	2219-T87	6061-T6	NO			1100-O	0	0.25	2.8	Y	0.5	N	0.41		2.8	0		43	ADP SM1	SS-P-001	08/19/85	
	4	0.13	0.06	2219-T87	6061-T6	NO			1100-O	0	0.25	3	Y	0.4	N	0.42		3	1		44	ADP SM1	SS-P-002	08/20/85	
	4	0.13	0.06	2219-T87	6061-T6	NO			1100-O	0	0.25	3.6	Y	0.5	N	0.42	3.6	3.7			395	MSFC	SS-PT4A	11/25/86	
	4	0.13	0.06	2219-T87	6061-T6	NO			1100-O	0	0.25	4.3	Y	0.2	Y	0.46	4.2	4.3			396	MSFC	SS-PT4B	11/26/86	
	4	0.13	0.06	2219-T87	6061-T6	NO			1100-O	0	0.25	4.9	Y	0.4	Y	0.49		4.9			45	ADP SM1	SS-P-003	08/23/85	
	4	0.13	0.06	2219-T87	6061-T6	NO			1100-O	0	0.25	5	Y	0.4		0.51		5	1		46	ADP SM1	SS-P-004	08/26/85	
	4	0.13	0.06	2219-T87	6061-T6	NO			1100-O	0	0.25	5.9	Y	0	Y	0.51	5.9	5.9	1		681	MSFC	EHSS-2B	03/04/88	PINHOLES, PLUS SPALL OF REAR WALL
	4	0.13	0.06	2219-T87	6061-T6	NO			1100-O	0	0.25	6.1	Y	0.8	Y	0.51	6.2	6	3		931		2004-C	02/16/90	SPALL AROUND HOLES IN REAR WALL
	4	0.13	0.06	2219-T87	6061-T6	NO			1100-O	0	0.25	6.4	S	0	Y	0.57	6.3	6.4	0		680	MSFC	EHSS-2A	03/02/88	COUNT SPALL AS FAILURE
	4	0.13	0.06	2219-T87	6061-T6	NO			1100-O	0	0.25	6.9	Y	0	N	0.58		6.9	0		47	ADP SM1	SS-P-005	08/28/85	
	4	0.13	0.06	2219-T87	6061-T6	NO			1100-O	0	0.25	6.9	Y	0	Y	0.55	6.9	6.9	1		939		2004-B	02/21/90	
	4	0.13	0.06	2219-T87	6061-T6	NO			1100-O	0	0.25	7	Y	0	Y	0.59		7	0		49	ADP SM1	SS-P-006A	08/30/85	COUNT SPALL AS PENETRATION
	4	0.13	0.06	2219-T87	6061-T6	NO			1100-O	0	0.25	7.1	Y	1	Y	0.57		7.1	0		176	ADP SM1	SS-P-034B	03/13/86	REAR PLATE SPLIT 1" L X 0.1" W
	4	0.13	0.06	2219-T87	6061-T6	NO			1100-O	0	0.25	7.2	Y	2	Y	0.57		7.2	1		941		2004-A	02/26/90	
68	4	0.13	0.06	2219-T87	6061-T6	NO			1100-O	0	0.3	6.5	Y	2	N	0.62		6.5	3		127	ADP SM1	SS-P-021A	01/09/86	
	4	0.13	0.06	2219-T87	6061-T6	NO			1100-O	0	0.3	6.6	Y	1.5	Y	0.62		6.6	2		126	ADP SM1	SS-P-021	01/09/86	
69	4	0.13	0.06	2219-T87	6061-T6	NO			1100-O	0	0.31	3.4	Y	1	Y	0.5	3.4	3.4			477	MSFC	SS-T2-8	02/24/87	
	4	0.13	0.06	2219-T87	6061-T6	NO			1100-O	0	0.31	4.4	Y	1.4	N	0.54	4.3	4.4			392	MSFC	SS-PT8A	11/20/86	
	4	0.13	0.06	2219-T87	6061-T6	NO			1100-O	0	0.31	4.4	Y	1.4	N	0.56	4.3	4.4			393	MSFC	SS-PT8B	11/21/86	
	4	0.13	0.06	2219-T87	6061-T6	NO			1100-O	0	0.31	4.6	Y	1.8	N	0.61	4.6	4.7			484	MSFC	SS-T2-6A	03/03/87	
	4	0.13	0.06	2219-T87	6061-T6	NO			1100-O	0	0.31	6.6	Y	1.3	Y	0.57	6.6	6.7	2		703	MSFC	EHSS-6C	06/09/88	SPALL AROUND EDGE OF HOLE

	standoff inch	rearwall gage inch	bumper gage inch	rearwall alloy	bumper alloy	mli present	mli location	prj. len to dia	prj. material	obliquity	projectile size	velocity avg km/s	rear penetr'n	rearhole inch	rearwall spall	bumper hole inch	vel hall km/s	vel xray km/s	witness penet.	rico con	test number	data source	test	date	comments
	4	0.13	0.06	2219-T87	6061-T6	NO			1100-O	0	0.31	6.6	Y	2	N	0.61	6.6		2		636	MSFC	EH3-A	09/21/87	BUMPER - .611" DIA. HOLE, 1" LOW, SOME DEBRIS, FEW DEBRIS HOLES. WALL - HOLE 2" X 1.5", METAL SPLIT 1" LONG & PEELED BACK SLIGHTLY. HEAVY CONCENTRATION OF CAVATIES OVER 5" DIA. DAMAGE AREA 9" DIA. AREA. WITNESS #1 - HOLE, 3.5" DIA. WITH PETALS PEELED B
	4	0.13	0.06	2219-T87	6061-T6	NO			1100-O	0	0.31	6.8	Y	8	N	0.66	6.7	6.8	2		676	MSFC	EH4-B	12/11/87	WALL: 5 PETALS, CRACKS 4-6" EACH
70	4	0.13	0.06	2219-T87	6061-T6	NO			1100-O	0	0.38	5.1	Y	2	Y	0.7	5	5.1			487	MSFC	SS-T2-18	03/04/87	
71	4	0.13	0.06	2219-T87	6061-T6	NO			1100-O	30	0.19	5.1	Y	0.2	N	0.46	5	5.2	0	NO CAV.	546	MARTIN	SS-162B	05/27/87	
	4	0.13	0.06	2219-T87	6061-T6	NO			1100-O	30	0.19	6.5	S	0	Y	0.55	6.5		0	CAVITIES	545	MARTIN	SS-162A	05/26/87	COUNT SPALL AS FAILURE
72	4	0.13	0.06	2219-T87	6061-T6	NO			1100-O	30	0.25	5.9	Y	0.8	N	0.6	5.8	5.9	2		303	MARTIN	SS-135A	08/26/86	
	4	0.13	0.06	2219-T87	6061-T6	NO			1100-O	30	0.25	6.7	Y	1	Y	0.56	6.6	6.8	1		305	MARTIN	SS-135C	08/27/86	
	4	0.13	0.06	2219-T87	6061-T6	NO			1100-O	30	0.25	6.8	Y	1.3	Y	0.54	6.8	6.9	2	CAVITIES	691	MSFC	EHSS-3C	04/15/88	REAR WALL HOLED PLUS SPALLED
	4	0.13	0.06	2219-T87	6061-T6	NO			1100-O	30	0.25	6.9	Y	1	N	0.56	6.8	6.9	2		306	MARTIN	SS-135D	08/28/86	
	4	0.13	0.06	2219-T87	6061-T6	NO			1100-O	30	0.25	7.2	Y	0.1	Y	0.65	7.1	7.2	0		304	MARTIN	SS-135B	08/27/86	
	4	0.13	0.06	2219-T87	6061-T6	NO			1100-O	30	0.25	7.2	Y	0.2	N	0.63	7.1	7.3	0		307	MARTIN	SS-135E	08/29/86	
73	4	0.13	0.06	2219-T87	6061-T6	NO			1100-O	30	0.31	7.1	Y	1.5	N	0.67	7.1	7.2	4	OK	336	MSFC	SS-EH1A	09/26/86	
74	4	0.13	0.06	2219-T87	6061-T6	NO			1100-O	45	0.19	3.2	N	0	N	0.42	3.2	3.2	0	CAVITIES	230	IWALL	SS-206E	06/17/86	
	4	0.13	0.06	2219-T87	6061-T6	NO			1100-O	45	0.19	3.7	C	0	N	0.46		3.7	0		220	IWALL	SS-206D	06/10/86	COUNT REAR SURFACE CRACK AS FAILURE
	4	0.13	0.06	2219-T87	6061-T6	NO			1100-O	45	0.19	4.8	Y	0.2	Y	0.46	4.8	4.8	1		217	IWALL	SS-206A	06/06/86	
	4	0.13	0.06	2219-T87	6061-T6	NO			1100-O	45	0.19	5.1	N	0	N	0.52		5.1	0		218	IWALL	SS-206B	06/09/86	
	4	0.13	0.06	2219-T87	6061-T6	NO			1100-O	45	0.19	5.4	Y	0.1	N	0.52		5.4	0		219	IWALL	SS-206C	06/09/86	
	4	0.13	0.06	2219-T87	6061-T6	NO			1100-O	45	0.19	6.2	N	0	N	0.53	6.1	6.2	0	CAVITIES	231	IWALL	SS-206F	06/18/86	
	4	0.13	0.06	2219-T87	6061-T6	NO			1100-O	45	0.19	7	Y	0.2	N	0.52	7	7	0	CAVITIES	510	MARTIN	SS-155A	04/09/87	
	4	0.13	0.06	2219-T87	6061-T6	NO			1100-O	45	0.19	7.4	Y	0.1	N	0.61	7.3	7.4	0	CAVITIES	720	MSFC	EHRP-8	07/28/88	
75	4	0.13	0.06	2219-T87	6061-T6	NO			1100-O	45	0.25	5.2	Y	0.6	N	0.63	5.2	5.2	3	CAVITIES	453	IWALL	SS-230C	02/03/87	
	4	0.13	0.06	2219-T87	6061-T6	NO			1100-O	45	0.25	5.6	Y	0.4	N	0.64	5.5	5.6	2	CAVITIES	456	IWALL	SS-230D	02/04/87	
	4	0.13	0.06	2219-T87	6061-T6	NO			1100-O	45	0.25	6.6	Y	0.3	N	0.7	6.5	6.6	1	CAVITIES	457	IWALL	SS-230E	02/05/87	
	4	0.13	0.06	2219-T87	6061-T6	NO			1100-O	45	0.25	7	Y	0.7	N	0.71	6.9	7.1	2	CAVITIES	445	MARTIN	SS-150A	01/27/87	
76	4	0.13	0.06	2219-T87	6061-T6	NO			1100-O	45	0.31	6.5	Y	1.2	Y	0.8	6.4	6.6	4	HOLE	466	MSFC	SS-002A	02/12/87	
	4	0.13	0.06	2219-T87	6061-T6	NO			1100-O	45	0.31	7	Y	0.5	N	0.83	7	7.1	4	CAVITIES	337	MSFC	SS-EH1B	09/26/86	
77	4	0.13	0.06	2219-T87	6061-T6	NO			1100-O	55	0.25	6.3	Y	0.3	Y	0.72		6.3	1		308	MARTIN	SS-136A	08/29/86	

	standoff inch	rearwall gage inch	bumper gage inch	rearwall alloy	bumper alloy	mli present	mli location		prj. len to dia	prj. material	obliquity	projectile size	velocity avg km/s		rear penetr'n	rearhole inch		rearwall spall	bumper hole inch	vel hall km/s	vel xray km/s	witness penet.	rico con	test number	data source	test	date	comments
	4	0.13	0.06	2219-T87	6061-T6	NO				1100-O	55	0.25	6.7	Y	0.3	N		0.69		6.7	1		310	MARTIN	SS-136C	09/02/86	
	4	0.13	0.06	2219-T87	6061-T6	NO				1100-O	55	0.25	7.2	C	0	Y		0.83	7.2	7.3	0		309	MARTIN	SS-136B	09/02/86	
78	4	0.13	0.06	2219-T87	6061-T6	NO				1100-O	60	0.19	7.4	N	0	N		0.68		7.4	0	2HOLES	517	MARTIN	SS-157A	04/16/87	
	4	0.13	0.06	2219-T87	6061-T6	NO				1100-O	60	0.19	8	Y	0.1	N		0.66	8	8.1	0	CAVITIES	717	MSFC	EHRP-7	07/25/88	
79	4	0.13	0.06	2219-T87	6061-T6	NO				1100-O	60	0.31	7.2	Y	0.3	N		1	7.1	7.2	0	HOLES	338	MSFC	SS-EH1C	09/29/86	
80	4	0.13	0.06	2219-T87	6061-T6	NO				1100-O	65	0.19	2.4	N	0	N		0.42	2.4	2.5	0	HOLE	509	IWALL	SS-231B	04/09/87	
	4	0.13	0.06	2219-T87	6061-T6	NO				1100-O	65	0.19	3.3	N	0	N		0.47	3.3	3.4	0	HOLE	508	IWALL	SS-231A	04/08/87	
	4	0.13	0.06	2219-T87	6061-T6	NO				1100-O	65	0.19	4.2	N	0	N		0.63		4.2		HOLE	516	MARTIN	SS-156C	04/16/87	
	4	0.13	0.06	2219-T87	6061-T6	NO				1100-O	65	0.19	6	C	0	N		0.63		6		HOLES	515	MARTIN	SS-156B	04/15/87	SURFACE CRACK ON BACK OF WALL
	4	0.13	0.06	2219-T87	6061-T6	NO				1100-O	65	0.19	7.1	N	0	N		0.75		7.1		HOLES	514	MARTIN	SS-156A	04/15/87	
	4	0.13	0.06	2219-T87	6061-T6	NO				1100-O	65	0.19	7.3	N	0	N		0.62	7.3	7.4	0	CAVITIES	721	MSFC	EHRP-9	07/29/88	
81	4	0.13	0.06	2219-T87	6061-T6	NO				1100-O	65	0.25	3.3	N	0	N		0.8	3.2	3.4	0	2HOLES	228	IWALL	SS-208C	06/16/86	
	4	0.13	0.06	2219-T87	6061-T6	NO				1100-O	65	0.25	4.3	Y	0.2	N		0.73	4.2	4.4	0		227	IWALL	SS-208B	06/13/86	
	4	0.13	0.06	2219-T87	6061-T6	NO				1100-O	65	0.25	5	N	0	N		0.82	4.9	5	0		226	IWALL	SS-208A	06/13/86	
	4	0.13	0.06	2219-T87	6061-T6	NO				1100-O	65	0.25	5.6	C	0	N		0.79		5.6	0	HOLES	229	IWALL	SS-208D	06/17/86	COUNT REAR SURFACE CRACK AS FAILURE
	4	0.13	0.06	2219-T87	6061-T6	NO				1100-O	65	0.25	6.5	Y	0.2	N		0.83	6.5	6.5	1	HOLES	264	IWALL	SS-208E	07/16/86	
82	4	0.13	0.06	2219-T87	6061-T6	NO				1100-O	65	0.31	6.6	Y	0.2	Y		1.21	6.6	6.6		HOLES	511	IWALL	SS-231C	04/10/87	
	4	0.13	0.06	2219-T87	6061-T6	NO				1100-O	65	0.31	7.3	Y	0.2	Y		1	7.1	7.3	0	HOLES	512	IWALL	SS-231D	04/13/87	
83	4	0.13	0.06	2219-T87	6061-T6	NO				1100-O	75	0.25	7.3	Y	0.2	N		1.11	7.2	7.4		CAVITIES	598	MSFC	EH1-B	07/27/87	
84	4	0.13	0.06	2219-T87	6061-T6	NO				1100-O	75	0.31	6.9	Y	0.2	N		1.28	6.8	7	1	HOLE	593		EH1-A	07/22/87	
	4	0.13	0.06	2219-T87	6061-T6	NO				1100-O	75	0.31	6.9	Y	0.1	N		1.32	6.9	7	1	HOLES	594		EH1-AA	07/23/87	
	4	0.13	0.06	2219-T87	6061-T6	NO				1100-O	75	0.31	6.9	Y	0.2	N		1.49	6.9	7		CAVITIES	597		EH1-AB	07/24/87	
	4	0.13	0.06	2219-T87	6061-T6	NO				1100-O	75	0.31	7.2	Y	0.2	N		1.41	7.1	7.2	1	HOLES	340	MSFC	SS-EH1D	09/30/86	
85	4	0.13	0.06	2219-T87	6061-T6	NO				6061-T6	0	0.3	7	Y	0.7	Y		0.61		7	2		81	ADP SM1	SS-P-017	10/17/85	
86	4	0.13	0.06	2219-T87	6061-T6	NO				6061-T6	45	0.25	3.2	Y	0.4	N		0.58		3.2	3		171	MARTIN	SS-113A	03/10/86	
87	4	0.13	0.06	2219-T87	6061-T6	NO				6061-T6	60	0.25	3.2	N	0	N		0.73		3.2			170	MARTIN	SS-113	03/10/86	
88	4	0.13	0.06	2219-T87	6061-T6	NO				6061-T6	60	0.3	3.3	N	0	N		0.87		3.3	0		172	MARTIN	SS-114	03/11/86	
89	4	0.13	0.06	2219-T87	6061-T6	NO				GLASS	0	0.38	5.4	N	0	N		1.5	5.4				557		SS-165B	06/04/87	PROJECTILE SHATTERED

	standoff inch	rearwall gage inch	bumper gage inch	rearwall alloy	bumper alloy	mli present	mli location	prj. len to dia	prj. material	obliquity	projectile size	velocity avg km/s	rear penet/rn	rearhole inch	rearwall spall	bumper hole inch	vel hail km/s	vel xray km/s	witness penet.	rico con	test number	data source	test	date	comments
	4	0.13	0.06	2219-T87	6061-T6	NO			GLASS	0	0.38	6.4	N	0	N	1.1	6.4				555		SS-165A	06/03/87	
90	4	0.13	0.06	2219-T87	6061-T6	NO			STEEL	0	0.13	7	Y	1	Y	0.37		7	2		388	MARTIN	SS-146A	11/07/86	
	4	0.13	0.06	2219-T87	6061-T6	NO			STEEL	0	0.13	7.4	Y	0.1	Y	0.36		7.4	1		389	MARTIN	SS-146B	11/07/86	
91	4	0.13	0.06	5456	6061-T6	NO			1100-O	0	0.25	6	Y	1	Y	0.52	6	6.1	1		678	MSFC	EHSS-1B	02/22/88	
	4	0.13	0.06	5456	6061-T6	NO			1100-O	0	0.25	6.4	Y	0.2	Y	0.55	6.3	6.5	1		679	MSFC	EHSS-1C	02/24/88	
	4	0.13	0.06	5456	6061-T6	NO			1100-O	0	0.25	6.9	N		Y	0.57	6.9	6.9	1		677	MSFC	EHSS-1A	02/18/88	
92	4	0.13	0.06	5456	6061-T6	NO			1100-O	0	0.31	6.6	Y	0.7	Y	0.65	6.5	6.6	2		695	MSFC	EHSS-6A	05/02/88	
	4	0.13	0.06	5456	6061-T6	NO			1100-O	0	0.31	6.6	Y	1.8		0.58	6.6	6.7	2		696	MSFC	EHSS-6B	05/09/88	
93	4	0.13	0.06	5456	6061-T6	NO			1100-O	25	0.25	5	Y	0.6		0.56	4.9	5	2		690	MSFC	EHSS-5B	04/12/88	
94	4	0.13	0.06	5456	6061-T6	NO			1100-O	30	0.25	6.8	Y	0.2	Y	0.64	6.7	6.9	1		683	MSFC	EHSS-3A	03/17/88	
	4	0.13	0.06	5456	6061-T6	NO			1100-O	30	0.25	7.1	Y	1.3	Y	0.66	7	7.1	2		686	MSFC	EHSS-3B	03/30/88	
95	4	0.13	0.06	5456	6061-T6	NO			1100-O	45	0.25	4.1	Y	0.4	N	0.53	4.1	4.1	2		689	MSFC	EHSS-5A	04/07/88	
	4	0.13	0.06	5456	6061-T6	NO			1100-O	45	0.25	5.6	Y	0.6	Y	0.67	5.5	5.6	1		712	MSFC	EHSS-4C	07/14/88	
	4	0.13	0.06	5456	6061-T6	NO			1100-O	45	0.25	6.8	Y	0.3		0.76	6.8	6.8	1		687	MSFC	EHSS-4A	04/01/88	
	4	0.13	0.06	5456	6061-T6	NO			1100-O	45	0.25	7	Y	0.5	Y	0.71	6.9	7	2		688	MSFC	EHSS-4B	04/04/88	
	4	0.13	0.06	5456	6061-T6	NO			1100-O	45	0.25	7.6	Y	0.2	Y	0.8	7.6	7.7	1		715	MSFC	EHRP-6	07/19/88	
96	4	0.13	0.06	5456	6061-T6	NO			1100-O	45	0.31	6.6	Y	1.3		0.84	6.6	6.6	2		697	MSFC	EHSS-7A	05/11/88	
	4	0.13	0.06	5456	6061-T6	NO			1100-O	45	0.31	6.8	Y	1	Y	0.81	6.8	6.9	2		707	MSFC	EHRP-3	06/30/88	
	4	0.13	0.06	5456	6061-T6	NO			1100-O	45	0.31	7	Y	1.4	Y	0.86	7	7.1	2		699	MSFC	EHSS-7B	05/17/88	
97	4	0.13	0.06	5456	6061-T6	NO			1100-O	60	0.25	7.7	Y	0.3		0.84	7.7	7.8	1		713	MSFC	EHRP-4	07/15/88	
98	4	0.13	0.06	5456	6061-T6	NO			1100-O	60	0.31	6.9	Y	0.4		1.2	6.9	7	1		705	MSFC	EHRP-1	06/28/88	
99	4	0.13	0.06	5456	6061-T6	NO			1100-O	65	0.25	4.3	Y	0.2		0.79	4.2	4.3	0		694	MSFC	EHSS-5D	04/28/88	
	4	0.13	0.06	5456	6061-T6	NO			1100-O	65	0.25	5.3	Y	0.1	Y	0.85	5.2	5.3	0		693	MSFC	EHSS-5C	04/20/88	
	4	0.13	0.06	5456	6061-T6	NO			1100-O	65	0.25	7.6	Y	0.3		0.87	7.5	7.6	1		714	MSFC	EHRP-5	07/18/88	
100	4	0.13	0.06	5456	6061-T6	NO			1100-O	65	0.31	6.9	Y	0.3		1.3	6.8	6.9	1		706	MSFC	EHRP-2	06/29/88	
101	4	0.13	0.06	5456	6061-T6	NO			1100-O	75	0.31	7.1	Y	0.2		1.43	7	7.2	0		701	MSFC	EHSS-8A	05/26/88	
102	4	0.13	0.06	2219-T87	6061-T6	YES	0.9		1100-O	0	0.38	6.6	Y	8	N	0.65	6.7	6.6	3		1002		3227-B	04/24/90	HOLE IN REARWALL 8" L X 2" WIDE, PETALLED OUT.
103	4	0.13	0.06	2219-T87	6061-T6	YES	2.0		1100-O	0	0.31	5	Y		N	0.57	5	5.1	1		1141		3402-D	10/16/90	WALL: 4 PETALS, PLUS CRATERS 20 LAYER MLI
	4	0.13	0.06	2219-T87	6061-T6	YES	2.0		1100-O	0	0.31	5.3	Y	0.3	N	0.58	5.3	5.3	1		1138		3401-D	10/11/90	WALL CRACKED ABOUT 1" EACH L/R, .8" EACH U/D. 30 LAYER MLI
	4	0.13	0.06	2219-T87	6061-T6	YES	2.0		1100-O	0	0.31	6.2	Y		N	0.61	6.1	6.2	0		1139		3401-C	10/15/90	30 LAYER MLI
	4	0.13	0.06	2219-T87	6061-T6	YES	2.0		1100-O	0	0.31	6.2	Y	0.3	N	0.61	6.2	6.2	0		1142		3402-C	10/17/90	WALL HOLED + 4 PETALS TO 1.75" LONG 20 LAYER MLI

C-18

	standoff inch	rearwall gage inch	bumper gage inch	rearwall alloy	bumper alloy	mli present	mli location	prj. len to dia	prj. material	obliquity	projectile size	velocity avg km/s	rear penetrn	rearhole inch	rearwall spall	bumper hole inch	vel hall km/s	vel xray km/s	witness penet.	rico con	test number	data source	test	date	comments
	4	0.13	0.06	2219-T87	6061-T6	YES	2.0		1100-O	0	0.31	7.1	Y	0.4	N	0.67	7.1	7.1	2		1144		3401-B	10/18/90	WALL HOLED PLUS 6 CRACKS TO 1.75" FROM IMPACT 30 LAYER MLI
	4	0.13	0.06	2219-T87	6061-T6	YES	2.0		1100-O	0	0.31	7.1	Y	0.4	N	0.66	7.1	7.2	2		1145		3402-B	10/19/90	WALL 5 CRACKS UP TO 1.25" LONG, PETALED 20 LAYER MLI
	4	0.13	0.06	2219-T87	6061-T6	YES	2.0		1100-O	0	0.31	7.2	Y	0.4	N	0.68	7.2	7.2	2		1143		3402-A	10/17/90	WALL HOLED PLUS 4 CRACKS TO 1.5" LONG FROM IMPACT 20 LAYER MLI
	4	0.13	0.06	2219-T87	6061-T6	YES	2.0		1100-O	0	0.31	7.2	Y		N	0.68	7.2	7.2	3		1140		3401-A	10/15/90	WALL: 5 PETALS W/CRACKS UP TO 2" 30 LAYER MLI
104	4	0.13	0.06	2219-T87	6061-T6	YES	2.0		1100-O	0	0.38	6.9	Y	1.8	N	0.66	6.9		3		1153		3404-B	10/26/90	7 WALL PETALS TO 3.5" RADIUS. 20 LAYER NEW MLI
	4	0.13	0.06	2219-T87	6061-T6	YES	2.0		1100-O	0	0.38	6.9	Y	2	N	0.66	6.9		3		1152		3404-A	10/25/90	5 WALL PETALS TO 3" RADIUS. 20 LAYER NEW MLI
105	4	0.13	0.06	2219-T87	6061-T6	YES	3.75		1100-O	0	0.19	3.8	C	0	N	0.43	3.8	3.8	0		1024		3305-C	05/21/90	REAR SURFACE CRACK COUNTED AS FAILURE
	4	0.13	0.06	2219-T87	6061-T6	YES	3.75		1100-O	0	0.19	4.2	N	0	N	0.4	4.2	4.2	0		1023		3305-B	05/18/90	
	4	0.13	0.06	2219-T87	6061-T6	YES	3.75		1100-O	0	0.19	4.6	N	0	N	0.38	4.6		0		1025		3305-A	05/21/90	
106	4	0.13	0.06	2219-T87	6061-T6	YES	3.75		1100-O	0	0.25	5.2	N	0	N	0.52	5.2	5.2	0		1026		3306-A	05/22/90	
	4	0.13	0.06	2219-T87	6061-T6	YES	3.75		1100-O	0	0.25	7	N	0	N	0.54	7		0		1031		3306-B	05/24/90	
	4	0.13	0.06	2219-T87	6061-T6	YES	3.75		1100-O	0	0.25	7	Y	0.1	N	0.51	7		0		1028		3306-D	05/23/90	
	4	0.13	0.06	2219-T87	6061-T6	YES	3.75		1100-O	0	0.25	7.1	Y	0.2	Y	0.52	7.1		0		1027		3306-C	05/22/90	
107	4	0.13	0.06	2219-T87	6061-T6	YES	3.75		1100-O	0	0.31	5.1	Y	0.8	N	0.67	5	5.1	2		1146		3403-D	10/19/90	WALL PETALED. 20 LAYER MLI
	4	0.13	0.06	2219-T87	6061-T6	YES	3.75		1100-O	0	0.31	6.2	Y	0.6	N	0.64	6.2	6.2	2		1147		3403-C	10/22/90	WALL: 5 PETALS W/CRACKS TO 1.2". 20 LAYER MLI
	4	0.13	0.06	2219-T87	6061-T6	YES	3.75		1100-O	0	0.31	7.1	Y	1	N	0.66	7.1	7.2	2		1148		3403-B	10/22/90	LITTLE WALL PETALING. 20 LAYER MLI
	4	0.13	0.06	2219-T87	6061-T6	YES	3.75		1100-O	0	0.31	7.2	Y	0.8	N	0.64	7.2	7.2	2		1149		3403-A	10/23/90	WALL PETALED TO 0.75" CRACKS. 20 LAYER NEW MLI
	4	0.13	0.06	2219-T87	6061-T6	YES	3.75		1100-O	0	0.31	7.2	Y	0.6	N	0.66	7.2	7.2	2		1150		MLI-BURN2	10/24/90	WALL PETALED TO 1.75" RADIUS. 20 LAYER OLD MLI
108	4	0.13	0.06	2219-T87	6061-T6	YES	3.75		1100-O	45	0.19	4.8	N	0	N	0.48	4.8	4.8	0		1032		3307-A	05/30/90	
	4	0.13	0.06	2219-T87	6061-T6	YES	3.75		1100-O	45	0.19	6.3	N	0	N	0.59	6.3	6.3	0		1033		3307-B	05/31/90	
109	4	0.13	0.06	2219-T87	6061-T6	YES	3.75		1100-O	45	0.25	5.2	Y	0	N	0.65	5.2	5.1	0		1034		3308-A	05/31/90	
	4	0.13	0.06	2219-T87	6061-T6	YES	3.75		1100-O	45	0.25	6.2	Y	0.3	N	0.56	6.2	6.2	1		1035		3308-B	06/01/90	3 HOLES: .26X.203, .27X.205, PINHOLE
110	4	0.13	0.06	2219-T87	6061-T6	YES	3.75		1100-O	75	0.31	7.1	N	0	N	1.37	7.1	7.1	0	F HOLED	1047		4002-D	06/18/90	SIDE RICOCHET PLATES VERY FINE CRATERS
111	4	0.13	0.06	2219-T87	6061-T6	YES	B		1100-O	0	0.31	7.1	Y	0.7	N	0.07	7.1	7.1			894		MLI-B1	12/11/89	MLI ON BUMPER
112	4	0.13	0.06	2219-T87	6061-T6	YES	B		1100-O	0	0.38	6.9	Y	2	N	0.75	6.9	6.8			896		MLI-B2	12/12/89	
	4	0.13	0.06	2219-T87	6061-T6	YES	B		1100-O	0	0.38	6.9	Y	2	Y	0.67	6.9	6.9	3		1000		3227-D	04/23/90	
113	4	0.13	0.06	2219-T87	6061-T6	YES	B--AL		1100-O	0	0.31	6.9	Y	0.8	Y	0.67	6.9	6.9			905		BLKT-AL-1	12/19/89	AL FOIL OF SAME AREAL WEIGHT AS MLI
114	4	0.13	0.06	2219-T87	6061-T6	YES	W	1	1100-O	0	0.2	3.1	Y	0.2	N	0.43	3	3.1			492	MSFC	SS-T2-13	03/09/87	
115	4	0.13	0.06	2219-T87	6061-T6	YES	W	1	1100-O	0	0.26	6.2	Y	1.3	N	0.6		6.2	6		132	ADP SM1	SS-P-022A	01/15/86	
116	4	0.13	0.06	2219-T87	6061-T6	YES	W		1100-O	0	0.19	2.2	Y	0.3	N	0.29		2.2			447	MSFC	MD-TEST-A	01/29/87	
	4	0.13	0.06	2219-T87	6061-T6	YES	W		1100-O	0	0.19	2.5	C	0	N	0.31		2.5	0		448	MSFC	MD-TEST-B	01/29/87	

	standoff inch	rearwall gage inch	bumper gage inch	rearwall alloy	bumper alloy	mli present	mli location	prj. len to dia	prj. material	obliquity	projectile size	velocity avg km/s	rear penet'n	rearhole inch	rearwall spall	bumper hole inch	vel hall km/s	vel xray km/s	witness panel	rico con	test number	data source	test	date	comments
	4	0.13	0.06	2219-T87	6061-T6	YES	W		1100-O	0	0.19	2.5	C	0	N	0.32	2.5	2.6			451		MD-TEST-A1	02/02/87	
	4	0.13	0.06	2219-T87	6061-T6	YES	W		1100-O	0	0.19	2.5	N	0	N	0.3		2.5	0		125	ADP SM1	SS-P-027F	01/06/86	
	4	0.13	0.06	2219-T87	6061-T6	YES	W		1100-O	0	0.19	2.8	N	0	N	0.32		2.8	0		120	ADP SM1	SS-P-027E	12/18/85	
	4	0.13	0.06	2219-T87	6061-T6	YES	W		1100-O	0	0.19	3.1	N	0	N	0.34		3.1	0		119	ADP SM1	SS-P-027D	12/17/85	
	4	0.13	0.06	2219-T87	6061-T6	YES	W		1100-O	0	0.19	3.7	N	0	N	0.38		3.7	0		118	ADP SM1	SS-P-027C	12/16/85	
117	4	0.13	0.06	2219-T87	6061-T6	YES	W		1100-O	0	0.25	2.9	Y	0.4		0.41		2.9	0		50	ADP SM1	SS-P-007	09/04/85	
	4	0.13	0.06	2219-T87	6061-T6	YES	W		1100-O	0	0.25	3	Y	0.4	Y	0.41		3	1		51	ADP SM1	SS-P-008	09/05/85	
	4	0.13	0.06	2219-T87	6061-T6	YES	W		1100-O	0	0.25	3	Y	0.2	N	0.42	3	3			480	MSFC	SS-T2-3	02/25/87	
	4	0.13	0.06	2219-T87	6061-T6	YES	W		1100-O	0	0.25	4	N	0	N	0.45		4	0		124	ADP SM1	SS-P-012D	01/03/86	
	4	0.13	0.06	2219-T87	6061-T6	YES	W		1100-O	0	0.25	4.3	Y	0.2	Y	0.45	4.3	4.4			479	MSFC	SS-T2-4	02/25/87	
	4	0.13	0.06	2219-T87	6061-T6	YES	W		1100-O	0	0.25	4.3	N	0	N	0.46		4.3	0		123	ADP SM1	SS-P-012C	01/02/86	
	4	0.13	0.06	2219-T87	6061-T6	YES	W		1100-O	0	0.25	5	N	0		0.5		5	0		53	ADP SM1	SS-P-010	09/09/85	
	4	0.13	0.06	2219-T87	6061-T6	YES	W		1100-O	0	0.25	5.2	N	0	N	0.5		5.2	0		179	ADP SM1	SS-P-034C-2	03/14/86	
	4	0.13	0.06	2219-T87	6061-T6	YES	W		1100-O	0	0.25	5.3	N	0		0.52		5.3	0		52	ADP SM1	SS-P-009	09/06/85	
	4	0.13	0.06	2219-T87	6061-T6	YES	W		1100-O	0	0.25	6.6	N	0		0.58		6.6	0		54	ADP SM1	SS-P-011	09/11/85	
	4	0.13	0.06	2219-T87	6061-T6	YES	W		1100-O	0	0.25	6.8	N	0		0.55		6.8	0		57	ADP SM1	SS-P-012B	09/12/85	
118	4	0.13	0.06	2219-T87	6061-T6	YES	W		1100-O	0	0.3	5.9	Y	2	N	0.59		5.9	1		130	ADP SM1	SS-P-021D	01/13/86	AFT PLATE CRACKED THROUGH-THICKNESS 1" UP, 1" LEFT, 1" RIGHT. PART-THROUGH CRACKS UP TO 2" UP, 3" LEFT, 3" RIGHT.
	4	0.13	0.06	2219-T87	6061-T6	YES	W		1100-O	0	0.3	6.6	N	0	N	0.61		6.6	0		129	ADP SM1	SS-P-021C	01/10/86	
	4	0.13	0.06	2219-T87	6061-T6	YES	W		1100-O	0	0.3	6.9	N	0	N	0.63		6.9	0		128	ADP SM1	SS-P-021B	01/10/86	
119	4	0.13	0.06	2219-T87	6061-T6	YES	W		1100-O	0	0.31	3.3	Y	0.6	N	0.49	3.2	3.3			478	MSFC	SS-T2-7	02/24/87	SOME CRACKS AROUND HOLE
	4	0.13	0.06	2219-T87	6061-T6	YES	W		1100-O	0	0.31	3.3	Y	0.7	N	0.55	3.2	3.3			488	MSFC	SS-T2-7A	03/05/87	PETALING AND CRACKS
	4	0.13	0.06	2219-T87	6061-T6	YES	W		1100-O	0	0.31	5.6	Y	1	N	0.6	5.6	5.7	0		485	MSFC	MD-TEST-D	03/03/87	
	4	0.13	0.06	2219-T87	6061-T6	YES	W		1100-O	0	0.31	6.1	Y	11	N	0.6	6.1	6.2	2		675	MSFC	EH4-A	12/01/87	
	4	0.13	0.06	2219-T87	6061-T6	YES	W		1100-O	0	0.31	6.6	Y	10	N	0.62	6.6	6.7			618	MSFC	EH2-C	08/25/87	BUMPER - .619" DIA. HOLE, 1" LOW, .6" RIGHT, SOME DEBRIS. BUMPER BENT OUT .6" AT CENTER. WALL - MATERIAL SPLIT 5" DOWN, 5" UP, & 3" TO THE RIGHT. SINK 3.5" DIA. & 1" DEEP. WALL PANEL BENT OUT FOR .4". MLI - HOLE 6" DIA. & FLUFFED OUT

	standoff inch	rearwall gage inch	bumper gage inch	rearwall alloy	bumper alloy	mli present	mli location	prj. lan to dia	prj. material	obliquity	projectile size	velocity avg km/s	rear penet/n	rearhole inch	rearwall spall	bumper hole inch	vel hall km/s	vel xray km/s	witness penet.	rico con	test number	data source	test	date	comments
	4	0.13	0.06	2219-T87	6061-T6	YES	W		1100-O	0	0.31	6.7	Y	10	N	0.64	6.6	6.7			619	MSFC	EH2-D	08/26/87	BUMPER - .635" DIA. HOLE, 1" LOW, .2" RIGHT, 3 DEBRIS HOLES .15" DIA. BUMPER BENT OUTWARD .8" AT CENTER. WALL - HOLE, METAL SPLIT 5" UP, & 5" DOWN, 4" LEFT. PANEL BENT OUTWARD .8" AT EDGES. LARGE CAVITY 4" DIA. & 1" DEEP
	4	0.13	0.06	2219-T87	6061-T6	YES	W		1100-O	0	0.31	6.7	N	0	N	0.77	6.6	6.7			613	MSFC	EH2-B	08/14/87	BUMPER - .766" DIA. HOLE, 1" LOW, SOME DEBRIS. BENT OUT 1.1" AT CENTER. WALL - NO HOLE, CAVITY 6" DIA. AND .55" DEEP. MLI - HOLE 6" DIA. AND FLUFFED OUT.
	4	0.13	0.06	2219-T87	6061-T6	YES	W		1100-O	0	0.31	6.7	Y	9.3	N	0.63		6.7	0		844		3020-A	10/24/89	HOLE, METAL SPLIT 4 WAYS, HORIZONTAL-4.75" LEFT AND 4.5" RIGHT, VERTICAL-2.75" UP AND 2.75" DOWN. DOES NOT SEEM TO BE A PROJECTILE PENETRATION. 4 PETALS PUSHED OUT APPROX. 1.3"
	4	0.13	0.06	2219-T87	6061-T6	YES	W		1100-O	0	0.31	6.8	Y	4	N	0.58	6.7	6.9			620	MSFC	EH2-E	08/27/87	BUMPER - .584" DIA. HOLE, 1" LOW, .2" LEFT, SOME DEBRIS, BENT OUTWARD .55" AT CENTER. WALL - HOLE 3" X 4" WITH THE SECTION PEELED BACK.
	4	0.13	0.06	2219-T87	6061-T6	YES	W		1100-O	0	0.31	6.9	Y	7	N	0.7	6.9	6.9	1		859		N2PURGE1	11/07/89	METAL SPLIT 4 PETALS, CRACKS ALONG PETALS APPROX. 4", 3.5", 4.2" AND 2.8" LONG. DAMAGE IN CENTER AREA OF PETALS APPROX. 2" DIA OF SMALL CRATERS.
	4	0.13	0.06	2219-T87	6061-T6	YES	W		1100-O	0	0.31	6.9	Y	0.8	N	0.64	6.9	7			756		EHSS-M4	03/22/89	
	4	0.13	0.06	2219-T87	6061-T6	YES	W		1100-O	0	0.31	7.1	Y	5	N	0.63	7	7.1			606	MSFC	EH2-A	08/05/87	BUMPER - .634" DIA. HOLE, .9" LOW, .3" LEFT. FEW DEBRIS CAVITIES, ONE DEBRIS HOLE .2" DIA. BUMPER BENT OUTWARD 1". WALL - HOLE, METAL SPLIT 4 DIRECTIONS LENGTH 5", 3.5", 4", AND 4". (NO PRESSURE READINGS)
	4	0.13	0.06	2219-T87	6061-T6	YES	W		1100-O	0	0.31	7.1	Y	11	N	0.65	7.1	7.2	0		834		3020-B	10/13/89	METAL SPLIT, NO PROJECTILE HOLE, LARGE SINK APPROX. 1" DEEP AND 6" DIA, WITH SPLIT IN BOTTOM, SPLIT IN METAL HORIZONTAL APPROX. 5.5" BOTH WAYS. SPLIT OPEN APPROX. .5" AT BOTTOM OF SINK.
	4	0.13	0.06	2219-T87	6061-T6	YES	W		1100-O	0	0.31	7.2	N	0	N	0.65	7.2	7.3			845		3021-A	10/24/89	NO HOLE, SINK APPROX. 5" DIA AND .5" DEEP, FEW SMALL CRATERS. PUSHED OUT ON REAR, NO DIMPLES.
120	4	0.13	0.06	2219-T87	6061-T6	YES	W		1100-O	0	0.38	4.6	Y	5.5	N	0.61	4.6	4.6			491	MSFC	SS-T2-17	03/09/87	PETALING
	4	0.13	0.06	2219-T87	6061-T6	YES	W		1100-O	0	0.38	6.8	Y	6	N	0.7	6.8	6.8	3		997		3227-A	04/19/90	REARWALL PETALLED
121	4	0.13	0.06	2219-T87	6061-T6	YES	W		1100-O	30	0.19	2.2	N	0	N	0.43		2.2			836		3022-A	10/16/89	NO HOLE, CRATER IN PROJECTILE PATH APPROX. .25" DIA AND LESS THAN .050" DEEP, SLIGHT DIMPLE ON REAR. FEW SMALL CRATERS.
	4	0.13	0.06	2219-T87	6061-T6	YES	W		1100-O	30	0.19	3.4	N	0	N	0.37		3.4			835		3022-B	10/16/89	NO HOLE, CRATER APPROX .3" X .25" IN PROJ PATH WITH LARGE DIMPLE ON REAR. FEW SMALL CRATERS UNDER BUMPER HOLE.
	4	0.13	0.06	2219-T87	6061-T6	YES	W		1100-O	30	0.19	4.1	Y	0.3	N	0.41		4.1			842		3022-C	10/23/89	HOLE 0.338" DIA. ONE CRATER APPROX. .2" DIA AND .05" DEEP IN PROJECTILE PATH. SEVERAL SMALL CRATERS IN AREA APPROX. 3.5" DIA.
	4	0.13	0.06	2219-T87	6061-T6	YES	W		1100-O	30	0.19	4.9	Y	0.2	N	0.44	4.9	4.9	1		843		3022-D	10/23/89	2 HOLES IN PROJECTILE PATH, .21" X .13" AND .15" X .70" WITH FEW SMALL CRATERS FROM HOLE UP TO AREA UNDER BUMPER HOLE.

	standoff inch	rearwall gage inch	bumper gage inch	rearwall alloy	bumper alloy	mli present	mli location		proj. len to dia	proj. material	obliquity	projectile size	velocity avg km/s		rear penet'rn	rearhole inch		rearwall spall	bumper hole inch	vel hall km/s	vel xray km/s	witness penet.	rico con	test number	data source	test	date	comments
122	4	0.13	0.06	2219-T87	6061-T6	YES	W			1100-O	30	0.25	6.2		Y	0		N	0.61	6.2	6.2			839		3023-B	10/19/89	PIN HOLE BOTTOM OF CRATER .18" WIDE X .13" DEEP WITH CRACK IN DIMPLE ON REAR. SEVERAL CRATERS IN APPROX. 3" DIA AREA UP TO .15" DIA X .07" DEEP WITH FEW DIMPLES ON REAR.
	4	0.13	0.06	2219-T87	6061-T6	YES	W			1100-O	30	0.25	7		N	0		N	0.62	6.9	7			840		3023-A	10/20/89	NO HOLE, SINK AREA APPROX. 2.5" DIA X .15" DEEP WITH SMALL CRATER IN SINK AREA UP TO .15" DIA, VERY SMALL SIMPLES ON REAR.
123	4	0.13	0.06	2219-T87	6061-T6	YES	W			1100-O	30	0.31	7		Y	7		N	0.73	7	7	0		841		3024-B	10/20/89	PROJECTILE HOLE WITH SPLIT HORIZONTALLY ACCROSS METAL
124	4	0.13	0.06	2219-T87	6061-T6	YES	W			1100-O	45	0.19	3.2		N	0		N	0.47		3.2	0	CAVITIES	386	IWALL	SS-230B	11/06/86	
	4	0.13	0.06	2219-T87	6061-T6	YES	W			1100-O	45	0.19	4.4		N	0		N	0.48		4.4	0	CAVITIES	385	IWALL	SS-230A	11/05/86	
125	4	0.13	0.06	2219-T87	6061-T6	YES	W			1100-O	45	0.25	3.2		Y	0.4		N	0.58		3.2	2	CAVITIES	242	IWALL	SS-205E	06/27/86	
	4	0.13	0.06	2219-T87	6061-T6	YES	W			1100-O	45	0.25	4.2		Y	0.2		N	0.61	4.1	4.2	0	CAVITIES	238	IWALL	SS-205A	06/24/86	
	4	0.13	0.06	2219-T87	6061-T6	YES	W			1100-O	45	0.25	4.6		Y	0.2		N	0.65	4.6	4.6	0	1HOLE	239	IWALL	SS-205B	06/25/86	
	4	0.13	0.06	2219-T87	6061-T6	YES	W			1100-O	45	0.25	5.3		Y	0.3		N	0.6		5.3	1	CAVITIES	240	IWALL	SS-205C	06/25/86	
	4	0.13	0.06	2219-T87	6061-T6	YES	W			1100-O	45	0.25	6.3		C	0		N	0.63	6.2	6.4	0	SPRAY	241	IWALL	SS-205D	06/26/86	COUNT REAR SURFACE CRACK AS FAILURE
	4	0.13	0.06	2219-T87	6061-T6	YES	W			1100-O	45	0.25	7		Y	0		N	0.7	6.9	7.1			847		3027-A	10/26/89	PIN HOLE, IN PROJECTILE PATH, ONE CRATER APPROX. .16" DIA X .08" DEEP WITH DIMPLE ON REAR, SEVERAL OTHER SMALL CRATERS IN AREA. MANY VERY SMALL CRATERS UNDER BUMPER HOLE.
126	4	0.13	0.06	2219-T87	6061-T6	YES	W			1100-O	45	0.3	6.3		Y	1.1		N	0.81	6.2	6.4	2	CAVITIES	284	IWALL	SS-212B	08/06/86	
127	4	0.13	0.06	2219-T87	6061-T6	YES	W			1100-O	45	0.31	3.1		Y	0.2		N	0.74	3	3.1	0	CAVITIES	525	MSFC	SS-320	04/28/87	CRACK IN C. 0.25" CAVITY
	4	0.13	0.06	2219-T87	6061-T6	YES	W			1100-O	45	0.31	3.7		Y	0.6		N	0.74	3.7	3.8	2	CAVITIES	599	MSFC	SS-303A	07/27/87	
	4	0.13	0.06	2219-T87	6061-T6	YES	W			1100-O	45	0.31	4.3		Y	0.3		N	0.77	4.1	4.4	1	CAVITIES	528	MSFC	SS-325	05/01/87	
	4	0.13	0.06	2219-T87	6061-T6	YES	W			1100-O	45	0.31	6.5		Y	0.2		N	0.81	6.4	6.5	0	CAVITIES	467	MSFC	SS-002B	02/12/87	
	4	0.13	0.06	2219-T87	6061-T6	YES	W			1100-O	45	0.31	7.1		Y	1.1		N	0.84	7	7.1	1 / +		846		3028-A	10/25/89	METAL HAS SMALL CRACK FROM ONE EDGE OF HOLE APPROX .7" LONG. SEVERAL CRATERS AROUND HOLE UP TO .2" DIA AND .07" DEEP, WITH FEW DIMPLES ON REAR. MANY VERY SMALL CRATERS UNDER BUMPER HOLE WITH NO DIMPLES ON REAR. #2 WITNESS HAS
128	4	0.13	0.06	2219-T87	6061-T6	YES	W			1100-O	45	0.35	5.9		Y	1.1		N	0.86	5.9	5.9	4	CAVITIES	282	IWALL	SS-211B	08/05/86	
	4	0.13	0.06	2219-T87	6061-T6	YES	W			1100-O	45	0.35	7		Y	1.3		N	0.91	6.8	7.1	4	CAVITIES	283	IWALL	SS-211D	08/06/86	
129	4	0.13	0.06	2219-T87	6061-T6	YES	W			1100-O	65	0.19	3.9		N	0		N	0.44		3.9			848		3029-C	10/26/89	NO, HOLE NO DAMAGE IN PROJ PATH. FEW CRATERS UNDER BUMPER HOLE AND FOR APPROX. 3" IN DIRECTION OF PROJ TRAVEL. 3 CRATERS APPROX. .15" DIA AND .05" DEEP WITH SMALL DIMPLES ON REAR.
130	4	0.13	0.06	2219-T87	6061-T6	YES	W			1100-O	65	0.25	3.5		N	0		N	0.91		3.5			849		3030-A	10/30/89	NO HOLE, NO DAMAGE IN PROJ PATH, FEW CRATERS UNDER BUMPER HOLE AND FOR APPROX. 3" IN DIRECTION OF PROJ TRAVEL. 2 CRATERS APPROX. .17" DIA X .06" DEEP WITH DIMPLES ON REAR, OTHER CRATERS SMALLER.
	4	0.13	0.06	2219-T87	6061-T6	YES	W			1100-O	65	0.25	4.3		N	0		N	0.69	4.2	4.4	0	HOLES	274	IWALL	SS-209A	07/25/86	

	standoff inch	rearwall gage inch	bumper gage inch	rearwall alloy	bumper alloy	mli present	mli location	prj. len to dia	prj. material	obliquity	projectile size	velocity avg km/s	rear penetrn	rearhole inch	rearwall spall	bumper hole inch	vel halt km/s	vel xray km/s	witness penet.	rico con	test number	data source	test	date	comments
	4	0.13	0.06	2219-T87	6061-T6	YES	W		1100-O	65	0.25	6.4	N	0	N	0.87	6.3	6.4	0	HOLES	275	IWALL	SS-209B	07/31/86	
	4	0.13	0.06	2219-T87	6061-T6	YES	W		1100-O	65	0.25	7.3	N	0	N	0.77	7.3	7.4	0	HOLES	276	IWALL	SS-209D	07/31/86	
131	4	0.13	0.06	2219-T87	6061-T6	YES	W		1100-O	65	0.3	5.7	Y	0.2	N	0.88	5.6	5.9	0	HOLES	249	IWALL	SS-207A	07/03/86	
	4	0.13	0.06	2219-T87	6061-T6	YES	W		1100-O	65	0.3	6.3	Y	0.1	N	0.92	6.3	6.5	0	HOLES	271	IWALL	SS-207B	07/23/86	
	4	0.13	0.06	2219-T87	6061-T6	YES	W		1100-O	65	0.3	7	N	0	N	1.02	7	7.1	0	HOLES	273	IWALL	SS-207C	07/24/86	
132	4	0.13	0.06	2219-T87	6061-T6	YES	W		1100-O	65	0.31	3.5	N	0	N	0.92		3.5			851		3031-B	11/01/89	NO HOLE, VERY LITTLE DAMAGE IN PROJ PATH. CRATERS UNDER BUMPER HOLE OVER AN AREA APPROX. 3.5" DIA. FEW OF THE LARGER CRATERS UP TO .2" DIA AND .9" DEEP WITH DIMPLES ON REAR
	4	0.13	0.06	2219-T87	6061-T6	YES	W		1100-O	65	0.31	7	N	0	N	1.11	7	7.1			850		3031-C	10/31/89	NO HOLE, ALMOST NO DAMAGE IN PROJ PATH. FEW VERY LIGHT CRATERS. MANY CRATERS UNDER BUMPER HOLE OVER AN AREA APPROX 5" WIDE X 3.5" LONG PROJ TRAVEL. SEVERAL CRATER APPROX. .15" DIA X .07" DEEP WITH SMALL DIMPLES ON REAR
133	4	0.13	0.06	2219-T87	6061-T6	YES	W		1100-O	65	0.35	5.7	Y	0.1	N	1.13	5.7	5.7	0	HOLES	280	IWALL	SS-210B	08/04/86	
	4	0.13	0.06	2219-T87	6061-T6	YES	W		1100-O	65	0.35	6.9	Y	0.2	N	1.4	6.8	7.1	1	HOLES	281	IWALL	SS-210D	08/05/86	
134	4	0.13	0.06	2219-T87	6061-T6	YES	W--AL		1100-O	0	0.31	6.8	Y	0.6	N		6.9	6.8			909		BLKT-AL-2	01/03/90	AL FOIL INSTEAD OF MLI
135	4	0.13	0.06	2219-T87	2219-T87	YES			1100-O	0	0.31	6.9	Y	3	N	0.62	6.9	7	2		543	MSFC	PR-EH2	05/20/87	
	4	0.13	0.06	2219-T87	2219-T87	YES			1100-O	0	0.31	7	Y	3	N	0.62	7	7.1	2		542	MSFC	PR-EH1	05/20/87	
136	4	0.13	0.06	5456H116	6061-T6	YES			1100-O	0	0.31			1.5		0.73	6.9	7.1			745		EHSS-M1	03/04/89	
	4	0.13	0.06	5456H116	6061-T6	YES			1100-O	0	0.31					0.65	6.9	7.1			747		EHSS-M3	03/06/89	
137	4	0.13	0.06	5456H116	6061-T6	YES			1100-O	45	0.31			0.4		0.85	7	7.2			746		EHSS-M2	03/06/89	
138	4	0.13	0.08	2219-T87	6061-T6	NO			1100-O	0	0.19	2	N	0	N	0.32		2	0		166	MARTIN	SS-109D	03/04/86	
	4	0.13	0.08	2219-T87	6061-T6	NO			1100-O	0	0.19	2.6	S	0	Y	0.35		2.6			165	MARTIN	SS-109C	03/04/86	COUNT SPALL AS PENETRATION
	4	0.13	0.08	2219-T87	6061-T6	NO			1100-O	0	0.19	3.1	Y	0.3	N	0.35		3.1	2		134	MARTIN	SS-101	01/16/86	
	4	0.13	0.08	2219-T87	6061-T6	NO			1100-O	0	0.19	3.6	N	0	N	0.39		3.6	0		164	MARTIN	SS-109B	03/03/86	
	4	0.13	0.08	2219-T87	6061-T6	NO			1100-O	0	0.19	3.7	Y	0.2	N	0.37		3.7	1		135	MARTIN	SS-101A	01/17/86	
	4	0.13	0.08	2219-T87	6061-T6	NO			1100-O	0	0.19	4.1	N	0	N	0.43		4.1	0		163	MARTIN	SS-109A	03/03/86	
	4	0.13	0.08	2219-T87	6061-T6	NO			1100-O	0	0.19	4.3	C	0	N	0.44		4.3	0		136	MARTIN	SS-101B	01/21/86	COUNT REAR SURFACE CRACK AS FAILURE
	4	0.13	0.08	2219-T87	6061-T6	NO			1100-O	0	0.19	7.4	N	0	N	0.53		7.4	0		153	MARTIN	SS-109	02/14/86	
139	4	0.13	0.08	2219-T87	6061-T6	NO			1100-O	0	0.3	7.2	Y	0	Y	0.72		7.2	0		137	MARTIN	SS-102	01/21/86	

	standoff inch	rearwall gage inch	bumper gage inch	rearwall alloy	bumper alloy	mli present	mli location	prj. len to dia	prj. material	obliquity	projectile size	velocity avg km/s	rear penetrn	rearhole inch	rearwall spall	bumper hole inch	vel hall km/s	vel xray km/s	witness penet.	rico con	test number	data source	test	date	comments
140	4	0.13	0.08	2219-T87	6061-T6	NO			1100-O	0	0.35	6.8	Y	0.8	Y	0.74		6.8	4		155	MARTIN	SS-107	02/19/86	
141	4	0.13	0.08	2219-T87	6061-T6	NO			1100-O	45	0.25	6.9	Y	0.3	N	0.72	6.8	6.9	0	HOLE	461	MARTIN	SS-151A	02/09/87	
142	4	0.13	0.08	2219-T87	6061-T6	NO			1100-O	45	0.31	6.6	Y	0.4	N	0.83	6.6	6.6	2	CAVITIES	463	MSFC	SS-001A	02/10/87	
143	4	0.13	0.08	2219-T87	6061-T6	NO			1100-O	45	0.35	3.5	Y	0.6	N	0.81		3.5	0		149	MARTIN	SS-105	02/06/86	REAR WALL HIT OVER THICK PART OF SAMPLE HOLDER
	4	0.13	0.08	2219-T87	6061-T6	NO			1100-O	45	0.35	6.8	Y	1.3	N	0.93		6.8	6		157	MARTIN	SS-106	02/21/86	
144	4	0.13	0.08	2219-T87	6061-T6	NO			1100-O	60	0.35	4.1	Y	0.4	N	1.05		4.1	1		150	MARTIN	SS-105A	02/07/86	
	4	0.13	0.08	2219-T87	6061-T6	NO			1100-O	60	0.35	6.8	Y	0.3	N	1.14		6.8	1		158	MARTIN	SS-106-1	02/24/86	
145	4	0.13	0.08	2219-T87	6061-T6	NO			1100-O	60	0.38	6.7	Y	0.5	N	1.28		6.7	3		160	MARTIN	SS-106A	02/26/86	
146	4	0.13	0.08	2219-T87	6061-T6	NO			1100-O	75	0.35	3.9	N	0	N	1.4		3.9	0		151	MARTIN	SS-105B	02/11/86	
	4	0.13	0.08	2219-T87	6061-T6	NO			1100-O	75	0.35	6.7	Y	0.1	N	1.53		6.7	0		159	MARTIN	SS-106-2	02/25/86	
147	4	0.13	0.08	2219-T87	6061-T6	NO			1100-O	75	0.38	6.7	Y	0.2	N	1.77		6.7	2		161	MARTIN	SS-106B	02/27/86	
148	4	0.13	0.08	2219-T87	6061-T6	NO			6061-T6	0	0.3	7.1	Y	0.8	Y	0.71		7.1	1		152	MARTIN	SS-110	02/12/86	
149	4	0.13	0.08	5456H116	6061-T6	W			LEXAN	0	0.5			6		0.98	6.4	6.4			920		FLASH-2	01/16/90	20 LAYERS AL FOIL INSTEAD OF MLI
150	4	0.13	0.08	2219-T87	6061-T6	YES	3.75		1100-O	0	0.25	5	Y	0.2	Y	0.51	5		0		1029		3301-E	05/23/90	
151	4	0.13	0.08	2219-T87	6061-T6	YES	3.75		1100-O	0	0.31	6.2	Y	2	N	0.66	6.2		2		1030		3302-E	05/24/90	
152	4	0.13	0.08	2219-T87	6061-T6	YES	3.75		1100-O	45	0.19	3.3	N	0	N	0.46	3.3	3.3	0	CRATERED	1058		4109-A	07/03/90	
	4	0.13	0.08	2219-T87	6061-T6	YES	3.75		1100-O	45	0.19	4.1	N	0	N	0.47		4.1	0	CRATERED	1059		4109-B	07/05/90	
	4	0.13	0.08	2219-T87	6061-T6	YES	3.75		1100-O	45	0.19	5.7	Y	0.1	Y	0.52	5.7	5.7	0		1021		3303-D	05/17/90	
	4	0.13	0.08	2219-T87	6061-T6	YES	3.75		1100-O	45	0.19	6.1	N	0	N	0.54	6.1		0		1016		3303-C	05/11/90	
	4	0.13	0.08	2219-T87	6061-T6	YES	3.75		1100-O	45	0.19	6.4	Y	0.1	N	0.56	6.4	6.4			1014		3303-A	05/09/90	
	4	0.13	0.08	2219-T87	6061-T6	YES	3.75		1100-O	45	0.19	6.5	N	0	N	0.56	6.5	6.5	0	CRATERED	1060		4109-C	07/05/90	RICOCHET CRATERS < 0.05"D
	4	0.13	0.08	2219-T87	6061-T6	YES	3.75		1100-O	45	0.19	6.8	N	0	N	0.57	6.8	6.8	0		1015		3303-B	05/10/90	
	4	0.13	0.08	2219-T87	6061-T6	YES	3.75		1100-O	45	0.19	7.4	N	0	N	0.59	7.5	7.4	0	SPRAYED	1062		4109-D	07/09/90	
153	4	0.13	0.08	2219-T87	6061-T6	YES	3.75		1100-O	45	0.25	3.3	N	0	N	0.58	3.3	3.3	0	CRATERED	1064		4110-A	07/10/90	
	4	0.13	0.08	2219-T87	6061-T6	YES	3.75		1100-O	45	0.25	4	N	0	N	0.62	4	4	0	CRATERED	1065		4110-B	07/11/90	

	standoff inch	rearwall gage inch	bumper gage inch	rearwall alloy	bumper alloy	mli present	mli location	prj. lan to dia	prj. material	obliquity	projectile size	velocity avg km/s	rear penetrn	rearhole inch	rearwall spall	bumper hole inch	vel hall km/s	vel xray km/s	witness panel. rico con	test number	data source	test	date	comments
	4	0.13	0.08	2219-T87	6061-T6	YES	3.75		1100-O	45	0.25	5.8	Y	0.1	N	0.75	5.8	5.8	0 CRATERED	1068		4110-C	07/12/90	SM. CRATERS ON RICO. PLATE UP TO 0.07"DIA X 0.03"DEEP
	4	0.13	0.08	2219-T87	6061-T6	YES	3.75		1100-O	45	0.25	6.1	Y	0.2	N	0.71	6.2	6	0	1017		3304-A	05/11/90	
	4	0.13	0.08	2219-T87	6061-T6	YES	3.75		1100-O	45	0.25	6.2	Y	0.4	N	0.72	6.3	6.1	1	1018		3304-B	05/14/90	BUMPER HOLE .722" X .568", 0.6" LOW, 0.4" LEFT. NO DEBRIS.
	4	0.13	0.08	2219-T87	6061-T6	YES	3.75		1100-O	45	0.25	6.9	Y	0.4	N	0.66	6.8	6.9	1	1019		3304-C	05/14/90	BUMPER: HOLE 0.661" X 0.590" OBLONG, 1" LOW, 1.1" RIGHT.
	4	0.13	0.08	2219-T87	6061-T6	YES	3.75		1100-O	45	0.25	6.9	Y	0.1	Y	0.69	6.9	6.8	0	1020		3304-D	05/17/90	BUMPER HOLE .693"X.611" OBLONG, 0.3" LOW, 0.2" RIGHT. NO DEBRIS.
	4	0.13	0.08	2219-T87	6061-T6	YES	3.75		1100-O	45	0.25	6.9	N	0	N	0.71	7	6.9	0 CRATERED	1069		4110-D	07/13/90	RICO PLATE SMALL CRATERS UP TO 0.1" DIA X 0.03"DEEP
154	4	0.13	0.08	2219-T87	6061-T6	YES	3.75		1100-O	45	0.31	2.9	Y	0.3	N	0.7		2.9	0 CRATERED	1070		4111-A	07/16/90	RICO PLATE CRATERS UP TO 0.1" DIA X 0.03" DEEP
	4	0.13	0.08	2219-T87	6061-T6	YES	3.75		1100-O	45	0.31	3.2	Y	0.5	N	0.68	3.2	3.2	3 CRATERED	1051		4003-C	06/21/90	
	4	0.13	0.08	2219-T87	6061-T6	YES	3.75		1100-O	45	0.31	3.2	Y	0.5	N	0.71	3.2	3.2	3 CRATERED	1042		4001-A	06/13/90	
	4	0.13	0.08	2219-T87	6061-T6	YES	3.75		1100-O	45	0.31	3.4	Y	0.7	N	0.7	3.4	3.4	3 F CRATER	1048		4003-A	06/19/90	FRONT RICOCHET PLATE CRATERED.
	4	0.13	0.08	2219-T87	6061-T6	YES	3.75		1100-O	45	0.31	3.9	Y	0.6	N	0.73	3.9	3.9	2 CRATERED	1071		4111-B	07/18/90	RICO PLATE CRATERS UP TO 0.1" DIA X 0.03" DEEP
	4	0.13	0.08	2219-T87	6061-T6	YES	3.75		1100-O	45	0.31	4.3	Y	0.9	N	0.76	4.3	4.2	2 CRATERS	1040		4001-B	06/12/90	LEFT RICOCHET PANEL CRATERED OVERALL ABOVE BUMPER.
	4	0.13	0.08	2219-T87	6061-T6	YES	3.75		1100-O	45	0.31	6	Y	0.6	Y	0.83		6	3 CRATERED	1072		4111-C	07/19/90	RICO PLATE CRATERS UP TO 0.11" DIA X 0.05" DEEP. WALL SPALL AROUND HOLE 0.07" WIDE
	4	0.13	0.08	2219-T87	6061-T6	YES	3.75		1100-O	45	0.31	6.1	Y	0.8	N	0.85	6.1	6.1	2 CRATERED	1041		4001-C	06/12/90	L&R RICOCHET PANELS CRATERED OVERALL
	4	0.13	0.08	2219-T87	6061-T6	YES	3.75		1100-O	45	0.31	6.2	Y	0.6	N	0.79	6.2	6.3	1 CRATERED	1050		4003-D	06/20/90	2 HOLES IN WALL: 0.6X0.3, 0.21D
	4	0.13	0.08	2219-T87	6061-T6	YES	3.75		1100-O	45	0.31	6.3	Y	0.6	N	0.79	6.3	6.3	2 CRATERED	1049		4003-B	06/19/90	4 HOLES, .57X.35, .5X.3, .25D, .05D
	4	0.13	0.08	2219-T87	6061-T6	YES	3.75		1100-O	45	0.31	6.7	Y	0.3	N	0.83	6.7	6.7	1 CRATERED	1043		4001-D	06/13/90	
	4	0.13	0.08	2219-T87	6061-T6	YES	3.75		1100-O	45	0.31	6.8	Y	0.2	N	0.77	6.8		0 CRATERED	1073		4111-D	07/19/90	RICO PLATE CRATERS UP TO 0.1" DIA X 0.03" DEEP
155	4	0.13	0.08	2219-T87	6061-T6	YES	3.75		1100-O	60	0.19	3.3	N	0	N	0.55	3.3	3.4	0 CRATERED	1074		4112-A	07/20/90	RICO PLATE CRATERS UP TO 0.11" DIA X 0.04" DEEP
	4	0.13	0.08	2219-T87	6061-T6	YES	3.75		1100-O	60	0.19	4	N	0	N	0.52	4.1	4	0 CRATERED	1075		4112-B	07/20/90	ONE RICO CRATER 0.1" DIA X 0.1" DEEP, OTHERS 0.03" DEEP MX
	4	0.13	0.08	2219-T87	6061-T6	YES	3.75		1100-O	60	0.19	5.9	N	0	N	0.6	5.9	5.9	0 CRATERED	1076		4112-C	07/23/90	RICO PLATE CRATERS UP TO 0.15" DIA X 0.05" DEEP
	4	0.13	0.08	2219-T87	6061-T6	YES	3.75		1100-O	60	0.19	7.5	N	0	N	0.69	7.5	7.5	0 CRATERED	1077		4112-D	07/23/90	RICO PLATE CRATERS UP TO 0.12" DIA X 0.04" DEEP
156	4	0.13	0.08	2219-T87	6061-T6	YES	3.75		1100-O	60	0.25	3	N	0	N	0.65		3	0 CRATERED	1078		4113-A	07/24/90	RICO PLATE CRATERS UP TP 0.13" DIA X 0.08" DEEP
	4	0.13	0.08	2219-T87	6061-T6	YES	3.75		1100-O	60	0.25	3.8	N	0	N	0.7	3.8	3.8	0 CRATERED	1079		4113-B	07/25/90	
	4	0.13	0.08	2219-T87	6061-T6	YES	3.75		1100-O	60	0.25	6.3	Y	0.1	N	0.78	6.3	6.3	0 CRATERED	1080		4113-C	07/25/90	
	4	0.13	0.08	2219-T87	6061-T6	YES	3.75		1100-O	60	0.25	7.1	N	0	N	0.78	7.1	7.1	0 CRATERED	1082		4113-D	07/26/90	
157	4	0.13	0.08	2219-T87	6061-T6	YES	3.75		1100-O	60	0.31	3.1	N	0	N	0.83	3.1	3.2	0 CRATERED	1083		4114-A	07/27/90	
	4	0.13	0.08	2219-T87	6061-T6	YES	3.75		1100-O	60	0.31	4	N	0	N	1	4		0 CRATERED	1084		4114-B	07/27/90	
	4	0.13	0.08	2219-T87	6061-T6	YES	3.75		1100-O	60	0.31	5.9	Y	0	N	0.97	5.9	5.9	0 CRATERED	1085		4114-C	08/02/90	
	4	0.13	0.08	2219-T87	6061-T6	YES	3.75		1100-O	60	0.31	7.4	Y	0.1	Y	0.71	7.4	7.4	0 CRATERED	1086		4114-D	08/02/90	
158	4	0.13	0.08	2219-T87	6061-T6	YES	3.75		1100-O	75	0.19	3.1	N	0	N	0.63	3.1	3.2	0 CRATERED	1089		4115-A	08/06/90	
	4	0.13	0.08	2219-T87	6061-T6	YES	3.75		1100-O	75	0.19	4.1	N	0	N	0.35	4.1	4.1	0 CRATERED	1088		4115-B	08/03/90	
	4	0.13	0.08	2219-T87	6061-T6	YES	3.75		1100-O	75	0.19	6.1	N	0	N	0.47	6.1	6.1	0 CRATERED	1090		4115-C	08/07/90	
	4	0.13	0.08	2219-T87	6061-T6	YES	3.75		1100-O	75	0.19	7.3	N	0	N	0.51	7.3	7.3	0 CRATERED	1091		4115-D	08/07/90	
159	4	0.13	0.08	2219-T87	6061-T6	YES	3.75		1100-O	75	0.25	2.9	N	0	N	0.63	2.9	2.9	0 CRATERED	1092		4116-A	08/08/90	
	4	0.13	0.08	2219-T87	6061-T6	YES	3.75		1100-O	75	0.25	4.5	N	0	N	0.84	4.5	4.5	0 CRATERED	1093		4116-B	08/09/90	

	standoff inch	rearwall gage inch	bumper gage inch	rearwall alloy	bumper alloy	mil present	mil location	prj. len to dia	prj. material	obliquity	projectile size	velocity avg km/s	rear penetrn	rearhole inch	rearwall spall	bumper hole inch	vel hall km/s	vel xray km/s	witness penet.	rico con	test number	data source	test	date	comments
	4	0.13	0.08	2219-T87	6061-T6	YES	3.75		1100-O	75	0.25	6.2	N	0	N	0.96	6.2	6.2	0	CRATERED	1094		4116-C	08/14/90	
	4	0.13	0.08	2219-T87	6061-T6	YES	3.75		1100-O	75	0.25	7.4	N	0	N	0.72	7.4	7.3	0	CRATERED	1095		4116-D	08/15/90	
160	4	0.13	0.08	2219-T87	6061-T6	YES	3.75		1100-O	75	0.31	3.1	N	0	N	0.91	3.1	3.1	0	CRATERED	1096		4117-A	08/15/90	
	4	0.13	0.08	2219-T87	6061-T6	YES	3.75		1100-O	75	0.31	3.2	N	0	N	1.48	3.2	3.2	0	CRATERED	1052		4004-A	06/22/90	
	4	0.13	0.08	2219-T87	6061-T6	YES	3.75		1100-O	75	0.31	3.2	N	0	N	1.01	3.2	3.2	0	F HOLED	1046		4002-A	06/15/90	SIDE RICOCHET PLATES SPRAYED W/PARTICLES
	4	0.13	0.08	2219-T87	6061-T6	YES	3.75		1100-O	75	0.31	4	N	0	N	1.06	4	4	0	CRATERED	1044		4002-B	06/14/90	
	4	0.13	0.08	2219-T87	6061-T6	YES	3.75		1100-O	75	0.31	4.1	Y	0.4	N	1.1	4.1	4.1	0	CRATERED	1097		4117-B	08/24/90	
	4	0.13	0.08	2219-T87	6061-T6	YES	3.75		1100-O	75	0.31	6	N	0	N	1.24	6	6	0	CRATERED	1098		4117-C	08/24/90	
	4	0.13	0.08	2219-T87	6061-T6	YES	3.75		1100-O	75	0.31	6.1	Y	0.1	N	1.33	6.1	6.1	0	CRATERED	1053		4004-B	06/25/90	
	4	0.13	0.08	2219-T87	6061-T6	YES	3.75		1100-O	75	0.31	6.2	C	0	N	1.25	6.2	6.2	0	HOLE	1054		4004-C	06/26/90	COUNT REAR SURFACE CRACK AS FAILURE
	4	0.13	0.08	2219-T87	6061-T6	YES	3.75		1100-O	75	0.31	6.3	Y	0.2	N	1.35	6.3	6.3	0	F HOLED	1045		4002-C	06/14/90	SIDE RICOCHET PLATES SPRAYED W/PARTICLES, FRONT HOLED
	4	0.13	0.08	2219-T87	6061-T6	YES	3.75		1100-O	75	0.31	6.4	N	0	N	1.21	6.4	6.3	0	HOLE .1D	1056		4002-E	07/02/90	
	4	0.13	0.08	2219-T87	6061-T6	YES	3.75		1100-O	75	0.31	7.1	N	0	N	1.44	7.2	7	0	CRATERED	1103		4117-D	09/04/90	
161	4	0.13	0.08	2219-T87	6061-T6	YES	B		1100-O	0	0.25	3.9	Y	0.1	N	0.5	3.9	3.8	0		1005		3301-A	05/02/90	
	4	0.13	0.08	2219-T87	6061-T6	YES	B		1100-O	0	0.25	4.3	Y	0.4	N	0.49		4.3	3		1006		3301-B	05/02/90	
	4	0.13	0.08	2219-T87	6061-T6	YES	B		1100-O	0	0.25	5.5	N	0	N	0.59	5.5	5.5	0		1008		3301-D	05/04/90	
	4	0.13	0.08	2219-T87	6061-T6	YES	B		1100-O	0	0.25	6.3	N	0	N	0.55	6.3	6.3	0		1007		3301-C	05/03/90	
162	4	0.13	0.08	2219-T87	6061-T6	YES	B		1100-O	0	0.31	6.2	Y	0.3	N	0.7	6.2	6.2	1		1010		3302-A	05/07/90	
	4	0.13	0.08	2219-T87	6061-T6	YES	B		1100-O	0	0.31	6.4	Y	1	N	0.66	6.4	6.4	1		1011		3302-B	05/07/90	
	4	0.13	0.08	2219-T87	6061-T6	YES	B		1100-O	0	0.31	6.7	Y	0.6	N	0.73	6.7	6.6	0		1012		3302-C	05/08/90	
163	4	0.13	0.08	2219-T87	6061-T6	YES	W		1100-O	0	0.25	3.4	N	0	N	0.47		3.4			853		3033-B	11/02/89	NO HOLE, DAMAGE AREA APPROX. 3.5" DIA WITH SINK AREA APPROX 1.5" DIA AND .15" DEEP, CRATERS IN SINK AREA UP TO .15" DIA X .06" DEEP, WITH SEVERAL DIMPLES ON REAR.
	4	0.13	0.08	2219-T87	6061-T6	YES	W		1100-O	0	0.25	3.8	N	0	N	0.47	3.9	3.8			852		3033-A	11/01/89	NO HOLE, MOST OF CRATERS OVER AND AREA APPROX. 2" DIA. FEW SMALL CRATERS OVER A 4" DIA AREA. FEW OF THE CRATERS IN THE CENTER ARE UP TO .2" DIA AND .1" DEEP. ONE CRATER HAS A DIMPLE ON REAR WITH A CRACK IN METAL. SEVERAL SMAL DIMPLES ON REAR.
	4	0.13	0.08	2219-T87	6061-T6	YES	W		1100-O	0	0.25	5.6	C	0	N	0.56	5.6	5.6			869		3033-C	11/13/89	NO HOLE, ONE CRATER .226" DIA X .06" DEEP, DIMPLE ON REAR WITH CRACK IN METAL. VERY SMALL CRATERS OVER AN AREA OF 4" DIA. COUNT CRACK AS FAILURE
164	4	0.13	0.08	2219-T87	6061-T6	YES	W		1100-O	0	0.3	3.8	Y	0.2	N	0.57		3.8	0		141	MARTIN	SS-102D	01/24/86	
	4	0.13	0.08	2219-T87	6061-T6	YES	W		1100-O	0	0.3	4.7	C	0	N	0.61		4.7	0		140	MARTIN	SS-102C	01/23/86	COUNT REAR SURFACE CRACK AS FAILURE
	4	0.13	0.08	2219-T87	6061-T6	YES	W		1100-O	0	0.3	5.4	N	0	N	0.67		5.4	0		138	MARTIN	SS-102A	01/22/86	
	4	0.13	0.08	2219-T87	6061-T6	YES	W		1100-O	0	0.3	6	N	0	N	0.65		6	0		139	MARTIN	SS-102B	01/23/86	

	standoff inch	rearwall gage inch	bumper gage inch	rearwall alloy	bumper alloy	mli present	mli location	prj. len to dia	prj. material	obliquity	projectile size	velocity avg km/s	rear penetrn	rearhole inch	rearwall spall	bumper hole inch	vel hall km/s	vel xray km/s	witness penet.	rico con	test number	data source	test	date	comments
165	4	0.13	0.08	2219-T87	6061-T6	YES	W		1100-O	0	0.31	3.7	Y	0.3	N	0.57		3.7	0		855		3034-B	11/03/89	HOLE APPROX. .25" DIA WITH CRACK IN METAL APPROX. 1.3" LEFT, 1.5" RIGHT, .5" UP, AND .5" DOWN. CRATERS OVER SINK AREA APPROX. 4" DIA. SINK APPROX. .45" DEEP. CRATERS UP TO .15" DIA X .07" DEEP.
	4	0.13	0.08	2219-T87	6061-T6	YES	W		1100-O	0	0.31	4.5	Y	0.5	N	0.62	4.5	4.4	0		854		3034-A	11/02/89	HOLE APPROX .5" X .15" WITH METAL CRACK APPROX. 1.5" LEFT, 1.4" RIGHT, AND .6" UP. SINK APPROX. 4" DIA WITH APPROX 2: DIA COVERED WITH CRATERS UP TO .13" DIA AND .5" DEEP.
	4	0.13	0.08	2219-T87	6061-T6	YES	W		1100-O	0	0.31	5.6	Y	5.5	N	0.66	5.6	5.6	0		856		3034-C	11/03/89	PANEL SPLIT, CRACK 3" LONG LEFT, 2.5" LONG RIGHT, AND 2.3" LONG DOWN, SINK AREA APPROX. 5" DIA X .8" DEEP. MANY SMALL CRATER IN CENTER OF SINK COVERING APPROX. 3" DIA. METAL SEPARATED APPROX. .3" AT CENTER.
166	4	0.13	0.08	2219-T87	6061-T6	YES	W		1100-O	45	0.19	5.3	Y	0.2	N	0.53	5.3	5.3	0		863		3035-A	11/08/89	HOLE .215" DIA IN PROJ PATH, VERY LITTLE OTHER DAMAGE IN PROJ PATH. FEW CRATERS UNDER BUMPER HOLE, 4 SMALL DIMPLES ON REAR.
	4	0.13	0.08	2219-T87	6061-T6	YES	W		1100-O	45	0.19	5.9	C	0	N	0.57		5.9			864		3035-B	11/08/89	NO HOLE, ONE CRATER UNDER BUMPER HOLE .15" DIA X .14" DEEP WITH A CRACK IN THE DIMPLE ON REAR (COUNT CRACK AS FAILURE). FEW SMALL CRATERS UNDER BUMPER HOLE. fEW SMALL CRATER IN PROJ PATH WITH VERY SLIGHT DIMPLES ON REAR.
167	4	0.13	0.08	2219-T87	6061-T6	YES	W		1100-O	45	0.25	5.6	Y	0.3	N	0.66	5.5	5.6	1		857		3036-A	11/06/89	2 HOLES IN PROJ PATH, ONE PIN HOLE IN CRATER APPROX. .170" DIA. ONE HOLE APPROX .346" X .265", FEW CRATER OVER AREA APPROX. 2" DIA AND UP TO .12" DIA AND .06" DEEP. FEW CRATERS UNDER BUMPER HOLE OVER AREA APPROX. 2" HORZ X 4" VERT., ONE DIMPLE ON BACK A
	4	0.13	0.08	2219-T87	6061-T6	YES	W		1100-O	45	0.25	6.4	N	0	N	0.75	6.4	6.4			858		3036-B	11/06/89	NO HOLE, FEW CRATERS IN PROJECTIL PATH AND UNDER BUMPER HOLE. SLIGHTLY DEEPER CRATERS IN PROJ PATH. CRATERS IN PROJ PATH UP TO .15" DIA AND .05" DEEP.
168	4	0.13	0.08	2219-T87	6061-T6	YES	W		1100-O	45	0.31	3	Y	0.4	N	0.7	3	3.1	2	CAVITIES	526	MSFC	SS-321	04/28/87	
	4	0.13	0.08	2219-T87	6061-T6	YES	W		1100-O	45	0.31	4.3	Y	0.4	N	0.76	4.2	4.3	3	CAVITIES	529	MSFC	SS-326	05/01/87	
	4	0.13	0.08	2219-T87	6061-T6	YES	W		1100-O	45	0.31	6.5	Y	0.4	N	0.83	6.5	6.6	0	CAVITIES	464	MSFC	SS-001B	02/10/87	
	4	0.13	0.08	2219-T87	6061-T6	YES	W		1100-O	45	0.31	7.1	Y	0.1	N	0.86	7.1	7.1	0		861		3037-A	11/07/89	HOLE APPROX. .08" DIA IN PROJ PATH, DAMAGE AREA APPROX. 2" DIA WITH A FEW CRATERS UP TO .15" DIA X .06" DEEP. FEW VERY SMALL CRATERS UNDER BUMPER HOLE.
169	4	0.13	0.08	2219-T87	6061-T6	YES	W		1100-O	65	0.19	5.1	N	0	N	0.69	5	5.1			870		3038-A	11/13/89	NO HOLE, FEW CRATERS UNDER BUMPER HOLE, ONE CRATER .15" DIA X .05" DEEP. DAMAGE IN PROJ PATH.
	4	0.13	0.08	2219-T87	6061-T6	YES	W		1100-O	65	0.19	6.4	N	0	N	0.7	6.4	6.4			871		3038-B	11/14/89	NO HOLE, SLIGHT DAMAGE UNDER BUMPER HOLE, NO DAMAGE IN PROJ PATH, FEW CRATERS UNDER BUMPER HOLE UP TO .156" DIA AND .03" DEEP. FEW VERY SMALL SIMPLES ON REAR.

	standoff inch	rearwall gage inch	bumper gage inch	rearwall alloy	bumper alloy	mli present	mli location	prj. len to dia	prj. material	obliquity	projectile size	velocity avg km/s	rear penetrn	rearhole inch	rearwall spall	bumper hole inch	vel hail km/s	vel xray km/s	witness penet.	rico con	test number	data source	test	date	comments
170	4	0.13	0.08	2219-T87	6061-T6	YES	W		1100-O	65	0.25	4.6	N	0	N	0.73	4.5	4.6			867		3039-B	11/10/89	NO HOLE, FEW CRATERS, ONE CRATER .170" DIA AND .09" DEEP. 5 OTHER CRATERS UP TO .2" DIA AND .04" DEEP. ALL DAMAGE UNDER BUMPER HOLE. FEW DIMPLES ON REAR.
	4	0.13	0.08	2219-T87	6061-T6	YES	W		1100-O	65	0.25	5.7	Y	0.1	N	0.82	5.7	5.6	0		866		3039-A	11/10/89	HOLE .090" UNDER BUMPER HOLE SEVERAL CRATER UP TO .075" DIA X .050" DEEP, FEW SMALL DIMPLES ON REAR.
	4	0.13	0.08	2219-T87	6061-T6	YES	W		1100-O	65	0.25	6.3	Y	0.2	N	0.87	6.3	6.3	1		868		3039-C	11/13/89	2 HOLES .192" AND .175" DIA, ALL DAMAGE UNDER BUMPER HOLE, FEW CRATERS UP TO .125" DIA AND .07" DEEP. DAMAGE AREA APPROX. 4" DIA.
171	4	0.13	0.08	2219-T87	6061-T6	YES	W		1100-O	65	0.31	6.3	N	0	N	0.93	6.3	6.3			498	MSFC	SS-004A	03/26/87	
	4	0.13	0.08	2219-T87	6061-T6	YES	W		1100-O	65	0.31	6.9	Y	0.2	N	1.87	6.9	6.9	0		865		3040-A	11/09/89	2 HOLES UNDER BUMPER HOLE .140" X .180" AND .115" DIA. DAMAGE AREA APPROX. 4.5" DIA. CRATER UP TO .16" DIA X .1" DEEP, 2 CRATERS WITH SLIGHT CRACK IN DIMPLES ON REAR
172	4	0.13	0.08	2219-T87	6061-T6	YES	W		LEXAN	0	0.5	6.3	Y	8	N	1.02	6.3				919		FLASH-1	01/15/90	20 LAYERS AL FOIL INSTEAD OF MLI
173	4	0.13	0.13	2219-T87	2219-T87	NO			1100-O	0	0.25	4.4	Y	0.2	Y	0.56	4.4	4.4	1		333	MSFC	SS-139B	09/24/86	
	4	0.13	0.13	2219-T87	2219-T87	NO			1100-O	0	0.25	5	N		Y	0.61	5	5.1	0		332	MSFC	SS-139A	09/24/86	
174	4	0.16	0.06	2219-T87	6061-T6	YES	W		1100-O	45	0.25	2.9	N	0	N	0.54	3	2.9	0	CAVITIES	595	MSFC	SS-301	07/23/87	
175	4	0.16	0.06	2219-T87	6061-T6	YES			1100-O	45	0.31	4.4	N		N	0.71	4.3	4.5	0	CAVITIES	605	MSFC	SS-303B	07/31/87	
	4	0.16	0.06	2219-T87	6061-T6	YES			1100-O	45	0.31	4.7	N		N	0.73	4.6	4.7	0	CAVITIES	592	MSFC	SS-303	07/22/87	
176	4	0.16	0.06	2219-T87	6061-T6	YES			1100-O	45	0.38	6.4	Y	2.1	N	0.89	6.3	6.5	2	3HOLES	596	MSFC	SS-306	07/24/87	
177	4	0.19	0.03	2219-T87	6061-T6	NO			1100-O	0	0.25	6.6	Y	0.1	Y	0.44	6.5	6.7	1		500	IWALL	SS-228D	03/30/87	
	4	0.19	0.03	2219-T87	6061-T6	NO			1100-O	0	0.25	7	Y	0.1	Y	0.45	6.9	7	2		499	IWALL	SS-228C	03/27/87	
178	4	0.19	0.04	2219-T87	6061-T6	NO			1100-O	0	0.25	4.5	Y	0.1	Y	0.41	4.5	4.6	0		316	IWALL	SS-214D	09/05/86	
	4	0.19	0.04	2219-T87	6061-T6	NO			1100-O	0	0.25	4.8	Y	0.1	Y	0.41	4.7	4.8	0		313	IWALL	SS-214C	09/04/86	
	4	0.19	0.04	2219-T87	6061-T6	NO			1100-O	0	0.25	5.6	N		Y	0.42	5.6	5.7	0		311	IWALL	SS-214A	09/03/86	
179	4	0.19	0.04	2219-T87	6061-T6	NO			1100-O	15	0.25	4.9	Y	0.3		0.4	4.9	5	1		312	IWALL	SS-214B	09/03/86	
180	4	0.19	0.04	2219-T87	6061-T6	NO			1100-O	45	0.25	6.1	Y	0.3	N	0.63		6.1	1	CAVITIES	441	IWALL	SS-217C	01/21/87	
	4	0.19	0.04	2219-T87	6061-T6	NO			1100-O	45	0.25	6.5	Y	0.2	Y	0.58		6.5	1	CAVITIES	442	IWALL	SS-217D	01/22/87	
	4	0.19	0.04	2219-T87	6061-T6	NO			1100-O	45	0.25	7.1	Y	0.5	Y	0.58		7.1	2	CAVITIES	443	IWALL	SS-217E	01/23/87	
181	4	0.19	0.04	2219-T87	6061-T6	NO			1100-O	45	0.31	6.6	Y	1	N	0.75	6.5	6.7	4	CAVITIES	329	IWALL	SS-217A	09/22/86	
	4	0.19	0.04	2219-T87	6061-T6	NO			1100-O	45	0.31	7.1	Y	1.1	N	0.72		7.1	4	CAVITIES	331	IWALL	SS-217B	09/23/86	
182	4	0.19	0.04	2219-T87	6061-T6	YES			1100-O	0	0.35	4.6	Y	0.5	N	0.49	4.6	4.7	3		314	IWALL	SS-215A	09/04/86	
	4	0.19	0.04	2219-T87	6061-T6	YES			1100-O	0	0.35	5.5	Y	0.4	N	0.52		5.5	1		315	IWALL	SS-215B	09/05/86	
	4	0.19	0.04	2219-T87	6061-T6	YES			1100-O	0	0.35	6.1	Y	0.3	N	0.53	6.1	6.2	1		325	IWALL	SS-215D	09/16/86	
	4	0.19	0.04	2219-T87	6061-T6	YES			1100-O	0	0.35	6.2	N		N	0.54	6.1	6.3	0		324	IWALL	SS-215C	09/16/86	

	standoff inch	rearwall gage inch	bumper gage inch	rearwall alloy	bumper alloy	mli present	mli location		prj. lan to dia	prj. material	obliquity	projectile size	velocity avg km/s	rear penetrn	rearhole inch	rearwall spall	bumper hole inch	vel hall km/s	vel xray km/s	witness penet.	rico con	test number	data source	test	date	comments
183	4	0.19	0.04	2219-T87	6061-T6	YES				1100-O	45	0.35	5.8	Y	0.7	N	0.58	5.7	5.8	4		326	IWALL	SS-218A	09/19/86	
	4	0.19	0.04	2219-T87	6061-T6	YES				1100-O	45	0.35	6.3	Y	0.7	N	0.8	6.2	6.4	4	HOLES	327	IWALL	SS-218B	09/19/86	
	4	0.19	0.04	2219-T87	6061-T6	YES				1100-O	45	0.35	6.8	Y	1.2	N	0.84	6.8	6.9	4	CAVITIES	328	IWALL	SS-218C	09/22/86	
184	4	0.19	0.08	2219-T87	6061-T6	NO				1100-O	0	0.25	4.4	Y	0.2	Y	0.49		4.4	1		439	IWALL	SS-213C	01/16/87	
	4	0.19	0.08	2219-T87	6061-T6	NO				1100-O	0	0.25	5.1	N		Y	0.54		5.1	0		440	IWALL	SS-213D	01/20/87	
185	4	0.19	0.08	2219-T87	6061-T6	NO				1100-O	0	0.31	4.9	Y	0.3	Y	0.62	5	4.9	3		334	IWALL	SS-213A	09/25/86	
	4	0.19	0.08	2219-T87	6061-T6	NO				1100-O	0	0.31	5.8	Y	0.4	Y	0.65	5.7	5.9	0		335	IWALL	SS-213B	09/25/86	
186	4	0.19	0.08	2219-T87	6061-T6	NO				1100-O	45	0.31	6.9	Y	0.3	Y	0.84	6.9	7	1	CAVITIES	465	IWALL	SS-216C	02/11/87	
187	4	0.19	0.08	2219-T87	6061-T6	NO				1100-O	45	0.35	6	Y	1.3	N	0.89	5.9	6.1	4		317	IWALL	SS-216A	09/08/86	
	4	0.19	0.08	2219-T87	6061-T6	NO				1100-O	45	0.35	6.5	Y	1.6	N	0.9	6.5	6.6	4	CAVITIES	318	IWALL	SS-216B	09/08/86	
188	4	0.19	0.08	2219-T87	6061-T6	YES				1100-O	0	0.31	3.1	Y	0.5	Y	0.51		3.1	2		421	IWALL	SS-229B	12/19/86	
	4	0.19	0.08	2219-T87	6061-T6	YES				1100-O	0	0.31	3.6	Y	0.3	Y	0.55		3.6	0		422	IWALL	SS-229C	12/19/86	
	4	0.19	0.08	2219-T87	6061-T6	YES				1100-O	0	0.31	5.3	N		N	0.63		5.3	0		420	IWALL	SS-229A	12/18/86	
189	4	0.19	0.08	GR/E	6061-T6	YES	W			1100-O	0	0.31	3.8	Y	1.2		0.56	3.7	3.8	0		1039		CRW-4	06/08/90	1.2 DIA HOLE, 1-4 FRONT PLIES, 4 REAR PLIES DAMAGED
	4	0.19	0.08	GR/E	6061-T6	YES	W			1100-O	0	0.31	4.7	Y	1.5	N	0.61	4.7	4.7	0		1038		CRW-3	06/07/90	HOLE .7X1.5
	4	0.19	0.08	GR/E	6061-T6	YES	W			1100-O	0	0.31	5.4	Y	2		0.67	5.4	5.4	0		1037		CRW-2	06/04/90	HOLE .5X2, 1-3 TOP PLIES DAMAGED, 4-5 REAR PLIES DAMAGED
	4	0.19	0.08	GR/E	6061-T6	YES	W			1100-O	0	0.31	5.7	N	0		0.66	5.7	5.7			1036		CRW-1	06/01/90	FRONT: 3 PLIES DAMAGED
190	4	0.2	0.08	2219-T87	6061-T6	NO				1100-O	0	0.35	6.7	Y	0.4	Y	0.73		6.7	4		156	MARTIN	SS-107A	02/20/86	
191	4	0.23	0.08	2219-T87	6061-T6	NO				1100-O	0	0.35	6.8	Y	0.4	Y	0.73		6.8	2		162	MARTIN	SS-107B	02/28/86	
192	4	0.25	0.13	2219-T87	2219-T87	NO				1100-O	0	0.25	4	Y	0.1	Y	0.53		4	1		369	MARTIN	SS-144C	10/23/86	
	4	0.25	0.13	2219-T87	2219-T87	NO				1100-O	0	0.25	4.5	Y	0.4	Y	0.57		4.5	1		368	MARTIN	SS-144B	10/23/86	
	4	0.25	0.13	2219-T87	2219-T87	NO				1100-O	0	0.25	4.9	N		Y	0.61		4.9	0		367	MARTIN	SS-144A	10/22/86	
193	5	0.13	0.08	316SS	6061-T6	NO				1100-O	0	0.25	6.7	N	0	N	0.57	6.6	6.7		N	1119		DEBRIS-Z1	09/18/90	MOMENTUM SENSOR TEST #1
194	5	0.13	0.08	316SS	6061-T6	NO				1100-O	0	0.38	6.8	N	0	N	0.48	6.8	6.7		N	1120		DEBRIS-Z2	09/19/90	MOMENTUM SENSOR TEST #2
195	6	0.13	0.06	2219-T87	6061-T6	NO			1	6061-T6	0	0.26	7.1	Y	3.8	N	0.65		7.1	3		82	ADP SM1	SS-P-018RV	10/18/85	
196	6	0.13	0.06	2219-T87	6061-T6	NO				1100-O	0	0.13	2.9	N	0	N	0.23		2.9	0		67	ADP SM1	SS-P-015	09/27/85	
	6	0.13	0.06	2219-T87	6061-T6	NO				1100-O	0	0.13	3	N	0	N	0.23		3	0		70	ADP SM1	SS-P-015C	10/02/85	

	standoff inch	rearwall gage inch	bumper gage inch	rearwall alloy	bumper alloy	mli present	mli location	prj. len to dia	prj. material	obliquity	projectile size	velocity avg km/s	rear penetrn	rearhole inch	rearwall spall	bumper hole inch	vel hall km/s	vel xray km/s	witness penet.	rico con	test number	data source	test	date	comments
197	6	0.13	0.06	2219-T87	6061-T6	NO			1100-O	0	0.19	3.3	Y	0.1	N	0.36		3.3	0		71	ADP SM1	SS-P-014D	10/03/85	
	6	0.13	0.06	2219-T87	6061-T6	NO			1100-O	0	0.19	3.7	N	0	N	0.38		3.7	0		65	ADP SM1	SS-P-014B	09/25/85	
	6	0.13	0.06	2219-T87	6061-T6	NO			1100-O	0	0.19	3.7	Y	0.2	N	0.3		3.7	1		63	ADP SM1	SS-P-014	09/23/85	
	6	0.13	0.06	2219-T87	6061-T6	NO			1100-O	0	0.19	3.8	Y	0.2	N	0.36	3.8	3.7	0		960		2001-A	03/15/90	
	6	0.13	0.06	2219-T87	6061-T6	NO			1100-O	0	0.19	3.9	Y	0.2	Y	0.36	3.9	3.9	0		962		2001-	03/16/90	
	6	0.13	0.06	2219-T87	6061-T6	NO			1100-O	0	0.19	4.1	S	0	Y	0.36	4.1	4.1			961		2001-C	03/15/90	COUNT SPALL AS FAILURE
	6	0.13	0.06	2219-T87	6061-T6	NO			1100-O	0	0.19	4.2	Y	0.2	N	0.39		4.2	1		64	ADP SM1	SS-P-014A	09/24/85	
198	6	0.13	0.06	2219-T87	6061-T6	NO			1100-O	0	0.25	4.8	Y	0.2	Y	0.35		4.8	1		58	ADP SM1	SS-P-013	09/17/85	
	6	0.13	0.06	2219-T87	6061-T6	NO			1100-O	0	0.25	4.9	Y	0.5		0.55		4.9			59		SS-P-13A	09/17/85	
	6	0.13	0.06	2219-T87	6061-T6	NO			1100-O	0	0.25	5.8	Y	0.6	Y	0.53		5.8	2		61	ADP SM1	SS-P-013C	09/19/85	
	6	0.13	0.06	2219-T87	6061-T6	NO			1100-O	0	0.25	6.1	Y	0.2	Y	0.5	6.1	6.1	1		929		2002-A	02/15/90	
	6	0.13	0.06	2219-T87	6061-T6	NO			1100-O	0	0.25	6.2	S	0	Y	0.63		6.2	0		60	ADP SM1	SS-P-013B	09/18/85	COUNT SPALL AS PENETRATION
	6	0.13	0.06	2219-T87	6061-T6	NO			1100-O	0	0.25	6.5	Y	0.1	Y	0.57	6.5	6.5	0		930		2002-B	02/15/90	
	6	0.13	0.06	2219-T87	6061-T6	NO			1100-O	0	0.25	6.7	Y	0.2	Y	0.53	6.8	6.7	1		940		2002-C	02/22/90	SPALL AROUND HOLES IN WALL
	6	0.13	0.06	2219-T87	6061-T6	NO			1100-O	0	0.25	7.1	Y	0.2	Y	0.55		7.1	0		949		2003-A	03/05/90	WALL: 5 HOLES, SPALL AROUND HOLES
199	6	0.13	0.06	2219-T87	6061-T6	NO			1100-O	0	0.3	6.6	Y	0.1	Y	0.6		6.6	1		89	ADP SM1	SS-P-020C	11/01/85	
	6	0.13	0.06	2219-T87	6061-T6	NO			1100-O	0	0.3	7	S	0	Y	0.65		7	0		88	ADP SM1	SS-P-020B	10/30/85	COUNT SPALL AS PENETRATION
200	6	0.13	0.06	2219-T87	6061-T6	NO			1100-O	0	0.31	4.7	Y	1.5	Y	0.63	4.7	4.8			489	MSFC	SS-T2-20	03/06/87	
201	6	0.13	0.06	2219-T87	6061-T6	NO			1100-O	0	0.35	6.7	Y	2	Y	0.66		6.7	1		168	ADP SM1	SS-P-035	03/06/86	
202	6	0.13	0.06	2219-T87	6061-T6	NO			1100-O	5	0.25	6	N	0	N	0.58	6	6			959		2003-A1	03/14/90	
	6	0.13	0.06	2219-T87	6061-T6	NO			1100-O	5	0.25	6.6	Y	0.4	Y	0.51	6.6	6.6	1		956		2003-B1	03/12/90	SPALL AROUND HOLES IN WALL
	6	0.13	0.06	2219-T87	6061-T6	NO			1100-O	5	0.25	7.1	Y	0.4	Y	5.56	7.1	7.1	0		944		2003-B	02/28/90	SPALL AROUND HOLES IN WALL
	6	0.13	0.06	2219-T87	6061-T6	NO			1100-O	5	0.25	7.3	Y	1.4	Y	0.59	7.3	7.3	1		945		2003-C	02/28/90	
203	6	0.13	0.06	2219-T87	6061-T6	NO			6061-T6	0	0.19	2.3	Y	0.3	N	0.3		2.3	2		122	ADP SM1	SS-P-025B	12/22/85	
	6	0.13	0.06	2219-T87	6061-T6	NO			6061-T6	0	0.19	2.6	N	0	N	0.33		2.6	0		104	ADP SM1	SS-P-025C	11/25/85	
	6	0.13	0.06	2219-T87	6061-T6	NO			6061-T6	0	0.19	3.3	N	0	N	0.35		3.3	0		103	ADP SM1	SS-P-025A	11/22/85	
	6	0.13	0.06	2219-T87	6061-T6	NO			6061-T6	0	0.19	3.7	N	0	N	0.37		3.7	0		102	ADP SM1	SS-P-025	11/21/85	

	standoff inch	rearwall gage inch	bumper gage inch	rearwall alloy	bumper alloy	mli present	mli location	prj. len to dia	prj. material	obliquity	projectile size	velocity avg km/s	rear penet'n	rearhole inch	rearwall spall	bumper hole inch	vel hall km/s	vel xray km/s	witness penet.	rico con	test number	data source	test	date	comments
204	6	0.13	0.06	2219-T87	6061-T6	NO			6061-T6	0	0.25	5.8	Y	0.1	N	0.53		5.8	0		97	ADP SM1	SS-P-024C	11/13/85	
	6	0.13	0.06	2219-T87	6061-T6	NO			6061-T6	0	0.25	5.9	Y	0.1	Y	0.52		5.9	0		100	ADP SM1	SS-P-024F	11/20/85	
	6	0.13	0.06	2219-T87	6061-T6	NO			6061-T6	0	0.25	6	Y	0	Y	0.53		6			98		SS-P-24D	11/14/85	COUNT SPALL AS PENETRATION
205	6	0.13	0.06	2219-T87	6061-T6	NO			6061-T6	0	0.3	5.1	Y	1	Y	0.54		5.1	2		72	ADP SM1	SS-P-016	10/04/85	
	6	0.13	0.06	2219-T87	6061-T6	NO			6061-T6	0	0.3	6	Y	1	N	0.57		6	2		73		SS-P-016A	10/04/85	
	6	0.13	0.06	2219-T87	6061-T6	NO			6061-T6	0	0.3	6.3	Y	1	Y	0.58		6.3	1		74	ADP SM1	SS-P-016B	10/07/85	
	6	0.13	0.06	2219-T87	6061-T6	NO			6061-T6	0	0.3	6.6	Y	0.8	Y	0.6		6.6	1		75	ADP SM1	SS-P-016C	10/08/85	
	6	0.13	0.06	2219-T87	6061-T6	NO			6061-T6	0	0.3	6.8	Y	1	Y	0.62		6.8	0		77	ADP SM1	SS-P-016E	10/10/85	
	6	0.13	0.06	2219-T87	6061-T6	NO			6061-T6	0	0.3	7.2	Y	0	Y	0.65		7.2	0		79	ADP SM1	SS-P-016G	10/15/85	COUNT SPALL AS PENETRATION
206	6	0.13	0.06	2219-T87	AL-LI	NO			1100-O	0	0.31	3.5	Y	0.8	N	0.47		3.5	3		360		SS-219A	10/15/86	
207	6	0.13	0.06	2219-T87	6061-T6	YES	W		1100-O	0	0.13	2.1	N	0	N	0.21		2.1	0		69	ADP SM1	SS-P-015B	10/01/85	
208	6	0.13	0.06	2219-T87	6061-T6	YES	W		1100-O	0	0.19	2.8	Y	0.3	N	0.33		2.8	0		107	ADP SM1	SS-P-014E	12/02/85	
	6	0.13	0.06	2219-T87	6061-T6	YES	W		1100-O	0	0.19	3	N	0	N	0.34		3	0		106	ADP SM1	SS-P-014F	12/02/85	
	6	0.13	0.06	2219-T87	6061-T6	YES	W		1100-O	0	0.19	3.7	N	0	N	0.38		3.7	0		66	ADP SM1	SS-P-014C	09/26/85	
209	6	0.13	0.06	2219-T87	6061-T6	YES	W		1100-O	0	0.25	3.9	C	0	N	0.48		3.9	0		108	ADP SM1	SS-P-013E	12/03/85	COUNT REAR SURFACE CRACK AS FAILURE
	6	0.13	0.06	2219-T87	6061-T6	YES	W		1100-O	0	0.25	6	N	0	N	0.55		6	0		62	ADP SM1	SS-P-013D	09/20/85	
210	6	0.13	0.06	2219-T87	6061-T6	YES	W		1100-O	0	0.3	4.3	Y	1	N	0.48		4.3	2		93	ADP SM1	SS-P-020G	11/06/85	0-
	6	0.13	0.06	2219-T87	6061-T6	YES	W		1100-O	0	0.3	4.7	Y	0.5	N	0.54		4.7	0		114	ADP SM1	SS-P-020H	12/12/85	
	6	0.13	0.06	2219-T87	6061-T6	YES	W		1100-O	0	0.3	5	N	0	N	0.55		5	0		92	ADP SM1	SS-P-020F	11/05/85	
211	6	0.13	0.06	2219-T87	6061-T6	YES	W		1100-O	0	0.31	2.9	Y	0.8	N	0.57	2.9	2.9			496	MSFC	SS-T2-19B	03/11/87	PETALED
	6	0.13	0.06	2219-T87	6061-T6	YES	W		1100-O	0	0.31	3	Y	0.3	N	0.53	3	3			490	MSFC	SS-T2-19A	03/06/87	
	6	0.13	0.06	2219-T87	6061-T6	YES	W		1100-O	0	0.31	4.1	N	0	N	0.58	4.1	4.1			486	MSFC	SS-T2-19	03/04/87	
212	6	0.13	0.06	2219-T87	6061-T6	YES	W		1100-O	0	0.35	6.3	N	0	N	0.64		6.3	0		169	ADP SM1	SS-P-035B	03/07/86	

	standoff inch	rearwall gage inch	bumper gage inch	rearwall alloy	bumper alloy	mli present	mli location	prj. len to dia	prj. material	obliquity	projectile size	velocity avg km/s	rear penetr'n	rearhole inch	rearwall spall	bumper hole inch	vel hall km/s	vel xray km/s	witness penet.	rico con	test number	data source	test	date	comments
213	6	0.13	0.06	2219-T87	6061-T6	YES	W		6061-T6	0	0.19	1.6	S	0	Y	0.27		1.6	0		105	ADP SM1	SS-P-025D	11/26/85	COUNT SPALL AS PENETRATION
214	6	0.13	0.06	2219-T87	6061-T6	YES	W		6061-T6	0	0.25	4.3	S	0	Y	0.46		4.3	0		101	ADP SM1	SS-P-024G	11/21/85	COUNT SPALL AS PENETRATION
215	6	0.13	0.06	2219-T87	6061-T6	YES	W		6061-T6	0	0.3	3.4	Y	0.3	N	0.49		3.4	2		110	ADP SM1	SS-P-016M	12/04/85	
	6	0.13	0.06	2219-T87	6061-T6	YES	W		6061-T6	0	0.3	3.8	Y	0.3	N	0.51		3.8	3		111	ADP SM1	SS-P-016N	12/10/85	
	6	0.13	0.06	2219-T87	6061-T6	YES	W		6061-T6	0	0.3	4.2	Y	0.3	N	0.51		4.2	1		112	ADP SM1	SS-P-016P	12/11/85	
	6	0.13	0.06	2219-T87	6061-T6	YES	W		6061-T6	0	0.3	4.8	N	0	N	0.54		4.8	0		109	ADP SM1	SS-P-016L	12/03/85	
	6	0.13	0.06	2219-T87	6061-T6	YES	W		6061-T6	0	0.3	6.7	N	0	N	0.59		6.7	0		85	ADP SM1	SS-P-016K	10/25/85	
	6	0.13	0.06	2219-T87	6061-T6	YES	W		6061-T6	0	0.3	6.7	N	0	N	0.6		6.7	0		84	ADP SM1	SS-P-016J	10/22/85	
	6	0.13	0.06	2219-T87	6061-T6	YES	W		6061-T6	0	0.3	7.1	N	0	N	0.61		7.1	0		80	ADP SM1	SS-P-016H	10/16/85	
216	6	0.13	0.08	2219-T87	6061-T6	NO			1100-O	0	0.3	6.6	Y	0.2	Y	0.63	6.4	6.7	2		206	MARTIN	SS-121-2	05/22/86	
	6	0.13	0.08	2219-T87	6061-T6	NO			1100-O	0	0.3	6.8	Y	0.1	Y	0.66	6.7	6.9			205	MARTIN	SS-121-1	05/21/86	
217	6	0.13	0.08	2219-T87	6061-T6	YES	W		1100-O	0	0.35	5.7	Y	12	N	0.63		5.7	2		173	ADP SM1	SS-P-035C	03/11/86	SPLIT IN TWO.
218	6	0.19	0.19	2219-T87	2219-T87	NO			6061-T6	0	0.5	6	Y	4	N	1.3	5.9	6.1	2		648	MSFC	SS-185A	10/14/87	BUMBER - 1.303" DIA. HOLE WITH RING KNOCKED OUT .1" WIDE AND .080" DEEP FRONT AND BACK. NO DEBRIS HOLES , SOME DEBRIS, .5" LEFT, .7" LOW. WALL - HOLE SECTION 3" X 4" KNOCKED OUT. 1/3 OF SECTION BROKE OFF, THE REMAINING PORTION OF SECTION HANGING BY 1" S
219	8	0.25	0.13	2219-T87	2219-T87	NO			1100-O	0	0.25	3.4	N			0.5	3.4	3.4			353	MARTIN	SS-142A	10/09/86	
220	8	0.25	0.13	2219-T87	2219-T87	NO			1100-O	0	0.31	2.9	N		Y	0.55	2.8	2.9			356	MARTIN	SS-143B	10/10/86	
	8	0.25	0.13	2219-T87	2219-T87	NO			1100-O	0	0.31	3.8	N		N	0.63	3.8	3.9			355	MSFC	SS-143A	10/10/86	
221	12	0.13	0.03	2219-T87	6061-T6	YES	W		1100-O	0	0.19	4.3	Y	0.3	N	0.29		4.3	1		876		3119-A	11/16/89	2 HOLES, FEW VERY SMALL CRATERS
	12	0.13	0.03	2219-T87	6061-T6	YES	W		1100-O	0	0.19	4.8	N	0	N	0.3	4.8	4.8			877		3119-B	11/17/89	NO HOLE, FEW SMALL CRATERS
	12	0.13	0.03	2219-T87	6061-T6	YES	W		1100-O	0	0.19	5.5	Y	0.1	N	0.31	5.6	5.5			988		3222-A	04/11/90	
222	12	0.13	0.03	2219-T87	6061-T6	YES	W		1100-O	0	0.25	4.9	Y	0.2	Y	0.4	5	4.9	0		874		3120-A	11/15/89	3 HOLES, FEW CRATERS, PIN HOLE & SPALLING OFF REAR,
	12	0.13	0.03	2219-T87	6061-T6	YES	W		1100-O	0	0.25	5.4	Y	0.1	N	0.44	5.4	5.5			875		3120-B	11/16/89	HOLE IN BOTTOM, MOST DAMAGE IN .5" DIA AREA

	standoff inch	rearwall gage inch	bumper gage inch	rearwall alloy	bumper alloy	mli present	mli location	prj. len to dia	prj. material	obliquity	projectile size	velocity avg km/s	rear penet'n	rearhole inch	rearwall spall	bumper hole inch	vel hall km/s	vel xray km/s	witness panel.	rico con	test number	data source	test	date	comments
	12	0.13	0.03	2219-T87	6061-T6	YES	W		1100-O	0	0.25	6.2	Y	0.3	Y	0.38	6.2	6.1	0		986		3221-A	04/10/90	SPALL AROUND SOME HOLES AND ON DIMPLES
	12	0.13	0.03	2219-T87	6061-T6	YES	W		1100-O	0	0.25	6.4	Y	0.2	Y	0.4	6.4	6.4	0		987		3221-B	04/10/90	SPALL AROUND HOLES
223	12	0.13	0.03	2219-T87	6061-T6	YES	W		1100-O	0	0.31	4.6	Y	0.5	N	0.46	4.6	4.6	2		873		3121-B	11/15/89	5 HOLES, SEVERAL CRATERS WITH DIMPLES ON REAR, DAMAGE
	12	0.13	0.03	2219-T87	6061-T6	YES	W		1100-O	0	0.31	5.6	Y	0	N	0.46	5.6	5.6			872		3121-A	11/14/89	2 PIN HOLES, SINK AREA, CRATERS OVER AREA, SEVERAL DIMPLES
	12	0.13	0.03	2219-T87	6061-T6	YES	W		1100-O	0	0.31	6	Y	0.1	Y	0.47	6				984		3220-A	04/06/90	
	12	0.13	0.03	2219-T87	6061-T6	YES	W		1100-O	0	0.31	6.5	Y	0.2	N	0.47	6.5	6.5	0		985		3220-B	04/09/90	
224	12	0.13	0.03	2219-T87	6061-T6	YES	W		1100-O	0	0.38	5.9	Y	0.7	N	0.5	5.9	5.8	2		993		3225-A	04/17/90	HOLE, METAL SPLIT, PETALS PUSHED OUT ON REAR
	12	0.13	0.03	2219-T87	6061-T6	YES	W		1100-O	0	0.38	5.9	Y	0.5	N	0.5	5.9	5.9	1		992		3225-B	04/16/90	HOLE, METAL SPLIT, METAL MISSSING FROM CENTER, 4 PETALS PUSHED
	12	0.13	0.03	2219-T87	6061-T6	YES	W		1100-O	0	0.38	6.2	Y	1.5	N	0.53	6.2	6.2	1		1009		3225-C	05/04/90	
225	12	0.13	0.03	2219-T87	6061-T6	YES	W		1100-O	45	0.19	4.9	Y	0.3	N	0.45	4.9	5	0		900		3122-C	12/14/89	HOLE, 6 SM CRATERS NEAR HOLE, SM CRATER UNDER BUMPER HOLE
	12	0.13	0.03	2219-T87	6061-T6	YES	W		1100-O	45	0.19	5.5	N	0	N	0.47	5.4	5.5			901		3122-D	12/15/89	
	12	0.13	0.03	2219-T87	6061-T6	YES	W		1100-O	45	0.19	6.3	N	0	N	0.45	6.3	6.3	0		895		3122-B	12/11/89	NO HOLE, 10 CRATERS, 3 DIMPLES ON REAR, FEW SMALL CRATERS UNDER BUMPER HOLE
	12	0.13	0.03	2219-T87	6061-T6	YES	W		1100-O	45	0.19	7.4	N	0	N	0.57	7.4	7.4			890		3122-A	12/06/89	NO HOLE, 1 SMALL CRATER IN PROJECTILE PATH
226	12	0.13	0.03	2219-T87	6061-T6	YES	W		1100-O	45	0.25	7.2	Y	0.3	Y	0.62	7.2	7.2	2		888		3123-A	12/05/89	HOLE, 1 PIN HOLE IN CRATER W/SPALL OFF DIMPLE ON REAR, 5 CRATERS
	12	0.13	0.03	2219-T87	6061-T6	YES	W		1100-O	45	0.25	7.6	Y	0.2	Y	0.6	7.6	7.6	0		889		3123-B	12/05/89	2 HOLES, FEW CRATERS W/DIMPLES ON REAR, NO DAM UNDER BUMPER HOLE
227	12	0.13	0.03	2219-T87	6061-T6	YES	W		1100-O	45	0.31	5	Y	0.7	N	0.68	5	4.9	2		884		3124-A	11/27/89	HOLE, 2 CRATERS W/DIMPLES ON REAR, FEW SMALL CRATERS.
	12	0.13	0.03	2219-T87	6061-T6	YES	W		1100-O	45	0.31	6.2	Y	0.7	N	0.77	6.2	6.2	2		885		3124-B	11/28/89	5 HOLES, FEW CRATERS W/DIMPLE ON REAR, FEW UNDER BUMPER HOLE
	12	0.13	0.03	2219-T87	6061-T6	YES	W		1100-O	45	0.31	6.7	Y	0.6	N	0.72	6.7	6.6	2		886		3124-C	11/29/89	5 HOLES IN PROJECTILE PATH, FEW SMALL CRATERS
228	12	0.13	0.04	2219-T87	6061-T6	TPS	TPS		1100-O	0	0.31	6.8	N	0	N	0.55	6.8	6.9			732		GRIT-11	08/18/88	
229	12	0.13	0.04	2219-T87	6061-T6	TPS	TPS		1100-O	0	0.38	6.7	Y	0.2	N	0.56	6.6	6.7	0		729		GRIT-8	08/15/88	
230	12	0.13	0.06	2219-T87	6061-T6	TPS	TPS		1100-O	0	0.38	5.9	Y	0.1	N	0.64	5.8	5.9	0		731		GRIT-10	08/17/88	
231	12	0.13	0.06	2219-T87	6061-T6	YES	W		1100-O	0	0.19	3.6	Y	0.2	N	0.36		3.6	0		882		3128-A	11/22/89	HOLE .2" DIA, FEW SMALL CRATER SCATTERED OVER PANEL
	12	0.13	0.06	2219-T87	6061-T6	YES	W		1100-O	0	0.19	4.2	N	0	N	0.39	4.2	4.2			883		3128-B	11/22/89	NO HOLE,SCATTERING SM CRATERS,FEW VERY SM CRATERS TO EDGE PANEL
232	12	0.13	0.06	2219-T87	6061-T6	YES	W		1100-O	0	0.25	4.3	Y	0.4	N	0.45	4.3	4.3	0		880		3129-A	11/20/89	5 HOLES, FEW CRATERS, FEW VERY SM CRATERS OUT TO EDGE OF PANEL
	12	0.13	0.06	2219-T87	6061-T6	YES	W		1100-O	0	0.25	4.8	Y	0.2	Y	0.47	4.8	4.8	1		881		3129-B	11/21/89	2 HOLES W/SPALLING OFF REAR
	12	0.13	0.06	2219-T87	6061-T6	YES	W		1100-O	0	0.25	5.2	Y	0.1	Y	0.49	5.2	5.2	0		990		3224-A	04/13/90	
	12	0.13	0.06	2219-T87	6061-T6	YES	W		1100-O	0	0.25	5.3	N	0	N	0.53	5.3	5.3	0		989		3224-B	04/12/90	

C-33

	standoff inch	rearwall gage inch	bumper gage inch	rearwall alloy	bumper alloy	mli present	mli location	prj. len to dia	prj. material	obliquity	projectile size	velocity avg km/s	rear penet'n	rearhole inch	rearwall spall	bumper hole inch	vel hall km/s	vel xray km/s	witness penet.	rico con	test number	data source	test	date	comments
233	12	0.13	0.06	2219-T87	6061-T6	YES	W		1100-O	0	0.31	4.6	Y	0.3	N	0.56	4.6	4.6	0		879		3130-B	11/20/89	4 HOLES
	12	0.13	0.06	2219-T87	6061-T6	YES	W		1100-O	0	0.31	5.3	C	0	N	0.58	5.3	5.3			878		3130-A	11/17/89	NO HOLE,SOME DAMAGE,FEW CRATERS W/DIMPLES,2 DIMPLES W/SM CRACKS. COUNT REAR SURFACE CRACKS AS FAILURES.
	12	0.13	0.06	2219-T87	6061-T6	YES	W		1100-O	0	0.31	5.9	N	0	N	0.62	5.9	5.9	0		991		3223-A	04/16/90	
234	12	0.13	0.06	2219-T87	6061-T6	YES	W		1100-O	0	0.38	5.6	Y	0.9	Y	0.64	5.6	5.5	1		994		3226-B	04/17/90	3 HOLES, SPALL AROUND HOLES, FEW SMALL CRATERS OUTSIDE MLI BLNKS
	12	0.13	0.06	2219-T87	6061-T6	YES	W		1100-O	0	0.38	5.6	Y	0.1	N	0.63	5.6	5.6	0		995		3226-A	04/18/90	3 HOLES, 2 HOLES TOGETHER IN CENTER W/METAL PUSHED UP ON REAR
	12	0.13	0.06	2219-T87	6061-T6	YES	W		1100-O	0	0.38	6	S	0	Y	0.64	6	5.9	0		996		3226-C	04/18/90	COUNT SPALL AS FAILURE
	12	0.13	0.06	2219-T87	6061-T6	YES	W		1100-O	0	0.38	6.6	N	0	N	0.66	6.6	6.6	0		998		3227-C	04/20/90	
235	12	0.13	0.06	2219-T87	6061-T6	YES	W		1100-O	45	0.19	3.6	N	0	N	0.46		3.6			918		3131-C	01/11/90	
	12	0.13	0.06	2219-T87	6061-T6	YES	W		1100-O	45	0.19	3.9	N	0	N	0.49	3.9	3.9			903		3131-B	12/18/89	
	12	0.13	0.06	2219-T87	6061-T6	YES	W		1100-O	45	0.19	4.1	N	0	N	0.5	4.1	4.1			902		3131-A	12/15/89	
236	12	0.13	0.06	2219-T87	6061-T6	YES	W		1100-O	45	0.25	5.4	Y	0.3	N	0.67	5.4	5.3	1		915		3132-A	01/09/90	
	12	0.13	0.06	2219-T87	6061-T6	YES	W		1100-O	45	0.25	6.4	Y	0.2	N	0.69	6.4	6.4	0		917		3132-C	01/10/90	
	12	0.13	0.06	2219-T87	6061-T6	YES	W		1100-O	45	0.25	7	N	0	N	0.69	7	7			916		3132-B	01/09/90	
237	12	0.13	0.06	2219-T87	6061-T6	YES	W		1100-O	45	0.31	6.3	Y	0.3	Y	0.82	6.4	6.3	1		910		3133-B	01/04/90	
	12	0.13	0.06	2219-T87	6061-T6	YES	W		1100-O	45	0.31	6.8	Y	0.6	N	0.82	6.8	6.8	2		914		3133-D	01/08/90	
	12	0.13	0.06	2219-T87	6061-T6	YES	W		1100-O	45	0.31	6.9	Y	0.3	N	0.82	6.9	6.9	1		911		3133-C	01/05/90	
238	12	0.13	0.06	2219-T87	6061-T87	YES	W		1100-O	45	0.31	5.1	Y	0.4	N	0.76		5.1	1		904		3133-A	12/19/89	
239	12	0.13	0.08	2219-T87	6061-T6	NO			1100-O	0	0.35	6.9	Y	0.2	N	0.69		6.9	0		154	MARTIN	SS-108	02/18/86	
240	12	0.13	0.13	2219-T87	2219-T87	NO			1100-O	0	0.5	6.1	Y	0.1	N	1.08	6.1				661	MSFC	SS-189B	11/02/87	
	12	0.13	0.13	2219-T87	2219-T87	NO			1100-O	0	0.5	6.1	Y	0.2	N	1.07	6.1	6.2	1		660	MSFC	SS-189A	10/30/87	
241	12	0.13	0.13	2219-T87	2219-T87	TPS			1100-O	0	0.38					0.95	6.7	6.7			722		GRIT-1	08/03/88	
	12	0.13	0.13	2219-T87	2219-T87	TPS			1100-O	0	0.38					0.95	6.8	6.9			723		GRIT-2	08/04/88	
242	12	0.13	0.13	2219-T87	2219-T87	TPS			1100-O	0				0.2		1.15	6.4	6.5			727		GRIT-6	08/11/88	
243	12	0.13		2219-T87	B-CLOTH	TPS			1100-O	0	0.13					0.17	7.4	7.5			728		GRIT-7	08/12/88	
244	12	0.19	0.19	2219-T87	2219-T87	NO			6061-T6	0	0.5	5.3	Y	0.1	Y	1.22	5.2	5.4			647	MARTIN	SS-184B	10/08/87	BUMBER - 1.216" DIA. HOLE WITH RING .1" WIDE AND .08" DEEP AROUND HOLE FRONT AND BACK. SOME DEBRIS, 1.5" LOW, .5" LEFT. WALL - 2 HOLES, .1" DIA. IN A CAVIVITY .25" DIA. AND LOCATED AT 11:00 O'CLOCK AND 3" FROM CENTER. SECOND HOLE .050" DIA. IN A CAVITY

	standoff inch	rearwall gage inch	bumper gage inch	rearwall alloy	bumper alloy	mli present	mli location	prj. len to dia	prj. material	obliquity	projectile size	velocity avg km/s	rear penet'n	rearhole inch	rearwall spall	bumper hole inch	vel hall km/s	vel xray km/s	witness penet.	rico con	test number	data source	test	date	comments
	12	0.19	0.19	2219-T87	2219-T87	NO			6061-T6	0	0.5	5.7	N	0	Y	1.25		5.7			646	MARTIN	SS-184A	10/07/87	BUMBER - 1.253" DIA. HOLE, WITH A RING .1" WIDE AND .80" DEEP KNOCKED OFF AROUND THE HOLE, .7" LOW, .2" LEFT. SOME DEBRIS BUT NO DEBRIS HOLES. WALL - NO HOLE, SPALLING OFF 3 DIMPLES ON BACK FEW OTHER DIMPLES WITH CRACKED METAL. DIMPLES ON BACK OVER 80%
245	12	0.13	0.06	2219-T87	6061-T6	TPS	TPS		1100-O	0	0.38	6.8	N	0	N	0.68	6.7	6.9			726		GRIT-5	08/10/88	
246	36	0.13	0.13	PLEXIGLA	2219-T87	NO			1100-O	0	0.31	5.5	Y	0.1	N	0.73		5.5	0		364	MSFC	PT-1	10/20/86	

WHIPPLE_EXCEL DATA

Translated from Lotus by L.Thompson (714) 896-4495

Whipple Database

	Shot No.	Site	Proj. Mat'l	Proj. Dia. (cm)	Proj. Dens. (g/cc)	Proj. Mass (g)	Vel. (km/sec)	Impact Angle (deg)	Normal Vel. (km/sec)	Bumper Mat'l	Bumper Thk (cm)	tb/d	Bumper Dens. (g/cc)	Spacing (cm)	S/d	Wall Th'k (cm)	tw/d	Wall Mat'l	Yield Stress (ksi)	(tb+tw)/d	Category
1	4613	JSC-orig	Glass	0.079	2.25	0.00059	7.13	0	7.13	Al2024T3	0.025	0.32	2.796	5.08	64	0.025	0.32	Al2024-T3	47	0.640	E2
2	4637	JSC-orig	Glass	0.079	2.25	0.00059	7.22	0	7.22	Aluminum	0.015	0.19	2.78	5.08	64	0.025	0.32	Al2024-T3	47	0.512	E4
3	4638	JSC-orig	Glass	0.079	2.25	0.00059	7.53	0	7.53	Aluminum	0.015	0.19	2.78	7.62	96	0.025	0.32	Al2024-T3	47	0.512	E4
4	4658	JSC-orig	Al1100	0.079	2.71	0.00071	7.25	0	7.25	Aluminum	0.015	0.19	2.78	5.08	64	0.025	0.32	Al2024-T3	47	0.512	E4
5	4679	JSC-orig	Al1100	0.079	2.71	0.00071	7.16	0	7.16	Aluminum	0.051	0.64	2.78	7.62	96	0.025	0.32	Al2024-T3	47	0.960	D2
6	4681	JSC-orig	Al1100	0.079	2.71	0.00071	7.34	0	7.34	Aluminum	0.051	0.64	2.78	2.54	32	0.041	0.51	Al2024-T3	47	1.152	D2
7	4691	JSC-orig	Glass	0.159	2.54	0.0053	7.25	0	7.25	Aluminum	0.051	0.32	2.78	7.62	48	0.041	0.26	Al2024-T3	47	0.576	E4
8	4695	JSC-orig	Glass	0.159	2.54	0.0053	7.56	0	7.56	Aluminum	0.051	0.32	2.78	5.08	32	0.064	0.40	Al2024-T3	47	0.720	E2
9	4706	JSC-orig	Glass	0.159	2.54	0.0053	7.26	0	7.26	Aluminum	0.025	0.16	2.78	7.62	48	0.041	0.26	Al2024-T3	47	0.416	E4
10	4709	JSC-orig	Glass	0.159	2.54	0.0053	7.26	0	7.26	Aluminum	0.025	0.16	2.78	5.08	32	0.064	0.40	Al2024-T3	47	0.560	E2
11	4736	JSC-orig	Al1100	0.159	2.71	0.0057	7.31	0	7.31	Aluminum	0.051	0.32	2.78	7.62	48	0.041	0.26	Al2024-T3	47	0.576	E4
12	4738	JSC-orig	Al1100	0.159	2.71	0.0057	7.20	0	7.20	Aluminum	0.051	0.32	2.78	5.08	32	0.064	0.40	Al2024-T3	47	0.720	E1
13	A201	JSC-orig	Glass	0.079	2.25	0.00059	6.70	0	6.70	Al1100-H14	0.030	0.38	2.713	7.62	96	0.030	0.38	Al1100-H14	17	0.768	E4
14	A250	JSC-orig	Glass	0.079	2.25	0.00059	6.52	0	6.52	Al7075-T6	0.030	0.38	2.796	2.54	32	0.030	0.38	Al7075-T6	68	0.768	E2
15	A337	JSC-orig	Glass	0.079	2.25	0.00059	5.44	0	5.44	Aluminum	0.025	0.32	2.78	2.54	32	0.025	0.32	Al2024-T4	47	0.640	E1
16	A358	JSC-orig	Glass	0.040	2.25	7.36E-05	5.56	0	5.56	Al2024-T4	0.015	0.38	2.796	2.54	64	0.015	0.38	Al2024-T4	47	0.768	E1
17	AV26	AVCO	Glass	0.127	2.25	0.0024	5.72	0	5.72	Al7178T6	0.041	0.32	2.823	2.54	20	0.041	0.32	Al7178-T6	78	0.640	D1
18	1376	JSC-HIRL	Al1100	0.079	2.713	0.00071	7.20	0	7.20	Al6061T6	0.064	0.80	2.713	3.33	42	0.635	8.00	Al1100	10	8.800	E1
19	1378	JSC-HIRL	Al1100	0.040	2.713	0.00009	8.00	0	8.00	Al6061T6	0.064	1.60	2.713	3.33	84	0.635	16.00	Al1100	10	17.600	E1
20	1403	JSC-HIRL	Al1100	0.079	2.713	0.00071	3.55	0	3.55	Al6061-0	0.015	0.19	2.713	2.54	32	0.064	0.80	Al2024-T3	47	0.992	D4
21	1421	JSC-HIRL	Al2017T4	0.079	2.796	0.00073	6.40	45	4.53	Al6061-0	0.015	0.19	2.713	2.54	32	0.064	0.80	Al6061-T6	36	0.992	C2
22	1423	JSC-HIRL	Al2017T4	0.079	2.796	0.00073	7.04	45	4.98	Al6061-0	0.015	0.19	2.713	2.54	32	0.064	0.80	Al2024-T3	47	0.992	C4
23	1425	JSC-HIRL	Al1100	0.079	2.713	0.00071	6.13	45	4.33	Al6061-0	0.015	0.19	2.713	2.54	32	0.064	0.80	Al2024-T3	47	0.992	C4
24	1431	JSC-HIRL	Al2024T3	0.081	2.796	0.00078	6.57	45	4.65	Al6061-0	0.015	0.19	2.713	2.54	31	0.064	0.78	Al2024-T3	47	0.971	C4
25	1435	JSC-HIRL	Al2017T4	0.080	2.796	0.00076	6.52	0	6.52	Al6061-0	0.015	0.19	2.713	2.54	32	0.064	0.79	Al2024-T3	47	0.980	E2
26	1436	JSC-HIRL	Al1100	0.079	2.713	0.00069	6.60	0	6.60	Al6061-0	0.015	0.19	2.713	2.54	32	0.030	0.39	Al2024-T3	47	0.582	C4
27	1444	JSC-HIRL	Al2017T4	0.079	2.796	0.00072	3.72	0	3.72	Al6061-0	0.015	0.19	2.713	2.54	32	0.064	0.80	Al2024-T3	47	0.998	A3/D4
28	1449	JSC-HIRL	Al2024T4	0.081	2.796	0.00079	3.01	0	3.01	Al6061-0	0.015	0.19	2.713	2.54	31	0.064	0.78	Al2024-T3	47	0.967	A3
29	1450	JSC-HIRL	Al1100	0.079	2.713	0.00071	3.89	0	3.89	Al6061-0	0.015	0.19	2.713	2.54	32	0.064	0.80	Al2024-T3	47	0.992	D4
30	1452	JSC-HIRL	Al1100	0.079	2.713	0.00071	3.21	0	3.21	Al6061-0	0.015	0.19	2.713	2.54	32	0.064	0.80	Al2024-T3	47	0.992	D4
31	1453	JSC-HIRL	Al2017T4	0.080	2.796	0.00074	3.14	0	3.14	Al6061-0	0.015	0.19	2.713	2.54	32	0.064	0.80	Al2024-T3	47	0.988	D4
32	1462	JSC-HIRL	Al2024T4	0.081	2.796	0.00077	6.85	45	4.84	Al6061-0	0.015	0.19	2.713	2.54	31	0.064	0.79	Al2024-T3	47	0.975	C4
33	1463	JSC-HIRL	Al2017T4	0.079	2.796	0.00072	6.20	45	4.38	Al6061-0	0.015	0.19	2.713	2.54	32	0.064	0.80	Al2024-T3	47	0.998	C4
34	1468	JSC-HIRL	Al2017T4	0.081	2.796	0.00078	6.70	0	6.70	Al6061-0	0.015	0.19	2.713	2.54	31	0.030	0.38	Al2024-T3	47	0.565	E2
35	1470	JSC-HIRL	Al1100	0.080	2.713	0.00072	6.50	0	6.50	Al6061-0	0.015	0.19	2.713	2.54	32	0.064	0.80	Al2024-T3	47	0.988	E2/C2
36	1472	JSC-HIRL	Al1100	0.079	2.713	0.00071	6.30	0	6.30	Al6061-0	0.015	0.19	2.713	2.54	32	0.064	0.80	Al2024-T3	47	0.992	E2/C2
37	1473	JSC-HIRL	Al1100	0.079	2.713	0.00071	6.40	0	6.40	Al6061-0	0.015	0.19	2.713	2.54	32	0.030	0.38	Al2024-T3	47	0.576	E4/C4
38	1475	JSC-HIRL	Al2017T4	0.040	2.796	9.15E-05	7.99	0	7.99	Al3003-0	0.010	0.26	2.74	1.27	32	0.025	0.64	Al3003-H14	21	0.896	F3
39	1476	JSC-HIRL	Al2017T4	0.040	2.796	9.15E-05	8.06	0	8.06	Al3003-0	0.010	0.26	2.74	1.27	32	0.027	0.68	Al3003-H14	21	0.936	F3
40	1481	JSC-HIRL	Al2017T4	0.040	2.796	9.15E-05	7.10	0	7.10	Al3003-0	0.010	0.26	2.74	1.27	32	0.010	0.26	Al3003-H12	18	0.512	F4
41	1486	JSC-HIRL	Al2017T4	0.040	2.713	8.88E-05	7.90	0	7.90	Al3003-0	0.010	0.26	2.74	1.27	32	0.015	0.38	Al3003-H12	18	0.640	F3/E2
42	1487	JSC-HIRL	Al1100	0.040	2.713	8.88E-05	7.30	0	7.30	Al3003-0	0.010	0.26	2.74	1.27	32	0.015	0.38	Al3003-H12	18	0.640	F3/E2
43	1488	JSC-HIRL	Al1100	0.040	2.713	8.88E-05	7.30	0	7.30	Al3003-0	0.010	0.26	2.74	1.27	32	0.015	0.38	Al3003-H12	18	0.640	F3/E2
44	1499	JSC-HIRL	Al1100	0.082	2.713	0.00078	3.70	0	3.70	Al6061-0	0.015	0.19	2.713	2.54	31	0.064	0.78	Al2024-T3	47	0.962	A3/D4
45	1644	JSC-HIRL	CuBe	0.018	8.24	0.000024	7.97	0	7.97	Al6061-T6	0.064	3.57	2.796	2.54	143	0.025	1.43	Al3003-H12	18	5.000	E2
46	A150	JSC-HIRL	Al1100	0.318	2.713	0.0455	6.45	0	6.45	Al6061T6	0.081	0.26	2.713	5.08	16	0.159	0.50	Al2024-T3	47	0.756	D4
47	A151	JSC-HIRL	Al1100	0.318	2.713	0.0455	6.60	0	6.60	Al6061T6	0.081	0.26	2.713	5.08	16	0.127	0.40	Al2024-T3	47	0.656	D4
48	A235	JSC-HIRL	Al2017T4	0.318	2.796	0.0469	6.98	0	6.98	Al1100	0.056	0.18	2.713	10.16	32	0.159	0.50	Al2024-T3	47	0.676	E3
49	A240	JSC-HIRL	Al2017T4	0.318	2.796	0.0469	6.58	0	6.58	Al6061T6	0.081	0.26	2.713	10.16	32	0.127	0.40	Al2024-T3	47	0.656	E2
50	A315	JSC-HIRL	Al1100	0.317	2.713	0.0453	6.08	45	4.30	Al6061T6	0.081	0.26	2.713	5.08	16	0.127	0.40	Al2024-T3	47	0.657	C5

WHIPPLE_EXCEL DATA

Translated from

K=tw*(Y/70)^.5*S^.5*(pp*pb)^-1/6*Vn^-1*M^-1/3
K"=tw*(Y/70)^.5*S^.5*(pp*pb)^-1/6*Vn^-1*M^-1/3*d^-.5

K=tw*(Y/70)^.5*S^.5*(pp*pb)^
K"=tw*(Y/70)^.5*S^.5*(pp*pb)^-1/6*Vn^-1*M^-1/3*d^-.5

	Shot No.	Damage Description	JSC Whipple Eqns. dcrit (cm)	dcrit-d (cm)	Fail? 1=Y, 0=N)	Perf. Pred.	Safe Acc?	Pred. Accurate?	Comments	dc/d	K	K"	JSC Whipple Ec Category (cm)
1	4613	No perfs or spall;v.fine filament craters	0.094	0.0143	0	0	1	1		1.180	0.0578	0.2050	0.096806
2	4637	No tear or hole;v.small perfs in 2.7cm ring	0.093	0.0136	1	0	0	0		1.171	0.0571	0.2027	0.098579
3	4638	No tear or hole;v.small perfs in 4.4cm ring	0.103	0.0241	1	0	0	0		1.303	0.0671	0.2380	0.119325
4	4658	No tear or hole,v.small perfs in 2.7cm ring	0.087	0.0077	1	0	0	0		1.097	0.0518	0.1839	0.093167
5	4679	No tear or perfs; small central dimples	0.101	0.0212	0	0	1	1		1.267	0.0643	0.2281	0.104367
6	4681	No tear or perfs; small central dimples	0.094	0.0144	0	0	1	1		1.182	0.0579	0.2055	0.100454
7	4691	No tear or hole; 3 small perfs	0.139	-0.0194	1	1	1	1		0.878	0.0524	0.1316	0.148133
8	4695	No tear or perfs; small central craters	0.159	0.0007	0	0	1	1		1.004	0.0642	0.1610	0.18161
9	4706	No tear or hole; perf ring 3.4 cm; 4 perfs	0.139	-0.0195	1	1	1	1		0.877	0.0524	0.1314	0.14928
10	4709	No tear or perfs; 2cm dimple ring	0.164	0.0050	0	0	1	1		1.032	0.0668	0.1677	0.175167
11	4736	No tear or hole; perf ring 5.6 cm; 4 perfs	0.136	-0.0231	1	1	1	1		0.854	0.0503	0.1264	0.14628
12	4738	No tear,hole or perfs; small central craters	0.161	0.0024	0	0	1	1		1.015	0.0652	0.1637	0.169118
13	A201	No hole or spall; 1 perf	0.084	0.0041	1	0	0	0		1.052	0.0546	0.1938	0.083503
14	A250	No hole or spall; near perf	0.090	0.0106	0	0	1	1		1.133	0.0645	0.2288	0.089947
15	A337	No hole, spall or perfs	0.059	-0.0201	0	1	1	0		0.746	0.0536	0.1902	0.059247
16	A358	No hole, spall or perfs	0.042	0.0022	0	0	1	1		1.054	0.0629	0.3155	0.041838
17	AV26	No hole or spall; front surface eroded	0.102	-0.0247	0	1	1	0		0.805	0.0655	0.1837	0.102258
18	1376	Many craters, no spall	0.389	0.3097	0	0	1	1		4.901	0.4891	1.7359	0.406226
19	1378	Many craters, no spall	0.363	0.3230	0	0	1	1		9.138	0.8803	4.4190	0.445023
20	1403	Small perf., spall bubbles/dimples	0.060	-0.0197	1	1	1	1		0.752	0.1877	0.6662	0.05971
21	1421	No perf., craters and dimples	0.082	0.0028	0	0	1	1		1.035	0.1269	0.4506	0.082155
22	1423	Small perf., spall bubbles/dimples	0.097	0.0181	1	0	0	0		1.228	0.1319	0.4680	0.097474
23	1425	Small perf., spall bubbles/dimples	0.088	0.0090	1	0	0	0		1.114	0.1538	0.5458	0.088386
24	1431	3 perfs, craters/dimples	0.092	0.0112	1	0	0	0		1.138	0.1383	0.4859	0.092227
25	1435	No tear or hole; dimples	0.120	0.0392	0	0	1	1		1.488	0.0994	0.3507	0.11959
26	1436	~14 perfs. (small)	0.075	-0.0036	1	1	1	1		0.954	0.0489	0.1745	0.074974
27	1444	1 large perf. (1.8x1.4 mm), some dmpls	0.062	-0.0165	1	1	1	1		0.791	0.1774	0.6315	0.06241
28	1449	1 large perf. (1.8 mm)	0.048	-0.0335	1	1	1	1		0.588	0.2126	0.7451	0.047911
29	1450	1 pinhole perf. (0.5mm), craters/dimples	0.067	-0.0127	1	1	1	1		0.841	0.1713	0.6082	0.066706
30	1452	Large hole (1.7mm); little projectile breakup	0.053	-0.0267	1	1	1	1		0.664	0.2076	0.7368	0.052714
31	1453	Large hole (1.7mm); little projectile breakup	0.051	-0.0291	1	1	1	1	Vel Estimated	0.635	0.2083	0.7380	0.050566
32	1462	1 perf. (1.2x.6mm); dmpls (4)	0.095	0.0146	1	0	0	0		1.181	0.1333	0.4690	0.095353
33	1463	1 perf. (1.3mm); dmpls (6)	0.088	0.0092	1	0	0	0		1.116	0.1506	0.5359	0.088097
34	1468	No tear or hole; dimples	0.075	-0.0055	0	1	1	0		0.932	0.0461	0.1620	0.07549
35	1470	No perf, dimples (2)	0.120	0.0407	0	0	1	1		1.510	0.1021	0.3614	0.120411
36	1472	No perf, dimples (7)	0.116	0.0369	0	0	1	1		1.465	0.1058	0.3754	0.116295
37	1473	Small perfs (13), diffuse impact pattern	0.072	-0.0070	1	1	1	1		0.912	0.0500	0.1774	0.072398
38	1475	No perfs; v. slight impulsive bulge	0.039	-0.0007	0	1	1	0		0.982	0.0310	0.1557	0.048868
39	1476	No perfs; v. slight impulsive bulge	0.040	0.0007	0	0	1	1		1.017	0.0327	0.1640	0.051377
40	1481	Several perfs; impulsive bulge with dimples	0.022	-0.0179	1	1	1	1		0.548	0.0129	0.0649	0.022243
41	1486	No perfs; impulsive bulge with dimples	0.027	-0.0129	0	1	1	0		0.675	0.0177	0.0888	0.032756
42	1487	No perfs; impulsive bulge with dimples	0.028	-0.0114	0	1	1	0		0.712	0.0191	0.0961	0.030293
43	1488	No perfs; impulsive bulge with dimples	0.028	-0.0114	0	1	1	0		0.712	0.0191	0.0961	0.030293
44	1499	1 large perf. (1.5x1.3 mm), some dmpls	0.063	-0.0191	1	1	1	1		0.767	0.1746	0.6101	0.062796
45	1644	No perf, craters & dimples	0.033	0.0147	0	0	1	1		1.829	0.0528	0.3956	0.037404
46	A150	No hole, detached spall, through crack	0.281	-0.0370	1	1	1	1		0.884	0.0913	0.1621	0.28054
47	A151	Hole, detached spall, cracks	0.247	-0.0703	1	1	1	1		0.779	0.0714	0.1267	0.247242
48	A235	No hole or tear; 1 spall split	0.377	0.0596	0	0	1	1		1.188	0.1175	0.2086	0.377068
49	A240	No hole or tear; attached spall	0.304	-0.0133	0	1	1	0		0.958	0.0998	0.1770	0.304218
50	A315	7 Perfs. (max 8.1x3.8mm)	0.197	-0.1199	1	1	1	1	16mil 3003-0 wit: 48 perfs	0.622	0.1097	0.1948	0.197262

Translated from Lotus by L.Thompson (714) 896-4495

Whipple Database

	Shot No.	Site	Proj. Mat'l	Proj. Dia. (cm)	Proj. Dens. (g/cc)	Proj. Mass (g)	Vel. (km/sec)	Impact Angle (deg)	Normal Vel. (km/sec)	Bumper Mat'l	Bumper Thk (cm)	tb/d	Bumper Dens. (g/cc)	Spacing (cm)	S/d	Wall Th'k (cm)	tw/d	Wall Mat'l	Yield Stress (ksi)	(tb+tw)/d	Category
51	A316	JSC-HIRL	Al1100	0.317	2.713	0.0452	5.99	45	4.24	Al6061T6	0.081	0.26	2.713	5.08	16	0.159	0.50	Al2024-T3	47	0.758	C5
52	A481	JSC-HIRL	Al2017T4	0.318	2.796	0.0469	6.38	0	6.38	Al1100	0.056	0.18	2.713	12.7	40	0.127	0.40	Al6061-T6	36	0.576	E4
53	A558	JSC-HIRL	Al2017T4	0.318	2.796	0.0469	2.64	0	2.64	Al1100	0.056	0.18	2.713	12.7	40	0.483	1.52	Al6061-T6	36	1.696	D2/C2
54	A570	JSC-HIRL	Al2017T4	0.318	2.796	0.0469	2.48	0	2.48	Al1100	0.056	0.18	2.713	12.7	40	0.635	2.00	Al1100-0	10	2.176	D2/C2
55	A689	JSC-HIRL	Al2017T4	0.318	2.796	0.0469	6.5	45	4.60	Al1100	0.056	0.18	2.713	10.16	32	0.160	0.50	Al2024-T3	47	0.680	C5
56	A690	JSC-HIRL	Al2017T4	0.318	2.796	0.0469	5.65	45	4.00	Al1100	0.056	0.18	2.713	10.16	32	0.160	0.50	Al2024-T3	47	0.680	C5
57	A939	JSC-HIRL	Al2O3	0.317	3.9	0.0650	5.67	0	5.67	Al1100	0.056	0.18	2.713	12.7	40.1	0.160	0.50	Al2024-T3	47	0.681	D3
58	A1005	JSC-HIRL	Al2017T4	0.318	2.796	0.0472	5.86	0	5.86	Al3003H12	0.064	0.20	2.74	10.16	31.9	0.081	0.26	Al2024-T3	47	0.455	D5/E4
59	A1076	JSC-HIRL	Al2017T4	0.200	2.796	0.0117	6.37	0	6.37	Al1100	0.064	0.32	2.713	6.0	30	0.041	0.20	Al6061-T6	36	0.521	E4
60	A1077	JSC-HIRL	Al2017T4	0.200	2.796	0.0117	6.77	0	6.77	Al1100	0.041	0.20	2.713	6.0	30	0.064	0.32	Al6061-T6	36	0.521	E2
61	A1112	JSC-HIRL	Al2017T4	0.318	2.796	0.0469	6.20	45	4.38	Al1100	0.051	0.16	2.713	10.16	32	0.318	1.00	Al2024-T3	47	1.160	D5
62	A1114	JSC-HIRL	Al2017T4	0.318	2.796	0.0469	6.21	0	6.21	Al1100	0.051	0.16	2.713	10.16	32	0.159	0.50	Al2024-T3	47	0.660	E4
63	A1184	JSC-HIRL	Al2017T4	0.238	2.796	0.0198	6.34	45	4.48	Al1100	0.041	0.17	2.713	7.62	32	0.318	1.33	Al2024-T3	47	1.504	C2
64	A1193	JSC-HIRL	Al2017T4	0.318	2.796	0.0469	6.25	0	6.25	Al1100	0.051	0.16	2.713	10.16	32	0.203	0.64	Al6061-T6	36	0.800	E4
65	A1195	JSC-HIRL	Al2017T4	0.318	2.796	0.0469	5.97	45	4.22	Al1100	0.051	0.16	2.713	10.16	32	0.483	1.52	Al6061-T6	36	1.680	C2
66	A1196	JSC-HIRL	Al2017T4	0.200	2.796	0.0117	7.20	0	7.20	Al1100	0.036	0.18	2.713	6.35	31.8	0.159	0.79	Al2024-T3	47	0.972	E2
67	A1199	JSC-HIRL	Al2017T4	0.200	2.796	0.0117	5.70	0	5.70	Al1100	0.036	0.18	2.713	6.35	31.8	0.483	2.41	Al6061-T6	36	2.591	E1
68	A1210	JSC-HIRL	Al2017T4	0.318	2.796	0.0469	6.27	0	6.27	Al1100	0.051	0.16	2.713	10.16	32	0.203	0.64	Al2024-T3	47	0.800	E3
69	A1211	JSC-HIRL	Al2017T4	0.200	2.796	0.0117	5.06	0	5.06	Al1100	0.036	0.18	2.713	6.35	31.8	0.483	2.41	Al6061-T6	36	2.591	E1
70	A1221	JSC-HIRL	Al2017T4	0.200	2.796	0.0117	5.42	0	5.42	Al1100	0.036	0.18	2.713	6.35	31.8	0.318	1.59	Al2024-T3	47	1.765	E1
71	A1222	JSC-HIRL	Al2017T4	0.200	2.796	0.0117	4.48	0	4.48	Al1100	0.036	0.18	2.713	6.35	31.8	0.318	1.59	Al2024-T3	47	1.765	E2
72	A1281	JSC-HIRL	Nylon	0.318	1.145	0.0192	6.70	0	6.70	Al1100	0.025	0.08	2.713	10.16	32	0.081	0.26	Al2024-T3	47	0.336	E4
73	A1331	JSC-HIRL	Al2017T4	0.319	2.796	0.0473	6.58	0	6.58	Al1100	0.056	0.18	2.713	10.16	31.9	0.160	0.50	Al2024-T3	47	0.678	E2
74	A1332	JSC-HIRL	Al1100	0.317	2.713	0.0453	6.47	0	6.47	Al1100	0.056	0.18	2.713	10.16	32.0	0.127	0.40	Al6061-T6	36	0.577	D5/E4
75	A1333	JSC-HIRL	Al2024T4	0.315	2.796	0.0458	6.58	0	6.58	Al1100	0.056	0.18	2.713	10.16	32.2	0.127	0.40	Al6061-T6	36	0.580	D4/E4
76	A1334	JSC-HIRL	Al2017T4	0.317	2.796	0.0468	6.25	0	6.25	Al1100	0.056	0.18	2.713	10.16	32.0	0.127	0.40	Al6061-T6	36	0.576	D5/E4
77	A1342	JSC-HIRL	Al2017T4	0.318	2.796	0.0469	3.96	0	3.96	Al6061T6	0.127	0.40	2.713	10.16	32.0	0.318	1.00	Al2219-T87	52	1.400	E2/D2
78	A1343	JSC-HIRL	Al2017T4	0.359	2.796	0.0678	3.72	0	3.72	Al6061T6	0.127	0.35	2.713	10.16	28.3	0.318	0.88	Al2219-T87	52	1.238	E2/D2
79	A1344	JSC-HIRL	Al2017T4	0.358	2.796	0.0674	3.19	0	3.19	Al6061T6	0.127	0.35	2.713	10.16	28.4	0.318	0.89	Al2219-T87	52	1.241	D4
80	A1347	JSC-HIRL	Al2017T4	0.358	2.796	0.0673	2.93	0	2.93	Al6061T6	0.127	0.35	2.713	10.16	28.4	0.318	0.89	Al2219-T87	52	1.241	D4
81	A1360	JSC-HIRL	Al2017T4	0.357	2.796	0.0667	5.96	75	1.54	Al6061T6	0.051	0.14	2.713	10.16	28.4	0.127	0.36	Al2024-T3	47	0.498	C2
82	A1363	JSC-HIRL	Al2017T4	0.357	2.796	0.0667	6.20	0	6.20	Al7075T6	0.064	0.18	2.796	10.16	28.4	0.127	0.36	Al7075-T73	56	0.533	D4
83	B31	JSC-HIRL	Al2017T4	0.635	2.796	0.3748	7.08	0	7.08	Al6061T6	0.127	0.20	2.713	20.32	32	0.229	0.36	Al6061-T6	36	0.560	E2
84	B37	JSC-HIRL	Al2017T4	0.635	2.796	0.3748	6.39	0	6.39	Al2024T3	0.159	0.25	2.796	10.16	16	0.318	0.50	Al6061-T6	36	0.750	E4
85	B71	JSC-HIRL	Al2017T4	0.635	2.796	0.3748	6.77	0	6.77	Al6061T6	0.127	0.20	2.796	10.16	16	0.254	0.40	Al2024-T3	47	0.600	D5/F5
86	B72	JSC-HIRL	Al2017T4	0.635	2.796	0.3748	7.22	0	7.22	Al6061T6	0.127	0.20	2.796	10.16	16	0.318	0.50	Al2219-T87	52	0.700	D3
87	B73	JSC-HIRL	Al2017T4	0.635	2.796	0.3748	6.80	0	6.80	Al6061T6	0.127	0.20	2.796	10.16	16	0.318	0.50	Al6061-T6	36	0.700	D5/F5
88	B74	JSC-HIRL	Al2017T4	0.634	2.796	0.3730	7.20	60	3.60	Al6061T6	0.127	0.20	2.796	10.16	16.0	0.318	0.50	Al2219-T87	52	0.701	C5
89	GM-1	GMRL	Aluminum	0.318	2.713	0.0455	6.8	0	6.80	Al1100	0.064	0.20	2.713	5.08	16.0	0.318	1.00	Al7075-T6	68	1.200	D1
90	D1584	GMRL	Aluminum	0.318	2.713	0.0455	7.4	30	6.41	Al1100	0.064	0.20	2.713	5.08	16.0	0.159	0.50	Al7075-T6	68	0.700	C3
91	D1585	GMRL	Aluminum	0.318	2.713	0.0455	7.4	45	5.23	Al1100	0.064	0.20	2.713	5.08	16.0	0.159	0.50	Al7075-T6	68	0.700	C5
92	D1586	GMRL	Aluminum	0.318	2.713	0.0455	7.4	60	3.70	Al1100	0.064	0.20	2.713	5.08	16.0	0.159	0.50	Al7075-T6	68	0.700	C3
93	GM-5	GMRL	Aluminum	0.318	2.713	0.0455	7.4	30	6.41	Al1100	0.102	0.32	2.713	5.08	16.0	0.159	0.50	Al7075-T6	68	0.820	C2
94	GM-6	GMRL	Aluminum	0.318	2.713	0.0455	7.4	45	5.23	Al1100	0.102	0.32	2.713	5.08	16.0	0.159	0.50	Al7075-T6	68	0.820	C5
95	GM-7	GMRL	Aluminum	0.318	2.713	0.0455	7.4	60	3.70	Al1100	0.102	0.32	2.713	5.08	16.0	0.159	0.50	Al7075-T6	68	0.820	C4
96	GM-8	GMRL	Aluminum	0.318	2.713	0.0455	7.4	30	6.41	Al1100	0.159	0.50	2.713	5.08	16.0	0.159	0.50	Al7075-T6	68	1.000	C2
97	GM-9	GMRL	Aluminum	0.318	2.713	0.0455	7.4	45	5.23	Al1100	0.159	0.50	2.713	5.08	16.0	0.159	0.50	Al7075-T6	68	1.000	C4
98	GM-10	GMRL	Aluminum	0.318	2.713	0.0455	7.57	45	5.35	Al1100	0.064	0.20	2.713	5.08	16.0	0.318	1.00	Al7075-T6	68	1.200	C3
99	GM-11	GMRL	Aluminum	0.318	2.713	0.0455	7.57	60	3.79	Al1100	0.064	0.20	2.713	5.08	16.0	0.318	1.00	Al7075-T6	68	1.200	C2
100	GM-12	GMRL	Aluminum	0.318	2.713	0.0455	7.57	45	5.35	Al1100	0.102	0.32	2.713	5.08	16.0	0.318	1.00	Al7075-T6	68	1.320	C2

WHIPPLE_EXCEL DATA

Translated from

K=tw*(Y/70)^.5*S^.5*(pp*pb)^-1/6*Vn^-1*M^-1/3
K*=tw*(Y/70)^.5*S^.5*(pp*pb)^-1/6*Vn^-1*M^-1/3*d^-.5

K=tw*(Y/70)^.5*S^.5*(pp*pb)^
K*=tw*(Y/70)^.5*S^.5*(pp*pb)^-1/6*Vn^

	Shot No.	Damage Description	JSC Whipple Eqns. dcrit (cm)	dcrit-d (cm)	Fail? 1=Y, 0=N)	Perf Pred.	Safe Acc?	Pred. Accurate?	Comments	dc/d	K	K*	JSC Whipple Ec Category (cm)
51	A316	4 Perfs. (max 10.7x2.3mm)	0.226	-0.0910	1	1	1	1	16mil 3003-0 wit: 11 perfs	0.713	0.1394	0.2476	0.225761
52	A481	No hole; att'd spall 0.5cm dia; thru crack	0.286	-0.0310	1	1	1	1		0.902	0.1007	0.1787	0.286466
53	A558	No Perf (?)	0.287	-0.0302	0	1	1	0		0.905	0.9245	1.6407	0.218443
54	A570	No Perf (?)	0.221	-0.0966	0	1	1	0		0.696	0.6825	1.2112	0.141647
55	A689	6 Perfs: 7x5mm max	0.255	-0.0627	1	1	1	1		0.803	0.1799	0.3193	0.254797
56	A690	4 Perfs: 3 interconnected 12mmx5mm	0.223	-0.0941	1	1	1	1		0.704	0.2070	0.3674	0.223402
57	A939	Detached spall (7x10mm)	0.280	-0.0370	1	1	1	1		0.883	0.1384	0.2458	0.279839
58	A1005	Perfs (25): 3.2x4.4mm max., many dmpls	0.197	-0.1216	1	1	1	1		0.618	0.0714	0.1265	0.19671
59	A1076	Numerous perforations and spall dimples	0.108	-0.0921	1	1	1	1		0.539	0.0353	0.0789	0.107858
60	A1077	No perfs, numerous spall (attached) dimples	0.152	-0.0479	0	1	1	0		0.761	0.0519	0.1161	0.152132
61	A1112	Perforated, hole 6mm, surface cratered	0.395	0.0779	1	0	0	0		1.245	0.3743	0.6643	0.395434
62	A1114	Thin spall 1cm dia; 2 perfs	0.327	0.0099	1	0	0	0		1.031	0.1321	0.2345	0.327352
63	A1184	No hole; large craters and attached spall	0.378	0.1403	0	0	1	1		1.589	0.4227	0.8662	0.378433
64	A1193	No hole or tear; thin spall 2 mm dia; 1 perf	0.356	0.0386	1	0	0	0		1.122	0.1471	0.2610	0.356084
65	A1195	No hole, large craters and spall (attached)	0.475	0.1576	0	0	1	1		1.496	0.5171	0.9177	0.475074
66	A1196	No tear,hole or perfs; small central craters	0.317	0.1174	0	0	1	1		1.587	0.1430	0.3198	0.334038
67	A1199	Too thick; central and ring craters	0.502	0.3021	0	0	1	1		2.511	0.4806	1.0748	0.502148
68	A1210	No tear, hole or perfs; thin spall 2.5 mm dia	0.391	0.0735	1	0	0	0		1.232	0.1675	0.2973	0.391023
69	A1211	Too thick; central and ring craters	0.444	0.2436	0	0	1	1		2.218	0.5414	1.2107	0.443584
70	A1221	Too thick; central and ring craters	0.389	0.1893	0	0	1	1		1.946	0.3800	0.8497	0.389284
71	A1222	Beginning central and ring spallation	0.315	0.1154	0	0	1	1		1.577	0.4597	1.0279	0.315386
72	A1281	Many small, dispersed perforations	0.309	-0.0086	1	1	1	1		0.973	0.0980	0.1739	0.308874
73	A1331	No perf, s. bulge, craters, dimples	0.353	0.0348	0	0	1	1		1.109	0.1253	0.2220	0.353385
74	A1332	Perfs (7): 2.5 mm max., ring perfs	0.274	-0.0428	1	1	1	1	.025" Al3003H14 wit: 1 dmpl	0.865	0.0902	0.1602	0.274343
75	A1333	Perfs (4): 0.7 mm max., ring perfs	0.277	-0.0381	1	1	1	1	.025" Al3003H14 wit: s.crater	0.879	0.0879	0.1566	0.277104
76	A1334	Perfs (12): 3x2 mm max., ring perfs	0.260	-0.0570	1	1	1	1	.025" Al3003H14 wit: 1 dmpl	0.820	0.0919	0.1632	0.260433
77	A1342	No perfs, craters & dimples	0.341	0.0237	0	0	1	1		1.075	0.4358	0.7733	0.341307
78	A1343	No perfs, craters & dimples	0.319	-0.0399	0	1	1	0		0.889	0.4102	0.6845	0.319212
79	A1344	1 Perf (<1mm), 8mm det. spall, 4mm thru crack	0.270	-0.0879	1	1	1	1	Wit .025" Al3003H14: lrg dmpl	0.755	0.4794	0.8010	0.27042
80	A1347	1 Perf (.6 mm), 6mm det. spall	0.257	-0.1015	1	1	1	1	Wit .025"Al3003H14:perf/split (5mmx1m	0.717	0.5222	0.8725	0.246484
81	A1360	No perf, ~30 dmpls	0.561	0.2042	0	0	1	1		1.572	0.3782	0.6329	0.384406
82	A1363	8 perfs (max 1.5 mm), det.spall (13x7mm)	0.299	-0.0585	1	1	1	1	Wit .025"Al3003H14:5-6 dmpls, no perf	0.836	0.1022	0.1710	0.2987
83	B31	Central and ring dimples/spallation	0.552	-0.0832	0	1	1	0		0.869	0.1033	0.1296	0.563672
84	B37	Small hole, detached spall (30 mm dia.)	0.501	-0.1344	1	1	1	1		0.788	0.1118	0.1403	0.500553
85	B71	Petalled Hole (~11mm), Det.Spall (37mm)	0.498	-0.1367	1	1	1	1	Wit (.04" Al2024): large dmpls	0.785	0.0965	0.1211	0.498269
86	B72	No perf, detached spall (35 x 28 mm)	0.606	-0.0287	1	1	1	1	Wit (.04" Al2024): dmpls	0.955	0.1189	0.1493	0.639234
87	B73	Perf, split (20 mm long), det. spall(40x30mm)	0.531	-0.1036	1	1	1	1	Wit (.04" Al2024): dmpls	0.837	0.1051	0.1319	0.531444
88	B74	3 Perfs (11x6mm max), craters, det. spall	0.507	-0.1265	1	1	1	1	Wit (.04" Al2024): dmpls	0.800	0.2389	0.3001	0.507439
89	GM-1	No perf or spall	0.530	0.2124	0	0	1	1		1.669	0.2084	0.3698	0.529897
90	D1584	No perf, detached spall	0.317	-0.0003	1	1	1	1		0.999	0.1105	0.1962	0.317151
91	D1585	Perf (~5x2mm)	0.281	-0.0362	1	1	1	1		0.886	0.1354	0.2403	0.281314
92	D1586	No perf, detached spall	0.293	-0.0245	1	1	1	1		0.923	0.1915	0.3398	0.292954
93	GM-5	No perf or detached spall	0.320	0.0029	0	0	1	1		1.009	0.1105	0.1962	0.320449
94	GM-6	Perf	0.293	-0.0242	1	1	1	1		0.924	0.1354	0.2403	0.293259
95	GM-7	Perf	0.324	0.0064	1	0	0	0		1.020	0.1915	0.3398	0.323925
96	GM-8	No perf or detached spall	0.325	0.0079	0	0	1	1		1.025	0.1105	0.1962	0.325358
97	GM-9	Perf	0.311	-0.0065	1	1	1	1		0.980	0.1354	0.2403	0.311035
98	GM-10	No perf, detached spall	0.464	0.1463	1	0	0	0		1.461	0.2647	0.4698	0.483759
99	GM-11	No perf or detached spall	0.496	0.1781	0	0	1	1		1.561	0.3743	0.6644	0.495635
100	GM-12	No perf or detached spall	0.475	0.1571	0	0	1	1		1.495	0.2647	0.4698	0.47458

Translated from Lotus by L.Thompson (714) 896-4495

Whipple Database

	Shot No.	Site	Proj Mat'l	Proj Dia (cm)	Proj Dens (g/cc)	Proj Mass (g)	Vel (km/sec)	Impact Angle (deg)	Normal Vel (km/sec)	Bumper Mat'l	Bumper Thk (cm)	tb/d	Bumper Dens (g/cc)	Spacing (cm)	S/d	Wall Th'k (cm)	tw/d	Wall Mat'l	Yield Stress (ksi)	(tb+tw)/d	Category
101	GM-13	GMRL	Aluminum	0.318	2.713	0.0455	7.57	60	3.79	Al1100	0.102	0.32	2.713	5.08	16.0	0.318	1.00	Al7075-T6	68	1.320	C2
102	GM-14	GMRL	Aluminum	0.318	2.713	0.0455	7.57	45	5.35	Al1100	0.159	0.50	2.713	5.08	16.0	0.318	1.00	Al7075-T6	68	1.500	C2
103	GM-15	GMRL	Aluminum	0.318	2.713	0.0455	7.57	60	3.79	Al1100	0.159	0.50	2.713	5.08	16.0	0.318	1.00	Al7075-T6	68	1.500	C2
104	GM-16	GMRL	Aluminum	0.318	2.713	0.0455	7.62	30	6.60	Al1100	0.064	0.20	2.713	5.08	16.0	0.635	2.00	Al7075-T6	68	2.200	C2
105	GM-17	GMRL	Aluminum	0.318	2.713	0.0455	7.62	45	5.39	Al1100	0.064	0.20	2.713	5.08	16.0	0.635	2.00	Al7075-T6	68	2.200	C2
106	A86/1	ARC	Al2017T4	0.953	2.796	1.2651	6.65	0	6.65	Al2024T3	0.159	0.17	2.796	30.48	32	0.635	0.67	Al2024-T351	47	0.833	D1
107	A86/2	ARC	Al2017T4	0.953	2.796	1.2651	6.64	0	6.64	Al2024T3	0.318	0.33	2.796	30.48	32	0.229	0.24	Al2024-T3	47	0.573	F2
108	A86/3	ARC	Al2017T4	0.953	2.796	1.2651	6.65	0	6.65	Al2024T3	0.159	0.17	2.796	30.48	32	0.229	0.24	Al2024-T3	47	0.407	F4
109	A86/4	ARC	Al2017T4	0.953	2.796	1.2651	6.40	0	6.40	Al2024T3	0.483	0.51	2.796	30.48	32	0.229	0.24	Al2024-T3	47	0.747	E4
110	1732	ARC	Al2017T4	0.953	2.796	1.2651	6.47	0	6.47	Al2024T3	0.159	0.17	2.796	30.48	32	0.318	0.33	Al2024-T3	47	0.500	F4
111	1761	ARC	Al2017T4	0.953	2.796	1.2651	6.50	45	4.60	Al2024T3	0.159	0.17	2.796	30.48	32	0.318	0.33	Al6061-T6	36	0.500	C5
112	1868	ARC	Al2017T4	0.953	2.796	1.2651	7.10	0	7.10	Al2024T3	0.159	0.17	2.796	30.48	32	0.318	0.33	Al6061-T6	36	0.500	F3
113	1869	ARC	Al2024T4	0.893	2.796	1.0436	6.70	0	6.70	Al2024T3	0.159	0.18	2.796	15.24	17.1	0.127	0.14	Al2024-T3	47	0.320	D5
114	1870	ARC	Al2024T4	0.954	2.796	1.2697	6.53	0	6.53	Al2024T3	0.159	0.17	2.796	15.24	16.0	0.483	0.51	Al6061-T6	36	0.673	D5
115	1871	ARC	SS316	0.955	7.86	3.5872	5.44	0	5.44	Al2024T3	0.318	0.33	2.796	30.48	31.9	0.635	0.66	Al6061-T6	36	0.997	E5
116	1872	ARC	SS316	0.955	7.86	3.5870	5.45	0	5.45	Al2024T3	0.318	0.33	2.796	45.72	47.9	0.635	0.66	Al6061-T6	36	0.997	E5
117	1873	ARC	Al2017T4	0.953	2.796	1.2681	6.89	0	6.89	Al2024T3	0.081	0.09	2.796	30.48	32.0	0.635	0.67	Al6061-T6	36	0.751	E2
118	1874	ARC	SS316	0.955	7.86	3.5870	5.45	0	5.45	Al2024T3	0.318	0.33	2.796	30.48	31.9	0.635	0.66	Al2024-T351	47	0.997	E5
119	1875	ARC	Al2017T4	0.953	2.796	1.2651	6.75	0	6.75	Al2024T3	0.159	0.17	2.796	30.48	32	0.318	0.33	Al6061-T6	36	0.500	F3
120	1894	ARC	Al2017T4	0.953	2.796	1.2651	6.74	45	4.77	Al2024T3	0.159	0.17	2.796	30.48	32	0.795	0.83	Al2024-T351	47	1.001	C4
121	1895	ARC	Al2017T4	0.953	2.796	1.2651	6.89	0	6.89	Al2024T3	0.159	0.17	2.796	30.48	32	0.318	0.33	Al6061-T6	36	0.500	F3
122	1899	ARC	Al2017T4	0.953	2.796	1.2651	6.83	0	6.83	Al2024T3	0.159	0.17	2.796	15.24	16	0.635	0.67	Al2024-T351	47	0.833	D3
123	1907	ARC	Al2017T4	1.270	2.796	2.9988	6.53	0	6.53	Al2024T3	0.318	0.25	2.796	50.80	40	0.483	0.38	Al2024-T351	47	0.630	E4
124	1913	ARC	Al2017T4	1.270	2.796	2.9988	6.71	0	6.71	Al2024T3	0.318	0.25	2.796	50.80	40	0.483	0.38	Al6061-T6	36	0.630	D2
125	1917	ARC	Al2017T4	0.953	2.796	1.2651	6.72	0	6.72	Al2024T3	0.159	0.17	2.796	22.86	24	0.483	0.51	Al2024-T351	47	0.673	D2
126	1918	ARC	Al2017T4	0.953	2.796	1.2651	6.83	0	6.83	Al2024T3	0.159	0.17	2.796	38.10	40	0.318	0.33	Al2024-T3	47	0.500	E2
127	1921	ARC	Al2017T4	1.270	2.796	2.9988	6.80	0	6.80	Al2024T3	0.159	0.13	2.796	22.86	18	0.635	0.50	Al2024-T351	47	0.625	D3
128	MD15	MDAC	Aluminum	0.884	2.78	1.0053	7.08	0	7.08	Al2024T351	0.229	0.26	2.796	26.52	30	0.201	0.23	Al2024-T351	47	0.486	E3
129	MD27	MDAC	Aluminum	1.908	2.78	10.1106	7.15	0	7.15	Al2024T351	0.406	0.21	2.796	28.58	15.0	2.827	1.48	Al2024-T351	47	1.695	D2
130	MD28	MDAC	Aluminum	1.908	2.78	10.1106	7.08	0	7.08	Al2024T351	0.406	0.21	2.796	57.15	30.0	0.968	0.51	Al2024-T351	47	0.720	E2
131	MD29	MDAC	Aluminum	1.908	2.78	10.1106	7.08	0	7.08	Al2024T351	0.406	0.21	2.796	76.2	39.9	0.622	0.33	Al2024-T351	47	0.539	E3
132	MD31	MDAC	Aluminum	1.908	2.78	10.1106	7.15	0	7.15	Al2024T351	0.813	0.43	2.796	57.15	30.0	0.800	0.42	Al2024-T351	47	0.845	E2
133	1675	Burch-BAC	Al2017	0.635	2.796	0.3748	4.97	0	4.97	Al2024T3	0.102	0.16	2.796	7.62	12.0	0.051	0.08	Al2024-T4	47	0.240	C5
134	1676	Burch-BAC	Al2017	0.635	2.796	0.3748	5.79	0	5.79	Al2024T3	0.102	0.16	2.796	7.62	12.0	0.051	0.08	Al2024-T4	47	0.240	C5
135	1677	Burch-BAC	Al2017	0.635	2.796	0.3748	5.33	30	4.62	Al2024T3	0.102	0.16	2.796	7.62	12.0	0.051	0.08	Al2024-T4	47	0.240	C5
136	1678	Burch-BAC	Al2017	0.635	2.796	0.3748	5.09	45	3.60	Al2024T3	0.102	0.16	2.796	7.62	12.0	0.051	0.08	Al2024-T4	47	0.240	C5
137	1679	Burch-BAC	Al2017	0.635	2.796	0.3748	5.24	30	4.54	Al2024T3	0.203	0.32	2.796	7.62	12.0	0.051	0.08	Al2024-T4	47	0.400	C5
138	1680	Burch-BAC	Al2017	0.635	2.796	0.3748	5.27	45	3.73	Al2024T3	0.203	0.32	2.796	7.62	12.0	0.051	0.08	Al2024-T4	47	0.400	C5
139	1681	Burch-BAC	Al2017	0.635	2.796	0.3748	5.09	30	4.41	Al2024T3	0.406	0.64	2.796	7.62	12.0	0.051	0.08	Al2024-T4	47	0.720	C5
140	1682	Burch-BAC	Al2017	0.635	2.796	0.3748	5.36	45	3.79	Al2024T3	0.406	0.64	2.796	7.62	12.0	0.051	0.08	Al2024-T4	47	0.720	C5
141	1683	Burch-BAC	Al2017	0.635	2.796	0.3748	5.09	60	2.55	Al2024T3	0.102	0.16	2.796	7.62	12.0	0.051	0.08	Al2024-T4	47	0.240	C5
142	1684	Burch-BAC	Al2017	0.635	2.796	0.3748	5.24	60	2.62	Al2024T3	0.203	0.32	2.796	7.62	12.0	0.051	0.08	Al2024-T4	47	0.400	C5
143	1685	Burch-BAC	Al2017	0.635	2.796	0.3748	5.09	60	2.55	Al2024T3	0.406	0.64	2.796	7.62	12.0	0.051	0.08	Al2024-T4	47	0.720	C5
144	1686	Burch-BAC	Al2017	0.635	2.796	0.3748	5.36	30	4.65	Al2024T3	0.102	0.16	2.796	15.24	24.0	0.051	0.08	Al2024-T4	47	0.240	C5
145	1687	Burch-BAC	Al2017	0.635	2.796	0.3748	5.12	45	3.62	Al2024T3	0.102	0.16	2.796	15.24	24.0	0.051	0.08	Al2024-T4	47	0.240	C5
146	1688	Burch-BAC	Al2017	0.635	2.796	0.3748	4.63	60	2.32	Al2024T3	0.102	0.16	2.796	15.24	24.0	0.051	0.08	Al2024-T4	47	0.240	C5
147	1689	Burch-BAC	Al2017	0.635	2.796	0.3748	5.09	45	3.60	Al2024T3	0.102	0.16	2.796	22.86	36.0	0.051	0.08	Al2024-T4	47	0.240	C5
148	1690	Burch-BAC	Al2017	0.635	2.796	0.3748	4.97	60	2.48	Al2024T3	0.102	0.16	2.796	22.86	36.0	0.051	0.08	Al2024-T4	47	0.240	C5
149	1691	Burch-BAC	Al2017	0.635	2.796	0.3748	4.57	70	1.56	Al2024T3	0.102	0.16	2.796	7.62	12.0	0.051	0.08	Al2024-T4	47	0.240	C5
150	1692	Burch-BAC	Al2017	0.635	2.796	0.3748	3.41	45	2.41	Al2024T3	0.102	0.16	2.796	7.62	12.0	0.051	0.08	Al2024-T4	47	0.240	C5

WHIPPLE_EXCEL DATA

Translated from

K=tw*(Y/70)^.5*S^.5*(pp*pb)^-1/6*Vn^-1*M^-1/3
K'=tw*(Y/70)^.5*S^.5*(pp*pb)^-1/6*Vn^-1*M^-1/3*d^-.5

K=tw*(Y/70)^.5*S^.5*(pp*pb)*
K"=tw*(Y/70)^.5*S^.5*(pp*pb)*

	Shot No.	Damage Description	JSC Whipple Eqns. dcrit (cm)	dcrit-d (cm)	Fail? 1=Y, 0=N)	Perf. Pred.	Safe Acc?	Pred. Accurate?	Comments	dc/d	K	K"	JSC Whipple Eq BLC Category (cm)
101	GM-13	No perf or detached spall	0.525	0.2075	0	0	1	1		1.653	0.3743	0.6644	0.524963
102	GM-14	No perf or detached spall	0.491	0.1732	0	0	1	1		1.546	0.2647	0.4698	0.490734
103	GM-15	No perf or detached spall	0.569	0.2512	0	0	1	1		1.791	0.3743	0.6644	0.568745
104	GM-16	No perf or detached spall	0.830	0.5124	0	0	1	1		2.614	0.4294	0.7621	0.829883
105	GM-17	No perf or detached spall	0.770	0.4522	0	0	1	1		2.424	0.5259	0.9334	0.7697
106	A86/1	No hole or spall; front surface erosion	1.288	0.3352	0	0	1	1		1.352	0.2835	0.2905	1.287739
107	A86/2	No hole or tear; impulsive dent;1 incip spall	0.657	-0.2953	0	1	1	0		0.690	0.1022	0.1047	0.657206
108	A86/3	Dented with 0.16 cm crack; incip spall ring	0.651	-0.3011	1	1	1	1		0.684	0.1021	0.1046	0.651404
109	A86/4	No hole or tear; perf ring; no central spall	0.645	-0.3075	1	1	1	1		0.677	0.1061	0.1087	0.644964
110	1732	Dented with 3 cracks; 3 sm perfs; thin spall	0.783	-0.1692	1	1	1	1	JSC A86/5	0.822	0.1457	0.1493	0.783329
111	1761	Perfs (20): Max ~30mm x 12 mm	0.514	-0.4381	1	1	1	1	Wit .063" Al. 3 perfs (1.5mm)	0.540	0.1795	0.1839	0.514377
112	1868	Dented; no tear or spall; A1732 w/6061-T6	0.782	-0.1703	0	1	1	0		0.821	0.1162	0.1191	0.803666
113	1869	Perforated (L/D=3 proj., hit parallel)	0.356	-0.5374	1	1	1	1	.125" Al 3rd perf. @ 6"	0.398	0.0424	0.0449	0.355892
114	1870	Perforated, 55 mm diameter spall	0.768	-0.1852	1	1	1	1	Wit .125 Al6061: dented	0.806	0.1356	0.1389	0.768434
115	1871	Cooking cutter perf (7 mm dia)	0.652	-0.3033	1	1	1	1	Wit .125 Al6061:	0.682	0.1804	0.1846	0.651949
116	1872	Cooking cutter perf (7 mm dia)	0.732	-0.2230	1	1	1	1	Wit .125 Al6061: bul,cr,dmpl	0.767	0.2205	0.2256	0.732212
117	1873	No perf	1.229	0.2757	0	0	1	1		1.289	0.2393	0.2451	1.228938
118	1874	Cooking cutter perf (103 mm dia)	0.714	-0.2415	1	1	1	1	Wit .125 Al6061: bul,cr,dmpl	0.747	0.2057	0.2105	0.713689
119	1875	Dented; no tear or spall; #1868 w/ 2mm press.	0.755	-0.1971	0	1	1	0		0.793	0.1222	0.1252	0.755435
120	1894	2 perfs (0.9 and 0.5 cm)	1.097	0.1441	1	0	0	0		1.151	0.4953	0.5075	1.096637
121	1895	Dented; no tear or spall; #1868 repeat	0.775	-0.1778	0	1	1	0		0.813	0.1197	0.1227	0.774727
122	1899	No hole or tear; thin, 5cm detached spall	1.060	0.1071	0	0	1	1		1.112	0.1952	0.2000	1.059555
123	1907	No tear; 1 perf 0.48cm; attached spall	1.244	-0.0262	1	1	1	1		0.979	0.2125	0.1885	1.243794
124	1913	No tear or spall; some impulsive denting	1.177	-0.0933	0	1	1	0		0.927	0.1810	0.1606	1.176681
125	1917	No hole or tear; attached spall with crack	0.989	0.0361	0	0	1	1		1.038	0.1847	0.1892	0.988596
126	1918	No hole or perf; ring & central incip spalls	0.901	-0.0510	0	1	1	0		0.946	0.1543	0.1581	0.901479
127	1921	No hole or tear; thin 7.6cm detached spall	1.204	-0.0659	1	1	1	1		0.948	0.1801	0.1598	1.204124
128	MD15	No hole or tear; discrete spallations	0.603	-0.2806	1	1	1	1		0.683	0.0848	0.0902	0.615616
129	MD27	No hole or tear; attached spall, split	3.585	1.6766	0	0	1	1		1.879	0.5691	0.4120	3.712186
130	MD28	No hole or tear; attached spall dimples	2.225	0.3166	0	0	1	1		1.166	0.2782	0.2014	2.272769
131	MD29	No hole or tear; incip spalls, some detached	1.824	-0.0838	1	1	1	1		0.956	0.2066	0.1496	1.864576
132	MD31	No hole or tear; attached spall dimples	1.947	0.0388	0	0	1	1		1.020	0.2278	0.1649	2.018569
133	1675	Perforated (2")	0.123	-0.5124	1	1	1	1	4 20mil 2024T3 wit perf LOF	0.193	0.0228	0.0286	0.12257
134	1676	Perforated (2.2")	0.138	-0.4972	1	1	1	1	3.3 20mil 2024T3 wit perf LOF	0.217	0.0195	0.0245	0.137846
135	1677	Perforated (2.1"x2.6")	0.124	-0.5114	1	1	1	1	4.3 20mil 2024T3 wit perf LOF	0.195	0.0245	0.0307	0.12357
136	1678	Perforated (1.8"x2.6")	0.126	-0.5094	1	1	1	1	4.1 20mil 2024T3 wit perf LOF	0.198	0.0314	0.0394	0.125587
137	1679	Perforated (2.8")	0.159	-0.4759	1	1	1	1	3.3 20mil 2024T3 wit perf LOF	0.251	0.0249	0.0313	0.159073
138	1680	Perforated (2.0"x3.7")	0.186	-0.4489	1	1	1	1	3.3 20mil 2024T3 wit perf LOF	0.293	0.0303	0.0381	0.186091
139	1681	Perforated (3.0"x3.5")	0.234	-0.4008	1	1	1	1	3 20mil 2024T3 wit perf LOF	0.369	0.0257	0.0322	0.234203
140	1682	Perforated (2.8"x3.5")	0.298	-0.3367	1	1	1	1	3 20mil 2024T3 wit perf LOF	0.470	0.0298	0.0374	0.298316
141	1683	Perforated (1.7"x2.7")	0.184	-0.4509	1	1	1	1	6 20mil 2024T3 wit perf LOF	0.290	0.0444	0.0558	0.166545
142	1684	Perforated (1.7"x2.5")	0.290	-0.3449	1	1	1	1	3.2LOF & 4Norm 20mil wit perf	0.457	0.0432	0.0542	0.276444
143	1685	Perforated	0.512	-0.1228	1	1	1	1	1.5LOF & 5.8Norm 20mil perf	0.807	0.0444	0.0558	0.49595
144	1686	Perforated (2.5"x3.5")	0.141	-0.4939	1	1	1	1	3.3LOF 20mil 2024T3 wit perf	0.222	0.0344	0.0432	0.141118
145	1687	Perforated (1.2"x2")	0.132	-0.5027	1	1	1	1	4.7LOF 20mil 2024T3 wit perf	0.208	0.0442	0.0554	0.132273
146	1688	Perforated (0.8"x1.4")	0.195	-0.4397	1	1	1	1	4LOF 20mil 2024T3 wit perf	0.308	0.0691	0.0867	0.159748
147	1689	Perforated (0.5"x0.9")	0.136	-0.4988	1	1	1	1	5LOF 20mil 2024T3 wit perf	0.214	0.0544	0.0683	0.136207
148	1690	Perforated	0.187	-0.4481	1	1	1	1	4LOF 20mil 2024T3 wit perf	0.294	0.0789	0.0990	0.157489
149	1691	Perforated (1.1"x1.8")	0.359	-0.2762	1	1	1	1	3.8LOF 20mil 2024T3 wit perf	0.565	0.0723	0.0908	0.265551
150	1692	Perforated (0.7"x0.9")	0.137	-0.4980	1	1	1	1	7LOF 20mil 2024T3 wit perf	0.216	0.0469	0.0588	0.113493

WHIPPLE_EXCEL DATA

Translated from Lotus by L.Thompson (714) 896-4495

Whipple Database

	Shot No.	Site	Proj. Mat'l	Proj. Dia. (cm)	Proj. Dens. (g/cc)	Proj. Mass (g)	Vel. (km/sec)	Impact Angle (deg)	Normal Vel. (km/sec)	Bumper Mat'l	Bumper Thk (cm)	tb/d	Bumper Dens. (g/cc)	Spacing (cm)	S/d	Wall Th'k (cm)	tw/d	Wall Mat'l	Yield Stress (ksi)	(tb+tw)/d	Category
151	1693	Burch-BAC	Al2017	0.318	2.796	0.0469	4.48	45	3.17	Al2024T3	0.102	0.32	2.796	7.62	24.0	0.025	0.08	Al2024-T4	47	0.400	C5
152	1694	Burch-BAC	Al2017	0.318	2.796	0.0469	5.82	45	4.12	Al2024T3	0.102	0.32	2.796	7.62	24.0	0.051	0.16	Al2024-T4	47	0.480	C5
153	1695	Burch-BAC	Al2017	0.635	2.796	0.3748	5.36	45	3.79	Al2024T3	0.102	0.16	2.796	7.62	12.0	0.102	0.16	Al2024-T4	47	0.320	C5
154	1696	Burch-BAC	Al2017	0.635	2.796	0.3748	5.33	45	3.77	Al2024T3	0.102	0.16	2.796	7.62	12.0	0.102	0.16	Al2024-T4	47	0.320	C5
155	1697	Burch-BAC	Al2017	0.635	2.796	0.3748	5.64	45	3.99	Al2024T3	0.051	0.08	2.796	7.62	12.0	0.051	0.08	Al2024-T4	47	0.160	C5
156	1699	Burch-BAC	Al2017	0.635	2.796	0.3748	4.05	60	2.03	Al2024T3	0.051	0.08	2.796	7.62	12.0	0.051	0.08	Al2024-T4	47	0.160	C5
157	1702	Burch-BAC	Al2017	0.318	2.796	0.0469	3.96	60	1.98	Al2024T3	0.102	0.32	2.796	7.62	24.0	0.051	0.16	Al2024-T4	47	0.480	C5
158	1703	Burch-BAC	Al2017	0.318	2.796	0.0469	4.18	60	2.09	Al2024T3	0.102	0.32	2.796	7.62	24.0	0.025	0.08	Al2024-T4	47	0.400	C5
159	1705	Burch-BAC	Al2017	0.635	2.796	0.3748	4.54	45	3.21	Al2024T3	0.051	0.08	2.796	7.62	12.0	0.051	0.08	Al2024-T4	47	0.160	C5
160	1706	Burch-BAC	Al2017	0.635	2.796	0.3748	5.49	60	2.74	Al2024T3	0.051	0.08	2.796	7.62	12.0	0.051	0.08	Al2024-T4	47	0.160	C5
161	1707	Burch-BAC	Al2017	0.635	2.796	0.3748	5.30	30	4.59	Al2024T3	0.102	0.16	2.796	7.62	12.0	0.051	0.08	Al2024-T4	47	0.240	C5
162	1708	Burch-BAC	Al2017	0.635	2.796	0.3748	5.52	45	3.90	Al2024T3	0.102	0.16	2.796	7.62	12.0	0.051	0.08	Al2024-T4	47	0.240	C5
163	1709	Burch-BAC	Al2017	0.635	2.796	0.3748	5.21	60	2.61	Al2024T3	0.102	0.16	2.796	7.62	12.0	0.051	0.08	Al2024-T4	47	0.240	C5
164	1710	Burch-BAC	Al2017	0.635	2.796	0.3748	5.12	30	4.43	Al2024T3	0.203	0.32	2.796	7.62	12.0	0.051	0.08	Al2024-T4	47	0.400	C5
165	1711	Burch-BAC	Al2017	0.635	2.796	0.3748	5.21	45	3.69	Al2024T3	0.203	0.32	2.796	7.62	12.0	0.051	0.08	Al2024-T4	47	0.400	C5
166	1712	Burch-BAC	Al2017	0.635	2.796	0.3748	5.30	60	2.65	Al2024T3	0.203	0.32	2.796	7.62	12.0	0.051	0.08	Al2024-T4	47	0.400	C5
167	1713	Burch-BAC	Al2017	0.635	2.796	0.3748	5.24	30	4.54	Al2024T3	0.406	0.64	2.796	7.62	12.0	0.051	0.08	Al2024-T4	47	0.720	C5
168	1714	Burch-BAC	Al2017	0.635	2.796	0.3748	5.36	45	3.79	Al2024T3	0.406	0.64	2.796	7.62	12.0	0.051	0.08	Al2024-T4	47	0.720	C5
169	1715	Burch-BAC	Al2017	0.635	2.796	0.3748	4.69	60	2.35	Al2024T3	0.406	0.64	2.796	7.62	12.0	0.051	0.08	Al2024-T4	47	0.720	C5
170	1716	Burch-BAC	Al2017	0.635	2.796	0.3748	5.21	30	4.51	Al2024T3	0.051	0.08	2.796	5.08	8.0	0.051	0.08	Al2024-T4	47	0.160	C5
171	1717	Burch-BAC	Al2017	0.635	2.796	0.3748	5.00	45	3.53	Al2024T3	0.051	0.08	2.796	5.08	8.0	0.051	0.08	Al2024-T4	47	0.160	C5
172	1719	Burch-BAC	Al2017	0.635	2.796	0.3748	5.12	30	4.43	Al2024T3	0.051	0.08	2.796	12.7	20.0	0.051	0.08	Al2024-T4	47	0.160	C5
173	1721	Burch-BAC	Al2017	0.635	2.796	0.3748	5.46	60	2.73	Al2024T3	0.051	0.08	2.796	12.7	20.0	0.051	0.08	Al2024-T4	47	0.160	C5
174	1722	Burch-BAC	Al2017	0.635	2.796	0.3748	3.23	0	3.23	Al2024T3	0.051	0.08	2.796	7.62	12.0	0.051	0.08	Al2024-T4	47	0.160	C5
175	1723	Burch-BAC	Al2017	0.635	2.796	0.3748	3.57	0	3.57	Al2024T3	0.102	0.16	2.796	7.62	12.0	0.051	0.08	Al2024-T4	47	0.240	C5
176	1724	Burch-BAC	Al2017	0.635	2.796	0.3748	3.78	0	3.78	Al2024T3	0.203	0.32	2.796	7.62	12.0	0.051	0.08	Al2024-T4	47	0.400	C5
177	1725	Burch-BAC	Al2017	0.318	2.796	0.0469	5.30	30	4.59	Al2024T3	0.051	0.16	2.796	2.54	8.0	0.051	0.16	Al2024-T4	47	0.320	C5
178	1726	Burch-BAC	Al2017	0.635	2.796	0.3748	5.27	30	4.57	Al2024T3	0.102	0.16	2.796	7.62	12.0	0.102	0.16	Al2024-T4	47	0.320	C5
179	1727	Burch-BAC	Al2017	0.635	2.796	0.3748	5.15	45	3.64	Al2024T3	0.102	0.16	2.796	7.62	12.0	0.102	0.16	Al2024-T4	47	0.320	C5
180	1728	Burch-BAC	Al2017	0.635	2.796	0.3748	5.30	60	2.65	Al2024T3	0.102	0.16	2.796	7.62	12.0	0.102	0.16	Al2024-T4	47	0.320	C5
181	1171	ESA	Aluminum	0.2	2.713	0.0114	3.3	30	2.86	Al2024T3	0.150	0.75	2.796	20	100.0	0.150	0.75	Al2219-T851	46	1.500	D2
182	1172	ESA	Aluminum	0.2	2.713	0.0114	3.3	45	2.33	Al2024T3	0.150	0.75	2.796	20	100.0	0.150	0.75	Al2219-T851	46	1.500	D2
183	1173	ESA	Aluminum	0.2	2.713	0.0114	3.3	60	1.65	Al2024T3	0.150	0.75	2.796	20	100.0	0.150	0.75	Al2219-T851	46	1.500	D1
184	1647	ESA	Aluminum	0.4	2.713	0.0909	7	0	7.00	Al2024T3	0.200	0.50	2.796	15	37.5	0.150	0.38	Al2219-T851	46	0.875	D3
185	1648	ESA	Aluminum	0.4	2.713	0.0909	7.1	0	7.10	Al2024T3	0.200	0.50	2.796	20	50.0	0.150	0.38	Al2219-T851	46	0.875	D2
186	1650	ESA	Aluminum	0.4	2.713	0.0909	7.1	0	7.10	Al2024T3	0.200	0.50	2.796	30	75.0	0.150	0.38	Al2219-T851	46	0.875	D2
187	1716	ESA	Aluminum	0.5	2.713	0.1776	3.2	0	3.20	Al2024T3	0.150	0.30	2.796	20	40.0	0.150	0.30	Al2219-T851	46	0.600	D4
188	1717	ESA	Aluminum	0.5	2.713	0.1776	3.2	0	3.20	Al2024T3	0.180	0.36	2.796	20	40.0	0.318	0.64	Al2219-T851	46	0.995	D4
189	1718	ESA	Aluminum	0.5	2.713	0.1776	3.1	0	3.10	Al2024T3	0.200	0.40	2.796	20	40.0	0.600	1.20	Al2219-T851	46	1.600	D2
190	1720	ESA	Aluminum	0.5	2.713	0.1776	5.6	0	5.60	Al2024T3	0.150	0.30	2.796	20	40.0	0.150	0.30	Al2219-T851	46	0.600	D4
191	1721	ESA	Aluminum	0.5	2.713	0.1776	5.8	0	5.80	Al2024T3	0.180	0.36	2.796	20	40.0	0.318	0.64	Al2219-T851	46	0.995	D2
192	1720	ESA	Aluminum	0.5	2.713	0.1776	5.8	0	5.80	Al2024T3	0.200	0.40	2.796	20	40.0	0.600	1.20	Al2219-T851	46	1.600	D1
193	1724	ESA	Aluminum	0.5	2.713	0.1776	6.5	0	6.50	Al2024T3	0.150	0.30	2.796	20	40.0	0.150	0.30	Al2219-T851	46	0.600	D3
194	1725	ESA	Aluminum	0.5	2.713	0.1776	6.4	0	6.40	Al2024T3	0.180	0.36	2.796	20	40.0	0.318	0.64	Al2219-T851	46	0.995	D2
195	1726	ESA	Aluminum	0.5	2.713	0.1776	6.4	0	6.40	Al2024T3	0.200	0.40	2.796	20	40.0	0.600	1.20	Al2219-T851	46	1.600	D1
196	1729	ESA	Aluminum	1.0	2.713	1.4205	3.1	0	3.10	Al2024T3	0.180	0.18	2.796	20	20.0	0.318	0.32	Al2219-T851	46	0.498	D5
197	1730	ESA	Aluminum	1.0	2.713	1.4205	3.1	0	3.10	Al2024T3	0.200	0.20	2.796	20	20.0	0.600	0.60	Al2219-T851	46	0.800	D5
198	1739	ESA	Aluminum	0.5	2.713	0.1776	3.2	0	3.20	Al2024T3	0.180	0.36	2.796	20	40.0	0.318	0.64	Al2219-T851	46	0.995	D4
199	1762	ESA	Aluminum	0.4	2.713	0.0909	3.1	0	3.10	Al2024T3	0.200	0.50	2.796	20	50.0	0.150	0.38	Al2219-T851	46	0.875	C5
200	1763	ESA	Aluminum	0.4	2.713	0.0909	2.7	0	2.70	Al2024T3	0.200	0.50	2.796	30	75.0	0.150	0.38	Al2219-T851	46	0.875	C5

WHIPPLE_EXCEL DATA

Translated from

	Shot No.	Damage Description	JSC Whipple Eqns. dcrit (cm)	dcrit-d (cm)	Fail? 1=Y, 0=N)	Perf. Pred.	Safe Acc?	Pred. Accurate?	Comments	dc/d	K=tw*(Y/70)^.5*S^.5*(pp*pb)^-1/6*Vn^-1*M^-1/3 K=tw*(Y/70)^.5*S^.5*(pp*pb)^-1/6*Vn^-1*M^-1/3*d^-.5 K	K"	JSC Whipple Ec Category	K=tw*(Y/70)^.5*S^.5*(pp*pb)^ K"=tw*(Y/70)^.5*S^.5*(pp*pb)^ ELC Whipple Ec (cm)
151	1693	Perforated (0.6"x0.7")	0.100	-0.2180	1	1	1	1	4LOF 10mil 2024T3 wit perf	0.314	0.0357	0.0634	0.099546	
152	1694	Perforated (0.7"x1.3")	0.131	-0.1866	1	1	1	1	3LOF 20mil 2024T3 wit perf	0.412	0.0550	0.0975	0.130865	
153	1695	Perforated (1.4"x2.6")	0.178	-0.4571	1	1	1	1	3LOF 40mil 2024T3 wit perf	0.280	0.0596	0.0748	0.177867	
154	1696	Perforated (1.2"x2.2")	0.177	-0.4576	1	1	1	1	3LOF 40mil 2024T3 wit perf	0.279	0.0600	0.0753	0.177352	
155	1697	Perforated (1.5"x2.3")	0.102	-0.5334	1	1	1	1	6LOF 20mil 2024T3 wit perf	0.160	0.0284	0.0356	0.101634	
156	1699	Perforated (1.8"x1.8")	0.147	-0.4884	1	1	1	1	5.1LOF 20mil 2024T3 wit perf	0.231	0.0558	0.0700	0.103296	
157	1702	Perforated	0.216	-0.1019	1	1	1	1	2LOF 20mil 2024T3 wit perf	0.679	0.1142	0.2027	0.167338	
158	1703	Perforated	0.174	-0.1438	1	1	1	1	3.5LOF 10mil 2024T3 wit perf	0.547	0.0542	0.0962	0.146624	
159	1705	Perforated (1"x0.7")	0.087	-0.5485	1	1	1	1	5.5LOF 20mil 2024T3 wit perf	0.136	0.0352	0.0442	0.08653	
160	1706	Perforated (1"x0.8")	0.121	-0.5139	1	1	1	1	3.5LOF 20mil 2024T3 wit perf	0.191	0.0412	0.0517	0.111504	
161	1707	Perforated (2.2"x2.8")	0.123	-0.5118	1	1	1	1	3.5LOF 20mil 2024T3 wit perf	0.194	0.0246	0.0309	0.123163	
162	1708	Perforated (1.5")	0.129	-0.5063	1	1	1	1	4.3LOF 20mil 2024T3 wit perf	0.203	0.0290	0.0364	0.128666	
163	1709	Perforated (0.9"x1.1")	0.181	-0.4537	1	1	1	1	3.5LOF 20mil 2024T3 wit perf	0.286	0.0434	0.0545	0.16646	
164	1710	Perforated (1.8"x2.4")	0.159	-0.4760	1	1	1	1	3.3LOF 20mil 2024T3 wit perf	0.250	0.0255	0.0320	0.159022	
165	1711	Perforated (1.1"x2.2")	0.186	-0.4486	1	1	1	1	3.1LOF 20mil 2024T3 wit perf	0.294	0.0307	0.0385	0.186431	
166	1712	Perforated (0.8"x0.5")	0.288	-0.3470	1	1	1	1	3.6LOF 20mil 2024T3 wit perf	0.454	0.0427	0.0535	0.275635	
167	1713	Perforated (2.2"x2.1")	0.230	-0.4046	1	1	1	1	3LOF 20mil 2024T3 wit perf	0.363	0.0249	0.0313	0.230439	
168	1714	Perforated (0.4"x1.8")	0.298	-0.3367	1	1	1	1	2.7LOF & 3.6Norm .02 wit perf	0.470	0.0298	0.0374	0.298316	
169	1715	Perforated	0.539	-0.0959	1	1	1	1	3.9Norm .02 2024T3 wit perf	0.849	0.0482	0.0605	0.510878	
170	1716	Perforated (1"x0.9")	0.095	-0.5397	1	1	1	1	5.1LOF 20mil 2024T3 wit perf	0.150	0.0205	0.0257	0.095265	
171	1717	Perforated (0.8"x0.8")	0.090	-0.5449	1	1	1	1	6.1LOF 20mil 2024T3 wit perf	0.142	0.0261	0.0328	0.090115	
172	1719	Perforated (1.6"x1.7")	0.112	-0.5232	1	1	1	1	4.3LOF 20mil 2024T3 wit perf	0.176	0.0329	0.0413	0.111778	
173	1721	Perforated (0.8"x1")	0.122	-0.5135	1	1	1	1	3.8LOF 20mil 2024T3 wit perf	0.191	0.0535	0.0672	0.109306	
174	1722	Perforated (0.4")	0.065	-0.5698	1	1	1	1	7.7LOF 20mil 2024T3 wit perf	0.103	0.0350	0.0439	0.065175	
175	1723	Perforated (0.9")	0.097	-0.5385	1	1	1	1	5.6LOF 20mil 2024T3 wit perf	0.152	0.0317	0.0398	0.096544	
176	1724	Perforated (1.8")	0.142	-0.4925	1	1	1	1	5.2LOF 20mil 2024T3 wit perf	0.224	0.0299	0.0376	0.142461	
177	1725	Perforated (0.7"x0.6")	0.085	-0.2323	1	1	1	1	3.3LOF 20mil 2024T3 wit perf	0.268	0.0284	0.0505	0.085187	
178	1726	Perforated (1.3"x1.8")	0.179	-0.4556	1	1	1	1	4.5LOF 40mil 2024T3 wit perf	0.283	0.0495	0.0622	0.179437	
179	1727	Perforated (1"x1.4")	0.174	-0.4607	1	1	1	1	4.9LOF 40mil 2024T3 wit perf	0.274	0.0621	0.0779	0.174265	
180	1728	Perforated (0.6"x1.1")	0.239	-0.3964	1	1	1	1	3.6LOF 40mil 2024T3 wit perf	0.376	0.0853	0.1071	0.217756	
181	1171	Buckled	0.197	-0.0026	0	1	1	0		0.987	0.6038	1.3501	0.182004	
182	1172	Buckled	0.272	0.0718	0	0	1	1		1.359	0.7395	1.6535	0.194552	
183	1173	No perf. or spall	0.470	0.2698	0	0	1	1		2.349	1.0458	2.3384	0.276779	
184	1647	Spall, buckled	0.415	0.0145	1	0	0	0		1.036	0.1067	0.1688	0.414638	
185	1648	Buckled	0.452	0.0519	0	0	1	1		1.130	0.1215	0.1921	0.462968	
186	1650	Buckled	0.517	0.1173	0	0	1	1		1.293	0.1488	0.2353	0.530662	
187	1716	Perf., spall, buckled; witness buckled	0.181	-0.3185	1	1	1	1		0.363	0.2157	0.3050	0.181499	
188	1717	Perf., buckled; witness buckled	0.296	-0.2038	1	1	1	1		0.592	0.4565	0.6457	0.296192	
189	1718	Buckled	0.448	-0.0520	0	1	1	0		0.896	0.8906	1.2595	0.448002	
190	1720	Perf., spall, buckled; witness buckled	0.355	-0.1449	1	1	1	1		0.710	0.1233	0.1743	0.3551	
191	1721	Buckled	0.608	0.1083	0	0	1	1		1.217	0.2519	0.3562	0.608296	
192	1720	No perf. or spall	0.934	0.4340	0	0	1	1		1.868	0.4760	0.6732	0.933983	
193	1724	Spall, buckled	0.420	-0.0798	1	1	1	1		0.840	0.1062	0.1502	0.420201	
194	1725	Buckled	0.680	0.1803	0	0	1	1		1.361	0.2283	0.3228	0.68032	
195	1726	No perf. or spall	1.042	0.5420	0	0	1	1		2.084	0.4314	0.6101	1.041979	
196	1729	Perf., spall, buckled	0.284	-0.7158	1	1	1	1		0.284	0.2356	0.2356	0.284188	
197	1730	Perf., spall, buckled	0.448	-0.5520	1	1	1	1		0.448	0.4453	0.4453	0.448002	
198	1739	Backwall perforated, .5mm witness dented	0.296	-0.2038	1	1	1	1		0.592	0.4565	0.6457	0.296192	
199	1762	2 Perfs (max: 7 mm)	0.199	-0.2010	1	1	1	1		0.497	0.2783	0.4401	0.198982	
200	1763	1 Perf (dia.: 6 mm)	0.206	-0.1944	1	1	1	1		0.514	0.3914	0.6188	0.16763	

Translated from Lotus by L.Thompson (714) 896-4495

Whipple Database

	Shot No.	Site	Proj. Mat'l	Proj. Dia. (cm)	Proj. Dens. (g/cc)	Proj. Mass (g)	Vel. (km/sec)	Impact Angle (deg)	Normal Vel. (km/sec)	Bumper Mat'l	Bumper Thk (cm)	tb/d	Bumper Dens. (g/cc)	Spacing (cm)	S/d	Wall Th'k (cm)	tw/d	Wall Mat'l	Yield Stress (ksi)	(tb+tw)/d	Category
201	1764	ESA	Aluminum	0.4	2.713	0.0909	3.2	0	3.20	Al2024T3	0.200	0.50	2.796	30	75.0	0.150	0.38	Al2219-T851	46	0.875	C5
202	1765	ESA	Aluminum	0.4	2.713	0.0909	3.4	0	3.40	Al2024T3	0.200	0.50	2.796	15	37.5	0.150	0.38	Al2219-T851	46	0.875	C4
203	1780	ESA	Aluminum	0.5	2.713	0.1776	5.7	30	4.94	Al2024T3	0.180	0.36	2.796	20	40.0	0.318	0.64	Al2219-T851	46	0.995	D4
204	1784	ESA	Aluminum	0.5	2.713	0.1776	5.7	45	4.03	Al2024T3	0.180	0.36	2.796	20	40.0	0.318	0.64	Al2219-T851	46	0.995	D2
205	1785	ESA	Aluminum	0.5	2.713	0.1776	5.6	60	2.80	Al2024T3	0.180	0.36	2.796	20	40.0	0.318	0.64	Al2219-T851	46	0.995	D2
206	1788	ESA	Aluminum	0.5	2.713	0.1776	6.5	0	6.50	Al2024T3	0.180	0.36	2.796	20	40.0	0.200	0.40	Al2219-T851	46	0.760	D2
207	1795	ESA	Aluminum	1.0	2.713	1.4205	3.1	0	3.10	Al2024T3	0.200	0.20	2.796	20	20.0	1.000	1.00	Al2219-T851	46	1.200	D3
208	1815	ESA	Aluminum	0.5	2.713	0.1776	5.3	0	5.30	Al2024T3	0.150	0.30	2.796	20	40.0	0.250	0.50	Al2219-T851	46	0.800	D4
209	1821	ESA	Aluminum	0.5	2.713	0.1776	6.2	0	6.20	Al2024T3	0.150	0.30	2.796	20	40.0	0.250	0.50	Al2219-T851	46	0.800	D2
210	1822	ESA	Aluminum	0.5	2.713	0.1776	6.4	0	6.40	Al2024T3	0.180	0.36	2.796	15	30.0	0.318	0.64	Al2219-T851	46	0.995	D2
211	1824	ESA	Aluminum	0.5	2.713	0.1776	3.2	0	3.20	Al2024T3	0.150	0.30	2.796	20	40.0	0.318	0.64	Al2219-T851	46	0.935	D5
212	1825	ESA	Aluminum	0.5	2.713	0.1776	1.6	0	1.60	Al2024T3	0.150	0.30	2.796	20	40.0	0.318	0.64	Al2219-T851	46	0.935	D5
213	1826	ESA	Aluminum	0.5	2.713	0.1776	5.7	0	5.70	Al2024T3	0.150	0.30	2.796	20	40.0	0.100	0.20	Al2219-T851	46	0.500	D4
214	1827	ESA	Aluminum	0.5	2.713	0.1776	7.3	0	7.30	Al2024T3	0.150	0.30	2.796	20	40.0	0.100	0.20	Al2219-T851	46	0.500	D4
215	6266	ESA	Aluminum	1.0	2.713	1.4205	5.2	0	5.20	Al2024T3	0.200	0.20	2.796	20	20.0	0.600	0.60	Al2219-T851	46	0.800	D5
216	6267	ESA	Aluminum	1.0	2.713	1.4205	5.2	0	5.20	Al2024T3	0.180	0.18	2.796	20	20.0	0.318	0.32	Al2219-T851	46	0.498	D5
217	6274	ESA	Aluminum	1.0	2.713	1.4205	5.6	0	5.60	Al2024T3	0.200	0.20	2.796	20	20.0	0.600	0.60	Al2219-T851	46	0.800	D5

WHIPPLE_EXCEL DATA

Translated from

K=tw*(Y/70)^.5*S^.5*(pp*pb)^-1/6*Vn^-1*M^-1/3
K*=tw*(Y/70)^.5*S^.5*(pp*pb)^-1/6*Vn^-1*M^-1/3*d^-.5

K=tw*(Y/70)^.5*S^.5*(pp*pb)^
K*=tw*(Y/70)^.5*S^.5*(pp*pb)^

Shot No.		Damage Description	JSC Whipple Eqns. dcrit (cm)	dcrit-d (cm)	Fail? 1=Y, 0=N)	Perf. Pred.	Safe Acc?	Pred. Accurate?	Comments	dc/d	K	K*	BLC JSC Whipple Ec Category (cm)
201	1764	1 Perf (dia.: 7 mm)	0.209	-0.1911	1	1	1	1		0.522	0.3302	0.5221	0.208883
202	1765	Small perf holes and spall	0.215	-0.1854	1	1	1	1		0.537	0.2198	0.3475	0.214608
203	1780	Perforation, spall, buckled	0.525	0.0251	1	0	0	0		1.050	0.2960	0.4186	0.525123
204	1784	Buckled	0.474	-0.0256	0	1	1	0		0.949	0.3625	0.5126	0.474417
205	1785	Buckled	0.548	0.0482	0	0	1	1		1.096	0.5218	0.7379	0.513492
206	1788	Buckled	0.510	0.0099	0	0	1	1		1.020	0.1416	0.2002	0.509909
207	1795	Spall	0.659	-0.3406	1	1	1	1		0.659	0.7422	0.7422	0.659351
208	1815	Perf. (1mm), spall, buckled	0.463	-0.0371	1	1	1	1		0.926	0.2170	0.3070	0.462877
209	1821	Buckled	0.557	0.0575	0	0	1	1		1.115	0.1855	0.2624	0.557456
210	1822	Buckled	0.622	0.1218	0	0	1	1		1.244	0.1977	0.2796	0.621845
211	1824	Perf. (6mm), buckled	0.282	-0.2179	1	1	1	1		0.564	0.4565	0.6457	0.28205
212	1825	Perf. (5.5mm), buckled	0.383	-0.1173	1	1	1	1		0.765	0.9131	1.2913	0.084031
213	1826	Perf., spall, buckled	0.280	-0.2195	1	1	1	1		0.561	0.0807	0.1142	0.280457
214	1827	Perf. (1mm), buckled	0.339	-0.1614	1	1	1	1		0.677	0.0630	0.0891	0.363924
215	6266	Perf., spall, buckled	0.826	-0.1740	1	1	1	1		0.826	0.2655	0.2655	0.825988
216	6267	Perf., spall, buckled	0.536	-0.4637	1	1	1	1		0.536	0.1405	0.1405	0.536272
217	6274	Perf., spall, buckled	0.898	-0.1020	1	1	1	1		0.898	0.2465	0.2465	0.897985

NASA JSC
Hypervelocity Impact Research Laboratory (HIRL)

Translated from Lotus by L. Thompson (714) 896-4495

Aluminum Mesh Double-Bumper Shots

. MESH, AL 2ND BUMPER, KEVLAR OR SPECTRA INTERMEDIATE, AL REAR WALL

		PROJECTILE CONDITIONS							TARGET CONDITIONS								
Shot No.	Site	Mat'l	Dia. (cm)	Density (g/cc)	Mass (g)	Vel. (km/sec)	Impact Angle (deg)	Vn (km/sec)	1st Bumper Mat'l	1st Areal Density (g/cm^2)	2nd Bumper Mat'l	2nd Areal Density (g/cm^2)	Intermediate Layer Mat'l (# sheets)	Intermed. Areal Density (g/cm^2)	Total Bump+I A.D. (g/cm^2)	Overall Spacing (cm)	Back-Wall Mat'l
A954	JSC-HIRL	AI2017T4	0.318	2.796	0.0469	6.39	0	6.39	Almesh 30x30 .012" wire	0.051	AI6061-0	0.110	Spectra 618(2)	0.056	0.217	5.08	AI2024T3
A962	JSC-HIRL	AI2017T4	0.320	2.796	0.0478	6.38	0	6.38	Almesh 30x30 .012" wire	0.051	AI6061-0	0.083	Spectra 618(3)	0.084	0.218	5.08	AI2024T3
A963	JSC-HIRL	AI2017T4	0.320	2.796	0.0478	6.35	0	6.35	Almesh 30x30 .012" wire	0.051	AI6061-0	0.083	Spectra 618(2)	0.056	0.190	5.08	AI2024T3
A971	JSC-HIRL	AI2017T4	0.317	2.796	0.0464	6.62	0	6.62	Almesh 30x30 .012" wire	0.051	AI6061-0	0.083	Spectra 618(2)	0.056	0.190	10.16	AI3003H12
A978	JSC-HIRL	AI2017T4	0.318	2.796	0.0473	6.58	0	6.58	Almesh 30x30 .012" wire	0.051	AI6061-0	0.083	Spectra 618(2)	0.056	0.190	10.16	AI6061-0
A1060	JSC-HIRL	AI2017T4	0.318	2.796	0.0469	6.32	0	6.32	Almesh 30x30 .012" wire	0.051	AI6061-0	0.083	Spectra 618(2)	0.056	0.190	10.16	AI2024T3
A1061	JSC-HIRL	AI2017T4	0.318	2.796	0.0469	6.11	45	4.32	Almesh 30x30 .012" wire	0.051	AI6061-0	0.083	Spectra 618(2)	0.056	0.190	10.16	AI2024T3
A1068	JSC-HIRL	AI2017T4	0.318	2.796	0.0469	5.87	60	2.94	Almesh 30x30 .012" wire	0.051	AI6061-0	0.083	Spectra 618(2)	0.056	0.190	10.16	AI3003H12
A1069	JSC-HIRL	AI2017T4	0.318	2.796	0.0469	6.08	45	4.30	Almesh 30x30 .012" wire	0.051	AI6061-0	0.083	Spectra 618(2)	0.056	0.190	10.16	AI3003H12
A1111	JSC-HIRL	AI2017T4	0.318	2.796	0.0469	6.02	60	3.01	Almesh 30x30 .012" wire	0.051	AI6061-0	0.083	Spectra 618(3)	0.084	0.218	10.16	AI2024T3
A1275	JSC-HIRL	AI2017T4	0.318	2.796	0.0469	5.9	0	5.90	Almesh 30x30 .013" wire	0.057	AI6061-0	0.083	Spectra 618(2)	0.056	0.196	10.16	AI2024T3
A1276	JSC-HIRL	AI2017T4	0.318	2.796	0.0469	6.2	0	6.20	Almesh 50x50 .009" wire	0.0304	AI6061-0	0.083	Kevlar 095(2)	0.056	0.169	10.16	AI2024T3
A1285	JSC-HIRL	AI2017T4	0.318	2.796	0.0469	6.42	0	6.42	Almesh 50x50 .009" wire	0.0304	AI6061-0	0.083	Kevlar 095(2)	0.056	0.169	10.16	AI2024T3
A1289	JSC-HIRL	AI2017T4	0.318	2.796	0.0469	6.24	0	6.24	Almesh 50x50 .009" wire	0.0304	AI6061-0	0.083	Spectra 618(2)	0.056	0.169	10.16	AI2024T3
A1351	JSC-HIRL	AI2017T4	0.239	2.796	0.01989	4.46	45	3.15	Almesh 50x50 .009" wire	0.0304	AI6061-0	0.083	Kevlar710(2)	0.064	0.177	10.16	AI2024T3
A1364	JSC-HIRL	AI2017T4	0.357	2.796	0.06672	6	75	1.55	Almesh 50x50 .009" wire	0.0304	AI6061-0	0.083	Kevlar710(2)	0.064	0.177	5.08	AI2024T3
1414	JSC-HIRL	AI2017T4	0.079	2.796	0.00073	3.5	0	3.50	Almesh 50x50 .009" wire	0.051	AI6061-0	0.083	Spectra 618 (2)	0.056	0.190	10.16	AI2024T3
1418	JSC-HIRL	AI2017T4	0.079	2.796	0.00073	4.1	0	4.10	Almesh 50x50 .009" wire	0.051	AI6061-0	0.083	Spectra 618 (2)	0.056	0.190	10.16	AI2024T3
1650	JSC-HIRL	AI2017T4	0.160	2.796	0.00598	3	0	3.00	Almesh 50x50 .009" wire	0.0304	AI6061-0	0.083	Kevlar710(2)	0.064	0.177	10.16	AI2024T3
1651	JSC-HIRL	AI2017T4	0.149	2.796	0.00485	2.63	0	2.63	Almesh 50x50 .009" wire	0.0304	AI6061-0	0.083	Kevlar710(2)	0.064	0.177	10.16	AI2024T3
1652	JSC-HIRL	AI2017T4	0.160	2.796	0.00596	3.44	45	2.43	Almesh 50x50 .009" wire	0.0304	AI6061-0	0.083	Kevlar710(2)	0.064	0.177	10.16	AI2024T3
1653	JSC-HIRL	AI2017T4	0.160	2.796	0.00596	3.31	60	1.66	Almesh 50x50 .009" wire	0.0304	AI6061-0	0.083	Kevlar710(2)	0.064	0.177	10.16	AI2024T3
1654	JSC-HIRL	AI2017T4	0.160	2.796	0.00596	3.41	60	1.71	Almesh 50x50 .009" wire	0.0304	AI6061-0	0.083	Kevlar710(2)	0.064	0.177	10.16	AI2024T3
1655	JSC-HIRL	AI2017T4	0.143	2.796	0.00425	2.96	0	2.96	Almesh 50x50 .009" wire	0.0304	AI6061-0	0.083	Kevlar710(2)	0.064	0.177	10.16	AI2024T3
1656	JSC-HIRL	AI2017T4	0.125	2.796	0.00288	3.19	0	3.19	Almesh 50x50 .009" wire	0.0304	AI6061-0	0.083	Kevlar710(2)	0.064	0.177	10.16	AI2024T3
1660	JSC-HIRL	AI2017T4	0.160	2.796	0.00595	4.81	45	3.40	Almesh 50x50 .009" wire	0.0304	AI6061-0	0.083	Kevlar710(2)	0.064	0.177	10.16	AI2024T3
1661	JSC-HIRL	AI2017T4	0.160	2.796	0.00597	5.74	60	2.87	Almesh 50x50 .009" wire	0.0304	AI6061-0	0.083	Kevlar710(2)	0.064	0.177	10.16	AI2024T3
B27	JSC-HIRL	AI2017T4	0.635	2.796	0.374	6.69	0	6.69	Almesh 24x24 .023" wire	0.130	AI3003H14	0.174	Spectra 618(4)	0.112	0.416	20.32	AI2024T3
B77	JSC-HIRL	AI2017T4	0.635	2.796	0.374	7.53	0	7.53	Almesh 24x24 .023" wire	0.130	AI6061T6	0.172	Kevlar710(4)	0.128	0.430	10.16	AI2024T3
B81	JSC-HIRL	AI2017T4	0.634	2.796	0.3734	7.29	0	7.29	Almesh 24x24 .023" wire	0.130	AI6061T6	0.172	Kevlar710(4)	0.128	0.430	10.16	AI2024T3
4-1172	UDRI	AI2017T4	0.953	2.796	1.2651	6.65	0	6.65	Almesh 12x12 .032" wire	0.135	AI2024T3	0.284	Kevlar903(7)	0.161	0.580	30.48	AI2024T3

MDB_EXCEL DATA

Hypervel

Alumini

. MESH, AL 2ND BUMPE

Shot No.	Site	Wall Thick (cm)	Wall Areal Density (g/cm^2)	Yield Stress (ksi)	Damage Class	Wall Damage (P=Perforation, S=Detached Spall)	Total Areal Density (g/cm^2)	SN3-91-42 dcrit (cm)	dcrit-d (cm)	ratio dcrit/d	Predict Fail? (1=Y,0=N)	Fail?	Safety Accurate?	All Acc?	Comments	3<Vn<6 dcrit (cm)	Wire Thick (mm)	Min Ratio t1/d
A954	JSC-HIRL	0.079	0.222	47	F3	No P or S, some dimples	0.439	0.267	-0.050	0.841	1	0	1	0	Si=.25",1.5",.25"	0.291	0.305	0.096
A962	JSC-HIRL	0.079	0.222	47	F3	No P or S, bulge	0.440	0.267	-0.052	0.836	1	0	1	0	Si=.25",1.5",.25"	0.290	0.305	0.095
A963	JSC-HIRL	0.079	0.222	47	F3	No P or S, bulge	0.412	0.268	-0.052	0.838	1	0	1	0	Si=.25",1.5",.25"	0.290	0.305	0.095
A971	JSC-HIRL	0.064	0.174	18	F3	No P or S, bulge	0.364	0.329	0.013	1.040	0	0	1	1	Si=.25",3.5",.25"	0.391	0.305	0.096
A978	JSC-HIRL	0.064	0.172	8	F3	No P or S, bulge	0.362	0.287	-0.031	0.902	1	0	1	0	Si=.3",3.45",.25"	0.338	0.305	0.096
A1060	JSC-HIRL	0.079	0.222	47	F3	No P or S, s.bulge	0.412	0.426	0.108	1.340	0	0	1	1	Si=.375",3.25",.375"	0.466	0.305	0.096
A1061	JSC-HIRL	0.079	0.222	47	C2	No P or S, dmpls	0.412	0.289	-0.029	0.909	1	0	1	0	Si=.375",3.25",.375"	0.289	0.305	0.096
A1068	JSC-HIRL	0.064	0.174	18	C4	1 P, 1.3mm	0.364	0.181	-0.137	0.570	1	1	1	1	Si=.375",3.25",.375"	0.175	0.305	0.096
A1069	JSC-HIRL	0.064	0.174	18	C2	No P or S, dmpls	0.364	0.220	-0.097	0.694	1	0	1	0	Si=.375",3.25",.375"	0.220	0.305	0.096
A1111	JSC-HIRL	0.064	0.178	47	C2	No P or S, dmpls	0.395	0.234	-0.084	0.737	1	0	1	0	Si=.375",3.25",.375"	0.234	0.305	0.096
A1275	JSC-HIRL	0.041	0.114	47	F3	No P or S, bulge	0.309	0.338	0.020	1.064	0	0	1	1	Si=.5",3",.5"	0.338	0.330	0.104
A1276	JSC-HIRL	0.041	0.114	47	F3	No P or S, bulge	0.283	0.343	0.025	1.079	0	0	1	1	Si=.5",3",.5"	0.363	0.229	0.072
A1285	JSC-HIRL	0.030	0.085	47	F3	No P or S, bulge	0.254	0.308	-0.010	0.969	1	0	1	0	Si=.5",3",.5"	0.348	0.229	0.072
A1289	JSC-HIRL	0.030	0.085	47	F3	No P or S, bulge	0.254	0.311	-0.007	0.979	1	0	1	0	Si=.5",3",.5"	0.333	0.229	0.072
A1351	JSC-HIRL	0.051	0.142	47	C4	4 Ps, 1.5x1mm max	0.319	0.149	-0.089	0.626	1	1	1	1	Si=.5",3",.5"	0.149	0.229	0.096
A1364	JSC-HIRL	0.051	0.142	47	C1	No P or S, sm.dmpls	0.319	0.538	0.180	1.505	0	0	1	1	Si=.5",3",.5"	0.414	0.229	0.064
1414	JSC-HIRL	0.030	0.085	47	C1/C0	No P or S, No damage	0.275	0.123	0.044	1.556	0	0	1	1	Si=.5",3",.5"	0.123	0.229	0.288
1418	JSC-HIRL	0.030	0.085	47	C1/C0	No P or S, No damage	0.275	0.169	0.090	2.134	0	0	1	1	Si=.5",3",.5"	0.169	0.229	0.288
1650	JSC-HIRL	0.051	0.142	47	C4	2 Ps, 1.5x0.8mm & 0.7mm	0.319	0.099	-0.061	0.617	1	1	1	1	Si=.5",3",.5"	0.099	0.229	0.143
1651	JSC-HIRL	0.051	0.142	47	C4	1 P, 0.8mm	0.319	0.107	-0.042	0.719	1	1	1	1	Si=.5",3",.5"	0.065	0.229	0.153
1652	JSC-HIRL	0.051	0.142	47	C2	No P or S, dmpls	0.319	0.156	-0.003	0.979	1	0	1	0	Si=.5",3",.5"	0.093	0.229	0.143
1653	JSC-HIRL	0.051	0.142	47	C1	No P or S, no dmpls	0.319	0.277	0.117	1.733	0	0	1	1	Si=.5",3",.5"	0.109	0.229	0.143
1654	JSC-HIRL	0.051	0.142	47	C1	No P or S, no dmpls	0.319	0.272	0.112	1.701	0	0	1	1	Si=.5",3",.5"	0.112	0.229	0.143
1655	JSC-HIRL	0.051	0.142	47	C4	4 Ps, 1mm max	0.319	0.099	-0.043	0.697	1	1	1	1	Si=.5",3",.5"	0.095	0.229	0.160
1656	JSC-HIRL	0.051	0.142	47	C4	Small P, 0.7mm	0.319	0.116	-0.009	0.927	1	1	1	1	Si=.5",3",.5"	0.116	0.229	0.182
1660	JSC-HIRL	0.051	0.142	47	C2	No P or S, dmpls	0.319	0.169	0.009	1.057	0	0	1	1	Si=.5",3",.5"	0.169	0.229	0.143
1661	JSC-HIRL	0.051	0.142	47	C1/C0	No P or S, No damage	0.319	0.195	0.036	1.224	0	0	1	1	No perf of Kevlar, Si=.5",3'	0.183	0.229	0.143
B27	JSC-HIRL	0.079	0.222	47	F3	No P or S, bulge	0.638	0.663	0.028	1.045	0	0	1	1	Si=1",6",1"	0.801	0.584	0.092
B77	JSC-HIRL	0.180	0.504	47	F3	No P or S, bulge	0.935	0.528	-0.107	0.832	1	0	1	0	Si=1",2",1"	0.719	0.584	0.092
B81	JSC-HIRL	0.180	0.504	47	F3	No P or S, bulge	0.935	0.534	-0.101	0.841	1	0	1	0	Si=1",2",1"	0.696	0.584	0.092
4-1172	UDRI	0.180	0.504	47	F3	No P or S, s.bulge	1.084	1.144	0.192	1.201	0	0	1	1	Si=1.5",8.5",2"	1.372	0.813	0.085
											no.	6	31	19				
											count	31	31	31				
											%	19.4%	100.0%	61.3%				

MDB_EXCEL DATA

Hypervel

Alumini

. MESH, AL 2ND BUMPE

Shot No.	Site	Max Ratio t1/d	Wires per inch	Wires "Cut"	Ratio Shield to proj.	Ratio AD 1st to proj.	Ratio AD 2nd to proj.	Ratio Int. to proj.	Ratio AD 1&2 to proj.	Ratio AD B&I to proj.	Ratio Wall to proj.	Ratio W&I to proj.	2nd Thick (cm)	Ratio (t1 min+t2)/ proj dia
A954	JSC-HIRL	0.192	30	3.8	0.495	0.057	0.124	0.063	0.182	0.245	0.250	0.313	0.041	0.224
A962	JSC-HIRL	0.191	30	3.8	0.492	0.057	0.093	0.094	0.150	0.244	0.248	0.342	0.030	0.191
A963	JSC-HIRL	0.191	30	3.8	0.461	0.057	0.093	0.063	0.150	0.212	0.248	0.311	0.030	0.191
A971	JSC-HIRL	0.193	30	3.7	0.411	0.058	0.093	0.063	0.151	0.214	0.197	0.260	0.030	0.193
A978	JSC-HIRL	0.191	30	3.8	0.406	0.057	0.093	0.063	0.150	0.213	0.193	0.256	0.030	0.191
A1060	JSC-HIRL	0.192	30	3.8	0.464	0.057	0.093	0.063	0.151	0.214	0.250	0.313	0.030	0.192
A1061	JSC-HIRL	0.192	30	3.8	0.464	0.057	0.093	0.063	0.151	0.214	0.250	0.313	0.030	0.192
A1068	JSC-HIRL	0.192	30	3.8	0.410	0.057	0.093	0.063	0.151	0.214	0.196	0.259	0.030	0.192
A1069	JSC-HIRL	0.192	30	3.8	0.410	0.057	0.093	0.063	0.151	0.214	0.196	0.259	0.030	0.192
A1111	JSC-HIRL	0.192	30	3.8	0.445	0.057	0.093	0.095	0.151	0.245	0.200	0.295	0.030	0.192
A1275	JSC-HIRL	0.208	30	3.8	0.348	0.064	0.093	0.063	0.157	0.220	0.128	0.191	0.030	0.200
A1276	JSC-HIRL	0.144	50	6.3	0.318	0.034	0.093	0.063	0.127	0.190	0.128	0.191	0.030	0.168
A1285	JSC-HIRL	0.144	50	6.3	0.286	0.034	0.093	0.063	0.127	0.190	0.096	0.159	0.030	0.168
A1289	JSC-HIRL	0.144	50	6.3	0.286	0.034	0.093	0.063	0.127	0.190	0.096	0.159	0.030	0.168
A1351	JSC-HIRL	0.192	50	4.7	0.478	0.046	0.124	0.096	0.170	0.265	0.213	0.309	0.030	0.224
A1364	JSC-HIRL	0.128	50	7.0	0.320	0.030	0.083	0.064	0.113	0.177	0.142	0.206	0.030	0.149
1414	JSC-HIRL	0.576	50	1.6	1.239	0.230	0.373	0.252	0.602	0.855	0.384	0.636	0.030	0.672
1418	JSC-HIRL	0.576	50	1.6	1.239	0.230	0.373	0.252	0.602	0.855	0.384	0.636	0.030	0.672
1650	JSC-HIRL	0.286	50	3.1	0.714	0.068	0.185	0.143	0.253	0.396	0.318	0.461	0.030	0.334
1651	JSC-HIRL	0.307	50	2.9	0.766	0.073	0.198	0.154	0.271	0.425	0.341	0.494	0.030	0.358
1652	JSC-HIRL	0.286	50	3.1	0.715	0.068	0.185	0.143	0.253	0.397	0.318	0.461	0.030	0.334
1653	JSC-HIRL	0.286	50	3.1	0.715	0.068	0.185	0.143	0.253	0.397	0.318	0.461	0.030	0.334
1654	JSC-HIRL	0.286	50	3.1	0.715	0.068	0.185	0.143	0.253	0.397	0.318	0.461	0.030	0.334
1655	JSC-HIRL	0.320	50	2.8	0.800	0.076	0.207	0.160	0.284	0.444	0.356	0.517	0.030	0.374
1656	JSC-HIRL	0.365	50	2.5	0.911	0.087	0.236	0.183	0.323	0.505	0.405	0.588	0.030	0.426
1660	JSC-HIRL	0.286	50	3.1	0.715	0.068	0.185	0.143	0.253	0.397	0.318	0.462	0.030	0.334
1661	JSC-HIRL	0.286	50	3.1	0.714	0.068	0.185	0.143	0.253	0.396	0.318	0.461	0.030	0.334
B27	JSC-HIRL	0.184	24	6.0	0.360	0.073	0.098	0.063	0.171	0.234	0.125	0.188	0.064	0.192
B77	JSC-HIRL	0.184	24	6.0	0.527	0.073	0.097	0.072	0.170	0.243	0.284	0.356	0.064	0.192
B81	JSC-HIRL	0.184	24	6.0	0.527	0.073	0.097	0.072	0.170	0.243	0.284	0.357	0.064	0.192
4-1172	UDRI	0.171	12	4.5	0.407	0.051	0.107	0.060	0.157	0.218	0.189	0.250	0.102	0.192

C-48

MS_EXCEL DATA

Eric L. Christiansen
NASA/Johnson Space Center
Mail Code SN3
Translated from Lotus by L.Thompson (714)896-4495

Multi-Shock Shield Database

Nextel Bumpers, Aluminum Rear Wall

	Projectile Parameters								Bumper				Back Wall			
Shot No.	Site	Mat'l	Dia. (cm)	Dens. (g/cc)	Mass (g)	Vel. (km/sec)	Obliquity (deg)	Vn (km/sec)	Mat'l	Number Sheets	Areal D. (g/cm^2)	Overall Spacing (cm)	Mat'l	Thk (cm)	Areal D. (g/cm^2)	Yield Stress (ksi)
A433	JSC	Al2017T4	0.3175	2.796	0.0469	6.6	0	6.6	Nextel	4	0.172	10.16	Al6061T6	0.079	0.215	36
A436	JSC	Al2017T4	0.3175	2.796	0.0469	6.55	0	6.55	Nextel	4	0.172	10.16	Al6061T6	0.079	0.215	36
A624	JSC	Al2017T4	0.3175	2.796	0.0469	6.6	0	6.6	Nextel	2	0.172	5.08	Al2024T3	0.127	0.355	47
A725	JSC	Al2017T4	0.3175	2.796	0.0469	6.17	0	6.17	Nextel	2	0.284	5.08	Al2024T3	0.127	0.355	47
A726	JSC	Al2017T4	0.3175	2.796	0.0469	5.93	0	5.93	Nextel	2	0.256	5.08	Al2024T3	0.127	0.355	47
A727	JSC	Al2017T4	0.3175	2.796	0.0469	6.14	0	6.14	Nextel	2	0.22	5.08	Al2024T3	0.127	0.355	47
A729	JSC	Al2017T4	0.3175	2.796	0.0469	6.14	0	6.14	Nextel	3	0.165	7.62	Al6061T6	0.079	0.215	36
A731	JSC	Al2017T4	0.3175	2.796	0.0469	6.15	0	6.15	Nextel	3	0.129	7.62	Al6061T6	0.079	0.215	36
A732	JSC	Al2017T4	0.3175	2.796	0.0469	6.15	0	6.15	Nextel	4	0.22	10.16	Al3003H12	0.064	0.174	18
A958	JSC	Al2O3	0.3175	3.9	0.0654	6	0	6	Nextel	5	0.258	12.7	Al2024T3	0.079	0.222	47
A1066	JSC	Al2017T4	0.3175	2.796	0.0469	6.34	60	3.17	Nextel AF26	4	0.172	10.16	Al2024T3	0.079	0.222	47
A1067	JSC	Al2017T4	0.3175	2.796	0.0469	5.91	45	4.18	Nextel AF26	4	0.172	10.16	Al2024T3	0.079	0.222	47
A1229	JSC	Al2017T4	0.3175	2.796	0.0469	6.49	0	6.49	Nextel AF26	4	0.172	10.16	Al2024T3	0.051	0.142	47
A1230	JSC	Al2017T4	0.3175	2.796	0.0469	6.32	0	6.32	Nextel AF26	4	0.172	10.16	Al6061T6	0.064	0.172	36
A1231	JSC	Al2017T4	0.3175	2.796	0.0469	6.39	0	6.39	Nextel AF26	4	0.172	10.16	Al2024T3	0.041	0.114	47
A1235	JSC	Al2017T4	0.3175	2.796	0.0469	6.24	0	6.24	Nextel AF26	4	0.172	10.16	Al2024T3	0.064	0.178	47
A1237	JSC	Al2017T4	0.3175	2.796	0.0469	6.2	0	6.2	Nextel AF26	4	0.172	7.62	Al2024T3	0.079	0.222	47
A1239	JSC	Al2017T4	0.3175	2.796	0.0469	4.87	0	4.87	Nextel AF26	4	0.172	10.16	Al2024T3	0.079	0.222	47
A1252	JSC	Al2017T4	0.3175	2.796	0.0469	6.23	0	6.23	Nextel AF26	4	0.172	5.08	Al6061T6	0.127	0.355	36
A1253	JSC	Al2017T4	0.3175	2.796	0.0469	6.51	0	6.51	Nextel AF26	4	0.172	5.08	Al2024T3	0.159	0.444	47
A1256	JSC	Al2017T4	0.3175	2.796	0.0469	6.47	0	6.47	Nextel AF26	4	0.172	10.16	Al2024T3	0.030	0.085	47
A1257	JSC	Al2017T4	0.3175	2.796	0.0469	6.32	0	6.32	Nextel AF26	4	0.172	10.16	Al2024T3	0.030	0.085	47
A1264	JSC	Al2017T4	0.3175	2.796	0.0469	5.47	0	5.47	Nextel AF26	4	0.172	10.16	Al2024T3	0.051	0.142	47
A1265	JSC	Al2017T4	0.238	2.796	0.0198	6.71	0	6.71	Nextel AF26	4	0.172	10.16	Al2024T3	0.064	0.178	47
A1283	JSC	Al2017T4	0.3175	2.796	0.0469	6.23	0	6.23	Nextel AF26	4	0.172	10.16	Al2024T3	0.030	0.085	47
A1284	JSC	Al2017T4	0.3175	2.796	0.0469	6.29	0	6.29	Nextel AF26	4	0.172	10.16	Al2024T3	0.030	0.085	47
A1291	JSC	Al2017T4	0.3175	2.796	0.0469	5.44	0	5.44	Nextel AF26	4	0.172	10.16	Al2024T3	0.051	0.142	47
A1312	JSC	Al2017T4	0.3	2.796	0.0395	5.58	0	5.58	Nextel AF26	4	0.172	10.16	Al2024T3	0.051	0.142	47
A1313	JSC	Al2017T4	0.28	2.796	0.0321	5.3	0	5.3	Nextel AF26	4	0.172	10.16	Al2024T3	0.051	0.142	47
A1314	JSC	Al2017T4	0.2805	2.796	0.0323	5.69	0	5.69	Nextel AF26	4	0.172	10.16	Al2024T3	0.051	0.142	47
A1315	JSC	Al2017T4	0.26	2.796	0.0257	5.59	0	5.59	Nextel AF26	4	0.172	10.16	Al2024T3	0.051	0.142	47
A1316	JSC	Al2017T4	0.2191	2.796	0.0154	4.9	0	4.9	Nextel AF26	4	0.172	10.16	Al2024T3	0.051	0.142	47
A1317	JSC	Al2017T4	0.3176	2.796	0.0469	6.23	45	4.41	Nextel AF26	4	0.172	10.16	Al2024T3	0.051	0.142	47

MS_EXCEL DATA

Eric L. Christians
NASA/Johnson S
Mail Code SN3
Translated from

Vn>6km/sec: K=mw*S^2*(Y/40)^0.5/(M*Vn) [sec/km] (K=43.1 for Nextel bumpers w/ Al rear wall)
Vn<6 km/sec: K2=mw*S*(Y/40)^0.5*Vn/M [km/sec-cm]
K3=mw*[S^2*[(Vn/3-1)+((2-Vn/(3*S^2))]]*(Y/40)^0.5/M [km/sec-cm]

Shot No.	Damage Class	Damage Description	Ratio AD Bumper to Proj.	Total Areal D. (g/cm^2)	K >6km/s	K2 <6km/s	K3 <6km/s	Comments
A433	F3	Bulged, intact	0.194	0.387	68.2			
A436	F3	Bulged, intact	0.194	0.387	68.7			
A624	F3	Bulged, intact	0.194	0.527	32.1			
A725	F3	Bulged, intact	0.320	0.639	34.4			
A726	F5	Bulged, perforated	0.288	0.611		247.5	549	
A727	F3	Bulged, intact	0.248	0.575	34.5			
A729	F5	Bulged, perforated	0.186	0.380	41.2			
A731	F5	Bulged, perforated	0.145	0.344	41.2			
A732	F3	Bulged, intact	0.248	0.394	41.8			
A958	F3	Bulged, intact	0.208	0.480	98.9			NEXTEL:1,1,1,1,2
A1066	C1/F1	No perf, surface craters only	0.194	0.394		165.4	1035	
A1067	C2	No perf, cratering & dimples	0.194	0.394		218.0	1196	
A1229	F3	Bulged (1 v.small dimple)	0.194	0.314	52.3			
A1230	F3	Bulged, intact	0.194	0.344	57.0			
A1231	F3	Bulged, intact	0.194	0.286	42.5			
A1235	F3	Bulged, intact	0.194	0.350	67.9			
A1237	F3	Bulged, intact	0.194	0.394	48.1			
A1239	C5	perforated (1 hole 1.5x1mm)	0.194	0.394		254.0	1306	
A1252	F5/D4	Bulged, Pet. Perf. (5 x 3 mm)	0.194	0.527	29.8			
A1253	F3	Bulged, intact	0.194	0.616	40.7			
A1256	F5	Bulged, perforated	0.194	0.257	31.5			Si=.75",.75",.75",1.75"
A1257	F5	Bulged, perforated	0.194	0.257	32.2			Si=.5",.75",.75",2"
A1264	F4/C4	Bulged, 7 perfs, max 1.8x1.5mm	0.194	0.314		182.6	897	
A1265	F1	No bulge, intact	0.258	0.350	149.8			
A1283	F4	Bulged, split (8mm)	0.194	0.257	32.7			Si=1",.5",.5",2"; frame size (115 x 120mm)
A1284	F5	Bulged, split (no dmpls/holes)	0.194	0.257	32.4			Si=1",.5",.5",2"; small frame (90 x 95 mm)
A1291	C4	5 perforations, Dmax=1.5 mm	0.194	0.314		181.6	894	Witness: craters & Al powder
A1312	F4/C4	bulge, 1 hole (1 mm) & dimples	0.205	0.314		220.8	1076	Witness: no craters, soot
A1313	C4	1 tiny pinhole (~.2mm) & 7 dimples	0.220	0.314		258.0	1282	Witness: no damage
A1314	F3/C2	Bulged, 2 dimples	0.219	0.314		275.6	1333	
A1315	F3/C2	Bulged, 11 small dimples	0.237	0.314		339.8	1655	
A1316	F3/C2	Bulged, 10 dimples (2 lrg)	0.281	0.314		498.0	2553	
A1317	F3/C2	s. bulge, 12 dimples (2 large)	0.194	0.314		147.0	788	

MS_EXCEL DATA

Eric L. Christiansen
NASA/Johnson Space Center
Mail Code SN3
Translated from Lotus by L.Thompson (714)896-4495

Multi-Shock Shield Database

Nextel Bumpers, Aluminum Rear Wall

	Projectile Parameters								Bumper				Back Wall			
Shot No.	Site	Mat'l	Dia. (cm)	Dens. (g/cc)	Mass (g)	Vel. (km/sec)	Obliquity (deg)	Vn (km/sec)	Mat'l	Number Sheets	Areal D. (g/cm^2)	Overall Spacing (cm)	Mat'l	Thk (cm)	Areal D. (g/cm^2)	Yield Stress (ksi)
A1318	JSC	Al2017T4	0.2806	2.796	0.0324	5.5	45	3.89	Nextel AF26	4	0.172	10.16	Al2024T3	0.051	0.142	47
A1319	JSC	Al2017T4	0.2992	2.796	0.0392	5.36	45	3.79	Nextel AF26	4	0.172	10.16	Al2024T3	0.051	0.142	47
A1320	JSC	Al2017T4	0.2595	2.796	0.0256	4.52	45	3.20	Nextel AF26	4	0.172	10.16	Al2024T3	0.051	0.142	47
A1322	JSC	Al2017T4	0.238	2.796	0.0198	4.53	45	3.20	Nextel AF26	4	0.172	10.16	Al2024T3	0.051	0.142	47
A1325	JSC	Al2017T4	0.2200	2.796	0.0156	4.7	45	3.32	Nextel AF26	4	0.172	10.16	Al2024T3	0.051	0.142	47
A1327	JSC	Al2017T4	0.3176	2.796	0.0469	4.00	0	4.00	Nextel AF26	4	0.344	20.32	Al2024T3	0.102	0.284	47
A1328	JSC	Al2017T4	0.3174	2.796	0.0468	2.91	0	2.91	Nextel AF26	4	0.344	20.32	Al2024T3	0.102	0.284	47
A1329	JSC	Al2017T4	0.3174	2.796	0.0468	4.82	45	3.41	Nextel AF26	4	0.344	20.32	Al2024T3	0.102	0.284	47
A1330	JSC	Al2017T4	0.3175	2.796	0.0468	3.62	45	2.56	Nextel AF26	4	0.344	20.32	Al2024T3	0.102	0.284	47
A1335	JSC	Al2017T4	0.3174	2.796	0.0468	5.57	60	2.79	Nextel AF26	4	0.172	10.16	Al2024T3	0.051	0.142	47
A1336	JSC	Al2017T4	0.2994	2.796	0.0393	6.27	60	3.14	Nextel AF26	4	0.172	10.16	Al2024T3	0.051	0.142	47
A1337	JSC	Al2017T4	0.2806	2.796	0.0323	5.46	60	2.73	Nextel AF26	4	0.172	10.16	Al2024T3	0.051	0.142	47
A1338	JSC	Al2017T4	0.2601	2.796	0.0258	5.49	60	2.75	Nextel AF26	4	0.172	10.16	Al2024T3	0.051	0.142	47
A1339	JSC	Al2017T4	0.3172	2.796	0.0467	4.75	60	2.38	Nextel AF26	4	0.172	10.16	Al2024T3	0.051	0.142	47
A1340	JSC	Al2017T4	0.3583	2.796	0.0674	6.24	60	3.12	Nextel AF26	4	0.172	10.16	Al2024T3	0.051	0.142	47
A1341	JSC	Al2017T4	0.3585	2.796	0.0675	6.13	0	6.13	Nextel AF26	4	0.172	10.16	Al2024T3	0.051	0.142	47
A1361	JSC	Al2017T4	0.3572	2.796	0.0667	6.09	75	1.58	Nextel AF26	4	0.172	10.16	Al2024T3	0.030	0.085	47
B39	JSC	Al2017T4	0.6265	2.796	0.3600	6.92	0	6.92	Nextel AF26	4	0.344	20.32	Al2024T3	0.081	0.227	47
B70	JSC	Al2017T4	0.6265	2.796	0.3600	7.07	0	7.07	Nextel AF26	4	0.344	20.32	Al2024T3	0.102	0.284	47
B75	JSC	Al2017T4	0.6343	2.796	0.3736	7.48	0	7.48	Nextel AF26	4	0.344	10.16	Al2024T3	0.254	0.710	47
B79	JSC	Al2017T4	0.6350	2.796	0.3748	7.76	0	7.76	Nextel AF26	4	0.43	10.16	Al2024T3	0.180	0.504	47
B80	JSC	Al2017T4	0.6340	2.796	0.3731	7.41	0	7.41	Nextel AF26	4	0.43	10.16	Al2024T3	0.180	0.504	47
B82	JSC	Al2017T4	0.6340	2.796	0.3730	7.51	0	7.51	AF26,BF54	3	0.302	10.16	Al2024T3	0.180	0.504	47
B83	JSC	Al2017T4	0.6340	2.796	0.3730	7.48	0	7.48	AF62,BF54	3	0.416	10.16	Al2024T3	0.180	0.504	47
B84	JSC	Al2017T4	0.6350	2.796	0.3748	7.29	0	7.29	AF62,26+BF54	3	0.459	10.16	Al2024T3	0.180	0.504	47
B85	JSC	Al2017T4	0.6340	2.796	0.3730	7.39	0	7.39	AF62,26+BF54	3	0.459	10.16	Al2024T3	0.180	0.504	47
B86	JSC	Al2017T4	0.6344	2.796	0.3738	7.34	0	7.34	62,26+62,2-62+	3	0.486	10.16	Al2024T3	0.180	0.504	47
B87	JSC	Al2017T4	0.6342	2.796	0.3734	7.51	0	7.51	AF26:2,3,3,3	4	0.473	10.16	Al2024T3	0.180	0.504	47
B88	JSC	Al2017T4	0.6342	2.796	0.3734	7.06	0	7.06	:2,2,2,4(2/Balli	4	0.447	10.16	Al2024T3	0.180	0.504	47
B89	JSC	Al2017T4	0.6350	2.796	0.3748	7.22	0	7.22	AF26:2,2,2,2	4	0.344	10.16	Al2024T3	0.254	0.710	47
B95	JSC	Al2017T4	0.6350	2.796	0.3748	7.36	0	7.36	\F62(2),AF26(5	2	0.415	10.16	Al2024T3	0.229	0.639	47
1512	JSC	Al2017T4	0.1599	2.796	0.00598	3.26	0	3.26	Nextel AF26	4	0.172	10.16	Al2024T3	0.051	0.142	47
1513	JSC	Al2017T4	0.1598	2.796	0.00597	4.33	0	4.33	Nextel AF26	4	0.172	10.16	Al2024T3	0.051	0.142	47
1523	JSC	Al2017T4	0.1253	2.796	0.00288	3.94	0	3.94	Nextel AF26	4	0.172	10.16	Al2024T3	0.051	0.142	47

MS_EXCEL DATA

Eric L. Christians
NASA/Johnson S
Mail Code SN3
Translated from

Vn>6km/sec: K=mw*S^2*(Y/40)^0.5/(M*Vn) [sec/km] {K=43.1 for Nextel bumpers w/ Al rear wall}
Vn<6 km/sec: K2=mw*S*(Y/40)^0.5*Vn/M [km/sec-cm]
K3=mw*{S^2*[(Vn/3-1)+((2-Vn/(3*S^2))]}*(Y/40)^0.5/M [km/sec-cm]

Shot No.	Damage Class	Damage Description	Ratio AD Bumper to Proj.	Total Areal D. (g/cm^2)	K >6km/s	K2 <6km/s	K3 <6km/s	Comments
A1318	C2	14 dimples (2 large)	0.219	0.314		188.1	1065	
A1319	C4	2 Perls (max=1 mm) 12 dimples	0.206	0.314		151.2	867	Witness: no damage
A1320	C4	7 Perls (max=2x1.5 mm) 15 dmpl	0.237	0.314		195.5	1219	Witness: craters
A1322	C4	1 Perls (2x1.5 mm) 13 dmpl	0.258	0.314		253.5	1578	Witness: craters & dimples
A1325	C2	15 dimples (3 large)	0.280	0.314		333.7	2039	
A1327	C2	No perforation, craters & dmpl	0.387	0.628		533.9	6150	
A1328	C5	3 perls, Max 3 mm	0.388	0.628		389.1	5222	Witness: 1 hole (1 mm), cr.
A1329	C1	No perforation, s. cratering	0.388	0.628		455.4	5648	
A1330	C2	No perforation, craters & dmpl	0.388	0.628		341.9	4917	
A1335	C1/F1	No perls, s.craters only	0.194	0.314		93.0	623	
A1336	C1/F1	No perls, no cratering	0.205	0.314		124.8	786	4th Nextel was perforated
A1337	C2	No perls, craters & 2 dmpls	0.219	0.314		132.1	895	
A1338	C2	No perls, craters & 1 dmpl	0.237	0.314		166.8	1126	
A1339	C2	No perls, craters & 5 dmpls	0.194	0.314		79.5	583	
A1340	C2	No perls, craters & 5 dmpls	0.172	0.314		72.5	457	
A1341	F5	Large petalled perf (25mm)	0.172	0.314	38.4			Wit: perf (3x2mm); some secondaries
A1361	C0	No perf, No damage	0.172	0.257		22.2	211	No perf of 4th Nextel
B39	F4	Bulge, 2 small perf(1.5mm max)	0.196	0.571	40.8			Many secondarys (Redo)
B70	F3	Deep bulge (~8mm)	0.196	0.628	50.0			Center of wall bulge has dmpl
B75	F5	Pet Perf (12x15mm),s.cratering	0.194	1.054	28.4			Si=1.5",.75",.75",1";Wit:dmpl, molten splash
B79	D5	Perf (~12 mm)	0.242	0.934	19.4			1/4Sabot (Redo), AF26:3,2,2,3;.04"Wit:8mm perls
B80	F5	Pet Perf (~30mm), 70mm cracks	0.243	0.934	20.4			AF26:3,2,1,4; .04"Wit:splash (no perf)
B82	F5	Petalled Perf (~50mm)	0.170	0.806	20.1			AF26,AF26,2*BF54; Wit:2 perls (3/4" max)
B83	F5	Petalled Perf (~40mm)	0.235	0.920	20.2			AF62,AF62,2*BF54; Wit:no perf, dimples
B84	F5	Petalled Perf (~25mm)	0.259	0.963	20.6			AF62,AF62,AF26+2*BF54; Wit:no perf; Si=1.5",1.5",
B85	F5	Petalled Perf (~25mm)	0.259	0.963	20.5			AF62,AF62,AF26+2*BF54; Wit:no perf; Si=1.3",1.3"
B86	F5	Petalled Perf (~20x30mm), particulates	0.274	0.990	20.6			Wit: s.bulge, no perf; AF62,AF26+AF62,AF26+2*AF(
B87	F5	Petalled Perf (~35x45mm), impulsive	0.267	0.977	20.1			Wit: no perf, no dmpls; Si=1",1",1",1"
B88	F5	Petalled Perf (~50x20mm), particulates	0.252	0.951	21.4			Wit: no perf, 5 s.dmpls; (2)AF26, (2)AF26, (2)AF2
B89	F5	Petalled Perf (~15x19mm), particulates/holes in petals	0.194	1.054	29.4			Wit: no perf, many dmpls; Si=1",1",1",1"
B95	F4	Bulge, 1 s. perf (1.6 mm)	0.234	1.054	25.9			Wit: no perf; Si=2",2"
1512	C4	3 Perls (max=1.2 mm), dimples	0.385	0.314		852.8	5261	Witness: craters & dimples
1513	C2	No perforation, dimples	0.385	0.314		1134.6	6126	
1523	C2	No perf., dimples (1 Large)	0.491	0.314		2140.0	12053	

MS_EXCEL DATA

Eric L. Christiansen
NASA/Johnson Space Center
Mail Code SN3
Translated from Lotus by L.Thompson (714)896-4495

Multi-Shock Shield Database

Nextel Bumpers, Aluminum Rear Wall

	Projectile Parameters								Bumper				Back Wall			
Shot No.	Site	Mat'l	Dia. (cm)	Dens. (g/cc)	Mass (g)	Vel. (km/sec)	Obliquity (deg)	Vn (km/sec)	Mat'l	Number Sheets	Areal D. (g/cm^2)	Overall Spacing (cm)	Mat'l	Thk (cm)	Areal D. (g/cm^2)	Yield Stress (ksi)
1525	JSC	Al2017T4	0.1488	2.796	0.00482	3.89	0	3.89	Nextel AF26	4	0.172	10.16	Al2024T3	0.051	0.142	47
1526	JSC	Al2017T4	0.1598	2.796	0.00597	3.32	45	2.35	Nextel AF26	4	0.172	10.16	Al2024T3	0.051	0.142	47
1528	JSC	Al2017T4	0.1599	2.796	0.00598	4.57	45	3.23	Nextel AF26	4	0.172	10.16	Al2024T3	0.051	0.142	47
1540	JSC	Al2017T4	0.1595	2.796	0.00594	3.57	30	3.09	Nextel AF26	4	0.172	10.16	Al2024T3	0.051	0.142	47
1550	JSC	Al2017T4	0.1600	2.796	0.00600	4.24	30	3.67	Nextel AF26	4	0.172	10.16	Al2024T3	0.051	0.142	47
1585	JSC	Al2017T4	0.1596	2.796	0.00595	3.57	60	1.79	Nextel AF26	4	0.172	10.16	Al2024T3	0.051	0.142	47
1586	JSC	Al2017T4	0.1598	2.796	0.00597	4.81	60	2.41	Nextel AF26	4	0.172	10.16	Al2024T3	0.051	0.142	47
1587	JSC	Al2017T4	0.1596	2.796	0.00595	3.79	0	3.79	Nextel AF26	4	0.344	10.16	Al2024T3	0.102	0.284	47
1588	JSC	Al2017T4	0.1252	2.796	0.00287	3.77	0	3.77	Nextel AF26	4	0.172	10.16	Al2024T3	0.051	0.142	47
1589	JSC	Al2017T4	0.1597	2.796	0.00596	3.45	0	3.45	Nextel AF26	4	0.172	10.16	Al2024T3	0.051	0.142	47
1590	JSC	Al2017T4	0.1256	2.796	0.00290	4.04	0	4.04	Nextel AF26	4	0.172	10.16	Al2024T3	0.051	0.142	47
1591	JSC	Al2017T4	0.1154	2.796	0.00225	4.14	0	4.14	Nextel AF26	4	0.172	10.16	Al2024T3	0.051	0.142	47
1594	JSC	Al2017T4	0.1156	2.796	0.00226	2.85	0	2.85	Nextel AF26	4	0.172	10.16	Al2024T3	0.051	0.142	47
1595	JSC	Al2017T4	0.1154	2.796	0.00225	4.1	0	4.10	Nextel AF26	4	0.172	10.16	Al2024T3	0.051	0.142	47
1597	JSC	Al2017T4	0.1157	2.796	0.00227	3.44	0	3.44	Nextel AF26	4	0.172	10.16	Al2024T3	0.051	0.142	47
1598	JSC	Al2017T4	0.1001	2.796	0.00147	4.27	0	4.27	Nextel AF26	4	0.172	10.16	Al2024T3	0.051	0.142	47
1603	JSC	Al2017T4	0.1001	2.796	0.00147	3.79	0	3.79	Nextel AF26	4	0.172	10.16	Al2024T3	0.051	0.142	47
1604	JSC	Al2017T4	0.0997	2.796	0.00145	3.62	0	3.62	Nextel AF26	4	0.172	10.16	Al2024T3	0.051	0.142	47
1625	JSC	Al2017T4	0.1006	2.796	0.00149	3.39	0	3.39	Nextel AF26	4	0.172	10.16	Al2024T3	0.051	0.142	47
1628	JSC	Al2017T4	0.1004	2.796	0.00148	2.47	0	2.47	Nextel AF26	4	0.172	10.16	Al2024T3	0.051	0.142	47
1632	JSC	Al2017T4	0.0794	2.796	0.00073	3.08	0	3.08	Nextel AF26	4	0.172	10.16	Al2024T3	0.051	0.142	47
1635	JSC	Al2017T4	0.0804	2.796	0.00076	2.68	0	2.68	Nextel AF26	4	0.172	10.16	Al2024T3	0.051	0.142	47
1636	JSC	Nylon	0.2373	1.14	0.00798	3.2	0	3.20	Nextel AF26	4	0.172	10.16	Al2024T3	0.051	0.142	47
1637	JSC	Nylon	0.2387	1.14	0.00812	3.16	0	3.16	Nextel AF26	4	0.172	10.16	Al2024T3	0.051	0.142	47
1638	JSC	Nylon	0.2399	1.14	0.00824	3.15	0	3.15	Nextel AF26	4	0.172	10.16	Al2024T3	0.051	0.142	47
1639	JSC	Nylon	0.2361	1.14	0.00786	3.78	0	3.78	Nextel AF26	4	0.172	10.16	Al2024T3	0.051	0.142	47
1640	JSC	Al2017T4	0.1596	2.796	0.00595	2.97	30	2.57	Nextel AF26	4	0.172	10.16	Al2024T3	0.051	0.142	47
1641	JSC	Al2017T4	0.1485	2.796	0.00479	2.90	30	2.51	Nextel AF26	4	0.172	10.16	Al2024T3	0.051	0.142	47
1642	JSC	Al2017T4	0.1489	2.796	0.00483	3.01	30	2.61	Nextel AF26	4	0.172	10.16	Al2024T3	0.051	0.142	47
1643	JSC	Al2017T4	0.1486	2.796	0.00480	3.36	45	2.38	Nextel AF26	4	0.172	10.16	Al2024T3	0.051	0.142	47
?	ARC	Al2017T4	0.9525	2.796	1.26512	6.5	0	6.50	Nextel AF26	4	0.516	30.48	Al2024T3	0.229	0.639	47
1150	UDRI	Al2017T4	0.9525	2.796	1.26512	6.77	0	6.77	Nextel AF26	4	0.516	30.48	Al6061T6	0.229	0.620	36
1151	UDRI	Al2017T4	0.9525	2.796	1.26512	6.78	0	6.78	Nextel AF62	5	0.500	38.1	Al6061T6	0.229	0.620	36
1152	UDRI	Al2017T4	0.9525	2.796	1.26512	6.78	0	6.78	Nextel BF54	4	0.434	30.48	Al6061T6	0.229	0.620	36

MS_EXCEL DATA

Eric L. Christians
NASA/Johnson S
Mail Code SN3
Translated from

Vn>6km/sec: K=mw*S^2*(Y/40)^0.5/(M*Vn) [sec/km] (K=43.1 for Nextel bumpers w/ Al rear wall)
Vn<6 km/sec: K2=mw*S*(Y/40)^0.5*Vn/M [km/sec-cm]
K3=mw*[S^2*[(Vn/3-1)+((2-Vn/(3*S^2))]*(Y/40)^0.5/M [km/sec-cm]

Shot No.	Damage Class	Damage Description	Ratio AD Bumper to Proj.	Total Areal D. (g/cm^2)	K >6km/s	K2 <6km/s	K3 <6km/s	Comments
1525	C2	No perf., dimples	0.414	0.314		1262.5	7152	
1526	C4	1 Perf (1.5x1 mm)	0.385	0.314		615.1	4540	Witness: dimple
1528	C2	No perf., dimples (2 large)	0.385	0.314		845.3	5239	
1540	C4	1 Perf (1.8x1.5mm), dimples	0.386	0.314		814.2	5162	Witness: 1.5x.7 mm hole
1550	C2	No perf., dimples (1 large)	0.384	0.314		957.3	5572	
1585	C1	No perf., v.slight cratering	0.385	0.314		469.3	4104	Barely perforated 4th Nextel
1586	C1	No perf., no craters, clean	0.385	0.314		630.2	4586	Barely perforated 3rd Nextel
1587	C1	No perf., cratering	0.771	0.628		1992.8	11427	
1588	C4	2 Perfs (max=1.8 mm)	0.492	0.314		2054.8	11812	Witness: craters & 3 dimples
1589	C5	1 Perf (3 mm), 3 dimples	0.385	0.314		905.5	5431	Witness: 1 perf (2mm) & 10dmp
1590	C2	No perf., 1 dimple	0.490	0.314		2179.2	12134	
1591	C2	No perf., 5 dimples (3 lrg)	0.533	0.314		2878.3	15852	
1594	C5	1 Perf (3 mm)	0.532	0.314		1972.6	13055	Witness: 7 dimples (1 lrg)
1595	C1	No perf., v.slight cratering	0.533	0.314		2850.5	15767	
1597	C4	1 perf (1.3x1 mm), dimples	0.531	0.314		2370.5	14239	Witness: craters, 3 small dmp
1598	C1	No perf., v.slight cratering	0.614	0.314		4543.9	24685	Barely perforated 4th Nextel
1603	C1	No perf., 3 dimples (1 lrg)	0.614	0.314		4033.1	23126	
1604	C1	No perf., 1 small dimple	0.617	0.314		3905.3	22885	
1625	C2	No perf., 2 small dimples	0.612	0.314		3559.0	21533	
1628	C4	1 Perf (~1.2 mm circ)	0.613	0.314		2610.7	18710	Wit: no perf, dmpls & melt
1632	C1	No perf	0.775	0.314		6580.8	41801	Secondary impact (half sabot)
1635	C2/D2	No perf, 1 impact: dimple	0.765	0.314		5516.1	37754	
1636	A2	No perf, 1 large dmpl (D=3mm)	0.636	0.314		627.3	3907	Slug DxL:.0798"x.0854"; est Vel
1637	C2	No perf, surface marks, s.dmpl	0.632	0.314		608.8	3816	Nylon Slug: D=.0798",L=.0869"
1638	C1	No perf, surface marks	0.629	0.314		598.0	3755	Nylon Slug: D=.0798",L=.0882"
1639	C1	No perf, no damage	0.639	0.314		752.3	4319	DxL:.0798"x.0882";4thNex no-perf
1640	C5/A3	1 perf (2.4 x 1.6 mm), dmpls	0.385	0.314		676.2	4736	Wit: perf (1.6x1.2 mm), dmpls
1641	C4/A3	1 perf (2 mm), dmpls	0.414	0.314		820.2	5822	Wit: no perf, dmpls
1642	C5/A3	1 perf (2.4x2 mm), dmpls	0.413	0.314		844.2	5868	Wit: pinhole (~0.4 mm), dmpls
1643	C4/A3	1 perf (2x1.1 mm), 2dmpls	0.414	0.314		774.3	5675	Wit: pinhole (~0.4 mm), dmpls
?	F3	No perf., bulge, molten splash	0.194	1.155	78.3			Chk Shot No., Vel.,M
1150	F3	No perf., bulge, molten splash	0.194	1.136	63.8			Chk Proj Mass
1151	F3	No perf., bulge, molten splash	0.188	1.120	99.6			Chk Proj Mass
1152	F3	No perf., bulge, molten splash	0.163	1.054	63.7			Chk Proj Mass

MS_EXCEL DATA

Eric L. Christiansen
NASA/Johnson Space Center
Mail Code SN3
Translated from Lotus by L.Thompson (714)896-4495

Multi-Shock Shield Database

Nextel Bumpers, Aluminum Rear Wall

	Projectile Parameters								Bumper				Back Wall			
Shot No.	Site	Mat'l	Dia. (cm)	Dens. (g/cc)	Mass (g)	Vel. (km/sec)	Obliquity (deg)	Vn (km/sec)	Mat'l	Number Sheets	Areal D. (g/cm^2)	Overall Spacing (cm)	Mat'l	Thk (cm)	Areal D. (g/cm^2)	Yield Stress (ksi)
1153	UDRI	Al2017T4	0.9525	2.796	1.26512	6.75	0	6.75	AF62 & BF54	4	0.417	30.48	Al6061T6	0.203	0.551	36
1154	UDRI	Al2017T4	0.9525	2.796	1.26512	6.94	0	6.94	AF62 & BF54	4	0.417	30.48	Al6061T6	0.203	0.551	36
1170	UDRI	Al2017T4	0.9525	2.796	1.26512	6.72	0	6.72	Nextel AF40	4	0.342	30.48	Al6061T6	0.203	0.551	36
1173	UDRI	Al2017T4	0.9525	2.796	1.26512	6.67	0	6.67	Nextel AF62	4	0.400	22.86	Al6061T6	0.203	0.551	36
1174	UDRI	Al2017T4	0.9525	2.796	1.26512	6.57	0	6.57	Nextel AF40	5	0.427	38.1	Al6061T6	0.203	0.551	36
1250	UDRI	Al2017T4	0.9549	2.796	1.27480	6.73	0	6.73	Nextel BF54	4	0.434	30.48	Al6061T6	0.203	0.551	36
1251	UDRI	Al2017T4	0.9549	2.796	1.27490	6.80	0	6.80	Nextel AF40	5	0.427	30.48	Al6061T6	0.203	0.551	36
1253	UDRI	Al2017T4	0.9550	2.796	1.27500	6.76	0	6.76	(3) AF26	4	0.516	30.48	Al6061T6	0.160	0.434	36
1293	UDRI	Al2017T4	0.9550	2.796	1.27500	6.67	0	6.67	AF62	4	0.400	30.48	Al6061T6	0.229	0.620	36

MS_EXCEL DATA

Eric L. Christians
NASA/Johnson S
Mail Code SN3
Translated from

Vn>6km/sec: K=mw*S^2*(Y/40)^0.5/(M*Vn) [sec/km] {K=43.1 for Nextel bumpers w/ Al rear wall}
Vn<6 km/sec: K2=mw*S*(Y/40)^0.5*Vn/M [km/sec-cm]
K3=mw*[S^2*|(Vn/3-1)+((2-Vn/(3*S^2))]*(Y/40)^0.5/M [km/sec-cm]

Shot No.	Damage Class	Damage Description	Ratio AD Bumper to Proj.	Total Areal D. (g/cm^2)	K >6km/s	K2 <6km/s	K3 <6km/s	Comments
1153	F4	Small perf. (trailing debris?)	0.157	0.968	56.9			2 AF62, 2 BF54 (Chk Mass)
1154	F4	Small perf. (trailing debris?)	0.157	0.968	55.3			2 AF54, 2 BF62 (Chk Mass)
1170	F5	Large petalled hole	0.128	0.893	57.2			Wit: molten splash (Chk M)
1173	F5	Large petalled hole	0.150	0.951	32.4			Wit: molten splash (Chk M)
1174	F4	Small perf. (trailing debris?)	0.160	0.978	91.3			(Chk M, S)
1250	F4	Pin hole, 3/4" deep bulge	0.162	0.985	56.6			(Chk Wit.)
1251	F4	3 Cracks(L=3.5"-4"),deep bulge	0.160	0.978	56.0			Si=2",2",2",3",3" (Chk Wit)
1253	F4	3 Perfs (1.6-2.5 mm), d. bulge	0.193	0.950	44.4			Wit: s.hole
1293	F3	No perf. Bulge, molten splash	0.150	1.020	64.3			

Appendix D

MODELING THE RESPONSE OF A THIN SHEET DUE TO A HYPERVELOCITY DEBRIS CLOUD IMPACT

D. J. GROVE AND A. M. RAJENDRAN
UNIVERSITY OF DAYTON RESEARCH INSTITUTE
DAYTON, OHIO 45469-0120

A spacecraft can be protected from hypervelocity meteoroid impacts through the use of a thin sacrificial shield, or bumper. The presence of a bumper shield causes the meteoroid to vaporize and expand before it reaches the rear (inner) wall of the space structure. Spreading the meteoroid's momentum over a larger surface area helps prevent a catastrophic failure of the rear wall. Additional protection may be achieved by placing intermediate blankets, such as honeycomb, fiber composites, etc., between the bumper and rear wall. The loading conditions on the rear wall due to the impact of debris that passes through the intermediate layers are extremely complex and difficult to measure or calculate. However, a simplistic approach to the loading calculation using an impulse based model proposed earlier by Wilkinson [1] seems to yield encouraging solutions to this complex problem. Recently, Rajendran and Elfer [2] presented a comprehensive summary on "Debris-Impact Protection of Space Structures".

In modeling the deflection of the rear wall due to a debris cloud impact, Wilkinson chose an impulse-velocity-based approach, in which the cloud imparts a sudden velocity to the rear wall. Thus, only the rear wall is modeled, and no attempt is made to model the physical details of the debris cloud. Assuming a 1:1 momentum transfer, Wilkinson proposed the following expression for the initial velocity of the rear wall:

$$V_i(r) = \xi \exp\left(\frac{-r^2}{2\Delta^2}\right) \tag{1}$$

where

$$\xi = \frac{m_p V_p}{4 m_r S^2 \tan^2 \theta} \tag{2}$$

and

$$\Delta = \left(\frac{2}{\pi}\right)^{\frac{1}{2}} S \tan \theta \tag{3}$$

In the above expressions, m_p and V_p are the mass and velocity of the projectile, respectively. S is the inner spacing between the bumper and the rear wall, m_r is the mass per unit area of the rear wall, and r is the radial distance from the center of the circular portion on the rear wall through which the momentum of the debris cloud is transferred. In this model, the parameters m_p, V_p, S, and m_r are known based on the experimental configuration. The only parameter that has to be determined from the experiments is the debris cloud's spray angle $\bar{\theta}$. Wilkinson presented an empirical expression for tan $\bar{\theta}$ as

$$\tan \bar{\theta} = \begin{cases} \beta \left(\dfrac{m_b}{\rho_p d_p} \right)^{\frac{1}{2}} & \dfrac{m_b}{\rho_p d_p} < 1 \\ \beta & \dfrac{m_b}{\rho_p d_p} \geq 1 \end{cases} \qquad (4)$$

where m_b is the mass per unit area of the bumper sheet, ρ_p is the density of the projectile, d_p is the diameter of the projectile, and β is an empirical parameter. Based on various hypervelocity experiments with lead and cadmium and hydrodynamic computer code calculations of vaporized aluminum, Wilkinson suggested a value of 0.6 for β.

After incorporating Wilkinson's model into the 2D STEALTH [3] finite difference code, numerous simulations were performed to evaluate the model for various impact velocities, bumper thicknesses, spacings between the bumper and rear wall, and rear wall yield strengths. Table 1 lists the configurations for the STEALTH simulations; the last column in the table lists the computed values of maximum effective strain (ε_{eff}^{max}) in the rear wall. The projectile, bumper, and rear wall were assumed to consist of aluminum, so $\rho_p = \rho_b = \rho_r = 2785$ kg/m^3 in all the simulations. Other constant simulation parameters were the rear wall thickness ($t_r = 3.175 \times 10^{-3}$ m) and Wilkinson's model parameter ($\beta = 0.392$).

TABLE 1

STEALTH SIMULATION CASES

Case	m_p (kg)	d_p (m)	V_p (m/s)	m_pV_p (kg-m/s)	t_b (m)	Y_r (Pa)	S (m)	Computed ε_{eff}^{max} (%)
1	1.0×10^{-3}	7.7216×10^{-3}	6500	6.500	2.032×10^{-3}	4.0×10^{8}	109.093×10^{-3}	19.40
2	2.0232×10^{-3}	9.7282×10^{-3}	6360	12.870	3.175×10^{-3}	4.0×10^{8}	298.450×10^{-3}	0.42
3	1.0×10^{-3}	7.7216×10^{-3}	6986	6.986	2.032×10^{-3}	4.0×10^{8}	109.093×10^{-3}	21.75
4	1.0×10^{-3}	7.7216×10^{-3}	6170	6.170	2.032×10^{-3}	4.0×10^{8}	109.093×10^{-3}	17.90
5	1.0×10^{-3}	7.7216×10^{-3}	6170	6.170	1.600×10^{-3}	4.0×10^{8}	109.525×10^{-3}	26.20
6	1.0×10^{-3}	7.7216×10^{-3}	1625	1.625	2.032×10^{-3}	4.0×10^{8}	77.1404×10^{-3}	8.00
7	1.0×10^{-3}	7.7216×10^{-3}	3250	3.250	2.032×10^{-3}	4.0×10^{8}	109.093×10^{-3}	7.40
8	1.0×10^{-3}	7.7216×10^{-3}	6500	6.500	2.032×10^{-3}	4.0×10^{8}	154.281×10^{-3}	5.90
9	1.0×10^{-3}	7.7216×10^{-3}	2600	2.600	2.032×10^{-3}	4.0×10^{8}	77.1404×10^{-3}	15.50
10	1.0×10^{-3}	7.7216×10^{-3}	5200	5.200	2.032×10^{-3}	4.0×10^{8}	109.093×10^{-3}	13.70
11	1.0×10^{-3}	7.7216×10^{-3}	10400	10.400	2.032×10^{-3}	4.0×10^{8}	154.281×10^{-3}	12.45
12	1.0×10^{-3}	7.7216×10^{-3}	3250	3.250	2.032×10^{-3}	4.0×10^{8}	77.1404×10^{-3}	20.90
13	1.0×10^{-3}	7.7216×10^{-3}	13000	13.000	2.032×10^{-3}	4.0×10^{8}	154.281×10^{-3}	18.10

TABLE 1 (continued)

STEALTH SIMULATION CASES

Case	m_p (kg)	d_p (m)	V_p (m/s)	m_pV_p (kg-m/s)	t_b (m)	Y_r (Pa)	S (m)	Computed ε_{eff}^{max} (%)
14	$1.0x10^{-3}$	$7.7216x10^{-3}$	4110	4.110	$2.032x10^{-3}$	$4.0x10^{8}$	$77.1404x10^{-3}$	30.00
15	$1.0x10^{-3}$	$7.7216x10^{-3}$	8220	8.220	$2.032x10^{-3}$	$4.0x10^{8}$	$109.093x10^{-3}$	28.30
16	$1.0x10^{-3}$	$7.7216x10^{-3}$	16440	16.440	$2.032x10^{-3}$	$4.0x10^{8}$	$154.281x10^{-3}$	27.00
17	$1.0x10^{-3}$	$7.7216x10^{-3}$	4875	4.875	$2.032x10^{-3}$	$4.0x10^{8}$	$77.1404x10^{-3}$	38.40
18	$1.0x10^{-3}$	$7.7216x10^{-3}$	9750	9.750	$2.032x10^{-3}$	$4.0x10^{8}$	$109.093x10^{-3}$	36.00
19	$1.0x10^{-3}$	$7.7216x10^{-3}$	19500	19.500	$2.032x10^{-3}$	$4.0x10^{8}$	$154.281x10^{-3}$	34.50
20	$1.0x10^{-3}$	$7.7216x10^{-3}$	5500	5.500	$2.032x10^{-3}$	$4.0x10^{8}$	$77.1404x10^{-3}$	44.50
21	$1.0x10^{-3}$	$7.7216x10^{-3}$	11000	11.000	$2.032x10^{-3}$	$4.0x10^{8}$	$109.093x10^{-3}$	41.75
22	$1.0x10^{-3}$	$7.7216x10^{-3}$	22000	22.000	$2.032x10^{-3}$	$4.0x10^{8}$	$154.281x10^{-3}$	39.75
23	$1.0x10^{-3}$	$7.7216x10^{-3}$	6500	6.500	$2.032x10^{-3}$	$4.0x10^{8}$	$77.1404x10^{-3}$	51.00
24	$1.0x10^{-3}$	$7.7216x10^{-3}$	13000	13.000	$2.032x10^{-3}$	$4.0x10^{8}$	$109.093x10^{-3}$	46.70
25	$1.0x10^{-3}$	$7.7216x10^{-3}$	26000	26.000	$2.032x10^{-3}$	$4.0x10^{8}$	$154.281x10^{-3}$	43.50
26	$1.0x10^{-3}$	$7.7216x10^{-3}$	8250	8.250	$2.032x10^{-3}$	$4.0x10^{8}$	$77.1404x10^{-3}$	56.70

TABLE 1 (concluded)

STEALTH SIMULATION CASES

Case	m_p (kg)	d_p (m)	V_p (m/s)	m_pV_p (kg-m/s)	t_b (m)	Y_r (Pa)	S (m)	Computed ε_{eff}^{max} (%)
27	$1.0x10^{-3}$	$7.7216x10^{-3}$	3250	3.250	$2.032x10^{-3}$	$3.0x10^{8}$	$109.093x10^{-3}$	8.55
28	$1.0x10^{-3}$	$7.7216x10^{-3}$	6500	6.500	$2.032x10^{-3}$	$3.0x10^{8}$	$109.093x10^{-3}$	24.30
29	$1.0x10^{-3}$	$7.7216x10^{-3}$	9750	9.750	$2.032x10^{-3}$	$3.0x10^{8}$	$109.093x10^{-3}$	41.70
30	$1.0x10^{-3}$	$7.7216x10^{-3}$	13000	13.000	$2.032x10^{-3}$	$3.0x10^{8}$	$109.093x10^{-3}$	49.50
31	$1.0x10^{-3}$	$7.7216x10^{-3}$	3250	3.250	$2.032x10^{-3}$	$5.0x10^{8}$	$109.093x10^{-3}$	6.53
32	$1.0x10^{-3}$	$7.7216x10^{-3}$	6500	6.500	$2.032x10^{-3}$	$5.0x10^{8}$	$109.093x10^{-3}$	16.50
33	$1.0x10^{-3}$	$7.7216x10^{-3}$	9750	9.750	$2.032x10^{-3}$	$5.0x10^{8}$	$109.093x10^{-3}$	31.50
34	$1.0x10^{-3}$	$7.7216x10^{-3}$	13000	13.000	$2.032x10^{-3}$	$5.0x10^{8}$	$109.093x10^{-3}$	44.10
35	$1.0x10^{-3}$	$7.7216x10^{-3}$	3250	3.250	$2.032x10^{-3}$	$6.0x10^{8}$	$109.093x10^{-3}$	5.45
36	$1.0x10^{-3}$	$7.7216x10^{-3}$	6500	6.500	$2.032x10^{-3}$	$6.0x10^{8}$	$109.093x10^{-3}$	14.30
37	$1.0x10^{-3}$	$7.7216x10^{-3}$	9750	9.750	$2.032x10^{-3}$	$6.0x10^{8}$	$109.093x10^{-3}$	27.10
38	$1.0x10^{-3}$	$7.7216x10^{-3}$	13000	13.000	$2.032x10^{-3}$	$6.0x10^{8}$	$109.093x10^{-3}$	40.80
39	$1.0x10^{-3}$	$7.7216x10^{-3}$	6807	6.807	$2.032x10^{-3}$	$4.0x10^{8}$	$109.093x10^{-3}$	20.90

The first five simulation cases corresponded to actual experiments, as indicated by Table 2. In each of these experiments, the rear wall consisted of 2219-T87 aluminum, and several intermediate layers of Kevlar cloth were placed between the bumper and rear wall. From split Hopkinson bar experiments, a critical strain to failure of 0.2 was determined for the 2219-T87 aluminum. Based on this failure strain, Wilkinson's model parameter β was calibrated to match experiments 4-0502 (no failure) and 4-0510 (failure), which had identical configurations except for their impact velocities. Using Wilkinson's model, the response of the rear wall was simulated for each of the five experiments. Figure 1 shows the computed strain histories (at the center of the rear wall) from the five simulations. Comparing these results with the experimental observations (last column of Table 2) reveals that Wilkinson's model correctly predicted (at least qualitatively) the rear wall response in experiments 4-0506, 4-0528, and 4-0529.

More recently, we incorporated Wilkinson's model into the EPIC-2 [4] finite element code and used it to simulate an experiment for which the final deformation and the bulged shape of the rear wall were available. In this experiment, the impact velocity was 6.5 km/s, the aluminum ball projectile was 9.525 mm in diameter, the 6061-T6 aluminum bumper shield was 2.032 mm thick, the ductile 5456-H116 aluminum rear wall was 3.175 mm thick, and the inner spacing between the bumper and rear wall was about 109 mm. As in previous experiments, intermediate layers of Kevlar cloth were placed between the bumper and rear wall. We simulated this experimental configuration and compared the results with experimental measurements [5]. We chose a value of β that produced the correct final thickness at the center of the thin sheet (rear wall). The simulated thickness reduction elsewhere in the sheet compared well with the experimental results, as illustrated by Figure 2.

We performed additional calculations to determine the effects of varying the boundary conditions on the thin sheet. We simulated a free boundary, a fixed boundary, and a boundary that was fixed in the vertical (z) direction and free in the

TABLE 2

EXPERIMENTS

Simulation Case Number	Experiment Case Number	Experimentally Observed Rear Wall Response
1	4-0502	Bulged; no failure
2	4-0506	Insignificant bulge
3	4-0510	Tearing
4	4-0528	Bulged; no failure
5	4-0529	Tearing

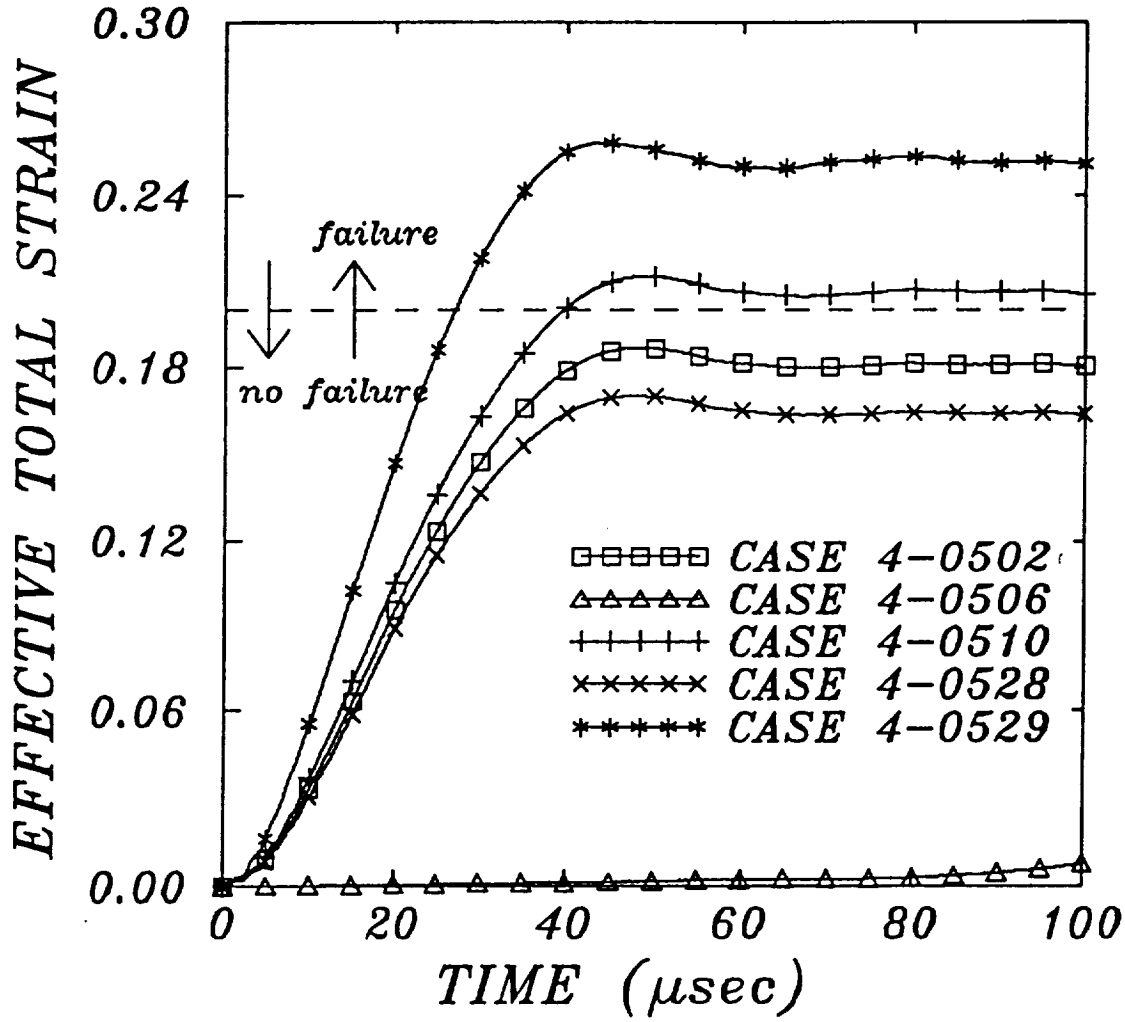

Figure 1. Calculated strain histories in rear wall

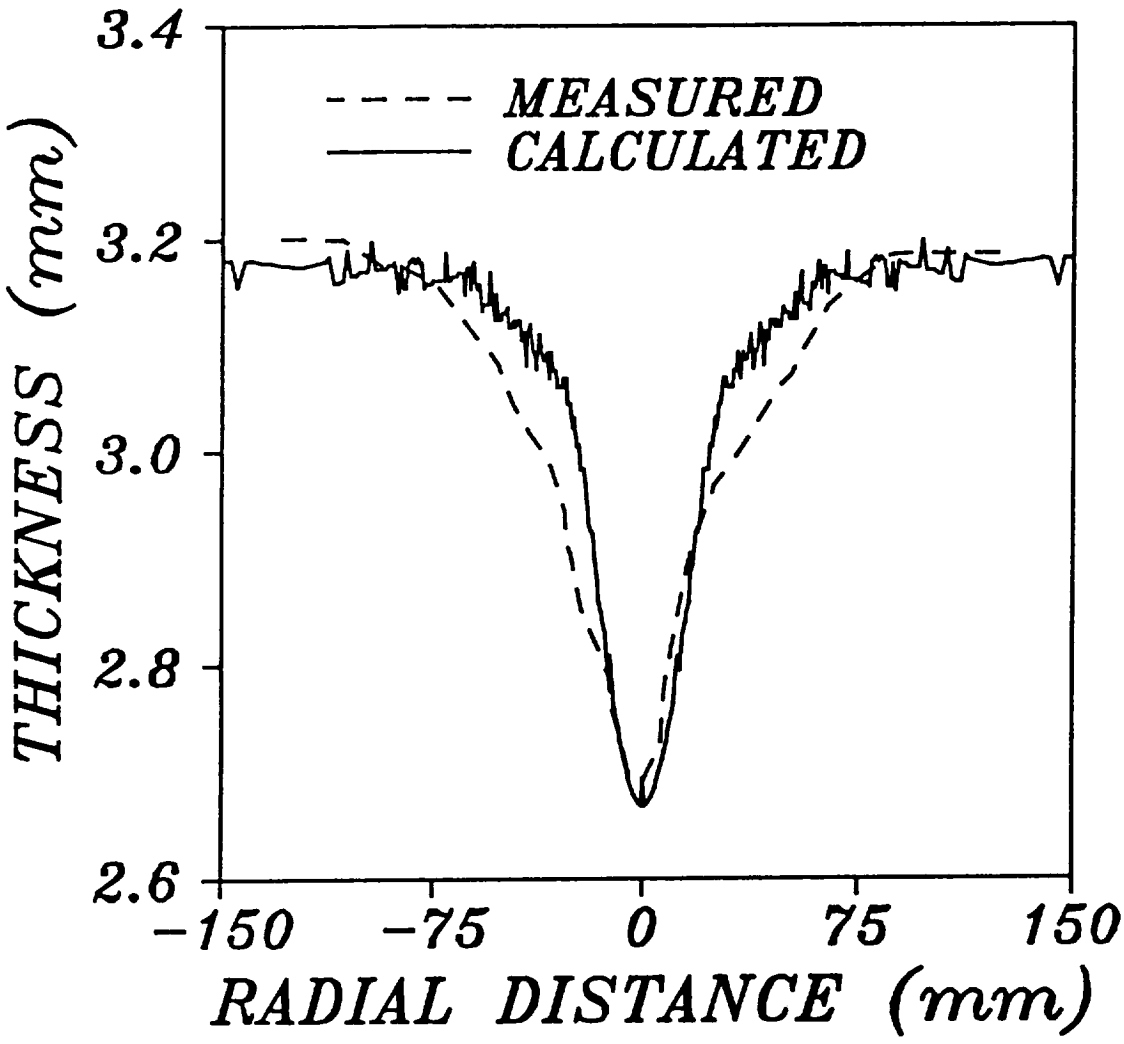

Figure 2. Comparison of final thickness profiles of rear wall

horizontal (r) direction. Since the simulations were all axisymmetric, the boundary conditions applied to the entire circumference of the circular thin sheet. In the actual experiment, the thin sheet was square and was held in place by a "picture frame" apparatus. The simulated shape of the rear wall deflection was sensitive to the boundary conditions imposed, and we were unable to achieve the amount of deflection measured by the experiment. However, the simulated thickness profile (see Figure 2) was independent of the boundary conditions.

Experimentally evaluating the effectiveness of various bumper shield configurations can be a time-consuming, expensive task. Since Wilkinson's model seems to generate a reasonable rear wall response, correlation of the above simulation results with some sort of design parameter may provide useful design criteria. Using ξ and Δ from Equations (2) and (3), we can define a dimensionless design parameter γ as follows:

$$\gamma = \frac{\xi^2 \rho_r e^{\left(\frac{t_r}{\Delta}\right)}}{Y_r} \tag{5}$$

where ρ_r, t_r, and Y_r are the density, thickness, and yield strength, respectively, of the rear wall. Using the results from the 39 STEALTH simulations, we plotted the maximum effective strains experienced by the rear wall (as predicted by the simulations, using Wilkinson's model) versus the corresponding γ values, as shown in Figure 3. There is definitely a correlation between γ and the maximum effective strain experienced by the rear wall. The "best fit" line shown in Figure 3 is a cubic polynomial, defined as follows:

$$\%\varepsilon_{eff}^{max} = 1.01152 + 18.2953\gamma - 2.35542\gamma^2 + 0.113756\gamma^3 \tag{6}$$

Alternatively, we can define γ as a function of ε_{eff}^{max}, so that a critical value of γ can

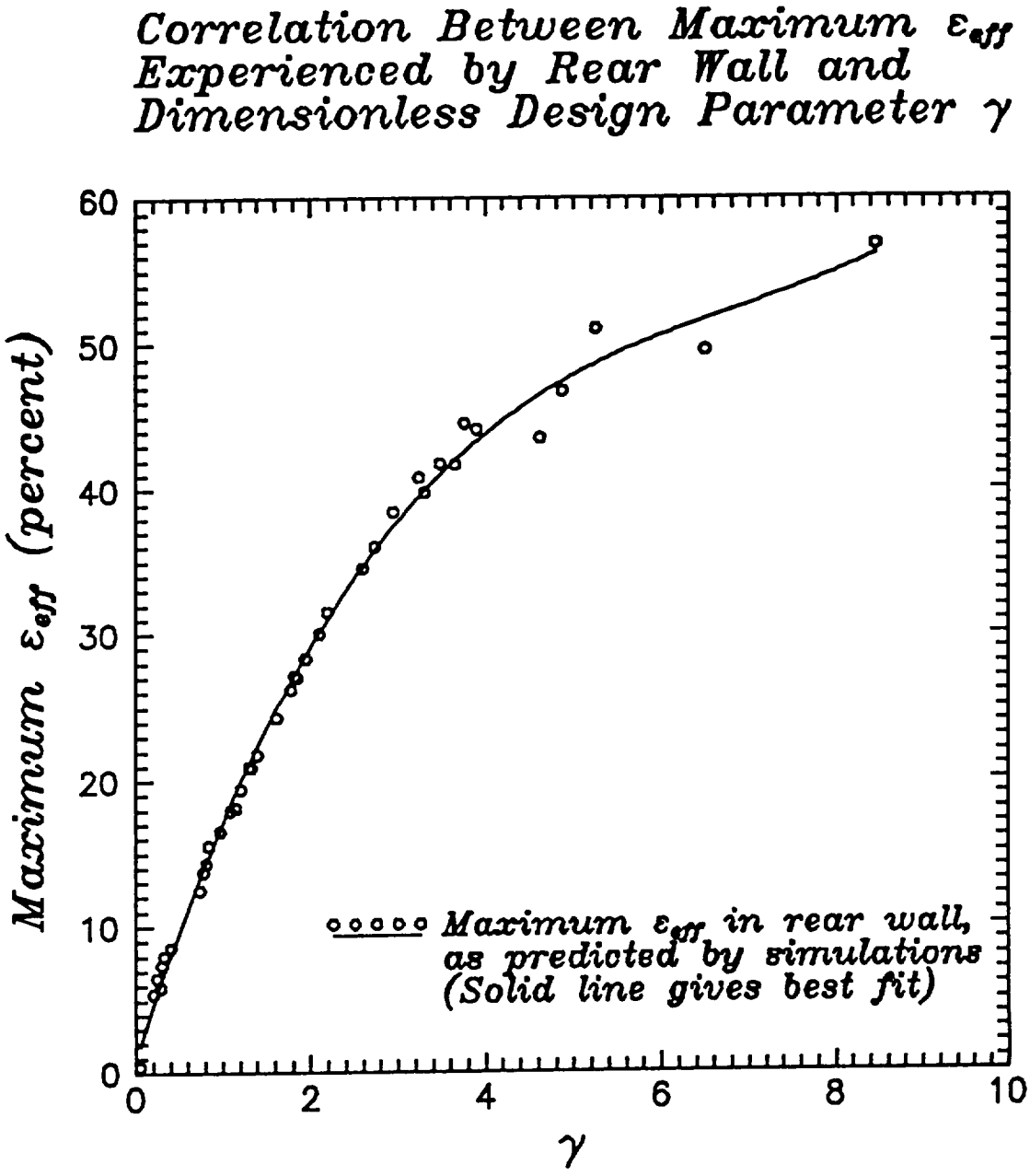

Figure 3. Correlation Between ε_{eff} in Rear Wall, as Predicted by Simulations, and Dimensionless Design Parameter γ.

be calculated from the critical ε_{eff} for rear wall failure. The resulting expression is a fourth degree polynomial:

$$\gamma = (-7.71338x10^{-3}) + (2.64191x10^{-2})(\%\varepsilon_{eff}^{max}) + (3.61467x10^{-3})(\%\varepsilon_{eff}^{max})^2 + (-1.24587x10^{-4})(\%\varepsilon_{eff}^{max})^3 + (1.74572x10^{-6})(\%\varepsilon_{eff}^{max})^4 \quad (7)$$

Knowing the critical ε_{eff} for rear wall failure, the bumper/rear wall geometry can then be designed so that γ is less than the critical value defined by Equation (7).

Using Equations (2)-(5) and (7), design curves were generated for various values of projectile momentum (M_p), rear wall thickness (t_r), rear wall strength (Y_r), and β. As in the simulations, the projectile, bumper, and rear wall materials were assumed to be aluminum. Each case considered four different levels of ε_{eff} for rear wall failure (0.10, 0.20, 0.30, and 0.40). For each rear wall failure strain, the inner spacing (S) between the bumper and rear wall was plotted as a function of the ratio of bumper thickness (t_b) to projectile diameter (d_p). Given β, t_r, Y_r, and anticipated values of M_p and d_p, these curves can be used to estimate the minimum S required for a given t_b (or the minimum t_b required for a given S). The various design curves are shown in Figures 4-84. Figure 4 provides the curves for the case when $\beta = 0.20$, $M_p = 6$ kg-m/s, $t_r = 1$ mm, and $Y_r = 0.20$ GPa. If the anticipated d_p is 2 mm and the desired t_b is 1 mm, then the S values corresponding to $t_b/d_p = 0.5$ reveal the critical inner spacings for the various rear wall failure strains. In this case ($t_b/d_p = 0.5$), for instance, the design curves predict that the rear wall will experience a maximum strain of 10% for an inner spacing of about 375 mm, and a maximum strain of 40% for an inner spacing of about 230 mm.

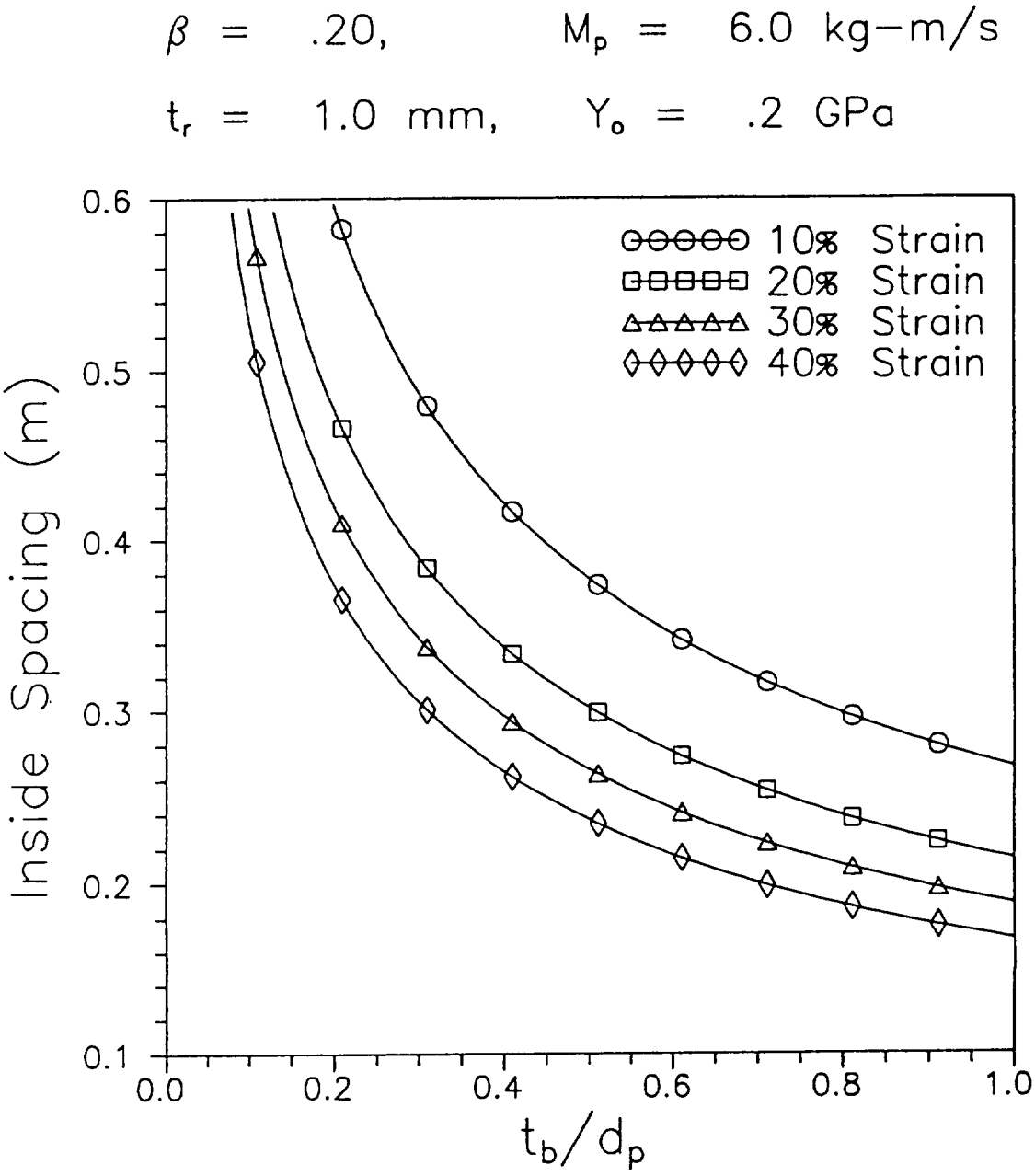

Figure 4. **Design Curves for $\beta = 0.2$, $M_p = 6$ kg-m/s, $t_r = 1$ mm, and $Y_r = 0.2$ GPa**

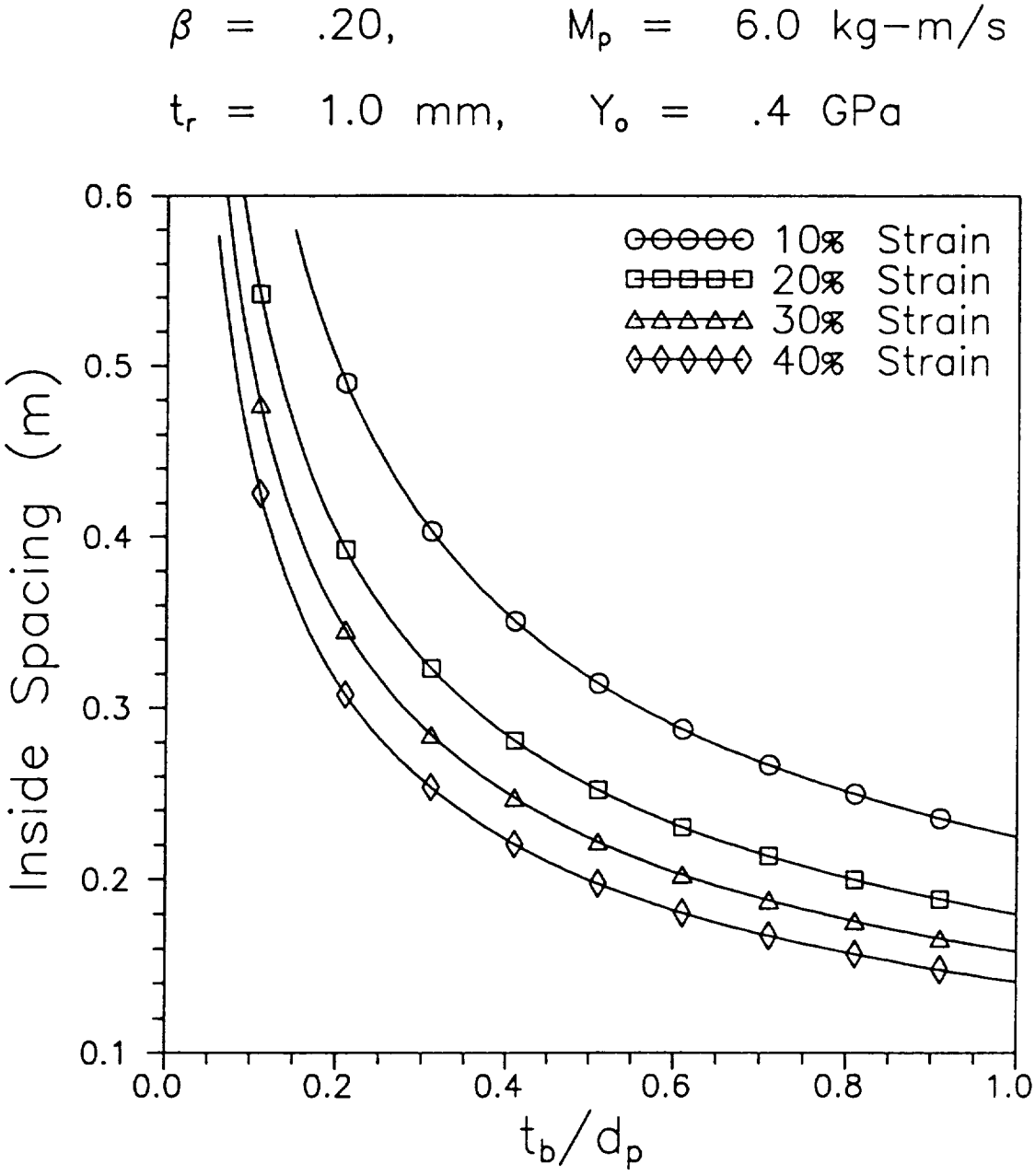

Figure 5. Design Curves for $\beta = 0.2$, $M_p = 6$ kg-m/s, $t_r = 1$ mm, and $Y_r = 0.4$ GPa

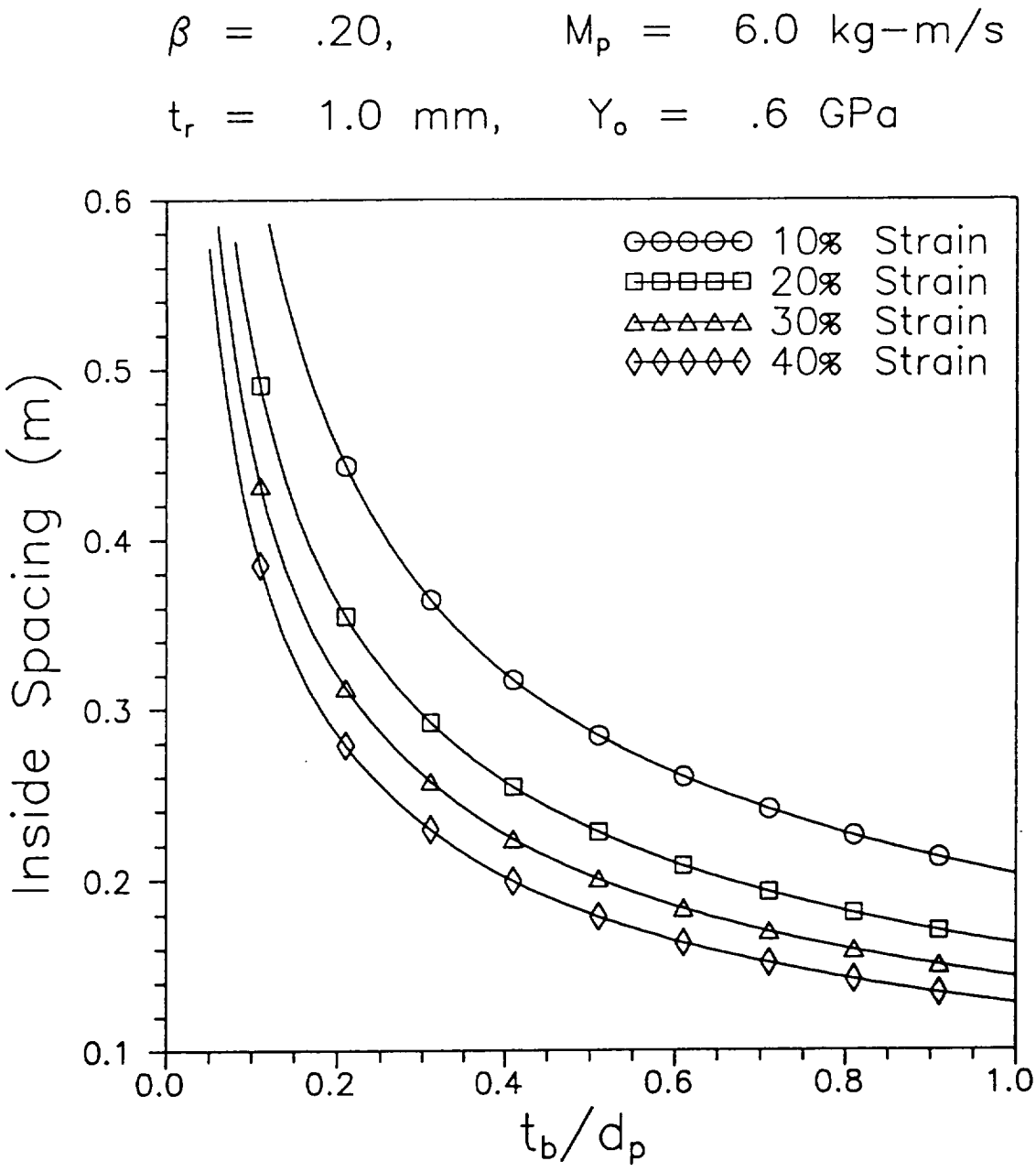

Figure 6. Design Curves for $\beta = 0.2$, $M_p = 6$ kg-m/s, $t_r = 1$ mm, and $Y_r = 0.6$ GPa

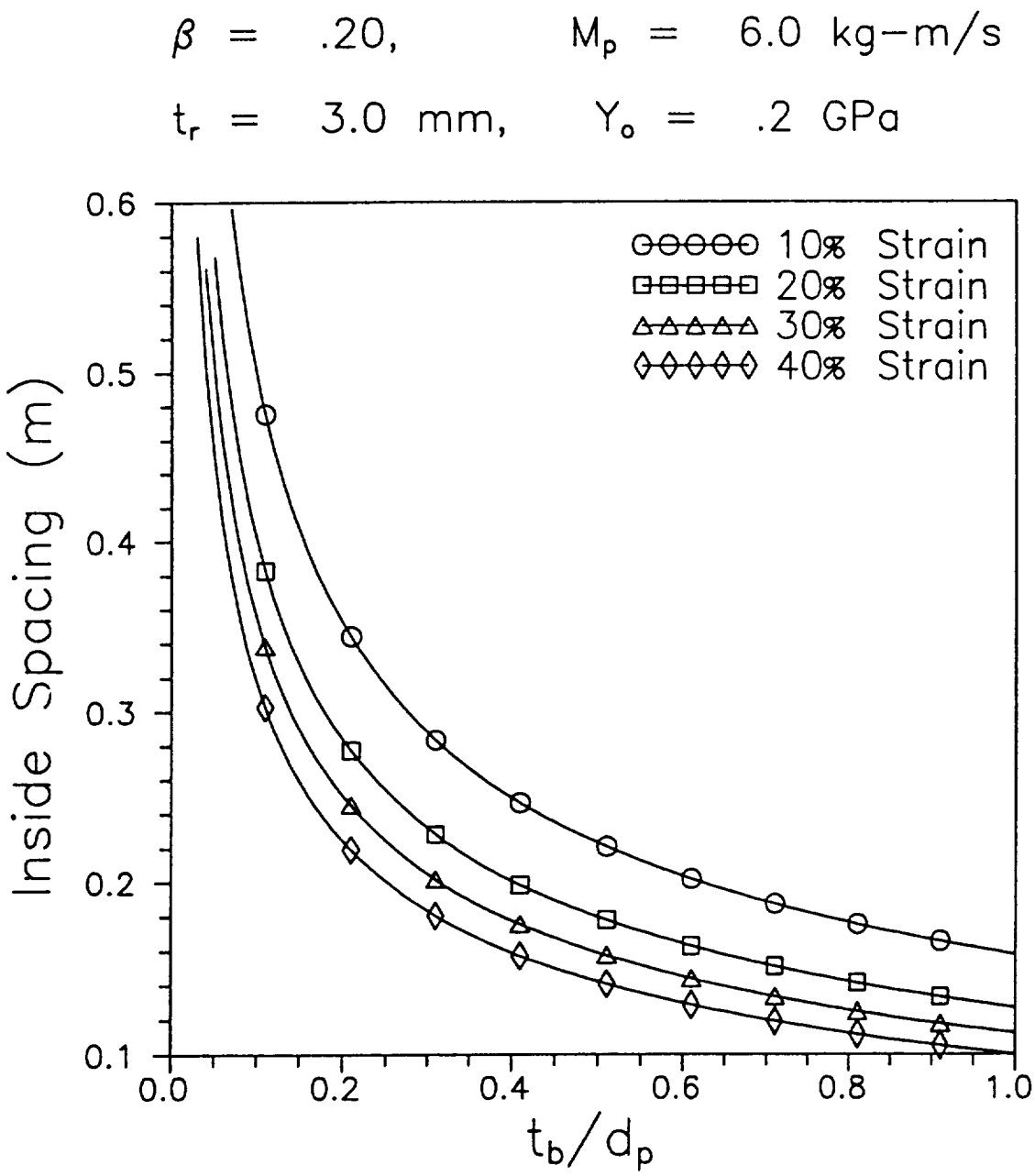

Figure 7. **Design Curves for $\beta = 0.2$, $M_p = 6$ kg-m/s, $t_r = 3$ mm, and $Y_r = 0.2$ GPa**

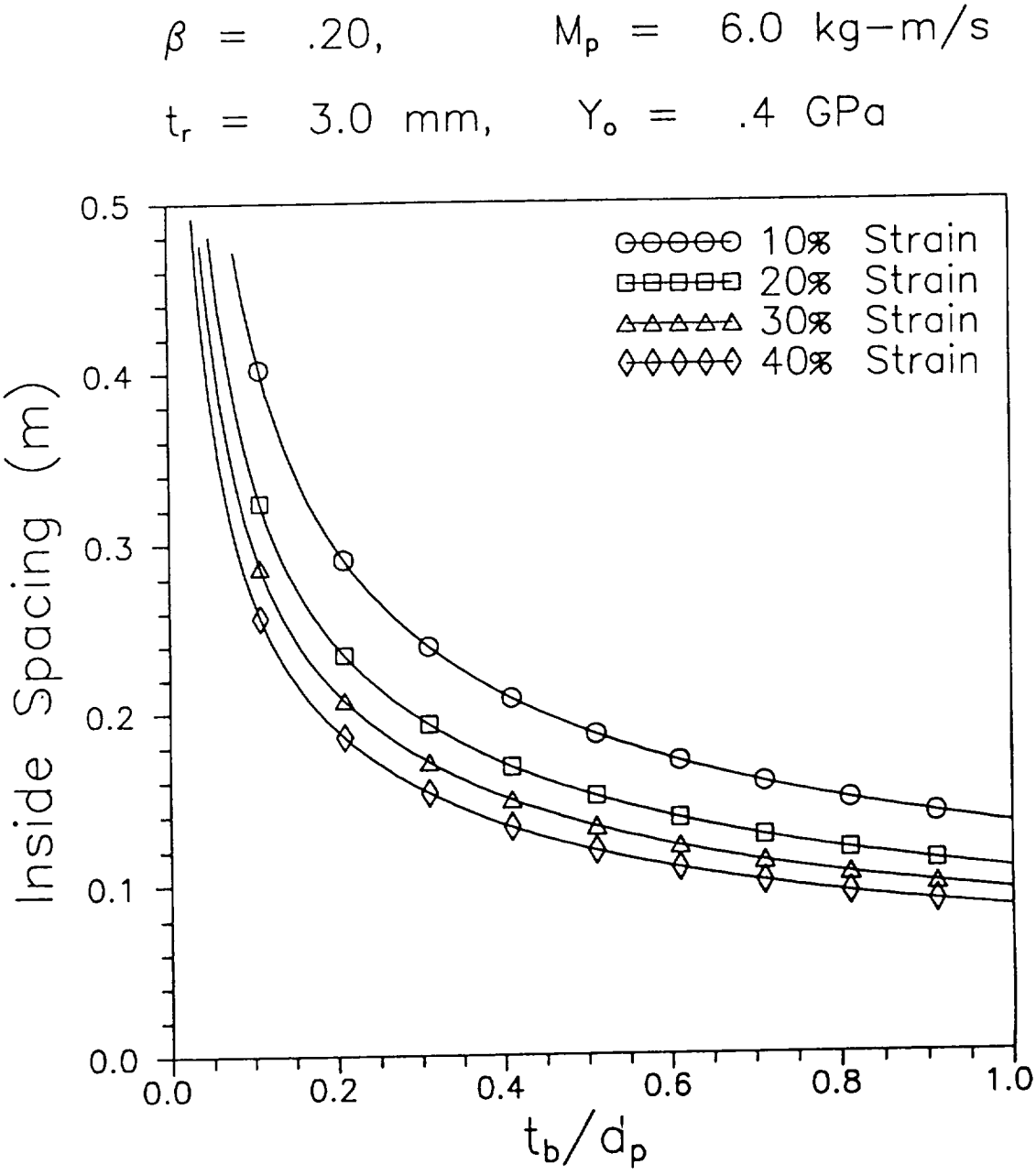

Figure 8. Design Curves for $\beta = 0.2$, $M_p = 6$ kg-m/s, $t_r = 3$ mm, and $Y_r = 0.4$ GPa

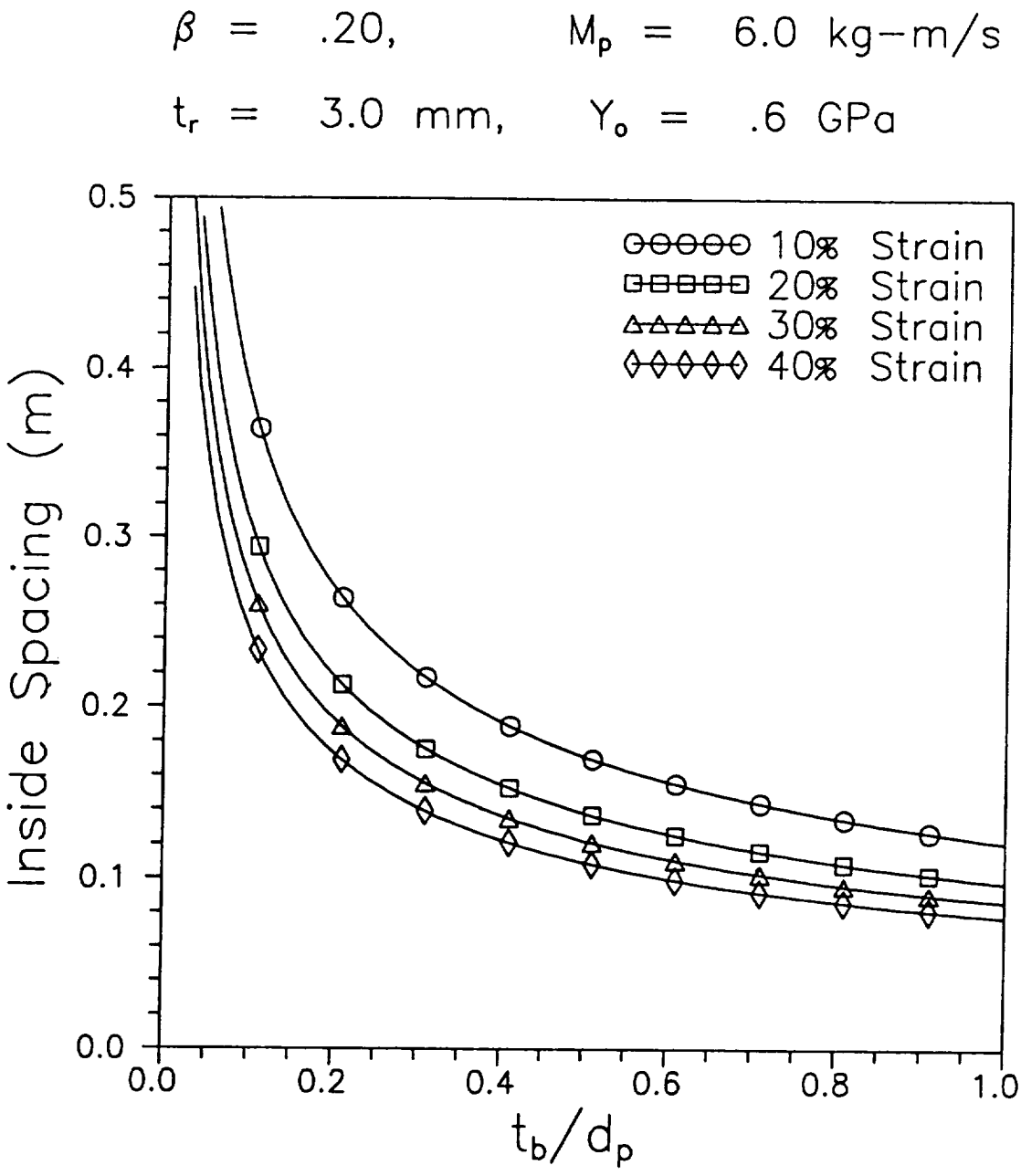

Figure 9. Design Curves for $\beta = 0.2$, $M_p = 6$ kg-m/s, $t_r = 3$ mm, and $Y_r = 0.6$ GPa

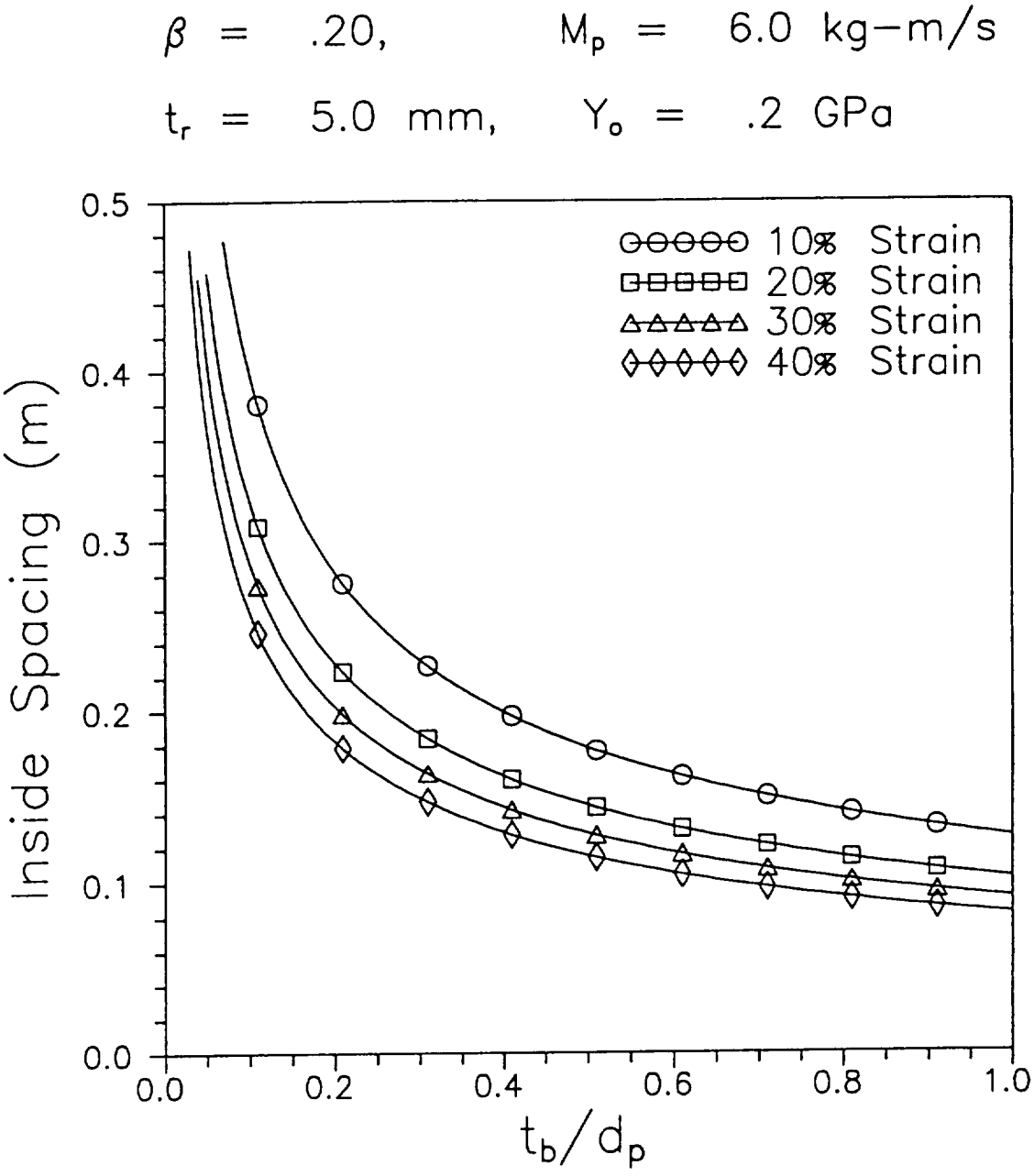

Figure 10. Design Curves for $\beta = 0.2$, $M_p = 6$ kg-m/s, $t_r = 5$ mm, and $Y_r = 0.2$ GPa

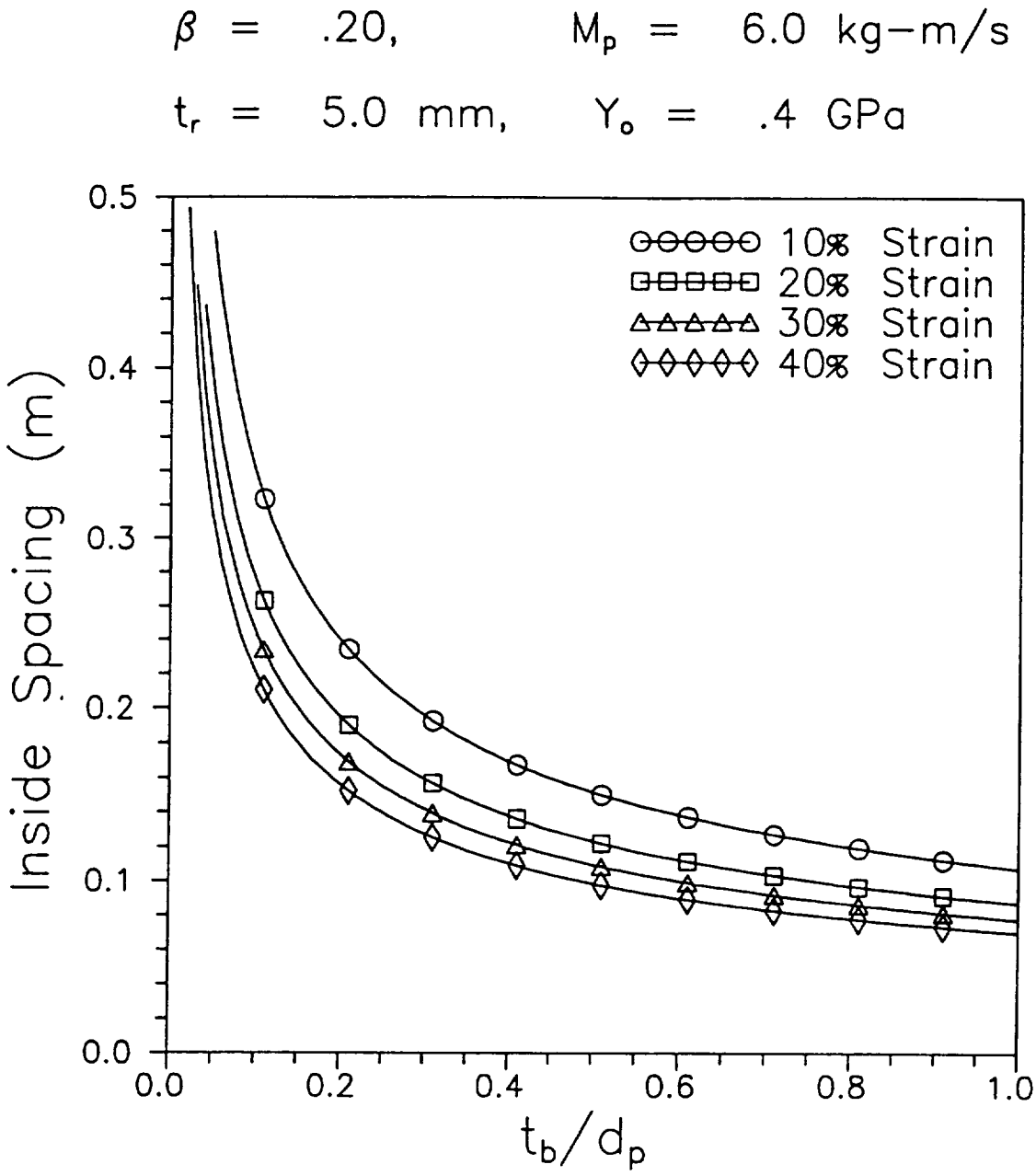

Figure 11. Design Curves for $\beta = 0.2$, $M_p = 6$ kg-m/s, $t_r = 5$ mm, and $Y_r = 0.4$ GPa

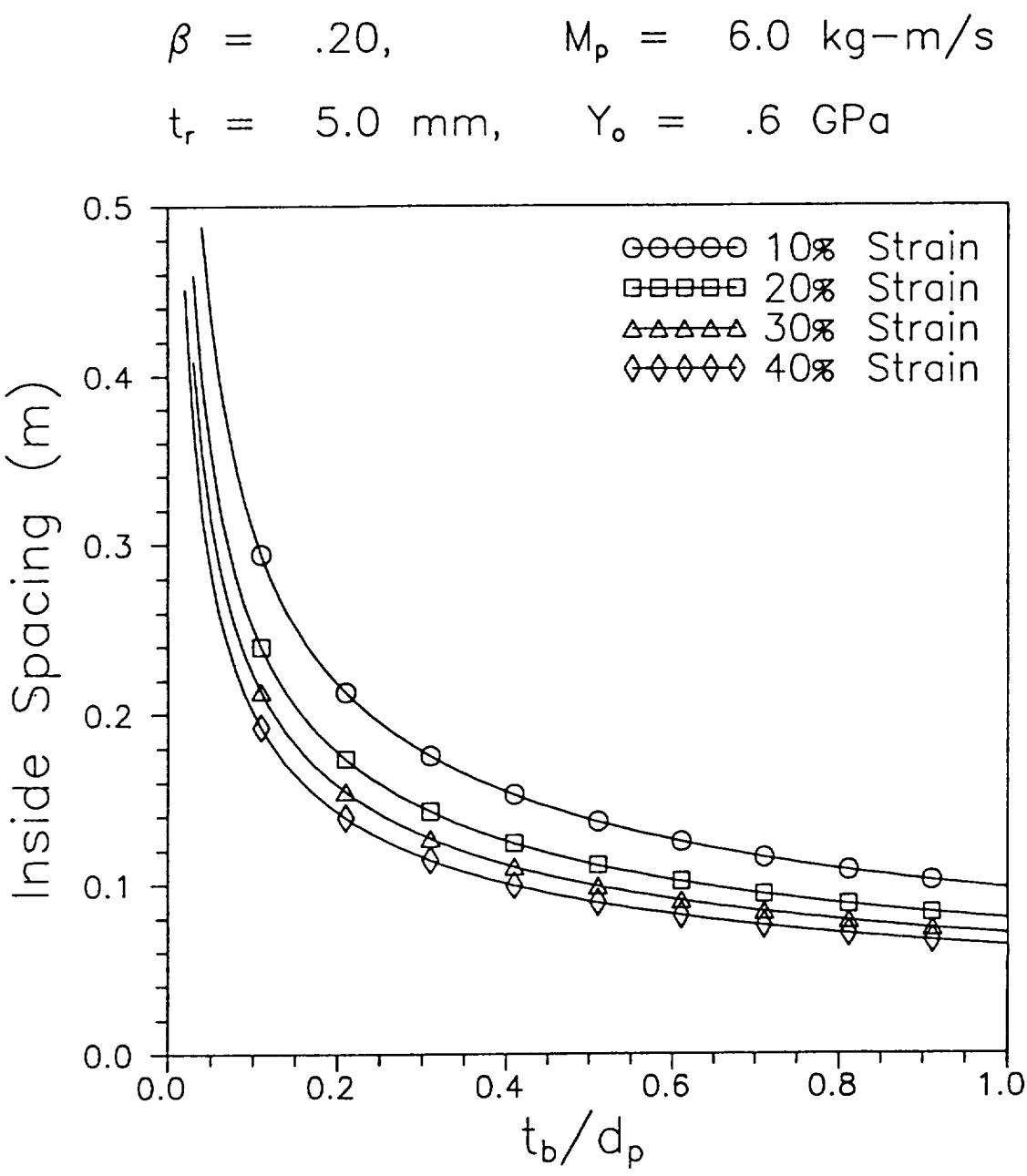

Figure 12. Design Curves for $\beta = 0.2$, $M_p = 6$ kg-m/s, $t_r = 5$ mm, and $Y_r = 0.6$ GPa

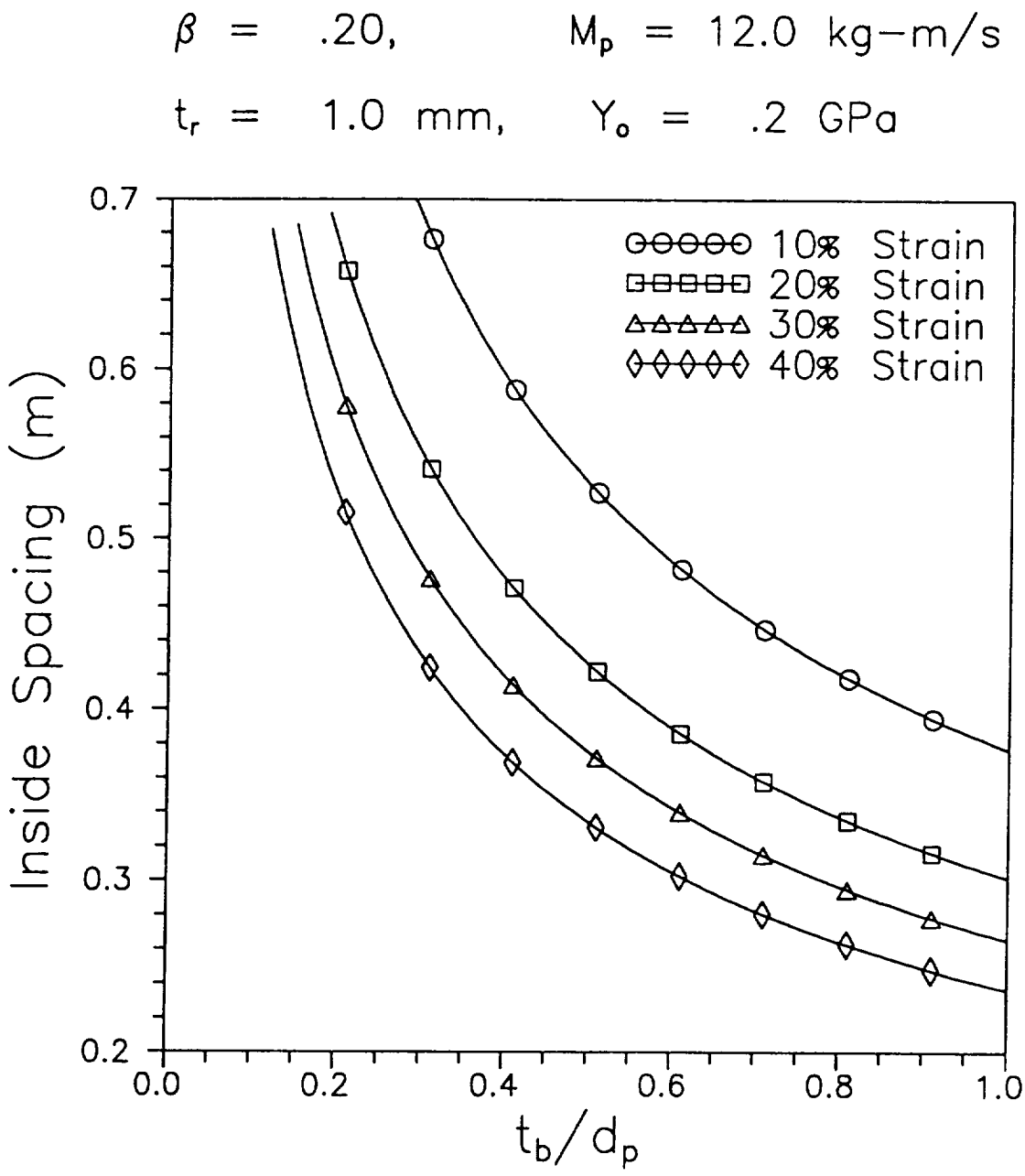

Figure 13. Design Curves for $\beta = 0.2$, $M_p = 12$ kg-m/s, $t_r = 1$ mm, and $Y_r = 0.2$ GPa

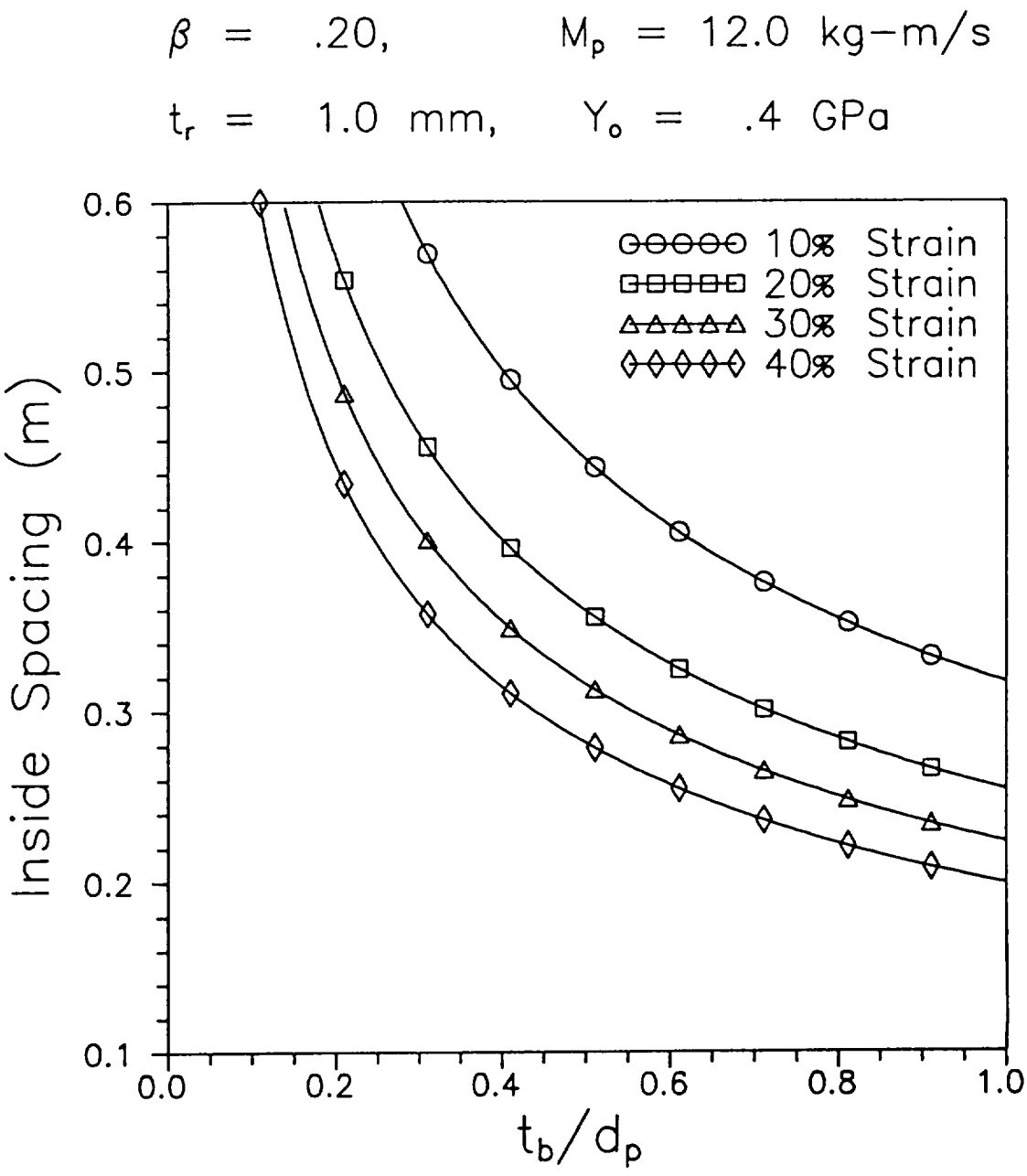

Figure 14. Design Curves for $\beta = 0.2$, $M_p = 12$ kg-m/s, $t_r = 1$ mm, and $Y_r = 0.4$ GPa

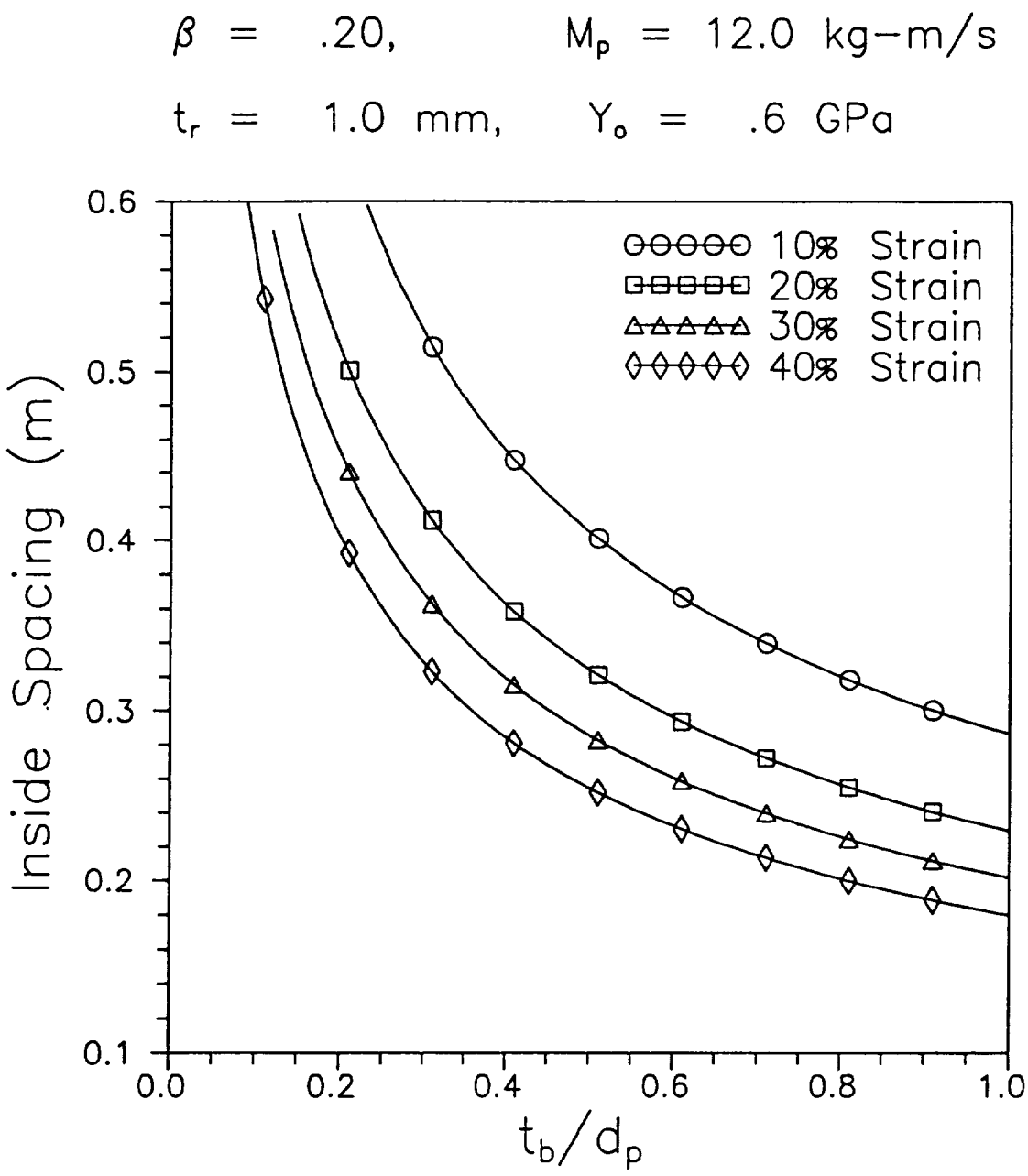

Figure 15. Design Curves for $\beta = 0.2$, $M_p = 12$ kg-m/s, $t_r = 1$ mm, and $Y_r = 0.6$ GPa

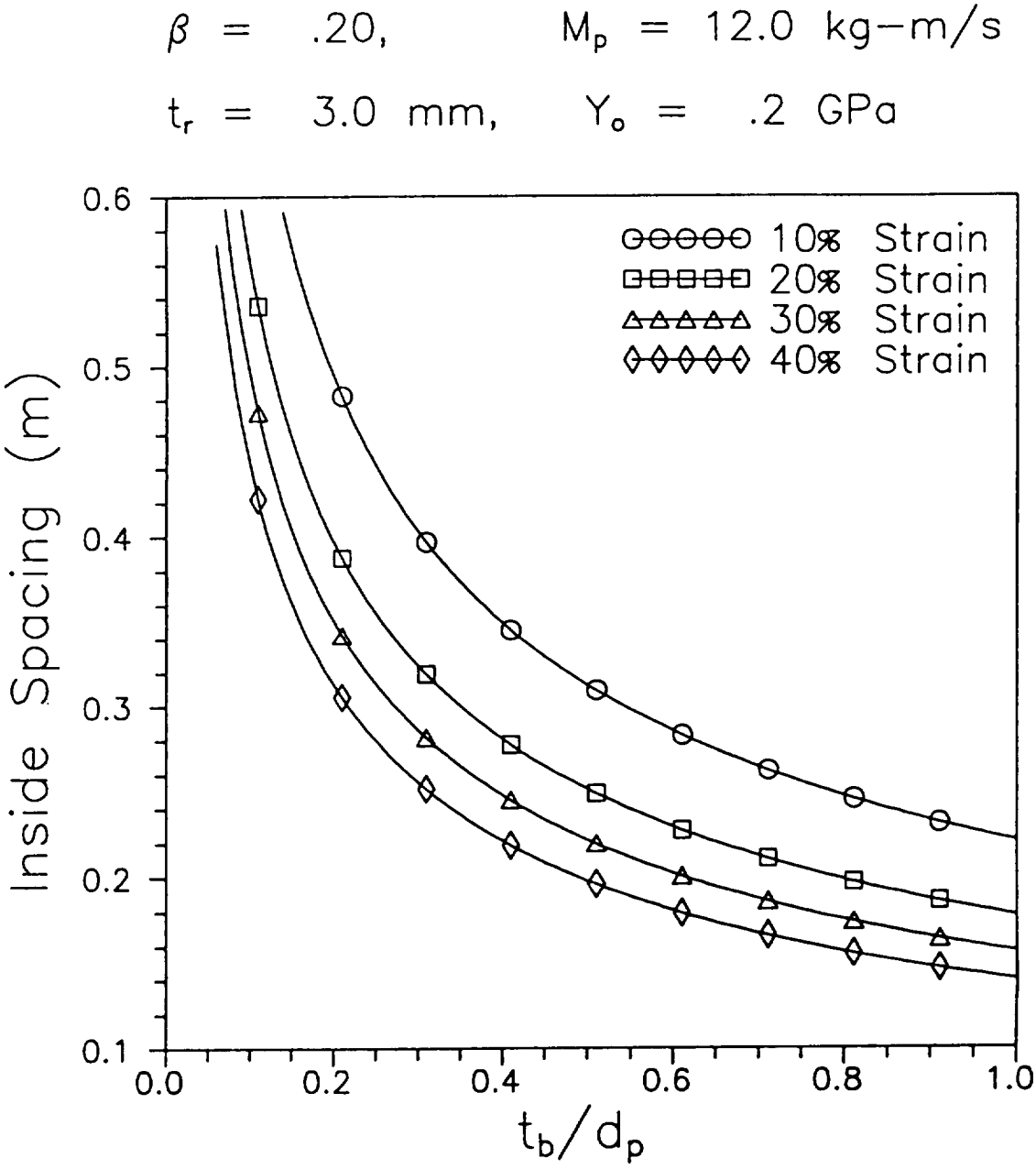

Figure 16. Design Curves for $\beta = 0.2$, $M_p = 12$ kg-m/s, $t_r = 3$ mm, and $Y_r = 0.2$ GPa

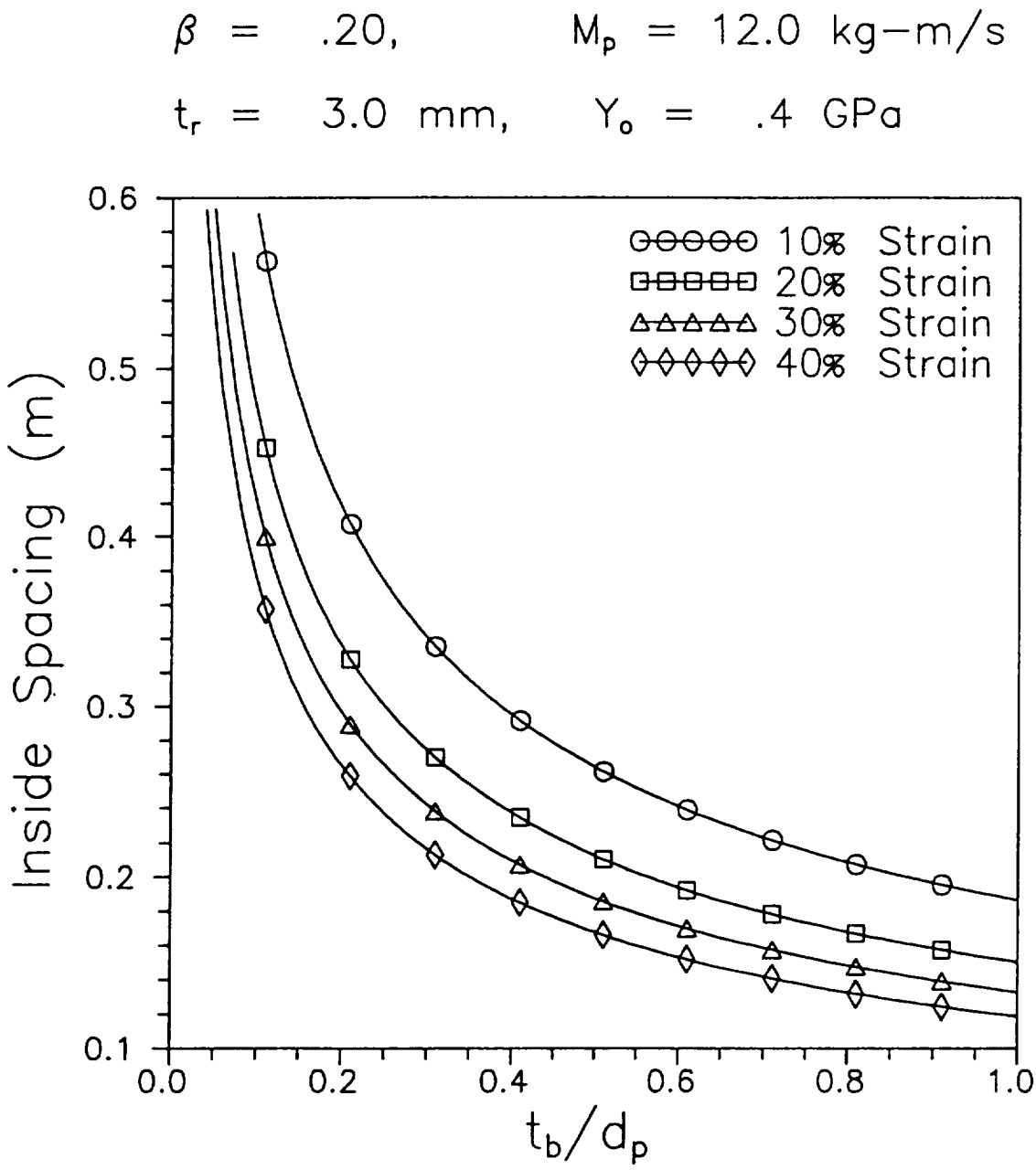

Figure 17. Design Curves for $\beta = 0.2$, $M_p = 12$ kg-m/s, $t_r = 3$ mm, and $Y_r = 0.4$ GPa

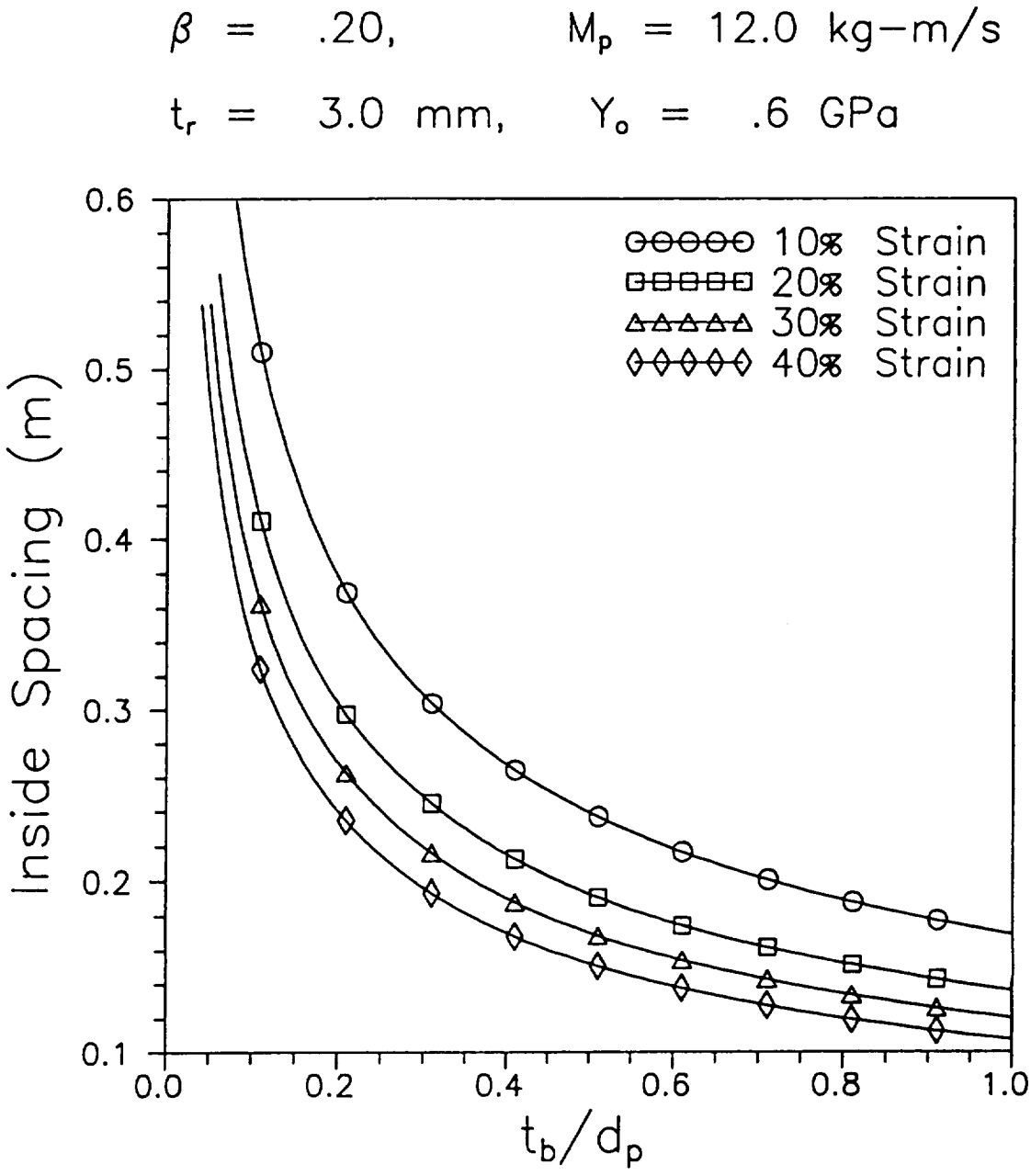

Figure 18. Design Curves for β = 0.2, M_p = 12 kg-m/s, t_r = 3 mm, and Y_r = 0.6 GPa

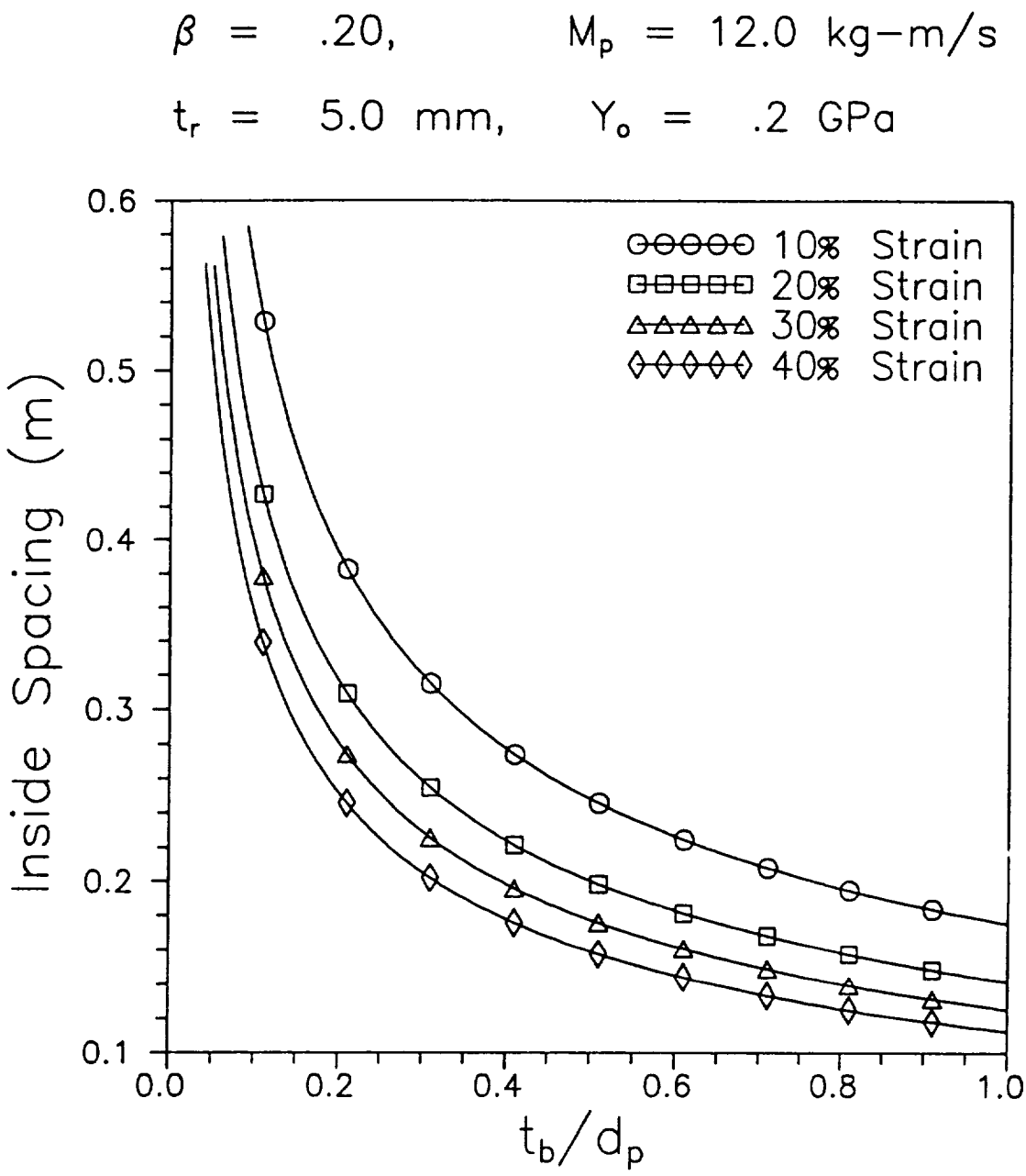

Figure 19. Design Curves for $\beta = 0.2$, $M_p = 12$ kg-m/s, $t_r = 5$ mm, and $Y_r = 0.2$ GPa

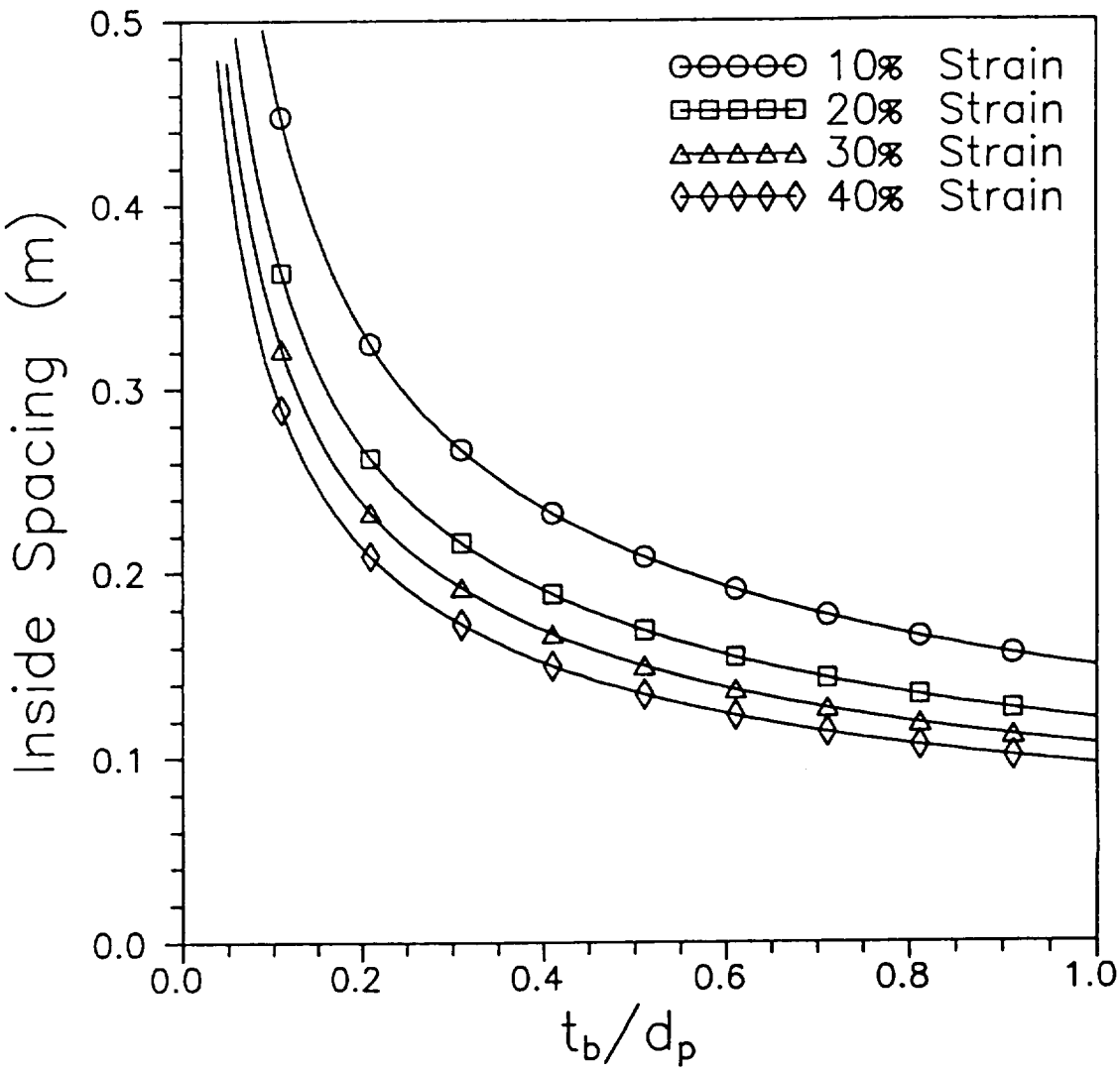

Figure 20. Design Curves for $\beta = 0.2$, $M_p = 12$ kg-m/s, $t_r = 5$ mm, and $Y_r = 0.4$ GPa

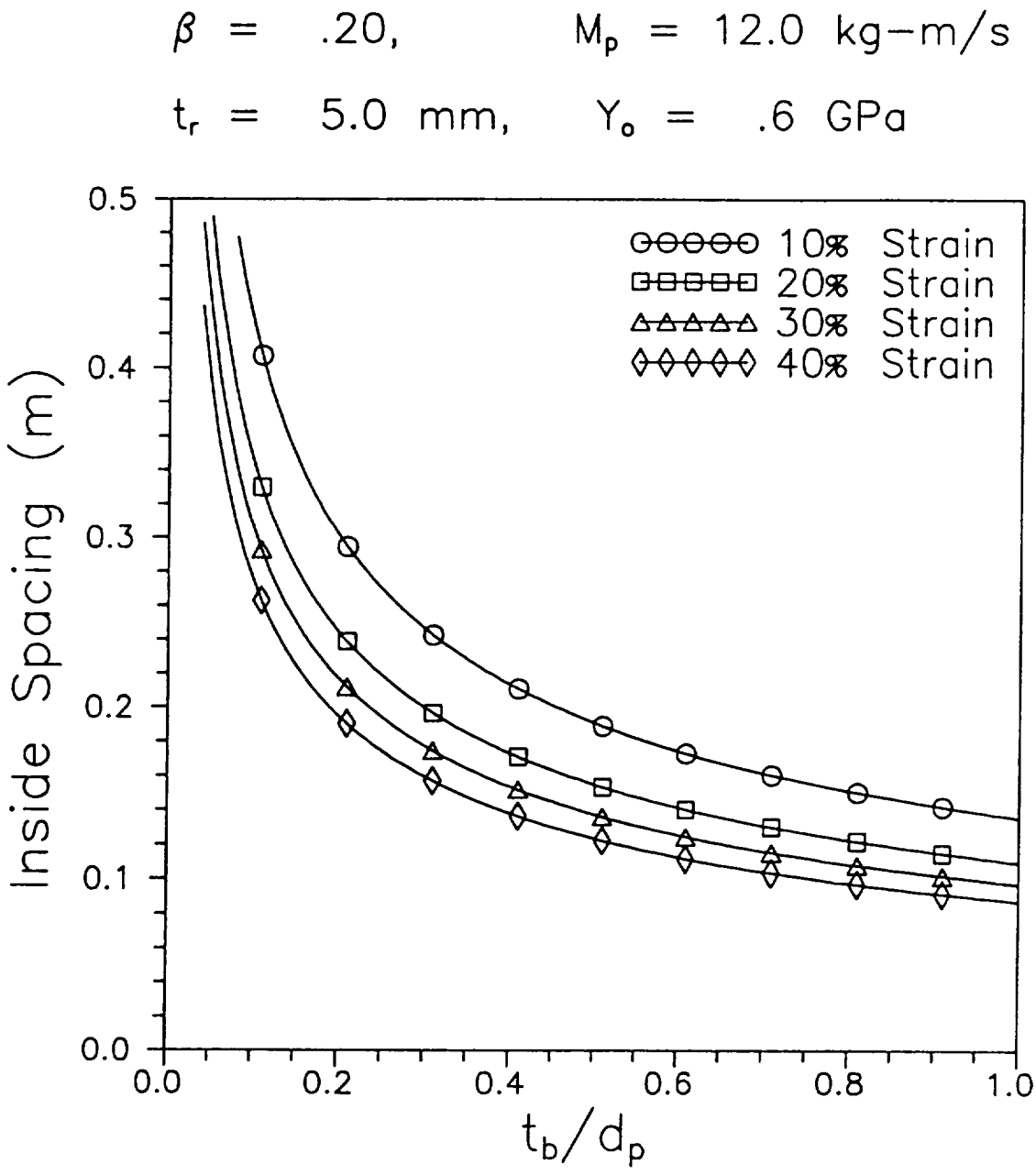

Figure 21. Design Curves for $\beta = 0.2$, $M_p = 12$ kg-m/s, $t_r = 5$ mm, and $Y_r = 0.6$ GPa

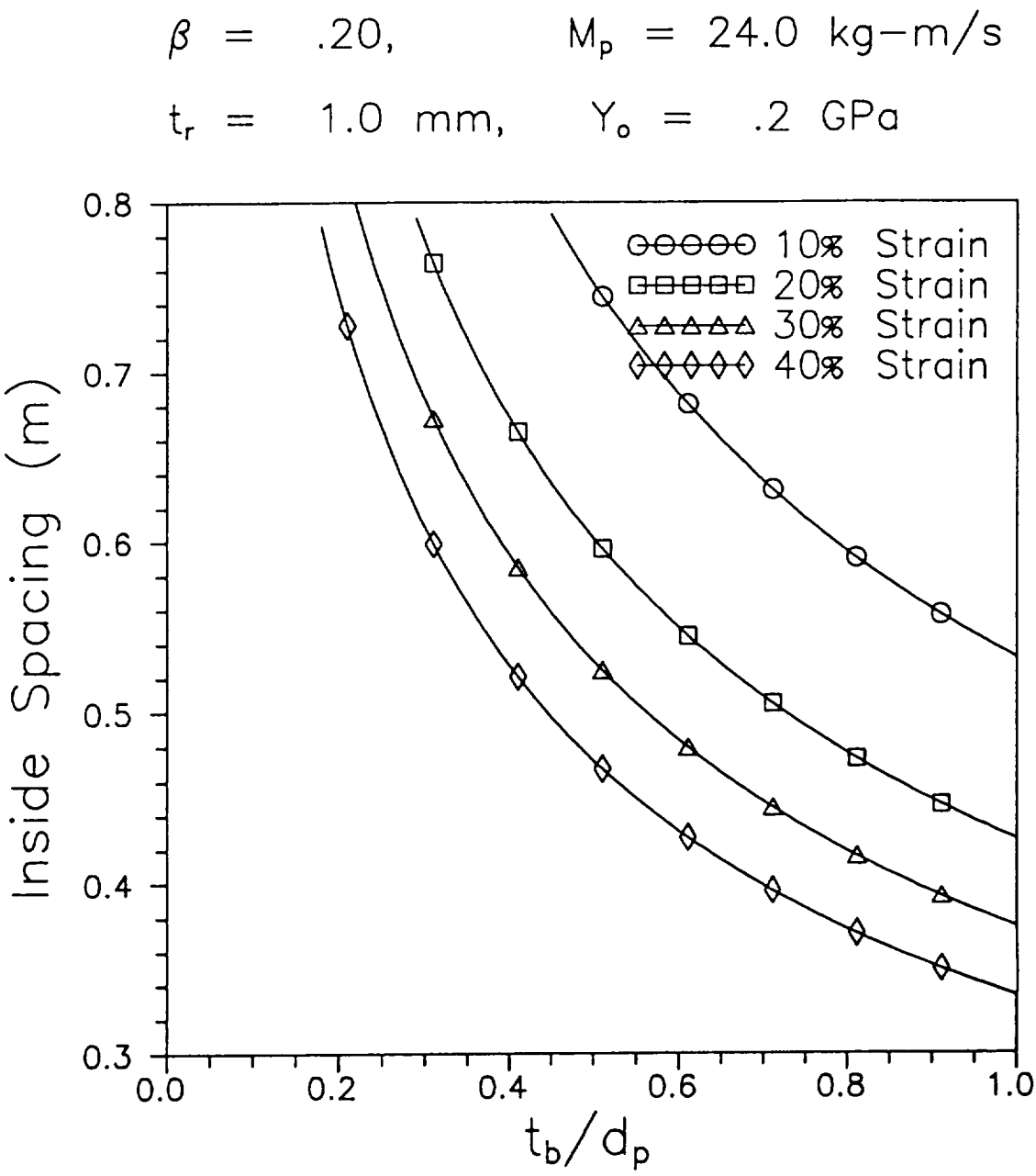

Figure 22. Design Curves for $\beta = 0.2$, $M_p = 24$ kg-m/s, $t_r = 1$ mm, and $Y_r = 0.2$ GPa

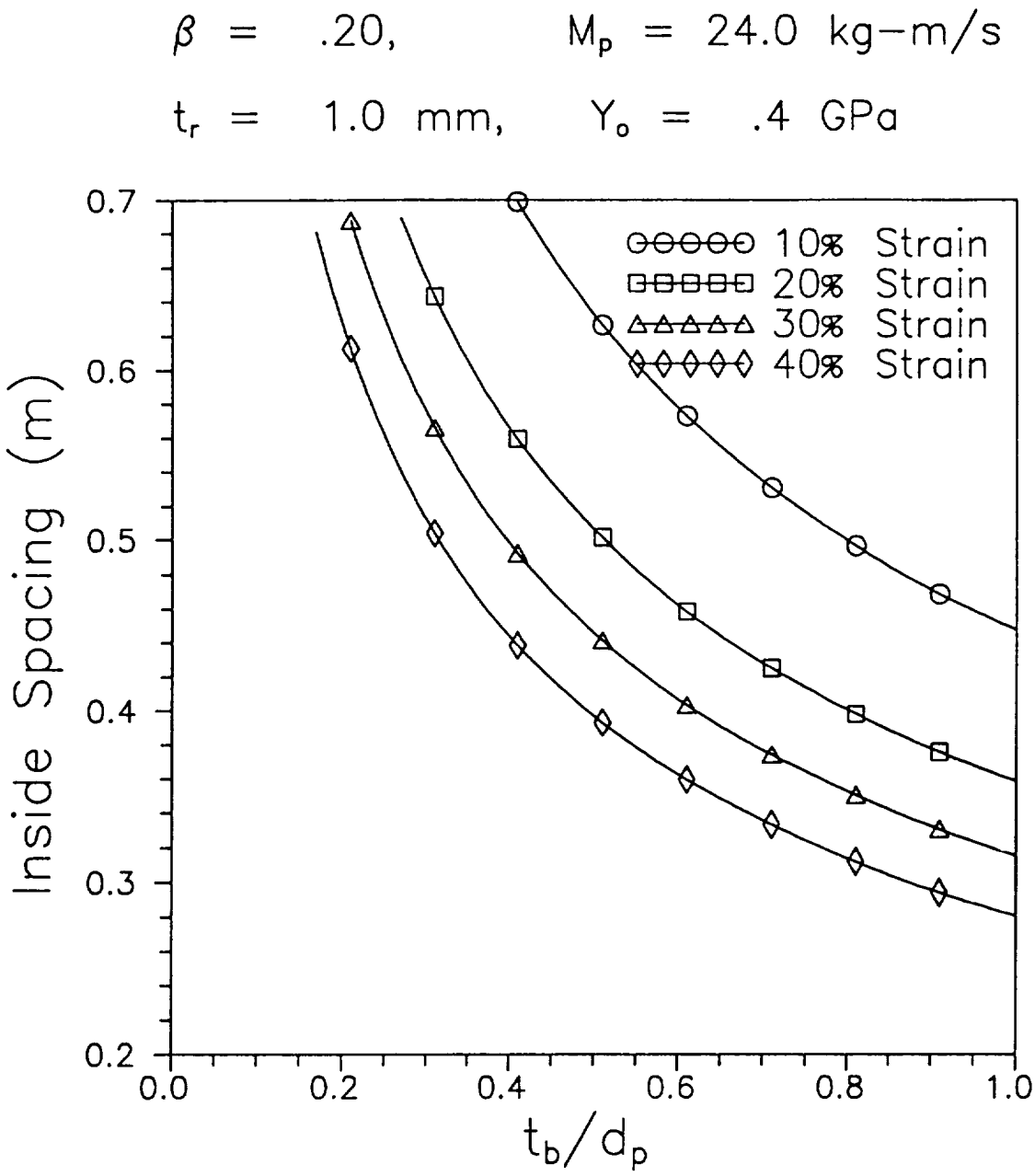

Figure 23. Design Curves for $\beta = 0.2$, $M_p = 24$ kg-m/s, $t_r = 1$ mm, and $Y_r = 0.4$ GPa

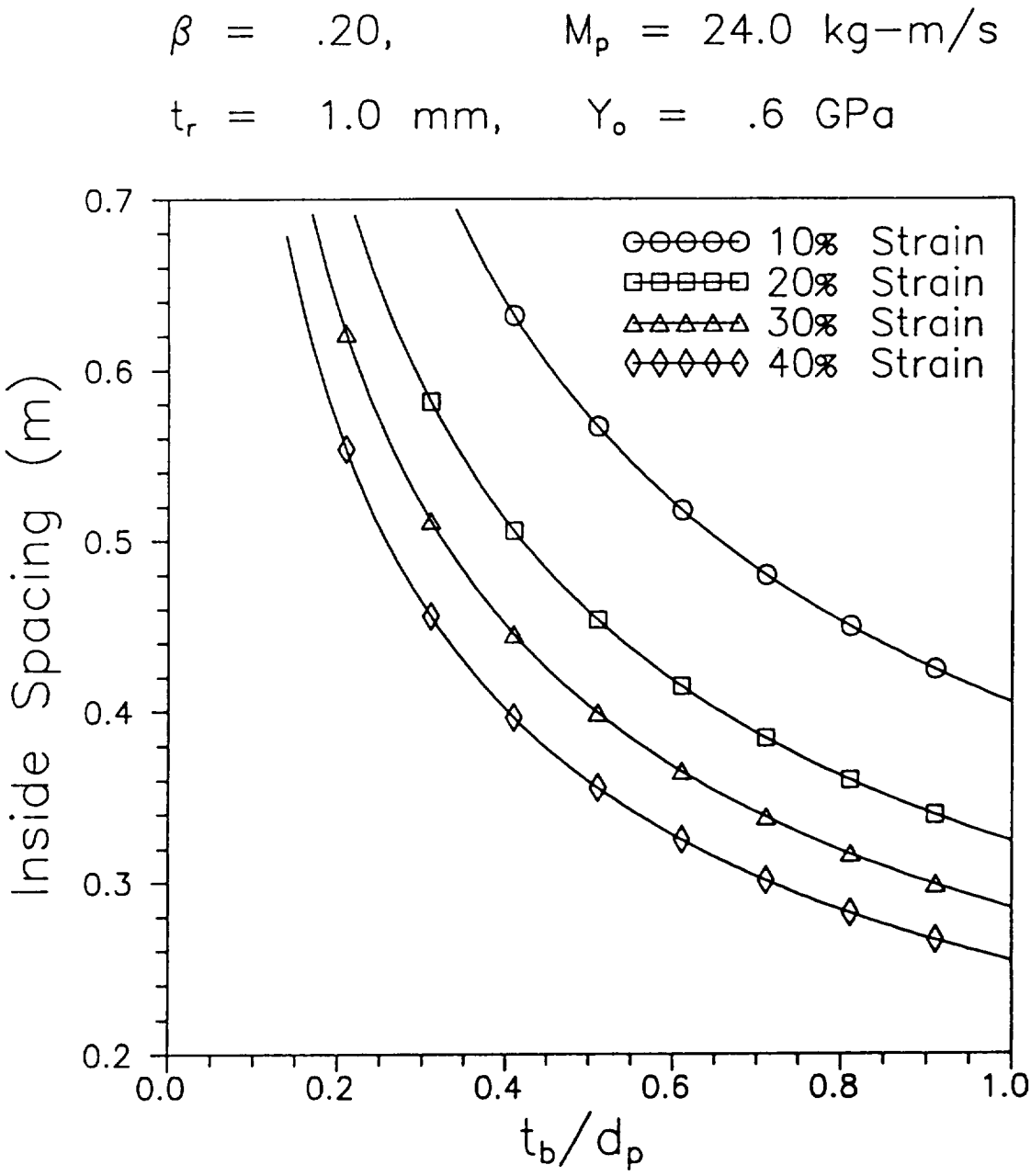

Figure 24. Design Curves for $\beta = 0.2$, $M_p = 24$ kg-m/s, $t_r = 1$ mm, and $Y_r = 0.6$ GPa

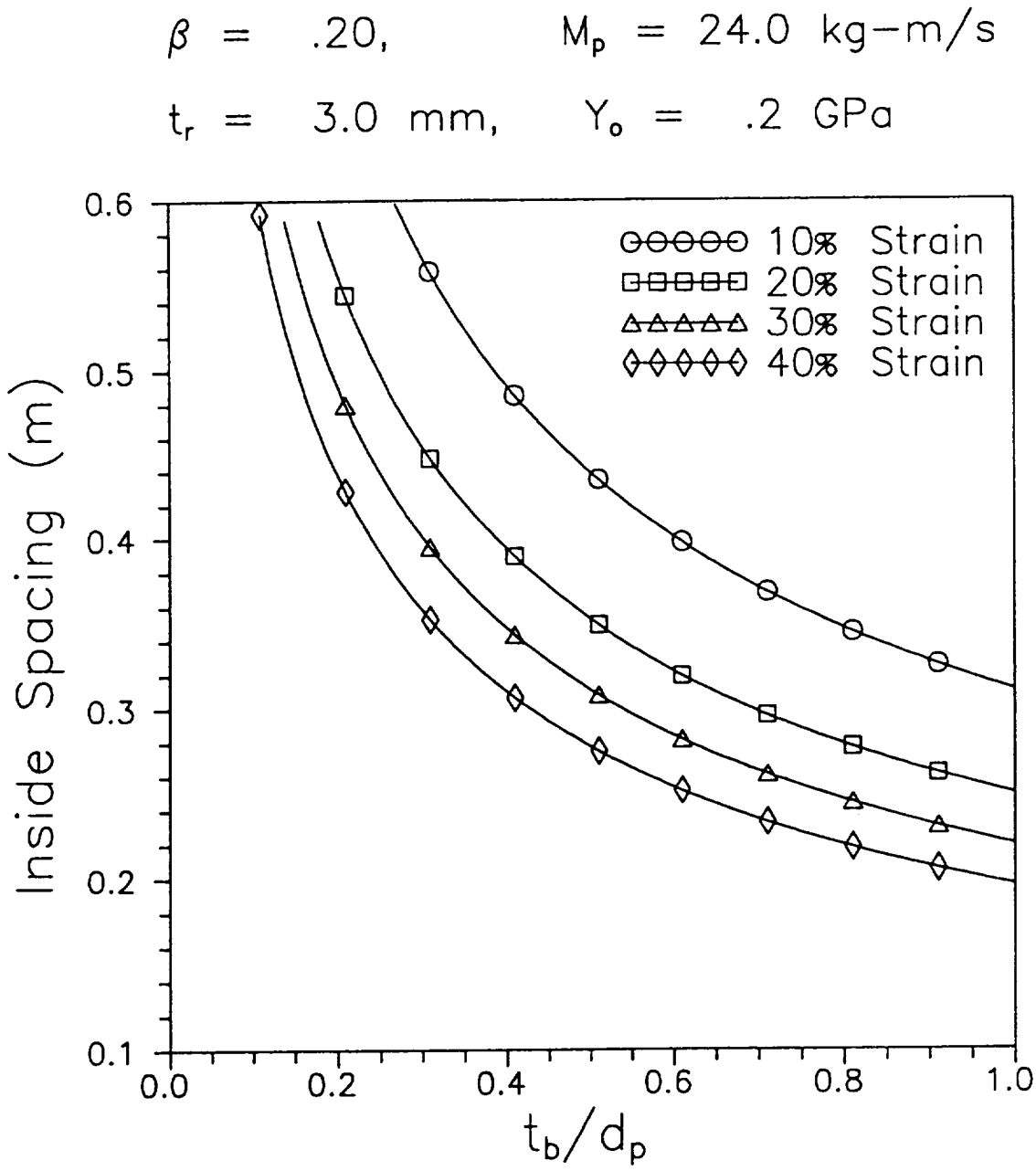

Figure 25. Design Curves for $\beta = 0.2$, $M_p = 24$ kg-m/s, $t_r = 3$ mm, and $Y_r = 0.2$ GPa

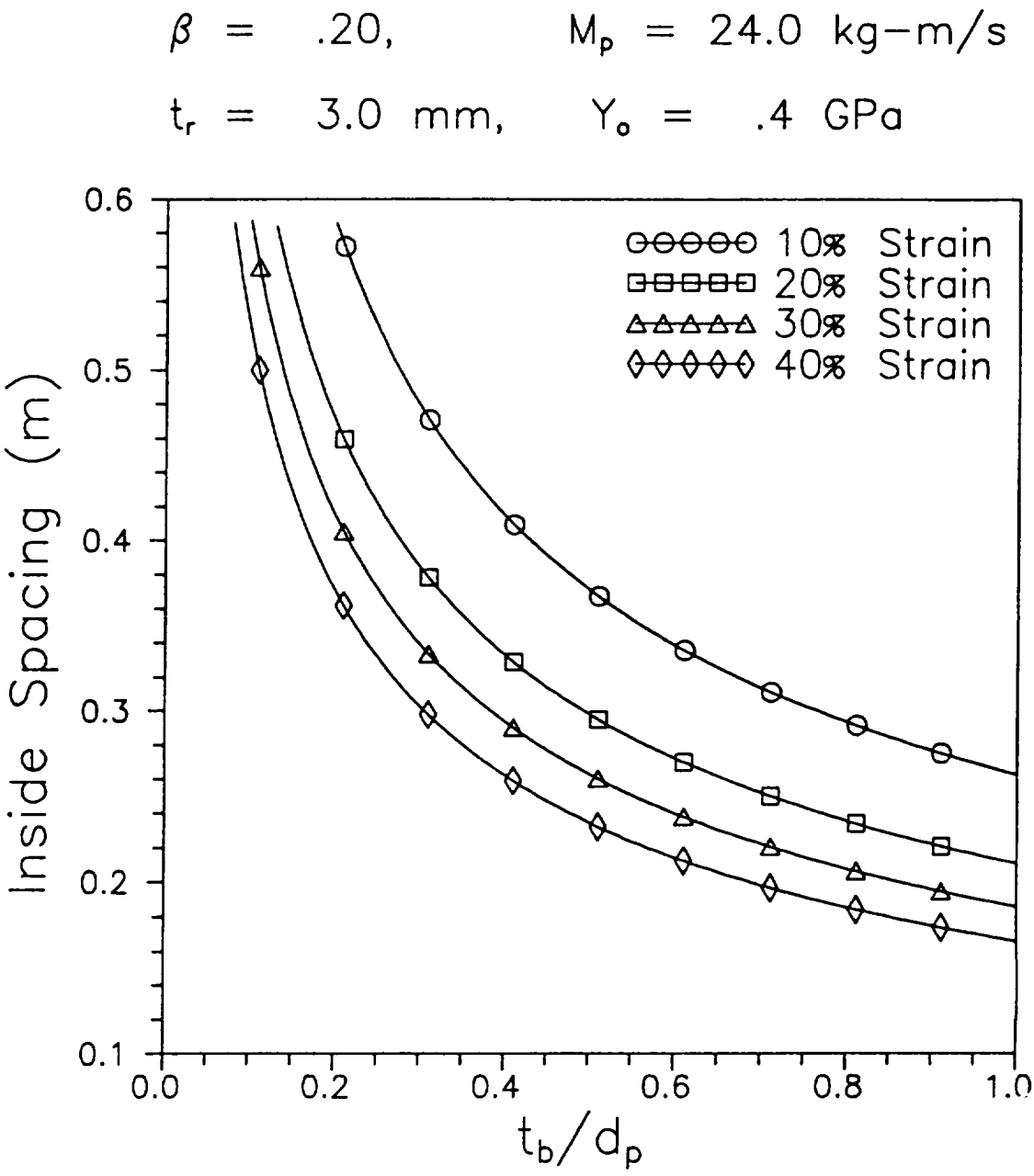

Figure 26. Design Curves for $\beta = 0.2$, $M_p = 24$ kg-m/s, $t_r = 3$ mm, and $Y_r = 0.4$ GPa

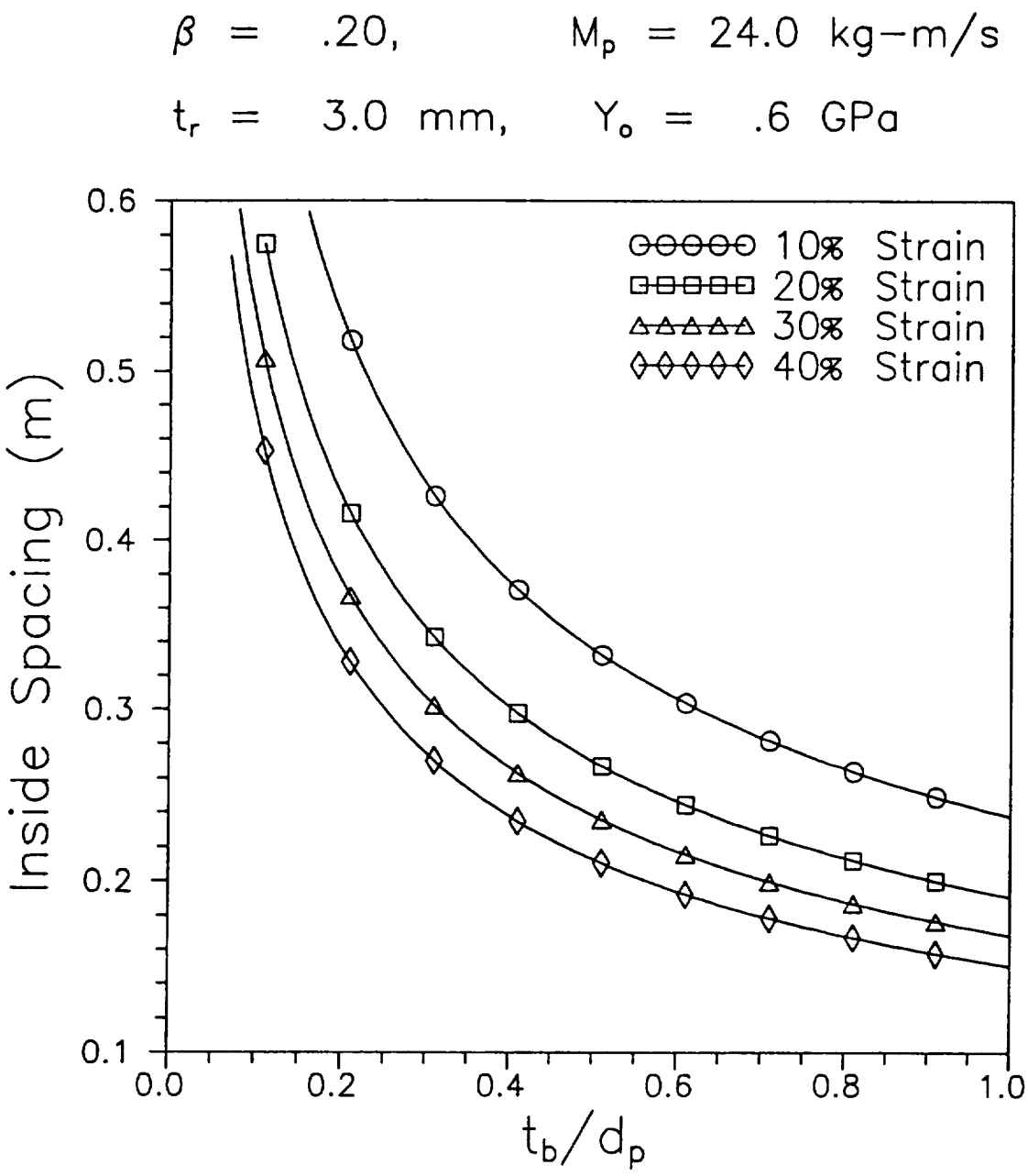

Figure 27. Design Curves for $\beta = 0.2$, $M_p = 24$ kg-m/s, $t_r = 3$ mm, and $Y_r = 0.6$ GPa

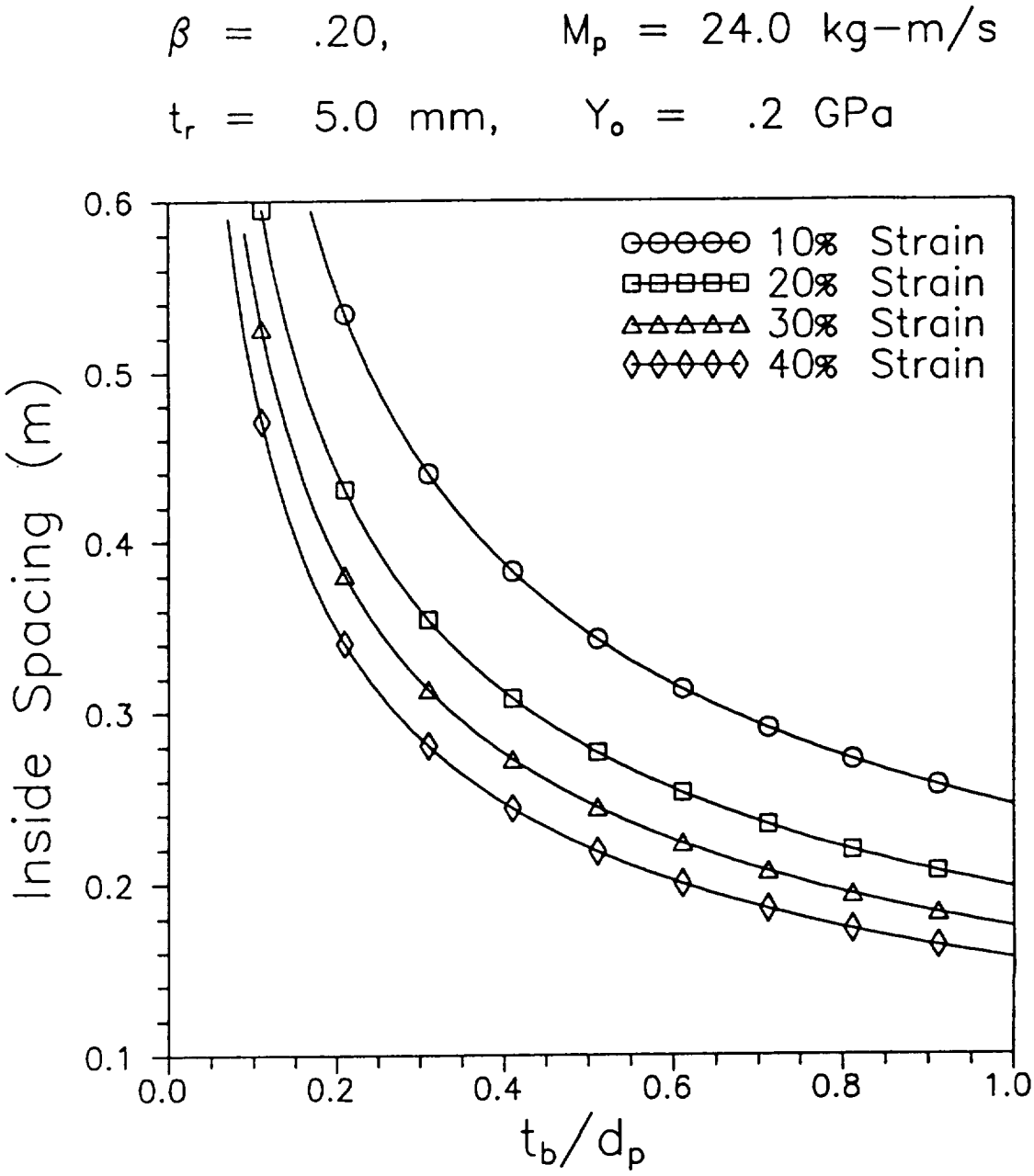

Figure 28. Design Curves for $\beta = 0.2$, $M_p = 24$ kg-m/s, $t_r = 5$ mm, and $Y_r = 0.2$ GPa

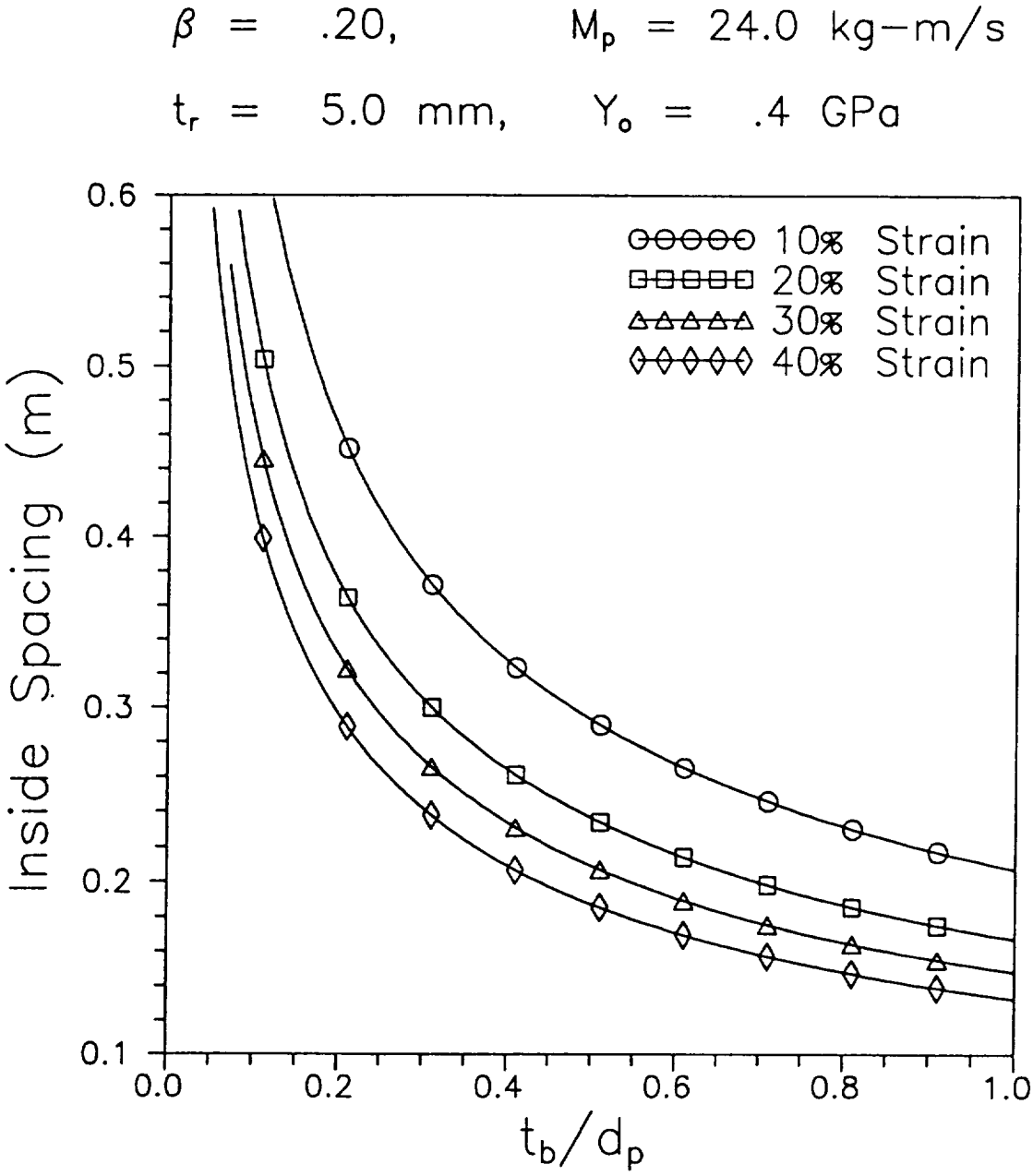

Figure 29. Design Curves for $\beta = 0.2$, $M_p = 24$ kg-m/s, $t_r = 5$ mm, and $Y_r = 0.4$ GPa

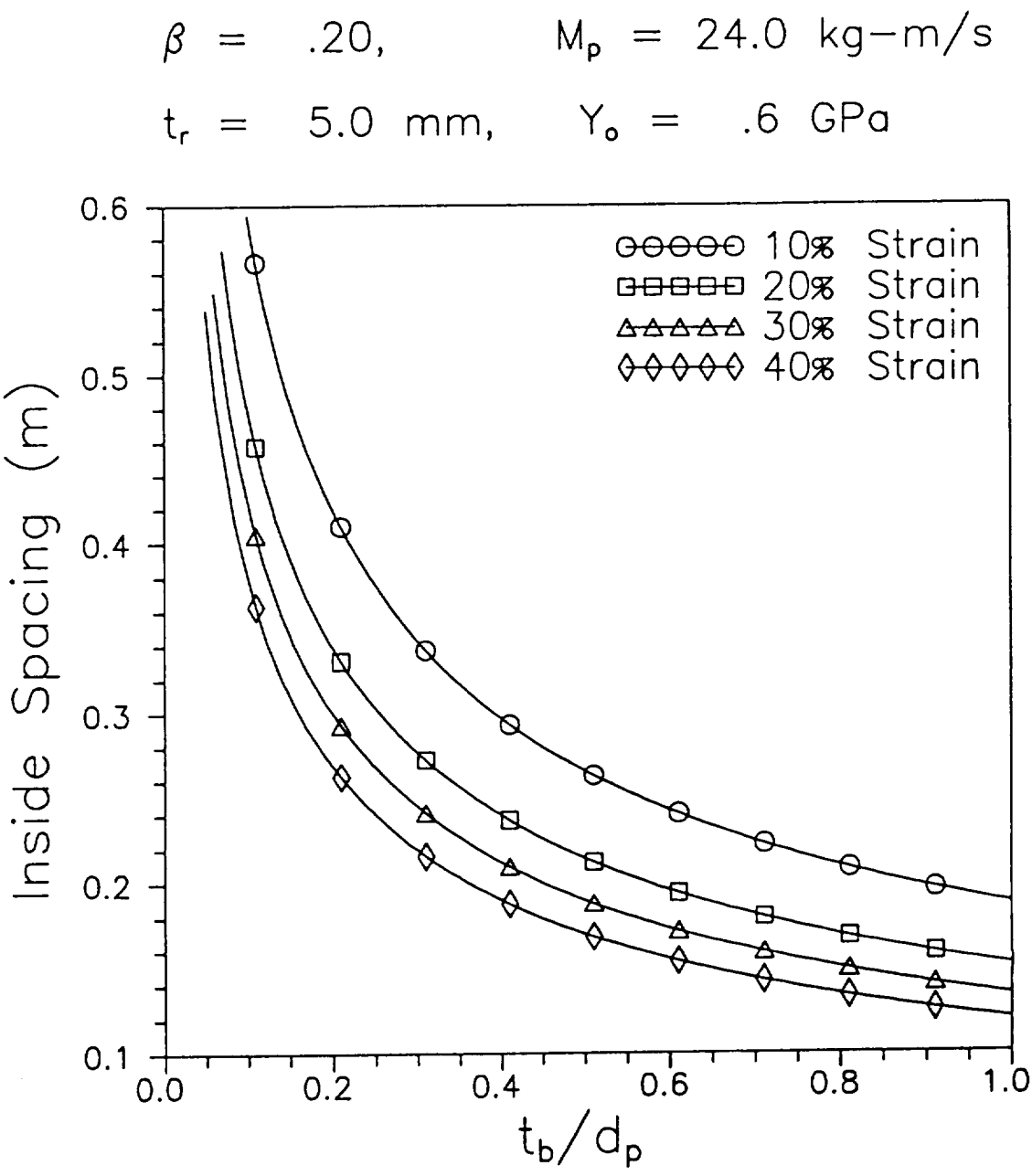

Figure 30. Design Curves for β = 0.2, M_p = 24 kg-m/s, t_r = 5 mm, and Y_r = 0.6 GPa

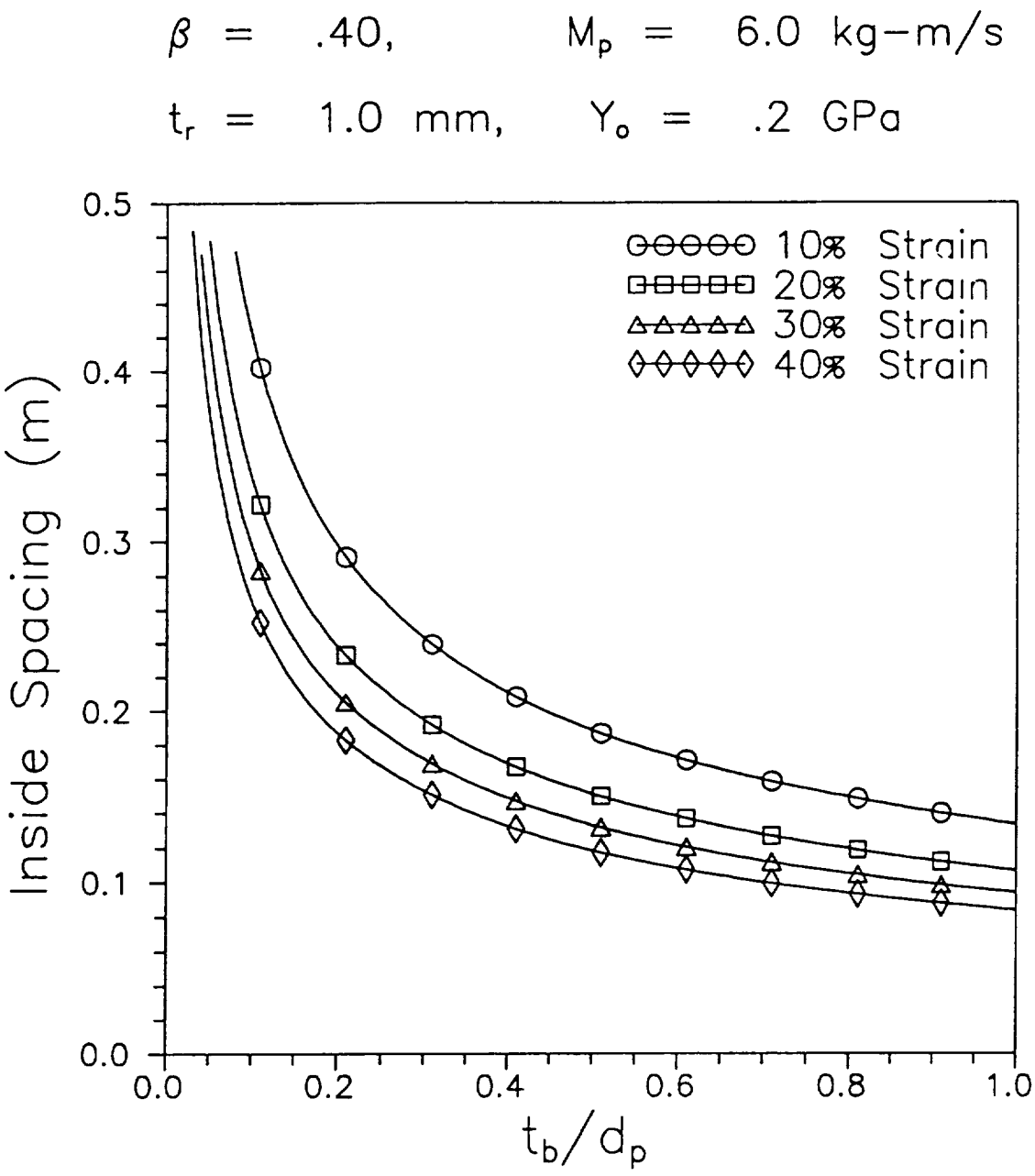

Figure 31. Design Curves for $\beta = 0.4$, $M_p = 6$ kg-m/s, $t_r = 1$ mm, and $Y_r = 0.2$ GPa

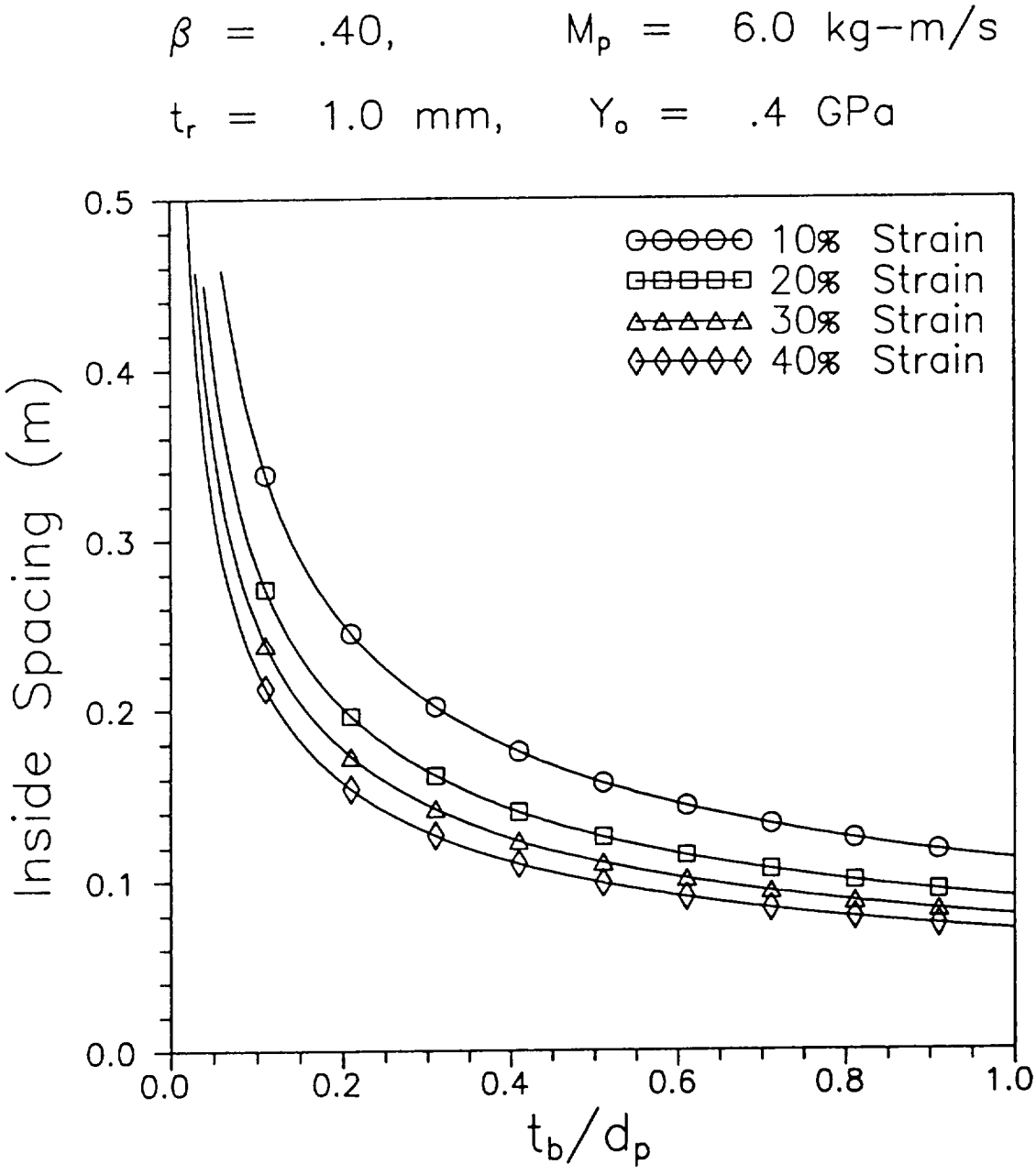

Figure 32. Design Curves for $\beta = 0.4$, M_p = 6 kg-m/s, t_r = 1 mm, and Y_r = 0.4 GPa

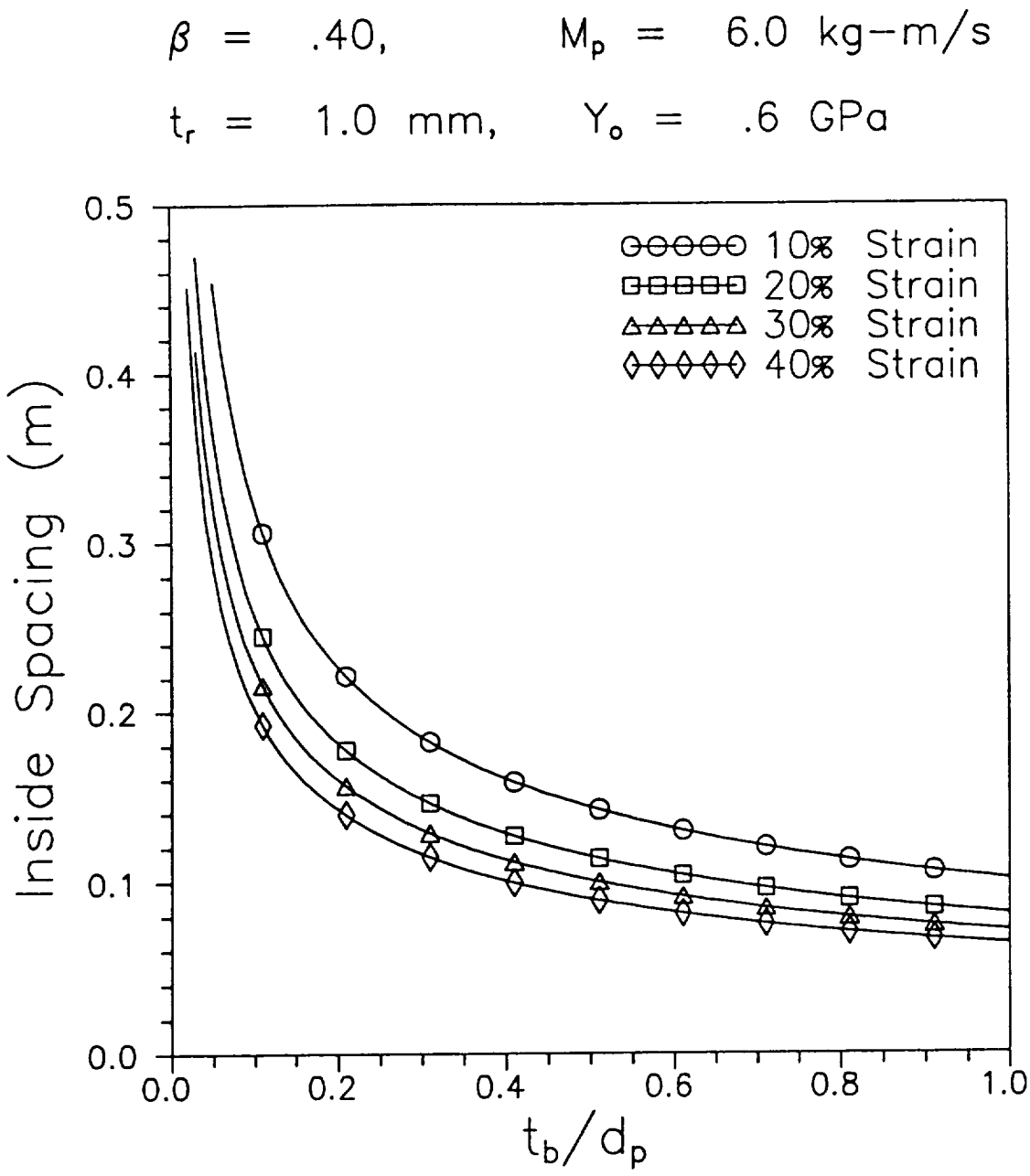

Figure 33. Design Curves for $\beta = 0.4$, $M_p = 6$ kg-m/s, $t_r = 1$ mm, and $Y_r = 0.6$ GPa

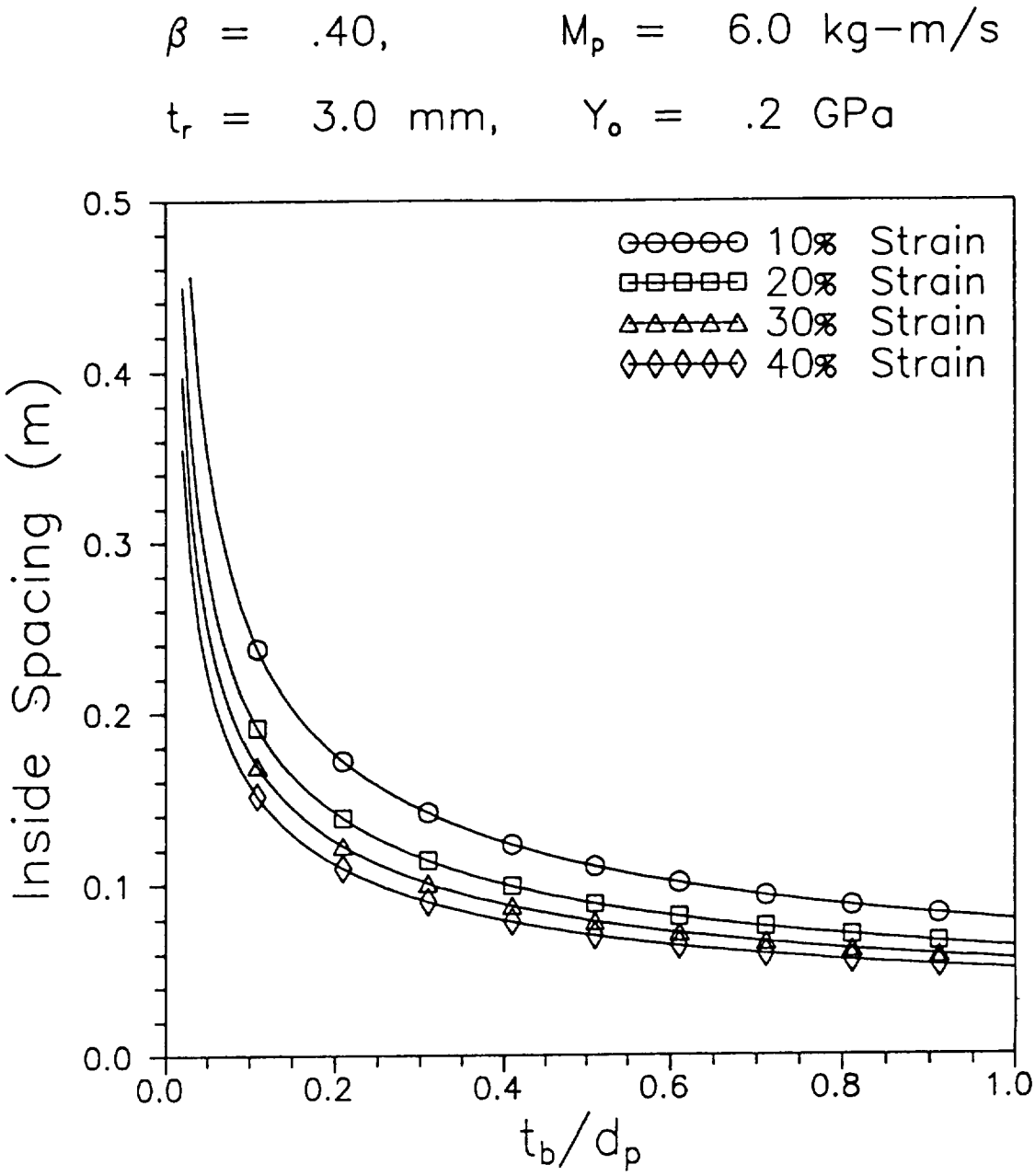

Figure 34. Design Curves for $\beta = 0.4$, M_p = 6 kg-m/s, t_r = 3 mm, and Y_r = 0.2 GPa

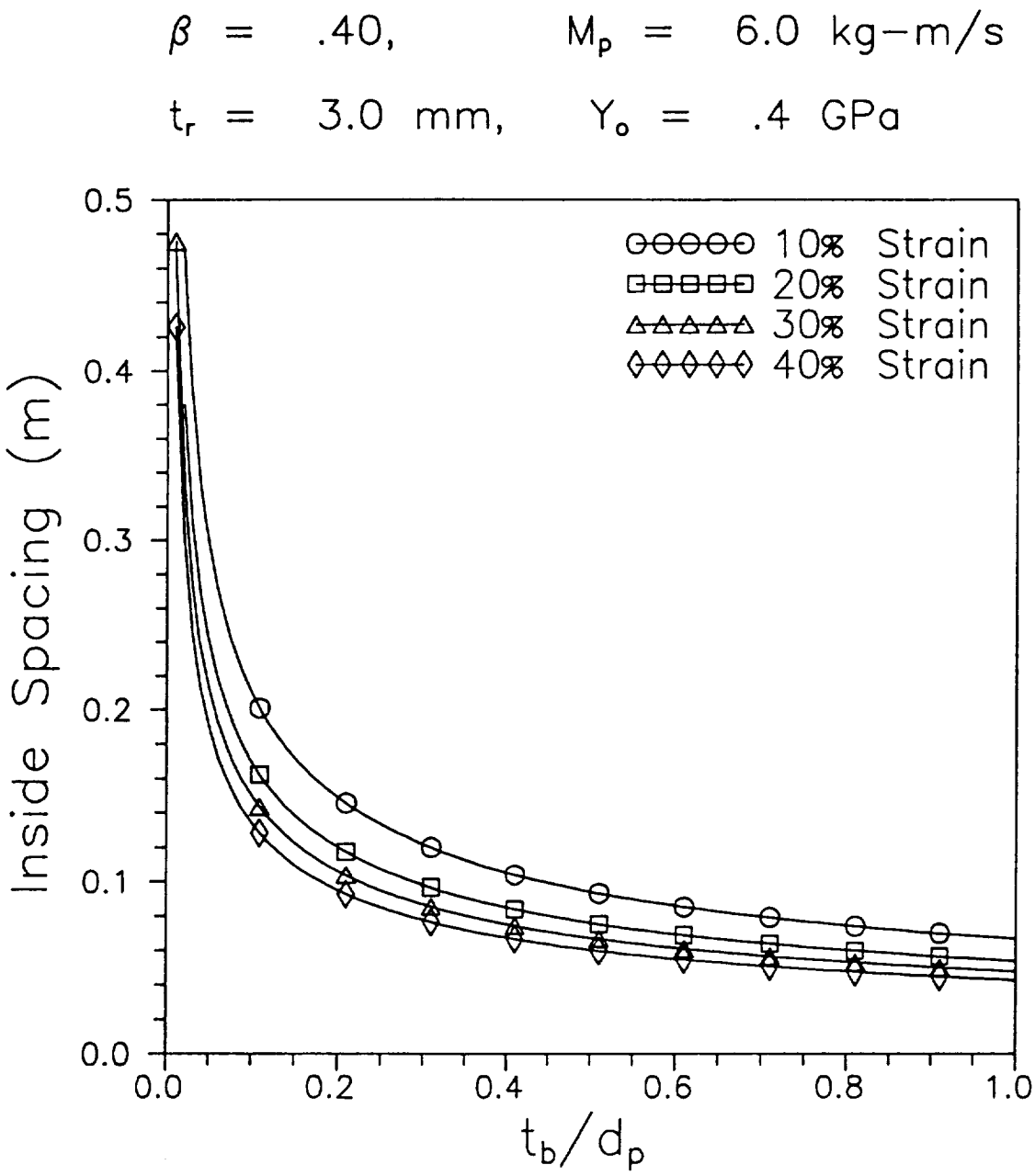

Figure 35. Design Curves for $\beta = 0.4$, $M_p = 6$ kg-m/s, $t_r = 3$ mm, and $Y_r = 0.4$ GPa

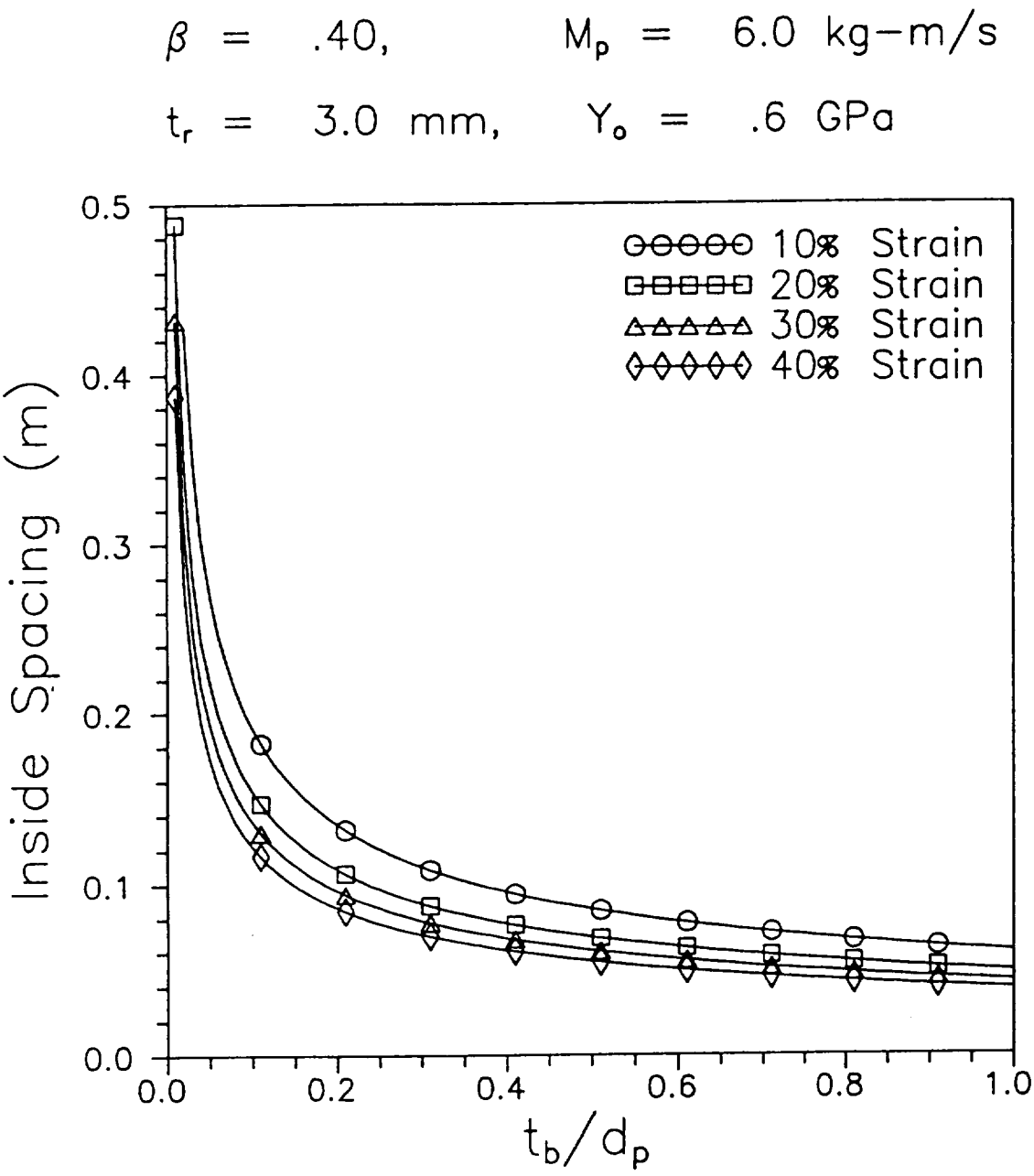

Figure 36. Design Curves for $\beta = 0.4$, $M_p = 6$ kg-m/s, $t_r = 3$ mm, and $Y_r = 0.6$ GPa

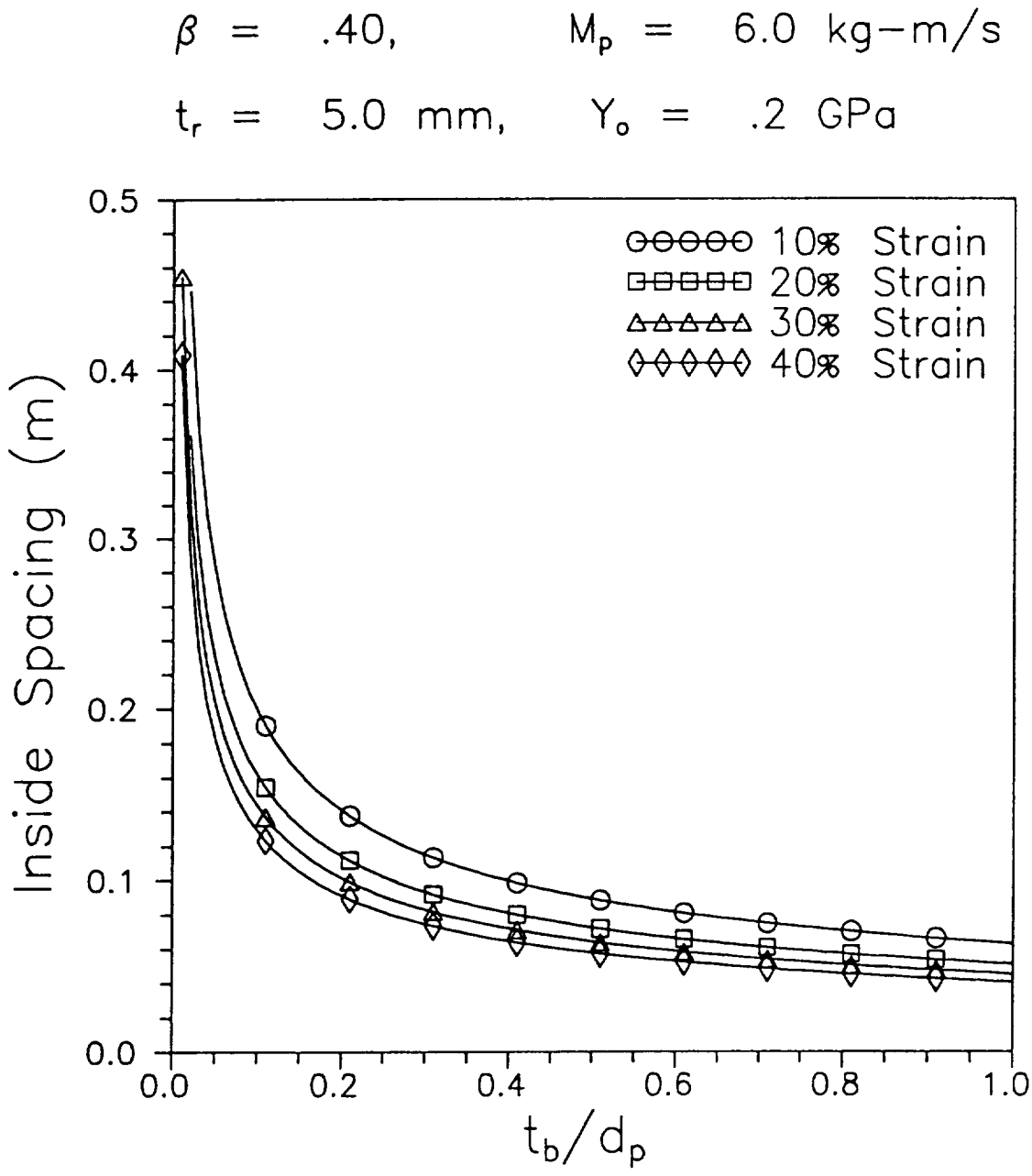

Figure 37. Design Curves for $\beta = 0.4$, $M_p = 6$ kg-m/s, $t_r = 5$ mm, and $Y_r = 0.2$ GPa

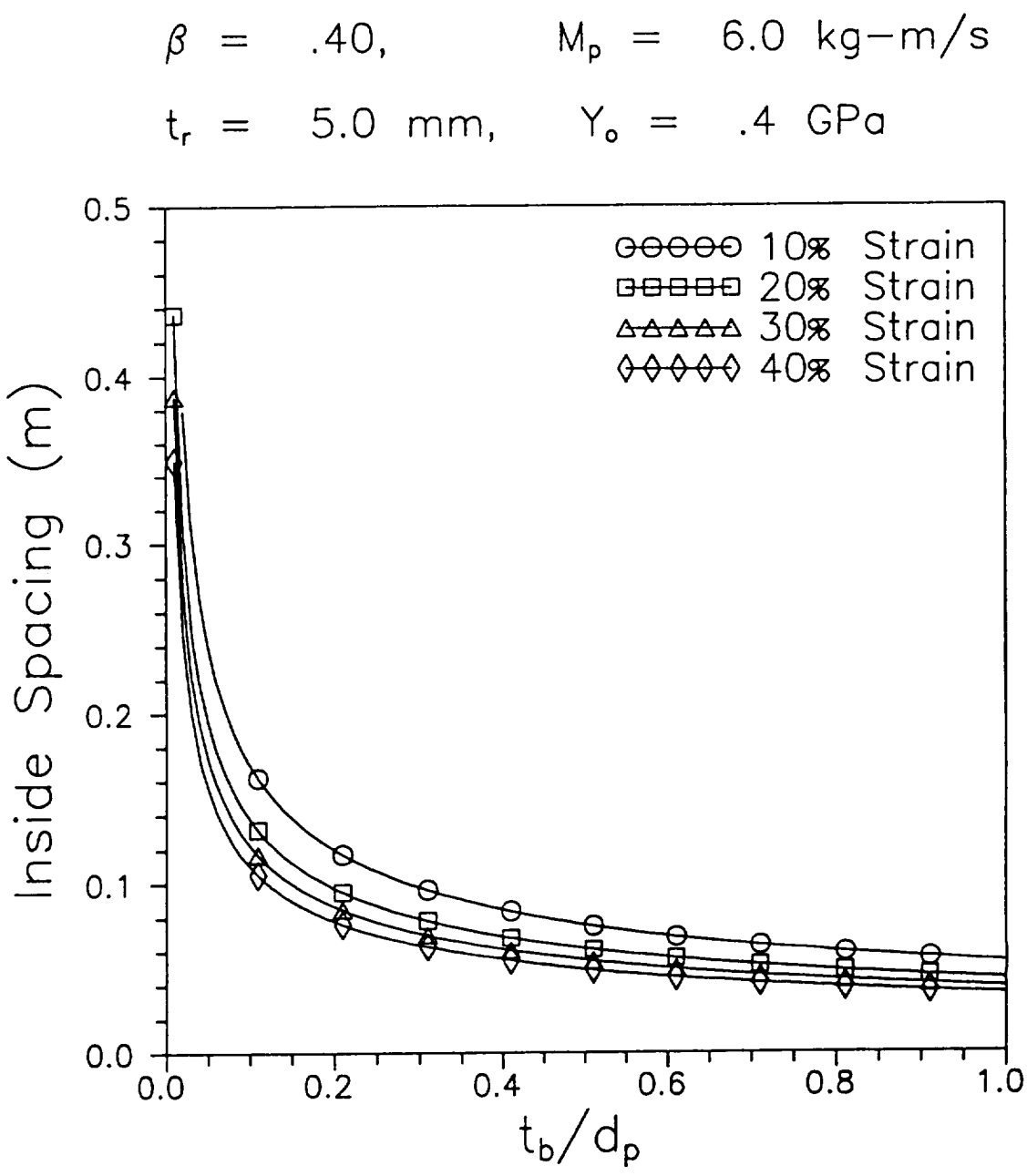

Figure 38. Design Curves for β = 0.4, M_p = 6 kg-m/s, t_r = 5 mm, and Y_r = 0.4 GPa

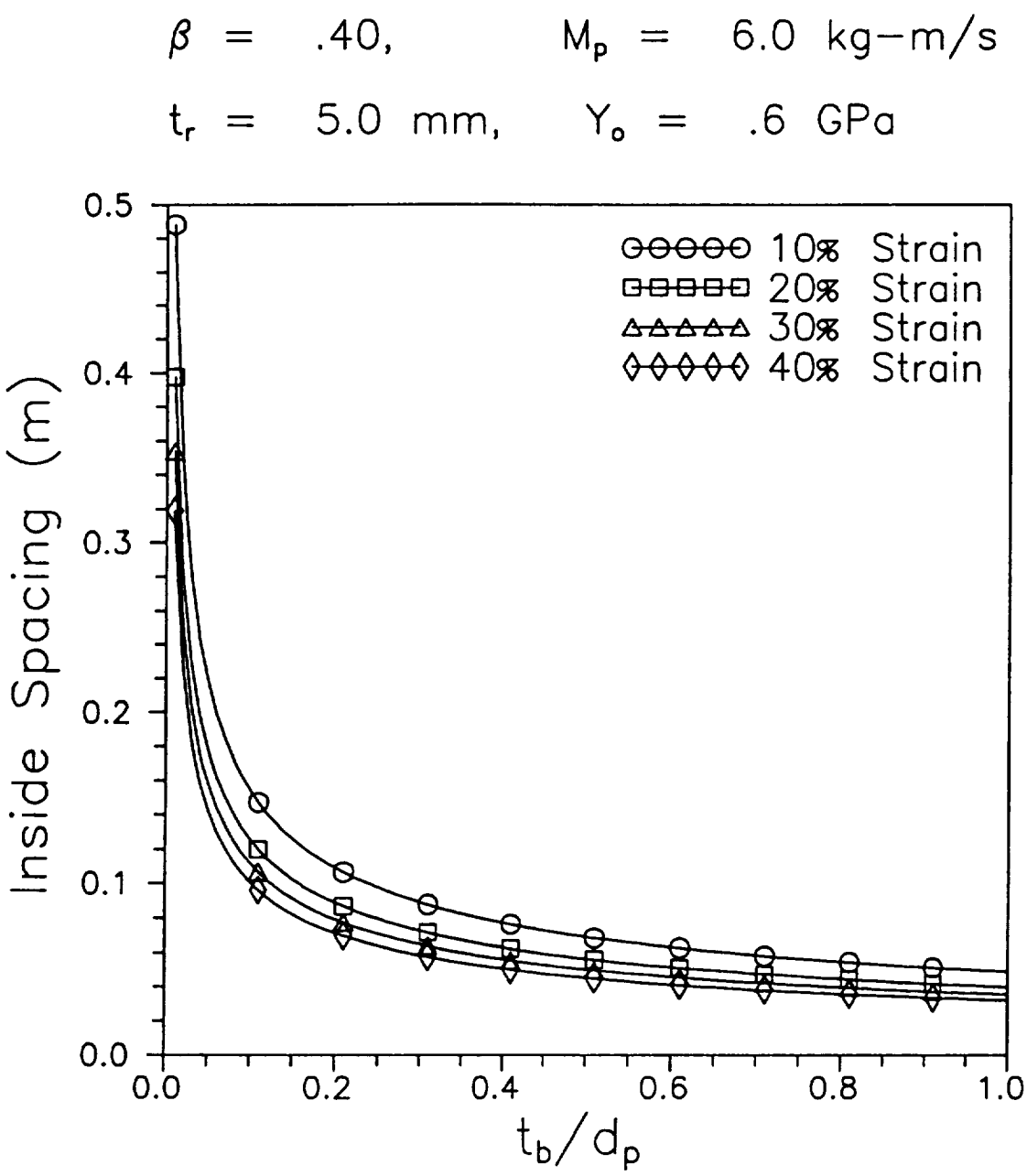

Figure 39. Design Curves for $\beta = 0.4$, $M_p = 6$ kg-m/s, $t_r = 5$ mm, and $Y_r = 0.6$ GPa

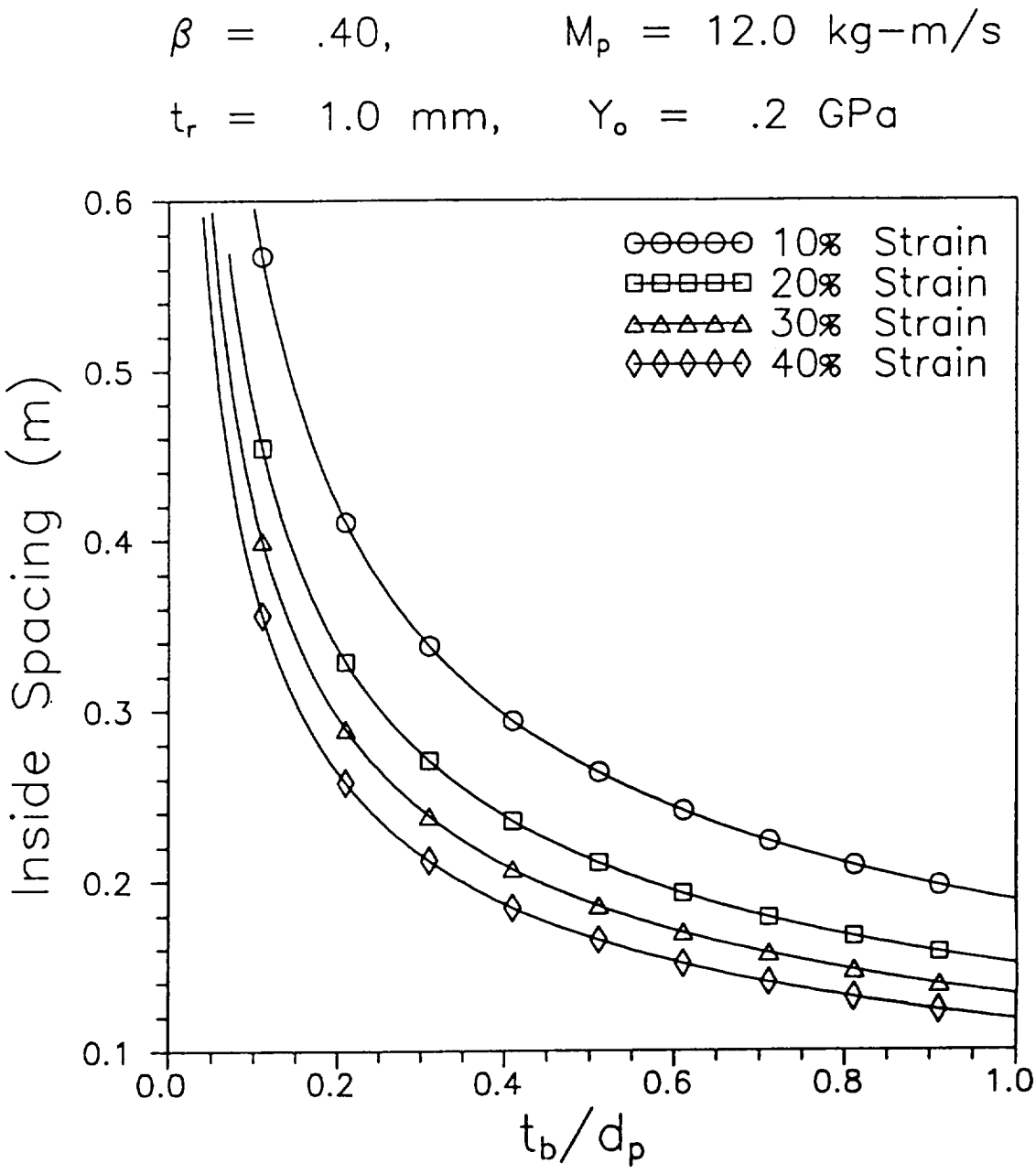

Figure 40. Design Curves for $\beta = 0.4$, $M_p = 12$ kg-m/s, $t_r = 1$ mm, and $Y_r = 0.2$ GPa

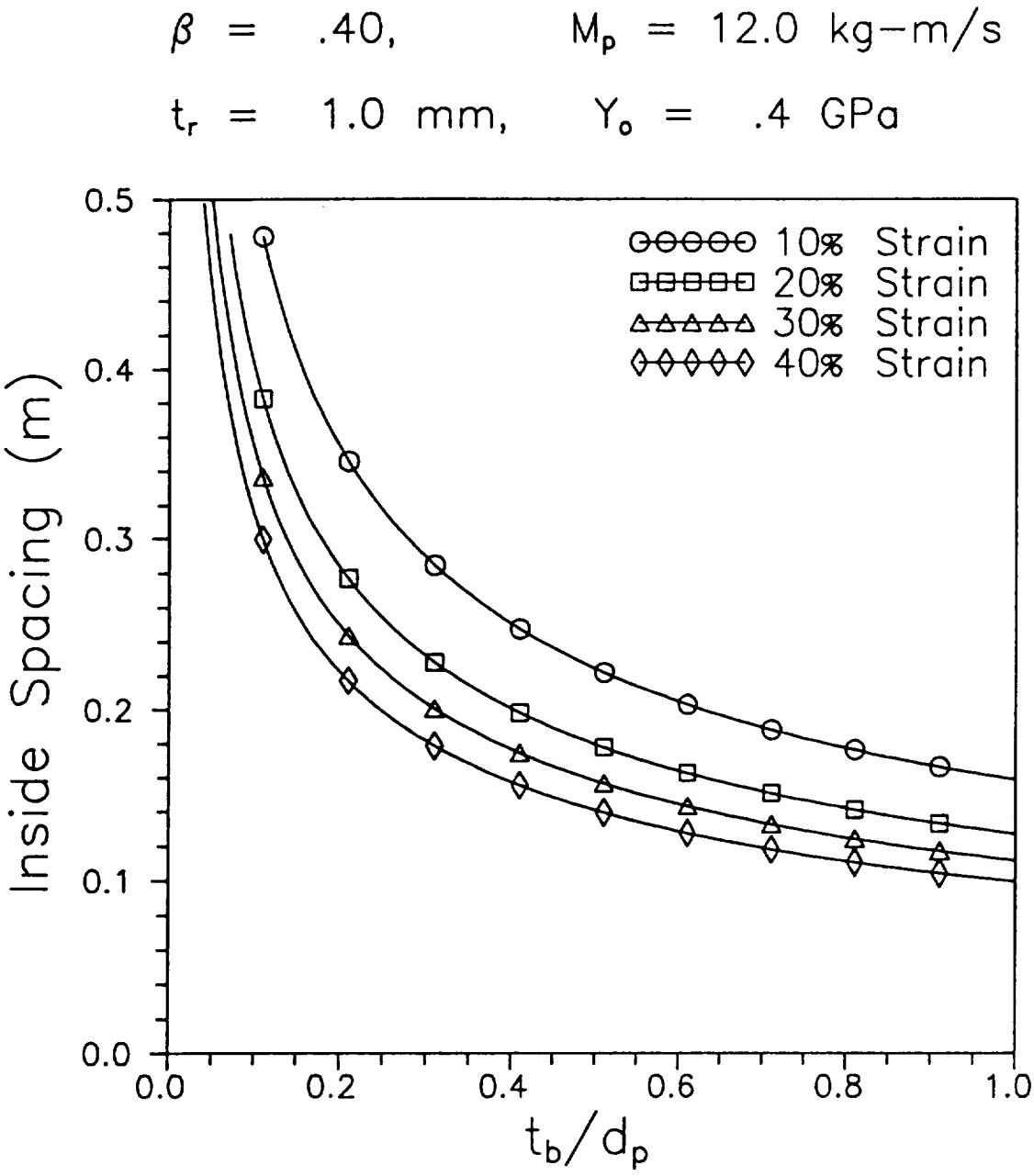

Figure 41. Design Curves for $\beta = 0.4$, $M_p = 12$ kg-m/s, $t_r = 1$ mm, and $Y_r = 0.4$ GPa

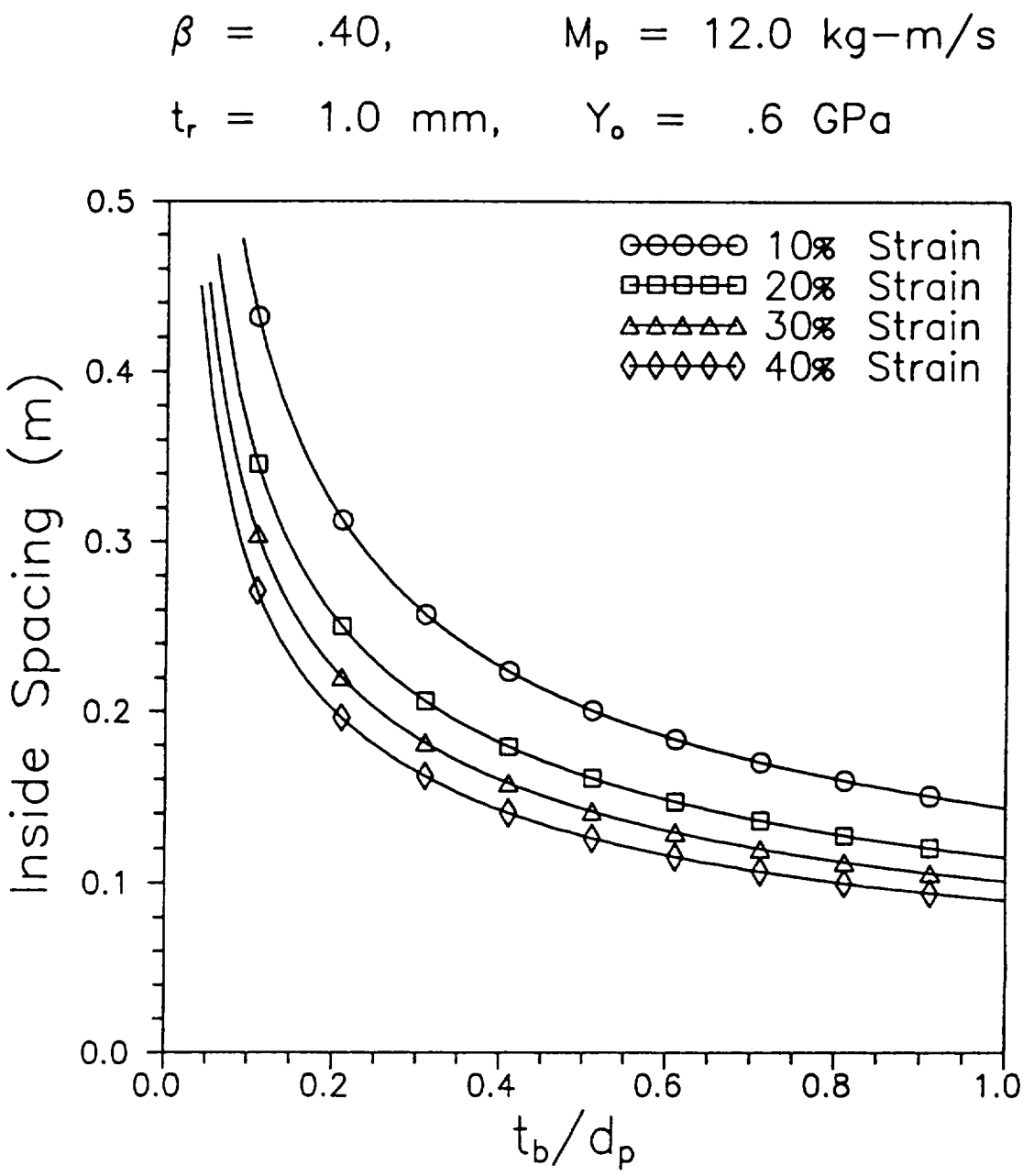

Figure 42. Design Curves for $\beta = 0.4$, $M_p = 12$ kg-m/s, $t_r = 1$ mm, and $Y_r = 0.6$ GPa

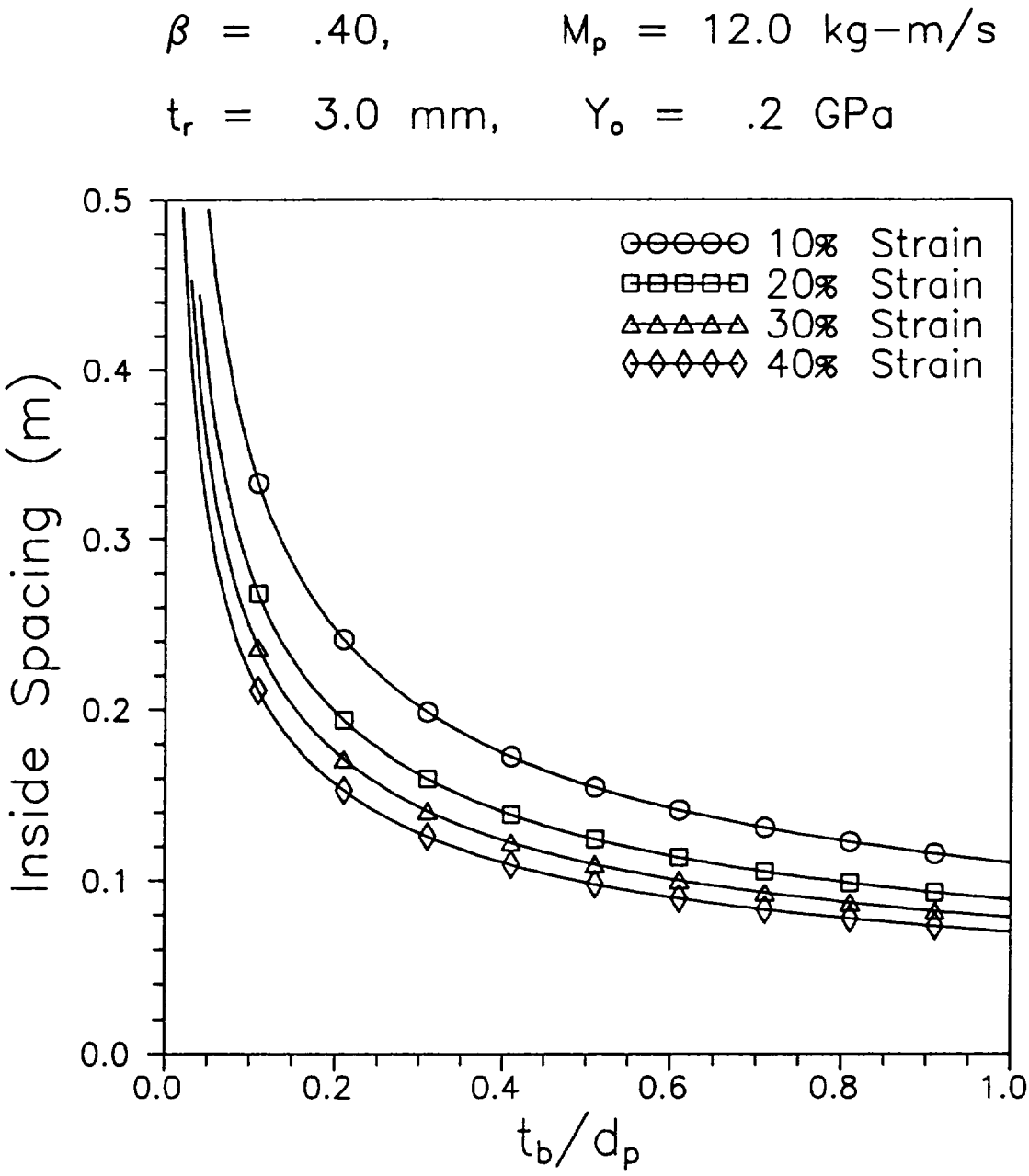

Figure 43. Design Curves for $\beta = 0.4$, $M_p = 12$ kg-m/s, $t_r = 3$ mm, and $Y_r = 0.2$ GPa

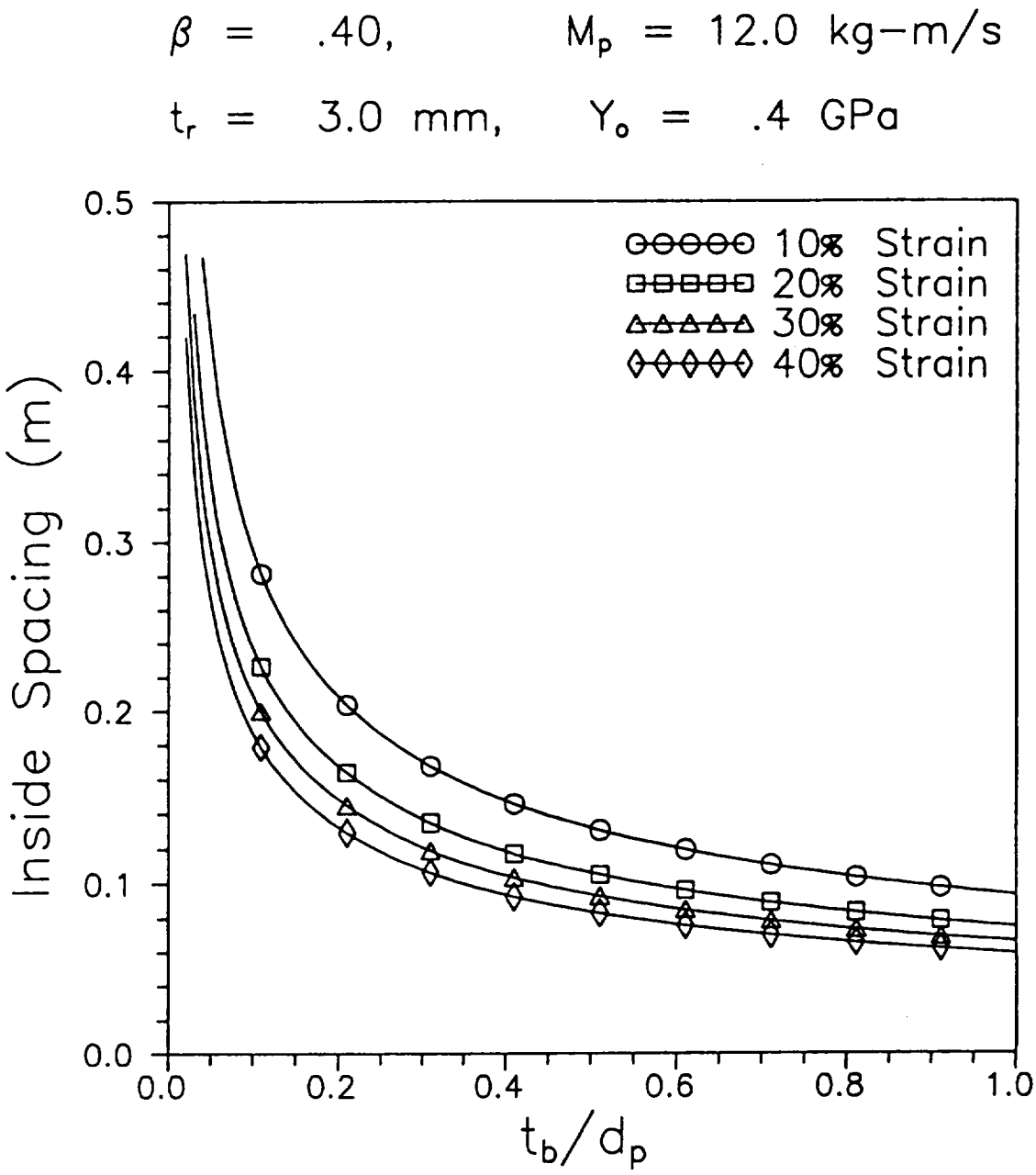

Figure 44. Design Curves for $\beta = 0.4$, $M_p = 12$ kg-m/s, $t_r = 3$ mm, and $Y_r = 0.4$ GPa

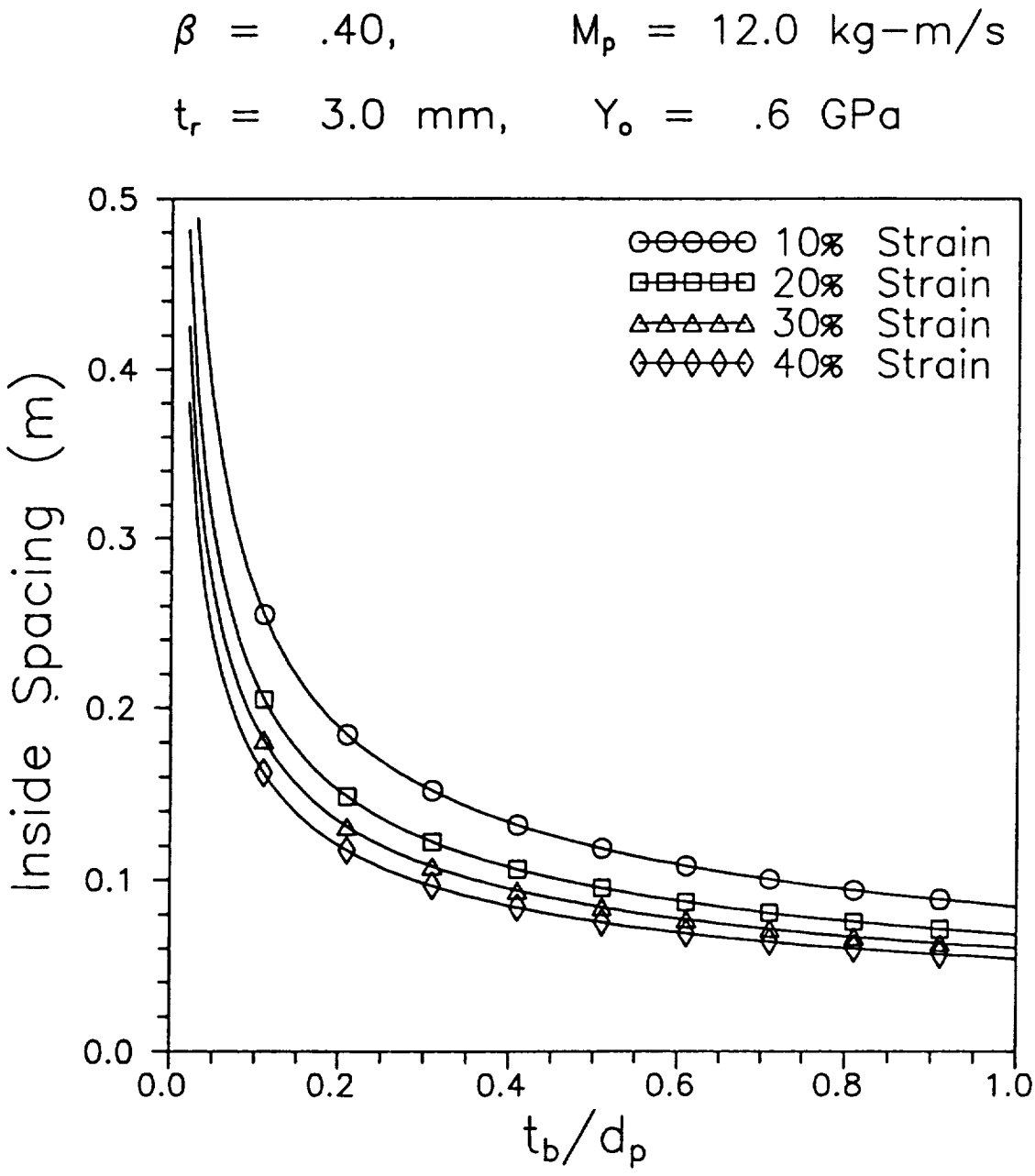

Figure 45. Design Curves for $\beta = 0.4$, $M_p = 12$ kg-m/s, $t_r = 3$ mm, and $Y_r = 0.6$ GPa

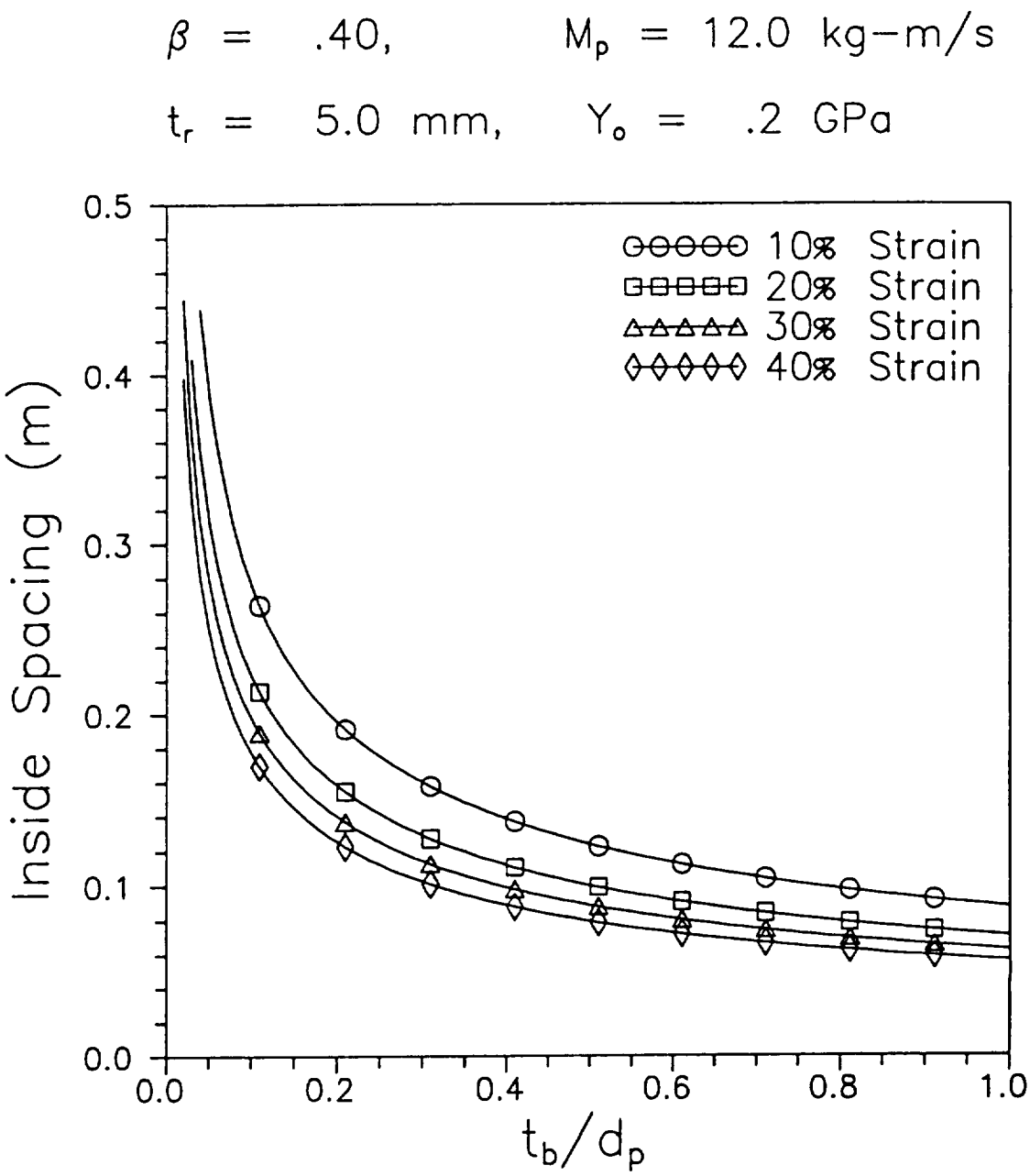

Figure 46. Design Curves for β = 0.4, M_p = 12 kg-m/s, t_r = 5 mm, and Y_r = 0.2 GPa

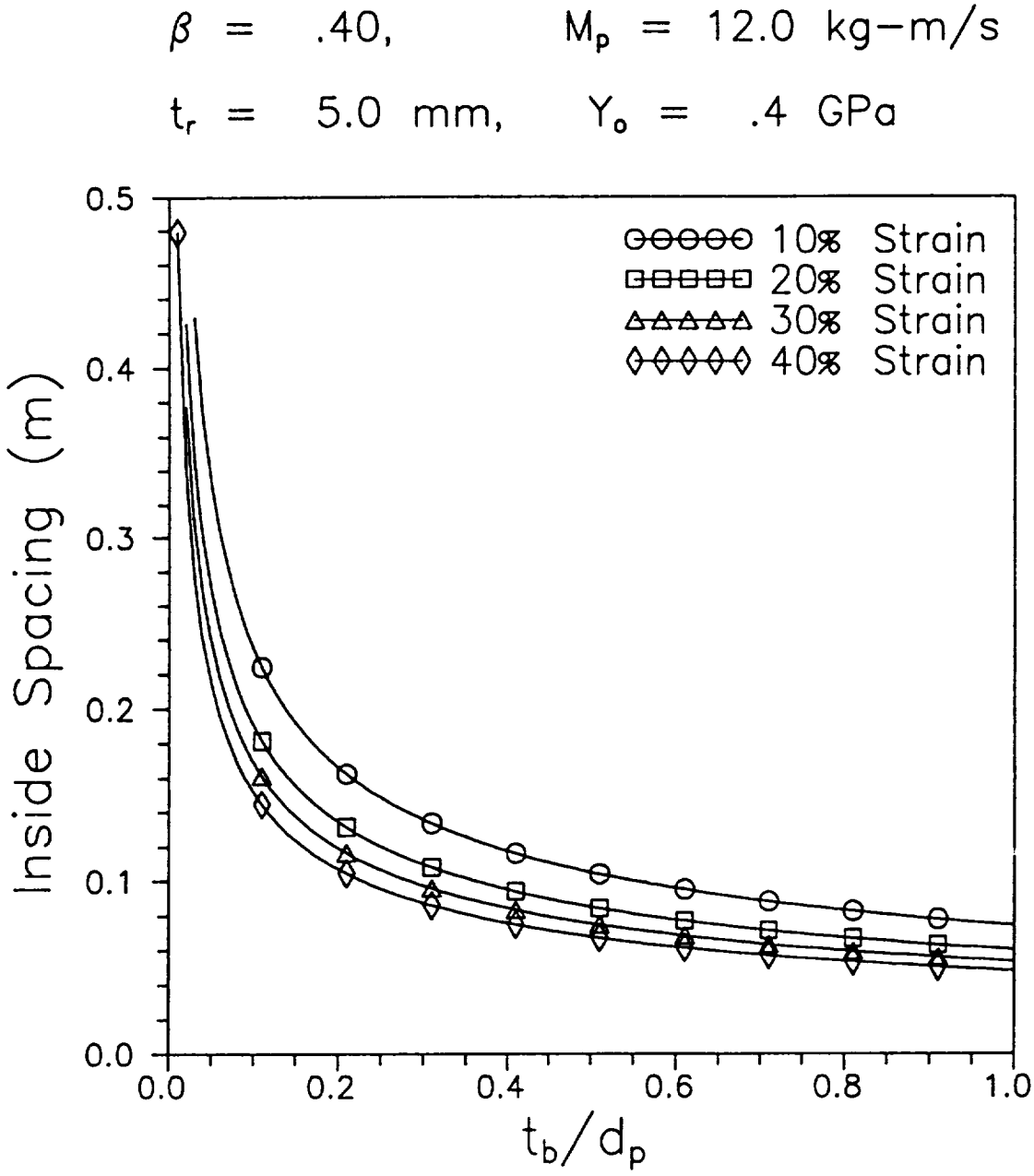

Figure 47. Design Curves for $\beta = 0.4$, $M_p = 12$ kg-m/s, $t_r = 5$ mm, and $Y_r = 0.4$ GPa

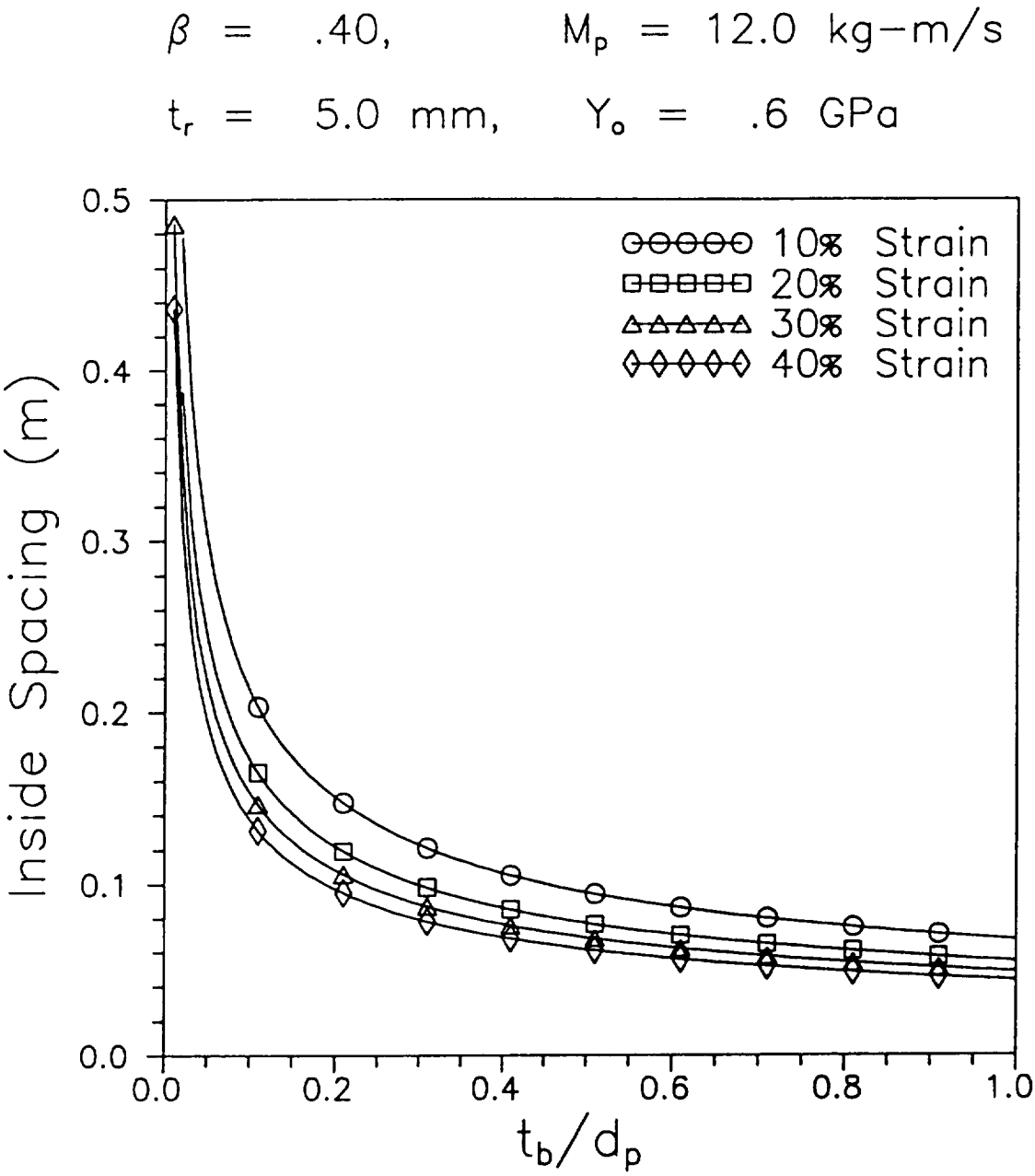

Figure 48. Design Curves for $\beta = 0.4$, $M_p = 12$ kg-m/s, $t_r = 5$ mm, and $Y_r = 0.6$ GPa

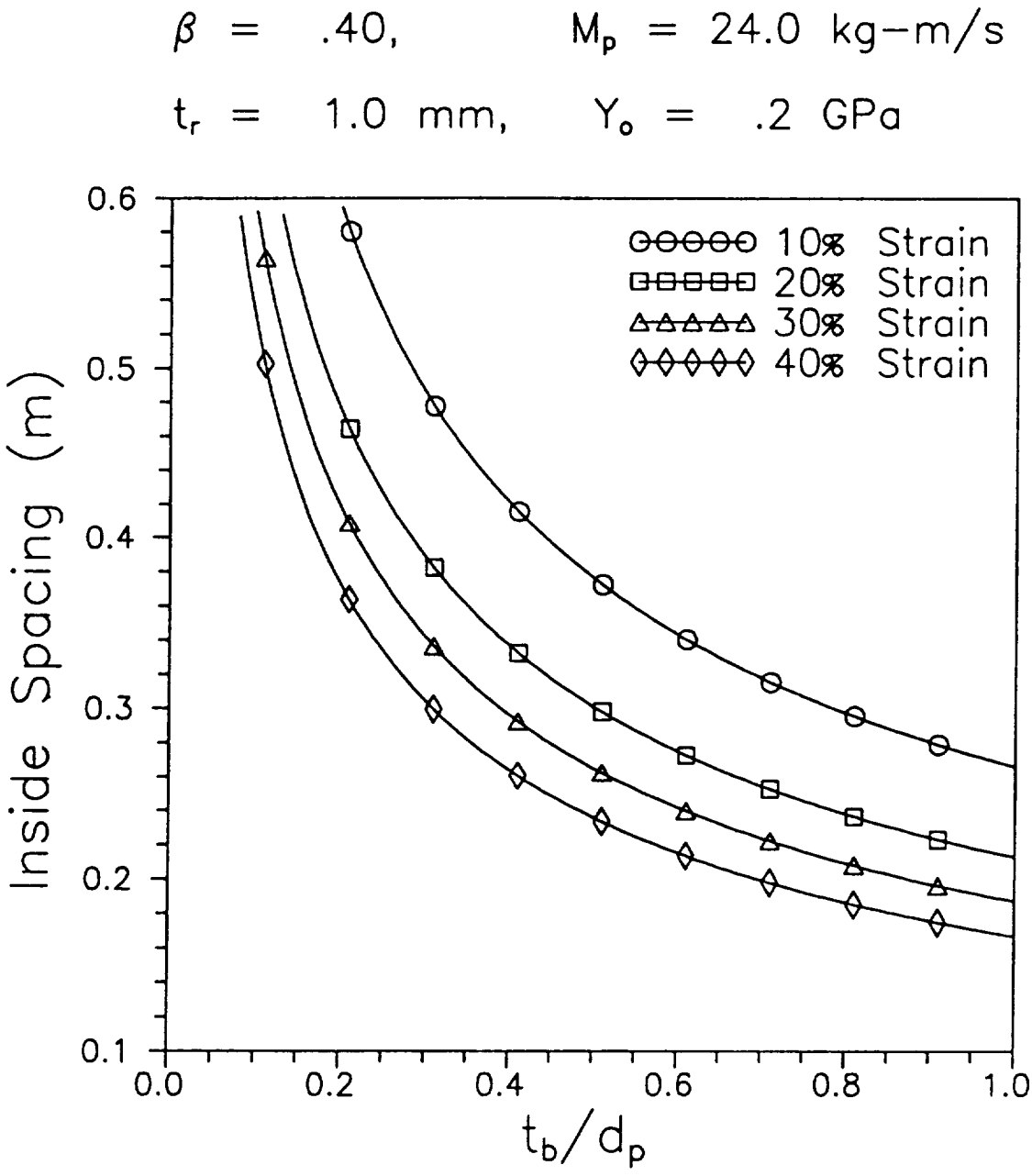

Figure 49. Design Curves for $\beta = 0.4$, $M_p = 24$ kg-m/s, $t_r = 1$ mm, and $Y_r = 0.2$ GPa

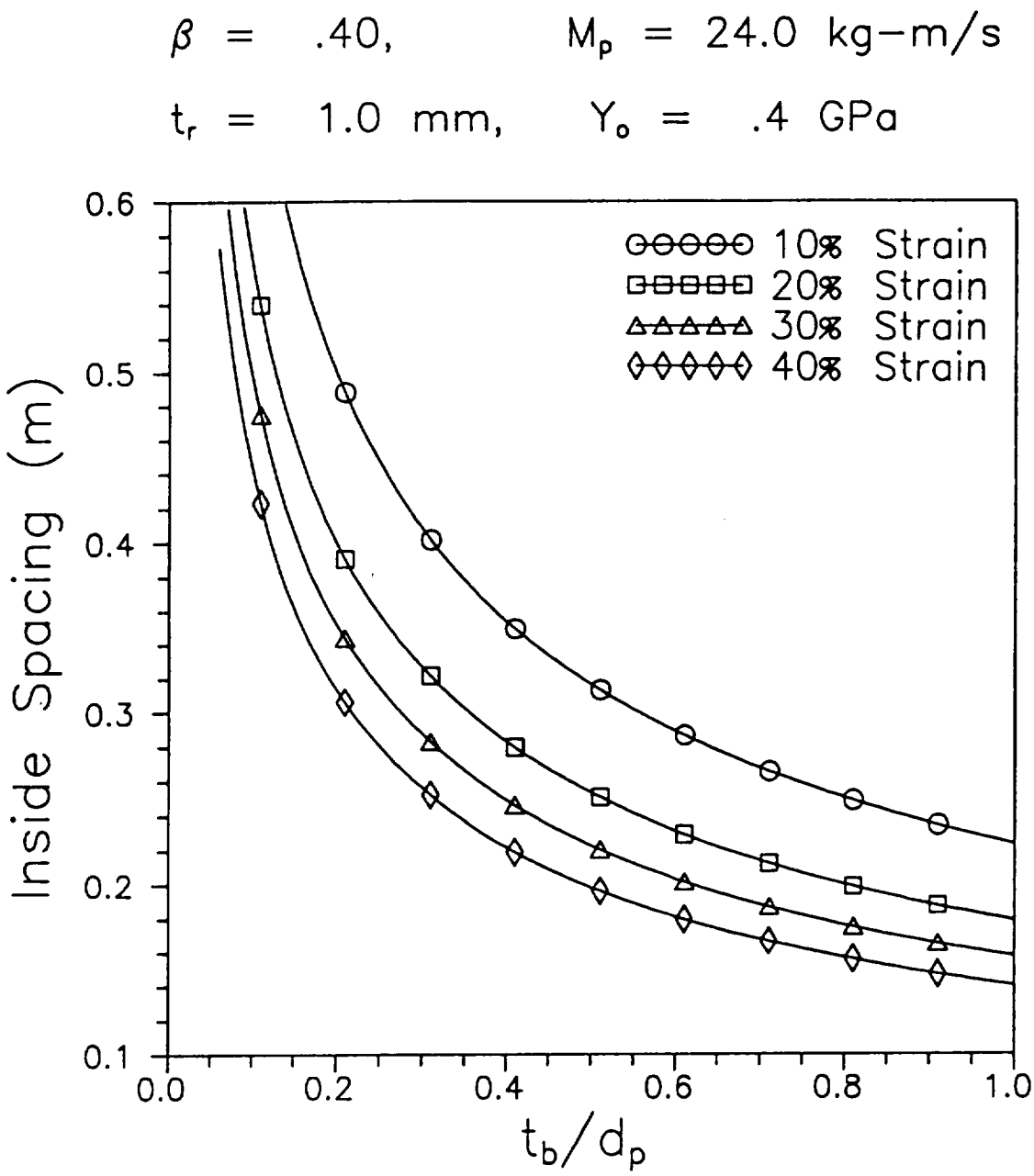

Figure 50. Design Curves for $\beta = 0.4$, $M_p = 24$ kg-m/s, $t_r = 1$ mm, and $Y_r = 0.4$ GPa

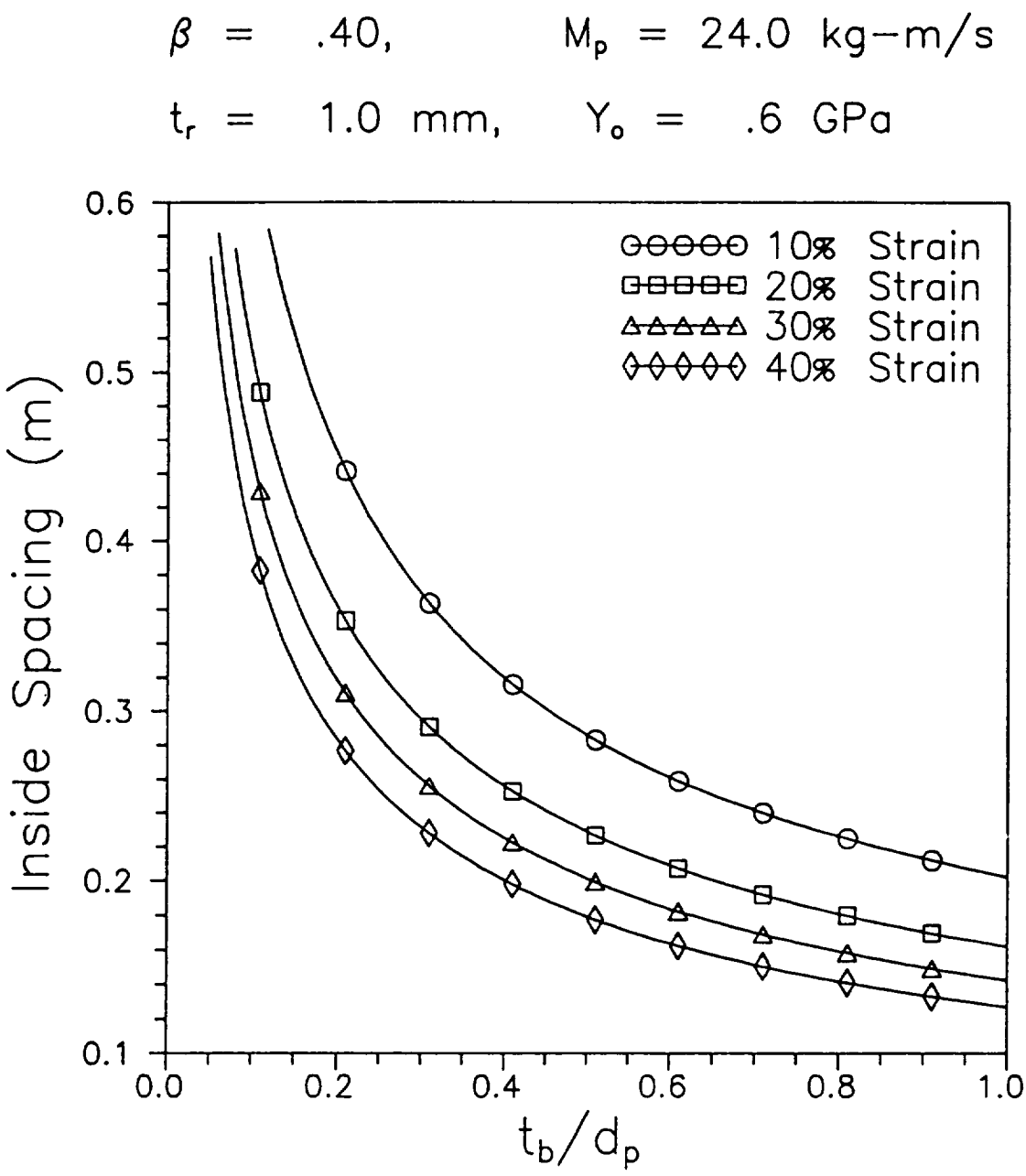

Figure 51. Design Curves for $\beta = 0.4$, $M_p = 24$ kg-m/s, $t_r = 1$ mm, and $Y_r = 0.6$ GPa

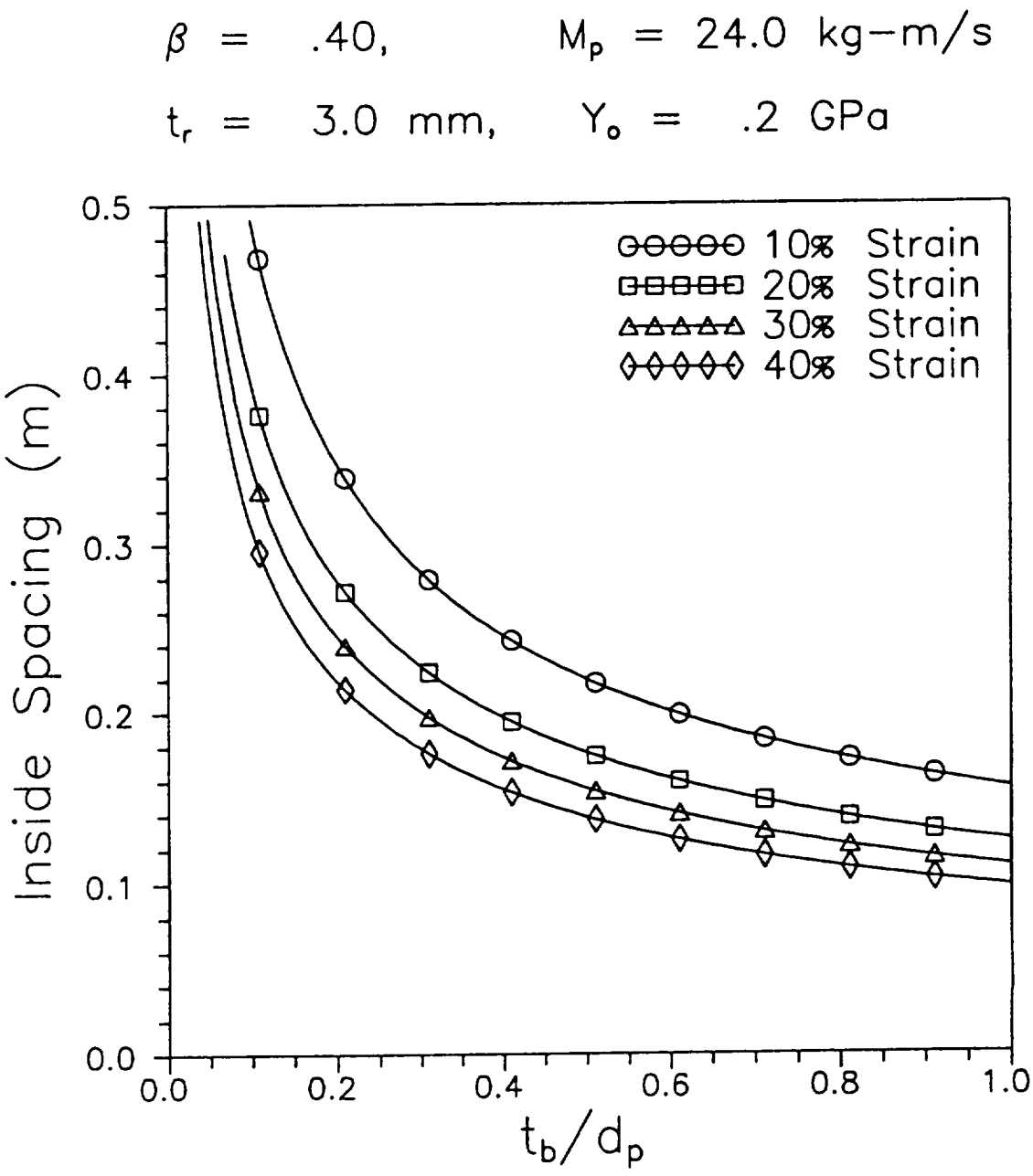

Figure 52. Design Curves for $\beta = 0.4$, $M_p = 24$ kg-m/s, $t_r = 3$ mm, and $Y_r = 0.2$ GPa

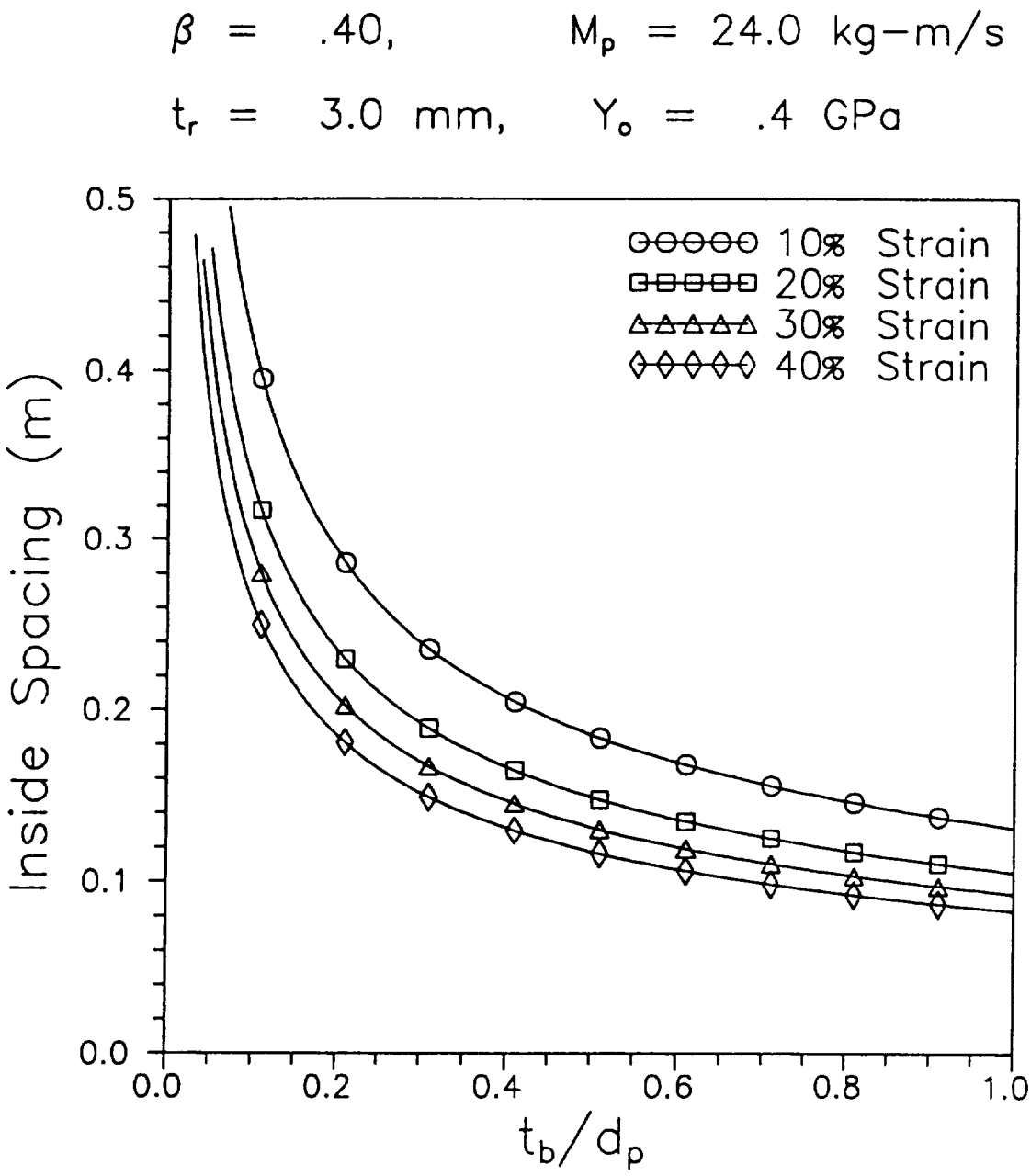

Figure 53. Design Curves for $\beta = 0.4$, $M_p = 24$ kg-m/s, $t_r = 3$ mm, and $Y_r = 0.4$ GPa

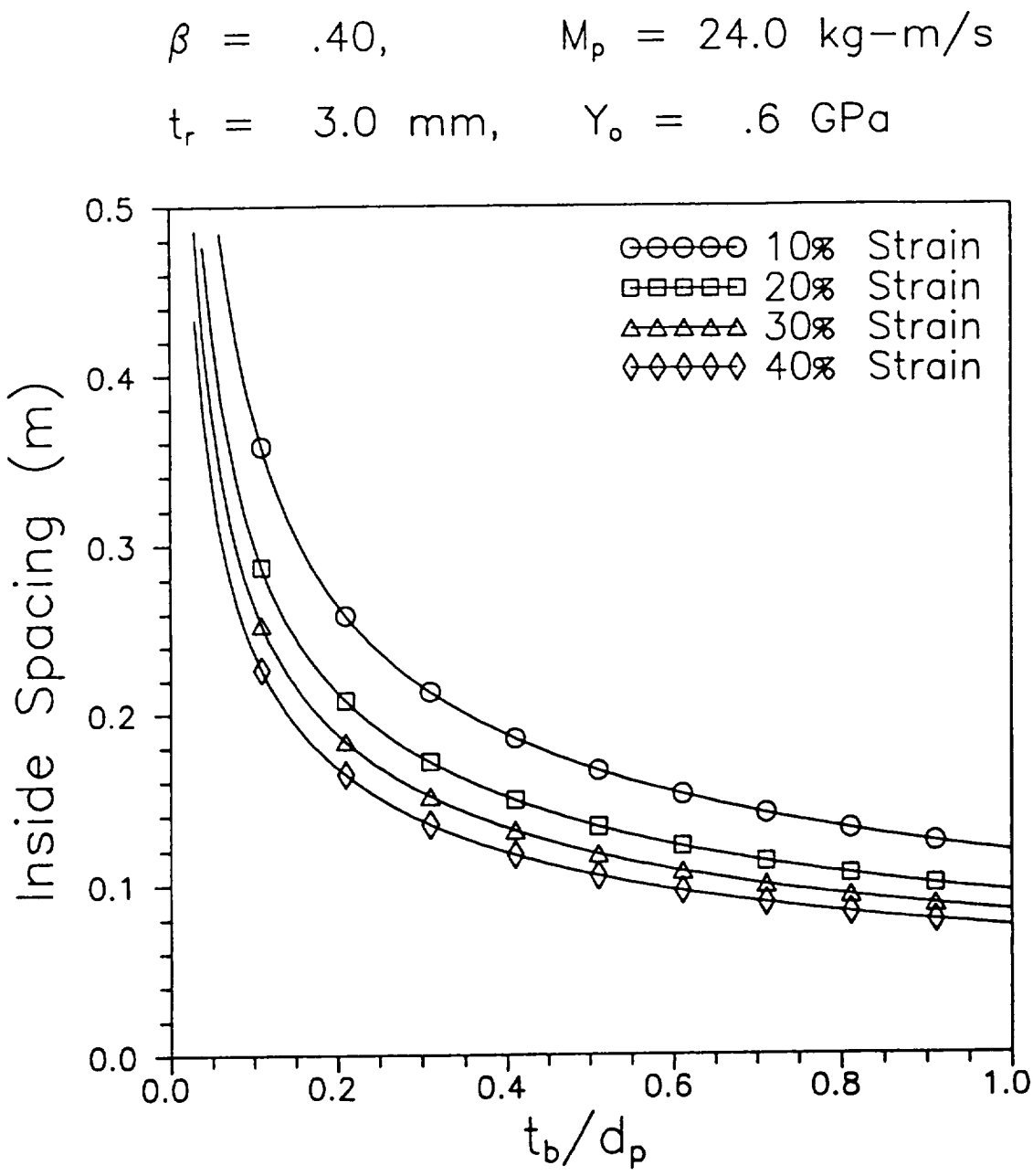

Figure 54. Design Curves for β = 0.4, M_p = 24 kg-m/s, t_r = 3 mm, and Y_r = 0.6 GPa

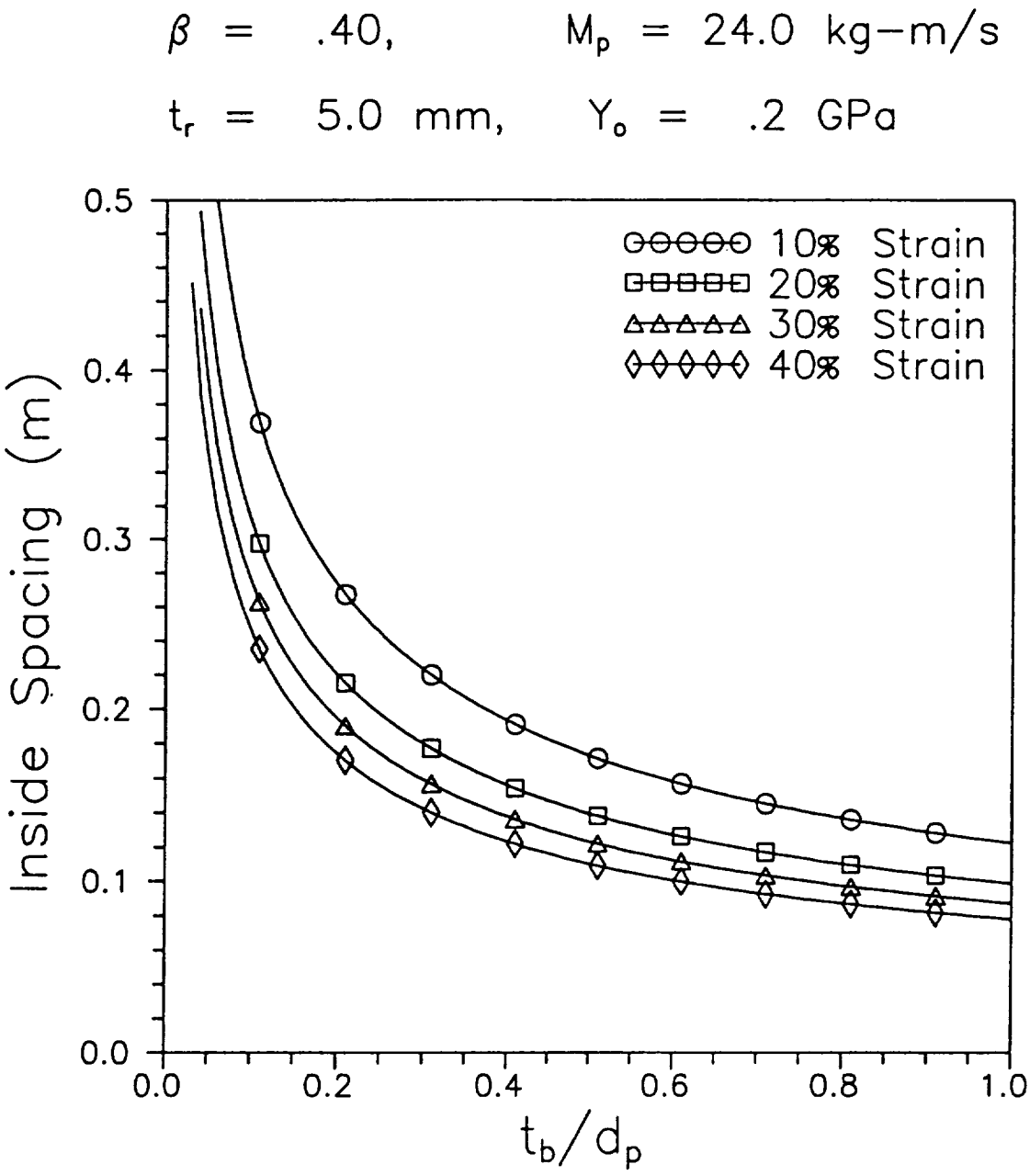

Figure 55. Design Curves for β = 0.4, M_p = 24 kg-m/s, t_r = 5 mm, and Y_r = 0.2 GPa

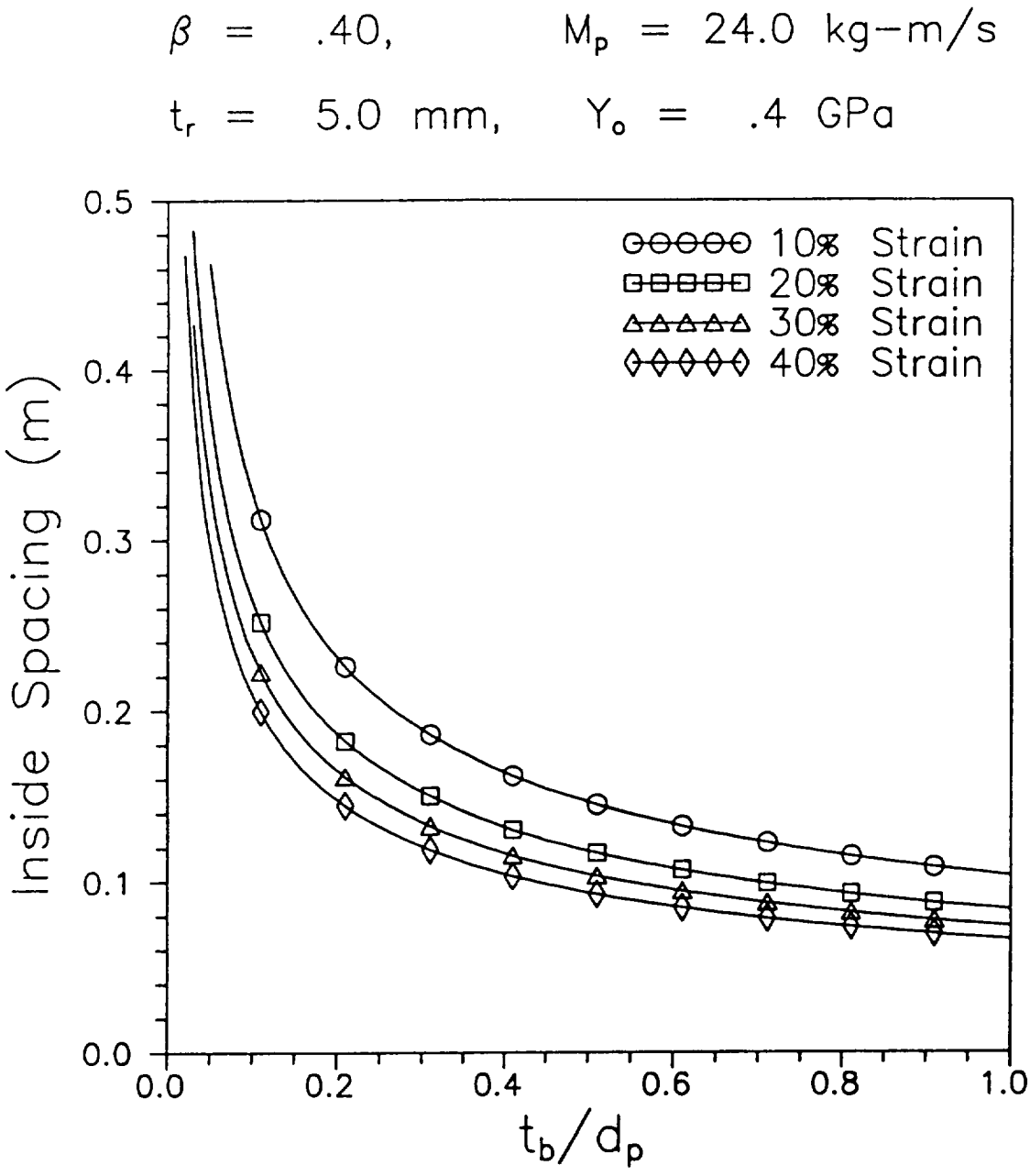

Figure 56. Design Curves for β = 0.4, M_p = 24 kg-m/s, t_r = 5 mm, and Y_r = 0.4 GPa

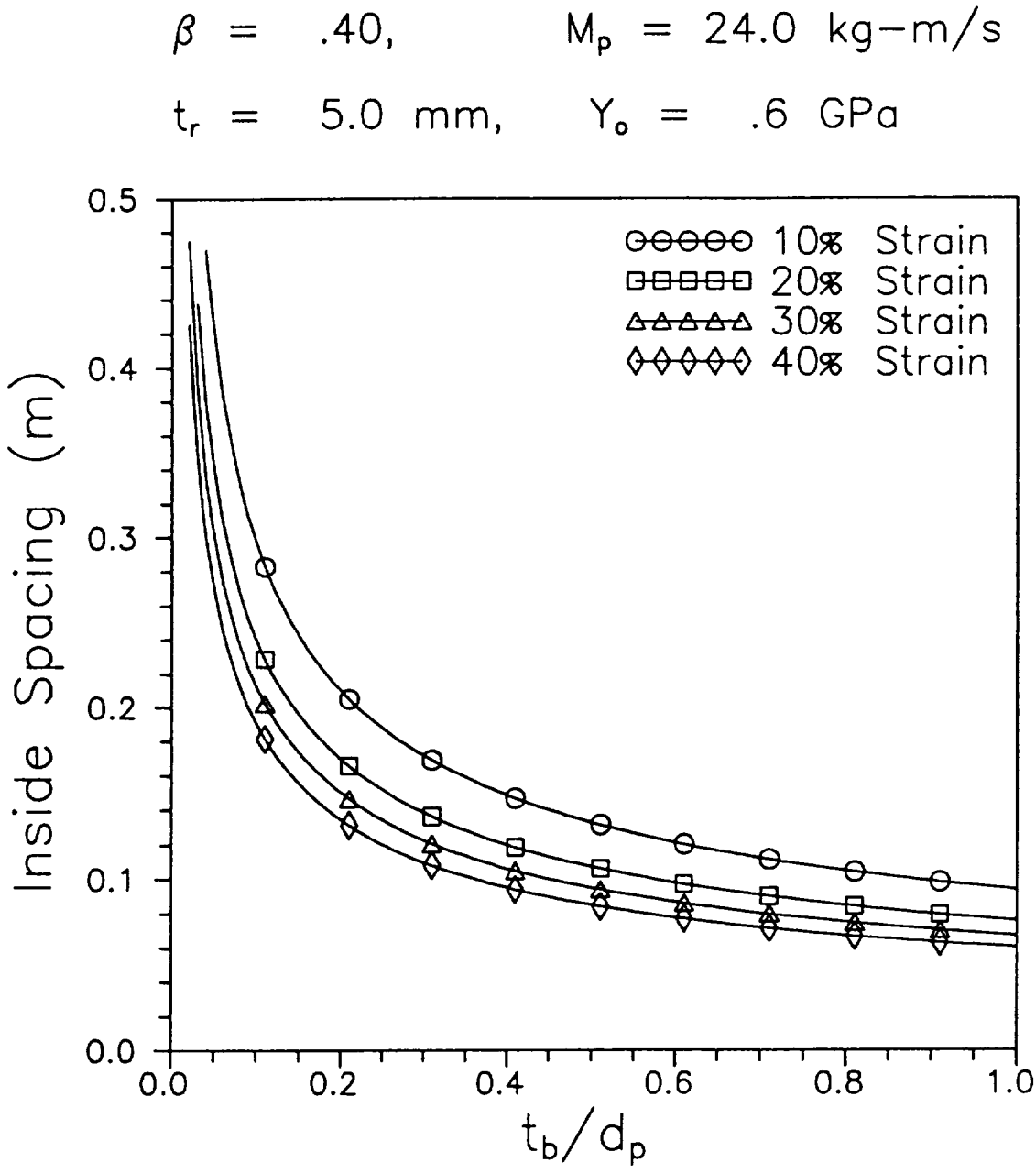

Figure 57. Design Curves for $\beta = 0.4$, $M_p = 24$ kg-m/s, $t_r = 5$ mm, and $Y_r = 0.6$ GPa

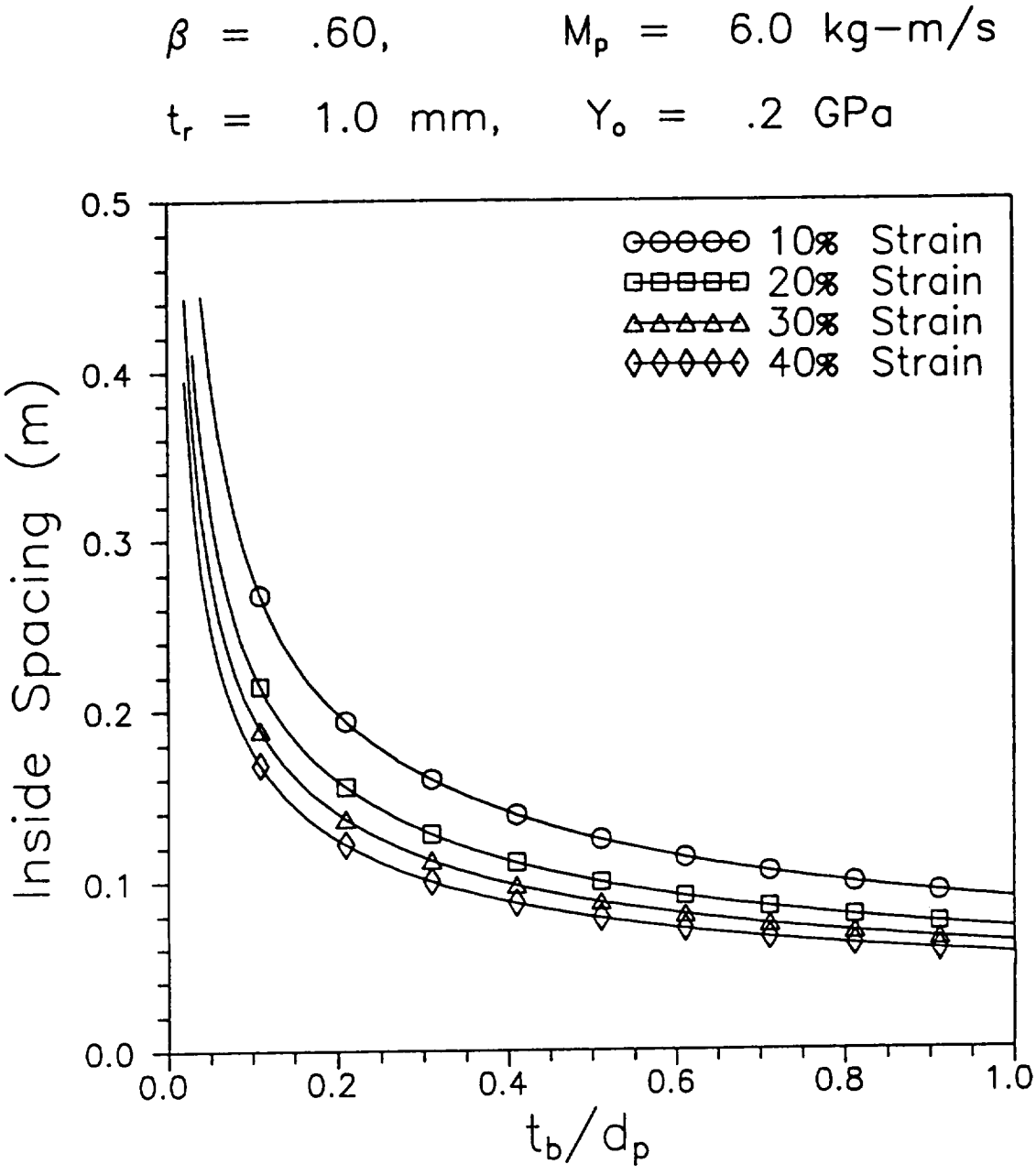

Figure 58. Design Curves for $\beta = 0.6$, $M_p = 6$ kg-m/s, $t_r = 1$ mm, and $Y_r = 0.2$ GPa

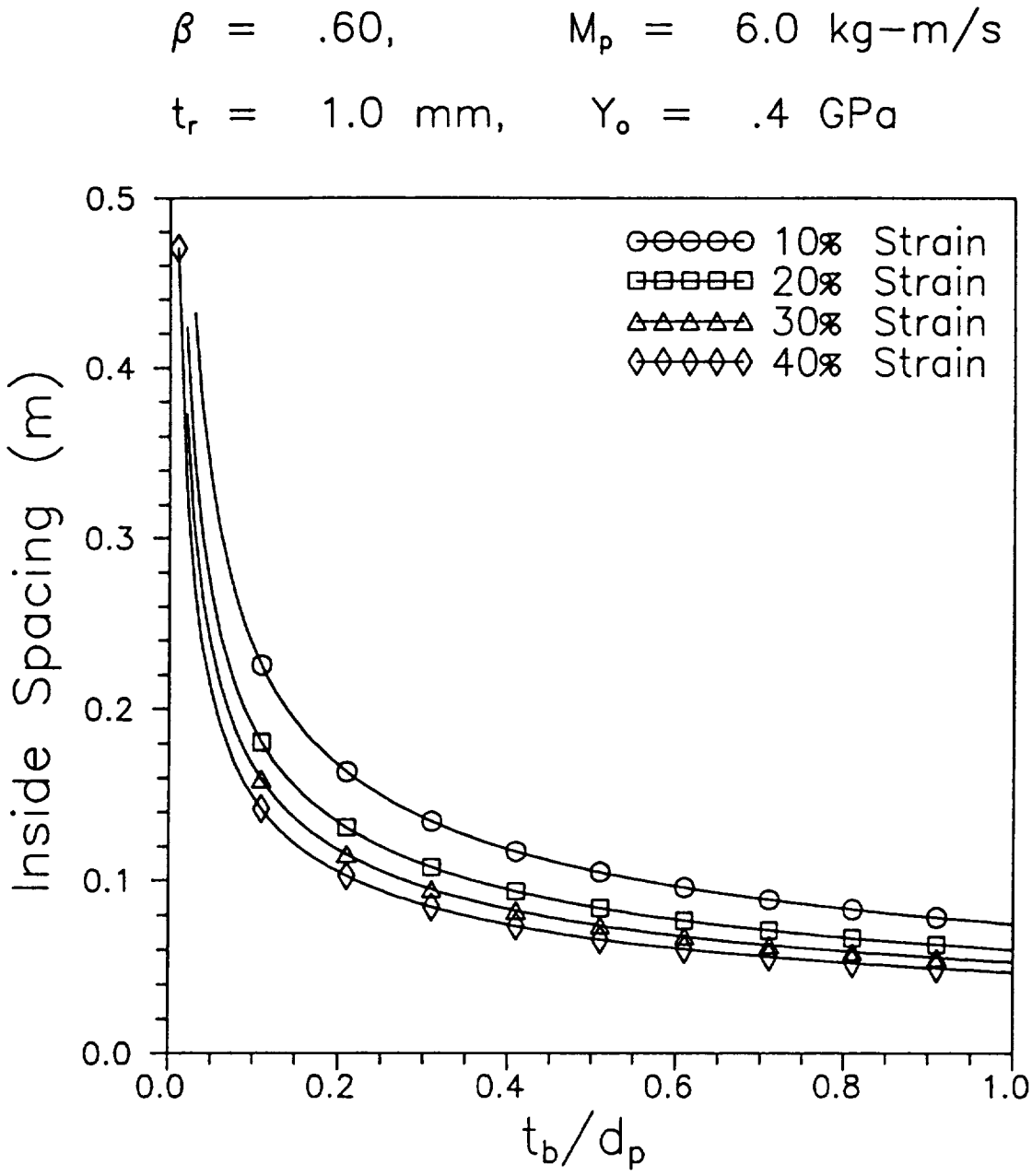

Figure 59. Design Curves for $\beta = 0.6$, $M_p = 6$ kg-m/s, $t_r = 1$ mm, and $Y_r = 0.4$ GPa

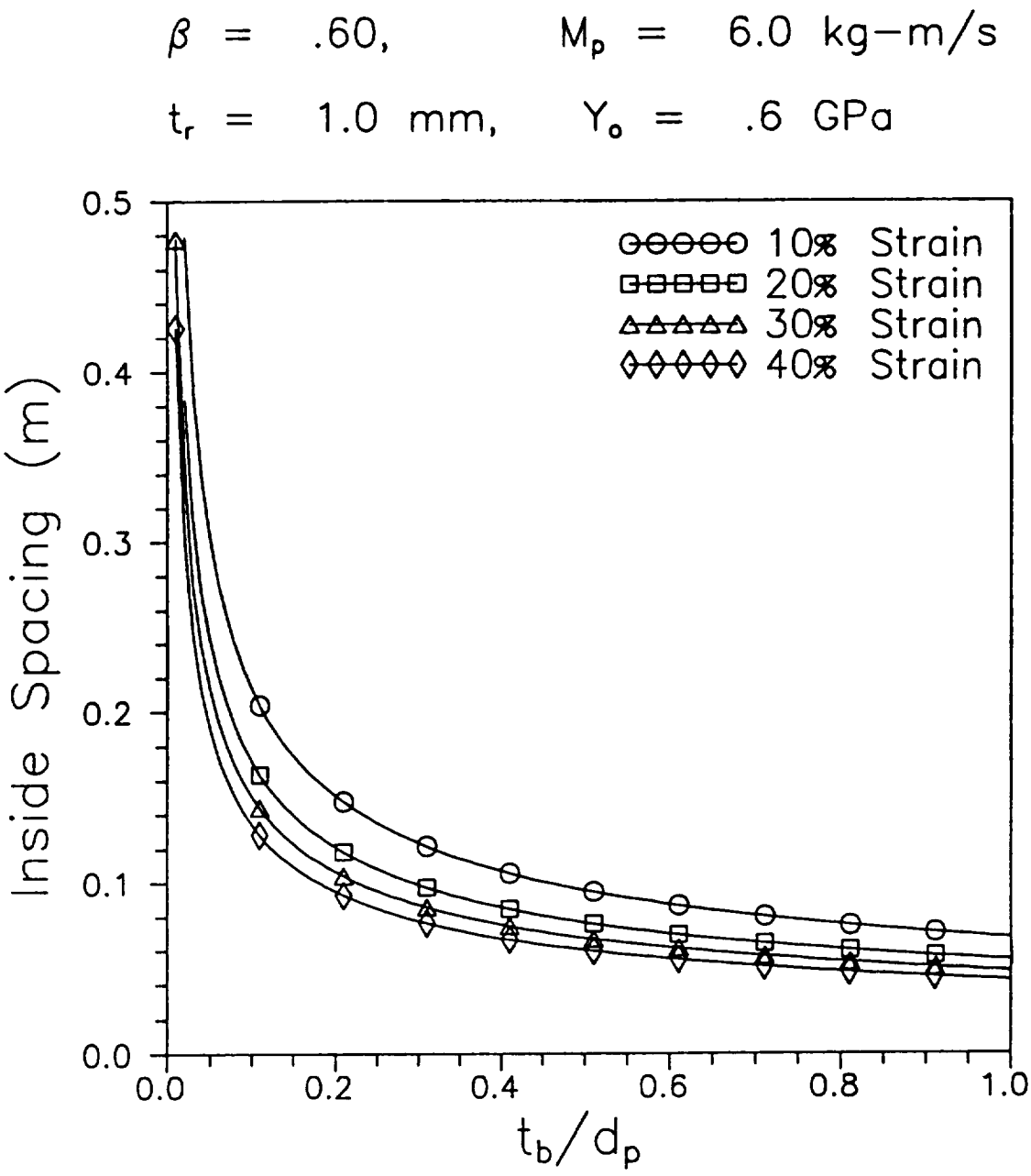

Figure 60. Design Curves for $\beta = 0.6$, $M_p = 6$ kg-m/s, $t_r = 1$ mm, and $Y_r = 0.6$ GPa

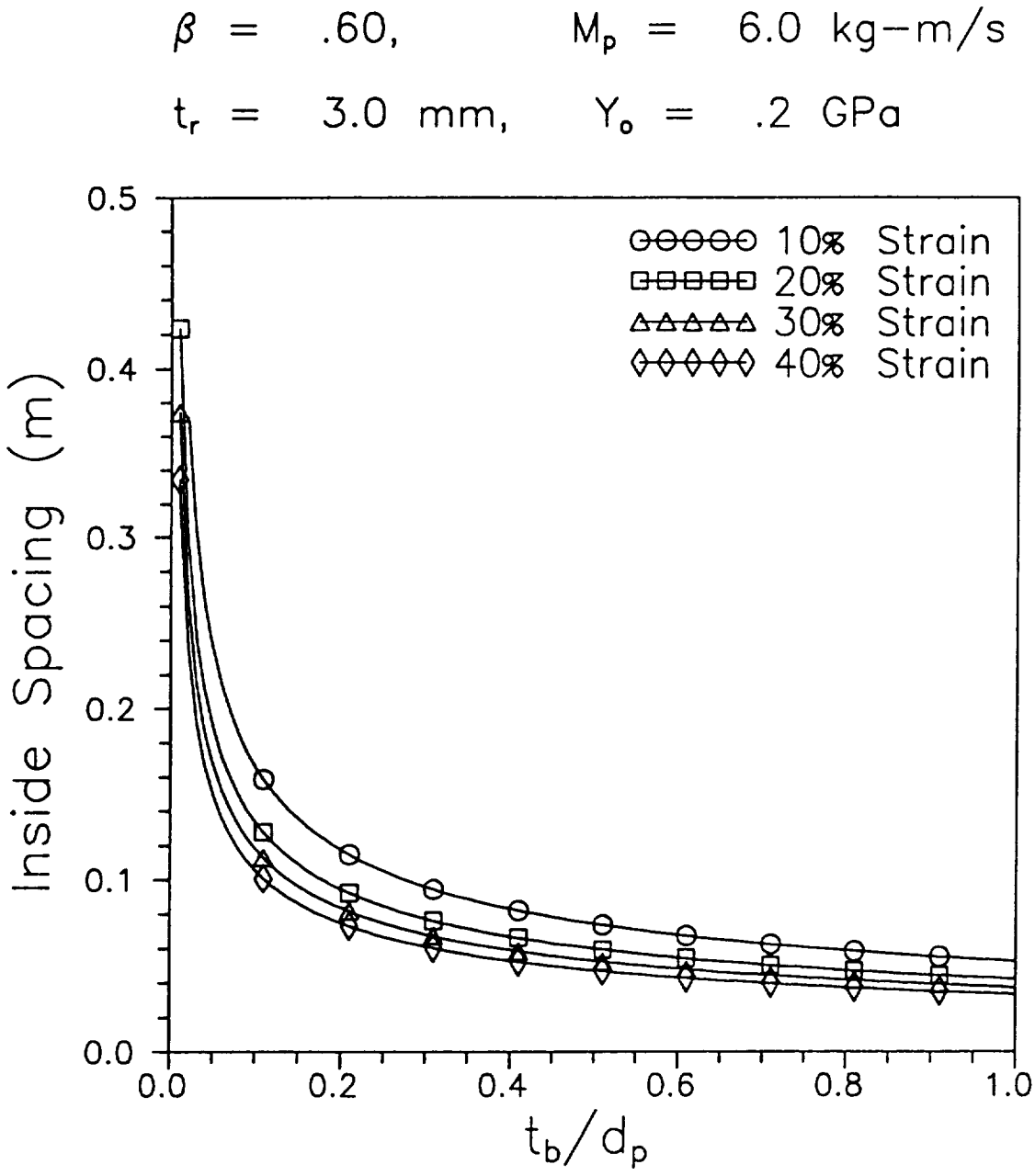

Figure 61. Design Curves for $\beta = 0.6$, $M_p = 6$ kg-m/s, $t_r = 3$ mm, and $Y_r = 0.2$ GPa

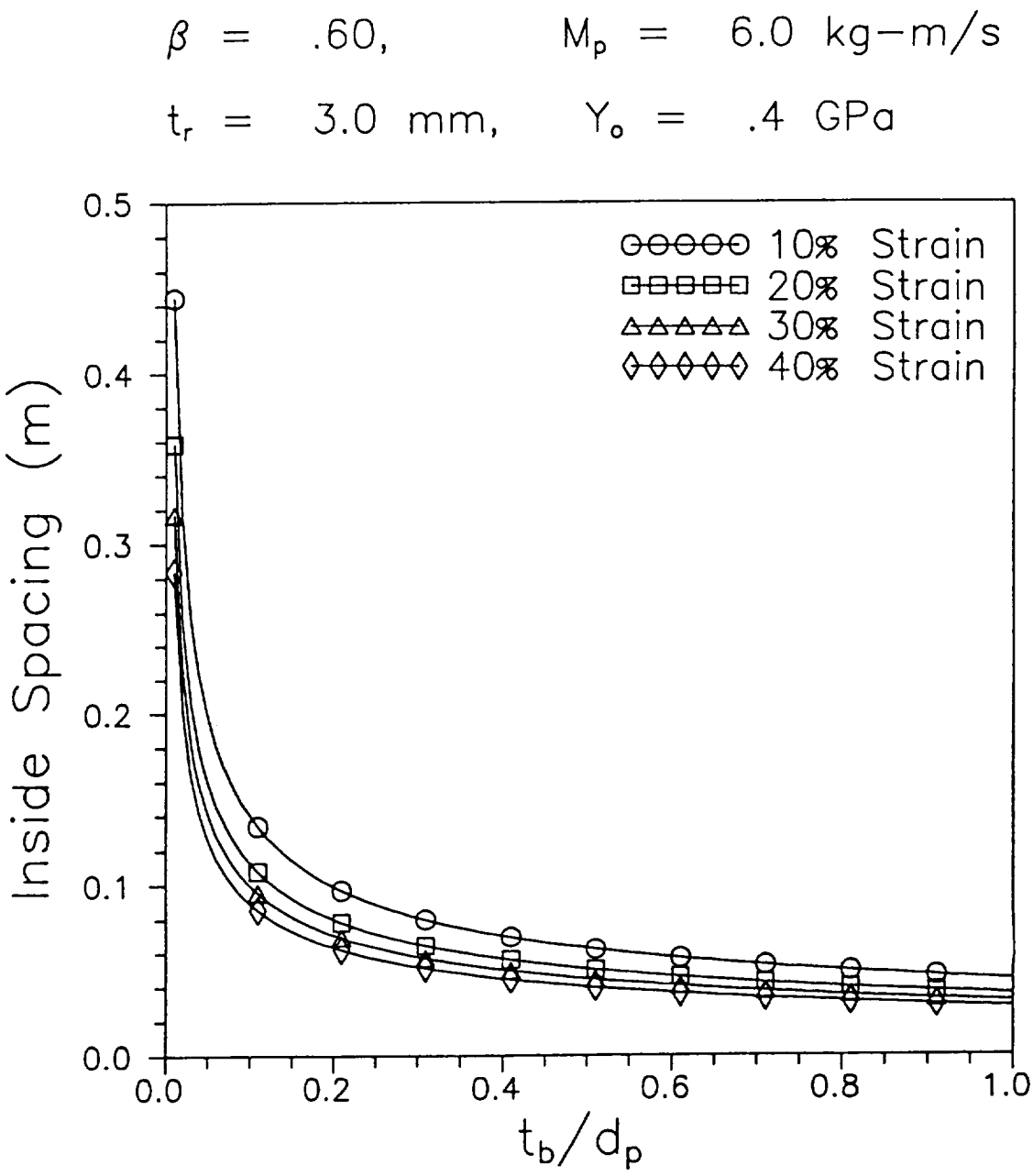

Figure 62. Design Curves for $\beta = 0.6$, $M_p = 6$ kg-m/s, $t_r = 3$ mm, and $Y_r = 0.4$ GPa

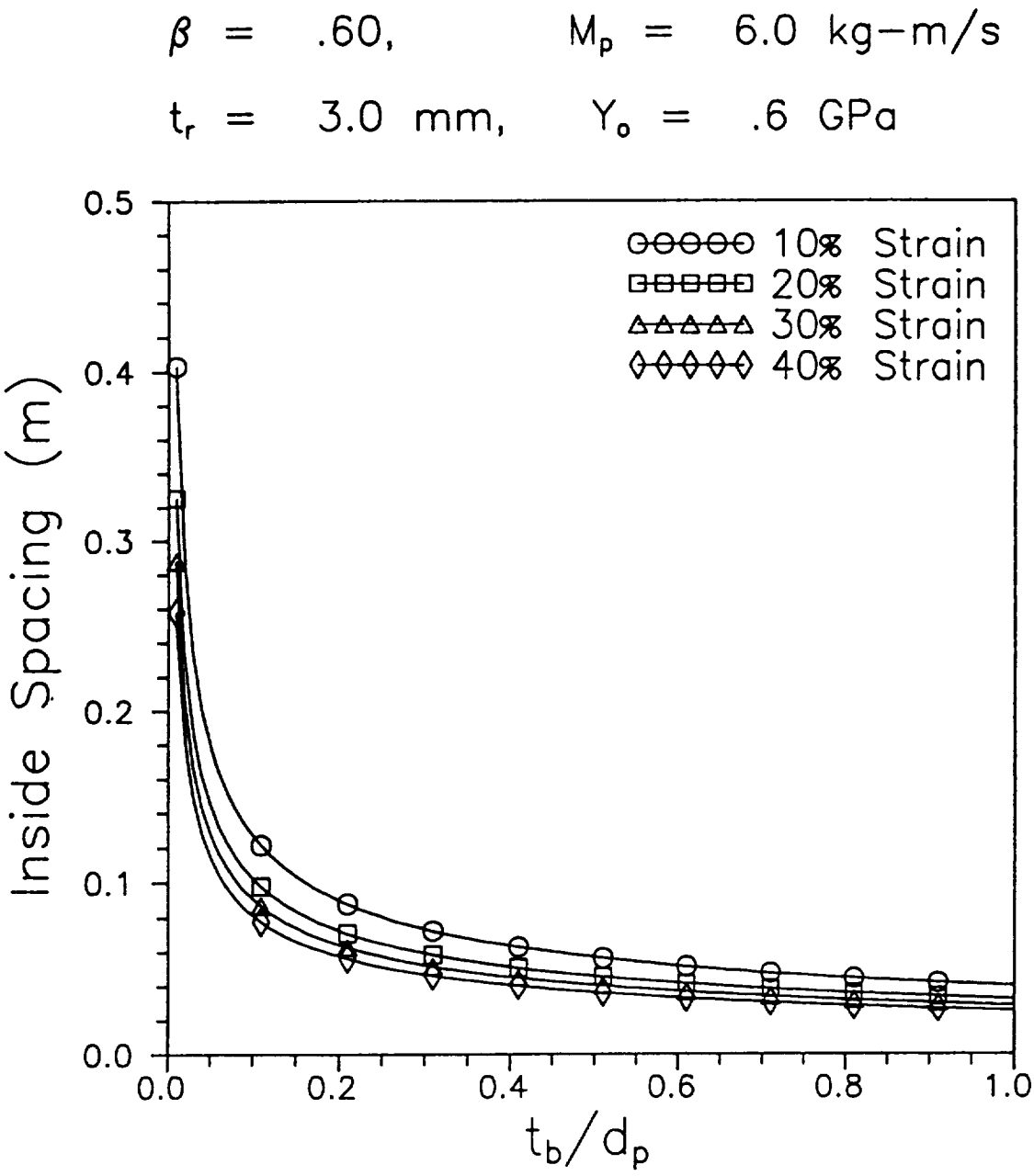

Figure 63. Design Curves for β = 0.6, M_p = 6 kg-m/s, t_r = 3 mm, and Y_r = 0.6 GPa

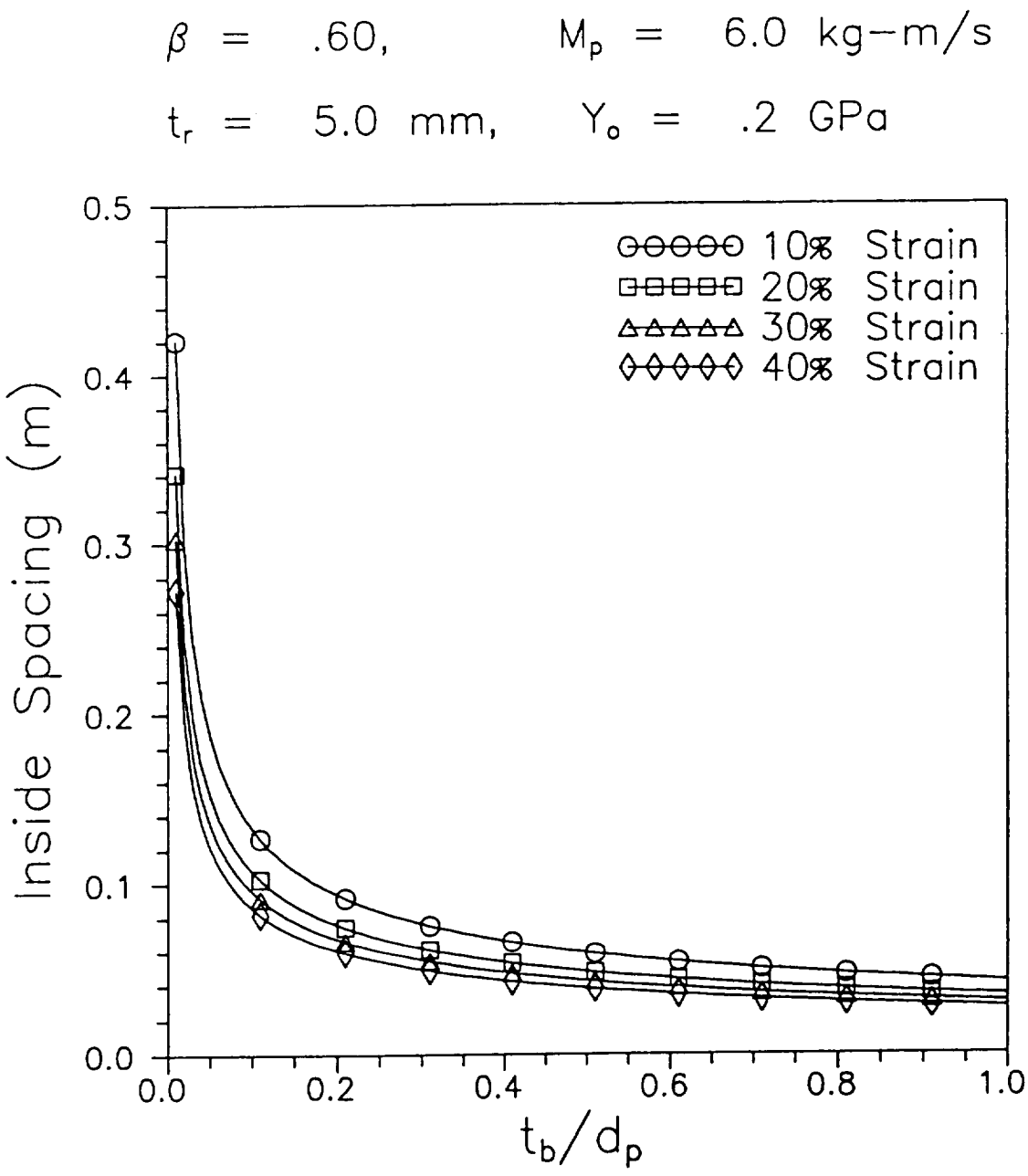

Figure 64. Design Curves for $\beta = 0.6$, $M_p = 6$ kg-m/s, $t_r = 5$ mm, and $Y_r = 0.2$ GPa

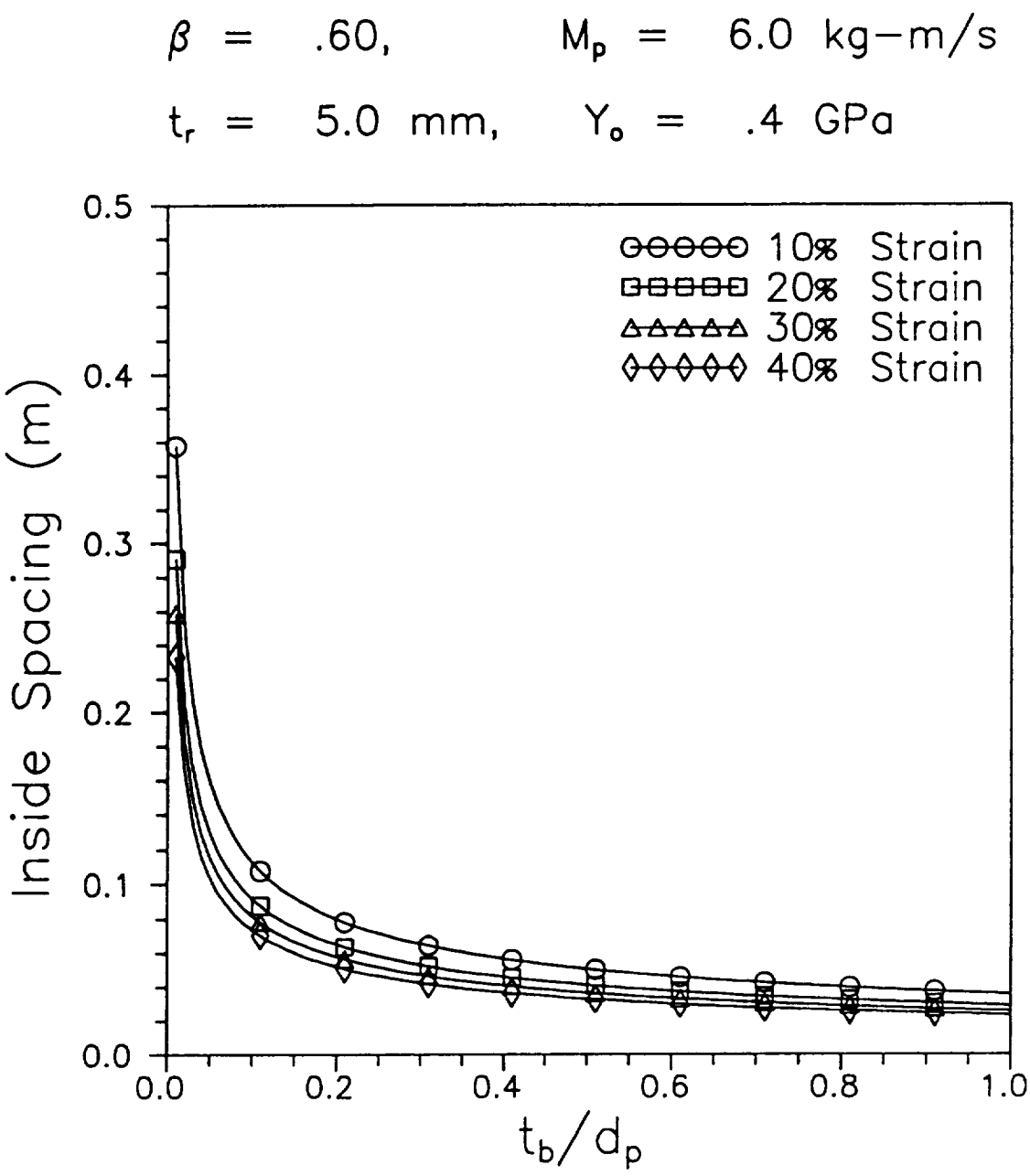

Figure 65. Design Curves for $\beta = 0.6$, $M_p = 6$ kg-m/s, $t_r = 5$ mm, and $Y_r = 0.4$ GPa

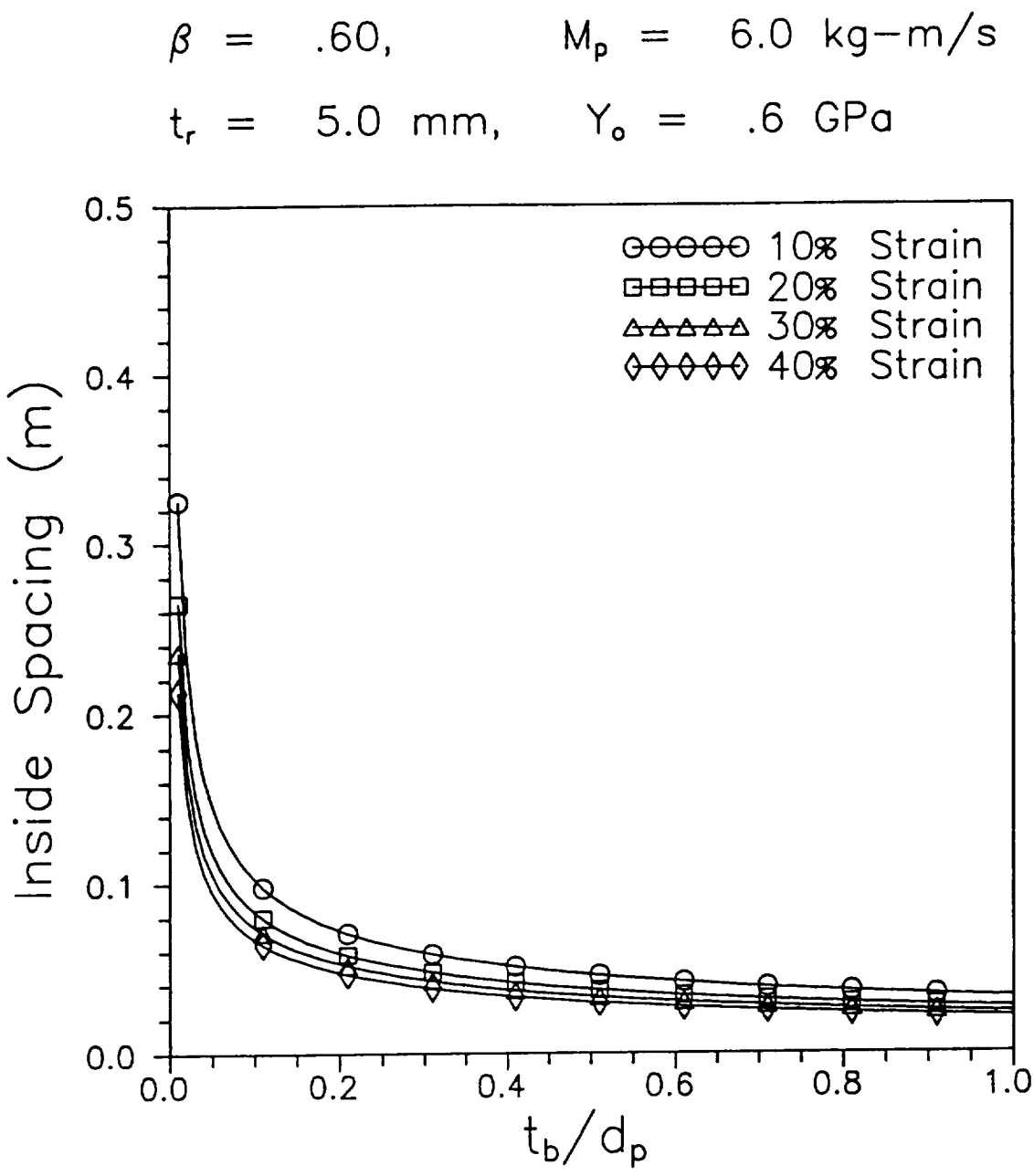

Figure 66. Design Curves for $\beta = 0.6$, $M_p = 6$ kg-m/s, $t_r = 5$ mm, and $Y_r = 0.6$ GPa

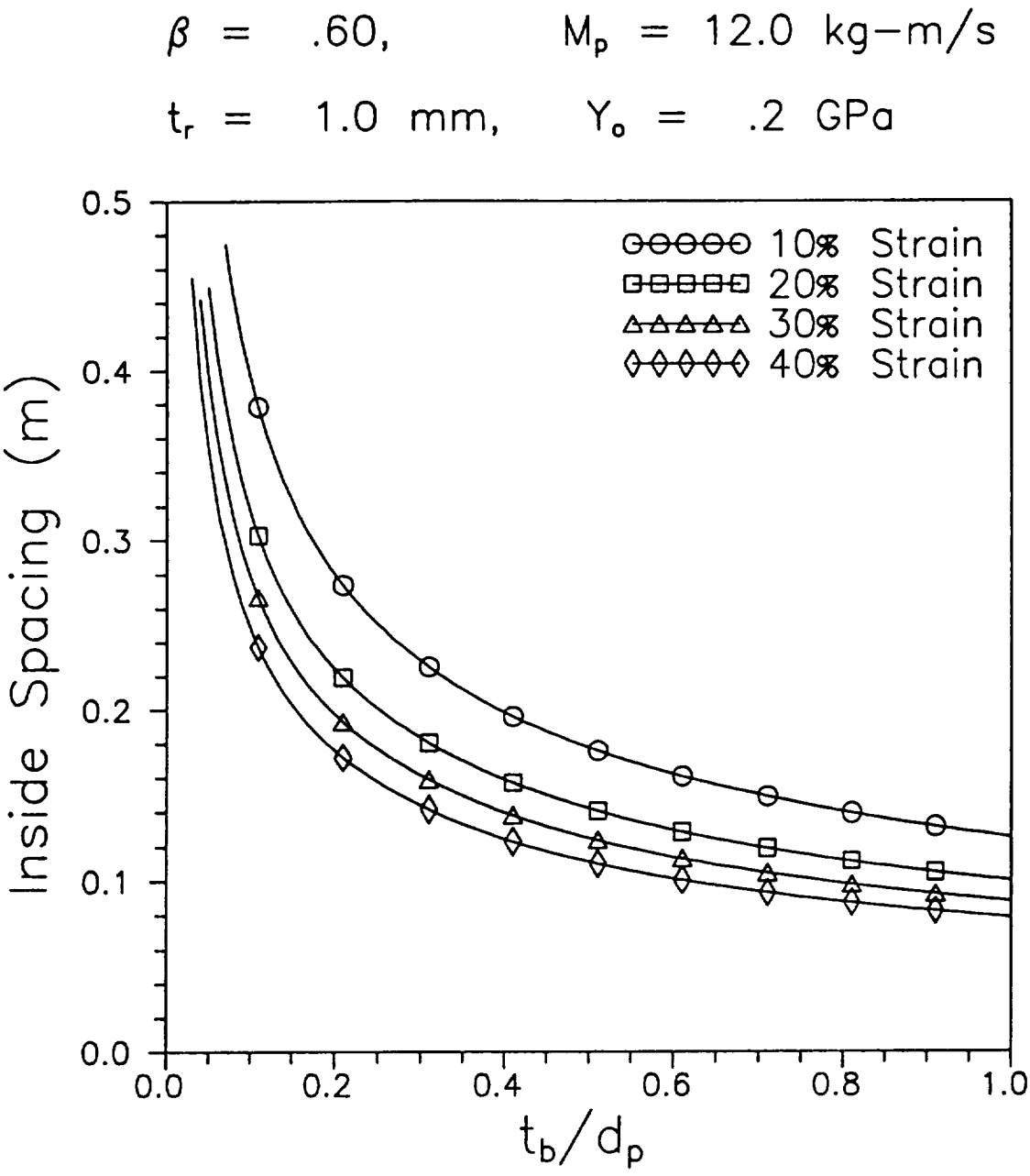

Figure 67. Design Curves for $\beta = 0.6$, $M_p = 12$ kg-m/s, $t_r = 1$ mm, and $Y_r = 0.2$ GPa

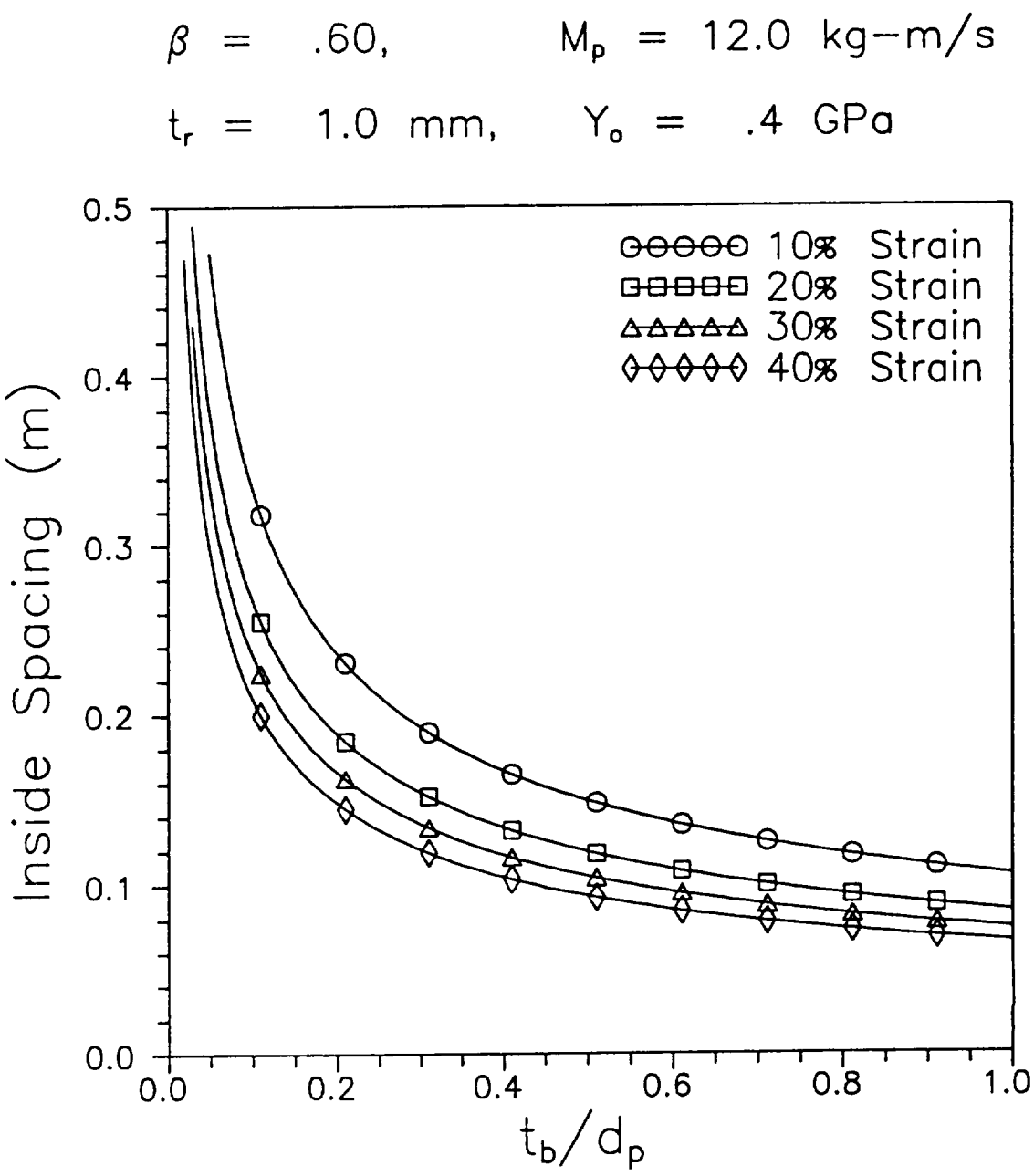

Figure 68. Design Curves for $\beta = 0.6$, $M_p = 12$ kg-m/s, $t_r = 1$ mm, and $Y_r = 0.4$ GPa

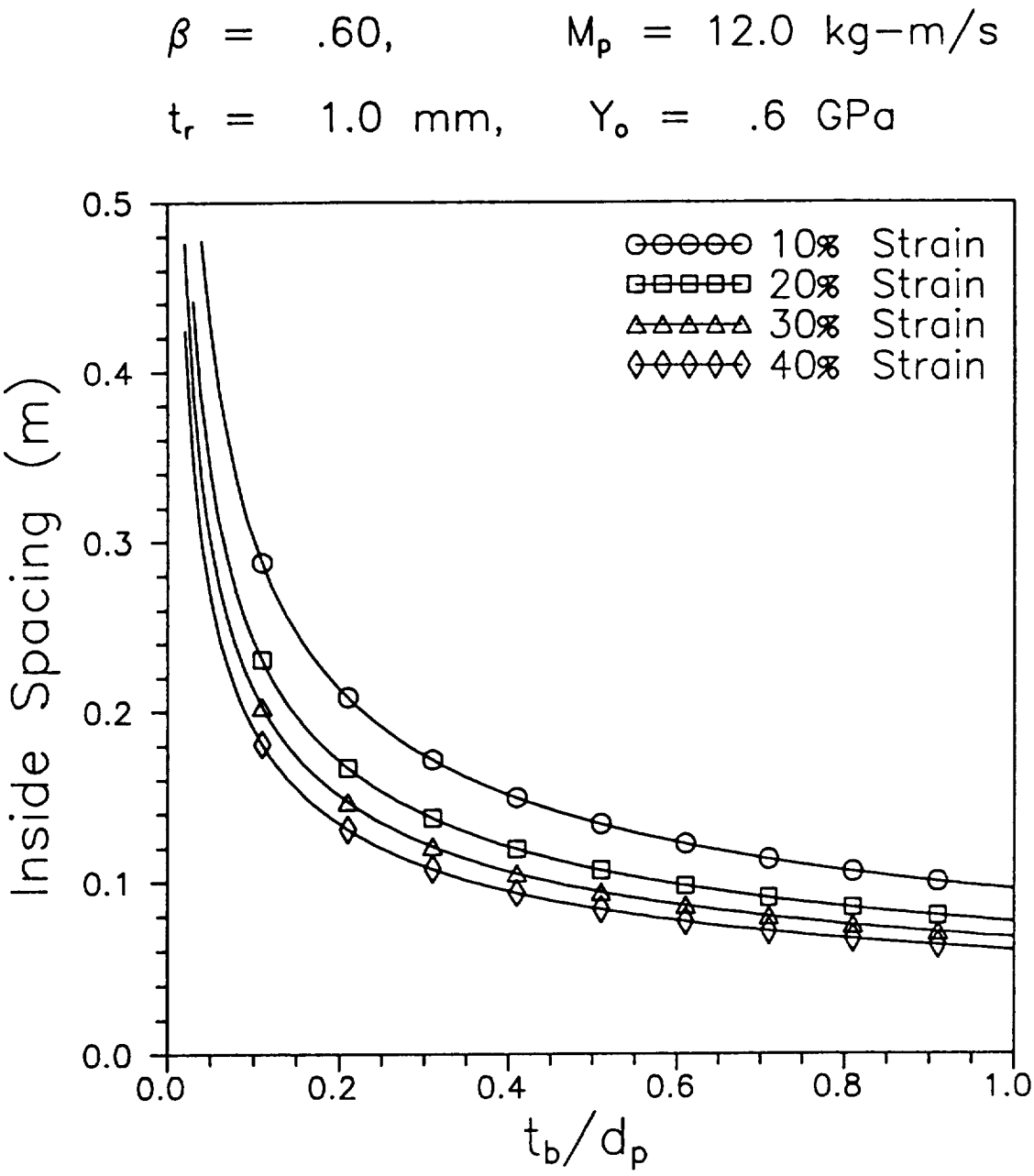

Figure 69. Design Curves for $\beta = 0.6$, $M_p = 12$ kg-m/s, $t_r = 1$ mm, and $Y_r = 0.6$ GPa

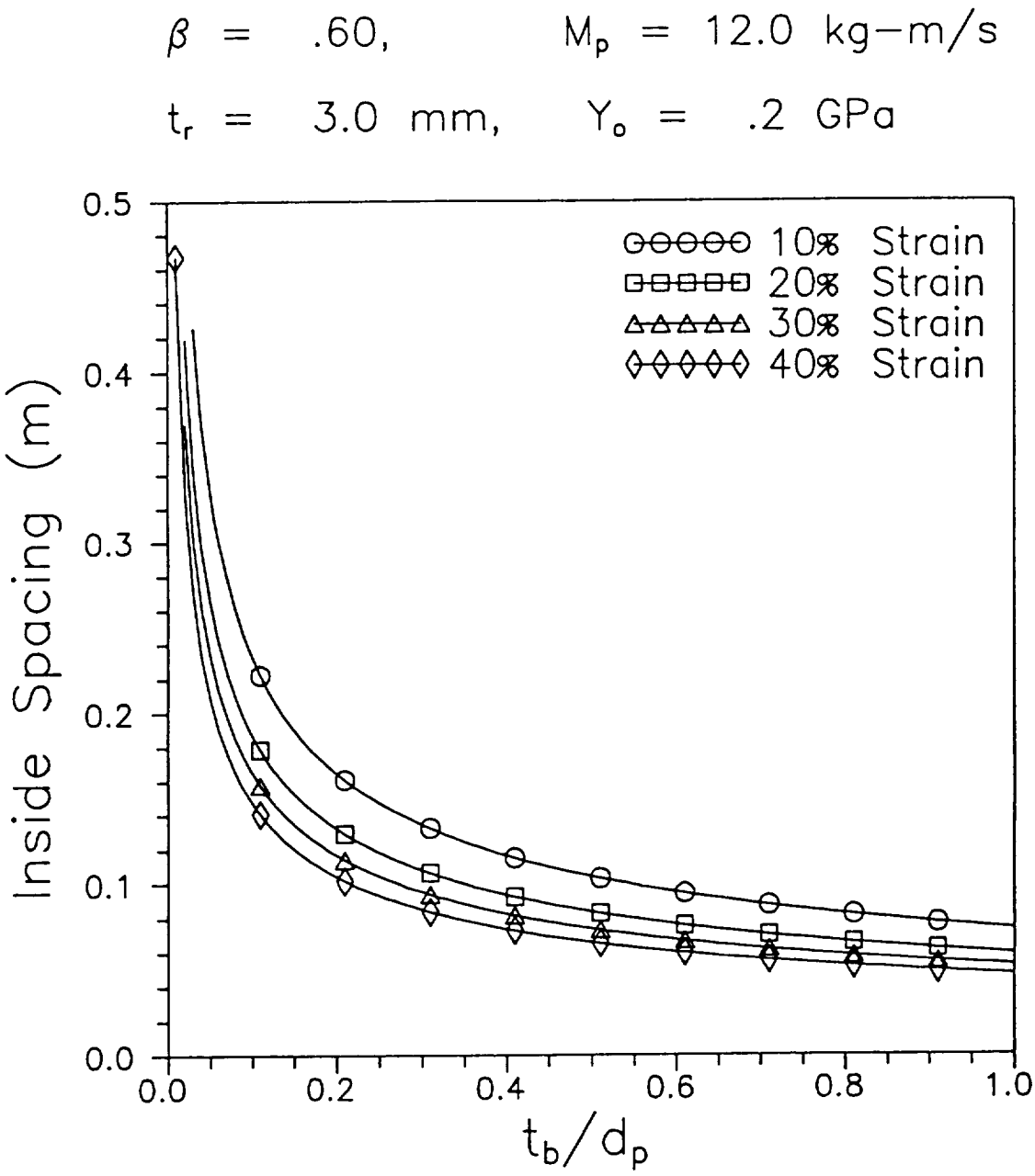

Figure 70. Design Curves for $\beta = 0.6$, $M_p = 12$ kg-m/s, $t_r = 3$ mm, and $Y_r = 0.2$ GPa

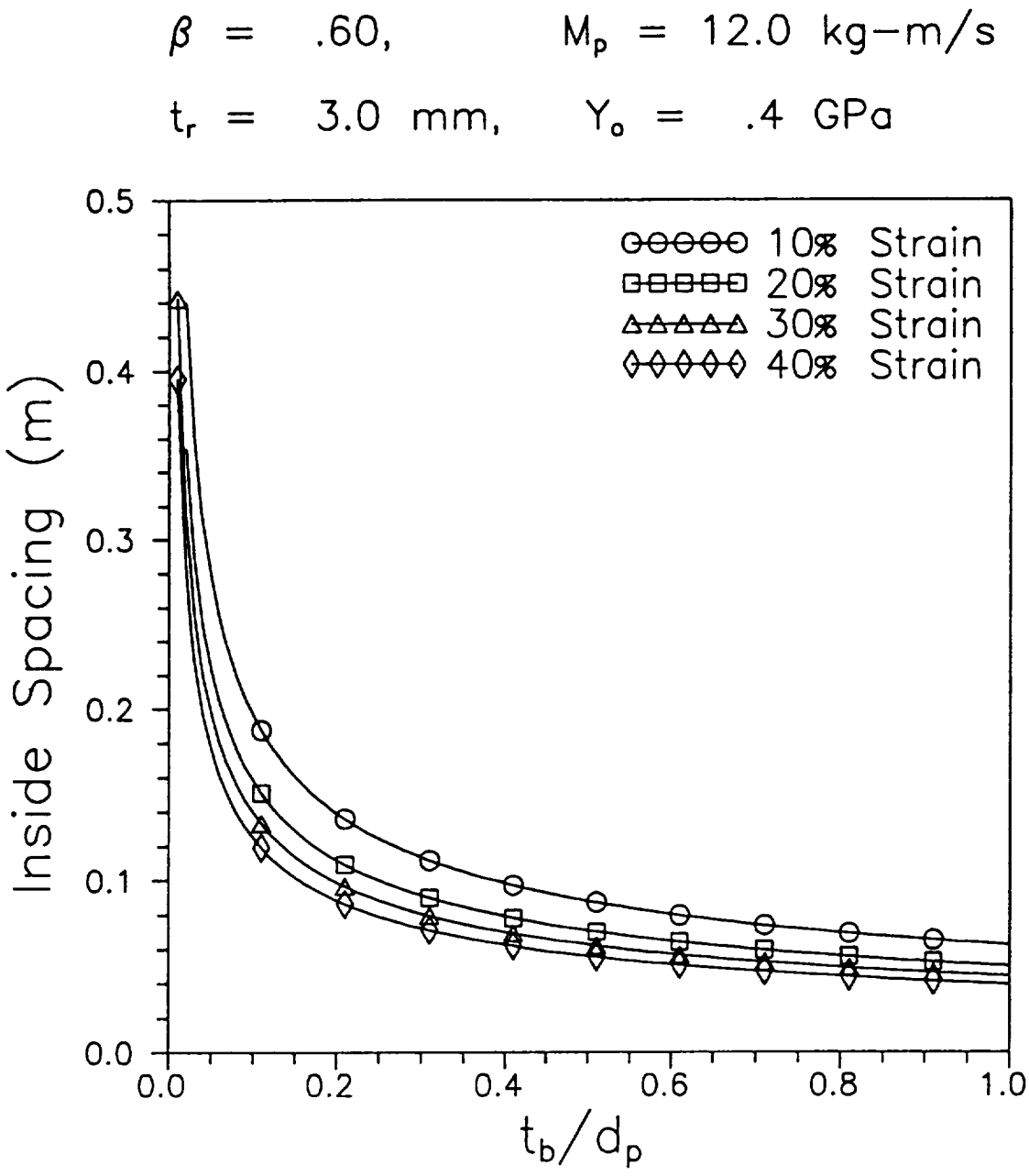

Figure 71. Design Curves for $\beta = 0.6$, $M_p = 12$ kg-m/s, $t_r = 3$ mm, and $Y_r = 0.4$ GPa

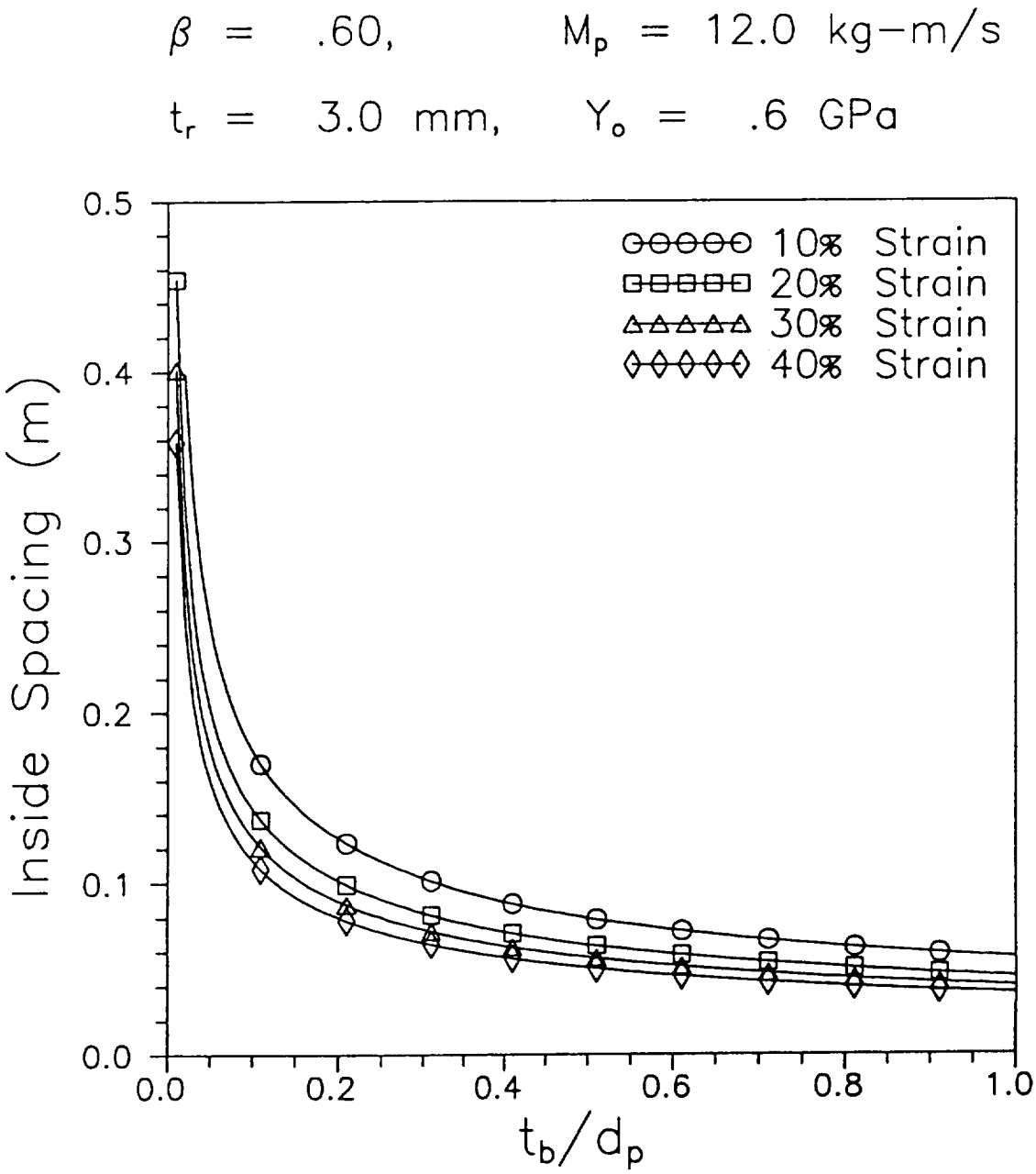

Figure 72. Design Curves for $\beta = 0.6$, $M_p = 12$ kg-m/s, $t_r = 3$ mm, and $Y_r = 0.6$ GPa

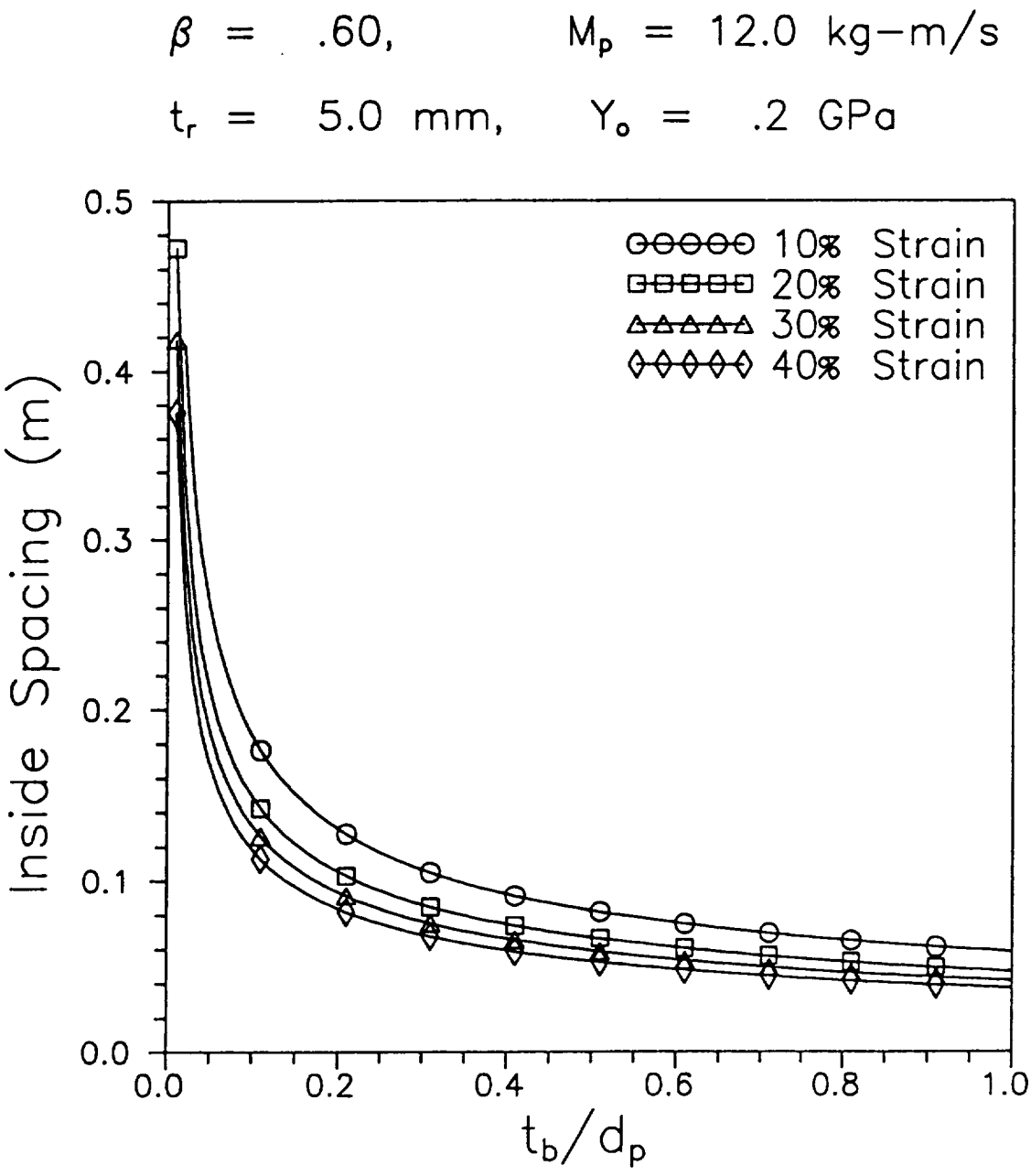

Figure 73. Design Curves for $\beta = 0.6$, $M_p = 12$ kg-m/s, $t_r = 5$ mm, and $Y_r = 0.2$ GPa

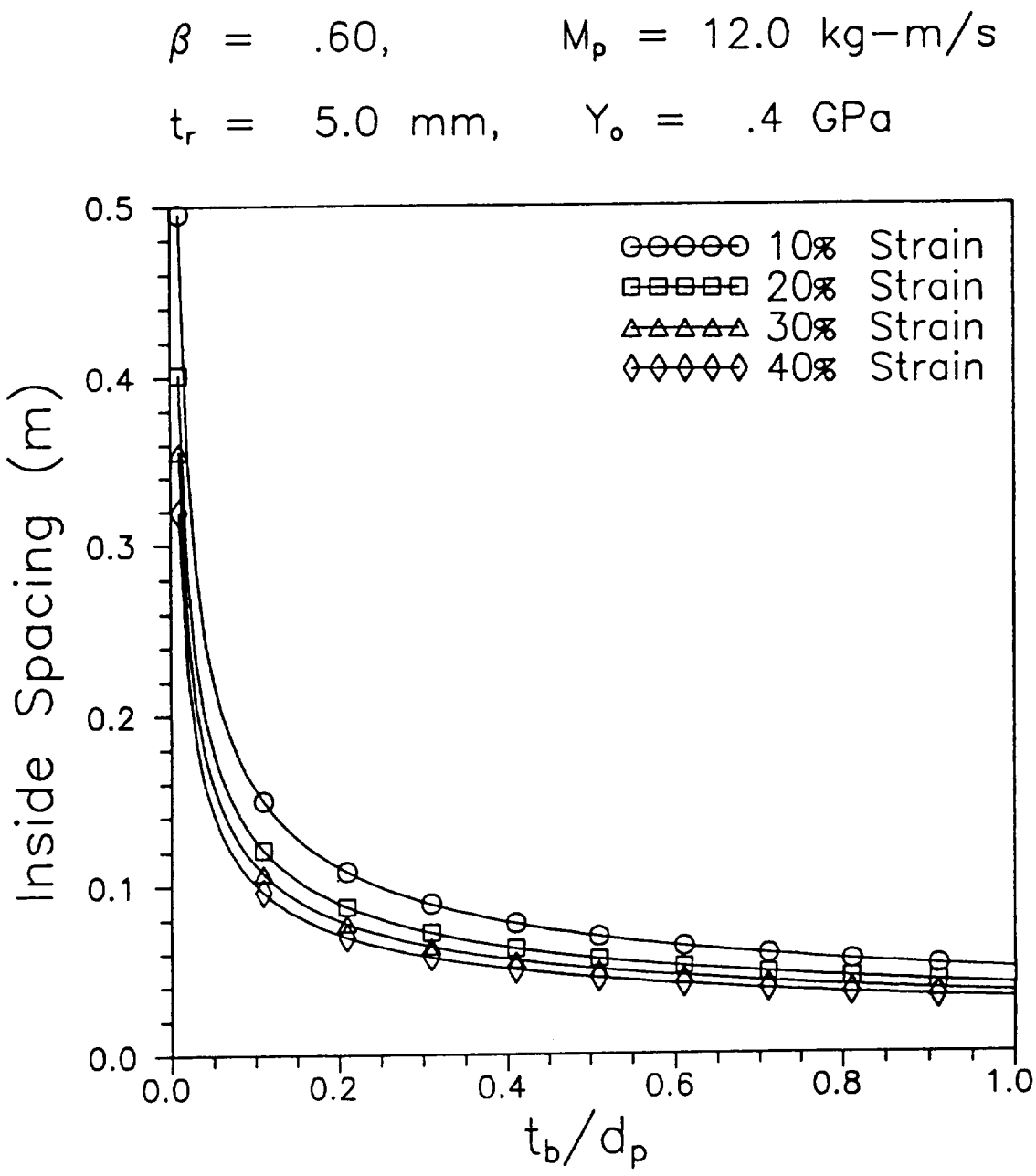

Figure 74. Design Curves for $\beta = 0.6$, $M_p = 12$ kg-m/s, $t_r = 5$ mm, and $Y_r = 0.4$ GPa

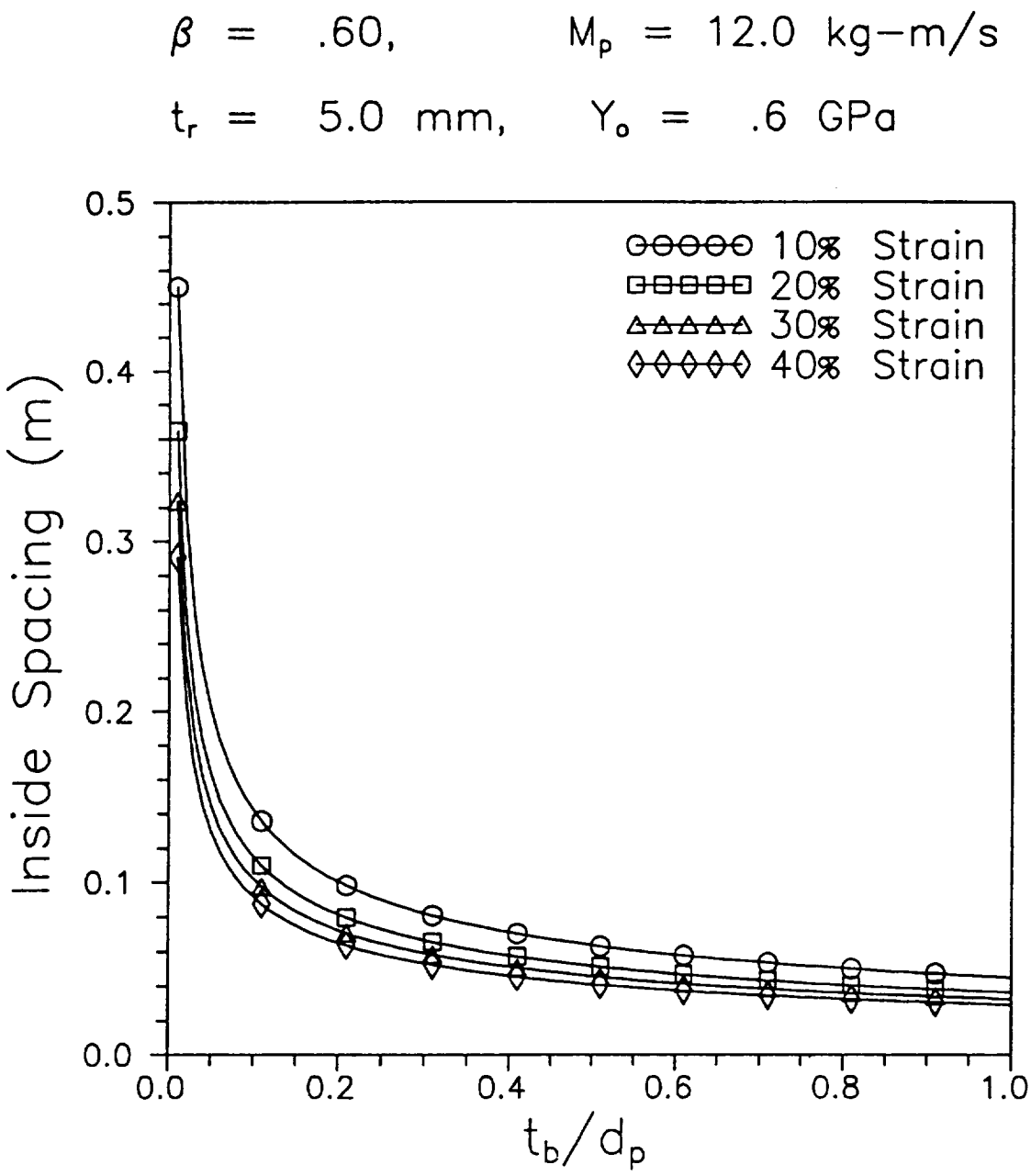

Figure 75. Design Curves for $\beta = 0.6$, $M_p = 12$ kg-m/s, $t_r = 5$ mm, and $Y_r = 0.6$ GPa

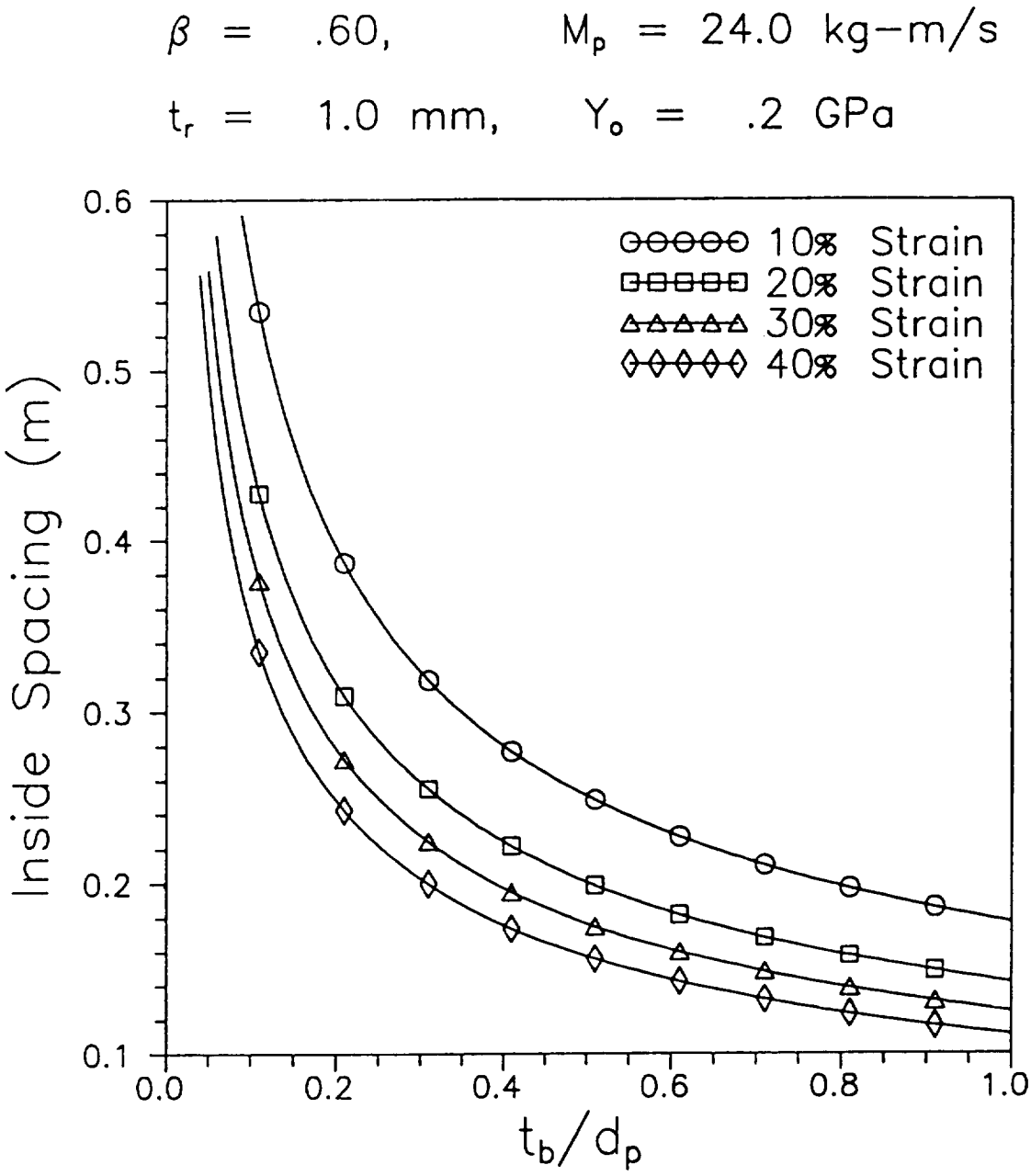

Figure 76. Design Curves for $\beta = 0.6$, $M_p = 24$ kg-m/s, $t_r = 1$ mm, and $Y_r = 0.2$ GPa

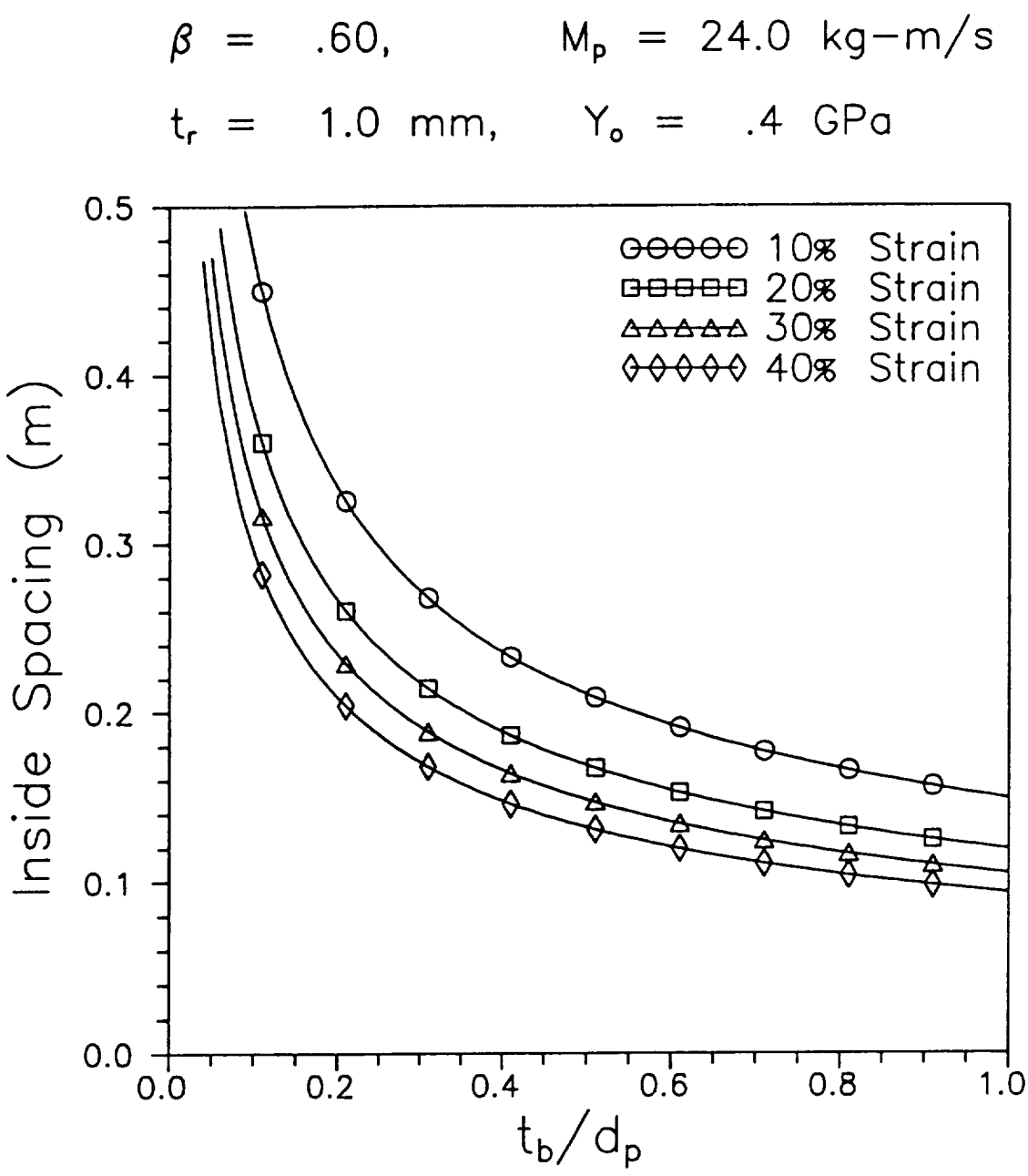

Figure 77. Design Curves for $\beta = 0.6$, $M_p = 24$ kg-m/s, $t_r = 1$ mm, and $Y_r = 0.4$ GPa

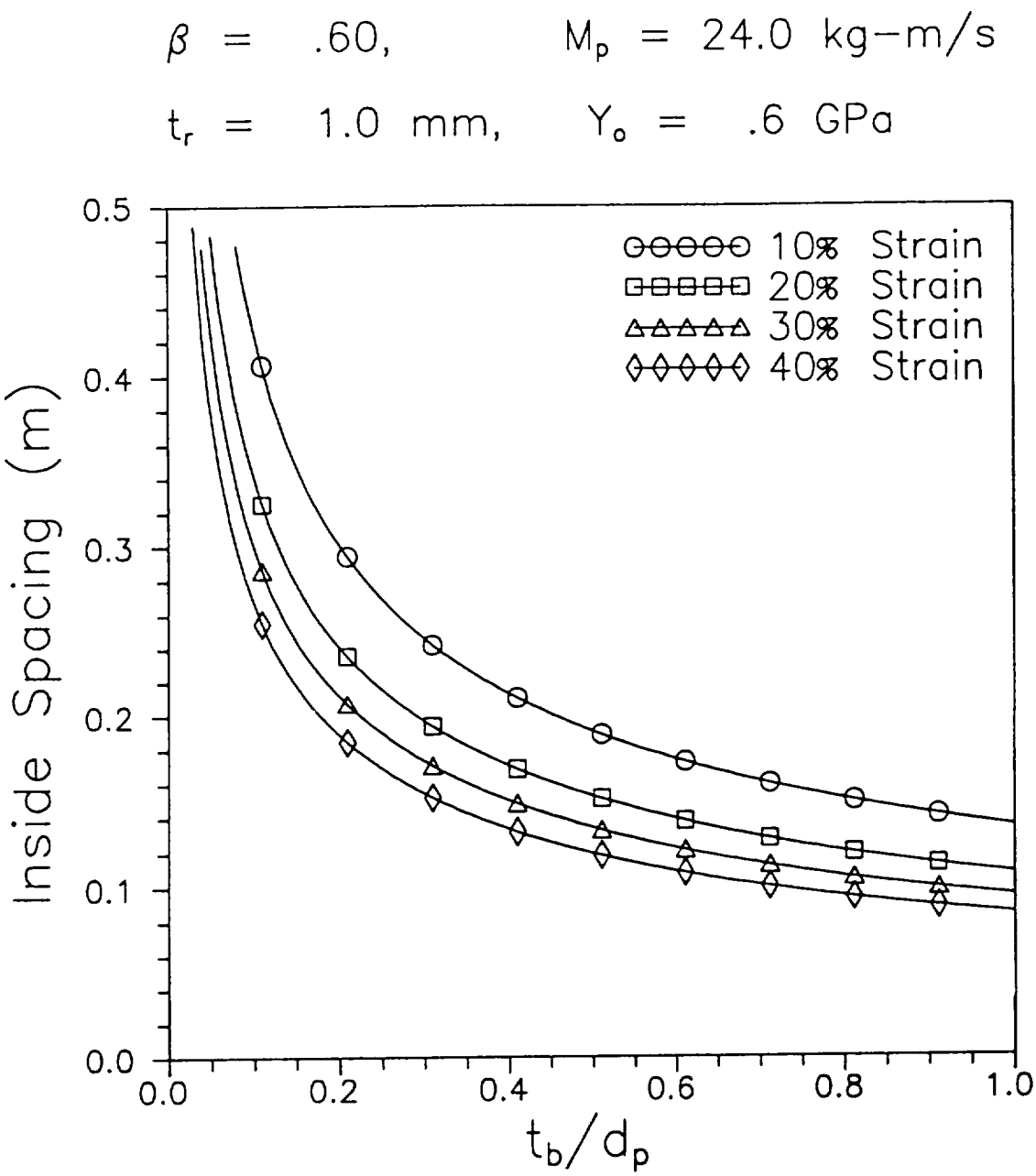

Figure 78. Design Curves for β = 0.6, M_p = 24 kg-m/s, t_r = 1 mm, and Y_r = 0.6 GPa

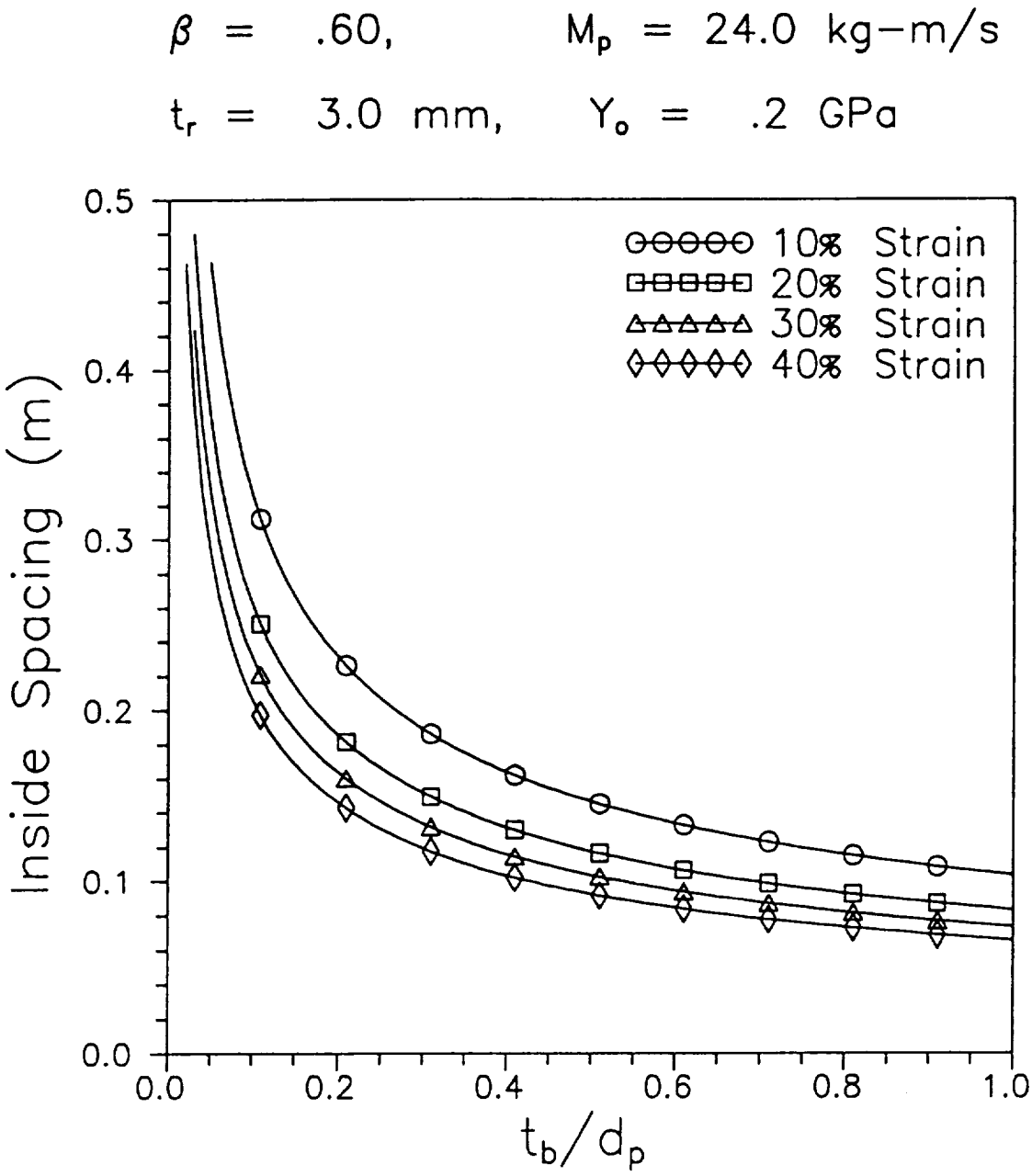

Figure 79. Design Curves for $\beta = 0.6$, $M_p = 24$ kg-m/s, $t_r = 3$ mm, and $Y_r = 0.2$ GPa

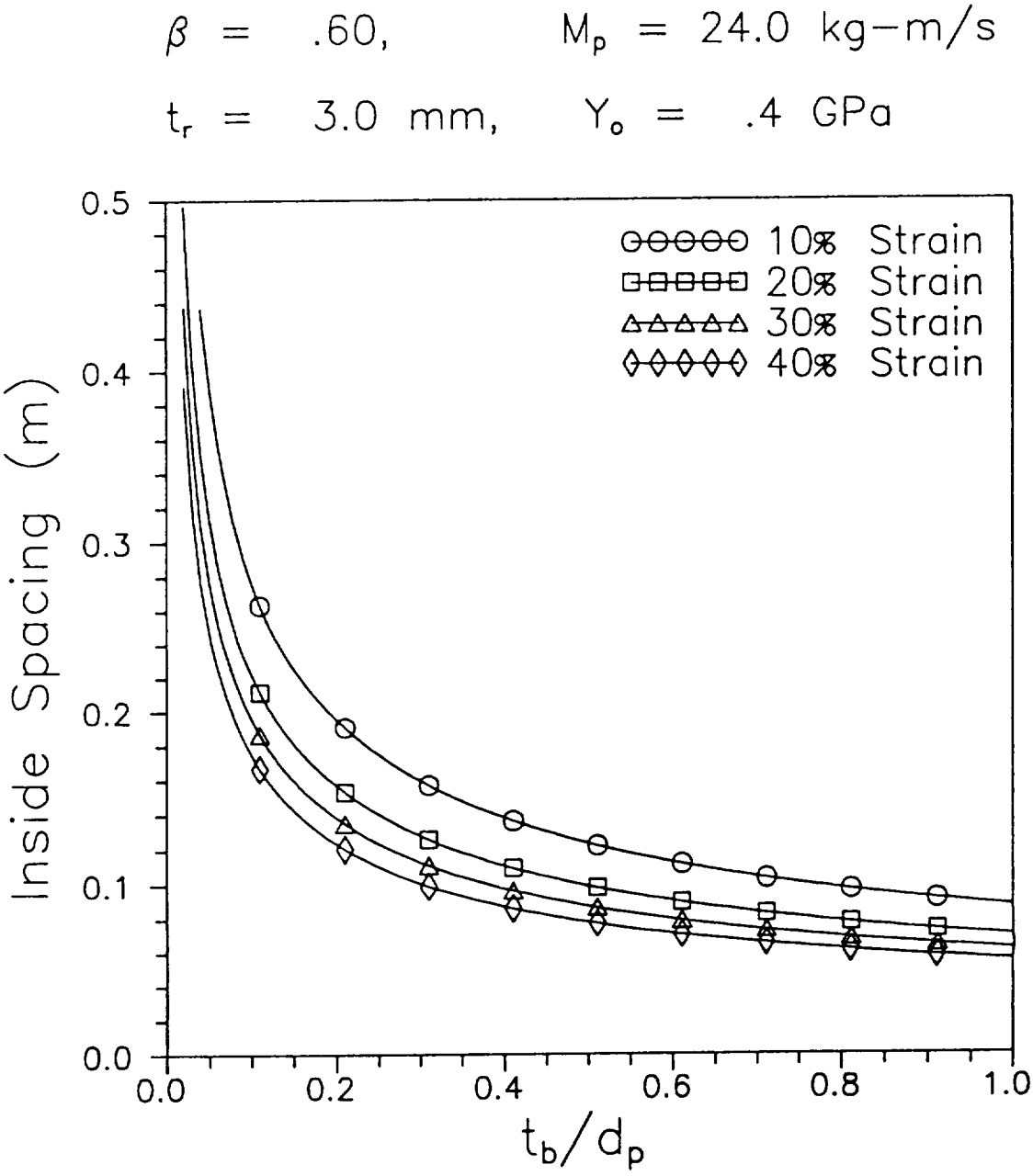

Figure 80. Design Curves for $\beta = 0.6$, $M_p = 24$ kg-m/s, $t_r = 3$ mm, and $Y_r = 0.4$ GPa

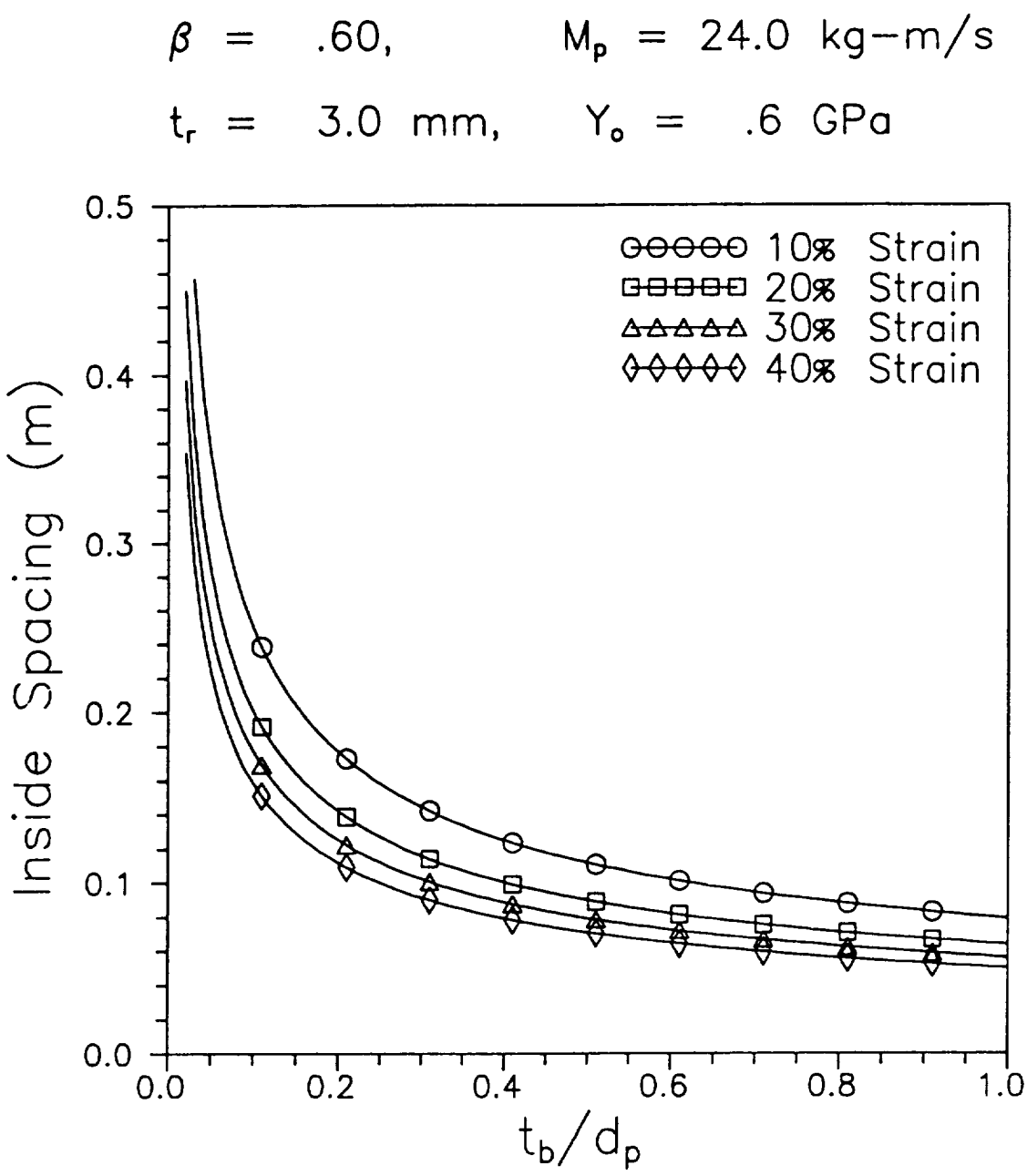

Figure 81. Design Curves for $\beta = 0.6$, $M_p = 24$ kg-m/s, $t_r = 3$ mm, and $Y_r = 0.6$ GPa

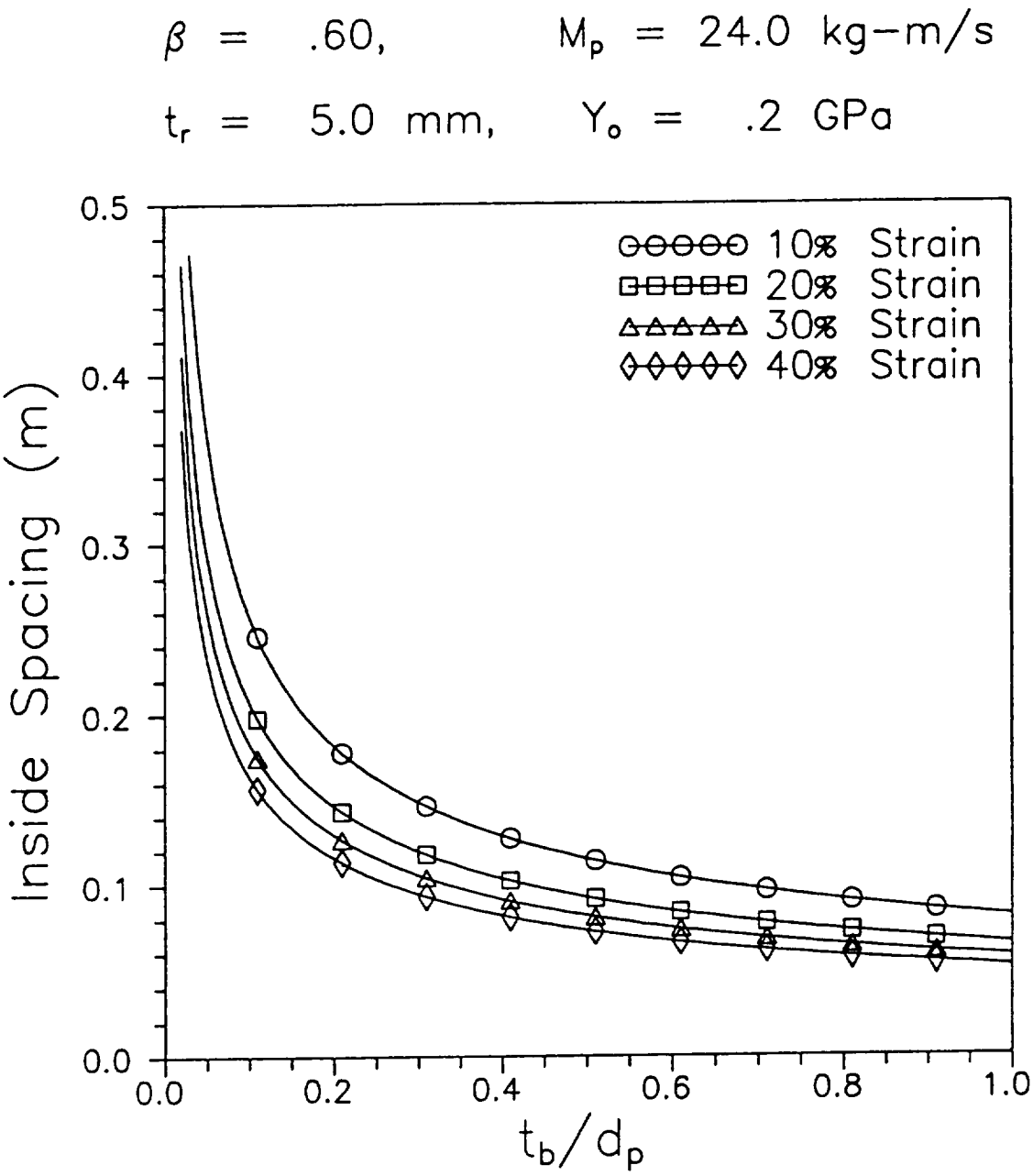

Figure 82. Design Curves for $\beta = 0.6$, $M_p = 24$ kg-m/s, $t_r = 5$ mm, and $Y_r = 0.2$ GPa

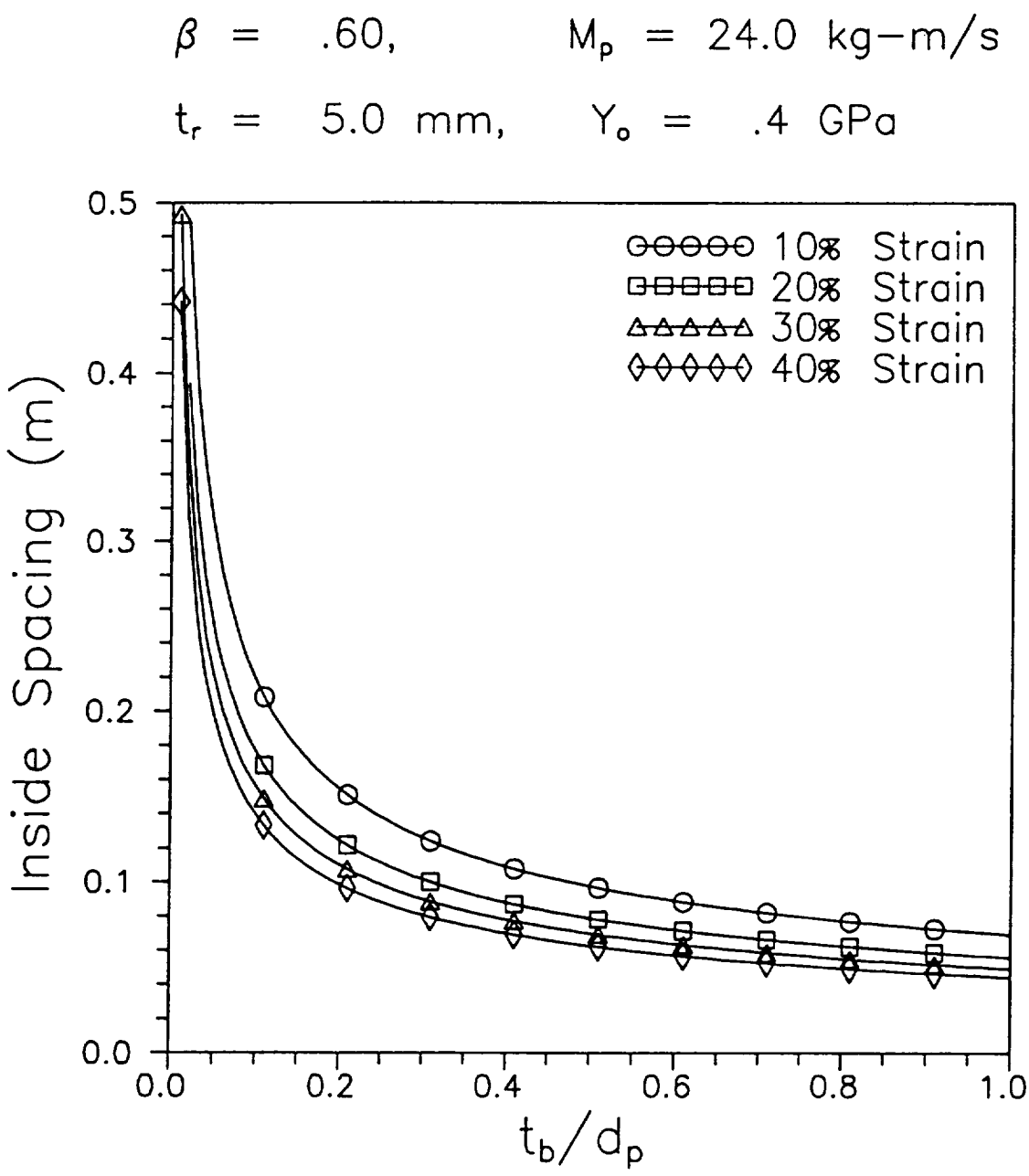

Figure 83. Design Curves for $\beta = 0.6$, $M_p = 24$ kg-m/s, $t_r = 5$ mm, and $Y_r = 0.4$ GPa

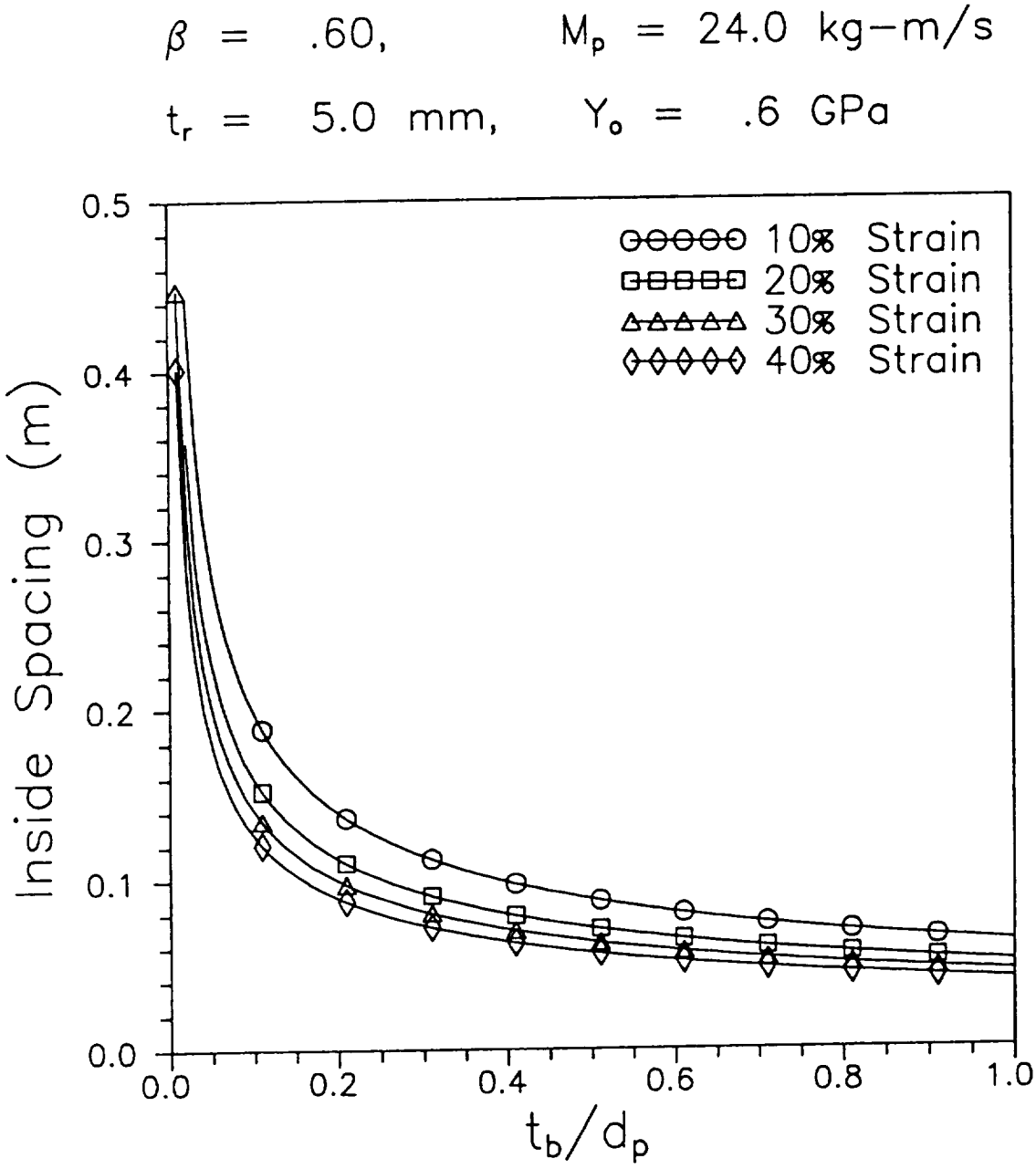

Figure 84. Design Curves for $\beta = 0.6$, $M_p = 24$ kg-m/s, $t_r = 5$ mm, and $Y_r = 0.6$ GPa

REFERENCES

1. J.P.D. Wilkinson, A penetration criterion for double-walled structures subject to meteoroid impact, AIAA 7 (10) (1969) 1937-1943.

2. A.M. Rajendran and N. Elfer, Debris-impact protection of space structures, Chapter 2, in: Structural Failure, eds. T. Wierzbicki and N. Jones (John-Wiley & Sons, Inc., 1989).

3. R. Hoffman, EPRI, NP-2080, (Nov. 1981).

4. G.R. Johnson and R.A. Stryk, Air Force Report No. AFATL-TR-86-51 (1986).

5. N. Elfer, unpublished works.

☆ U.S. GOVERNMENT PRINTING OFFICE – 1996 – 733-109/40010

REPORT DOCUMENTATION PAGE

Form Approved
OMB No. 0704-0188

Public reporting burden for this collection of information is estimated to average 1 hour per response, including the time for reviewing instructions, searching existing data sources, gathering and maintaining the data needed, and completing and reviewing the collection of information. Send comments regarding this burden estimate or any other aspect of this collection of information, including suggestions for reducing this burden, to Washington Headquarters Services, Directorate for Information Operations and Reports, 1215 Jefferson Davis Highway, Suite 1204, Arlington, Va 22202-4302, and to the Office of Management and Budget, Paperwork Reduction Project (0704-0188), Washington, DC 20503.

1. AGENCY USE ONLY (Leave Blank)	2. REPORT DATE	3. REPORT TYPE AND DATES COVERED
	February 1996	Contractor Report (Final)

4. TITLE AND SUBTITLE

Structural Damage Prediction and Analysis for Hypervelocity Impacts - Handbook

5. FUNDING NUMBERS

NAS8-38856

6. AUTHOR(S)

N. C. Elfer

7. PERFORMING ORGANIZATION NAME(S) AND ADDRESS(ES)

Lockheed Martin Marietta Manned Space Systems
P. O. Box 29304
New Orleans, LA 70189

8. PERFORMING ORGANIZATON REPORT NUMBERS

M-800

9. SPONSORING/MONITORING AGENCY NAME(S) AND ADDRESS(ES)

George C. Marshall Space Flight Center
Marshall Space Flight Center, Alabama 35812

10. SPONSORING/MONITORING AGENCY REPORT NUMBER

NASA CR-4706

11. SUPPLEMENTARY NOTES

Technical Monitor: Joel Williamsen, Structures and Dynamics Laboratory, Science and Engineering Directorate

12a. DISTRIBUTION/AVAILABILITY STATEMENT

Unclassified-Unlimited

Subject Category 18

12b. DISTRIBUTION CODE

13. ABSTRACT *(Maximum 200 words)*

This handbook reviews the analysis of structural damage on spacecraft due to hypervelocity impacts by meteoroid and space debris. These impacts can potentially cause structural damage to a Space Station module wall. This damage ranges from craters, bulges, minor penetrations, and spall to critical damage associated with a large hole, or even rupture. The analysis of damage depends on a variety of assumptions and the area of most concern is at a velocity beyond well controlled laboratory capability. In the analysis of critical damage, one of the key questions is how much momentum can actually be transfered to the pressure vessel wall. When penetration occurs without maximum bulging at high velocity and obliquities (if less momentum is deposited in the rear wall), then large tears and rupture may be avoided. In analysis of rupture effects of cylindrical geometry, biaxial loading, bending of the crack, a central hole strain rate and R-curve effects are discussed.

14. SUBJECT TERMS

aluminum alloys, bumpers, debris shields, fracture mechanics, hypervocity impacts, impact, meteoroids, orbital debris

15. NUMBER OF PAGES

320

16. PRICE CODE

A14

17. SECURITY CLASSIFICATION	18. SECURITY CLASSIFICATION OF THIS PAGE	19. SECURITY CLASSIFICATION OF ABSTRACT	20. LIMITATION OF ABSTRACT
Unclassified	Unclassified	Unclassified	Unlimited

National Aeronautics and
Space Administration
Code JTT
Washington, DC
20546–0001

Official Business
Penalty for Private Use, $300

Postmaster: If Undeliverable (Section 158 Postal Manual), Do Not Return